Universiteit Leiden
The Netherlands

# Mitochondria in chemical-induced toxicity

Stel, W. van der

**Citation**

Stel, W. van der. (2022, February 1). *Mitochondria in chemical-induced toxicity*. Retrieved from https://hdl.handle.net/1887/3270836

| | |
|---|---|
| Version: | Publisher's Version |
| License: | Licence agreement concerning inclusion of doctoral thesis in the Institutional Repository of the University of Leiden |
| Downloaded from: | https://hdl.handle.net/1887/3270836 |

**Note:** To cite this publication please use the final published version (if applicable).

# Mitochondria
## in chemical-induced toxicity

*Wanda van der Stel*

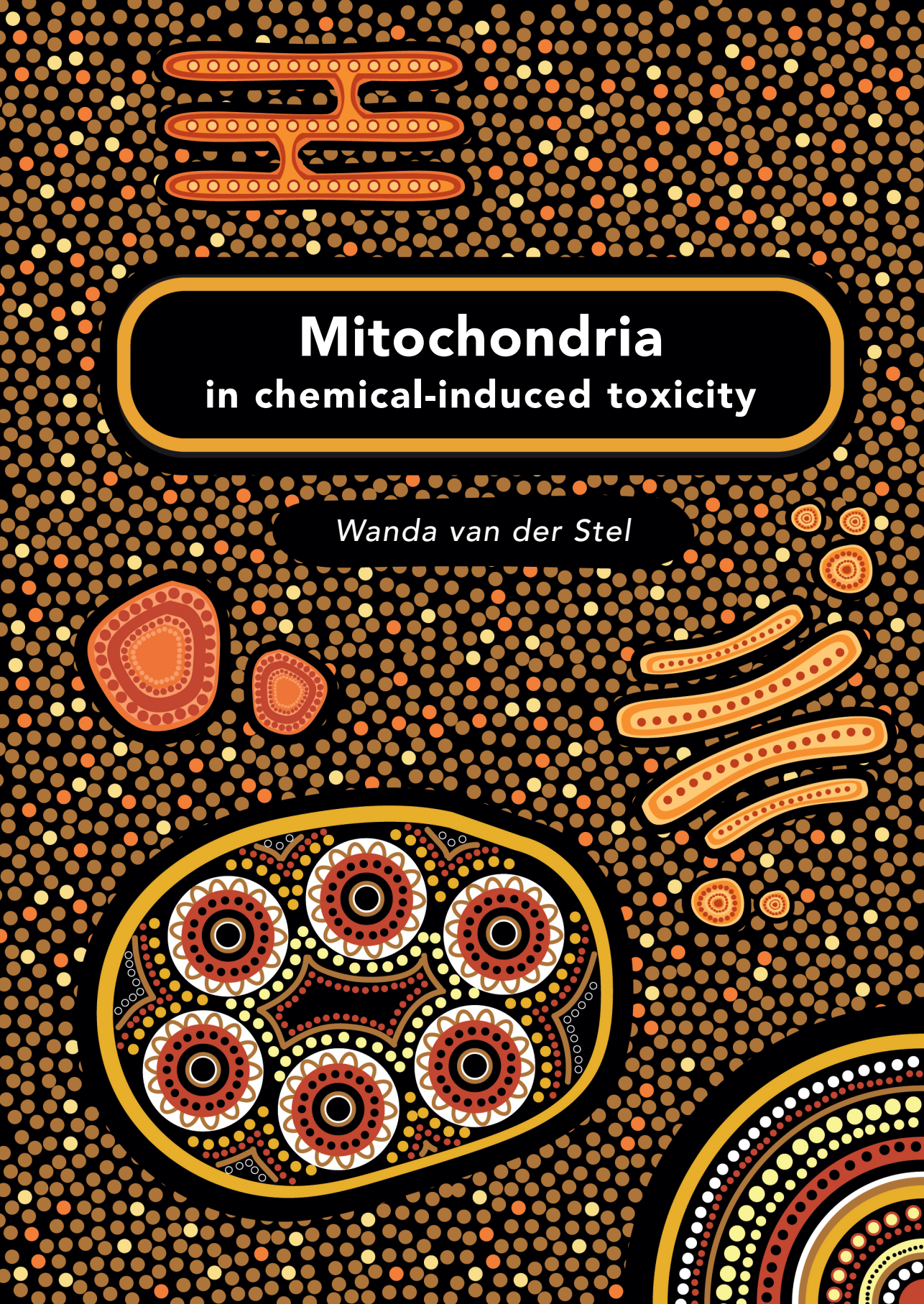

# Mitochondria

## in chemical-induced toxicity

Wanda van der Stel

Mitochondria in chemical-induced toxicity

ISBN: 978-94-6421-573-1

Cover design by Wanda van der Stel
Printed by Ipskamp Printing | proefschriften.net
Layout and design: Harma Makken, persoonlijkproefschrift.nl

© Wanda van der Stel, Leiden The Netherlands
All rights reserved. No part of this thesis may be reproduced, stored in a retrieval system, translated, or transmitted in any form or by any means now or hereafter known, electronic or mechanical, without permission in writing from the author

# Mitochondria

## in chemical-induced toxicity

PROEFSCHRIFT

ter verkrijging van de graad van doctor aan de Universiteit Leiden,

op gezag van rector magnificus prof. dr. ir. H. Bijl,

volgens besluit van het college voor promoties

te verdedigen op dinsdag 1 februari 2022

klokke 13:45

door

**Wanda van der Stel**

geboren op 4 oktober 1991 te Dordrecht, Nederland

**Promotor**

| | |
|---|---|
| Prof. dr. E.H.J. Danen | *Universiteit Leiden* |
| Prof. dr. B. van de Water | *Universiteit Leiden* |

**Promotion committee**

| | |
|---|---|
| Prof. dr. H. Irth (Chair) | *Universiteit Leiden* |
| Prof. dr. J.A. Bouwstra (Secretary) | *Universiteit Leiden* |
| Prof. dr. F.G. Russel | *Radboud Universiteit Nijmegen* |
| Prof. dr. H. Kamp | *BASF, Ludwigshafen Duitsland* |
| Prof. dr. T. Hankemeier | *Universiteit Leiden* |

This research was conducted at the Division of Drug Discovery and Safety of the Leiden Academic Centre for Drug Research (LACDR), Leiden University (Leiden, The Netherlands). The research was financially supported by the EU-ToxRisk project, grant agreement No 681002, funded by the European Union's Horizon 2020 research and innovation programme.

# Table of Contents

**Chapter 1**
General introduction, aim and scope of thesis 7

**Chapter 2**
Assessing mitochondria-related organ toxicity; using new approach methods in an adverse outcome pathway framework 19

**Chapter 3**
Multiparametric assessment of mitochondrial respiratory inhibition in HepG2 and RPTEC/TERT1 cells using a panel of mitochondrial targeting agrochemicals 61

**Chapter 4**
Mapping the cellular response to electron transport chain inhibitors reveals selective signaling networks triggered by mitochondrial perturbation 91

**Chapter 5**
Mitochondrial fragmentation through OPA1-cleavage in response to ETC inhibition is driven by a combination of reduced ATP and increased MMP 135

**Chapter 6**
Dynamic modeling of mitochondrial membrane potential upon exposure to mitochondrial inhibitors 163

**Chapter 7**
New approach methods (NAMs) supporting read-across: two neurotoxicity AOP-based IATA case studies 201

**Chapter 8**
Discussion and future perspectives 231

**Appendix**
References 242
Abbreviations 267
Nederlandse samenvatting 268
List of publications 272
About the author 275

# 1

# General introduction, aim and scope of thesis

Chemical-induced organ toxicity is a major concern in the development and societal application of chemicals, including pharmaceutical drugs, pesticides, industrial chemicals and cosmetics. In the last decades, the onset and progression of chemical-induced organ-toxicity have been linked to the perturbation of various cellular targets and processes, one of which is mitochondrial functioning. This is illustrated by a study involving 10,000 tested environmental chemicals and drugs (the TOX21 library) from which 15% perturbs mitochondrial respiration upon exposure [Attene-Ramos 2015, Xia 2018]. Mitochondria appear to be a major target after exposure to higher chemical concentrations in the case of liver, heart or kidney toxicity [Rana 2019]. Unraveling the mechanisms relating mitochondrial perturbations to organ-toxicity is essential to improve hazard identification and risk assessment for new and existing chemicals. This thesis elaborates on the development of quantitative markers for the assessment of chemically-induced mitochondrial perturbation. In this first chapter I will introduce the biological role of mitochondria, their susceptibility to perturbations and the role of perturbed mitochondria in development of organ failure. Furthermore, I will discuss how biomarkers of mitochondrial functioning could improve the mechanistic understanding of the progression of chemical-induced organ-toxicity and thereby support early stage risk assessment of chemicals.

## Mitochondria

Mitochondria are organelles essential for the energy production in eukaryotic cells. They are thought to originate from aerobic prokaryotes which established an endosymbiosis with the ancestors of today's eukaryotes. Although its precise trigger remains unknown, it is clear that this endosymbiosis provided the eukaryotic cell the opportunity to survive in more oxygen-rich atmospheres, develop into more complex architectures and support multi-cellular collaborations [Martin 2015]. In eukaryotic cells the mitochondrion consists of a double membrane enclosing the mitochondrial matrix with its unique circular DNA. This mitochondrial DNA (mtDNA) encodes for the majority of proteins and associated ribosomal RNAs involved in the oxygen-dependent production of energy via the electron transport chain (ETC). The double membranes provide the opportunity to create a proton gradient used to drive the production of energy carriers and the enclosed matrix is used to store ions like calcium. An energy carrier like ATP is of major importance for the effective functioning of active transport, signal transduction pathways and RNA/protein synthesis in the cell [Alberts 2002, Lynch 2015][1,2]. Active transport is a form of transport which consumes ATP to be able to transport molecules, like for example glucose, over membranes against a concentration or electrochemical gradient. ATP itself or the energy stored in ATP is also used to transport information concerning extracellular conditions from the cellular membranes into the cell, for instance signal transduction supported by

ATP-driven phosphorylation or the use of cAMP which is created from ATP. Not only transport and signaling requires the energy, also both RNA transcription and protein translation require the input of energy to allow the cell to assemble all proteins in the cell.

Furthermore, mitochondrial specific enzymes present in the mitochondrial matrix provide the necessary equipment to produce crucial building blocks, including amino acids, nucleotides, lipids, and Fe-S clusters, needed for protein translation, RNA transcription, membrane construction and enzyme functioning [Pfanner 2019, Friedman 2014]. All together this prominent role of the mitochondria in energy, amino acid, nucleotide and lipid production, makes the organelle the perfect sensor for the detection of abnormalities in the cellular homeostasis.



## Energy production in the cell

Energy required for cellular functioning is obtained from three sources: carbohydrates, proteins and fatty acids originating from our diet [Nelson 2017]. They are metabolized via an interplay between enzymatic reactions in the cytoplasm and mitochondria. Which of these three substrates is used depends on the availability in our food, the requirements of the cell itself, the presence of enzymes/substrates needed for all intermediate steps and the presence of oxygen.

Carbohydrate metabolism and especially glucose metabolism occurs in three successive metabolic steps: glycolysis, the citric acid cycle and mitochondrial respiration (figure 1). Glycolysis, an anaerobic process occurring in the cytoplasm of the cell, is the conversion of imported glucose via multiple enzymatic steps into pyruvate with a net yield of 2 ATP molecules. Pyruvate is subsequently transported into mitochondria by the mitochondrial pyruvate carriers 1 and 2 (MPC 1 and MPC2) [Bricker 2012], converted into 2-carbon acetyl-CoenzymeA (acetyl-CoA) and processed by the citric acid cycle: a series of metabolic steps resulting in the creation of NADH, $FADH_2$ and $CO_2$. The produced energy rich NADH and $FADH_2$ molecules are the fuel for the mitochondrial respiration. In an oxygen-poor environment cells rely completely on the less efficient ATP production via the glycolysis and do not shuttle pyruvate through the citric acid cycle, but instead convert pyruvate to lactate by fermentation.

Fatty acids are imported from the cytoplasm into the mitochondria where they are further metabolized. The import is through active transport for chain length longer than 14 carbons (carnitine carrier) [Indiveri 2011]. The complete metabolism of the fatty acid carbon chains is termed beta-oxidation, which is the gradual removal of all carbon pairs and coupling them to CoA resulting in acetyl-CoA. This process yields both NADH and $FADH_2$ molecules. Acetyl-CoA enters the citric acid cycle together

with the acetyl-CoA obtained from the glycolysis. In case of fasting, the intermediates of the citric acid cycle are depleted and the mitochondria start to produce ketone bodies from acetyl-CoA (ketogenesis). This form of energy production allows the beta-oxidation and mitochondrial respiration to continue without the need of the citric acid cycle. However, prolonged production of ketone bodies will result in an undesired drop in the pH of body fluids, eventually resulting in toxicity.

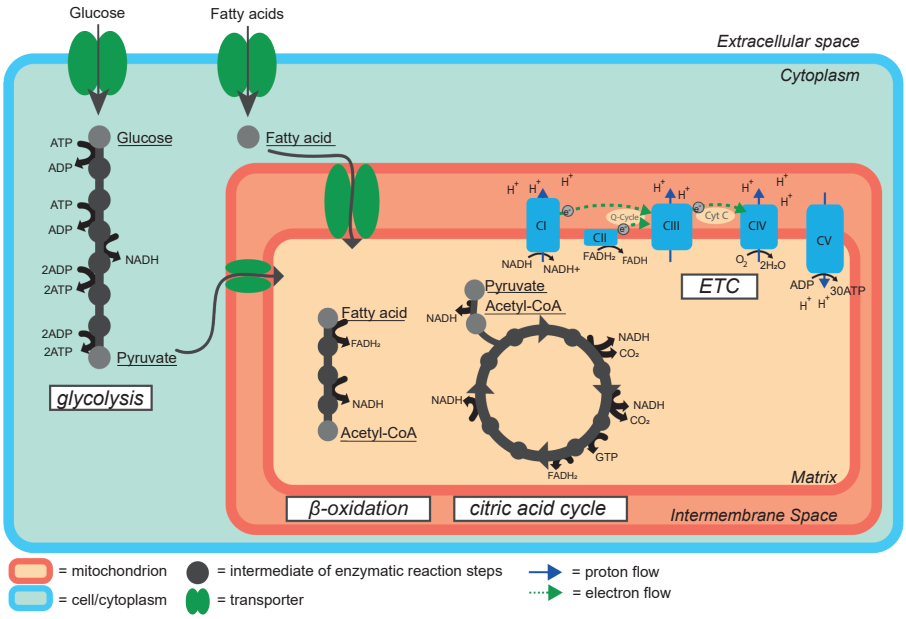


**Figure 1: Energy production in the cell from glucose and fatty acids**. Glucose and fatty acids are converted in the cytoplasm and mitochondria to ATP, NADH and $FADH_2$ via an interplay of glycolysis, β-oxidation, citric acid cycle and subsequently the electron transport chain (ETC). The intermediate steps in the glycolysis, β-oxidation and citric acid cycle are omitted for clarity and the protein complexes involved in the ETC are mitochondrial complex I, II, III, IV (respectively CI, CII, CIII, CIV and CV) .

The amino acids extracted from various proteins enter the citric acid cycle at various steps. In humans, there are two subgroups of amino acids: ketogenic amino acids, which can be converted to ketone bodies, and glucogenic amino acids, which can be used to create glucose and glycogen. The ketogenic amino acids are converted to acetyl-CoA and enter the citric acid cycle together with the acetyl-CoA created from carbohydrates and fat, while the glucogenic amino acids are pre-cursors for various intermediate substrates in the citric acid cycle or can be converted to pyruvate.

## Mitochondrial respiration (Electron transport chain)

The NADH and $FADH_2$ energy carriers that are created in the beta-oxidation and citric acid cycles are used in the mitochondrial respiration chain. To free the energy stored in

the electrons from NADH and $FADH_2$, they are passed over 4 protein complexes called the electron transport chain (ETC): complexes I (NADH dehydrogenase), II (Succinate dehydrogenase), III (Cytochrome bc1 complex) and IV (Cytochrome c oxidase), each transferring electrons from electron donors to electron acceptors. The energy that is released in these redox reactions is used to shuttle protons over complex I, III and IV from the mitochondrial matrix into the intermembrane space. Finally, low energy electrons are used by complex IV to reduce $O_2$ into $H_2O$, making the electron transport chain a form of aerobic energy production. The produced proton gradient drives the conversion of 30 ADP molecules to ATP in mitochondrial respiration chain complex V (ATPsynthase), making the mitochondrial respiration the major contributor to ATP production in the cell.



## Mitochondrial susceptibility towards damage

The central role of mitochondria in energy production and amino acid metabolism makes perturbation of these organelles a major risk factor in the cellular response to toxic chemicals. Furthermore, various features of the organelle itself, including the double membrane, the charged inner compartment and the presence of detoxifying enzymes and DNA, create vulnerability towards chemical toxicity [Meyer 2013].

Mitochondria are sensitive to the accumulation of chemical structures with various physicochemical properties within their matrix [Ross 2006, Battogtokh 2018]. Lipophilic compounds are attracted because of the lipid rich mitochondrial membranes, while cationic metals accumulate in the mitochondria because of the presence of a negative charged and a slightly alkaline matrix. Furthermore, the combination of lipophilic membranes and a charged/alkaline matrix attracts chemicals with amphiphilic properties. Besides accumulation of the parent chemical also the accumulation of metabolites bears the risk to disrupt mitochondrial integrity. The presence of metabolic enzymes in the mitochondria and the closely connected endoplasmic reticulum (ER) results in increased levels of reactive metabolites in the mitochondrial matrix [Sangar 2010].

Disruption of the mitochondrial membranes can also have secondary consequences. Under normal conditions the mitochondrial DNA is safely stored within the mitochondrial compartment. However, mitochondrial DNA leakage into the cytosol upon loss of mitochondrial integrity can trigger an undesired immune reaction targeted against free-nucleotides, causing or aggravating toxicity [Maekawa 2019].

Cells contain hundreds of mitochondria and therefore severe damage to a small fraction of these mitochondria will not immediately result in cytotoxicity and, consequently, tissue or organ malfunctioning [Alberts 2002]. The occurrence of

cytotoxicity upon chemical exposure largely depends on accumulation of damaged mitochondria and the speed by which the mitochondrial pool can restore itself. Single mitochondria possess an arsenal of options to restore homeostasis, including the activity of molecular chaperones to restore misfolded proteins [Munch 2018] and detoxifying enzymes to neutralize reactive parent chemicals and metabolites [Forred 2017, Holley 2011]. Furthermore, the pool of mitochondria in a cell provides the opportunity to cope with low amounts of damage via organelle interaction. The mitochondrial interaction is a balance between fusion – fusion of two or more organelles – and fission – splitting of one organelle into two or more – [Westermann 2010, Gaicomell 2020]. Together they provide the opportunity to exchange DNA and proteins, but also split off unrepairable components, which can be degraded specifically via the process termed mitophagy [Youle 2011, Hamacher-Brady 2016]. All processes combined make that the cell system can handle stress internally until a certain threshold is reached. Beyond this tipping point, the system will decide to sacrifice individual cells to save the organ and with that the species.

## Mitochondria as player in chemical-induced organ toxicity

As mentioned above, the cell and its mitochondria possess various adaptive mechanisms which can help to cope with limited amount of damage. However, acute high levels of perturbation or prolonged presence of damage can lead to organ toxicity. Tissues and organs which demonstrate high susceptibility towards toxicity include those involved in chemical metabolism and excretion. Disturbing either of these processes can result in accumulation of parent chemicals or its metabolites, as observed in liver and kidney [Doull's 2008]. Organs, like heart, kidney and muscle, with a high energy demand rely more heavily on mitochondrial respiration and are therefore more susceptible to mitochondrial specific organ toxicity [Pagliarini 2008, Wang 2010]. Finally, tissues, like neurons, with limited capacity to counteract the impaired mitochondrial respiration, via the upregulation of glycolysis, also demonstrate a higher occurrence of toxicity [Fernandez-Fernandez 2012, Zhao 2019].

Mitochondrial perturbation has been observed as off-target effect upon intake of various drug classes [Dykens 2007a, Dykens 2007b, Will 2019]. These chemicals can target various components of the mitochondria, including electron transport chain complexes, enzymes/ substrates, mitochondrial DNA, structural proteins or the mitochondrial permeability transition pores. Another subset of the chemicals affecting the mitochondria are designed to target mitochondria of others species (e.g. pesticides and piscicides like rotenone and antimycin), but demonstrate undesired affinity for human mitochondrial proteins.

The class of chemicals designed to interfere with mitochondrial respiration include pesticides manufactured to inhibit mitochondrial complex I of the ETC. Various retrospective studies speculate about an association between the hazard of developing Parkinson's-like diseases and prolonged exposure to complex I inhibitors, like rotenone [Tanner 2009, Tanner 2011, Nandipati 2016]. *In vivo* assessment of the toxicity of rotenone indicated the development of neuronal defects, which correlates with the possible development of neurological disorders [Betarbet 2000]. The occurrence of the undesired toxicity across species has led to environmental use restriction regulations in various countries [Gonzalez-Coloma 2013].



The undesired occurrence of mitochondrial perturbation as off-target effect upon exposure to chemicals has also led to usage restrictions (box warnings) or even withdrawal of chemicals and especially drugs from the market. The observed adversities are mostly occurring in the liver and heart, but malfunctioning of muscles, intestine or even systemic failure (development of lactic acidosis) have also been reported [Boelsterli 2007, Dykens 2017a, Dykens 2017b, Will 2019]. Examples of drugs withdrawn from the market include the liver injury inducing drugs nefazodone (anti-depressant), troglitazone (anti-diabetic) and trovafloxicin (antibiotic). An overrepresented class of drugs which have a box warning are commonly used pain medication drugs, including acetaminophen and NSAIDs (non-steroidal anti-inflammatory drugs) like, acetylsalicyl acid, celecoxib, diclofenac, ibuprofen, indomethacin, mefenamic acid, meloxicam, nabumetone, naproxen, nimusulide, piroxicam and sulindac.

## Mitochondria as biomarker for toxicity

In the past, a number of mitochondria perturbing agents have entered the market undetected. To reduce these incidences, industry introduced mitochondrial toxicity testing in their current chemical development pipelines [Dykens 2014]. However, to keep improving the mitochondrial risk assessment, it is important to validate existing biomarkers, introduce new candidates and to integrate them into structured risk assessment strategies.

To optimize the use of existing biomarkers and assays, it is important to select and validate their biological relevance. Currently, the assessment of the chemical impact on mitochondrial health is mostly based on biochemical readouts for the different mitochondrial processes, including oxidative phosphorylation (OXPHOS), metabolism, organelle dynamics, protein homeostasis, ion homeostasis and organelle degradation. These assays are specifically relevant for mitochondrial functioning and are therefore very suitable for the identification of direct and efficient inhibitors of mitochondrial targets. The assessed process can be relevant for mitochondrial functioning, however it is also important to consider the various *in vitro* parameters and their relationship

to the *in vivo/in human* situation. This includes among others the selection of the cell system, the environmental conditions and the moment of measurements. As mentioned above, tissues and their cell types vary greatly in their number of mitochondria and reliance on mitochondrial respiration. Moreover, the selected *in vitro* culture conditions affect mitochondrial respiration status and activity [Pagliarini 2008, Bogert 1992]. While assessing effects upon mitochondrial functioning *in vitro*, it is also important to keep in mind that *in vivo/in human* observed perturbation can be direct and indirect and one should adjust the assay and moment of measurement accordingly.

The introduction of new biomarkers is required to improve the quality and predictivity of mitochondrial toxicant detection. One of the main limitations of existing biochemical assays, used in the past, is that they cannot completely capture the interconnectivity between the mitochondria and the various organelles in the cell. Cytotoxicity occurring upon partial target interaction and prolonged or repeated exposures can be overlooked when assessing only mitochondrial targets. Incorporation of the mitochondrial interconnectivity via a combined strategy of assessing mitochondrial functioning and the correlated cellular responses could improve the identification of all mitochondrial perturbing agents. Opportunities to support biomarker identification are, among others, live confocal imaging and omics approaches.

Live confocal imaging using, among others, fluorescent tagged proteins provides the opportunity to follow multiple processes simultaneously over time in the same cell. The use of living intact cells enables tracking of signal transduction and protein expression, which includes valuable information allowing us to follow the development of adversity in a time-dependent manner [Wink 2017, Wink 2018].

Omics techniques can help bridge the gap between mitochondrial and cellular signaling present in single endpoint biochemical assays [Heijne 2005]. The assessment of the nuclear transcriptome gives information concerning regulation of essential mitochondrial components, and possible related cellular signaling [Joseph 2017 Cui 2010]. The mitochondrion-nucleus communication is a close connection exchanging information concerning the status of both organelles; this dynamic interaction could potentially produce an early biomarker for mitochondrial perturbation.

To support efficient and large-scale assessments of chemicals based on both existing and new biomarkers, the introduction of high throughput toxicity identification is required. Automated high throughput confocal imaging offers the opportunity to follow in a concentration- and time-dependent manner the effect of dozens of chemicals in all types of model systems using a variety of culture conditions. Furthermore, the establishment of cheaper alternatives for transcriptome analyses,

like the targeted transcriptome assessment of crucial genes in chemical-toxicity, also supports the assessment of chemical-induced time- and concentration-dependent alterations of the cellular response [Waldmann 2014, Limonciel 2018].

The addition of *in silico* assessments in any assay setup can support large scale pattern recognition, unbiased selection of predictive parameters or replace *in vitro* work. *In silico* set-ups can for example be used to pre-screen existing chemical libraries for the identification of pharmacophores susceptible for mitochondrial toxicity or chemical structures likely to bind to specific mitochondrial targets [Naven 2013, Troger 2020, Hemmerick 2020].



To be able to integrate the obtained high dimensional information into risk assessment and regulations, it is important to condense and structure information into documentation accepted by regulatory agencies (like an Integrated Approaches to Testing and Assessment (IATA) approach). One option to condense toxicological information is the use of the adverse outcome pathway (AOP) framework. AOPs are descriptions of adversity pathways divided in subsequent and essential events ranging from the interaction of a chemical with the cellular system to occurrence of adversity in tissue, organ or individual [Ankley 2010]. When integrating these mostly retrospective qualitative descriptions with all types of preferably *in vitro* data, it will be possible to create a quantitative description of adversity and provide a structured roadmap to perform targeted assessments for all types of toxicity [Oki 2019].

## Aim and scope of this thesis

This thesis aims to provide insights into the mechanisms underlying the occurrence of mitochondria-related organ toxicity. In **chapter 2**, we summarized the current knowledge concerning mitochondrial biomarker measurements and their use in a quantitative adverse outcome pathway approach. In **chapter 3**, we assembled an *in vitro* mitochondrial toxicity screening platform to systematically assess chemical-induced mitochondrial perturbation and applied it to assess the effects of chemical exposure upon two cell models: i) HepG2 cells, a liver carcinoma cell line; and ii) RPTEC-TERT1, an immortalized human renal proximal tubular epithelial cell line. Using a set of 23 prototypical ETC inhibitors we evaluated our testing platform for its performance. The introduction of more liver-like 3D cultured HepG2 cells improved the adversity predictions compared to 2D cultured HepG2 and made the outcomes comparable to results from RPTEC-TERT cells. In **chapter 4**, we systematically evaluated the effects of ETC inhibitors upon mitochondrial integrity using high content confocal imaging and targeted transcriptomic studies. High content imaging techniques revealed clear concentration- and time-dependent effects of mitochondrial complex I and III inhibitors exposure upon mitochondrial membrane potential and unfolded protein

response components. The targeted transcriptomic studies provided information for pathway and transcription factor enrichment studies and resulted in a gene profile specific for mitochondrial toxicants that was further evaluated for application in the assessment of drug-induced mitochondrial toxicity liability. In **chapter 5**, we evaluated changes in mitochondrial morphology as an early sign of mitochondrial toxicity. We studied the causal relationship between mitochondrial membrane potential with associated ATP production and mitochondrial morphology. These studies allowed us to get insight into the predictivity of the mitochondrial morphology for toxicity. In **chapter 6**, we used a combination of *in vitro* and *in silico* modeling (based on ordinary differential equations) to study the dynamics of mitochondrial membrane potential upon electron transport chain inhibitors exposures. We revealed that pharmacokinetics and proton leakage were essential parameters for the adjustment of the model to the different chemicals tested. In **chapter 7**, we addressed the possibilities of using chemical read across based on biological similarities for chemical risk assessment in the case of mitochondrial liabilities. Lastly, **Chapter 8**, provides a summary of all findings discussed in this thesis and outlines the implications and future perspectives of these studies.

# 2

# Assessing mitochondria-related organ toxicity

## using new approach methods in an adverse outcome pathway framework

Wanda van der Stel, Peter Bouwman, Bob van der Water, Erik Danen

*Manuscript in preparation*

**Over the last decades, mitochondrial-malfunctioning has been acknowledged as an important factor in the occurrence of chemical-induced organ toxicity. This implies that data concerning the relationship between mitochondrial perturbation and the development of organ failure need to be integrated in chemical risk assessment. The outcome of mitochondria related-toxicity depends on the severity of events and the concentration-time relationship between events. This can be captured using Adverse Outcome Pathways (AOPs) that bundle knowledge of (perturbed) biological processes in consecutive events, from chemical interaction to eventual adversity in organs. To allow the use of the AOP approach for chemical safety guidelines, it is important to select biologically relevant events and to move from qualitative descriptions to quantitative assessment. These events have to be properly specified and the AOP needs to be populate them with sufficient and robust quantitative data. In this review, we propose a core of mitochondrial key events that represent the major targets in mitochondrial toxicity and can be used to create AOP events. Furthermore, we review a set of methods for the evaluation of these mitochondrial key events, including the possibilities for integrating omics technologies. This set of methods is focused on *in vitro* assays to reduce the number of animal tests. Proper estimation of mitochondrial perturbation in the context of organ toxicity will support early-stage risk assessment of new and existing chemicals.**

**Keywords**: Mitochondria, quantitative adverse outcome pathway, risk assessment, methods, omics

## Introduction

In the last decades, mitochondrial involvement in the occurrence of chemical-induced organ toxicity has become increasingly clear. [Will 2014, Dykens 2007, Dykens 2007]. Mitochondria are multi-functional organelles, involved in supplying the cells with energy, creating building blocks like proteins and sugars and providing a storage compartment for ions. Perturbation of any of these mitochondrial functions can lead to cellular stress, cell death and eventually organ failure. To reduce the incidence of mitochondria-related organ failure upon use of pharmaceuticals and exposure to chemicals in general, it is important to improve early identification of mitochondrial toxicants.



Assessment of chemical-induced mitochondrial malfunctioning is nowadays included in the early phase of drug development but is less addressed during the design and production of other types of chemicals. To support and improve the integration of mitochondrial toxicity assessment in risk and hazard assessment of chemicals compounds, it is important to verify and create guidance concerning quality and usability of the mitochondrial toxicity data. One way to structure and link toxicity data is the use of adverse outcome pathways (AOPs) [Ankley 2010, Vinken 2013, Leist 2017]. AOPs describe, using a series of key events, the link between the occurrence of adverse effects and the initial chemical interaction with the cell. This structured representation of toxicological processes provides the opportunity to couple existing mitochondrial toxicity measurements to relevant biological events. The simplified presentation of biological processes provides a basis to clearly describe essential events in the process of cellular perturbation, organ failure and eventual human health issues.

In the past, AOPs have been used as a qualitative description of various key events leading to different types of organ toxicity based on existing data[3]. However, to allow implementation of the AOP framework into risk assessment for chemical-induced toxicity, it is essential to define and quantify the different events or event relationships. To be able to quantify the events, methods need to be selected that allow time and concentration dependent assessment of the changes within the biological processes belonging to the events. The use of quantitative AOPs (qAOPs) in toxicity assessments is promoted by the international Organization for Economic Co-operation and Development (OECD). The OECD already approved two qAOPs in the past and promotes the creation of new qAOPs by providing guidelines and various knowledge tools[4] [Foran 2019, Battistoni 2019].

In response to the OECD initiative, researchers have started to develop quantitative AOPs to assess an increasing number of human organ toxicities [Angrish 2017]. In particular mitochondrial toxicity assessment could benefit from the application of quantitative AOPs. Mitochondrial toxicity is characterized by series of thresholds which

need to be overcome before tissue injury occurs. Under normal conditions, these thresholds should protect the cell/organ from instant injury related to fluctuations in mitochondrial functioning. Injury originating from malfunctioning of mitochondrial processes occurs generally when most of the mitochondria of a cell are perturbed. One exception on this rule is mitochondrial stress which results in the release of mitochondrial DNA and with that causes an innate immune response [West 2015]. Cells can recover from a few malfunctioning mitochondria via the production of new mitochondria (biogenesis), exchange of functional proteins and/or genomic material between organelles (fission and fusion) and by discarding non-functional organelles (mitophagy). In this way, cells reduce the number of damaged mitochondria, while relying on the available pool of healthy mitochondria. However, when the number of damaged mitochondria is too large or the processes required to "cure" the mitochondrial pool are disturbed, cell death may be induced to remove defective cells from the tissue. Acute high levels or sustained presence of mitochondrial toxicants can eventually lead to organ toxicity.

This review will discuss the experimental assessment of mitochondrial toxicity and integrate this information in qAOPs for chemical risk assessment. The central part of this review will focus on the biologically relevant processes in mitochondrial toxicity and the range of assays available to measure their activity. Finally, we will briefly consider the use of mitochondrial toxicity assays in AOPs in a regulatory context.

## Quantifiable mitochondrial key events

The framework of AOPs provides a powerful tool to link molecular events to cellular perturbations and consequent organ malfunctioning. In order to link single events to interconnected networks of AOPs, it is crucial that the key event descriptions are specific for clearly defined biological processes. AOPs created using the OECD format are stored in de AOP-wiki database (https://aopwiki.org/), which thus far contains 303 AOPs and 1368 key event entries. 17 of these 1368 key events are related to mitochondrial functioning and can be grouped into mitochondrial damage/dysfunction (6 out of 17), ATP/electron transport/OXPHOS impairment (4 out of 17), metabolism related (3 out of 17) and mitochondrial DNA related issues (4 out of 17). As discussed by Dreier *et al* the mitochondria-related key events are redundant, and not properly specified.

In general, key events are divided into: 1) initiation events (molecular initiation event = first key event in AOP), 2) the adverse outcome (final key event in AOP), and 3) the remaining "in between" events (not first or last event). Mitochondrial key events belong to the group of early events, including the initiating and early key events. Most mitochondrial processes are interconnected, and consequently perturbation

of one process will eventually result in malfunctioning of others. This means that the initiating event for one chemical could be an in between event for other chemicals.

The integration of key events into qAOPs requires the selection of specific and reproducible assays. The assay selection depends on multiple factors: 1) Assay type: To reduce the need for animal experiments in early-stage risk assessment, it is preferred to select new approach methodologies (NAMs), including both *in vitro* and *in silico* approaches. 2) Capacity: Assay capacity can be an issue when there is a need for large scale high throughput perturbation assessments. 3) Complexity: Methods with complex production, optimization and safety steps are only suitable for specialized labs and are therefore less likely to be integrated in regulatory approved mitochondrial toxicity assessments.



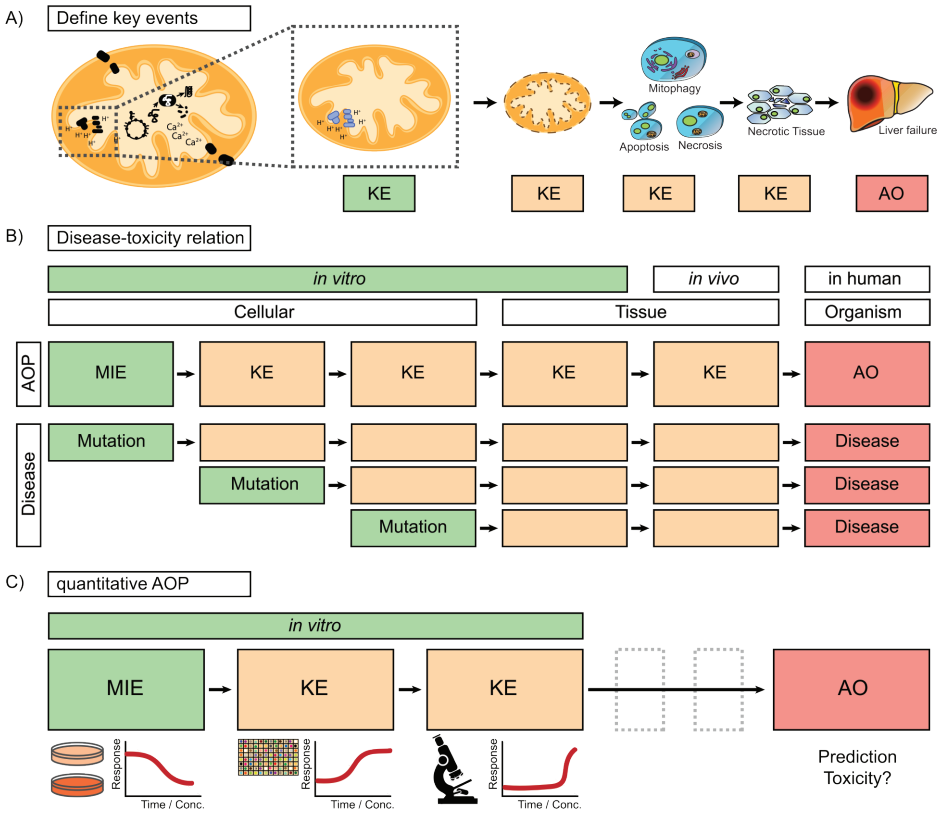


**Figure 1: AOP approach to define mitochondrial key events**
**A)** Illustration of the mitochondrial key event in an adverse outcome pathway (AOP) describing the relationship between mitochondrial perturbation and the occurrence of organ toxicity (in this case liver failure). **B)** Schematic representation of the key features in an AOP and the relationship to the occurrence of disease upon mutation in corresponding mitochondrial processes. **C)** Schematic representation of the steps in an AOP that can be quantified using *in vitro* methods to support risk assessment (prediction of toxicity).

In this review, we aim to subdivide the mitochondrial key events into six subgroups that can be used to support an AOP describing organ toxicity resulting from mitochondrial perturbation (figure 1A and figure 2): mitochondrial metabolism, oxidative phosphorylation (OXPHOS), mitochondrial dynamics, mitochondrial UPR, mitochondrial calcium homeostasis and mitochondrial degradation. To determine the relationship between mitochondrial process perturbation and adversity, we use available information from mitochondria-associated human diseases. It is well known that mutations of genes encoding mitochondrial proteins result in disease at various stages of life. This relationship between protein perturbation and disease is also likely to occur in case of chemical-induced perturbation of the same proteins (figure 1B). To enable integration of the defined key events into qAOPs and chemical risk assessment, we also address various established *in vitro* methodologies which can be linked to the defined events (figure 1C).

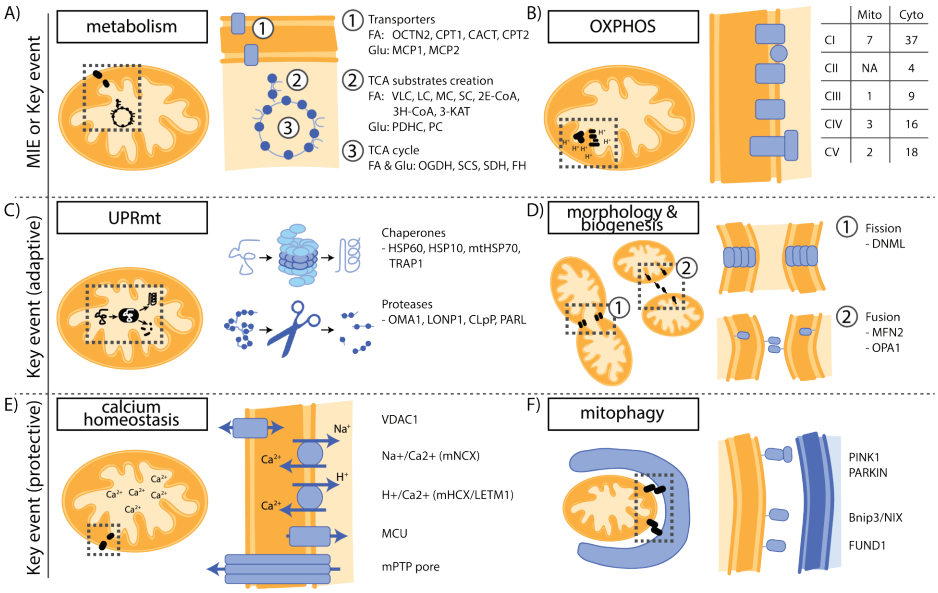


**Figure 2: Mitochondrial key events**

Illustrations of the six major mitochondrial key events: 1) metabolism, 2) OXPHOS, 3) UPRmt, 4) fission/fusion/biogenesis, 5) calcium homeostasis and 6) mitophagy. The individual illustrations per key event demonstrate perturbed components, which are frequently observed in diseases. The targets include for: A) *Mitochondrial metabolism*: Transporters and enzymes involved in TC substrate creation and the TCA cycle itself. B) *OXPHOS*: The different sub-proteins forming the proteins complexes I to V (CI-CV) which are coded by the mitochondrial or cellular genome. C) *UPRmt*: Chaperones and proteases. D) *Mitochondrial dynamics*: Proteins involved in the processes of fission and fusion. E) *Calcium homeostasis*: Various ion pumps and pores. F) *Mitophagy*: Proteins of 3 major pathways. The key events are structured based on the proposed type of key events and the location in the AOP (initiating event or subsequent key event). OXPHOS = oxidative phosphorylation, UPRmt = mitochondrial unfolded protein response.

**Mitochondrial metabolism – citric acid cycle (TCA cycle)**

*Description*

Cells require energy in the form of ATP, which is obtained from energy rich substrates including carbohydrates (e.g. glucose) and fatty acids [Smith 2017, Zhou 2018]. Acetyl-CoA, the starting material driving the TCA cycle in the matrix of the mitochondria, is generated, depending on available glucose levels, from pyruvate (itself derived from glucose via the glycolytic pathway) or from fatty acids (via beta-oxidation). The TCA cycle itself is a series of enzymatic reactions that result in the creation of NADH and $FADH_2$. Subsequently, under aerobic conditions NADH and $FADH_2$ are utilized to produce ATP in the oxidative phosphorylation. Notably, in low oxygen conditions cells will rely on the limited amount of ATP produced during the conversion of glucose to pyruvate in the glycolytic pathway. Cancer cells opt for this mechanism even when oxygen is not limited, referred to as the Warburg effect [DeBerardinis 2020].



*Disease*

Malfunctioning of the TCA cycle may ultimately result in mitochondrial encephalomyopathy. Mitochondrial encephalomyopathy manifest itself already in very young children and affects predominantly two tissue types both relying heavily on mitochondrial respiration, namely brain and muscle [DiMauro 1999, Merrit 2018]. Perturbations observed at the molecular level in these tissues are subdivided in three groups based on the perturbed biological process: substrate transport, preparation of substrates for the TCA cycle and the TCA cycle itself.

*Transporters:* Disorders or deficiencies caused by malfunctioning transport are in general autosomal recessive and the result of mutations in genes coding for the major transporter proteins of fatty acids (OCTN2, CPT1, CACT and CPT2) [Longo 2006] and pyruvate (MCP1 and MCP2[5,6,7] [Oonthonpan 2019]. Contrarily, increased expression of the fatty acid transporters (CPT/OCTN2), resulting in fatty acid accumulation, increases the risks for developing/ worsening other diseases, including infarcts and leukemia. Both diseases benefit from treatment with fatty acid transporter inhibitors, like ST1325 and R-(+)-Etomoxir [Liepinsh 2014, Abozguia 2006, Gugiatti 2018]. Decreased expression of the pyruvate transporters exacerbates cancer development by stimulating cell proliferation via a metabolic switch from mitochondrial respiration to glycolysis [Zhong 2015, Li 2017].

*TCA substrate creation:* Disturbance of the synthesis of acetyl-CoA, the substrate for the TCA cycle, causes a subset of metabolic deficiencies. Both pyruvate and fatty acid can be converted to acetyl-CoA. Pyruvate conversion occurs in the pyruvate dehydrogenase (PDH) complex or by pyruvate carboxylase (PC). Ineffective pyruvate conversion results in reliance on glycolysis for energy and excessive accumulation

of lactate (lactic acidosis)[8]. In fact, disruption of mitochondrial metabolism caused by inhibition of the PDH complex is a promising therapeutic strategy for patients suffering from bacterial infections [Zhou 2018]. Interestingly, PDH inhibition also demonstrated to be beneficial for pancreatic cancer patients illustrating the complex process of metabolic rewiring in cancer cells [Zacher 2011, Qin 2020, clinical trials: NCT03374852 and NCT01830322]. Fatty acid conversion into acetyl-CoA occurs in a stepwise process, removing 2 carbons in every cycle. This process is termed beta-oxidation. This process requires very long-, long-, medium- and short-chain acyl-CoA dehydrogenases (respectively VLC, LC, MC, SC). Other enzymes involved are the peroxisomal bifunctional protein 2-enoyl-CoA hydratase (2E-CoA)/ 3-hydroxyacyl-CoA (3H-CoA) dehydrogenase and 3-ketoacyl-CoA thiolase (3-KAT). [diMauro 1999, Merritt 2018]. Malfunctioning of any of these enzymes results in a combination of hypoglycemia, liver dysfunction, cardiomyopathy, skeletal myopathy and rhabdomyolysis. Conversely, stimulation of the switch from fatty acid to pyruvate metabolism by inhibiting the beta oxidation enzyme 3-KAT is used for the treatment of heart diseases [Sabbaha 2002].

*TCA cycle:* The TCA cycle consists of an interplay between nine enzymes. Metabolic disorders are mainly caused by recessive mutations in genes coding for α-Ketoglutarate Dehydrogenase (OGDH; conversion α-ketoglutarate to succinyl-CoA), succinyl-CoA synthetase (SCS; conversion of succinyl-CoA to succinate), succinate dehydrogenase (SDH; conversion succinate to fumarate) and fumarase (FH; conversion of fumarate to malate) [Rustin 1997]. Mutations in these genes manifest in central nervous system and muscles disorders, primarily in children up to 7 years. As described for the other enzymes involved in mitochondrial metabolism, TCA cycle enzymes are viewed as promising targets for cancer therapy. Various cancer types demonstrate mutations and/or overexpression of α-ketoglutarate dehydrogenase complex (KGDHC; OGDH is part of this complex) and/or isocitrate dehydrogenase (IDH2; conversion isocitrate to α-ketoglutarate) changing the TCA cycle usage. Inhibitors for both enzymes are currently being evaluated in phase II/III clinical trials (KGDHC inhibitor; CPI-613 and IDH2 inhibitors; AG221 and AG881) as treatment for multiple cancer types[9] [Anderson 2018].

*Chemical toxicity*

Chemical-induced perturbation of mitochondrial metabolism is observed upon exposure to a variety of chemicals and affects both fatty acid transport and beta-oxidation [Fromenty 2019]. For most mitochondrial toxicants, the molecular initiating event and the key events are unresolved. These include commonly used drugs such as acetaminophen, amiodarone and ibuprofen, which affect multiple steps in the mitochondrial metabolic pathways. However, the result of chemical-induced

mitochondrial toxicity is most often macrovascular and/or microvascular liver steatosis (development of an inflamed fatty liver).

Glucose metabolism and especially pyruvate conversion by the PDH complex is reported to be affected by psychoactive drugs [Sacks 1991]. Perturbation of the TCA cycle, more specifically inhibition of aconitase, by the chemotherapeutic agent fluorouracil, has been reported to result in neurotoxicity [Kwon 2010, Ki 2002, Pirzada 2000].

*Methods*

Assessment of mitochondrial metabolism is mostly focused on the activity of the enzymes involved and less on the substrate transport (table 1). Although transport protein deficiency can be assessed in patient materials using immunohistochemistry, this is not sufficient for the detection of chemical-induced protein malfunction. The assessment of TCA enzyme activity is achieved using radiolabeled substrates, or the spectral changes observed upon increased or decreased levels of NADH/COA. Radiolabeling of the TCA cycle is achieved by the addition of [$^{13/14}$C]-pyruvate or [$^{14}$C]-α-ketoglutarate followed by the detection of produced radio-labeled $CO_2$ or the other products of the TCA cycle. The use of radiolabeling is generally not desired and spectrometry measurements present an alternative. They rely on the differences in absorbance spectra between native and phosphorylated forms of substrates (NADHP/NADH) produced during metabolism or indirectly by addition of enzymes to stimulate the formation of NADHP from the available NADH. However, these spectrometry measurements demonstrate a lower signal-to-noise ratio and are more difficult to interpret than TCA cycle radiolabeling. Furthermore, the creation of NADH and some of the other metabolic intermediates is not limited to the mitochondria. Nonnenmacher *et al* optimized a method which only permeabilizes the outer cell membranes. The partially functional cells have easily accessible mitochondria and can be used for mitochondrial-compartment specific metabolic studies [Nonnenmacher 2017]. Finally, the specific process of beta-oxidation can be tracked based on the degradation of administered fatty acids. This can be achieved by using radiolabeled palmitic acid and assessing the introduction of [$^{14}$C] or [$^{3}$H] into downstream products. Another option is the assessment of fluorescence signal appearing upon oxidation of synthetic beta-oxidation substrates or the accumulation of fatty acids stained with fluorescent dyes into the various compartments of the cell.

*Integration into qAOPs*

In conclusion, perturbation of mitochondrial metabolism is observed in both disease and toxicity. The observed chemical-induced mutations in genes coding for metabolic components indicates that perturbation of mitochondrial metabolism is most likely an early key event or even molecular initiating event for both disease and toxicity.

**Table 1: Mitochondrial key events - part 1**

Table depicting mitochondrial key events and a subdivision of biological processes belonging to these specific key event. Per biological processes the table elaborates on: 1) methods available to assess related biological processes, 2) examples of the applied techniques, 3) specification of the technique mentioned in in the example, 4-11) columns assessing in detail the assay including the (dis)advantages that need to be considered when using these techniques in a AOP context. * Cells: Yes = Cellular assay/ No: Assay performed in tissue or with isolated enzymes; ** Life: Yes = Cellular assay without the need of lysation or permeabilsation of membranes; # Isol. Mito.: Yes = Assay can be performed in isolated mitochondria; $ Mod.: Yes = assay requires modification/transfection of used cell types; & Mito-target: Yes = Assay (for example tags) can be targeted specifically to the mitochondrial compartment. (Source numbers are provided at the end of the chapter).

| KE | Process | Method | | Examples | Specification | Cells * | Live ** | Isol. Mito. # | Label-free | Mod. $ | Mito-target & |
|---|---|---|---|---|---|---|---|---|---|---|---|
| Metabolism | TCA | Radio-labeling | | PDHc, CS, KDHc, FH | Integration of radio-labeled atoms into TCA substeps | Yes | No | N / Y | No | No | No |
| | | Optical spectrometry | | PDHc, CS, aconitase, IDH, KDHc, SCS-A, SDH, FH, MDH | Color spectrum changes caused by substrate conversion | N / Y | No | No | Yes | No | No |
| | Fatty acid oxidation | Radio-labeling | | [14C]- or [3H]-palmitic acid | Integration of radio-labeled atoms into fatty acids | Yes | No | No | No | No | No |
| | | Fluorescent labels | | Fluorescent fatty acid (FA) | Fluorescence upon metabolism of FP by FAO | Yes | Yes | No | No | No | No |
| | | | | Nile red, lipidTox, NBD | Accumulation of fatty acids in cellular compartments | Yes | Yes | No | No | No | No |
| OXPHOS | Oxygen consumption or localisation | Elektrodes | | Clark, microelektrodes | Oxygen concentration in liquid using a catalytic platinum surface | Yes | Yes | No | Yes | No | No |
| | | Oxygen sensors | Soluble (natural) | Myoglobulin, PPIX, NADH | Fluorescent spectrum change upon available oxygen level | Yes | Yes | No | Yes | No | No |
| | | | Soluble (natural/ plasmid) | Myo-mCherry | Myoglobin subunit introduced in FRET sensor | Yes | Yes | No | No | Yes | Yes |
| | | | Soluble (synthetic) | Various probes | Fluorescent spectrum change upon available oxygen level | Yes | Yes | No | No | No | No |
| | | | Static (synthetic) | Seahorse Analyzer | Plates containing oxygen sensitive FPs | Yes | Yes | No | Yes | No | No |
| | | | | Seahorse Analyzer (complex specific) | Seahorse plus membrane permeabilisation protocol | No | No | Yes | Yes | No | No |
| | | Electron paramagnetic resonance (EPR)/ Magnetic resonance imaging (MRI) | | Oxygen presence | EPR = free radicals using electron spin, MRI/NMR = presence of oxygen based on nuclear spin | No | No | No | No | No | No |
| | | ImmunoFluorescent (IF) staining | | Pimonidazole | Low O2 levels results in detactable reduced-pimonidazole | No | No | No | No | No | No |
| | | Near infrared spectrometry (NIRS) | | Hemoglobulin | Oxygen saturation of hemoglobulin in microvasculature | No | No | No | No | No | No |
| | Membrane potential | Potential sensitive dyes | | TMRE, JC1, mitoNr, MitoOrange, Rho123 | Potential dependent dyes accumulate in polarised mitochondria | Yes | Yes | No | No | No | Yes |

**Table 1: Mitochondrial key events - part 1** (continued)

| KE | Process | Method | | Examples | Advantage | Disadvantage | Source |
|---|---|---|---|---|---|---|---|
| Metabolism | TCA | Radio-labeling | | PDHc, CS, KDHc, FH | substrate specific, very acquirate | measurement in supernatant, radio-labeling | 1,2,3 |
| | | Optical spectrometry | | PDHc, CS, aconitase, IDH, KDHc, SCS-A, SDH, FH, MDH | natural occuring | measurement in supernatant, isolation of enzymes for specificty | 1, 4-8 |
| | Fatty acid oxidation | Radio-labeling | | [14C]- or [3H]-palmitic acid | substrate specific, very acquirate | radio-labeling, supernatant | 9, 10 |
| | | Fluorescent labels | | Fluorescent fatty acid (FA) | dynamic tracking, high through put options, complex cell systems, single cell | | 11 |
| | | | | Nile red, lipidTox, NBD | dynamic tracking, high through put options, complex cell systems, single cell | requires system with enough FA | 12, 13 |
| OXPHOS | Oxygen consumption or localisation | Elektrodes | | Clark, microelektrodes | non-invasive | not fit for high throuhput | 14-16 |
| | | Oxygen sensors | Soluble (natural) | Myoglobulin, PPIX, NADH | natural occuring | Noise-ratio high, because natural occuring | 17-19 |
| | | | Soluble (natural/plasmid) | Myo-mCherry | mcherry is stable and not toxic, FRET is very sensitive, complex cell systems, single cell | low signal-to-noise ratio, sensitive to environmental factors | 20 |
| | | | Soluble (synthetic) | Various probes | cheap, also plate reader assay, high throughput, single cell | | 21-27 |
| | | | Static (synthetic) | Seahorse Analyzer | OCR and ECAR measurement; kinetic measurement, stress test, semi high through put, complex cell systems | specialist equipment | 28-32 |
| | | | | Seahorse Analyzer (complex specific) | identification of complex specific inhibition | specialist equipment, not possible in complex cell systems | 33 |
| | | Electron paramagnetic resonance (EPR)/ Magnetic resonance imaging (MRI) | | Oxygen presence | | only tissue, not suitable for studies assessing MIE/ early KE in animal free studies | 34-41 |
| | | ImmunoFluorescent (IF) staining | | Pimonidazole | | only tissue, not suitable for studies assessing MIE/ early KE in animal free studies | 42, 43 |
| | | Near infrared spectrometry (NIRS) | | Hemoglobulin | | only tissue, not suitable for studies assessing MIE/ early KE in animal free studies | 44, 45 |
| | Membrane potential | Potential sensitive dyes | | TMRE, JC1, mitoNr, MitoOrange, Rho123 | dynamic tracking, high through put | nuclear staining required fo cells tracking after complete depolarisation; active removal of dye; dye quenching | 46-48 |

**Table 1: Mitochondrial key events - part 2**

Table depicting mitochondrial key events and a subdivision of biological processes belonging to these specific key event. Per biological processes the table elaborates on: 1) methods available to assess related biological processes, 2) examples of the applied techniques, 3) specification of the technique mentioned in in the example, 4-11) columns assessing in detail the assay including the (dis)advantages that need to be considered when using these techniques in a AOP context. * Cells: Yes = Cellular assay/ No: Assay performed in tissue or with isolated enzymes; ** Life: Yes = Cellular assay without the need of lysation or permeabilsation of membranes; # Isol. Mito.: Yes = Assay can be performed in isolated mitochondria; $ Mod.: Yes = assay requires modification/transfection of used cell types; & Mito-target: Yes = Assay (for example tags) can be targeted specifically to the mitochondrial compartment. (Source numbers are provided at the end of the chapter).

| KE | Process | Method | | Examples | Specification | Cells * | Live ** | Isol. Mito. # | Label-free | Mod. $ | Mito-target & |
|---|---|---|---|---|---|---|---|---|---|---|---|
| OXPHOS | ATP levels | Magnetization-transfer (MT) techniques | | 31P | Nuclear spin of P atoms | No | No | No | No | No | No |
| | | HPLC | | ADP/ATP ratio | Concentration of ATP or ADP effect the peak height of HPLC spectrum | Yes | No | No | No | No | No |
| | | Firefly luciferase based-assays | Solutions | ATPlite (luciferase based) | ATP to AMP conversion by luciferase with light as by-product | Yes | No | Yes | No | No | No |
| | | | Plasmids | mtLuc, cytLuc, pmeLuc, nucLuc | Targeted luciferase plasmids (same principle as ATPlite) | Yes | Yes | No | No | Yes | Yes |
| | | | Biosensors | Carbon nanotube (SWNT) | nanotube-luciferase conjugate, produced oxyluciferin effects NIR fluorescence of tube | Yes | Yes | No | No | No | No |
| | | Biosensors (ATP binding subunits) | Plasmids | FRET: Ateam, and many others (FoF1-ATP synthase e subunit) | ATP selective subunit used in FRET construct (2 FPs) | Yes | Yes | No | No | Yes | Yes |
| | | | | QUEEN: 1FP (FoF1-ATP synthase e subunit) | ATP selective subunit used in FRET construct (1 FP) | Yes | Yes | No | No | Yes | Yes |
| | | | | Perceval (GlnK1 subunit) | GLnk1 conformation change upon ATP binding results in confromation change of FP | Yes | Yes | No | No | Yes | Yes |
| | | | Probe | Aptamer | Oligonucleotide-ATP interaction results in conformation changes and with that fluorephore changes | Yes | Yes | No | No | No | No |
| | | Staining with small molecules | Spectrum shift | 1·2Zn (PPi specific molecule) | Change in fluorescence emission upon addition of PPi | Yes | Yes | No | No | No | No |
| | | | Signal upon interaction | ATP-red1, or based on eurpium, imidazolium | Fluorephore excitate light upon binding ATP (otherwise colorless) | Yes | Yes | No | No | No | No |
| | Complex activity | Optical Spectrometry | | Complex I, II, III, IV or V activity | Color spectrum changes caused by substrate conversion | No | No | Yes | Yes | No | No |
| mtUPR | Chaparone activity | Western blot or fluorescent labeled proteins under natural promotor | | Increase HSP60,HSP10, ClpP, ATF5 & no effect at BIP, HSP73, HSP72 | Presence/expression of mitoUPR specific proteins | Yes | No | No | No | No | No |
| | | Luciferase activity coupled to mtUPR TF | | Coupled to CHOP, Mure 1, Mure 2 | Luciferase activity upon mitoUPR specific TF activation | Yes | Yes | No | No | Yes | No |

**Table 1: Mitochondrial key events - part 2** (continued)

| KE | Process | Method | | Examples | Advantage | Disadvantage | Source |
|---|---|---|---|---|---|---|---|
| OXPHOS | ATP levels | Magnetization-transfer (MT) techniques | | 31P | | only tissue | 49-51 |
| | | HPLC | | ADP/ATP ratio | cell system independent | Samples collection required (tissue, cells) | 52, 53 |
| | | Firefly luciferase based-assays | Solutions | ATPlite (luciferase based) | plate reader assay, high throughput | measurement in lysate; effected by number of cells | 54, 55 |
| | | | Plasmids | mtLuc, cytLuc, pmeLuc, nucLuc | subcellular localisation, high throughput, single cell | | 56-58 |
| | | | Biosensors | Carbon nanotube (SWNT) | high signal-to-noise ratio | not compartment specific | 59 |
| | | Biosensors (ATP binding subunits) | Plasmids | FRET: Ateam, and many others (FoF1-ATP synthase e subunit) | can be compartment specific, single cell, high throuhput | low signal-to-noise ratio, sensitive to environmental factors | 60, 61 |
| | | | | QUEEN: 1FP (FoF1-ATP synthase e subunit) | no effect of growth, can be compartment specific, single cell, high through put, higher signal-to-noise ratio (than 2FPs)) | | 62 |
| | | | | Perceval (GlnK1 subunit) | ATP:ADP ratio, can be compartment specific, single cell, high throughput | sensitive to environmental factors | 63 |
| | | | Probe | Aptamer | single cell, high throughput | not compartment specific | 63 |
| | | Staining with small molecules | Spectrum shift | 1·2Zn (PPi specific molecule) | water soluble; pH insensitive, single cell, high throughput | not compartment specific | 65 |
| | | | Signal upon interaction | ATP-red1, or based on eurpium, imidazolium | single cell, high throughput | not compartment specific | 66-68 |
| | **Complex activity** | Optical Spectrometry | | Complex I, II, III, IV or V activity | natural occuring | isolated mitochondria | 69, 70 |
| mtUPR | **Chaparone activity** | Western blot or fluorescent labeled proteins under natural promotor | | Increase HSP60,HSP10, ClpP, ATF5 & no effect at BIP, HSP73, HSP72 | possible for any cell model, easily to combine with other markers | seperation between ER/mito response not 100% | 71 |
| | | Luciferase activity coupled to mtUPR TF | | Coupled to CHOP, Mure 1, Mure 2 | plate reader assay | seperation between ER/mito response not 100% | 71 |

**Table 1: Mitochondrial key events - part 3**

Table depicting mitochondrial key events and a subdivision of biological processes belonging to these specific key event. Per biological processes the table elaborates on: 1) methods available to assess related biological processes, 2) examples of the applied techniques, 3) specification of the technique mentioned in in the example, 4-11) columns assessing in detail the assay including the (dis)advantages that need to be considered when using these techniques in a AOP context. * Cells: Yes = Cellular assay/ No: Assay performed in tissue or with isolated enzymes; ** Life: Yes = Cellular assay without the need of lysation or permeabilsation of membranes; # Isol. Mito.: Yes = Assay can be performed in isolated mitochondria; $ Mod.: Yes = assay requires modification/transfection of used cell types; & Mito-target: Yes = Assay (for example tags) can be targeted specifically to the mitochondrial compartment. (Source numbers are provided at the end of the chapter).

| KE | Process | Method | | Examples | Specification | Cells * | Live ** | Isol. Mito. # | Label-free | Mod. $ | Mito-target & |
|---|---|---|---|---|---|---|---|---|---|---|---|
| Dynamics | Fission and Fusion | Immunofluorescent (IF) staining | | TOMM20, mtHSP70 | Staining of mitochondrial specific proteins | Yes | Yes | No | No | No | Yes |
| | | Mitochondrial compartment staining | Fluorescent dyes | Rho123, TMRM, mitoTracker | Mitochondrial dyes accumulate transient or stabile into mitochondria | Yes | Yes | No | No | No | Yes |
| | | | Plasmid (one FP) | mitoGFP, mitodsRED, mitoLoc etc… | Expression of mitochondrial targeted fluorphores | Yes | Yes | No | No | Yes | Yes |
| | | | Plasmid (photoactivatable) | mitoPAGFP | Photoactivation of a FP in invidual mitochondria to follow fusion | Yes | Yes | No | No | Yes | Yes |
| | | | 2 Plasmids (one FP) | Combined mGFP, mdsRed, or mBFP | Two populations of mitochondria transfected with 2 or more FPs | Yes | Yes | Yes | No | Yes | Yes |
| | | Cross link enzyme activity | 2 Plasmids (enzymes) | Cells expressing N- or C-terminus of enzyme | Two populations of mitochondria transfected N-/T-terminus of enzyme | Yes | Yes | Yes | No | Yes | Yes |
| | | Western blot | Protein localisation | Drp1 (cyto-mito) | Expression of mitochondrial specific proteins in mitochondrial fraction | Yes | No | No | No | No | Yes |
| | | | Protein cleavage | OPA1 (long-short) | Cleavage of OPA1 protein | Yes | No | No | No | No | No |
| | Biogenesis | TF activity measurment | Plasmid (one FP) | NRF1mitoGFP reporter plasmid | Nrf1 regulated expression of mito targeting plasmids | Yes | Yes | No | No | Yes | Yes |
| | | mtDNA vs nDNA | qPCR, MMqPCR, duplex qPCR | mtDNA genes vs nDNA gene | Expression of mitochondrial and nuclear gene | Yes | No | No | No | No | No |
| | | | ELISA, colorimetric, WB, cytrometry | COX1 (mtDNA) vs SDH-A (nDNA) | Expression of mitochondrial and nuclear DNA coded protein | Yes | No | No | No | No | No |
| | | Marker expression | Western blot, RTqPCR | PGC1A, NRF1, NRF2, TFAM | Expression of biogenesis specific proteins | Yes | No | No | No | No | No |

**Table 1: Mitochondrial key events - part 3** (continued)

| KE | Process | Method | | Examples | Advantage | Disadvantage | Source |
|---|---|---|---|---|---|---|---|
| Dynamics | Fission and Fusion | Immunofluorescent (IF) staining | | TOMM20, mtHSP70 | possible for any cell model, requires a lot of samples in conc, time dependent studies | one process, only useful when performed in living cells (fixation disrupts mitochondrial morphology) | 72, 73 |
| | | Mitochondrial compartment staining | Fluorescent dyes | Rho123, TMRM, mitoTracker | assessment of both fission and fusion | dyes ar einfluenced by environemntal factors (MMP) | 74 |
| | | | Plasmid (one FP) | mitoGFP, mitodsRED, mitoLoc etc… | assessment of both fission and fusion, not effected by environmental factors | | 75 |
| | | | Plasmid (photoactivatable) | mitoPAGFP | very high resolution (per mitochondria) | only fusion | 76, 77 |
| | | | 2 Plasmids (one FP) | Combined mGFP, mdsRed, or mBFP | difference fusion/ biogenesis and difference close proximity/fusion | higher resolution required to separate populations | 78 |
| | | Cross link enzyme activity | 2 Plasmids (enzymes) | Cells expressing N- or C-terminus of enzyme | plate reader assay | enzyme activity can be effected by chemicals | 79 |
| | | Western blot | Protein localisation | Drp1 (cyto-mito) | wb for specific celllular compartments | only fusion; measurement in lysate | 80-82 |
| | | | Protein cleavage | OPA1 (long-short) | post-translational changes are more dyamic than protien expression | only fission (conversion L-OPA1 -> S-OPA1); measurement in lysate | 83 |
| | Biogenesis | TF activity measurment | Plasmid (one FP) | NRF1mitoGFP reporter plasmid | | | 84 |
| | | mtDNA vs nDNA | qPCR, MMqPCR, duplex qPCR | mtDNA genes vs nDNA gene | directly related to nuc/mtDNA copy number | measurement in lysate | 85 |
| | | | ELISA, colorimetric, WB, cytrometry | COX1 (mtDNA) vs SDH-A (nDNA) | | measurement in lysate, protein expression depends on more than only the nuc/mtDNA copy number | 86, 87 |
| | | Marker expression | Western blot, RTqPCR | PGC1A, NRF1, NRF2, TFAM | possible for any cell model, requires a lot of samples in conc, time dependent studies | measurement in lysate | 88 |

**Table 1: Mitochondrial key events - part 4**

Table depicting mitochondrial key events and a subdivision of biological processes belonging to these specific key event. Per biological processes the table elaborates on: 1) methods available to assess related biological processes, 2) examples of the applied techniques, 3) specification of the technique mentioned in in the example, 4-11) columns assessing in detail the assay including the (dis)advantages that need to be considered when using these techniques in a AOP context. * Cells: Yes = Cellular assay/ No: Assay performed in tissue or with isolated enzymes; ** Life: Yes = Cellular assay without the need of lysation or permeabilsation of membranes; # Isol. Mito.: Yes = Assay can be performed in isolated mitochondria; $ Mod.: Yes = assay requires modification/transfection of used cell types; & Mito-target: Yes = Assay (for example tags) can be targeted specifically to the mitochondrial compartment. (Source numbers are provided at the end of the chapter).

| KE | Process | Method | | Examples | Specification | Cells * | Live ** | Isol. Mito. # | Label-free | Mod. $ | Mito-target & |
|---|---|---|---|---|---|---|---|---|---|---|---|
| Calcium homeostasis | Calcium flux | Calcium flux measurement (mitochondrial - targeted plasmids) | Luminescence | Aequorin, Berovin, Obelin, Phialidin, Mitrocomin, Mnemiopsin | Bio-luminescence upon binding to CA2+ | Yes | Yes | No | No | Yes | Yes |
| | | | FRET | Cameleon, G-CaMP & Tropin C biosensor | Ca2+ selective subunit (CaM/Troponin) used in FRET construct (1/2 FPs) | Yes | Yes | No | No | Yes | Yes |
| | | | Fluorescence | Camagroo | Conformational change of FP upon CA2+ to CaM subunit | Yes | Yes | No | No | Yes | Yes |
| | | | Ratiometric | Pericam, GEM-GECO1 | Similar principal as Camagroo, but with circular FP | Yes | Yes | No | No | Yes | Yes |
| | | | | GECO1 fused to MICU1, Cvsue, ROMO1 | Fluorescence measurement in mitochondrial subcompartments | Yes | Yes | No | No | Yes | Yes |
| | | Calcium flux measurment (dyes) | Fluorescence | Rhod-1, Rhod-2, Fluo-1, Fluo-2, Fluo-3, Fluo-4, etc… | FP intensity change upon binding of Ca2+ | Yes | Yes | No | No | No | No |
| | | | Ratiometric | Still-1, Still-2, Indo-1, Fura-1, Fura-2, Fura-3, etc... | FP intensity change upon binding of Ca2+ (dual emission/exitation) | Yes | Yes | No | No | No | No |
| Degradation | Mitophagy | pH detection (FP) | | mt-Keima, Rosella | pH dependent shift of FP spectrum | Yes | Yes | No | No | Yes | Yes |
| | | Co-localisation mitochondria/ lysosomes (IF or plasmid) | | Mito: dyes, cytochrome-c & lysosome: LAMP1, LC3, MAP1LC3B, SQSTM1 | Co-localisation of mitochondrial and lysosome labeled-proteins | Yes | Yes | No | No | Yes | No |
| | | Co-localisation mitochondria/ mitophagy proteins | | Mito: dyes, IF & mitophagy: Parkin2-FP | Detection of mitochondria tagged for degradation | Yes | Yes | No | No | Yes | No |
| | | Electron microscopy | | Mitochondrial and lysosome structures | Electrons as light source for high resolution images of cellular structures | Yes | Yes | No | Yes | No | No |

**Table 1: Mitochondrial key events - part 4** (continued)

| KE | Process | Method | | Examples | Advantage | Disadvantage | Source |
|---|---|---|---|---|---|---|---|
| Calcium homeostasis | Calcium flux | Calcium flux measurement (mitochondrial - targeted plasmids) | Luminescence | Aequorin, Berovin, Obelin, Phialidin, Mitrocomin, Mnemiopsin | plate reader assay | sensor is "utilized" upon usage, so requires constant expression, delayed dynamics | 89-97 |
| | | | FRET | Cameleon, G-CaMP & Tropin C biosensor | | endogenous CaM expression can effect efficiency | 96, 98-102 |
| | | | Fluorescence | Camagroo | | pH sensitive, endogenous CaM expression can effect efficiency | 96, 102-104 |
| | | | Ratiometric | Pericam, GEM-GECO1 | higher affinity for Ca2+ and larger dynamic range, than Cameleon and Camagroo | pH sensitive | 96, 102, 105-107 |
| | | | | GECO1 fused to MICU1, Cvsue, ROMO1 | labeling of multiple mito compartments | complex analysis and interpretation | 96, 102, 108, 109 |
| | | Calcium flux measurment (dyes) | Fluorescence | Rhod-1, Rhod-2, Fluo-1, Fluo-2, Fluo-3, Fluo-4, etc… | | localisation (some are more mitochondrial than others), equal loading is difficult | 96, 110-113 |
| | | | Ratiometric | Still-1, Still-2, Indo-1, Fura-1, Fura-2, Fura-3, etc... | less issues with probe loading, bleaching, optical path length, illumination intensity (compared to single emission/excitation) | localisation (some are mote mitochondrial than others) | 96, 114 |
| Degradation | Mitophagy | pH detection (FP) | | mt-Keima, Rosella | resistent to lysosomal degradation | double FP (rosella) are less stable than single FP (Keima based) | 115, 116 |
| | | Co-localisation mitochondria/ lysosomes (IF or plasmid) | | Mito: dyes, cytochrome-c & lysosome: LAMP1, LC3, MAP1LC3B, SQSTM1 | single cell resolution | detailed analysis required to confirm overlap | 117 |
| | | Co-localisation mitochondria/ mitophagy proteins | | Mito: dyes, IF & mitophagy: Parkin2-FP | single cell resolution | detailed analysis required to confirm overlap | 118-120 |
| | | Electron microscopy | | Mitochondrial and lysosome structures | high resolution | low throughput | 119, 121 |

*TCA:* Assessment of the TCA cycle enzyme activity using radiolabeling and spectrometry is possible for any cell model, because the metabolite/substrate assessment is performed in the supernatant. The use of radiolabeling requires special expertise and reduces the likelihood of integration into standard toolkit. Therefore, the use of reporter assays for TCA cycle enzyme activity would be more suitable for a standard qAOP approach. However, until now most reporter assays are not suitable for live cell assessments, precluding time-resolved analyses. The development of TCA cycle enzyme specific fluorescent ligands will provide the opportunity of real time monitoring and would also enhance enzyme specificity of read outs.

*FA:* Fatty acid oxidation is also measured using both radiolabeling and cell specific fluorescent dyes. Fluorescent dyes suitable for live measurements do support the assessment of fatty acid conversion and accumulation dynamics in cell systems with different complexities, including 2D, 3D, or co-cultures. A disadvantage of the use of fatty acid accumulation as a read out is that high amounts of fatty acid are required for the formation of detectable aggregates.

**OXPHOS – oxidative phosphorylation (mitochondrial respiration)**

*Description*

In the mitochondrial metabolic pathways, electrons are being pumped over various protein complexes in the mitochondrial inner membrane using flavin proteins. The electron flow supports the passage of protons over the same protein complexes, creating a proton gradient in the intermembrane space. Subsequently, the created surplus is channeled back into the matrix via the ATP synthase, which in turn uses the proton translocation to drive the conversion of more ADP into ATP [Alberts 2014].

*Disease*

Mitochondria contain a circular genome which encodes 14 proteins, 22 tRNAs and 2 rRNAs, all of which are part of the mitochondrial respiration machinery. The mitochondrial encoded proteins include 2 subunits of the ATP synthase (complex V), 3 subunits of complex IV, 1 subunit of complex III, 7 subunits of complex I and the protein humanin[10]. Mutations in the protein complex encoding genes, located in both the mitochondrial and the nuclear genome, will decrease OXPHOS capacity. The mutations identified in the mitochondrial genome can be both heteroplasmic and homoplasmic, and can be restricted to single tissues [Goodwin 2015, Wallace 2013]. Decreased OXPHOS capacity is associated with strokes, seizures, myopathy, impaired vision, liver failure or gastrointestinal abnormalities, which mostly manifest in childhood or early adolescence [Jacobs 2006, Merrit 2018]. The mitochondrial encoded micropeptide humanin was shown to be protective against starvation, oxidative stress and other injuries in *in vitro* systems [Yen 2012]. Reduction of functional

humanin, caused by mutations in the gene or age-related decreased expression, does not directly affect the OXPHOS capacity of the cell, but does result in the loss of its protective function which can worsen diseases such as Alzheimer, stroke, cardiovascular disease, metabolic diseases and cancer [Gong 2014].

*Chemical toxicity*

Inhibition of the mitochondrial respiration complexes has been reported for chemicals which also perturb fatty acid oxidation. This combined perturbation of OXPHOS and fatty acid oxidation is correlated with the transition of steatosis to steatohepatitis [Fromenty, 2019, Kaufmann 2005]. The chemicals which are known to interfere with mitochondrial respiration complexes are in many cases not inhibitors of just one protein complex. For instance, various liver toxicants demonstrated inhibition of multiple complexes *in vitro*, including Benzbromarone [Dykens 2008, Nadanaciva 2007], Diclofenac [Nadanaciva 2007, Acuna 2012, Ghosh 2016], Entacapone [Grünig 2017], Flutamine [Ball 2016], Metformin [Owen 2000, Nadanaciva 2007, Brunmair 2004], Nefazodone [Dykens 2008, Nadanaciva 2007] and Tolcapone [Grünig]. In addition, epidemiological studies indicate a relationship between neurological diseases (e.g., Parkinson) and exposure to pesticides designed to inhibit mitochondrial complexes [Dhillon 2008; Tanner 2011]. Mitochondrial complex inhibitors are widely used in pesticides, insecticides or fish poison[11] [Lümmen 1998, Bartlett 2001]. The lipophilic properties of for example the complex I targeting rotenone facilitate its uptake by gills and trachea and low concentrations can result in toxicity in fish in the form of cardiac and neurological failure and indicate a risk for human exposure [McKim 1991, Ling 2003].

*Methods*

Assessment of OXPHOS functioning can be based on mitochondrial membrane potential (1), oxygen homeostasis (2), ATP content (3) and protein complex activity (4) (table 1). 1) The driver of OXPHOS is the proton gradient over the mitochondrial inner membrane. This potential difference can be assessed using dyes that only accumulate in the mitochondria when there is a potential difference and are released into the cytoplasm during depolarization. 2) Oxygen consumption during ATP production can be monitored based on oxygen localization (in situ oxygenation) or oxygen consumption rates (OCR). Oxygen localization in various tissue types using electron paramagnetic resonance (EPR), immunofluorescence and spectrometry supports is assessed to study the local effects of a stroke, ischemia or cancer. In the context of chemical-induced perturbation the assessment of oxygen consumption is more informative for effects at the cellular level. Electrode measurements are based on amperometry, which means the detection of oxygen ions based on changes in an electric current. Alternatively, more sensitive oxygen sensors can be used, which rely on optical detection rather than electrochemical signals. The sensor can be soluble

or static. They are subdivided in endogenous (myoglobulin and NADH) or synthetic molecules that react with oxygen. 3) The end-product - ATP - of OXPHOS can be monitored using assays based on firefly luciferase, biosensors or small molecules. Firefly luciferase converts D-luciferin in the presence of ATP and $Mg^{2+}$ to oxyluciferin AMP and light. The amount of emitted light correlates with the amount of ATP used in the reaction. In the last decades, various ATP sensors have been developed which combine an ATP binding region (being parts of complex V or nucleotide strings) with single or double fluorophores (FRET). Researchers also developed small molecules, which upon interaction with ATP become fluorescent or demonstrate a shift in their emission spectrum. 4) The direct interaction with any of the complexes involved in the OXPHOS can be assessed using enzyme activity assays or complex specific respiration in isolated mitochondria or permeabilized cells using complex specific substrates and inhibitors.

*Integration into qAOP*

To summarize, mutations in almost all OXPHOS related genes are reported to result in lethality or diseases. The use of chemical inhibition of the complexes in pest control is expected to result in acute human toxicity. Indeed, a correlation between neurological disorders in humans upon prolonged exposure to OXPHOS inhibitors has been observed among farmers [Tanner 2011, Wang 2011]. In combination, with the above described direct relationship between OXPHOS protein malfunctioning and disease, it suggests that OXPHOS perturbation is a molecular initiating in both disease and toxicity.

Oxygen consumption is an important readout for the assessment of OXPHOS activity. The first oxygen specific electrodes for *in vivo* measurements were developed in the fifties. The next generation of oxygen consumption assays consists of oxygen sensitive fluorophores, with seahorse being the most recent, providing a non-invasive method to assess the behavior of both adhesive and non-adhesive cells upon changes in their environment. However, these techniques are less suitable for high-throughput measurements and are not used in live cell monitoring. The addition of the complex specific OCR measurements requires a successive addition of buffers and ligands and supports the accurate identification of complexes effected upon chemical exposure. However, the protocol makes it impossible to perform real-time assessments, which could be required when toxicity is not acute (chemicals which become toxic upon metabolism or accumulation).

Other assay options are the various soluble (mainly synthetic) probes and sensors for oxygen levels, membrane potential and ATP levels. They provide the opportunity to follow the distribution and presence of these markers in a high- throughput microscopy

setting on single cell level. The use of stable integrated sensors like single/multi-fluorophore FRET has the added value of organelle specificity. For example, subtle deviations in specific mitochondrial ATP dynamics could be more predictive for the outcome than overall cellular ATP levels, which are in some cell systems mostly driven by glycolysis. Most probes and biosensors are suitable for more complex cell systems but do require more elaborate and cell type specific optimization. This includes the effects of: environmental factors like pH (FRET sensors are pH sensitive), transporter expression (probes can be actively excreted) or cell behavior (e.g., influence of cell growth on read outs). Eventually, the probe and biosensor read out per cell could be linked in the same setup to later key events like cell death.



**Mitochondrial protein structure – UPR$^{mt}$**

*Description*

Mitochondria are largely independent organelles with their own genome and enclosed by double membranes. The majority of the mitochondrial proteins, including 84 out of 97 respiration complex proteins, are produced in the cytosol and have to be transported into the organelle by a variety of target-specific translocases. Subsequently, these proteins need to arrange into various large multi-protein complexes. To properly coordinate and control the protein arrangements, the mitochondria have a dedicated quality control system focused on translation and protein folding [Münch 2018, Qureshi 2017]. After the detection of misfolded proteins, the mitochondria initiate different responses, including upregulation of chaperone and proteasome activity, induction of antioxidant responses, and downregulation of pre-RNA processing/translation. All of these responses are focused on reduction of the number of improperly folded and assembled proteins [Münch 2018].

*Disease*

Mitochondrial UPR related diseases are divided into disorders affecting chaperones or proteases. Important mitochondrial chaperones include HSP60, HSP10, mtHSP70, and TRAP1 [Voos 2002, Yi 2018]. Malfunctioning of the HSP60-HSP10 complex caused by both autosomal dominant and recessive mutations in chaperone genes can result in neurological disorders, but in general results in embryonic lethality [Bross 2018].

Mitochondrial specific proteases include OMA1, LONP1, CLpP and PARL. Hyper-activation of OMA1, caused by mutations in *AFG3L2*, results in autosomal dominant optic atrophy or spinocerebellar ataxia, depending on the location of the mutation [Baderna 2020, Tulli 2019]. Autosomal recessive mutations in *LONP* cause neurological disorders or symptoms similar to mitochondrial metabolic diseases like lactic acidosis and muscle weakness [Dikoglu 2015, Strauss 2015, Peter 2018]. Malfunctioning of CLpP, caused by autosomal recessive mutations, results in Perrault syndrome, which is

associated with hearing loss and in some cases neurological problems [Brodie 2018]. Reduced levels of PARL are observed in obesity and Parkinson disease, but so far no causal link has been discovered [Chan 2013]. Myopathy due to decreased capacity of the mitochondrial UPR has been associated with aging and forms of Alzheimer disease [Shpilka 2018].

*Chemical induced toxicity*

Thus far, human mitochondrial UPR perturbing agents have not been reported. However, an *in vivo* screen in *C. elegans* of 1200 FDA approved chemicals identified Auranofin, Chlorprothixene HCl, Methacycline HCl and Minocycline as inducers of the mitochondrial unfolded protein response (mtUPR), based on HSP60 expression [Rauthan 2015]. By contrast, Yumnamcha *et al* did not observe any change in the expression of the mtUPR markers, LonP, YME1L1, mtHSP40 or PDIA upon Auranofin exposure of human retinal cells [Yumnamcha 2019].

*Methods*

Activation of the UPR can be assessed based on the activity of involved chaperones and proteases (table 1) [Jovaisaite 2015]. When assessing the mitochondrial UPR it is important to distinguish the responses triggered in the mitochondria from those coming from the ER or the cytoplasmic compartment. To assess chaperone activity, one could monitor the expression of transcription factors involved in the induction of the chaperone responses or the presence/localization of the chaperones themselves (both at the mRNA and protein levels). To distinguish mitochondrial UPR from ER UPR, a combination of several components from these responses should be analyzed.

*Integration into qAOPs*

In conclusion, development of adversity in the form of disease has been observed upon malfunctioning of several mitochondrial UPR specific proteins. Contrarily, no direct correlation has been found between chemical-induced adversity and any of these proteins. This in combination with the goal of the mtUPR, degradation of malfunction proteins like the ones observed upon mutations of genes involved in OXPHOS or metabolism, could indicate a possible more secondary role of the mtUPR in chemical adversity.

Specific assessment of the mtUPR is challenging, because of the interconnection of involved proteins between the ER, the cytosol and the mitochondria. The expression of especially mitochondrial specific chaperones and proteases, rather than ER specific UPR components, could indicate mitochondrial specific damage, but the close contact between these organelles renders this extremely difficult [Rowland 2012].

**Mitochondrial dynamics – fission/fusion and biogenesis**

*Description*

Mitochondria are dynamic organelles that adjust their morphology based on the energy requirements of cell. The mitochondrial morphology changes are divided into fission and fusion. Fission being the process of splitting mitochondria in smaller compartment, which enables transport of mitochondria and clearance of damaged parts. Fusion describing the process of mitochondrial merging into longer and interconnected structures, which facilitates ATP production and the exchange of materials between organelles [Westermann 2010, Youle 2011, Hamacher-Brady 2016, Giacomello 2020]. In addition, the process of fission is involved in the growth of the mitochondrial mass in the cell. Only splitting and merging of mitochondria should not result in a change in total mitochondrial mass. However, the cell can enlarge its mitochondrial mass via the process of biogenesis. Various cellular factors stimulate the replication of the mtDNA. Subsequently the mitochondria can split into two functional daughter mitochondria through fission [Jornayvaz 2010, Hock 2009].



*Disease*

If the fragile balance between fission and fusion is disturbed for a prolonged period it can lead to a drop in energy production causing cell and ultimately tissue dysfunction. Indeed, mutations in genes encoding components of the machinery controlling fission and fusion are observed in cardiovascular disease, amyotrophic lateral sclerosis and neurodegenerative diseases [Suárez-Rivero 2016, Chen 2009]. Neurodegenerative diseases can be divided into disorders caused by mutations in either fission related genes, *MFN2* or *OPA1*, or fusion related genes, *DNM1L*. Mutations in *MFN2* effects sensory and motor neurons in Charcot-Marie-Tooth (CMT) disease [Züchner 2004]. CMT is observed as an autosomal dominant, recessive and even X-linked dominant pattern[12]. Mutations in *OPA1* are associated with autosomal dominant optic atrophy, a disease affecting the retinal ganglia cells (*OPA1* is an abbreviation from optic atrophy type 1) [Delettre 2000, Alexander 2000]. In case of *DNM1L*, the major factor involved in fission, autosomal recessive and dominant negative mutations are observed. The location of the mutation determines the severity of the disease, which can lead to early childhood lethality or epileptic phenotypes and neurological disorders [Fahrner 2016]. There is also evidence that altered mitochondrial dynamics are involved in the progression of Huntington's disease (HD). Pharmacological inhibition of excessive fission is feasible in *in vitro* systems and mice and offers potentials for HD treatment [Reddy 2014]. Finally, alterations in the process of biogenesis are observed in diabetic patients [Nisoli 2007, Heinonen 2015].

*Chemical induced toxicity*

Changes in the expression of fission and fusion factors, but also altered mitochondrial morphology are observed upon exposure to various toxicants [Meyer 2017]. Perturbation of mitochondrial biogenesis occurs upon interference with mtDNA replication or translation of the related mitochondrial proteins. Both types of perturbation will prevent the production of new mitochondria. Vice versa, upregulation of mitochondrial biogenesis is also observed during toxicity and may represent a compensatory mechanism to counteract other types of mitochondrial perturbations [Zhond 2017].

*Methods*

The process of fission and fusion can be evaluated by manual or automated inspection of mitochondrial morphology, visualized using mitochondrial specific dyes, immune-fluorescent staining of mitochondrial proteins or stable integration of mitochondrial targeted and labeled plasmids (table 1). The localization (mitochondrial-cytoplasmic) or activation (e.g. cleavage of OPA1) of proteins crucial in the machinery of fission and/or fusion can be assessed using Western blot. Changes in biogenesis are monitored by comparing effects on mitochondrial mass and cellular mass. This can be done at the mRNA level, i.e. mitochondrial mRNA vs nuclear mRNA or at protein level, comparing amounts of proteins originating from mtDNA versus proteins originating from nuclear DNA (e.g. COX1 vs SDH-A).

*Integration into qAOP*

To summarize, perturbation of proteins regulating mitochondrial morphology has been observed as causal for several neurological disorders. Direct interaction of chemicals with mitochondrial morphology proteins has not been reported so far. However, the observation of changes in expression of these proteins is an indication of at least the occurrence of secondary responses to possibly counteract effects caused by interference with for example OXPHOS and mitochondrial metabolic pathways. Monitoring the dynamics of fission and fusion could therefore be an indicator of the significance of the perturbation in earlier key events.

Mitochondrial dynamics has been studied based on tracking shape and number of mitochondria. Mitochondrial number related to mitochondrial mass (quantity of for example membrane proteins or mitochondrial DNA) can be integrated in pipelines using all sorts of cell lines and simple plate readers. The assessment of fission/fusion ratio's is more challenging and requires sophisticated microscopy and time-lapse imaging, which is not always possible in every cell model.

In general, it is important to keep in mind that the assessment of mitochondrial morphology should: 1) be based on the fission/fusion ratio in multiple mitochondria

to prevent conclusions based on malfunctioning of individual mitochondria, which happens also under healthy conditions, 2) keep in mind spatial resolution, because acute effects can be cell type specific and location specific and 3) keep in mind time dynamics, because changes in morphology are constantly happening and some changes can be considered as temporal/protective.

When assessing specifically mitochondrial biogenesis it is important to distinguish between the number of mitochondria and the number of mtDNA copies. It is therefore required to additionally assess specifically the expression of mtDNA genes/proteins or study the exact copy number of mtDNA.



**Mitochondrial $Ca^{2+}$ homeostasis**

*Description*

$Ca^{2+}$ ions are important players in cellular signaling as second messengers, which makes their distribution and storage important factors in the maintenance of cellular functioning. The major storage of the $Ca^{2+}$ pool is in the ER. From the ER, $Ca^{2+}$ ions constantly shuttle to the mitochondria for storage and support of mitochondrial function including OXPHOS and metabolism, and regulation of cell migration, ROS signaling and regulation of cell death [Ben-Hail 2014, Paupe 2018, Prudent 2017, Görlach 2015, Wan 1989]. Mitochondrial $Ca^{2+}$ levels are regulated by 4 major transporters: VDAC1, the $Na^{+}$/$Ca^{2+}$ exchanger (mNCX), $H^{+}$/$Ca^{2+}$ exchanger (mHCX), the $Ca^{2+}$ uniporter (MCU) and the mitochondrial permeability transition pore (mPTP) [Phillips, 2016, Ben-Hail 2014, Giorgi 2018]. Besides its role in the regulation of $Ca^{2+}$ levels, mPTP is involved in transport of molecules smaller than 1.5kDa [Halestrap 2009].

*Disease*

Unbalanced distribution of $Ca^{2+}$ can affect all processes relying on this second messenger. Furthermore, an overload of $Ca^{2+}$ caused by irreversible opening of the $Ca^{2+}$ pores depolarizes the mitochondria and triggers apoptotic or necrotic cell death [Rasola 2011]. Dysregulation of the localization of $Ca^{2+}$, because of malfunctioning mitochondria, is observed in various diseases including diabetes, cardiovascular diseases, neurodegenerative diseases and metabolic diseases [Giorgi 2012]. For example mitochondrial metabolic diseases caused by inhibition of the PDH complex can be a result of changes in the $Ca^{2+}$ level [Lai 1988].

Mutations in the various mitochondrial transporter genes are rarely observed, with the exception of patients lacking *VDAC1* presenting with fatal mitochondrial encephalomyopathy [Huizing 1996]. Increased expression levels of transporters are correlated with development of cancer and neurological diseases. Overexpression of *MCU* correlates with increased proliferation of colorectal cancer [Liu 2020].

Overexpression of *VDAC1* supports anti-apoptotic activity in cancers, via interactions with hexokinases [Shoshan-Barmatz 2012]. In general, excessive $Ca^{2+}$ release aggravates the progression of various neurological diseases (Alzheimer, Parkinson and Huntington) and cardiac ischemia reperfusion-injury. The excessive release of $Ca^{2+}$ caused by changed transporter expression can be counteracted using pharmacological inhibition of the transporter [Dey 2020]. On the other hand, the involvement of the individual transporters in the development of a $Ca^{2+}$ overload is controversial, for example the NCX pump can revert its transport mode and therefore support both an in and outward flow of $Ca^{2+}$ [Samanta 2018].

Finally, perturbation of the mPTP protein complex or an occurrence of a $Ca^{2+}$ overload triggers the opening of the mPTP. This results in the release of soluble mitochondrial molecules with a molecular weight below 1.5kDa into the cytoplasm. This is combined with water intake based on the associated change in osmotic pressure. Opening of the pore for a short period supports regulation of the mitochondrial-cytoplasmic ion gradients. Prolonged opening contributes to $Ca^{2+}$ loss, a drop in of ATP synthesis and release of pro-apoptotic molecules, including cytochrome c, SMAC/DIABLO and Omi/HtrA2 [Garrido 2006]. Cytochrome C shuttles under normal condition between mitochondrial complex III and IV. However, upon release into the cytoplasm it stimulates, together with SMAC and Omi, the assembly of the apoptosome and the activation of the caspases responsible for the execution of apoptosis. The mPTP is therefore used as a target in cancer treatment [Olszewska 2013]. Furthermore, increased expression of mPTP components (CypD) is associated with neurodegenerative disease in *in* vitro and *in vivo* models [Rao 2014]. Although overexpressed mPTP may be targeted in neurological diseases, existing mPTP inhibitors are either too toxic or lack clinical effects.

*Chemical toxicity*

No toxicity has been identified thus far via direct interaction of chemicals with the $Ca^{2+}$ transport proteins. Possible mechanisms of $Ca^{2+}$ toxicity could include undesired formation of membrane pores. Some strains of bacteria produce pore-forming toxins that initiate a flux of $Ca^{2+}$ from the mitochondrial matrix into the cytosol [Bouillot 2018]. Bacterial infections accompanied by this type of toxins target mostly the immune system of the host cell [Los 2013].

*Methods*

Assessment of $Ca^{2+}$ homeostasis specifically in the mitochondria can be achieved using genetically encoded $Ca^{2+}$ sensitive FRET-, fluorescent-, ratiometric constructs or bioluminescent proteins that can be targeted to mitochondria (table 1). In addition, there is a range of dyes capable of detecting $Ca^{2+}$. However, most of them are not

specific for the mitochondria and require a combined staining with a dye or antibody targeting the mitochondria.

*Integration into qAOP*

To conclude, perturbation of $Ca^{2+}$ fluxes and storage are correlated with the severity of certain diseases. Excessive amounts of $Ca^{2+}$ aggravate diseases and can eventually trigger cell death. No chemicals have been reported to cause adversity by directly targeting the $Ca^{2+}$ distribution. This indicates that the perturbation of $Ca^{2+}$ rather belongs to a later key event than the molecular initiation event.

Assessment of $Ca^{2+}$ fluxes can be achieved using dyes and upon integration of $Ca^{2+}$ specific biosensors. A wide variety of options exits, which provides the opportunity to choose and optimize the assay for the cell type of interest. However, it also illustrates the difficulty of selecting a common strategy that would suit multiple cell types and models with different levels of complexity.



**Mitochondrial degradation - mitophagy**

*Description*

Cells are equipped with mechanisms to eliminate a surplus of unnecessary and/or malfunctioning structures and organelles using autophagy. Autophagy is defined as the process during which parts of the cytoplasmic content including organelles are engulfed by vesicles and eliminated. This process of organelle elimination is also referred to as mitophagy when it is specifically focused on mitochondria [Yuole 2011, Hamacher-Brady 2016, Palikaras 2018]. Under normal conditions mitophagy is also used to support cellular differentiation and maturation. Certain cell types change their mitochondrial content during development, sperm-derived mitochondria are for instance degraded in fertilized oocytes and red blood cells do not require mitochondria to properly function [Palikars 2018]. Under stress conditions – for example chemical exposure – mitophagy can be triggered by loss of mitochondrial membrane potential, nitrogen-starvation and hypoxia. Which proteins are involved in the mitophagy process depends on the trigger. The most common mitophagy pathway is centered around PINK1 (*PINK1/PARK6*) stabilization and Parkin (*PARK2/PRKN*) recruitment to the mitochondria. But under hypoxic conditions, cells rely on Bnip3/NIX and FUNDC1 driven mitophagy processes.

*Disease*

Malfunctioning of the mitophagy system has been observed in several diseases. Decreased activity is for example linked to heart disease and Parkinson disease, while hyper-activation correlates with improper blood/immune cell maturation and the induction of apoptosis [Palikars 2018]. About 10% of the Parkinson disease cases are

inherited [Thomas 2007]. A significant number of these cases demonstrate an autosomal recessive or dominant-negative mutation in in two gene involved in mitophagy, *PINK1* and *PRKN* [Valente 2004, Puschmann 2017, Kitada 1998, Balestrino 2020].

*Chemical induced toxicity*

Undesired excessive induction of mitophagy is observed upon exposure to different classes of chemicals, including some SIRT1-agonists, p53-inhibitors and PARP1-inhibitors [Georgakopoulos, 2017]. In general, the activation of mitophagy is a result of membrane potential loss and/or ROS formation, both originating from perturbation of OXPHOS. Another reported trigger is NAD+ accumulation, which is the result of malfunctioning mitochondrial metabolism. Often, massive activation of mitophagy is not triggered directly by chemicals but arises from chemical-induced perturbation of the above described key events.

*Methods*

While monitoring mitophagy it is important to clearly distinguish the observed effects from general autophagy (table 1). This can be achieved by performing co-staining of lysosome or proteins specific for mitophagy and mitochondrial markers. Other options are the use of mitochondrial targeted plasmids, including pH sensitive constructs, which will be triggered upon fusion with the low pH lysosome during mitophagy. In addition, mitophagy can be distinguished from general autophagy at high resolution when using electron microscopy.

*Integration into qAOP*

To summarize, mitophagy or specifically degradation of perturbed mitochondria is an end-stage in the process of mitochondrial malfunctioning. Enhanced levels of mitophagy are observed both in diseases and upon exposure to selected chemicals. Integration of mitophagy into mitochondrial AOPs would help to quantify the threshold between still functional cells and cells that are switching to cell death protocols. Quantifying the number of mitophagy events in a cell could distinguish between situations/exposures that would still allow recovery/adaptation and the moment at which cell/tissue are not be able to coop anymore.

## AOP wide quantification of biological events

In the last decades, the assessment of effects on mitochondrial function has been widely integrated in drug safety testing. Robust assessment of mitochondrial health can be based on biochemical readouts for the different mitochondrial-involved processes that can be coupled to key events, including respiration, energy-carrier production and byproduct formation.

Several additional sources of data can support these mechanism-based toxicity assessments. In the last decade various omics approaches, including metabolomics, transcriptomics and proteomics have successfully been used in addressing a variety of biological questions in all fields of biology and are recently also integrated into toxicity assessments [Brockmeier 2017, heijne 2005]. However, integration of these large-scale data sets is not yet common practice in a regulatory context. To support the use of omics techniques chemical safety regulation, it is important to enable integration of the dense information coming from omics technologies into toxicological pathways and relevant key events. This integration will make the obtained information more understandable and comprehensive, which is required for decision making [Hartung 2016].



The omics approaches can be used in an AOP context to: 1) monitor multiple components of pathways related to key events, 2) support identification of new key events, 3) perform cross-species extrapolation or to study preservation of responses between species and 4) feed information into biomarker identification programs. The use of expression patterns of a large unbiased set of transcripts, proteins and/or metabolites upon exposure to chemicals, specifically when they are chemically or biologically related, could support the identification of common markers and support prediction of toxicity [Kohonen 2017]. The identification of new biomarkers can help to specify existing AOPs.

**Metabolomics**

Metabolomics is the study of the metabolite profile of a cell system, tissue or body fluid and can serve as a measure for the effect of stressors upon any type of metabolism [Bouhifd 2013]. The assessment of metabolite levels can be an indicator for the adaptive responses initiated upon for instance chemically-induced shortage of certain substrates or a change in energy requirements.

*Methods*

Assessment of the metabolome is nowadays achieved using nuclear magnetic resonance (NMR) or mass spectrometry (MS). NMR detects molecules present in a sample based on the interaction of their nuclear spin with a magnetic field. MS uses the behavior of ions created from a metabolite in a magnetic field. Selection of the technology depends among others on the studied sample properties like polarity and abundance, the desired approach (targeted vs untargeted) and the available resources including money, time and space [Bouhifd 2013, Emwas 2015]. Metabolomics samples most often include the non-invasive collection of urine, blood and feces or the invasive extraction of a biopsy. Assessment of the metabolome *in vitro* is possible using cell lysates. The use of cell lysate requires the optimization of cell number to achieve enough signal for lowly abundant metabolites. In addition, the

*in vitro* culture conditions should be carefully selected because of the presence of a variety of anions and metabolites in growth media [Smith 2020]. In addition, when collecting metabolite profiles of different culture types (2D/3D cultured cell systems and non-adherent cells), sample preparation and cell environment affect the yield and purity and should be optimized per *in vitro* model. Extraction and collection methods affect specific metabolites varying in polarity, size and stability differently. Cell environments like gel materials used in 3D cultures require digestion before metabolites are available for analysis [Mushtaq 2014, Muschet 2016, Mathon 2019, Vuckovic 2012, Zukunft 2018].

Metabolomics studies can be designed to be targeted or untargeted. A targeted approach includes the collection and purification of a selected set of metabolites before the MS or NMR is used to quantify their abundance. The set of metabolites can be linked to metabolic pathways of interest, be predictive for certain toxicities/diseases or performance very well in species cross validation. Untargeted metabolomics is the relative assessment of all metabolites present in a sample compared to a control sample. It results in large amounts of data, which requires post-processing to distinguish noise from the real metabolites. This approach allows a relative quantification of the complete metabolic fingerprint; however, it is still challenging to identify individual metabolites. Recently, hybrid approaches combining targeted and untargeted mass spectrometry are under investigation, which could facilitate metabolite detection and identification [Chen 2020].

*Integration into qAOP*

Metabolites provide a fingerprint of the entire cellular response and therefore changes in their expression may provide a complete view on the studied toxicity. The obtained information could therefore be highly relevant in describing later key events and support even extrapolation to *in vivo* and human data collected in for example clinical settings. Metabolomic profiles support qAOP both when collected using targeted and untargeted approaches. The limited number of metabolites assessed with targeted approaches can be used to support key events describing specific metabolic pathways. Untargeted assessment of metabolites informs biomarker/key event identification, species/tissues/cell type comparisons and can be used to compare differences/similarities at a larger scale for chemicals with known and unknown mode of action in read across attempts [Van Ravenzwaay 2007, Van Ravenzwaay 2016].

Unfortunately, metabolomics studies are limited by the relatively few reference databases describing relationships between metabolic profiles and pathologies/toxicities. Changes in metabolic profiles are also observed upon physiological processes like growth, development and even feeding cycles. Reference profiles

should allow proper separation between desired and undesired changes. The Consortium for Metabolic Toxicology (COMET) and aBASF group company (in Germany based chemical industry cluster) started with the creation of metabolomics reference databases to describe metabolic variations in the context of chemical exposure [Lindon 2005, Bollard 2010, Spagou 2011, Van Ravenzwaay 2012]. Metabolic profiles are influenced by species and sex [Van Ravenzwaay 2012], indicating that these variables should be incorporated in reference panels to allow comparison studies and support extrapolation of responses in for example AOP approaches.

A few attempts to incorporate metabolomics data into AOP driven research have been reported concerning androgen receptor activation by spironolactone [Davis 2017], cross species extrapolation in plant species [Florez-Sarasa 2016] and nanoparticle toxicity [Bannuscher 2020].



*Mitochondrial studies using metabolomics*

In the field of mitochondrial research, metabolomics is already widely used, because of the central role of mitochondria in multiple metabolic pathways. Perturbation of mitochondrial metabolism will lead to changes in the detected metabolites, for instance when inhibition of mitochondrial respiration leads to a switch in cellular commitment from mitochondrial respiration to glycolysis [ref].

The human metabolome can be assessed in the entire cell or specifically in the mitochondria or cytoplasmic compartment. Around 10% of the known metabolites are unique for the mitochondria and 20% are unique for the cytoplasmic fraction [Pan 2018]. Variations in these unique sets could indicate compartment specific effects. These changes in metabolic profiles, compartment specific or not, should be properly mapped to allow identification of molecular initiating events or key events. An option to achieve these reference maps is the use of models representative for mitochondrial diseases, for instance by knocking out mitochondrial complexes in mice or *c. elegans* [Esterhuizen 2017, Pan 2018]. Various studies already demonstrated the possibilities for using metabolomics to identify mitochondrial involvement in diseases, e.g. in diabetic kidney disease [Li 2017, Buzkova 2018].

**Transcriptomics**

Transcriptomics studies changes in the expression of RNA transcripts in cells, tissues or organs [Lowe 2017]. The complete profile of RNA transcripts present at a specific moment in time informs about cellular modifications initiated in response to for example chemical induced stress. Most of the information can be derived from mRNAs. In addition, the study of other types of RNA, like non-coding RNA or miRNA, provides the opportunity to monitor quick modulation of the transcript profile caused by this subset of RNA. Changes in non-coding RNAs have been reported in case

of disease and upon exposure to chemicals [Dempsey 2017]. These changes could reflect the adaptation required in (early) responses during toxicity and are therefore considered as markers in regulatory toxicology and studied as possible therapeutic targets [Aigner 2016, Ratti 2020].

*Methods*

The transcriptome is generally studied using microarrays or RNA-sequencing. Microarrays assess a set of transcripts covert by the probes on the used chip. This set can be an interesting toxicity subset, the whole genome, a list of non-coding RNAs and could even contain various splicing variants as longs as it is possible to design transcript specific probes. The detection of the transcript abundance is based on the fluorescence signal coming from the hybridized transcripts-probes on predefined spots of the chip.

RNA-sequencing captures the exact sequence of every transcript without the need of transcript specific probes, which makes the technology excellent for detailed assessment of mutations, splice variants and "new" transcripts. The transcript detection is based on the high throughput sequencing of one nucleotide per round, where the four nucleotides have a unique fluorescent color [Lowe 2017]. A recent approach in the assessment of the transcriptome is TempO-seq. TempO-seq is a form of targeted sequencing, in which probes representing a subset of transcripts are used to select transcripts of interest and with that reduce the information density to be sequenced using RNA-sequencing technology [Mav 2018, Bushel 2018].

Samples suitable for the assessment of the transcriptome with any of these technologies only need to allow enough extraction of RNA [Lowe 2017]. Optimization of RNA extraction from any *in vitro* cell model includes selection of proper cell densities and lyses protocols. For instance, RNA-sequencing technologies require less RNA than microarrays. And similar to metabolomics, cell systems cultured in 3D-matrices require a more firm lysis protocol than 2D cultured or non-adherent cells.

*Integration into AOPs*

The transcripts are the tools of the cell to change protein expression (mRNA) or perform subtle changes to already transcribed mRNA (non-coding RNA) upon detection of malfunctioning. Understanding the cellular decisions, based on the induction of mRNA coding for proteins involved in adaptations, detoxification or cell death, will help to understand the toxic potential of a chemical and to indicate which events in de AOP are triggered with certain concentrations at specific timepoints.

In the last decades, transcriptomic data is increasingly used to obtain more mechanistic understanding in the occurrence and development of adversity. As discussed intensively by others, to enable the use of transcriptomics in regulatory chemical risk

assessment and regulatory decision making, it is necessary to standardize and evaluate data quality, storage and processing [Martens 2018, Buessen 2017]. Furthermore, to support integration of transcriptomics data into AOPs and biologically relevant key events, it is important to streamline data analysis into structured pipelines assessing not only individual genes, but also gene ontology enrichment, pathway (under/over) representations and co-regulated gene networks [Martens 2018, Nymark 2018, Serra 2020]. The integration of transcriptomics into AOP frameworks has been done in studies of various species and organs [Gust 2020, Gomes 2019, Lee 2019, Oki 2019]. Studies investigated the effects of substances like nanoparticles [Labib 20216] or followed development of chemical-induced diseases like cholestasis [Wolters 2016, Gijbels 2020].



*Mitochondrial studies using transcriptomics*

The use of transcriptome analysis upon chemical exposure could provide new insights for the assessment of mitochondrial toxicity. The early changes in transcript variations could reflect changes in cellular and mitochondrial biochemical reactions. Under normal and perturbed conditions there is a dynamic relationship between the nucleus and mitochondria [Quirós 2016]. Mitochondria and the nucleus are continuously interacting concerning the availability of energy, building blocks or storage places of ions, and the functional integrity of the mitochondria (for instance the mitochondrial membrane potential or mitochondrial DNA integrity). This constant communication initiated upon minimal changes in cellular-mitochondrial homeostasis could make it the perfect early marker for chemical toxicity. Monitoring this communication based on the mRNA transcriptome could provide valuable information concerning all these parallel processes and pick up the earliest signs for toxicity.

As discussed before, the expression of RNA transcripts originating from the mitochondrial genome can serve as indication of mitochondrial perturbation [Mercer 2011]. However, most of the mitochondrial proteins are encoded by the nuclear genome. Transcriptomic approaches monitoring the complete genome would provide information concerning all nuclear encoded mitochondrial proteins, and additionally give insights into the induction or inhibition of any other cellular process. For instance, the assessment of the cellular transcriptomic profile upon chemical exposure enabled the identification of toxic vs non-toxic concentrations of Manganese [Fernandes 2019] or chemicals that mimic disease states [Pearson 2016]. Furthermore, transcriptomic changes upon rotenone exposure helped to identify more detailed information concerning mode of action, recovery, and the threshold for cell death [Harris 2018].

*Integration of transcriptomics profiles into chemical assessments*

The integration of large-scale transcriptomic profiles into risk assessment requires more sophisticated data handling than the assessment of a small number of relevant

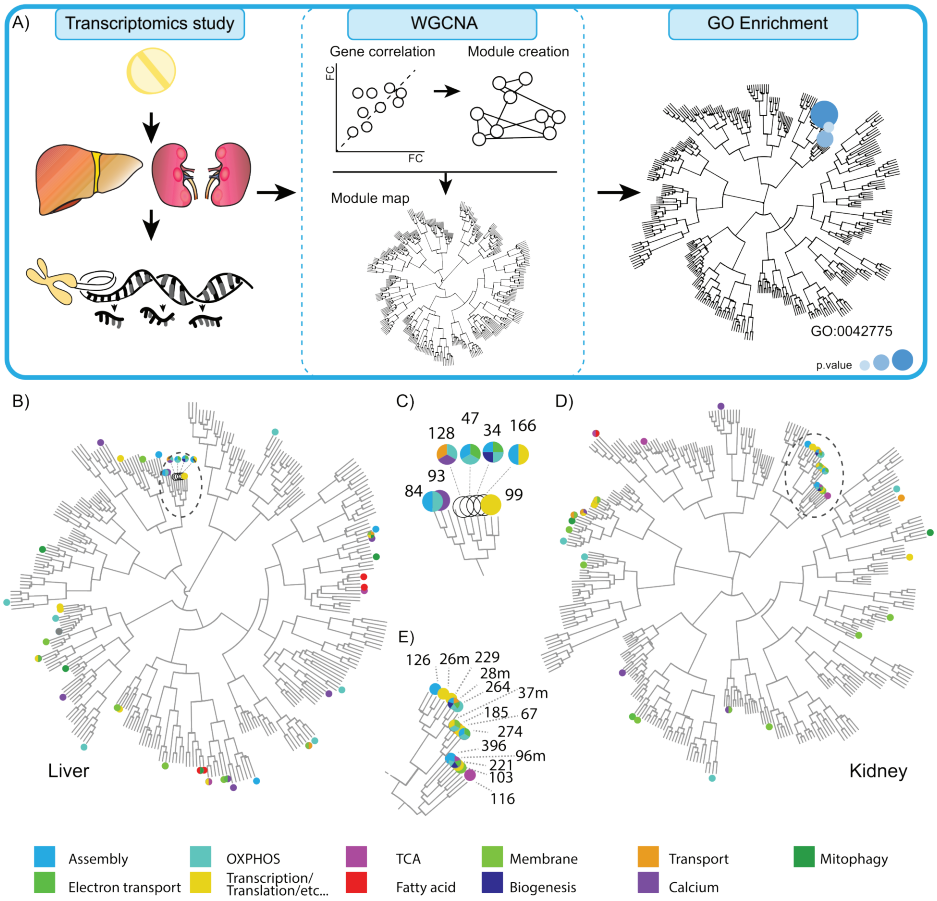


F)

| Module | Hubgene | Full name | Function |
|---|---|---|---|
| 34 | UQCR10 | Ubiquinol-Cytochrome C Reductase, Complex III SX | Mitochondrial subunit (complex III) |
| 47 | MRPS16 | Mitochondrial Ribosomal Protein S16 | Supports protein synthesis in the mitochondria |
| 84 | LOC301124 | NA | Cristae formation mitochondria * |
| 93 | Bloc1s1 | Biogenesis Of Lysosomal Organelles Complex 1 | Synthesis organelles of endosomal-lysosomal system |
| 99 | MRPL34 | Mitochondrial Ribosomal Protein L34 | Supports protein synthesis in the mitochondria |
| 128 | TMEM126B | Transmembrane Protein 126B | Component of mitochondrial complex I |
| 166 | SMIM8 | Small Integral Membrane Protein 8 | *No clear function defined* |

G)

| Module | Hubgene | Full name | Function |
|---|---|---|---|
| 26m | RGD1563941 | Chromosome 11 Open Reading Frame 71 | *No clear function defined* |
| 28m | NDUFB7 | NADH:Ubiquinone Oxidoreductase Subunit B7 | Mitochondrial subunit (complex I) |
| 37m | MRPL27 | Mitochondrial Ribosomal Protein L27 | Supports protein synthesis in the mitochondria |
| 67 | MRPS17 | Mitochondrial Ribosomal Protein S17 | Supports protein synthesis in the mitochondria |
| 96m | NDUFA9 | NADH:Ubiquinone Oxidoreductase Subunit A9 | Mitochondrial subunit (complex I) |
| 103 | MTFP1 | Mitochondrial Fission Process 1 | Mitochondrial dynamics |
| 116 | SLC13A2 | Solute Carrier Family 13 Member 2 | Succinate transporter * |
| 126 | SMIM8 | Small Integral Membrane Protein 8 | *No clear function defined* |
| 185 | TIMM13 | Translocase Of Inner Mitochondrial Membrane | Chaperone in import of proteins from cytoplasm |
| 221 | TFB2M | Transcription Factor B2, Mitochondrial | Mitochondrial specific transcription factor |
| 229 | PRELID3B | PRELI Domain Containing 3B | *No clear function defined* |
| 264 | NDUFA6 | NADH:Ubiquinone Oxidoreductase Subunit A6 | Mitochondrial subunit (complex I) |
| 274 | SMIM20 | Small Integral Membrane Protein 20 | Assembly Mitochondrial complex IV |
| 396 | DEPDC7 | DEP Domain Containing 7 | *No clear function defined* |

**Figure 3: Gene co-expression analysis**
**A)** Schematic representation of the performance of gene ontology (GO) enrich using a module network created using weighted co-regulated gene-network analysis. 1) the WGCNA analysis performed by Callegro *et al* unpublished work is based on microarray data for … compounds in both liver and kidney rat tissue, 2) the WGCNA analysis results is captured in a map depicting the hierarchical clustering of all identified gene modules and 3) The created network map can be used to study clustering of relevant mitochondrial GO term like GO:0042775 which represents mitochondrial ATP synthesis coupled electron transport. The color tone and the size represent the p.value per module for the selected GO term (the larger and darker the circle the more significant). **B)** Annotation of GO terms per module in the *in vivo* rat liver module map including GO terms describing 11 terms in combination with mitochondria. **C)** Zoom in on a branch of the *in vivo* rat liver map including a high density of mitochondria related labeled modules. **D)** Annotation of GO terms per module in the *in vivo* rat kidney module map including GO terms describing 11 terms in combination with mitochondria. **E)** Zoom in on a branch of the *in vivo* rat kidney map including a high density of mitochondria related labeled modules. **F)** Table depicting for the modules in C the hubgene and its function. **G)** Table depicting for the modules in E the hubgene and its function.

markers. One way to summarize the information from thou3sands of gene changes is the search for enrichment of terms belonging to predefined classes like gene ontologies or components of specific biological pathways as described in for instance KEGG, Reactome or Wikipathways [Ashburner 2000, Carbon 2021, Kanehisa 2000, Jassal 2020, Martens 2021]. Both an increase and a decrease in related terms can help to identify mode of action, adaptive vs toxic concentrations or off target effects.



Another option is the use of machine learning strategies, which enables the clustering of transcripts into biologically relevant and understandable subgroups without using predefined classes [Tarca 2007]. The subgroups can be defined using unsupervised and supervised methods, which support different types of comparisons. The unsupervised methods support clustering of for instance chemicals based on similarities of their induced gene expression pattern without prior knowledge. This information can be used in read across cases to predict the outcome of a target chemical based on a biological/chemical analogue (also called the source chemical). Supervised methods can be used to label new chemicals as inhibitors of for instance mitochondrial metabolism or OXPHOS based on expression patterns induced by treatment with chemicals known to inhibit these key events.

A widely used method to perform gene clustering by the unsupervised approach is gene co-expression analysis. Gene co-expression analysis assesses correlations between gene expression of all included genes and creates subgroups of genes (modules), which demonstrate correlated changes upon exposure to for example a chemical. This has been done in the past based on the microarray expression patterns obtained upon exposure to 170 chemicals, 3 concentrations, 3 time points and 3 different modules (primary human hepatocytes, rat liver slices and rat kidney slices) (available in the TG-GATES database) (figure 3A) [Callegaro 2021, Sutherland 2018, Igarashi 2015]. The obtained gene modules can be studied for their enrichment in gene ontology terms, like mitochondrial related processes (figure 3B (*in vivo* rat liver data) and D (*in vivo* rat kidney data)). Clustering of mitochondrial gene ontology terms is observed in gene modules created with *in vivo* data of rat both in the liver and kidney (figures 3C & F (*in vivo* rat liver data) and 3E & G (*in vivo* rat kidney data)). The expression patterns of these module clusters could be

included in the assessment of chemical-induced mitochondrial perturbation. A more supervised assessment including the defined module tree could include the inclusion of well-known mitochondrial toxicants into the teaching set of chemicals (at the moment mainly consisting of drugs), to create a module expression pattern that represents the selected class of chemicals. This profile could be used as a basis to identify chemicals with a similar mode of action.

**Proteomics**

Study of the cellular proteome upon chemical exposure creates the opportunity to follow both expression and compartment specific localization of proteins [Aslam 2017]. The increase in newly translated proteins correlates with the presence of newly transcribed mRNA. The total protein pool is not one-to-one correlated to the mRNA levels in the cell. Differences in protein expression in mammalian cells could only be captured for 40% using mRNA expression data [Tian 2004]. Protein levels are subject to variance in synthesis and degradation rates. On top of that protein functioning is also dependent on post-translational modifications, which adds a lot of extra information with more than 300 possible modifications [Zhao 2009]. The study of the proteome plus the related post-translational modifications informs about the reason for the actual observed phenotypic response, be it adaptation or adversity.

*Methods*

High through-put quantification of changes in the proteome is based on the relative expression of certain peptides between a test and control sample. Peptides present in the sample can be labeled using different methods: ICAT, ICPL, iTRAQ or SILAC [Shiio 2006, Schmidt 2005, Gan 2007, Ong 2017, Geiger 2011]. All labeling methods are based on the incorporation of a light atom in one sample and a heavy atom in the other, which can be for instance C12 vs C13 or H0 vs H1. The difference between the two atoms can be identified using tandem MS (MS/MS). Here, two MS analyze samples in series resulting in better separation/quantification of atoms with very similar sizes [Mclafferty 1980]. ICAT/ICPL labels consist of 1) an affinity tag, which can be used for extraction and with that reduction of complexity before the MS analysis, 2) linker with the light/heavy atom and 3) group reactive towards cysteine groups for ICAT and toward lysine groups and N-termini for ICPL. ICPL tags are designed with more than two types of heavy atoms creating the possibility to study more than two samples in one MS run. iTRAQ is a variant from ICPL, which also labels N-termini and protein side chains. They differ in their starting masses, because iTRAQ probes (one sample can be a multiplex of up to 8 different labels) all have the same mass. This results in one peak in the first MS run. The first MS run is followed by a fragmentation round resulting in up to 8 labels with different mass, which will be separated in the second

MS round. This approach helps to reduce the complexity and improves interpretation of the output of the first MS round. Finally, samples can also be labeled with light and heavy atoms before collection by using medium with amino acids containing light or heavy atoms (methods = SILAC).

Sample collection for proteomic studies requires the integration of an identifiable tag, as described above, but also the type of extraction requires consideration based on the study aim. For instance, extraction of membrane protein requires the use of specific detergents to solubilize the protein [Lee 2018]. Different types of detergents can have various effects on protein structure, charge or protein-protein interactions. Furthermore, inclusion of for example post-translational modification requires specific enrichment for the studied modification.



*Integration into AOPs*

The presence, expression levels and functionality of proteins, like detoxifying enzymes, during the chemical-exposure determines if a cell will be able to survive chemical-induced malfunctioning and additionally if this survival will be with or without permanent damage.

In the 21st century, proteomics is increasingly used in toxicology assessment and so far applied on drugs, natural products, industrial chemicals, metals and nanoparticles [Rabilloud 2015]. The data is used for identification of new biomarkers that are predictive for the occurrence of certain type of toxicity and their severity [Wetmore 2004]. The study of individual protein levels, like chemical targets, in multiple tissues can also be used to predict susceptibility of these particular tissues towards toxicity or predict susceptibility of specific individuals towards certain chemical-induced adversities [Van Summeren 2012, Kennedy 2008]. Besides single protein assessments, proteomics data can (like the transcriptomics data) be used for functional assessments (protein-protein interactions and enrichment of particular groups or pathways) and network analysis unraveling new interactions that drive machine learning approaches [Titz 2014].

It is also important to keep the high level of proteome complexity in mind. Proteins can be studied at multiple levels beyond the identification of amino acid sequences, including protein folding, post-translational modifications and protein-protein interactions. Thus far, the use of proteomics in toxicology is still challenging, because the technique does not yet support detection of low abundant proteins, very large-scale analyses, and, although further developed than metabolomics, the available reference databases for protein annotations are not complete [Manzoni 2018].

Integration of proteomics into AOPs, although limited, has been reported for example for endocrine disrupting agents [Johansson 2020], and triclosan [Guo 2018]. In addition, there is the option to study specifically post-translational modifications of the proteome, which was reported in an AOP context by Smith *et al* [Smith 2018].

*Mitochondrial studies using proteomics*

Starting from the 21st century proteomic studies have been used for the assessment of effects caused by various chemical substances. Rabilloud *et al* noted that a large number of these studies reported changes in the expression of mitochondria-related proteins (10 out of 31 drugs studies, 7 out 17 natural products studies, 14 out 30 industrial chemicals studies and 2 out of 19 nanoparticles studies) [Rabilloud 2015]. Identification of mitochondrial protein targets helps to find the potential mode of action of chemicals. However, time and concentration dependency should not be overlooked, because mitochondrial perturbation can be both the initiating event and a later key event.

Assessment of the proteome upon mitochondrial perturbation is usually only done for the mitochondrial proteome. The mitoproteome is studied in isolated mitochondria and provides information on the proteins within the mitochondrial membrane and matrix. However, this provides very limited information concerning the status of the mitochondria. The use of the whole proteome, including the mitochondrial proteins encoded by nuclear DNA and the transcription factors involved in mitochondrial retrograde and anterograde signaling, will provide more detailed information about the mitochondria and its responses upon stress [Kühl 2017].

**Combined omics approaches**

The combination of transcriptomic, proteomics and metabolomics studies provides multi-level information concerning the response of the cell to a chemical insult. Linking mRNA variations to changes in protein levels and eventually to excreted metabolite levels provides the opportunity to study the effect of a chemical-induced increase in gene expression upon adaptation/survival of cells/tissues/organs. What is the required change in mRNA expression before significant changes in protein expression are observed? Are these thresholds similar or distinct in different tissues? Do enriched pathways determined by transcriptomics result in actual pathway activity? Can transcriptional responses and subsequent proteomic alterations be linked to a more easily accessible marker for mitochondrial toxicity such as metabolomics analysis in body fluids of test species or people? Progress in this area will aid the development of quantitative AOPs.

Integration of all omics techniques into the assessment of effects induced by single chemicals has been done for example for cyclosporin A [Wilmes 2013], cisplatin [Von Stechow, Puigvert 2013 2013, Wilmes 2015, Späth 2019] and methapyrilene [Craig 2006]. This approach provides the opportunity to study the link between certain phenotypes, environmental factors and the cellular factors [Williams 2016]. Combination of transcriptomics, proteomics and metabolomics to identify biomarkers in an AOP driven approach has been described [Rodrigues 2018].

## Future perspective and conclusion



Nowadays chemical risk assessment faces the challenge of evaluating large numbers of chemicals that might affect human health. Over the years numerous assays have been developed to assess known risk factors in *in vitro* approaches, which should minimize the use of animal tests. Recently, more data-rich technologies like omics enter this arena of risk assessment. To make chemical risk assessment as efficient and coherent as possible, it is important to integrate these different methodologies in biologically relevant testing strategies. One way to do this is the use of AOPs. In this review, chemical-induced mitochondrial toxicity has been discussed using an AOP inspired approach. We highlight the importance of key event identification, the broad range of available key event specific assays and the integration of the methodologies into quantitative assessments.

The use of AOP relationships in risk assessments, and in particular in qAOPs, helps to link and quantify biological events observed during the development of adversity. The readout of one assay alone can easily miss specific types of toxicity, for instance toxicity resulting from concentration-/time-dependent accumulation or toxicity only occurring in specific cells/tissues. The combination of multiple related (as defined in a specific AOP) measurements will allow a broader readout and thereby help to create confidence about the identified chemical hazard.

The integration of omics technology is thus far not standard in regulatory chemical risk assessment. The technology is very data-rich and can provide a broad picture of cellular fitness, including interactions between signaling pathways and well-known toxicity markers. Simple assays are very valuable to study for instance target binding specificity and efficiency. Transcriptomics adds the opportunity to identify unexpected off-target effects which may otherwise only be discovered after running large sets of *in vitro* assays representing all facets of toxicology, which will eventually only lead to identification of known chemical-targets. In addition, the use of omics will also make it easier to detect (dis)similarities between chemicals, which can be used to categorize them into specific classes.

The AOP-driven biologically relevant combination of multiple targeted *in vitro* assays performed in cell types of different complexities and high throughput omics supports flagging of hazardous substances, that require further testing to study species/tissue specific metabolism, possible accumulation and tissue specific forms of toxicity. Omics technologies when applied in multiple cell systems also helps to add information concerning genetic diversity and the difference in overall cellular responses between multiple systems.

Although most of the established assay systems are very well suited for the identification of toxic and non-toxic conditions, their relevance for the human situation is not always clear. At the moment we still rely on animal-based approaches for final decision making, especially for chemicals which are not easily assigned toxic or non-toxic. To enable the use of AOP-driven combinations of target *in* vitro methodologies and omics technologies to their full potential, they require validation using large sets of diverse chemicals which will help to distinguish toxic from non-toxic conditions. This will improve flagging of the possible hazardous substances class and use the *in vitro* technologies to their full potential. Therefore, broadening our understanding of the opportunities and limitations of all available methodologies will support the assemble of biologically relevant testing strategies, and improve *in vitro* based chemical related (mitochondrial) risk-assessment.

## Reference numbers

1= Reisch 2007, 2= Kerr 2012, 3 = Nonnemacher 2017, 4 = Murphey 1967, 5 = Else 1988, 6 = Park 2000, 7 = Schwab 2005, 8 = Jones 2013, 9 = Huynh 2014, 10 = Ma 2020, 11 = Uchinomiya 2020, 12 = Grandl 2010, 13 = Wiederschain 2011, 14 = Clark 1953, 15 = Diepart 2009, 16 = Wu 2010, 17 = Wittenberg 1970, 18 = Anderson 1999, 19 = Mik 2008, 20 = Penjweini 2018, 21= Rumsey 1988, 22= Hynes 2003, 23 = Hynes 2006, 24 = Takahashi 2006, 25 = Will 2007, 26 = Dimitriev 2012, 27 = Wang 2014, 28 = Ferrick 2008, 29 = Gerencser 2009, 30 = Ribeiro 2014, 31 = Vivakaruni 2014, 32 = Yepez 2018, 33 = Van der Stel 2020, 34 = Kida 2004, 35 = Bobko 2009, 36 = Liu 2009, 37 = Diepart 2009, 38 = Williams 2009, 39 = Halevy 2010, 40 = Christen 2014, 41 = Danhier 2014, 42 = Kennedy 1997, 43 = Rosenberger 2009, 44 = Liu 2009, 45 = Banaji 2010, 46 = Perry 200, 47 = Lemaster 2007, 48 = Vos 2007, 49 = Befroy 2012, 50 = From 2017, 51 = Chen 2018, 49 = Befroy 2012, 50 = From 2017, 51 = Chen 2018, 52 = Manfredi 2002, 53 = Bhatt 2012, 54 = Wilson 1998, 55 = Crouch 1993, 56 = Contag 1997, 57 = Di Virgilop 2006, 58 = Rahendran 2016, 59 = Kim 2010, 60 = Imamura 2009, 61 = Depaoli 2019, 62 = Yaginuma 2014, 63 = Ozalp 2010, 64 = Berg 2009, 65 = Lee 2004, 66 = Xu 2009, 67 = Liu 2013, 68 = Wang 2016, 69 = Birch-Machin 2001, 70 = Spinazzi 2012, 71 = Durand 2017, 72 = Giedt 2016, 73 = Ouellet 2017, 74 = Harwig 2020, 75 = Vowinckel 2015 (e.g. mitoloc), 76 = Berman 2008, 77 = Karbowski 2015, 78 = Meeusen 2007, 79 = Jourdain 2010, 80= Smirnova 2001, 81 = Harder 2004, 82 = Gawlowski 2012, 83 = Baker 2014, 84 = Nilsson 2015, 85 = Hsieh 2018, 86 = Memon 2017, 87 = Fazzini 201, 88 = Popov 2020, 89 = Rizzuto 1992, 90 = Inouye 1993, 91 = Markova 2002, 92 = Fonteriz 2010, 93 = Jafarian 2011, 94 = Aghamaali 2011, 95 = Markova 2012, 96 = Bonora 2013, 97 = Bakayan 2016, 98 = Miyawaki 1997, 99 = Miyawaki 1999, 100 = Heim 2004, 101 = Garaschuk 2007, 102 = Palmer 2016, 103 = Baird 1999, 104 = Griesbeck 2001, 105 = Nagai 2001, 106 = Fonteriz 2010, 107 = Akimzhanov 2011, 108 = Zhao 2011, 109 = Waldeck-Weiemair 2019, 110 = Minta 1998, 111 = Thomas 2000, 112 = Fonteriz 2010, 113 = McKenzie 2017, 114 = Grynkiewicz 1985, 115 = Katayma 2011, 116 = Um 2018, 117 = Sargsyan 2015, 118 = Dolman 2013, 119 = Patergnani 2015, 120 = Hammerling 2017, 121 = Eskelinen 2011

# 3

# Multiparametric assessment of mitochondrial respiratory inhibition in HepG2 and RPTEC/TERT1 cells using a panel of mitochondrial targeting agrochemicals

Wanda van der Stel*, Giada Carta*, Julie Eakins, Salihanur Darici, Johannes Delp, Anna Forsby, Susanne Hougaard Bennekou, Iain Gardner, Marcel Leist, Erik H. J. Danen, Paul Walker, Bob van de Water#, Paul Jennings#

*Arch Toxicol. 2020 Aug;94(8):2707-2729; doi: 10.1007/s00204-020-02849-5*

**Evidence is mounting for the central role of mitochondria dysfunction in several pathologies including metabolic diseases, accelerated ageing, neurodegenerative diseases and in certain xenobiotic-induced organ toxicity. Assessing mitochondrial perturbations is not trivial and the outcomes of such investigations are dependent on the cell types used and assays employed. Here we systematically investigated the effect of Electron Transport Chain (ETC) inhibitors on multiple mitochondrial related parameters in two human cell types, HepG2 and RPTEC/TERT1. Cells were exposed to a broad range of concentrations of 20 ETC inhibiting agrochemicals and capsaicin, consisting of inhibitors of NADH dehydrogenase (Complex I, CI), succinate dehydrogenase (Complex II, CII) and cytochrome bc1 complex (Complex III, CIII). A battery of tests was utilised including viability assays, lactate production, mitochondrial membrane potential (MMP) and the Seahorse Bioanalyser which simultaneously measures extracellular acidification rate [ECAR] and oxygen consumption rate [OCR]. CI inhibitors caused a potent decrease in OCR, decreased mitochondrial membrane potential, increased ECAR and increased lactate production in both cell types. Twenty-four-hour exposure to CI inhibitors decreased viability of RPTEC/TERT1 cells and 3D spheroid cultured HepG2 cells in the presence of glucose. CI inhibitors decreased 2D HepG2 viability only in the absence of glucose. CII inhibitors had no notable effects in intact cells up to 10 μM. CIII inhibitors had similar effects to the CI inhibitors. Antimycin A was the most potent CIII inhibitor, with activity in the nanomolar range. The proposed CIII inhibitor cyazofamid demonstrated a mitochondrial uncoupling signal in both cell types. The study presents a comprehensive example of a mitochondrial assessment workflow and establishes measurable key events of ETC inhibition.**

**Keywords:** Mitochondria, Seahorse, ETC, ECAR, MMP, RPTEC/TERT1, HepG2

## Introduction

There is accumulating evidence that chemical-induced organ toxicity involves disruption of mitochondrial function more frequently than previously considered (Dykens 2007; Will 2007, Dreier 2019). Mitochondrial perturbations can have major effects on tissues and organs due to their key role in fatty acid metabolism, energy production and generation of reactive oxygen species (ROS). There are several mechanisms of direct mitochondrial perturbation including electron transport chain (ETC) inhibition, mitochondrial DNA damage, ROS, cardiolipin binding, Krebs Cycle inhibition, disturbances of fatty acid shuttling, beta oxidation inhibition and protonphoretic (uncoupling) activity (Boelsterli 2003). The subsequent dysfunction of these organelles can have several adverse effects, which is both dependent on the target tissue's reliance on mitochondrial function and the type of mitochondrial perturbation.



Various chemical classes may pose human liability for mitochondrial toxicity. Several drugs have been withdrawn from the market due to organ-toxicity, which have subsequently been proven or have strong evidence supporting a central role for mitochondrial perturbation (Nadanaciva 2007; Dykens 2007, Longo 2016; Eakins 2016, Grünig 2017). Compounds that fail late in clinical trials, or those that are withdrawn from the market are costly in terms of financial and time resources, but also on patient's health. The assessment of the potential of drug candidates to perturb mitochondria should be a fundamental parameter in the early stage of drug development to prevent later, often devastating, adverse drug reactions in patients. Furthermore, the agrochemical industry has harnessed a broad range of effective pesticides and fungicides that act via targeting individual complexes of the ETC. Selective inhibition of CI and CIII by model mitochondrial toxins, has been associated with adverse responses in pre-clinical species, including neurological defects (Cannon 2009). Therefore, a thorough assessment of mitochondrial toxicity could also provide important input for risk assessment in the case of industrial chemicals and environmental pollutants. While various divergent assays have been established to assess mitochondrial perturbations, there is no current consensus on the most appropriate assays to use, which combinations nor on the most appropriate cell types.

In this study we aimed to systematically assess the applicability of several assays which could eventually form the basis of a consensus mitochondrial toxicity testing platform. To this end we used two human cell lines, the renal RPTEC/TERT1 and the hepatic HepG2 cells. RPTEC/TERT1 are a non-cancerous human telomerase immortalised cell line that exhibit a differentiated oxidative phenotype when differentiated via contact inhibition (Auschauer 2013). The HepG2 cell line under standard 2D conditions

exhibit a highly proliferative phenotype but can be further differentiated under 3D spheroid conditions (Ramaiahgari 2014). We chose a panel of 20 agrochemicals which have been harnessed for the selective inhibition of ETC, consisting of inhibitors of NADH dehydrogenase (CI), succinate dehydrogenase (CII) and cytochrome bc1 complex (CIII). Capsaicin was also included due to its proposed CI activity (Satoh 1996). A battery of assays was utilised including assays monitoring viability, lactate production, mitochondrial membrane potential, and the simultaneous quantification of extracellular acidification and cellular oxygen consumption. While this study focuses on ETC inhibition, the combination of these assays has the potential to measure the majority, if not all, mitochondrial perturbations.

## Material and methods

### Chemicals

All tested compounds were purchased from Merck at one site (JRC, Ispra, Italy) and distributed to the testing laboratories. The catalogue no's are Capsaicin (Cat. No. M2028), Deguelin (D0817), Fenazaquin (31635), Fenpyroximate (31684), Pyridaben (46047), Pyrimidifen (35999), Rotenone (R8875), Tebufenpyrad (46438), Carboxin (45371), Fenfuram (45486), Flutolanil (N12004), Mepronil (33361), Thifluzamide (49792), Antimycin A (A8674), Azoxystrobin (3167), Cyazofamid (33874), Fenamidone (33965), Kresoxim-methyl (37899), Picoxystrobin (33568), Pyraclostrobin (33696), Trifloxystrobin (46477). The compounds are listed by class in Table 1 and structural information is provided in Figure 1. Stock solutions between 10 - 100 mM were created in dimethyl sulfoxide (DMSO) and stored at -20°C or -80°C until use. Treatment solutions were prepared freshly from DMSO stocks for each experiment and the final concentration of DMSO in the systems was 0.1% (v/v). For repeated administration the culture medium was removed and new medium with the compound was added every 24 hours.

### Cell culture

The human renal proximal tubule derived cell line RPTEC/TERT1, is a non-cancerous cell line which was immortalised by introduction of the catalytic unit of human telomerase (hTERT) (Wieser et al. 2008). These cells were obtained under licence from Evercyte GmBH, Vienna Austria. RPTEC/TERT1 grow in a monolayer and after reaching confluence become contact inhibited, enter cell cycle arrest and differentiate into a transporting epithelium (Aschauer et al. 2013). RPTEC/TERT1 at passage number between 72 and 95 were routinely cultured in 10 cm dishes (Sarstedt, 83.3902) at 37 ˚C in a 5% $CO_2$ humidified atmosphere. Cells were fed every second to third day with medium containing 1:1 mixture of Dulbecco's modified Eagle's medium (DMEM, no glucose, Invitrogen, 11966) and Ham's F-12 nutrient mix (Invitrogen, 21765), with a final

**Table 1: General properties of selected ETC complex I, II, and III inhibitors.**
***** refers to the subset of panel compounds in this study. **CI** (NADH:ubiquinone oxidoreductase), **CII** (succinate dehydrogenase), **CIII** (cytochrome $bc_1$ complex). **ClogP**: lipophilicity as reported by Delp et al. 2019. **Chemical group** from FRAC Code List © 2019. **Inhibitor**: type A- quinone antagonist, type B - semiquinone antagonist, type C -quinol antagonist, Qo-outside quinol oxidation pocket, Qi inside quinone reduction pocket, Pf-Qo sub-type I, Pm-Qo sub-type II.

| Compound | ETC complex inhibited | CAS number | Molecular weight (g/mol) | ClogP | Application | Chemical group | Inhibitor type | Putative binding site | References |
|---|---|---|---|---|---|---|---|---|---|
| Capsaicin* | I | 404-86-4 | 305,2 | 3,64 | topical analgesic, pepper spray agent | Phenol | Type C | Quinone binding pocket | (Degli Esposti1994; Tocilescu 2010) |
| Deguelin* | I | 522-17-8 | 394,14 | 4,26 | Insecticide | Flavonoid | | Quinone binding pocket | (Degli Esposti 1994) |
| Fenazaquin | I | 120928-09-8 | 306,17 | 5,51 | Insecticide/ acaricide | Quinazoline | Type A | Quinone binding pocket | (Wood 1996; Rgen 1999) |
| Fenpyroximate* | I | 134098-61-6 | 421,2 | 5,01 | Acaricide | Pyrazoles | Type A | Quinone binding pocket | (Rgen 1999; Ino 2003; Tocilescu 2010) |
| Pyridaben | I | 96489-71-3 | 364,14 | 5,24 | Insecticide/ acaricide | Pyrimidine | | Quinone binding pocket | (Schuler 1999) |
| Pyrimidifen* | I | 105779-78-0 | 377,19 | 5,03 | Insecticide/ acaricide | Pyrimidine | Type A | Quinone binding pocket | (Lümmen 1998; Rgen 1999) |
| Rotenone* | I | 83-79-4 | 394,14 | 4,1 | Insecticide | Flavonoid | Type B | Quinone binding pocket | (Esposti 1994; Tocilescu 2010) |
| Tebufenpyrad* | I | 119168-77-3 | 333,16 | 4,93 | Insecticide/ acaricide | Pyrazoles | | Quinone binding pocket | (Degli Esposti 1998) |
| Carboxin* | II | 5234-68-4 | 235,07 | 2,22 | Fungicide | Oxathiin-carboxamides | Qp | Quinone binding site | (Huang 2006; Horsefield 2006; Ruprecht 2009; Sierotzki 2013) |
| Fenfuram | II | 24691-80-3 | 201,08 | 2,24 | Fungicide | Furan- carboxamides | Qp | Quinone binding site | (Sierotzki 2013) |
| Flutolanil | II | 66332-96-5 | 323,11 | 3,7 | Fungicide | Phenyl-benzamides | Qp | Quinone binding site | (Sierotzki 2013) |
| Mepronil* | II | 55814-41-0 | 269,14 | 3,9 | Fungicide | Phenyl-benzamides | Qp | Quinone binding site | (Sierotzki 2013; Kluckova 2015) |
| Thifluzamide* | II | 130000-40-7 | 525,84 | 5,05 | Fungicide | Thiazole-carboxamides | Qp | Quinone binding site | (Sierotzki 2013) |
| Antimycin A* | III | 1397-94-0 | 548,27 | 4,41 | Piscicide | | Qi | Q-cycle | (Gao 2003; Esser 2004; Esser 2014; Zhao 2010) |
| Azoxystrobin* | III | 131860-33-8 | 403,12 | 2,5 | Fungicide | Methoxy-acrylates | Qo, Pm | Q-cycle | (Esser 2004, 2014; Zhao 2010) |
| Cyazofamid* | III | 120116-88-3 | 324,04 | 3,2 | Fungicide | Cyano-imidazole | Qi | Q-cycle | (Esser 2014) |
| Fenamidone | III | 161326-34-7 | 311,11 | 3,72 | Fungicide | Imidazolinones | Qo, Pf | Q-cycle | (Esser 2014) |
| Kresoxim-methyl | III | 143390-89-0 | 313,13 | 3,4 | Fungicide | Oximino-acetates | Qo, Pm | Q-cycle | (Esser 2004; Esser 2014; Zhao 2010) |
| Picoxystrobin* | III | 117428-22-5 | 367,1 | 3,81 | Fungicide | Methoxy-acrylates | Qo, Pm | Q-cycle | (Esser 2004; Esser 2014; Zhao 2010) |
| Pyraclostrobin* | III | 175013-18-0 | 387,1 | 3,99 | Fungicide | Methoxy-carbamates | Qo, Pm | Q-cycle | (Esser 2004; Esser 2014; Zhao 2010) |
| Trifloxystrobin | III | 141517-21-7 | 408,13 | 4,5 | Fungicide | Oximino-acetates | Qo, Pm | Q-cycle | (Esser 2004; Esser 2014; Zhao 2010) |

glucose concentration of 5 mM, supplemented with 2 mM glutamax (Thermofisher, 350500038), 5 µg/L insulin, 5 µg/L transferrin and 5 ng/L sodium selenite (Sigma-Aldrich, I1884), 100 U/mL penicillin and 100 µg/mL streptomycin (Merck, P4333), 10 ng/mL epithelial growth factor (Merck, E9644), 36 ng/mL hydrocortisone (Merck, E9644) and 0.5% foetal bovine serum (Gibco, 10720-106). For experiments cells were plated in required format plate, allowed to become contact inhibited and fed 24 h prior to treatment exposure. For experiments in galactose condition, cells were fed 24 h prior to experiment with culture medium (custom made DMEM/F12, PromoCell) in which 5 mM glucose was replaced with 5 mM galactose (Merck, G5388).

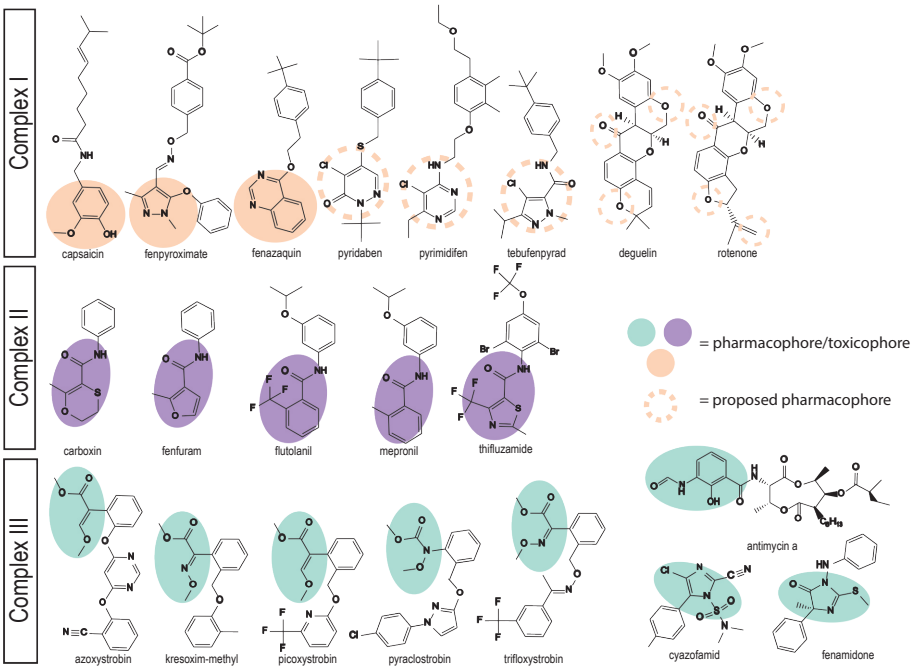


**Figure 1: Chemical structures of selected ETC complex I, II, and III inhibitors.**
Molecular structures of all assessed mitochondrial complex inhibitors organised based on their MoA (Table 1). The filled orange, purple and green areas highlight the region involved in the molecular recognition needed to perform the molecule´s activity for CI, CII and CIII inhibitors respectively. The dashed orange circles indicate the proposed regions of the pharmacophores for the remaining complex I inhibitors.

The HepG2 cell line, a human hepatocellular carcinoma, was obtained from ATCC (American Type Culture Collection, Wesel, Germany). HepG2 were cultured in Dulbecco's modified Eagle's medium (DMEM; 25 mM glucose, 4 mM L-glutamine, 1 mM sodium pyruvate) (Fisher Scientific, 11504496) supplemented with 10% (v/v) foetal bovine serum (Fisher Scientific, S181L-500), 25 U/ml penicillin and 25 µg/mL streptomycin (Fisher Scientific, 15070-063). Cells were maintained at 37˚C in a 5% $CO_2$ humidified atmosphere, fed every 2 to 3 days and passaged at approx. 80% confluence. For 2D

HepG2 culture the cells plated 48 h before exposures in 384 black µclear plates (Greiner Bio-One, 781 091) with a density of 10,000 cells/well. For galactose experiments, the medium was refreshed 24 h before exposure with galactose-containing medium. Galactose medium consist of glucose-free DMEM (Fisher Scientific, 11966-025), 10 mM galactose (Merck, G5388-100G), 1 mM sodium pyruvate (Sigma, P2256-100g), 10% (v/v) dialysed foetal bovine serum (GE healthcare, 26400-044), 25 U/ml penicillin and 25 µg/mL streptomycin (Fisher Scientific, 15070-063). The protocol for HepG2 3D culture was described previously (Ramaiahgari 2014). In short, Matrigel™ (BD biosciences, 354230) was diluted with ice cold PBS to 5 mg/ml. Ten microlitres was used to coat a 384 well Screenstar plate (Greiner, 781866). Cell were seeded at 1,000 cells per well in DMEM/Hams F12 (Thermo Fisher, 21041033) supplemented with 10% FBS, 25 U/ml penicillin and 25 µg/mL streptomycin. Culture medium was refreshed every 3-4 days and the culture was maintained for 21 days prior to dosing.



**Resazurin assay**

The resazurin reduction assay was conducted as previously described (Jennigs 2007). Briefly, a 880 µM resazurin stock solution (20X) was generated by dissolving 0.011 g resazurin (Merck, R7017), in 0.1 N NaOH and bringing to 50 ml in phosphate buffer and adjusting pH to 7.8. After exposure to compounds supernatant was replaced with 44 µM resazurin stock in cell culture medium and incubated for 1.5 h to 2h, at 37 °C in a 5% $CO_2$ humidified atmosphere. The conversion of resazurin to fluorescent resorufin was measured in a plate reader at excitation/emission 540/590 nm.

**Mitostress assay in intact cells with Seahorse XFe96 Bioanalyzer**

The Seahorse bioanalyzer simultaneously measures cellular oxygen consumption rates (OCR) and extracellular acidification rates (ECAR). The mitostress assay, utilises a sequential addition of modulators of the oxidative phosphorylation to assess key parameters of mitochondrial function. Subsequent injection of oligomycin (Merck, O4876), FCCP (Merck, C2920) and a mixture of rotenone (Merck, R8875) and antimycin A (Merck, A8674), provide information on ATP production, maximal respiration rates and non-mitochondrial respiration respectively. RPTEC/TERT1 cells were seeded onto Seahorse XF96 V3 PS Cell Culture Microplates (Agilent, 101085-004) at the density of 25,000 cells/well and allowed to differentiate for a minimum of two weeks before assay. It is worth noting here that RPTEC/TERT1 require longer differentiation times in the Seahorse plates, potentially due to sub-optimum gas exchange in the Seahorse culture plates. HepG2 cells were cultured at the density of 15,000 cells/well on collagen coated (2.5 µg/µL collagen IV, Merck, C7521) Seahorse Cell Culture Microplates two days prior to analysis.

**Table 2: IC50s and EC50s summary table of all experiments.**

Inhibitory and effective derived concentrations relative to all performed experiments. IC50s values were calculated with the in vitro toxicology on-line tool provided by the group of Prof. Leist, University of Konstanz (Krebs et al 2020), which calculates the curve fit applying a 4-parameter Hill model to the re-normalized datasets. The equation of the Hill model was solved for f(x) = 50% to determine the IC50s referring to the concentrations at which an inhibitory effect of 50% was observed. For endpoints increasing with treatment, EC50s values were calculated by fitting the curve without using a model but by using a point-to-point curve fit of re-normalized datasets. 1000 points were calculated with the X values ranging from lower to highest tested concentration. EC50s values were extrapolated from the curve and correspond to the concentrations at which an increased response of 50% was observed. NT- not tested, NR - no response.

| Compound | Complex | Viability (log10[M]) Glucose settings | | Viability (log10[M]) Galactose settings | | Cell death 1x 24h (log10[M]) | Cell death 5x 24h (log10[M]) | MMP (log10[M]) | | Lactate production (log10[M]) | | ECAR Basal (log10[M]) Intact cells | | OCR Basal (log10[M]) Intact cells | | OCR Maximal (log10[M]) Intact cells | | OCR Basal (log10[M]) Permeabilized cells | | |
|---|---|---|---|---|---|---|---|---|---|---|---|---|---|---|---|---|---|---|---|---|
| | | Resazurin | | Resazurin | | PI staining | PI staining | | | | | | | | | | | | | |
| | | RPTEC/ TERT1 | HepG2 | RPTEC/ TERT1 | HepG2 | HepG2 3D | HepG2 3D | RPTEC/ TERT1 | HepG2 | RPTEC/ TERT1 | HepG2 | RPTEC/ TERT1 | HepG2 | RPTEC/ TERT1 | HepG2 | RPTEC/ TERT1 | HepG2 | HepG2 (IC50) | | |
| | | IC50 | IC50 | IC50 | IC50 | EC50 | EC50 | EC50 | EC50 | EC50 | EC50 | EC50 | EC50 | IC50 | IC50 | IC50 | IC50 | CI | CII/CIII | CIV |
| Capsaicin | CI | > -5.00 | > -5.00 | -5,21 | > -5.00 | > -5.00 | > -5.00 | > -5.00 | > -5.00 | > -5.00 | > -5.00 | > -5.00 | -5,04 | > -5.00 | > -5.00 | > -5.00 | > -5.00 | -3,59 | NR | NR |
| Deguelin | CI | -6,33 | > -5.00 | -6,10 | -6,46 | -5,41 | -5,72 | -5,35 | -7,21 | -6,62 | -6,61 | -6,71 | -6,45 | -6,44 | -6,17 | -7,02 | -6,77 | -6,98 | NR | NR |
| Fenazaquin | CI | -5,37 | > -5.00 | NT | NT | NT | NT | > -5.00 | -6,55 | -6,06 | -6,07 | -6,05 | -5,62 | -5,84 | -5,59 | -6,44 | -6,42 | -6,74 | NR | NR |
| Fenpyroximate | CI | -6,73 | > -5.00 | -6,65 | -7,28 | -6,52 | -6,56 | -6,36 | -8,05 | -6,69 | -6,88 | -5,90 | -6,28 | -6,27 | -6,17 | -5,93 | -6,53 | -7,72 | NR | NR |
| Pyridaben | CI | -6,12 | > -5.00 | NT | NT | NT | NT | -5,46 | -8,19 | -6,56 | -6,85 | -5,81 | -5,31 | -5,91 | -5,49 | -6,40 | -5,82 | -7,37 | NR | NR |
| Pyrimidifen | CI | -6,93 | > -5.00 | -6,88 | -7,29 | -5,80 | -5,82 | -6,57 | -8,43 | -6,79 | -7,01 | -7,18 | -7,29 | -6,22 | -7,10 | -7,48 | -7,61 | -8,15 | NR | NR |
| Rotenone | CI | -6,77 | > -5.00 | -6,79 | -7,23 | -5,89 | -6,54 | -7,29 | -8,09 | -6,65 | -6,90 | -6,76 | -6,67 | -6,49 | -6,62 | -6,99 | -7,22 | -7,48 | NR | NR |
| Tebufenpyrad | CI | -6,78 | > -5.00 | -5,94 | -6,15 | > -5.00 | -5,13 | -5,44 | -7,29 | -6,05 | -6,84 | -6,15 | -6,49 | -5,79 | -6,07 | -6,61 | -6,68 | -5,26 | > -5.00 | NR |
| Carboxine | CII | > -5.00 | > -5.00 | > -5.00 | > -5.00 | > -5.00 | > -5.00 | > -5.00 | > -5.00 | > -5.00 | -6,92 | > -5.00 | > -5.00 | > -5.00 | > -5.00 | > -5.00 | > -5.00 | > -4.30 | -4,63 | NR |
| Fenfuram | CII | > -5.00 | > -5.00 | NT | NT | NT | NT | > -5.00 | > -5.00 | > -5.00 | > -5.00 | > -5.00 | > -5.00 | > -5.00 | > -5.00 | > -5.00 | > -5.00 | > -3.30 | > -3.30 | NR |
| Flutolanil | CII | > -5.00 | > -5.00 | NT | NT | NT | NT | > -5.00 | > -5.00 | > -5.00 | > -5.00 | > -5.00 | > -5.00 | > -5.00 | > -5.00 | > -5.00 | > -5.00 | NR | -4,16 | > -3.30 |
| Mepronil | CII | > -5.00 | > -5.00 | > -5.00 | > -5.00 | > -5.00 | > -5.00 | > -5.00 | > -5.00 | > -5.00 | > -5.00 | > -5.00 | > -5.00 | > -5.00 | > -5.00 | > -5.00 | > -5.00 | > -3.30 | -3,75 | NR |
| Thifluzamide | CII | > -5.00 | > -5.00 | > -5.00 | > -5.00 | > -5.00 | > -5.00 | > -5.00 | -5,06 | > -5.00 | > -5.00 | > -5.00 | > -5.00 | > -5.00 | > -5.00 | > -5.00 | > -5.00 | NR | -4,71 | NR |
| Antimycin A | CIII | -6,92 | > -5.00 | -7,15 | -7,53 | > -5.00 | -7,13 | -7,36 | -8,21 | -6,68 | -6,25 | -7,46 | -7,55 | -7,44 | -7,55 | -7,62 | -7,69 | -7,58 | -7,72 | NR |
| Azoxystrobin | CIII | > -5.00 | > -5.00 | > -5.00 | > -5.00 | > -5.00 | > -5.00 | -5,55 | -5,70 | -5,64 | -5,28 | -5,14 | > -5.00 | -5,04 | > -5.00 | -5,20 | > -5.00 | -4,50 | -4,77 | > -4.00 |
| Cyazofamid | CIII | > -5.00 | > -5.00 | > -5.00 | > -5.00 | > -5.00 | > -5.00 | -5,70 | > -5.00 | -5,42 | > -5.00 | -5,88 | > -5.00 | > -5.00 | > -5.00 | > -5.00 | > -5.00 | NR | NR | NR |
| Fenamidone | CIII | > -5.00 | > -5.00 | NT | NT | NT | NT | > -5.00 | -5,50 | -5,83 | -5,36 | -5,37 | -5,08 | -5,09 | -5,14 | -5,35 | -5,21 | -4,16 | -4,71 | NR |
| Kresoxim-methyl | CIII | > -5.00 | > -5.00 | NT | NT | NT | NT | > -5.00 | > -5.00 | > -5.00 | -6,69 | -5,28 | > -5.00 | -5,01 | -5,04 | -5,02 | > -5.00 | -5,25 | -5,21 | NR |
| Picoxystrobin | CIII | -5,47 | > -5.00 | -5,32 | -5,48 | > -5.00 | > -5.00 | > -5.00 | -6,14 | -6,32 | -6,26 | -5,88 | -5,04 | -5,35 | -5,63 | -5,77 | -5,30 | -5,16 | -5,40 | NR |
| Pyraclostrobin | CIII | -5,49 | > -5.00 | -5,85 | -6,04 | > -5.00 | > -5.00 | -5,75 | -6,31 | -6,42 | -6,32 | -6,12 | -5,93 | -5,90 | -5,86 | -6,22 | -5,76 | -6,07 | -6,41 | NR |
| Trifloxystrobin | CIII | > -5.00 | > -5.00 | NT | NT | NT | NT | > -5.00 | > -5.00 | -5,54 | > -5.00 | -5,42 | > -5.00 | -5,39 | > -5.00 | -5,37 | > -5.00 | -5,24 | -5,27 | > -4.00 |

The mitostress test was performed as described (Eakins 2016, Tilmant 2018). Immediately before the assay, cell culture medium was replaced with 180 µL of Seahorse XF Base Medium without phenol red (Agilent, 1003335-100), supplemented with 10 mM D-glucose (Merck, G7021), 5 mM HEPES (Merck, H4034), 2 mM sodium pyruvate (Merck, P5281) and 1 mM L-glutamine (Merck, G8540). Cells were allowed to equilibrate for 45 minutes in a non-$CO_2$ 37°C incubator, Agilent XFe96 sensor cartridge was hydrated 24 h prior to experiments with Seahorse XF Calibrant (Agilent, 100840-000) and both placed into the Seahorse Bioanalyser for assay. Compounds were injected sequentially. OCR was measured five times after test compound injection and three times for all injections. Each measurement consisted of a 3 min mix and subsequent 3 min read cycle. The sequence of injection was as follows, (A) test compound at 8 concentration points (1 in 5 dilutions starting at 10 µM final), (B) oligomycin (2 µM), (C) FCCP (2 µM) and (D) rotenone/antimycin A (0.5 µM each). OCR measurement was normalised to the baseline OCR measurement prior to compound addition. Measurements were performed in triplicate (3 wells) for each independent experiment.



**Mitochondrial complex assay with Seahorse XFe96 Bioanalyser**

The mitochondrial complex assay uses real time OCR measurement with sequential addition of specific complex substrates and/or inhibitors to identify the complex within the ETC that is inhibited. The assay principle explained in detail by Salabei et al. 2014, is to sequentially target specific electron chain complexes. In the first step cultured cells are permeabilised and provided with CI substrates. The test compound is injected and OCR measured. In the second step rotenone and succinate are added which simultaneously blocks CI while suppling substrates to CII. OCR is measured for the second time. In the third step Antimycin A together with ascorbate and tetramethyl phenylenediamine (TMPD) are added to simultaneously block CIII and supply CIV. A third and final OCR measurement is conducted. From the patterns of OCR inhibition, one can determine at which part of the ETC the compound is exhibiting its effect (Figure 4).

HepG2 cells were seeded at 20,000 cells/well on Seahorse XF96 V3 PS cell culture microplates (Agilent, 101085-004). The following day, cells were washed once in mitochondrial assay solution (MAS), containing 220 mM mannitol (Sigma, M9647), 70 mM sucrose (Sigma, S7903), 10 mM potassium phosphate (Sigma, P5655), 5 mM magnesium chloride (Sigma, M8266), 3 mM HEPES (Sigma, H0887) and 1 mM EGTA (Sigma, E4378) with 0.2% fatty acid-free BSA (Sigma, A8806). This solution was replaced with 180 µL MAS supplemented with 10 mM pyruvate (Sigma, 107360), 1 mM malate (Sigma, M0875), 4 mM ADP (Sigma, A5285), 0.2% fatty acid-free bovine serum albumin and 2 nM XF plasma membrane permeabilizer (PMP) (Agilent, 102504-100) and placed immediately into the Seahorse Bioanalyser. Each measurement consisted of a thirty

second mix and two minutes read cycle. Compounds were injected sequentially and OCR was measured twice. The sequence of injection was as follows, test compound, succinate (10 mM, Merck, S9512) and rotenone (2 μM, Chem Cruz, Sc203242) and TMPD (0.5 mM, Merck, T7394), ascorbate (10 mM, Merck, A5960) and antimycin A (2 μM, Merck, A8674). Complex inhibition was determined using the second OCR measurement after compound/vehicle injection, normalised to the baseline OCR measurements prior to compound addition. ETC inhibition is determined in decreased OCR. CI inhibition is confirmed if the inhibited OCR by injection A can be rescued after injection B. CII inhibition is determined if there is no inhibition after A, but inhibition after B. CIII inhibition is determined if there is inhibition after A and B, with recovery after C. OCR inhibition after injection C indicates effects downstream of CIII.

**Mitochondrial membrane potential (MMP) changes assays with JC-1**

JC-1 is a single excitation dual emission fluorescence-based assay, that allows for ratiometric semi-quantitative assessment of mitochondrial membrane potential (Perry 2011). For quantification of changes in MMP cells were pre-loaded, for approximately 1.5 h, with the JC-1 pre-loading solution containing 9 μM JC-1 (Invitrogen, 65-0851-38), 9 μL/mL Pluronic F-127 10% in water (Invitrogen, P6866) and 5 μM Cyclosporine A (CsA) (Merck, 30024), a P-glycoprotein (P-gp) inhibitor, to prevent dye extrusion due to the expression of efflux pumps in RPTEC/TERT1 cell line. After this incubation time cells were washed and exposed to test compounds dissolved in a JC-1 treatment solution containing 0.5 μM JC-1, 1.5 μL/mL Pluronic F-127 and 1 μM CsA for the desired time. We have previously determined that CsA at up to 5 μM has no adverse effect on RPTEC/TERT1 cells for up to 14 days (Wilmes 2013). Fluorescence was measured in a plate reader at excitation 492 nm and dual emission, 535 nm for monomers and 590 nm for dimers. Results are presented as the dimer/monomer ratio and expressed as percentage of untreated samples.

**Mitochondrial membrane potential plus cell death assay using live confocal imaging**

Rhodamine 123 (Rho123) (Merck, R8004) was used in a live confocal imaging setting for the assessment of effects at MMP. Rho123 localises to mitochondria and the decline in fluorescence is proportional to a decrease in MMP (Johnson 1980, 1981). HepG2 were seeded at 10,000 cells/30 μL/well in a 384-wells μCLEAR® black plate (Greiner Bio-One, 781 091). Two days post-seeding 30 μL complete HepG2 culture medium, containing 200 ng/μL Hoechst 33342 (Life technologies, H1399) and 1 μM Rho123, was added to the medium. After 1 h incubation at 37° C the medium was removed and 25 μL complete DMEM containing 0.2 μM Rho123 and 100 nM propidium iodide (PI) (Merck, P4170) was added, followed by 25 μL of medium containing 2X the desired concentration of test compound. The intensity of Hoechst, Rho123 and PI was monitored using live confocal imaging for 24 h using the 408, 488 and 561 nm laser

respectively. The confocal imaging was performed using a Nikon TiE2000 with perfect Focus System and xy-stage (Nikon, Amsterdam, The Netherlands). Quantification of the Hoechst, Rho123 and PI signal intensity and localization was performed using CellProfiler version 2.1.1 (Broad Institute, Cambridge, USA). The nuclear identification based on the Hoechst signal was performed using an internal created segmentation module (Di 2012), followed by a cytoplasmic identification based on a specific distance from these nuclei. The PI positive nuclei were identified by masking the previous segmented nuclei and the PI signal. More than 10% overlap was considered as PI positive. All CellProfiler analyses were stored as HDF5 files. The combination of an internal developed R script, run in Rstudio (Boston, USA) was used for data extraction including Rho123 signal intensity, fraction PI positive and nuclear count.



**Lactate assay**

The colorimetric assay for the lactate detection is based on the conversion of lactate to pyruvate by the lactate dehydrogenase (LDH) enzyme. The process is coupled with the active reduction of the co-factor NAD to NADH. NADH reduces N-methylphenazonium methyl sulphate (PMS) to PMSH which reduces p-iodonitrotetrazolium violet (INT) to its coloured product INTH (Babson and Phillips 1965) detectable in a plate reader. Cells were treated with test compounds for 24 h and at the end of the treatment supernatant medium was collected. Ten microliters of supernatant medium was added to 90 µL of reagent mix (80% TRAM buffer, 20% colour reagent, 3.3 mM β-NAD (Merck, N7004) and 0.33 µL/mL LDH (Merck, L2500)) and incubated light protected at room temperature for 5 to 10 mins. TRAM buffer contains 108 mM Triethanolamine HCl (Sigma, T9534), 10.7 mM EDTA-$Na_2$ (Merck, E4884), 42 mM $MgCl_2$ (Merck, M8266) in ddH20, pH 7.5. Colour reagent contains 1.63 mM PMS (Merck, P9625), 3.95 mM INT (Merck, I8377), 35% ethanol, 2% Triton-X-100 (Merck). Optical density was measured in a plate reader at 490 nm and lactate was quantified against a lactate standard curve (Fluka Chemika, 71718) using a spline fit / LOWESS (cubic spline) in GraphPad Prism.

**Cell death assay in 3D cultured HepG2**

At day 21 the culture medium was replaced by fresh medium containing the compounds in the desired concentration. During the single exposure scenario Hoechst (final concentration 667 ng/µL) was added to the exposure medium and after 24 h the medium was replaced with DMEM/F12 containing PI (final conc. 400 nM). For the repeat exposure scenario Hoechst was added to the $4^{th}$ exposure and PI to the $5^{th}$ exposure. Upon 1 h after PI-incubation for the single exposure scenario or 24 h after the $5^{th}$ repeated exposure, the Hoechst and PI staining were monitored in 11 z-planes using respectively the 408, and 561 nm lasers. The confocal imaging was performed using a Nikon TiE2000 with perfect Focus System and XY-stage (Nikon, Amsterdam,

**Table 3: Statistical significance of concentration responses relative to all performed experiments excluding ETC inhibition specificity assay.**

Significance levels were calculated comparing treatment responses to assay's specific control using one way ANOVA followed by a Dunnett's test, *p < 0.05. Light grey = chemical not tested in particular assay, Dark grey = not enough replicates to perform statistics. The numbers correspond to the used concentrations in µM: a = 0.000128, b = 0.0064, c = 0.0032, d = 0.016, e = 0.08, f = 0.4, 7 = g and h = 10.

| Compound | Complex | Viability Glucose settings | | | | | | | | | | | | | | | | Viability Galactose settings | | | | | | | | | | | | | | | | Cell death (1x 24h) | | | | | | | | Cell death (5x 24h) | | | | | | | | MMP | | | | | | | | | | | | | | | |
|---|---|---|---|---|---|---|---|---|---|---|---|---|---|---|---|---|---|---|---|---|---|---|---|---|---|---|---|---|---|---|---|---|---|---|---|---|---|---|---|---|---|---|---|---|---|---|---|---|---|---|---|---|---|---|---|---|---|---|---|---|---|---|---|---|---|
| | | Resazurin | | | | | | | | | | | | | | | | Resazurin | | | | | | | | | | | | | | | | PI staining | | | | | | | | PI staining | | | | | | | | | | | | | | | | | | | | | | | | | |
| | | RPTEC/TERT1 | | | | | | | | HepG2 | | | | | | | | RPTEC/TERT1 | | | | | | | | HepG2 | | | | | | | | HepG2 3D | | | | | | | | HepG2 3D | | | | | | | | RPTEC/TERT1 | | | | | | | | HepG2 | | | | | | | |
| | | a | b | c | d | e | f | g | h | a | b | c | d | e | f | g | h | a | b | c | d | e | f | g | h | a | b | c | d | e | f | g | h | a | b | c | d | e | f | g | h | a | b | c | d | e | f | g | h | a | b | c | d | e | f | g | h | a | b | c | d | e | f | g | h |
| Capsaicin | CI | | | | | | | | | | | | | | | | | | | | | | | | | | | | | | | | | | | | | | | | | | | | | | | | | | | | | | | | | | | | | | | | | | |
| Deguelin | CI | | | | | | | * | * | | | | | | | * | * | | | | | | * | * | | | | | | | * | * | * | | | | | | * | * | | | | | | | * | * | | | | | | * | * | * | * | | | | | * | * | * | * |
| Fenazaquin | CI | | | | | | | * | * | | | | | | | | | | | | | | | | | | | | | | | | | | | | | | | | | | | | | | | | | | | | | | | | | | | | | | | | | | |
| Fenpyroximate | CI | | | | | | * | * | * | | | | | | | | | | | | * | * | * | | | | | | * | * | * | * | * | | | | | | * | * | * | | | | | | * | * | * | * | * | * | * | * | * | * | * | * | * | * | * | * | * | * | * | * |
| Pyridaben | CI | | | | | | * | * | * | | | | | | | | | | | | | | | | | | | | | | | | | | | | | | | | | | | | | | | | | | | | | | | | | | | | | | | | | |
| Pyrimidifen | CI | | | | | * | * | * | * | | | | | | | | | | | * | * | * | * | | | | | | * | * | * | * | * | | | | | | * | * | | | | | | | * | * | | | | | | * | * | * | * | * | * | * | * | * | * | * | * |
| Rotenone | CI | | | | | | * | * | * | | | | | | | * | * | | | * | * | * | * | | | | | | * | * | * | * | * | | | | | | * | * | * | | | | | | * | * | * | * | * | * | * | * | * | * | * | * | * | * | * | * | * | * |
| Tebufenpyrad | CI | | | * | * | * | * | * | | | | | | | | | | | | | | | | | | | | | | * | * | * | * | | | | | | | * | | | | | | | * | * | | | | | | * | * | * | * | | | | | * | * | * | * |
| Carboxine | CII | | | | | | | | | | | | | | | | | | | | | | | | | | | | | | | | | | | | | | | | | | | | | | | | | | | | | | | | | | | | | | | | | | |
| Fenfuram | CII | | | | | | | * | | | | | | | | * | * | | | | | | | | | | | | | | | | | | | | | | | | | | | | | | | | | | | | | | | | | | | | | | | | | |
| Flutolanil | CII | | | | | | | | | | | | | | | | | | | | | | | | | | | | | | | | | | | | | | | | | | | | | | | | | | | | | | | | | | | | | | | | | | * |
| Mepronil | CII | | | | | | | | | | | | | | | | | | | | | | | | | | | | | | | | | | | | | | | | | | | | | | | | | | | | | | | | | | | | | | | | | | * |
| Thifluzamide | CII | | | | | | | | | | | | | | | | | | | | | | | | | | | | | | | | | | | | | | | | | | | | | | | | | | | | | | | | | | | | | | | | | | * |
| Antimycin A | CIII | | | | | * | * | * | * | | | | | | | | | | | | * | * | * | | | | | | * | * | * | * | * | | | | | * | * | * | * | * | | | | | * | * | * | * | * | | | | | * | * | * | * | * | | | | | * | * | * | * |
| Azoxystrobin | CIII | | | | | | | * | | | | | | | | | | | | | | | | | | | | | | | | | * | | | | | | | | | | | | | | | | | | | | | | | | | | | | | | | | | | * | * |
| Cyazofamid | CIII | | | | | | | * | | | | | | | | | | | | | | | | | | | | | | | | | | | | | | | | | | | | | | | | | | | | | | | | | | | | | | | | | | | |
| Fenamidone | CIII | | | | | | | * | | | | | | | | | | | | | | | | | | | | | | | | | | | | | | | | | | | | | | | | | | | | | | | | | | | | | | | | | | | * |
| Kresoxim-methyl | CIII | | | | | | | | | | | | | | | | | | | | | | | | | | | | | | | | | | | | | | | | | | | | | | | | | | | | | | | | | | | | | | | | | |
| Picoxystrobin | CIII | | | | | | * | * | | | | | | | | | | | | | * | * | * | | | | | | | | | * | * | | | | | | | | | | | | | | | | | | | | | | | | | | | | | | | | | * | * | * |
| Pyraclostrobin | CIII | | | | | | * | * | | | | | | | | * | * | | | | | * | * | | | | | | | | | * | * | | | | | | | | | | | | | | | | | | | | | | | | | | | | | | | | | * | * | * |
| Trifloxystrobin | CIII | | | | | | | * | | | | | | | | | | | | | | | | | | | | | | | | | | | | | | | | | | | | | | | | | | | | | | | | | | | | | | | | | | | |

**Table 3: Statistical significance of concentration responses relative to all performed experiments excluding ETC inhibition specificity assay.** (continued)

| Compound | Complex | Lactate production | | | | | | | | | | | | | | | | ECAR basal | | | | | | | | | | | | | | | | OCR basal | | | | | | | | | | | | | | OCR Maximal | | | | | | | | | | | | | | |
|---|---|---|---|---|---|---|---|---|---|---|---|---|---|---|---|---|---|---|---|---|---|---|---|---|---|---|---|---|---|---|---|---|---|---|---|---|---|---|---|---|---|---|---|---|---|---|---|---|---|---|---|---|---|---|---|---|---|---|---|---|---|---|---|
| | | RPTEC/TERT1 | | | | | | | | HepG2 | | | | | | | | RPTEC/TERT1 | | | | | | | | HepG2 | | | | | | | | RPTEC/TERT1 | | | | | | | | HepG2 | | | | | | | | RPTEC/TERT1 | | | | | | | | HepG2 | | | | | | | |
| | | a | b | c | d | e | f | g | h | a | b | c | d | e | f | g | h | a | b | c | d | e | f | g | h | a | b | c | d | e | f | g | h | a | b | c | d | e | f | g | h | a | b | c | d | e | f | g | h | a | b | c | d | e | f | g | h | a | b | c | d | e | f | g | h |
| Capsaicin | CI | | | | | | | | | | | | | | | | * | | | | | | | | | | | | | | | | * | | | | | | * | | * | | | | | | | | * | | | | | | | | | | | | | | | | * |
| Deguelin | CI | | | | | | * | * | * | | | | | | * | * | * | | | | | * | * | * | | | | | | * | * | * | | | | | | * | * | * | * | | | | | | * | * | * | * | | | | | | * | * | * | * | | | | | * | * | * | * |
| Fenazaquin | CI | | | | | | * | * | * | | | | | | | * | * | | | | | * | * | | | | | | | * | * | * | | | | | | * | * | * | * | | | | | | * | * | * | * | | | | | | * | * | * | * | | | | | * | * | * | * |
| Fenpyroximate | CI | | | | * | * | * | * | | | | | | | | * | * | | | | | * | * | | | | | | | * | * | * | | | | | | * | * | * | * | | | | | | * | * | * | * | | | | | | * | * | * | * | | | | | * | * | * | * |
| Pyridaben | CI | | | | | | * | * | * | | | | | | | * | * | | | | | * | * | | | | | | | * | * | * | | | | | | * | * | * | * | | | | | | * | * | * | * | | | | | | * | * | * | * | | | | | * | * | * | * |
| Pyrimidifen | CI | | | | | | * | * | * | | | | | | | | * | | | | | * | * | * | | | | | * | * | * | * | * | | | | | * | * | * | * | * | | | | | * | * | * | * | * | | | | | * | * | * | * | * | | | * | * | * | * | * | * |
| Rotenone | CI | | | | | | * | * | * | | | | | | * | | | | | | | * | * | * | | | | | | * | * | * | * | | | | | * | * | * | * | * | | | | | * | * | * | * | * | | | | | * | * | * | * | * | | | | | * | * | * | * |
| Tebufenpyrad | CI | | | | | | | | | | | | | | * | * | * | | | | | * | * | | | | | | | * | * | * | * | | | | | * | * | * | * | * | | | | | * | * | * | * | * | | | | | * | * | * | * | * | | | * | * | * | * | * | * |
| Carboxine | CII | | | | | | | | | | | | | | | | | | | | | | | | | | | | | | | | | | | | | * | * | | * | | | | | | | | | | | | | * | * | | | | | | | | | | | | | | |
| Fenfuram | CII | | | | | | | | | | | | | | | | | | | | | | | | | * | * | * | * | | | | | | | | | | | | | | | * | | | | | | | | | | | | | | | | | | | | | | | | |
| Flutolanil | CII | | | | | | | | | | | | | | | | * | | | | | | | | | | | | | | | | | * | | | | | * | | | | | | * | * | | | | | | | | | | | | | | | | | | | | |
| Mepronil | CII | | | | | | | | | | | | | | | | | | | | | | | | | | | | | | | * | * | | | | | | | | | | * | * | * | | | | * | | | | | | | | | | | | | | | | | |
| Thifluzamide | CII | | | | | | | | * | | | | | | | | | | | | | | | | | | | * | | | | | | | | | * | | | | | | | | | | | | | | | | | | | | | | | | | | | | |
| Antimycin A | CIII | | | | * | * | * | * | | | | | | | | | * | | | | * | * | * | * | | | | | * | * | * | * | * | | | | | * | * | * | * | * | | | | | * | * | * | * | * | | | | | * | * | * | * | * | | | | | * | * | * | * |
| Azoxystrobin | CIII | | | | | | * | * | | | | | | | | | * | | | | | * | * | | | | | | | * | * | * | | | | | | * | * | * | | | | | | | | * | * | | | | | | | | | | | | | | | | * |
| Cyazofamid | CIII | | | | | | | | * | | | | | | | | | | | | | * | * | * | * | | | | | | | | | | | | | | | * | * | | | | | | | | | | | | | | | | | | | | | | | | |
| Fenamidone | CIII | | | | | | * | * | | | | | | | | | * | | | | | | | | * | | | | | | * | * | * | | | | | | | | * | * | | | | | | | | * | * | | | | | | | | | | | | | | * | * |
| Kresoxim-methyl | CIII | | | | | | * | * | | | | | | | | | | | | | | | | | * | | | | | | | | | | | | | | | | * | | | | | | | | | | | | | | | | | | | | | | | | * |
| Picoxystrobin | CIII | | | | | | * | * | | | | | | | * | * | | | | | | * | * | | | | | * | | * | * | * | | | | | | * | * | * | | * | * | * | * | * | * | * | * | | | | | | | | | | | | | | * | * |
| Pyraclostrobin | CIII | | | | | | * | * | | | | | | | * | * | | | | | | * | * | | | | | | | * | * | * | | | | | | * | * | * | | | | | | | * | * | * | | | | | | | | | | | | | | | * | * |
| Trifloxystrobin | CIII | | | | | | | * | | | | | | | | * | | | | | | | * | | * | | | | | | * | * | * | | | * | | * | * | * | * | | | | | | | | | | | | | | | | | | | | | | | | |

The Netherlands). Quantification of the Hoechst and PI signal localization was performed using Nis Elements Analysis software. First a max projection was created of all z-stacks. The overlapping areas between Hoechst and PI in the projection picture were assessed based on a manually curated intensity threshold. Finally, the fraction of spheroids positive for PI staining was determined.

**Microarray in HepG2 cells**

Transcriptomic data of a previous HepG2 study from the de Water lab was used to interrogae potenial differences in glycolysis gene expression in 3D cultured cells (Hiemstra 2019). The study compared 2D at day 3 and 3D for 3, 7, 14, 21, 28 days. The Affymetrix HT Human Genome U133 plus platform was used and the original CEL files are stored at GEO (Number: GSE128763). Here we pulled out the genes from the Panther glycolysis pathway[13]. Values are represented as fold changes of HepG2 cells cultured in matrix gel for 3, 7, 14, 21 or 28 days over HepG2 cells cultured on plastic for 3 days.

**Data normalization and Statistical analysis**

All results are average of 2 to 3 independent experiments. Each independent experiment is referred to as biological replicate and include at least two technical replicates. A first normalisation is applied by representing responses as percentage of 0.1% DMSO treated samples (control) for the following assays: resazurin reduction, lactate production, Rho123, JC-1, PI staining. For those assays a second normalization was applied setting as 100% (upper or lower asymptote for inhibition or activation curves respectively) the average of at least 2 non-effective concentrations (if applicable), to be able to calculate the BMC (Table 2) according to the benchmark concentration concept of in vitro toxicology (Krebs 2020). For assays performed in Seahorse, basal OCR/ECAR responses were normalised as percentage of measurements before treatment injection. Maximal OCR was normalised as percentage of maximal respiration of control samples (0.1% DMSO treated). ECAR was normalised by setting the lower asymptote of the response curve to 0%, corresponding to the 100% ECAR prior to compound injection (basal acidification), and the upper asymptote to 100%, corresponding to the maximal ECAR induction (oligomycin response). Variation in all performed assays was calculated and represented as standard deviation (SD). Curves were fit using the non-liner regression four parameters Hill model. BMC were calculated using the *in vitro* toxicology on-line tool provided by the group of Prof. Leist, University of Konstanz (Krebs 2020). Significance levels were calculated comparing treatment responses to assay´s specific control using one way ANOVA followed by a Dunnett's test, $*p < 0.05$ (Table3, Table 4). Data analysis was performed using Rstudio (Boston, USA) using R 3.6.0 and included the following packages dplyr (Wickham 2011), tidyr (Wickham 2016), data.table (Dowle 2016), multcomp (Hothorn 2008) and stats.

**Table 4: Statistical significance of concentration responses relative to MRC complex inhibition specificity assay.**
Significance levels were calculated comparing responses to assay controls using one way ANOVA followed by a Dunnett's test, *p < 0.05. Light grey = chemical not tested in particular assay. The numbers correspond to the used concentrations in µM: a = 0.00001, b = 0.0001, c = 0.001, d = 0.00316, e = 0.01, f = 0.316, g = 0.1, h = 0.316, i = 0.5, j = 1, k = 1.58, l = 3.16, m = 5, n = 10, o = 15.8, p = 31.6, q = 50, r = 100, s = 158 and t = 500.

| Compound | Complex | OCR basal - Permeabilised cells | | |

# Results

## Effects of various selective ETC complex inhibitors on viability and OCR

In both cell lines mitochondrial and metabolic parameters were measured upon exposure to a broad concentration range of in total 21 mitochondrial ETC CI, CII and CIII inhibitors. The capacity of cells to reduce resazurin is widely used as a viability assay, due to its ease of use and low cost (Jennings 2004, 2007). Resazurin reduction was measured in both cell types after 24 h exposure of test compounds at a range of concentrations up to 10 µM. Cell viability decreased in a concentration dependent manner upon exposure to 15 out of 21 complex inhibitors in the RPTEC/TERT1 cell line, whereas only rotenone mildly affected the viability of HepG2 cells (Figure 2). The CII inhibitors and capsaicin did not affect resazurin reduction up to 10 µM in a 24 h exposure.

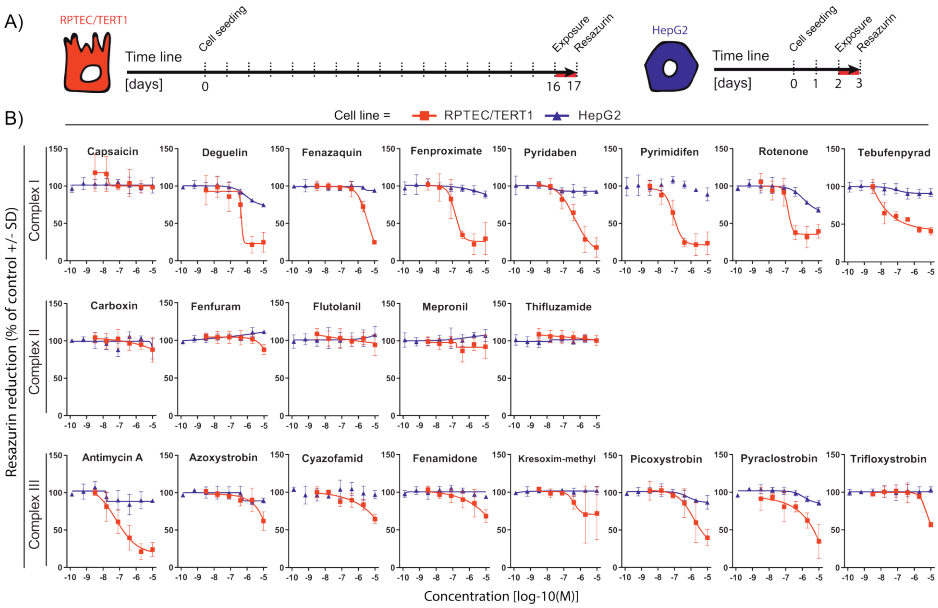


**Figure 2: Effect of compound exposure on cellular viability as measured by resazurin reduction.**
**A)** Schematic representation of the experimental setup in RPTEC/TERT1 and HepG2 cells, the red line represents the exposure time. **B)** Concentration response curves of resazurin reduction in RPTEC/TERT1 and HepG2 cells exposed for 24 h to a range of concentrations (1.28E-10, 6.40E-10, 3.20E-9, 1.60E-8, 8.00E-8, 4.00E-7, 2.00E-6, 1.00E-5 M) of complex I, complex II and complex III inhibitors of the ETC. RPTEC/TERT1 (red) and HepG2 (blue). Values are represented as percentage of vehicle controls (0.1% DMSO) and further normalized to the average of at least two non-effective concentrations (if applicable) set as 100%. Measurements are average of at least three independent experiments ± SD. Connecting lines are non-linear fits (Y=Bottom + (Top-Bottom)/(1+10^((LogIC50-X)*HillSlope))).

Mitochondrial oxygen consumption rate (OCR) was quantified in intact RPTEC/TERT1 and HepG2 cells using the Seahorse XFe96 Bioanalyzer (Agilent). OCR was quantified for 30 minutes immediately after test compound injection to estimate the effect of

compound on basal respiration. After 30 mins, oligomycin was injected to estimate mitochondrial ATP production. Thereafter FCCP was injected to provide maximal mitochondrial respiration. Finally, rotenone and antimycin A were injected to assess non-mitochondrial respiration (Figure 3). Comparison of untreated cells revealed a 2.2 fold higher maximal respiration rates in RPTEC/TERT1 cells compared to HepG2 cells (RPTEC/TERT1 337.4% basal OCR ± 72.9, HepG2 159.4% basal OCR ± 26.8) (Figure 3 B).

CI inhibitors, except for capsaicin, induced a concentration dependent decrease in basal and maximal OCR in both cell lines (Figure 3 D and E). The effects were comparable in both cell types with pyrimidifen being the most potent of the entire CI class. None of the CII inhibitors exhibited an effect in basal OCR. However, some of the compounds including thifluzamide showed a tendency to increase maximal respiration at higher concentrations in RPTEC/TERT1 cells (Figure 3 D and E). CIII inhibitors exhibited a dose dependent decrease in basal and maximal OCR, in both cell types with the exception of cyazofamid (Figure 3 D and E). Antimycin A was the most potent of the CIII class. Cyazofamid demonstrated a strong uncoupling effect, with a more pronounced effect in RPTEC/TERT1 cells (Figure 3 D). Note the Y axis in Figure 3 D is extended to 300% due to this effect, where all other graphs have a scale from 0 to 180%. The Seahorse mitostress OCR plots for cyazofamid are provided in Figure 3 F, which more clearly show the uncoupling effect at 2 and 10 μM in both cell types.



**Mitochondrial ETC complex inhibition specificity**

To confirm the specificity of the various ETC inhibitors and to rule out confounding pharmacokinetic effects such as lack of transport or metabolism, Seahorse measurements were conducted in permeabilised HepG2 cells with sequential addition of paired ETC complex substrates and inhibitors (Figure 4). All CI inhibitors including capsaicin (50 μM and above) exhibited the expected CI specificity pattern i.e. inhibition of OCR after injection and recovery with succinate. All CII inhibitors exhibited CII specificity pattern i.e. no (or less potent) OCR inhibition after direct injection but OCR inhibition after succinate/rotenone injection. However, only carboxin and thifluzamide exhibited activity at or below 10 μM. CIII inhibition is determined by OCR inhibition after compound injection, no recovery with succinate, but recovery with ascorbate/TMPD. Antimycin A, kresoxim-methyl, picoxystrobin, pyraclostrobin and trifloxystrobin conformed to this pattern, while azoxystrobin and fenamidone were only partially rescued with ascorbate/TMPD. Cyazofamid exhibited a CII inhibition pattern but only at 100 μM.

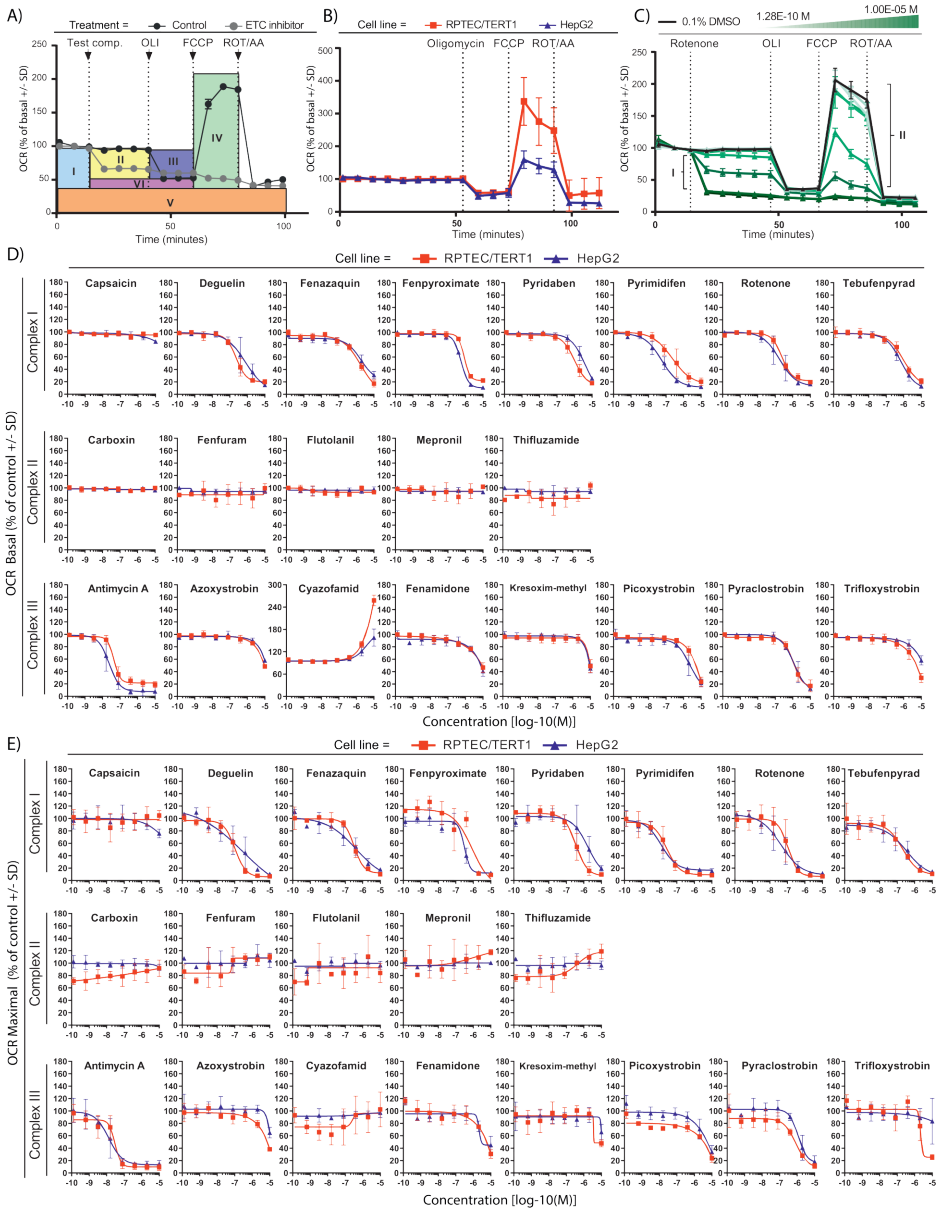
A)
Treatment =
Control
ETC inhibitor
Test comp.
OLI
FCCP
ROT/AA
OCR (% of basal +/- SD)
Time (minutes)
B)
Cell line =
RPTEC/TERT1
HepG2
Oligomycin
FCCP
ROT/AA
OCR (% of basal +/- SD)
Time (minutes)
C)
0.1% DMSO
1.28E-10 M
1.00E-05 M
Rotenone
OLI
FCCP
ROT/AA
OCR (% of basal +/- SD)
Time (minutes)
D)
Cell line =
RPTEC/TERT1
HepG2
OCR Basal (% of control +/- SD)
Complex I
Capsaicin
Deguelin
Fenazaquin
Fenpyroximate
Pyridaben
Pyrimidifen
Rotenone
Tebufenpyrad
Complex II
Carboxin
Fenfuram
Flutolanil
Mepronil
Thifluzamide
Complex III
Antimycin A
Azoxystrobin
Cyazofamid
Fenamidone
Kresoxim-methyl
Picoxystrobin
Pyraclostrobin
Trifloxystrobin
Concentration [log-10(M)]
E)
Cell line =
RPTEC/TERT1
HepG2
OCR Maximal (% of control +/- SD)
Complex I
Capsaicin
Deguelin
Fenazaquin
Fenpyroximate
Pyridaben
Pyrimidifen
Rotenone
Tebufenpyrad
Complex II
Carboxin
Fenfuram
Flutolanil
Mepronil
Thifluzamide
Complex III
Antimycin A
Azoxystrobin
Cyazofamid
Fenamidone
Kresoxim-methyl
Picoxystrobin
Pyraclostrobin
Trifloxystrobin
Concentration [log-10(M)]

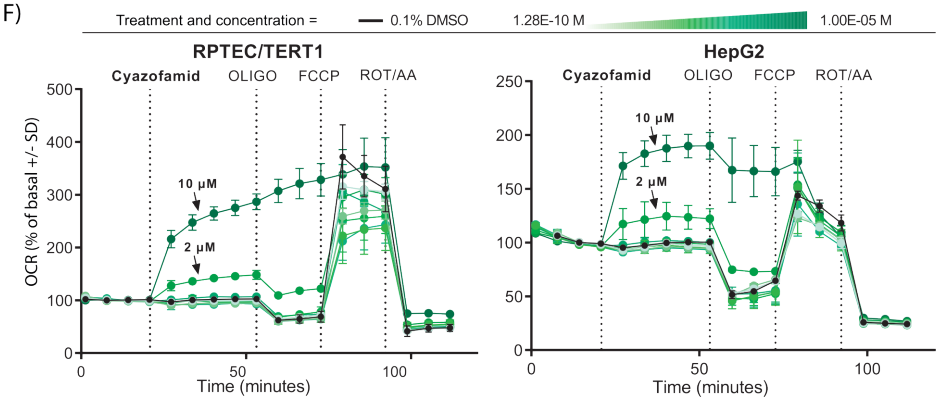


**Figure 3: Oxygen consumption rates in untreated and treated RPTEC/TERT1 and HepG2 cells.**
Effect on key parameters of mitochondrial function measured as changes in OCR with the Seahorse analyser upon 30 min exposure to range of concentrations (1.28E-10, 6.40E-10, 3.20E-9, 1.60E-8, 8.00E-8, 4.00E-7, 2.00E-6, 1.00E-5 M) of complex I, complex II and complex III inhibitors of the ETC in RPTEC/TERT1 and HepG2 cells . **A)** Overview of measurable parameters after subsequent injections of test compound and modulators of the oxidative phosphorylation of the mitostress assay in HepG2 cells. Respiration is first measured at the basal level of test system (I). Decrease in OCR upon test compound injection, indicate inhibition of the mitochondrial respiration (II). Changes in OCR upon oligomycin addition, indicate the portion of oxygen employed in ATP production (III). OCR increases after the protonophore addition indicates the maximal ability of the cell to increase mitochondrial respiration (IV). Addition of antimycin A and rotenone allows for identification of non-mitochondrial respiration (V). The difference between oligomycin and rotenone/antimycin response indicates the remaining basal respiration not coupled with ATP production to be attributed to proton leakage (VI). Arrows indicate time of injections. **B)** OCR changes after mitostress test conducted in 0.1% DMSO control samples in RPTEC/TERT1 and HepG2. Data are represented as mean of at least seven independent experiments, expressed as percentage of basal respiration ± SD. **C)** Representative response upon exposure to rotenone (1.28E-10, 6.40E-10, 3.20E-9, 1.60E-8, 8.00E-8, 4.00E-7, 2.00E-6, 1.00E-5 M) in HepG2 cells showing a dose dependent effect in basal (I) and maximal (II) respiration rates. **D-E)** Plots of concentration responses in terms of oxygen consumption rates extrapolated from the mitostress test of panel compounds. Data represents the mean of two independent experiments ± SD. All measurements were normalized for basal respiration prior to compound injection, slopes are generated by plotting dose responses of the direct oxygen consumption inhibition (OCR basal, D) and inhibition of the uncoupler stimulated respiration (OCR maximal respiration, E), the latter further represented as percentage of untreated controls samples. **F)** Response of the mitostress assay after treatment with different concentrations of cyazofamid (1.28E-10, 6.40E-10, 3.20E-9, 1.60E-8, 8.00E-8, 4.00E-7, 2.00E-6, 1.00E-5 M). The two highest concentrations indicate the uncoupling effect of the compound in the two cell systems.

3

## Monitoring mitochondrial membrane potential (MMP)

Live cell imaging was used to measure MMP in HepG2 utilising Rho123, whereas JC-1 dimer/monomer ratio measured with a plate reader was used to assess changes in MMP in RPTEC/TERT1 cells. For reasons we did not elucidate Rho123 was unresponsive in RPTEC/TERT1 cells and hence the JC-1 dye was used. A decrease in Rho123 intensity is representative for reduced MMP, while JC-1 red/green ratio shifts to the green with decreasing MMP (Figure 5 A). MMP decreased in a concentration dependent manner in both cell types with CI inhibitors, except for capsaicin (Figure 5 B). CII inhibitors did not decrease MMP in RPTEC/TERT1 cells; flutolanil and mepronil actually increased it. In HepG2 cells, flutolanil, mepronil and thifluzamide decreased MMP, but only at the highest concentrations. Exposure to all CIII inhibitors, except for kresoxim-methyl and trifloxystrobin, led to decreased MMP in both cell systems.

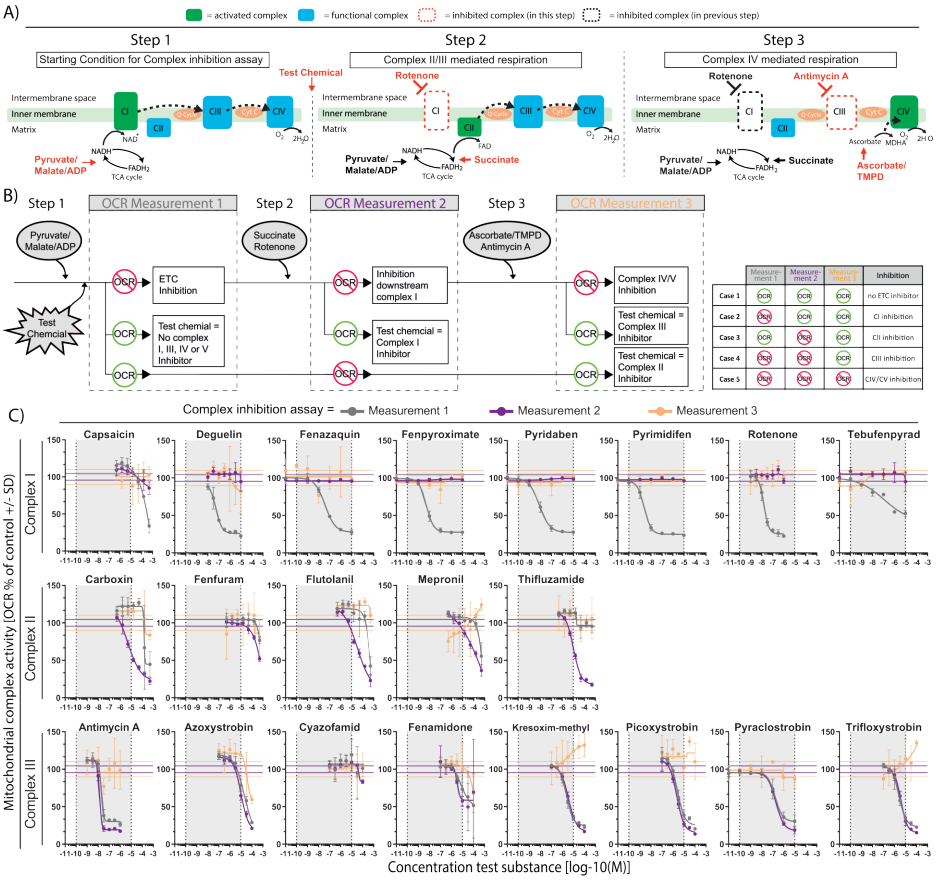


**Figure 4: Identification of ETC target using the mitochondrial complex assay.**

**A)** Schematic representation of the ETC complex inhibition assay. The complex inhibition assay consists of a sequential injection (in the same well) of substrates and/or inhibitors to determine specific complex inhibition. Initially cells are treated with permeabilizing agent and CI substrates (pyruvate/malate/ADP) (**Step 1**). Cells are subsequently injected with test chemical, followed by a second injection with CII substrate (succinate) and CI inhibitor (rotenone) simultaneously (**Step 2**), and finally a complex IV substrate (ascorbate/TMPD) and CIII inhibitor (antimycin A) is added (**Step 3**), followed by ORC measurement. **B)** Schematic representation of expected OCR responses upon test compound and sequential assay substrates and/or inhibitors addition. Following test chemical injection, OCR is measured (**measurement 1, grey line**). Decreased OCR indicates an inhibition of the ETC (unknown complex), no effect on OCR indicates either inhibition of CII, case 3 (established in the next assay measurements) or no ETC inhibition (case 1). Addition of rotenone and succinate at step 2, blocks CI and drives CII respectively. OCR is measured after step 2 (**measurement 2, purple line**). A rescue in decreased OCR indicates the test compound as CI inhibitor (case 2), a continuation in the drop of OCR indicates the site of inhibition is downstream of CI and a decrease in OCR where not observed previously indicates CII inhibition (case 3). Addition of antimycin A and ascorbate/TMPD at step 3, blocks CIII and drives CIV respectively. OCR is measured after step 3 (**measurement 3, orange line**). A rescue in decreased OCR indicates the test compound as CIII inhibitor (case 4) or confirms the test compound as CII inhibitor (case 3), a continuation in the drop of OCR indicates CIV or CV as the site of inhibition (case 5). **C)** Plots of dose responses in OCR for panel compounds in HepG2 cells. OCR is expressed as percentage of baseline response prior to compound exposure, data is mean of 3 independent experiments ± SD. A drop in measurement 1 OCR (grey line) alone indicates inhibition of complex I, drop in measurement 2 OCR (purple line) alone indicates CII inhibition and drop in measurement 1 and measurement 2 together indicates CIII inhibition. A drop in measurement 3 OCR (orange line) indicates CIV or CV inhibition and/or off target effects.

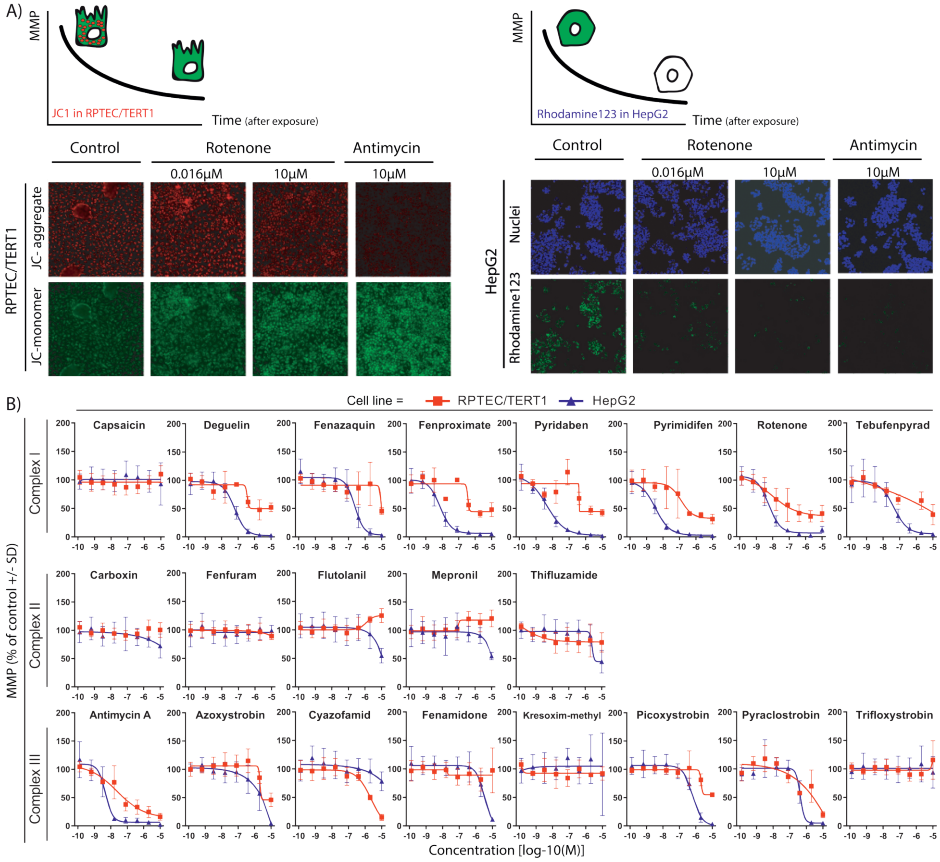


**Figure 5: Effect of compound exposure on mitochondrial membrane potential.**
Effect on mitochondrial membrane polarization by assessment of changes in mitochondrial membrane potential upon 24 h exposure to range of concentrations (1.28E-10, 6.40E-10, 3.20E-9, 1.60E-8, 8.00E-8, 4.00E-7, 2.00E-6, 1.00E-5 M) of complex I, complex II and complex III inhibitors of the ETC in RPTEC/TERT1 and HepG2 cells. A) Schematic representation of mitochondrial membrane depolarization using JC-1 and Rho123 in RPTEC/TERT1 and HepG2 respectively and representative images of changes in mitochondrial membrane polarization in RPTEC/TERT (JC-1) and HepG2 (Rho123) upon exposure to vehicle control, rotenone and antimycin A. B) Concentration response curves of panel compounds in RPTEC/TERT1 (red) and HepG2 (blue). The Rho123 intensity and the intensity ratio for JC-1 were presented as percentage of 0.1% DMSO exposure. The data was further normalized to the average of at least two non-effective concentrations (if applicable). Measurements are expressed as average of at least three independent experiments ± SD.

## Increased glycolysis by inhibitors of CI and CIII.

Exposure to CI and CIII inhibitors for 24 hours resulted in an increase in supernatant lactate in both cell types, with the exception of capsaicin and kresoxim-methyl. No effect was observed when exposing cells to CII inhibitors at tested concentrations (Figure 6 A). Overall RPTEC/TERT1 cells showed a more pronounced increased glycolysis compared to HepG2 cells. Utilising the Seahorse measurement of ECAR, after direct injection of compounds, a rapid increase in response to CI and CIII inhibitors was observed, with no increase in ECAR for CII inhibitors (Figure 6 B-D). Similar ECAR responses were observed in both cell systems, although cyazofamid was

much more potent in RPTEC/TERT1 cells. Both cell types showed a robust increase in ECAR in response to oligomycin, however only RPTEC/TERT1 further increased ECAR in response to FCCP (Figure 6 C).

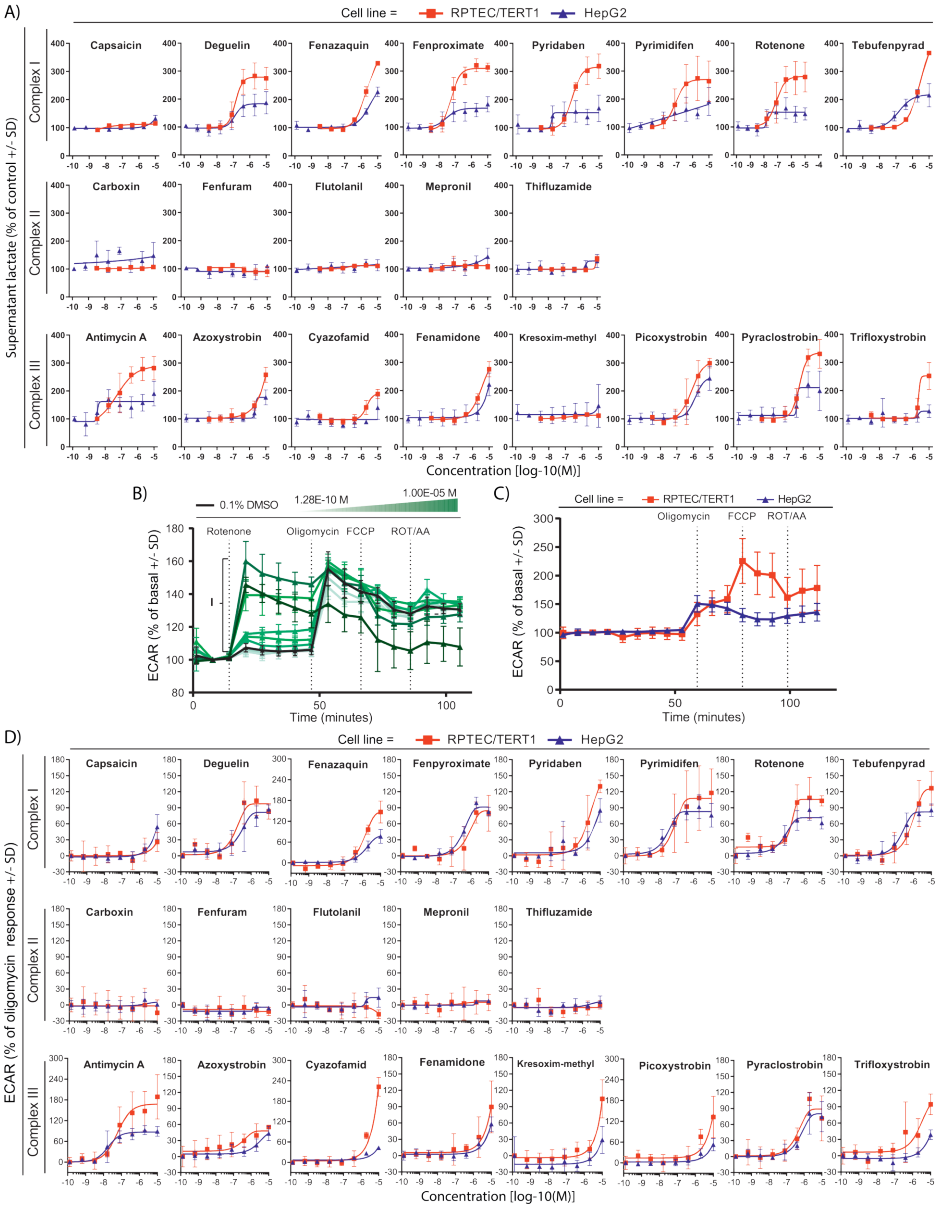

**Figure 6: Effect of compound exposure on extracellular lactate and extracellular acidification rates**. Glycolytic switch upon decreased mitochondrial respiration was indirectly assessed by measurements of supernatant lactate and the extracellular medium acidification after 24 h exposure to range of concentrations (1.28E-10, 6.40E-10, 3.20E-9, 1.60E-8, 8.00E-8, 4.00E-7, 2.00E-6, 1.00E-5 M) of complex I, complex II and complex III inhibitors of the ETC in RPTEC/TERT1 and HepG2 cells. **A)** Levels of lactate in the supernatant medium. Data are represented as percentage of 0.1% DMSO controls and re-normalized to the average of at least two non-effective concentrations (if applicable) set as 100%. **B)** Representative response to the testing concentration range of rotenone in HepG2 cells showing a dose dependent increase of medium acidification (I) reflecting the glycolytic turnover increase. **C)** Changes in ECAR after mitostress test conducted in 0.1% DMSO control samples in RPTEC/TERT1 and HepG2. Data are represented as mean of at least seven independent experiments, expressed as percentage of basal acidification ± SD. **D)** Plots of concentration responses of changes in ECAR after panel compounds injection. Data is mean of two independent experiments ± SD. Measurements are expressed as percentage of basal acidification and further normalized by setting the lower asymptote of the response curve to 0%, corresponding to the 100% ECAR prior to compound injection (basal acidification), and the upper asymptote to 100%, corresponding to the maximal ECAR induction (oligomycin response).

### Glu/Gal switch sensitises towards ETC inhibition induced toxicity in HepG2 cells but not RPTEC/TERT1 cells.

We evaluated the effect of glucose removal on the sensitivity of RPTEC/TERT1 and HepG2 cells to a restricted compound panel of CI and CIII inhibitors (Figure 7). Cells were switched from glucose to galactose containing medium one day before chemical exposure (Figure 7). Cell viability was measured after 24 h exposure to a subset of compounds. Replacing glucose with galactose had no clear effect on the viability to chemical exposure in RPTEC/TERT1 cells (Figure 7). In contrast, galactose conditions strongly sensitised HepG2 cells to the OCR active compounds, underlining the dependency of HepG2 cells on glycolysis under mitotoxicant induced stress conditions and making this system more comparable to the RPTEC/TERT1 cells (Figure 7).



### Effect of 3D spheroid culture and repeated exposures in HepG2 cells

There is evidence to suggest that HepG2 cells cultured in 3D spheroids results in decreased proliferation and reduced reliance on glucose (Hiemstra 2019). Thus we investigated if HepG2 3D spheroids had an increased sensitivity to the ETC inhibitors. We compared the effect of 24 h exposure to a range of concentrations of a set of CI, CII and CIII inhibitors in HepG2 monolayer and HepG2 spheroids (Figure 8 D). The combination of the cellular nuclear staining (Hoechst) and the cell death staining (PI), showed a substantial increase in cell death in HepG2 spheroids treated samples (Figure 8 D, blue curve) when compared to HepG2 monolayer treated cells (Figure 8 D, orange curve). This effect was more prominent in most of the CI inhibitors treated samples and antimycin A. In contrast, only visible for the highest concentration of pyraclostrobin in the remaining CIII inhibitors treated samples. Capsaicin and CII inhibition did not show increased sensitivity in spheroids compared to the 2D model.

Since 3D HepG2 can also be utilised over longer exposure periods, we investigated the effect of a 5 day repeated 24 h exposure (5 x 24 h) compared to the 24 h bolus exposure (1 x 24 h). The 5 X 24 h exposure, increased sensitivity to rotenone (EC50 127 nM 1x 24 h, 28 nM 5x 24 h) and antimycin A (EC50 >10 µM 1x 2 4h , 74 nM 5x 24 h ) (Figure 8 D, Table 2).

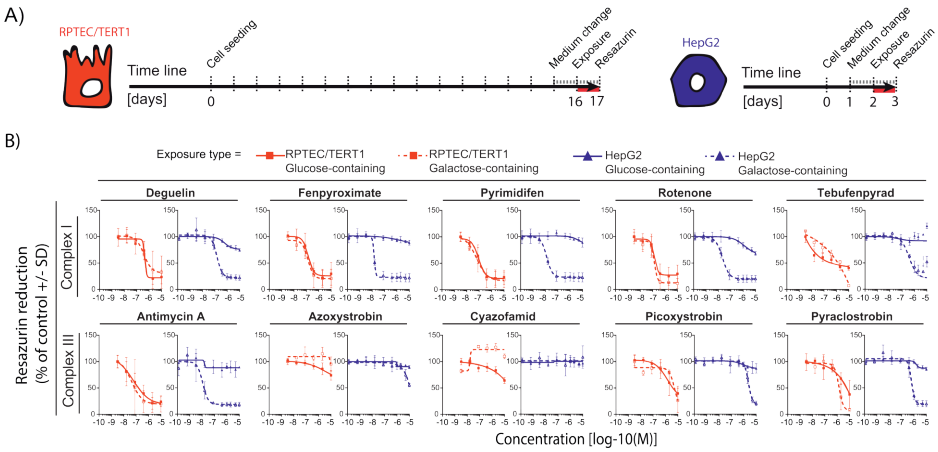


**Figure 7: Effect of medium glucose on compound induced alterations in cell viability**.
The effects of medium switch (glucose to galactose) in terms of cell viability was assessed in RPTEC/TERT1 and in HepG2 after 24h exposure to a range of concentrations (1.28E-10, 6.40E-10, 3.20E-9, 1.60E-8, 8.00E-8, 4.00E-7, 2.00E-6, 1.00E-5 M) of complex I, complex II and complex III inhibitors of the ETC. **A)** Schematic representation of the carbon source switch from glucose to galactose-containing medium in RPTEC/TERT1 (5 mM Glu/Gal) and HepG2 (25 mM Glu/Gal) respectively, the red line represents the exposure time. **B)** Plots of concentration responses in resazurin reduction. Measurements are expressed as percentage of vehicle controls (0.1% DMSO) and further normalized to the average of at least two non-effective concentrations (if applicable) set as 100%. Values are mean of two to four independent experiments ± SD. Connecting lines are non-linear fits (Y=Bottom + (Top-Bottom)/(1+10^((LogIC50-X)*HillSlope))).

## Correlation plots

In order to give an overview of the data and to explore the relationship between OCR/ECAR and the viability, lactate and MMP assays, correlation plots of all the data were generated (Figure 9). Matched data for 24 h resazurin reduction, 24 h MMP, 24 h supernatant lactate concentration and 30 min ECAR are plotted vs basal 30 min OCR data (Figure 9). In addition, 24 h lactate production is plotted vs 30 min basal ECAR (Figure 9). In RPTEC/TERT1 cells, acute basal OCR correlated with: 24 h viability, as measured by resazurin reduction (Figure 9 A and B) (glucose conditions $r^2 = 0.7723$, galactose conditions $r^2 = 0.8081$), with 24 h MMP, as measured by JC-1 ratio (Figure 9 C) ($r^2 = 0.6495$), with acute ECAR (Figure 9 D) (negative correlation, $r^2 = 0.8369$) and with 24 h supernatant lactate (Figure 9 E) (negative correlation, $r^2 = 0.8083$). Supernatant 24 h lactate correlated with acute ECAR (Figure 9 F) ($r^2 = 0.7339$). In HepG2 cells there was a poor correlation of acute basal OCR with 24 h viability under glucose conditions (Figure 9 A) ($r^2 = 0.4047$). However, this improved under galactose conditions (Figure 9 B) ($r^2 = 0.8217$). Acute basal OCR correlated: with MMP, as measured by Rho-123 (Figure 9 C) ($r^2 = 0.6661$), with acute basal ECAR (Figure 9 D) (negative correlation, $r^2 = 0.8867$) and with 24 h supernatant lactate (Figure 9 D) (negative correlation, $r^2 = 0.6395$). Supernatant lactate correlated with acute ECAR (Figure 9 C) ($r^2 = 0.649$), although the distribution range is smaller than in RPTEC/TERT1 cells.

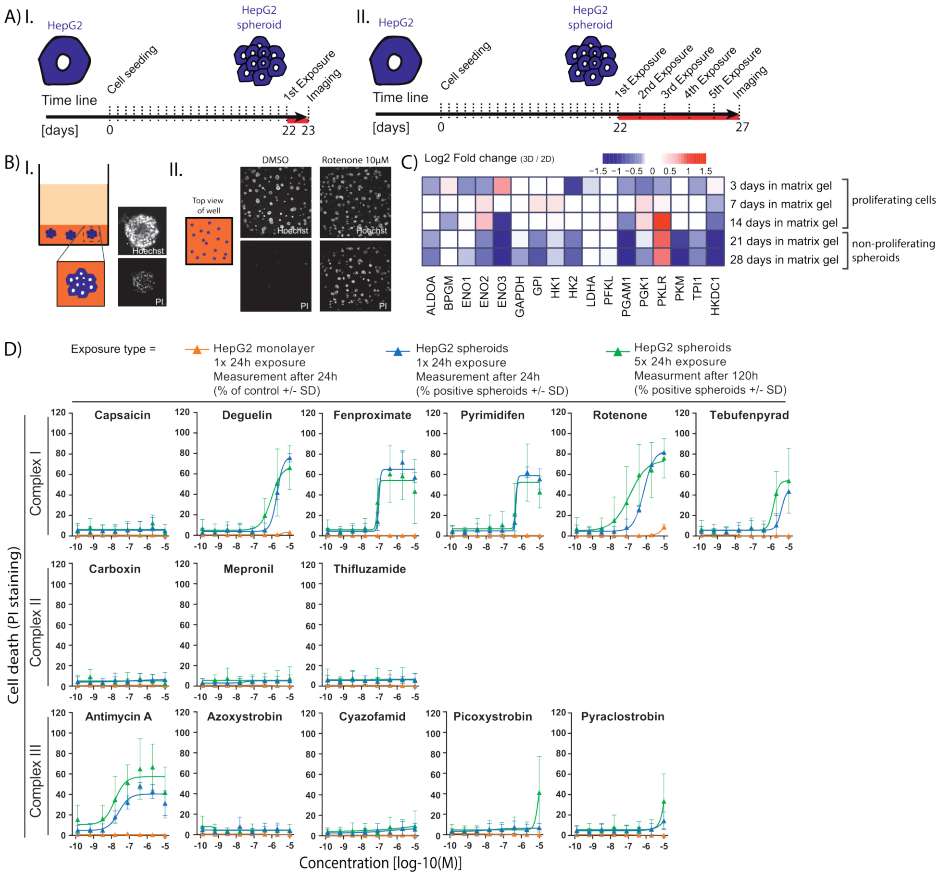


**Figure 8: Comparison of compound induced toxicity in 2D cultured HepG2 and 3D HepG2 spheroids.**
**A)** Schematic representation of cell culture/differentiation protocol and time of endpoint measurements in HepG2 spheroids treated with two exposure regimes; I = 1x 24 h exposure, measured after 24 h and II = 5x 24 h exposure, measured after 120 h. **B)** (I) Schematic representation of HepG2 spheroids in a 384 well, with a representative picture of a single spheroid stained with nuclear marker (Hoechst) and cell death marker (PI). (II) Representative images of a 384 well with spheroids cultured in glucose-containing medium followed by exposure to 10 µM rotenone or DMSO (24 h) and stained with nuclear marker and cell death marker. **C)** Heatmap of changes in glycolytic enzyme genes during HepG2 spheroids maturation, in medium containing glucose, showing the evolution toward a less glycolytic state. Log2 fold changes represent the expression of untreated HepG2 cells cultured in matrix gel (3D) at day 3, 7, 14 (proliferating cells) and 21, 28 (non-proliferating spheroids) over untreated HepG2 cells cultured on plastic (2D) for 3 days. **D)** Difference in the cytotoxicity responses upon treatment with a range of concentrations (1.28E-10, 6.40E-10, 3.20E-9, 1.60E-8, 8.00E-8, 4.00E-7, 2.00E-6, 1.00E-5 M) of CI, CII and CIII inhibitors of the ETC in HepG2 monolayer (2D) and HepG2 spheroids with a one time 24 h exposure or in 3D spheroids with a consecutive 5X 24 h exposure. All conditions are in glucose containing medium. Cell death endpoint was assessed with PI staining at the end of treatments. Values are expressed as percentage of PI positive cells/spheroids ± SD and are mean of two or three independent experiments.

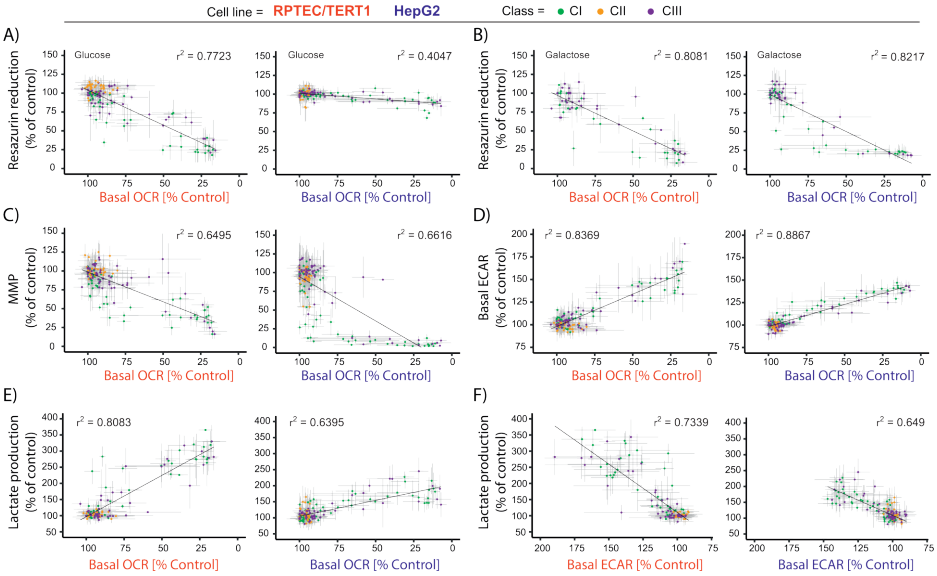


**Figure 9: Assay correlation plots.**
Graphs A to E show the correlation of the highly sensitive 30 min OCR Seahorse measurement with the other assays for all conditions. Each graph relates the OCR response, per compound and per concentration, to the one obtained with the correlating assay with the same treatment condition. Data include the mean of all replicates ± SD, slope´s $r^2$ values are provided. Classes are distinguished by colour, CI inhibitors (green), CII inhibitors (orange) and CIII inhibitors (purple). **A)** Basal 30 min OCR vs 24 h resazurin in glucose settings. **B)** Basal 30 min OCR vs 24 h resazurin in galactose settings. **C)** Basal 30 min OCR vs 24 h MMP. **D)** Basal 30 min OCR vs basal 30 min ECAR. **E)** Basal 30 min OCR vs 24 h supernatant lactate. **F)** This graph has the same metrics as the other graphs but shows the correlation of 30 min Seahorse ECAR measurement with 24 h supernatant lactate measurement. Note the X-axis is reversed for clarity.

## Discussion

We have assessed a panel of proposed ETC inhibitors in two human cell lines, with several assays and in various different modes to provide a basis for the establishment of a comprehensive workflow for assessing the impact of chemicals on mitochondrial function and the cellular consequences thereof.

Given the central role of mitochondria in energy metabolism, tissue health and ageing, there is increasing concern regarding the long-term effect that xenobiotics may have on mitochondrial function. Mitochondrial perturbations are likely to increase sensitivity to xenobiotics, decrease cellular repair mechanisms and contribute to both chronic disease states and accelerated ageing (Will 2019). The most direct method to assess mitochondrial activity is by measuring oxygen consumption rates (OCR). Situations that impair mitochondrial function, can lead to a decrease in cell viability, but usually there is first an increase in glycolytic rates. Altered glycolytic status can be quantified by assessing extracellular acidification rates (ECAR), or biochemically by measuring supernatant lactate (Limonciel 2011). The Seahorse bioanalyser coupled with the mitostress assay is becoming an industry standard for the quantification of OCR and ECAR (Divakaruni 2014; Eakins 2016, Tilmant 2018). Other methods to assess mitochondrial function include live cell

dyes, which under optimised conditions can be related to MMP or comparing toxicity in the presence and absence of glucose as an energy source.

Respiration rates were similarly affected in both RPTEC/TERT1 and HepG2 cells exposed for 30 minutes to the 21 compounds. In sharp contrast, the effect of ETC inhibition on cell viability after 24 h exposure was cell type and test system dependent. Differentiated RPTEC/TERT1 cell viability correlated with OCR inhibition independently of the presence of glucose. HepG2 cell viability correlated with OCR inhibition only in the absence of glucose. Interestingly, culturing HepG2 as 3D spheroids sensitised the cells to OCR inhibition in the presence of glucose. Previous studies have demonstrated that 3D spheroid culture of HepG2 cells, decreases proliferation, increases differentiation and increases sensitivity to various compounds with human drug-induced liver injury liability (Ramaiahgari 2014, Hiemstra 2019). Taken together the data suggest that proliferating cells are less reliant on oxidative phosphorylation as an energy source where glucose is not limiting and that 3D HepG2 cells switch towards an oxidative phosphorylation-mediated energy source.



With the exception of capsaicin, all of the CI inhibitors acutely reduced OCR and enhanced ECAR. In the mitochondrial complex assay, decreased OCR could be rescued with the addition of succinate confirming CI as the site of inhibition for these compounds. Pyrimidifen, deguelin and rotenone were the most potent CI compounds with IC50s in the nanomolar range. Capsaicin was also confirmed as a CI inhibitor, albeit with lower potency (LOEL 50 µM and IC50 approx. 260 µM).

CII inhibitors did not alter cell viability, basal OCR, ECAR or lactate production in living, non-permeabilised cells at concentrations up to 10 µM. However, in the permeabilised assay all compounds were confirmed as CII specific, albeit at concentrations, close to or above, the maximum concentration tested in intact cells. This difference can be attributed to the fact that CII activity is less critical for electron transfer and ATP production than CI and CIII and is neither required for CI to CIII electron transfer nor does it participate in proton pumping. CII gives a minor contribution to the Q-cycle compared to CI and therefore its inhibition can be totally (thifluzamide) or partially (carboxin, fenfuram, flutolanil and mepronil) masked from CI activity, depending on the strength of the CII inhibition. Indeed, it has been demonstrated that CII activity is more important for ATP generation where energy demand is high (Pfleger 2015) or when CI substrates are limiting (Salabei 2014). However, since CII is directly coupled to the Kreb's cycle, it would be expected that CII inhibition would eventually negatively impact OCR due to NADH and $FADH_2$ depletion, affecting CI and CII activity, respectively. Also, under our experimental settings pyruvate was present, which may be enough to supply the Krebs cycle until the succinate oxidation step, thus limiting

depletion of NADH. Flutolanil and mepronil do appear to slightly increase MMP in RPTEC/TERT1 cells, although this was not significant (Table 3). There was also a non-significant tendency of CII compounds to increase maximal OCR in RPTEC/TERT1 cells (Table 3). These effects are possibly a compensatory mechanism of CII inhibition leading to inner mitochondrial hyperpolarisation. However, further investigations would need to be conducted to address this possible mechanism specifically.

The mitochondrial complex assay confirmed CIII as the site of inhibition of 5 of the 8 compounds previously classified as CIII inhibitors. Contrary to how the system senses the electron flow from CII, CIII inhibition results in the total block of the Q-cycle as it receives electrons from both CI and CII; therefore concomitant inhibition of CI and succinate addition does not further decrease OCR when CIII inhibitors are applied. Azoxystrobin and fenamidone were only partially rescued by ascorbate/TMPD, which may indicate off target activity at CIV/CV or some other non-specific activity. Antimycin A was the most potent CIII inhibitor, with IC50s for most parameters in the nanomolar range. Since CIII receives electrons from both CI and CII, complete CIII inhibition would be expected to have a major impact, as it is the case for antimycin A. It appears we did not achieve full CIII inhibition for azoxystrobin, fenamidone, trifloxystrobin or kresoxim-methyl as OCR inhibition did not reach 100%. Surprisingly, cyazofamid did not inhibit OCR, on the contrary, it was the only test compound that demonstrated potent uncoupling effects, evidenced by an increase in basal OCR in the mitostress assay. Thus under our assay settings cyazofamid is a potent mitochondrial uncoupler and is therefore unlikely to be a classical CIII inhibitor as previously described (Li 2014). While cyazofamid is small and lipophilic, it does not conform to the primary characteristic of classical protonophoretic compounds such as FCCP and PCP, which are weak acids. This feature is necessary to facilitate the transfer a hydrogen from the inner membrane space to the mitochondrial matrix (Benz 1983). Thus, the protonophoretic effect of cyazofamid is potentially atypical and requires further attention to identify whether CIII is involved.

Risk assessment is intrinsically linked to exposure duration and frequency of the exposure. To assess the effects of repeated exposures to ETC inhibitors including possible sensitisation towards cellular toxicity, we exposed 3D HepG2 spheroids for 5 consecutive days to 24 hours administration to a selection of 14 of the ETC inhibitors and compared the results to a onetime 24 h exposure. Repeated exposure increased the toxic sensitivity for rotenone, tebufenpyrad, antimycin A, picoxystrobin and pyraclostrobin, but not to the other compounds tested. However, the increased sensitivity was minimal and does not fully justify the extra effort involved. This may be explained by the fact this set of compounds are very fast acting (within 5 mins) and are thus are unlikely to have accumulative effects of ETC inhibition upon sequential

exposures. Also, it is possible that unless there is a major inhibition of the ETC, compensatory mechanisms such as increased glucose utilisation can cover the energy deficit. We caution that this should not be assumed for other chemicals, in particular when mitochondrial toxicity is caused through indirect mechanisms, such as inhibition of mitochondrial DNA replication (Dykens 2007, Nadanaciva 2007).

A major current emphasis in transitioning mode of action toxicology to risk assessment regimes is the focus on adverse outcome pathways including identification of molecular initiating events (MIE) and key events (KE) leading to a particular pathology (Leist 2007). The current data supports a generic AOP framework for mitochondrial ETC inhibition, where CI and CIII inhibition directly leads to a decrease mitochondrial respiration. This leads almost immediately to an increase in glycolysis, which can accomplish energetic needs in cells less reliant on oxidative phosphorylation and where glucose is not limiting. Thus, CI or CIII inhibition is the MIE and decreased OCR is the initial KE and increased ECAR and/or increased supernatant lactate is the second KE. Decreases in MMP might be indicative of OCR inhibition although the correlation with OCR were not very strong. The Seahorse bioanalyser is an ideal method for the proposed AOP as it can simultaneously measure both KEs in real time. However, this becomes more cumbersome at longer exposures or repeated exposures, where supernatant lactate and cellular viability could be used to fill data gaps.



In summary, the study demonstrates the utility of two commonly used cell lines, together with OCR, ECAR, MMP, supernatant lactate and viability to establish critical values to assess chemical-induced ETC inhibition. HepG2 cells gave similar patterns with respect to OCR inhibition as differentiated RPTEC/TERT1, however glucose-free conditions or 3D spheroid culture were required to cause ETC inhibition-induced cytotoxicity in HepG2 cells. For studies investigating mitochondrial effects of compounds, we highly recommend the use of cell types and/or experimental conditions that favour oxidative metabolism over glycolysis. This is of particular importance when little is known about the test compound and more complicated mitochondrial perturbations than direct ETC inhibition are possible. Overall, the study presents a comprehensive example of a mitochondrial assessment workflow and establishes measurable key events of CI and CIII ETC inhibition.

**Acknowledgements**

This project was funded by the EU-ToxRisk project, grant agreement No 681002, funded by the European Union's Horizon 2020 research and innovation programme. We would like to thank all our EUToxRisk colleagues for their fruitful discussions and inputs. We especially want to thank Thomas Cole at the JRC for procuring and distributing the all 21 ETC inhibitors.

# 4

# Mapping the cellular response to electron transport chain inhibitors reveals selective signaling networks triggered by mitochondrial perturbation

Wanda van der Stel, Huan Yang, Nanette Vrijenhoek, Johannes P. Schimming, Giulia Callegaro, Giada Carta, Salihanur Darici, Johannes Delp, Anna Forsby, Andrew White, Sylvia le Dévédec, Marcel Leist, Paul Jennings, Joost Beltman, Bob van de Water#, Erik H.J. Danen#

*Archives of Toxicology, 2021, doi: 10.1007/s00204-021-03160-7*

**Mitochondrial perturbation is a key event in chemical-induced organ toxicities that is incompletely understood. Here, we studied how electron transport chain (ETC) complex I, II, or III (CI, CII and CIII) inhibitors affect mitochondrial functionality, stress response activation, and cell viability using a combination of high content imaging and TempO-Seq in HepG2 hepatocyte cells. CI and CIII inhibitors perturbed mitochondrial membrane potential (MMP) and mitochondrial and cellular ATP levels in a concentration- and time-dependent fashion and, under conditions preventing a switch to glycolysis attenuated cell viability, whereas CII inhibitors had no effect. TempO-Seq analysis of changes in mRNA expression pointed to a shared cellular response to CI and CIII inhibition. First, to define specific ETC inhibition responses, a gene set responsive towards ETC inhibition (and not to genotoxic, oxidative, or endoplasmic reticulum stress) was identified using targeted TempO-Seq in HepG2. Silencing of one of these genes, NOS3, exacerbated the impact of CI and CIII inhibitors on cell viability, indicating its functional implication in cellular responses to mitochondrial stress. Then by monitoring dynamic responses to ETC inhibition using a HepG2 GFP reporter panel for different classes of stress response pathways and applying pathway and gene network analysis to TempO-Seq data, we looked for downstream cellular events of ETC inhibition and identified the amino acid response (AAR) as being triggered in HepG2 by ETC inhibition. Through *in silico* approaches we provide evidence indicating that a similar AAR is associated with exposure to mitochondrial toxicants in primary human hepatocytes. Altogether, we i) unravel quantitative, time- and concentration resolved cellular responses to mitochondrial perturbation, ii) identify a gene set associated with adaptation to exposure to active ETC inhibitors, and iii) show that ER stress and an AAR accompany ETC inhibition in HepG2 and primary hepatocytes.**

**Keywords**: mitochondrial toxicity, ETC complex inhibitors, high content imaging, TempO-Seq, DILI

## Introduction

Accumulating evidence indicates that perturbation of mitochondria plays a role in the development of organ toxicity [Will 2014, Dykens 2007a, Dykens 2007b]. Disturbance of mitochondria upon chemical exposure has been monitored in the past based on changes in major functions of the mitochondria, including mitochondrial respiration and mitochondrial membrane potential (MMP) in both intact cells and isolated mitochondria [Porceddu 2012, Rana 2019, Zhang 2009]. The assay outcomes are predictive for occurrence and potency of the interaction between chemical and target. Nevertheless, assessment of the mitochondrial status alone does not cover all toxicity-associated abnormalities sufficiently. Unraveling the interaction between mitochondrial perturbation and cellular responses can shed light on the eventual chemical-induced adversity at organ level.



Mitochondria are the organelles responsible for energy metabolism through oxidative phosphorylation (OXPHOS), hormone synthesis and metabolism. Bidirectional signaling between mitochondria and the nucleus enables rapid feedback concerning the metabolic and energetic needs of both compartments [Han 2013, Monaghan 2015, Chandel 2014, Barbour 2014, Da Cunha 2015]. During oxidative phosphorylation, electrons flow through an electron transport chain (ETC) involving a series of enzyme complexes located in the mitochondrial double layered membrane, and ultimately, release the energy stored in fats and carbohydrates to produce ATP. This process relies on a MMP (i.e., a proton gradient leading to concentration and charge imbalance across the mitochondrial membrane), which is generated by proton pumps including ETC complexes I, III and IV (CI, CIII and CIV). Complex II (CII) represents an alternative entry point into the ETC in addition to CI but is itself not a proton-pump. CIV transfers the electrons to oxygen (and pumps protons), and complex V (CV) is the enzyme that uses the energy that can be extracted from the MMP to convert ADP into ATP [Alberts 2017].

Chemicals can perturb mitochondrial functioning via direct interaction with mitochondrial targets, or indirect via deprivation of building blocks and nutrients [Heiden 2009]. In general, cells possess an arsenal of adaptive stress response mechanisms to cope with toxic insults that give rise to among others reactive oxygen species [Sies 2017], cytoplasmic unfolded proteins [Ron 2017], and DNA damage [Giglia-Mari 2011]. In addition, cells have mitochondrial damage specific responses including upregulation of mitochondrial biogenesis [Jornayvaz 2010, Hock 2009], induction of mitochondrial-specific unfolded protein response (UPR) [Münch 2018, Qureshi 2017], adaptation of mitochondrial fission and fusion [Westermann 2010, Youle 2012], and removal of damaged mitochondria by mitophagy [Youle 2011, Hamacher-Brady 2016]. The outcome

of chemical-induced mitochondrial perturbation depends on the ability of cells to adapt and switch to alternative energy production via glycolysis [Merry 2016]. In the case that the cell cannot recover from the mitochondrial insult, apoptosis and/or necrosis will be induced to eliminate the damaged cells [Bock 2019]. Large numbers of apoptotic or necrotic cells will result in tissue damage and ultimately organ failure as seen for instance in drug-induced liver injury (DILI) [Pessayre 2012].

Combining the assessment of mitochondrial functionality with markers for a variety of cellular endpoints will generate information feeding into a mechanistic assessment of mitochondrial-related organ toxicity [van der Stel 2020]. Especially, time- and concentration-resolved exposure data can link the various involved processes, providing in depth mechanistic understanding and distinguish lethal from adaptive cellular responses to chemical exposures.

In this study, we systematically assessed the changes in mitochondrial and cellular signaling upon exposure to a panel of ETC inhibitors using HepG2 cells. We unravel quantitative, time- and concentration resolved mitochondrial and cellular responses to ETC inhibition providing mechanistic insight in mitochondrial toxicity. Using TempO-Seq, we first studied ETC inhibition specific responses and identify a gene set that is induced selectively upon exposure to ETC CI and CIII inhibitors, which could be used to flag compounds for mitochondria-related toxicity. Assessment of downstream cellular events of ETC inhibition using a HepG2 GFP reporter panel for different classes of stress response pathways and applying pathway and gene network analysis to TempO-Seq data we identify the amino acid response (AAR) as triggered in HepG2 by ETC inhibition. Through in silico approaches we provide evidence indicating that a similar AAR is associated with exposure to mitochondrial toxicants in primary hepatocytes (PHHs).

## Materials and Methods

### Chemicals

All tested chemicals were purchased via the European Union Reference Laboratory for alternatives to animal testing (Joint Research Centre, Ispra, Italy) and stored as stock solutions between 10-100 mM in dimethyl sulfoxide (DMSO) at -80°C until use. Treatment solutions were created in appropriate medium (DMSO 0.1% (v/v)) on the day of exposure. The selected chemicals included complex I inhibitors capsaicin (Cat. No. M2028), deguelin (D0817), fenazaquin (31635), fenpyroximate (31684), pyridaben (46047), pyrimidifen (35999), rotenone (R8875), tebufenpyrad (46438); complex II inhibitors carboxin (45371), fenfuram (45486), flutolanil (N12004), mepronil (33361), thifluzamide (49792) and complex III inhibitors antimycin A (A8674), azoxystrobin (3167),

cyazofamid (33874), fenamidone (33965), kresoxim-methyl (37899), picoxystrobin (33568), pyraclostrobin (33696), trifloxystrobin (46477). The included stress model compounds were CDDO-me (Cayman chemical; 11883), cisplatin (Ebewe pharma; 95199306), TNFα (R&D System-BioTechne; 210-TA-100) and tunicamycin (Merck; T7765). Seahorse experiments in HepG2 and RPTEC cells for these compounds have been previously published [van der Stel 2020].

**Cell culture**

HepG2 cells (ATCC; American Type Culture Collection, Wesel, Germany) were cultured in Dulbecco's modified Eagle's medium (DMEM) (Fisher Scientific, 11504496), supplemented with 10% (v/v) fetal bovine serum, 25 U/ml penicillin and 25 µg/mL streptomycin (FBS; South American, Fisher Scientific, S181L-500 & PenStrep, Fisher Scientific, 15070-063). Maintenance conditions were 37˚C in a 5% CO2 humidified atmosphere.



For experiments under conditions preventing glycolysis, medium was either replaced 1 day before the chemical exposures by glucose-free DMEM (Fisher Scientific, 11966-025) supplemented with 10 mM galactose (Sigma, G5388-100G) and 1 mM sodium pyruvate (Sigma, P2256-100g), or was enriched by medium containing 10 mM 2-deoxyglucose (Sigma-Aldrich, D8375-5G) at the moment of exposure.

**Generation of ATP-biosensor cells**

ATP dynamics was monitored using HepG2 cells expressing ATP-biosensors located in the mitochondria (Ateam1.03) or cytoplasm (mitAT1.03). For this, cDNA constructs were provided by Hiromi Imamura (Precursory Research for Embryonic Science, Japan Science and Technology Agency) [Imamura 2009] (Suppl. table 1). Constructs were introduced into HepG2 cells using lipofectamine2000 (INT) (Fisher Scientific, 11668-027). 8 µg DNA was combined with 10 µL of lipofectamine2000 in 500 µL serum free medium (SFM) to transfect 2*10^6 cells in a 6 cm dish. Cells were placed on G418 selection (PAA/Brunschwig chemie, P31-011) at 0.25 mg/ml and upon reaching confluency transferred to 10 cm dishes. Cells were kept on further selection at 0.5 mg/ml until colonies started to form. Colonies were picked, expanded and frozen to create a batch for usages (Suppl. Fig. 1A, B and C). Cells stably expressing H2B-RFP and either a CFP or a YFP construct were kindly provided by Dr. Y. Zhang, LACDR, Leiden University, NL and used to adjust imaging settings (Suppl. Fig. 1D). Localization of the FRET probes to their respective subcellular compartment (cytoplasm or mitochondria) was validated by microscopy.

**Confocal live cell imaging**

*Mitochondrial membrane potential*: MMP was assessed using Rhodamine123 (Rho123, Sigma Aldrich, R8004) by live confocal imaging. HepG2 cells were seeded in 384-wells µCLEAR® black plate (Greiner Bio-One, 781 091) at a density of 10,000 cells/well. Two days after seeding, cells were stained with 200 ng/µL Hoechst 33342 (Life technologies, H1399) and 1 µM Rho123. After 60-75 min incubation at 37° C the medium was refreshed into complete DMEM containing 0.2 µM Rho123, 100 nM propidium iodide (PI) (Sigma-Aldrich, P4170) and the desired concentration of the test chemicals. The signal intensity of Hoechst, Rho123 and PI (excitation wavelength respectively 408, 488 and 561 nm) were monitored hourly for 24 h. Note: the 24h time point MMP data, but not the full time-kinetics, have been previously published [van der Stel 2020]. Kinetic MMP data also serve as input for the development of a dynamic mathematical model; Yang et al, manuscript submitted.

*GFP-BAC reporters*: Cellular stress response activation was evaluated using HepG2 BAC-GFP reporter cell lines (ATF4-GFP, BIP-GFP, CHOP-GFP, P21-GFP, SRXN1-GFP and XBP1-GFP) [Wink 2017]. Cells were plated in 384-wells µCLEAR® black plate at a density of 10,000 cells/well. One day after seeding, cells were O/N stained with Hoechst 33342 and the medium was subsequently refreshed into complete DMEM containing the desired concentration of the test chemical. The signal intensity of Hoechst and GFP (408 and 488 nm) were monitored at 24, 48 and 72 h.

*Confocal live cell imaging of ATP-biosensor*: Cells stably transfected with cytoplasmic or mitochondrial ATP-biosensors were seeded in 96-wells µCLEAR® black (Greiner Bio-One, 655090) at a density of 20,000 cells/well. Two days post-seeding the cells were exposed to a concentration range of the test chemicals. The exposures were performed using DMEM without phenol red to improve signal-to-noise ratio (DMEM (Thermos Fisher, 12196590), supplemented with 10% (v/v) FBS, 25 U/mL penicillin, 25mg/mL streptomycin, 1 mM sodium pyruvate (Fisher Scientific, 11360070) and 4 mM L-glutamine (Fisher Scientific, 25030081). The signal intensity was monitored live every 5 minutes starting with untreated condition and followed by 2 h exposure with the desired test chemical. The ATP-biosensors were excited at 408 nm and the FRET-ratio was determined based on the emission at 408 and 488 nm.

All imaging was performed using a 20x objective on a Nikon TiE2000 with perfect Focus System, automated-stage, and controlled temp/$CO_2$ incubator (Nikon, Amsterdam, The Netherlands).

**Image analysis for MMP and BAC-reporter data**

Object identification and signal quantification were performed using CellProfiler version 2.1.1 [Kamentsky 2011]. A segmentation module [Di 2012] was used to segment nuclei objects based on the Hoechst signal. The cytoplasmic area was defined as the area around the nucleus to a maximal distance of 10 pixels (12.3 μM) or half the distance to the border of a neighbouring cell's nucleus. The signal intensity of Rho123, BIP-GFP, SRXN1-GFP and XBP1-GFP was quantified as the integrated pixel intensity in the cytoplasmic area. The signal intensity of ATF4-GFP, CHOP-GFP and P21-GFP was quantified as the integrated pixel intensity in the nuclear area. Nuclei were considered PI positive when the overlap of the nucleus with a PI object is larger than 10% of the nucleus area. All CellProfiler results were stored in HDF5 files and subsequently the data was extracted for further processing and visualisation using in house developed R scripts (run in Rstudio (Boston, USA) [Rstudio Team 2016]) and the following packages: rhdf5, data.table, plyr, dplyr, tydr, ggplot2, reshape2, stringr , shiny, ggvis, gridExtra and doParallel [Dowle 2019; Wickham 2007, 2011, 2016, 2019, 2020; Wickham et al 2021; Chang 2020, 2021; Auguie 2017; Microsoft corporation 2020].



**Image analysis for ATP-biosensor data**

The intensity quantification of the 408 and 488 nm emission images was performed using Ilastik version 1.1.9 [Berg 2019, Sommer 2011] and CellProfiler version 2.1.1. Background and foreground labels were based on manual curation of representative images of the 488 nm images and used for the creation of binary images of all conditions using Ilastik (Suppl. fig. 1E). The 408 and 488 nm intensity was monitored using CellProfiler in the region defined by the binary mask created with Ilastik. All CellProfiler results were saved as excel file and further processed in R.

**ATPlite assay and analysis**

ATP levels were assessed in whole cell lysates or in mitochondria after 2 h and 24 h exposures to chemicals. HepG2 cells were seeded in 96-wells μCLEAR® black plate at a density of 20,000 cells/well. The cells were stained with Hoechst33342 for 60 min, followed by exposure. 1 h before the end of the exposure period the complete well was imaged with a 10x objective and 7x6 montage using epifluorescence on a Nikon TiE2000 microscope with perfect focus system and xy-stage. After elapse of the exposure period, ATPlite 1-step Luminescence Assay reagent (PerkinElmer, 6016731) was added (1:1), followed by 2 min shaking and subsequent luminescence assessment using a FluoStar Optima plate reader (BMG Labtech). The epi-fluorescent pictures were used to normalize the data to the number of cells for each condition. Nuclear counting was performed using an in-house created macro for ImagePro software version 7.01 (Media Cybernetics). The macro performed watershed-based intensity

segmentation after background correction (flatten function and edgefilter). The segmented objects were filtered for size and shape using the following parameters: Edgefilter = 3, RemoveNarrowObjects = TRUE, Min-area = 15 pixels, Max-area = 4000 pixels, Intensity threshold = 1000 and Mean-Intensity = 0.1.

**ATP levels in mitochondria**

Mitochondrial specific ATP was assessed after permeabilizing the cell membranes [Zoeteweij 1994] (supplementary figure 2F). After the desired exposure period Hanks' buffer (Thermo Fisher 14175053) was supplemented with 5 mM HEPES, 250 mM sucrose (Thermo fisher s8600/63), 25 mM TRIS, 3 mM EGTA (Sigma Aldrich 4378), 5 mM $MgCl_2$ (Sigma Aldrich 8266), 5 mM succinate (Sigma Aldrich S2378) and 5 mM glutamate (Sigma Aldrich G5889) (37 °C, pH 7.3). 150 µM digitonin (Sigma Aldrich D5628) was added to permeabilize the cell membranes. After 30-45 sec exposure the buffer was replaced by PBS and the ATPlite 1step Luminescence Assay was performed as described above. The membrane permeabilization protocol was validated using confocal imaging. For this, cells were co-stained with Hoechst and 0.5 µM Rho123 and/or 0.05 µM Calcein-AM (VWR, 734-1434), to assess mitochondrial integrity (digitonin exposure should not affect the Rho123 intensity; Suppl. Fig. 1F and G) and loss of cell membrane integrity (digitonin exposure should result in the loss of Calcein-AM signal; Suppl. Fig. 1F, H and I). The Hoechst (408 nm) and Rho123/Calcein-AM (488 nm) signal intensity was monitored live every 10 sec just before and after addition of digitonin using a 20x objective on a Nikon TiE2000 with perfect focus system, automated-stage, and controlled temp/$CO_2$ incubator (Nikon, Amsterdam, The Netherlands).

**Transcriptomics**

HepG2 cells were plated into 96 wells plates (Costar, 3599) at a density of 50,000 cells/well. One day post-seeding medium was refreshed with complete DMEM containing the test chemicals. Plates were sealed with a gas permeable seal (IST, IST-124-080SS). After 24 h exposure, the wells were washed once with ice cold PBS (Sigma, D8537-500ml), lysed using TempO-Seq lysis buffer (Bioclavis) for 15 min at RT, and subsequently stored at -80 ˚C until shipment to BioClavis for TempO-Seq analysis [Yeakley 2017, Limonciel 2018]. TempO-Seq was performed using a panel of probes targeting the "S1500++" gene list established by the EU-ToxRisk consortium (https://www.eu-toxrisk.eu), which covers the S1500+ sentinel gene list from the U.S. Tox21 Federal collaboration [Mav 2018] and 587 additional probes including genes known to be affected in response to toxic insults and tissue relevant markers (Suppl. Table 2).

Expression data were returned by BioClavis as counts per probe per treatment. An in-house R script was developed to perform count normalization and determine differential

gene expression. The script includes the following steps: 1) load data and metadata, 2) determine library size (total number of reads per sample) and remove samples with a library size below 100.000 reads, 3) use the DESeq2 function to normalize counts (per probe calculate a ratio = *raw counts/geometric mean of that probe*, after which the median of the raw counts of each probe is divided by the median of all probe ratios for a treatment, and calculate differentially expressed genes (DEGs) considering cell line, treatment, concentration and time point), 4) create matrix of all comparisons between vehicle control and any of the other treatments. The analysis utilized the following packages gridExtra, stringr, ggplot2, pheatmap, reshape2, RColorBrewer, plyr, dplyr, tidyr, colorspace, scales, data.table, DESeq2, compare, readxl, PoiClaClu, hexbin, ggalt, vsn, org.GS.eg.db, annotationDbi [Kolde 2019; Neuwirth 2014; Zeileis 2020; Wickham 2019,2020; Wickham 2020; Love 2014; Murell 2015; Witten 2019; Carr 2021; Rudis 2017; Huber 2002; Carlson 2019; Pagès 2020].



**BMD express analysis: Williams trend test and BMD calculations**

Input for the BMD express software (version 2.3) [Phillips 2019] was the log2 of the normalized data. A Williams trend test was used to determine concentration responses (10,000 permutations; no filters). The output of the Williams trend test included a p-value per probe per treatment. Subsequently bench mark dose (BMD) [Haber 2018] values were determined based on the best model fit (lowest akaike information criterion (AIC)). The following parametric models were used to derive dose response curves: Power, linear, polynomial (2 parametric), Hill, and exponential (2 to 5 parametric) (maximum iterations = 250; confidence = 0.095; BMR factor = 1SD). The output of the BMD model fitting provided a "best model fit" per probe per treatment.

**Pathway analysis**

Gene ontology (GO)-term enrichment analysis was performed using the GOrilla website [Eden 2009]. For the analysis, the background file consisted of Ensembl IDs of all unique genes in the EU-ToxRisk panel and the significant set consisted of genes with p-adjusted <0.05; log2FC threshold of <-0.58 or >0.58; Williams trend test p-value <0.05.

**Transcription factor (TF) enrichment analysis**

A TF enrichment analysis was performed using the DoRothEA tool version 2 [Garcia-Alonso 2018]. The log2 normalized values were used as input for the analysis. For genes with multiple probes, an average fold change was calculated over all probes of the gene and used to determine z-scores (compared to DMSO). The Viper package was used to determine the TF enrichment including information with confidence set ABC [Alvarez 2016]. The Viper output consisted of a normalized enrichment score (NES) per transcription factor per treatment.

**Microarray data of HisOH in HepG2**

Microarray results of HepG2 cell exposed to 5mM HisOH for 4h were used to assess possible similarities in the induction of signaling pathways between HisOH and ETC inhibitors [Shan 2010]. The Affymetrix Human Genome U133 Plus 2.0 Array was used, and count files were stored at GEO (Number: GSE19495). We obtained log2FC and p-adjusted values using the GEO2R analysis provided by GEO. Values are log2FC of treated HepG2 versus medium control.

**TG-GATES data: Gene expression analysis**

Primary human hepatocyte (PHH) gene expression data was obtained from the open TG-GATES database: "Toxicogenomics Project and Toxicogenomics Informatics Project under CC Attribution-Share Alike 2.1 Japan" and processed as reported previously [Callegaro 2021]. Briefly, microarrays were jointly normalized using the Robust Multi-array Average (RMA) method (affy R package) [Gautier 2004] and probes were mapped to gene IDs with BrainArray chip description file (CDF) version 20[14]. Differential gene expression analysis was performed by building a linear model fit and computing the log-odds of differential expression by empirical Bayes moderation (limma R package) [Ritchie 2015].

**Real time PCR**

HepG2 cells were seeded into 24 wells plates (Costar) at a density of 200,000 cells/well. Two days post-seeding, medium was changed to complete DMEM containing the desired test chemical. After 24 h exposure the wells were washed with PBS and RNA was isolated using the NucleoSpin RNA kit (Marcherey-Nagel, 740955.25) according to manufacturer's protocol. cDNA was synthesized from 800 ng RNA per reaction using the RevertAid H Minus First Strand cDNA synthesis kit (Thermo Scientific, K1632). Real time PCR was performed using SYBR Green (Applied Biosystems, A25742) and KiCqstart SYBR green primers (Sigma) (Suppl. Table 3) using the QuantStudio 6 Flex Real-Time PCR System (ThermoFisher Scientific).

**RNA interference**

Transient knockdown of desired genes was achieved through reverse transfection with siGENOME Smartpool siRNAs (50 nM, from Dharmacon GE Healthcare). siRNAs were incubated with 0.3% INTERFERin transfection reagent (Westburg/PolyPlus, 409-50) for 20 min. Subsequently cells were seeded on top at a density of 23,000 cells per well (in a 96 wells µCLEAR® black plate). Medium was refreshed after 24h. All follow up assays were performed 72 h after transfection.

**Resazurin reduction assay**

The cell viability assessment using the resazurin reduction read out was performed as previously described [Jennings 2007, van der Stel 2020]. Briefly, after chemical exposure the medium from the cell culture was replaced with medium containing 44 µM resazurin. The conversion of resazurin to fluorescent resorufin was monitored after 1.5 to 2 h incubation at 37°C degrees in 5% $CO_2$ humidified atmosphere in a plate reader at excitation/emission 540/590 nm.



**Phenomenological modeling**

The phenomenological model for the MMP ($\Psi(t)$) data encompasses the following equation:

$$\Psi\,(t) = a\,exp\left(\frac{-t}{\tau}\right) + (1-a)\,.$$

Here, $a$ denotes the maximal reduction of the MMP. The MMP starts at a value of $\Psi(0) = 1$, and when $t \rightarrow \infty$, the MMP approaches $1-a$. We consider parameter $a$ to be chemical and concentration specific. The parameter τ denotes the MMP decay time constant, i.e., for large τ values the MMP drops slowly to the minimum (1- $a$ ). We consider τ to be only chemical specific, so its value is shared among the different concentrations.

We fitted the phenomenological model to the MMP data for each compound using the weighted least square approach, where τ and $a$ are free parameters to be tuned to minimize the cost function as a weighted sum of squared of difference between data and model predictions. To obtain a global optimum, we utilized 1000 sets of starting values for the parameters, which were sampled randomly as positive numbers. The resulting estimated $a$ values for all compounds were utilized during hierarchical clustering with the ward criterion [Ward 1963]. Moreover, we studied the relation between the sum of the $a$ values for all concentrations of a compound and corresponding logP value for that compound. The logP values were obtained from the PubChem database using the python package pubchempy[15].

### Statistical analysis

The R package DESeq2 was used to calculate the fold change compared to vehicle control per condition. The fold change values are represented with the standard error. P-adjusted values per condition were also calculated using DESeq2 based on the Wald test and Benjamini Hochberg correction. The significance threshold for the gene expression data was set at p-adjusted < 0.05.

A generalized linear model (glm) was used to compare the different variables (average abs log2F for yes/no *in vivo* mitochondrial toxicant + concentration (numeric) + time(numeric)) in the TG-GATES PHH dataset (package stats [R core team 2018]).

## Results

### Mitochondrial complex inhibitors differentially affect the MMP

To assess the effects of the various ETC inhibitors on the MMP dynamics, HepG2 cells were stained with Rho123 to monitor the MMP over a period of 24 h. The MMP decreased in a concentration and time dependent manner upon exposure to the CI inhibitor rotenone (Fig. 1A and B). A concentration range of various mitochondrial CI, CII and CIII inhibitors was evaluated for their effect on the MMP (Fig. 1C). Most complex I and III inhibitors, except for the weak CI-inhibitor capsaicin [Delp 2019, van der Stel 2020], decreased the MMP in a concentration and time dependent manner. CII inhibitors, CIII-inhibitors kresoxim-methyl and trifloxystrobin and the CIII-inhibitor/uncoupler cyazofamid [van der Stel 2020] only weakly affected the MMP at the highest concentration. Various highly potent CI inhibitors decreased the MMP already within the first 2 h of exposure.

To assess whether MMP dynamics were differentially perturbed by CI or CIII inhibitors, a phenomenological model was built and fitted to the data to capture compound and concentration dependent features of MMP decay (Fig. 1D and Suppl. Fig. 2). In this way, we estimated the maximal reduction of the MMP (*a*) that depended on the chemical and its concentration. Hierarchical clustering using the estimated maximal reduction per compound and concentration resulted in two major clusters: potent inhibitors vs chemicals with low potency/no effect (Fig. 1E). Based on the maximal reduction it was not possible to distinguish CI inhibitors from CIII inhibitors. However, per group of inhibitors, the maximal MMP reduction clearly depended on the lipophilicity (logP) of the inhibitors, i.e., the drop in the MMP is highest for compounds with high logP values (Fig. 1F). In general, the MMP drop of CI inhibitors depended more strongly on the logP value than CII and CIII inhibitors (Fig. 1G). In summary, our measurements on MMP dynamics suggest that CI and CIII inhibitors are more potent than CII inhibitors, and that this is in part correlated with the high lipophilicity of specific compounds.

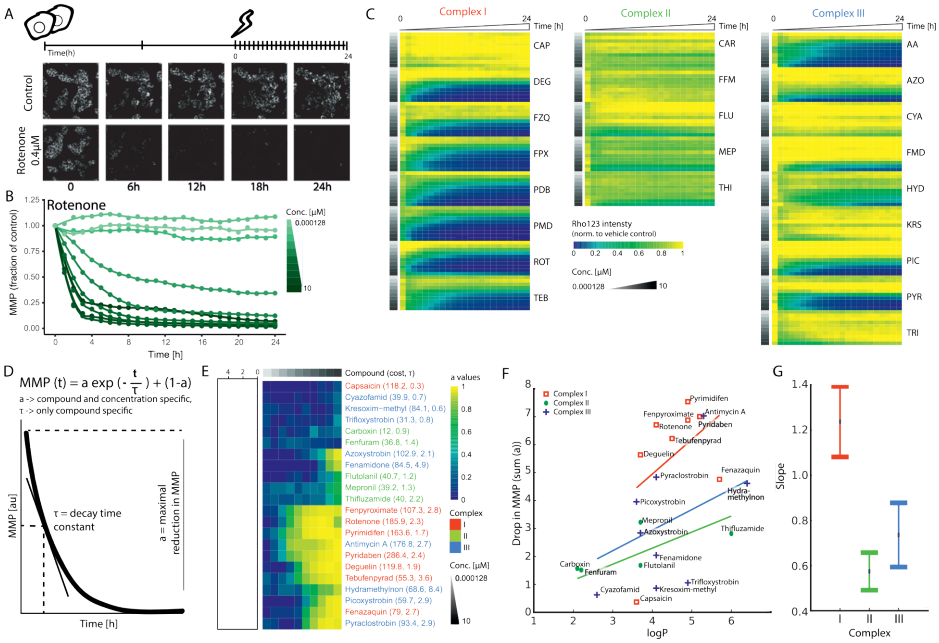


**Figure 1: Effect of various agrochemical mitochondrial respiratory chain inhibitors on mitochondrial membrane potential dynamics**

**A)** Schematic representation of the experimental set-up in HepG2 cells. Cells were seeded 2 days before exposure. At day 3 cells were stained with Hoechst33348 (nuclei) and Rho123 (MMP) followed by chemical exposure. Upon exposure cells were monitored every hour for 24h. Image panels demonstrate representative snapshots at 5 time points (0, 6, 12, 18 and 24 h) of Rho123 staining in vehicle control samples and upon exposure to 0.4 µM rotenone. **B)** Quantification of 1 replicate showing Rho123 intensity over time upon exposure to a concentration range of rotenone as fraction of the vehicle control. **C)** Heatmap including the Rho123 intensity over time upon exposure to a concentration range of 22 chemicals divided over CI (CAP= capsaicin, DEG = deguelin, FZQ = fenazaquin, FPX = fenpyroximate, PDB = pyridaben, PMD = pyrimidifen, ROT = rotenone, TEB = tebufenpyrad), CII (CAR = carboxin, FFM = fenfuram, FLU = flutolanil, MEP = mepronil, THI = thifluzamide) and CIII (AA = antimycin A, AZO = azoxystrobin, CYA = cyazofamid, FMD = fenamidone, HYD = hydra-methylnon, KRS = kresoxim-methyl, PIC = picoxystrobin, PYR = pyraclostrobin, TRI = trifloxystrobin) inhibitors. The values represent the geometric mean of 4 biological replicates, which is expressed as fraction of the measurements for the control condition. **D)** Phenomenological model describing MMP dynamics measured using Rho123. The equation describes exponential decay towards a minimal MMP, with $\tau$ representing a chemical specific MMP decay time constant and $a$ representing the maximal reduction of the MMP which is chemical and concentration dependent. **E)** Clustering heatmap generated with the Wald algorithm showing the estimated ***a*** value per compound and per concentration for in total 22 complex inhibitors plus the cost and $\tau$ value per compound. **F)** Correlation plot comparing the logP value with the sum of all determined *a* values per inhibitor. The logP values were collected from Pubchem. The correlation line is an ordinary-linear-least square regression between logP and the sum of all *a* values of an inhibitor ($r^2$-values: I = 0.899, II = 0.923 and III = 0.770). The Python package used for the regression line is statsmodels [Seabold 2010]. **G)** Estimated regression line slopes (±standard error) for the data from F. Colored names (C, E), symbols (F) and error bars (G) denote (CI (red), CII (green) or CIII (blue) inhibitors).

## Inhibition of glycolysis causes loss of viability in presence of complex I and III but not complex II inhibitors

Like primary liver tissue, HepG2 cells can increase their anaerobic non-mitochondrial respiration rate using glycolysis and do this more extensively than primary liver cells [Rodriguez-Enriquez 2001]. We prevented the increase in glycolytic rate in response to mitochondrial insult by switching the cells from glucose- to galactose-containing medium or inhibited glycolysis using the competitive inhibitor 2-deoxyglucose (2DG) [Marroquin 2007, Kamalian 2015, Korga 2019, Pietzke 2014] (Fig. 2A). While HepG2

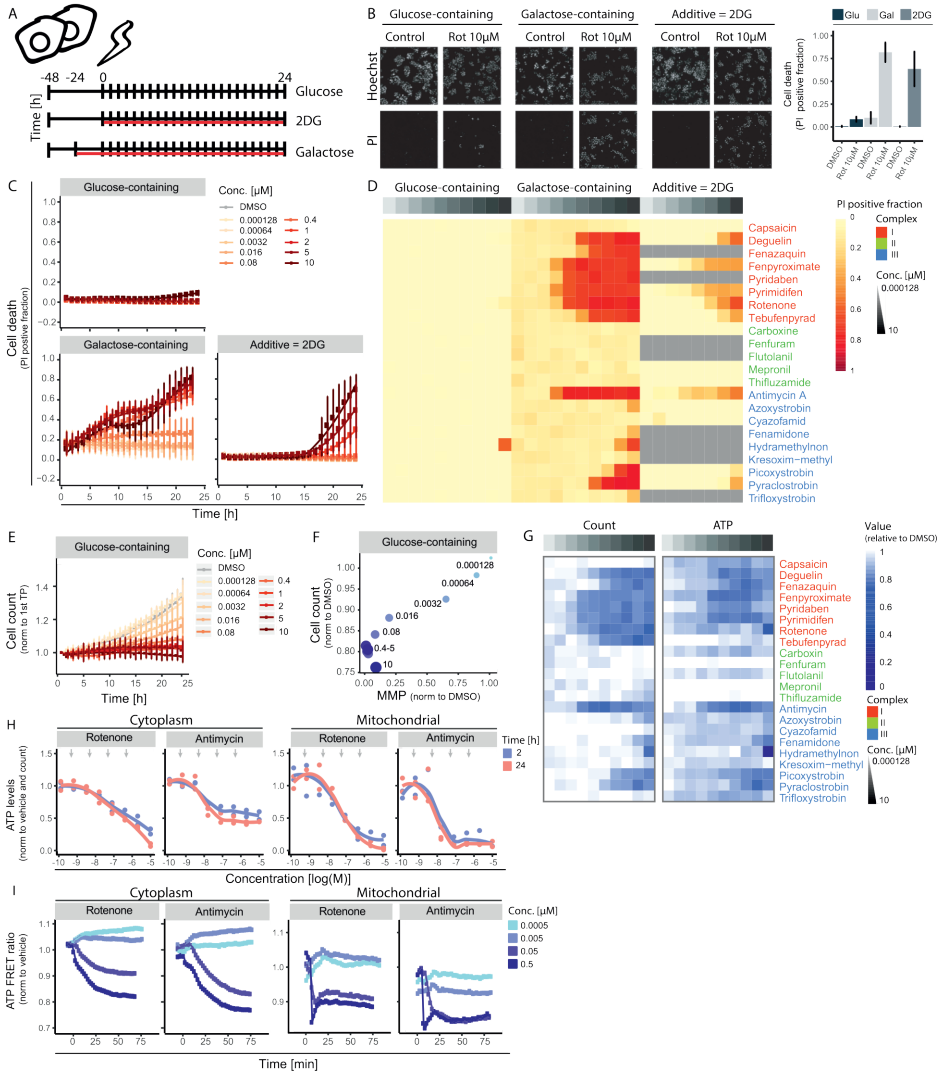


**Figure 2: Effect of various agrochemical MRC inhibitors on cell viability and ATP levels**

**A)** Schematic representation of different culture conditions. For all conditions, cells were seeded in glucose containing medium 2 days before the chemical exposure. 1) Glucose-containing medium: 2 days after seeding the medium is changed into new glucose-containing medium during the exposure. 2) Glucose-containing medium supplemented with 2DG: At the moment of chemical exposure 10 mM of 2DG was added into the wells. 3) Galactose-containing medium: Medium is refreshed into galactose-containing medium 1 day after seeding. 1 day later the chemical exposure is performed in galactose-containing medium. **B)** Representative images (of Hoechst and PI) plus PI positive fraction quantification of HepG2 cells exposed of 24 h to the vehicle control or 10 µM rotenone in 3 different medium conditions. **C)** 24 h live cell death measurement based on PI positive fraction upon exposure to concentration range of rotenone in 3 medium conditions. Values are mean ± SD of 3 biological replicates. **D)** Heatmap showing PI positive fraction upon exposure to concentration ranges of 22 complex inhibitors in 3 medium conditions (glucose-containing, galactose-containing and addition of 2DG). Values are a mean of 3 biological replicates. Grey cells in the 2DG medium condition were not tested. **E)** Nuclear count data in glucose-containing medium upon exposure to a concentration range of rotenone. Values were normalized to the 1st time point and represent a mean ± SD of 3 biological replicates. **F)** Correlation plot comparing MMP at 24 h (geometric mean normalized to DMSO) to cell ratio between 1st and last time point (normalized to DMSO) after exposure to a concentration range of rotenone. Values are mean of 4 biological replicates. Labels represent corresponding concentration in µM. **G)** Heatmap showing total cytoplasmic ATP levels and nuclear count ratio between first and last time point after exposure to concentration ranges of 22 complex inhibitors in glucose containing medium. Values are normalized to vehicle control and represent a mean ± SD for 2 biological (ATP levels) or 3 biological (nuclear count) replicates. **H)** Concentration-response curve of total ATP levels in the

cytoplasm (left two panels) and in mitochondria (right two panels) comparing rotenone or antimycin exposure to vehicle control at 2 h and 24 h. Values are normalized to nuclear count and represent a biological triplicate ± SD Arrows depict the concentrations used in Figure 2I. **I)** Time response curve of ATP-FRET ratio in the cytoplasm (left two panels) and mitochondria (right two panels) comparing 4 indicated concentrations of rotenone or antimycin to vehicle control over a period of 2 hours. Values are from 1 biological replicate, see supplementary figure 2D and E for 2nd biological replicates.

cells tolerated exposure to rotenone in glucose-containing medium, preventing the increase in glycolytic rates and inhibition of glycolysis itself sensitized these cells to adversity caused by CI inhibition as shown by propidium iodide staining (Fig. 2B). The use of galactose medium sensitized the cells to cell death to a larger extent and at earlier time points than the addition of 2DG to the medium (Fig. 2C). Perturbation of glycolytic capacity of the cell did lead to sensitization to cell death in response to both CI and CIII inhibitors, but no difference could be observed between the two inhibitor classes other than potency variability (Fig. 2D). No sensitization of HepG2 to CII inhibitors upon perturbation of the glycolytic capacity using either 2DG or galactose-containing medium was observed. These findings indicate that HepG2 cells can be stimulated to largely rely on mitochondrial respiration and under those conditions, inhibition of CI or CIII but not of CII reduces cell viability.



**Attenuation of mitochondrial ATP production and proliferation in presence of complex I and III but not complex II inhibitors**

The ability of HepG2 cells to tolerate ETC inhibition in glucose-containing medium allowed us to study the response to CI and CIII inhibitors in more detail at any desired moment after exposure. Despite the absence of cell death in glucose-containing medium (Fig. 2B), cell proliferation was attenuated in a concentration- and time-dependent manner by rotenone (Fig. 2E). The observed decrease in proliferation correlated to inhibition of MMP (Fig. 2F). Assessment of relative cell count upon exposure to the panel of CI, CII and CIII inhibitors also confirmed the correlation between a drop in proliferation and perturbation of the MMP (Fig. 2G left panel and Fig. 1C).

Next, the effect of CI and CIII inhibition on ATP concentration was evaluated in the cytoplasm and mitochondria using the ATPlite assay. Exposure to both CI (rotenone) and CIII (antimycin) inhibitors resulted in a concentration dependent decrease of total cytoplasmic ATP levels at 2h, which was still the case at 24h. (Fig. 2H left two panels). The concentration dependent decrease in ATP levels in the mitochondria resembled the pattern observed in the cytoplasm (figure 2H right two panels). We therefore only examined the total cytoplasmic ATP for the entire set of CI, CII and CIII inhibitors (Fig. 2G right panel). In general CI and CIII inhibitor exposure resulted in a drop in ATP which correlated with decreased proliferation. CII inhibitors did not exhibit a pronounced concentration-dependent decrease.

Finally, to assess the dynamics of the ATP levels (sum of production and degradation) in the cytoplasm and in the mitochondria, cells lines were created by stable integration of ATP-FRET probes localized in the cytoplasm or mitochondria. These allowed dynamic monitoring of ATP changes upon chemical exposure as exemplified using to CI (rotenone) and III inhibitors (antimycin) (Suppl. Fig. 1A-D). Assessment of the temporal dynamics using both ATP-FRET probes over a period of 75min confirmed the concentration-dependent decrease in ATP (Fig. 2I, Suppl. Fig. 2D and E). Cytoplasmic ATP levels dropped between the moment of exposure and the following 75 min in a concentration-dependent manner for CI and CIII inhibitors rotenone and antimycin. The ATP drop in the mitochondrial compartment was much faster than in the cytoplasm and already reached a minimum within the first 10 min.

In summary, our measurements demonstrated that exposure to CI and CIII inhibitors in glucose-containing medium resulted in a quick concentration-dependent drop in cytoplasmic and mitochondrial ATP, which was correlated with the inhibition of MMP and, when glycolysis is suppressed, by inhibition of cell proliferation.

**A gene signature for mitochondrial toxicants**

Having established that ETC CI and III inhibitors similarly attenuate MMP and mitochondrial ATP production, we collected targeted TempO-Seq transcriptomics data using the S1500++ probe set, which expands the U.S. Tox21 S1500+ sentinel list with probes targeting genes known to be affected in response to toxic insults and tissue relevant markers to further analyze the cellular response towards ETC inhibition. A concentration-dependent increase in the number of differentially expressed genes (DEGs) was observed in response to CI and CIII inhibitors whereas CII inhibitors did not affect overall gene expression (Suppl. Fig. 3A). Notably, the potency difference between the various chemicals with respect to the number of DEGs, correlated inversely with MMP perturbation (Suppl. Fig. 3B). To evaluate if concentration-dependent regulation of individual genes was correlated to the effects of inhibitors on MMP, for each probe we determined the benchmark concentration (BMC = the lowest concentration at which the probe count was changed more than 1x standard deviation (up or down) compared to the control condition). Indeed, accumulation plots of all BMC values per probe, measured upon exposure to the various ETC inhibitors, demonstrated an increase around the concentration at which also the MMP BMC was observed (Suppl. Fig. 3C).

We considered whether a signature of unique genes could achieve separation between the various mitochondrial complex inhibitors. To enable selection of candidate genes for the different complex inhibitors, DEGs were filtered based on p-adjusted values, fold change values, and their concentration-response correlation (William's trend test) (Fig. 3A).

Thereafter, a group of gene probes (299) was selected that was affected by any active ETC inhibitor (inactive = capsaicin, carboxin, cyazofamid, mepronil and thifluzamide) (Suppl. Fig. 3D). We subdivided the probe set across CI, CII and CIII inhibitors and defined genes affected specifically by CI or CIII inhibitors, respectively 302 and 193 probes (Fig. 3B). Using this approach, no genes were identified that responded to all compounds within one class but not to any compounds of another class (Suppl. Fig. 3E and F).

While no subclass specific DEGs were found, the individual gene expression patterns could still be used to create a gene signature for mitochondrial perturbation. We subdivided the probe set along "active inhibitors" (CI: deguelin, fenpyroximate, pyrimidifen, rotenone, tebufenpyrad and CIII: antimycin, azoxystrobin, picoxystrobin, pyraclostrobin), "inactive inhibitors" with non to minimal effect upon proliferation (capsaicin, carboxin, cyazofamid, mepronil and thifluzamide) and "model compounds" (CDDO-me (oxidative stress response), cisplatin (DNA damage response), TNFα (inflammation) and tunicamycin (unfolded protein response)). This resulted in 382 probes affected specifically by one or more active mitochondrial toxicants and not by the positive controls or "inactive" inhibitors (Fig. 3C). 23 of these 382 probes were affected by all individual "active inhibitors" (Fig. 3D). The identified hits exhibited a concentration response relationship upon exposure to the various "active inhibitors" (Fig. 3E) and a BMC value which was less than or equal to the BMC values for the MMP data (Fig. 3F) and previously determined basal oxygen consumption rate (OCR) [van der Stel 2020] (Fig. 3G).

To establish a robust mitochondrial toxicant gene signature, we selected 7 hits from the 23 probes unique for the ETC inhibitor induced effects upon the mitochondria (Table 1). The selection criterion was a log2FC of > 2 or < -2 or a direct link to mitochondria, which would facilitate detection when used as biomarker (Suppl. Fig. 3G and H). To assess the possible involvement of the selected signature genes in the modulation of mitochondrial toxicity, rotenone treatments were combined with RNA interference. We focused on the signature genes that were upregulated (*CYP3A5, KLHL24, NOS3* or *PFKP*) and used RNA interference to address their role. The depletion of *PFKP* itself resulted in a slight reduction of viability while the other siRNAs had no effect under non-treated conditions (Fig. 3H). *NOS3* depletion led to an increased sensitivity towards rotenone, suggesting that NOS3 is involved in an adaptive response during ETC inhibitor treatment (Fig. 3I). Depletion of the other signature genes did not significantly impact on rotenone-induced cytotoxicity.

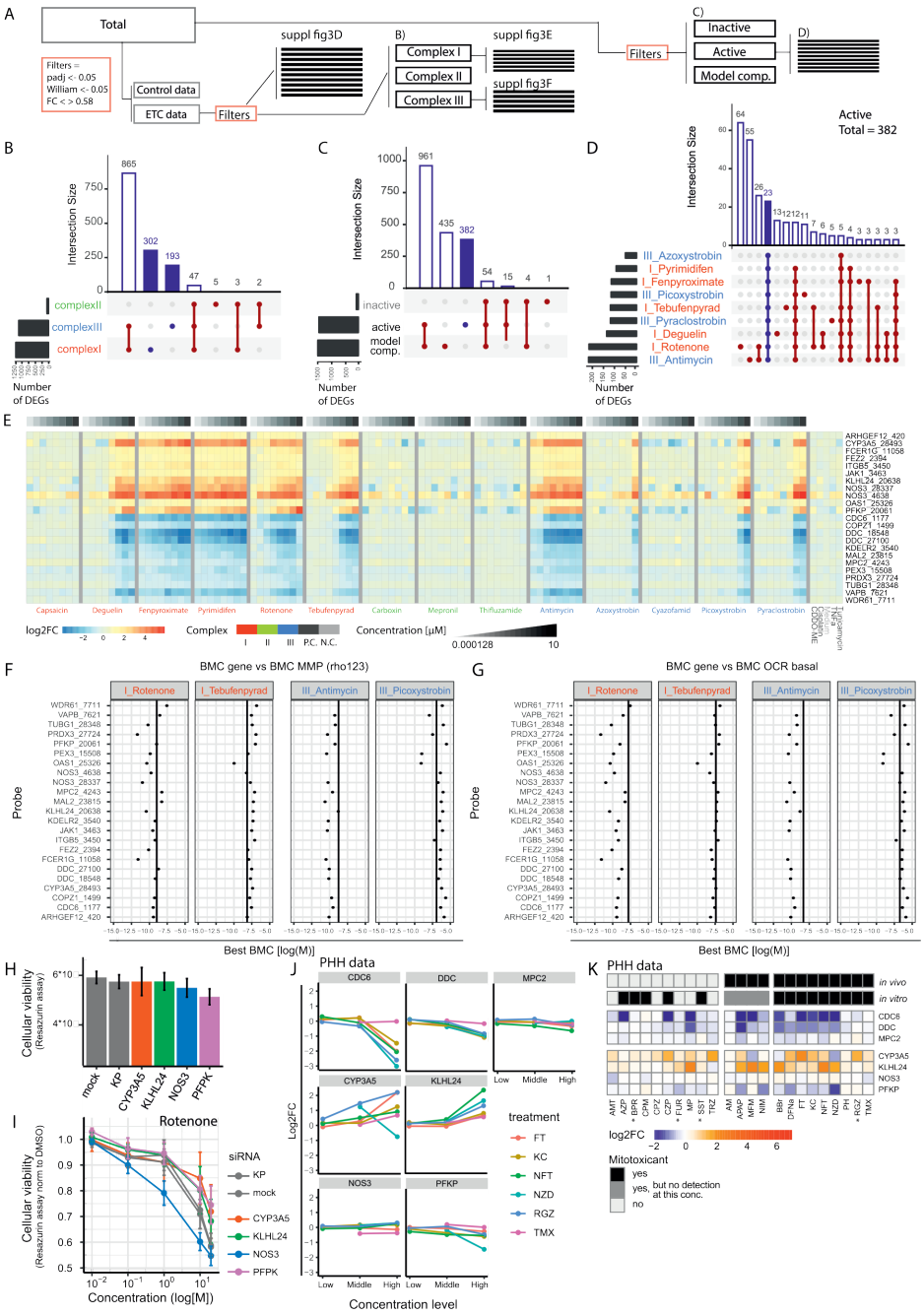
A
Total
Filters =
padj <- 0.05
William <- 0.05
FC < > 0.58
Control data
ETC data
Filters
suppl fig3D
B)
Complex I
Complex II
Complex III
suppl fig3E
suppl fig3F
Filters
C)
Inactive
Active
Model comp.
D)
B
Intersection Size
complexII
complexIII
complexI
Number of DEGs
C
Intersection Size
Inactive
active
model comp.
Number of DEGs
D
Intersection Size
Active
Total = 382
III_Azoxystrobin
I_Pyrimidifen
I_Fenpyroximate
III_Picoxystrobin
I_Tebufenpyrad
III_Pyraclostrobin
I_Deguelin
I_Rotenone
III_Antimycin
Number of DEGs
E
Capsaicin
Deguelin
Fenpyroximate
Pyrimidifen
Rotenone
Tebufenpyrad
Carboxin
Mepronil
Thifluzamide
Antimycin
Azoxystrobin
Cyazofamid
Picoxystrobin
Pyraclostrobin
log2FC
Complex
I II III P.C. N.C.
Concentration [µM]
0.000128
10
F
BMC gene vs BMC MMP (rho123)
I_Rotenone
I_Tebufenpyrad
III_Antimycin
III_Picoxystrobin
Probe
Best BMC [log(M)]
G
BMC gene vs BMC OCR basal
I_Rotenone
I_Tebufenpyrad
III_Antimycin
III_Picoxystrobin
Probe
Best BMC [log(M)]
H
Cellular viability
(Resazurin assay)
mock
KP
CYP3A5
KLHL24
NOS3
PFPK
I
Rotenone
Cellular viability
(Resazurin assay norm to DMSO)
siRNA
KP
mock
CYP3A5
KLHL24
NOS3
PFPK
Concentration (log[M])
J
PHH data
CDC6
DDC
MPC2
CYP3A5
KLHL24
NOS3
PFKP
Log2FC
treatment
FT
KC
NFT
NZD
RGZ
TMX
Low
Middle
High
Concentration level
K
PHH data
in vivo
in vitro
CDC6
DDC
MPC2
CYP3A5
KLHL24
NOS3
PFKP
AMT
AZP
BPR
CPM
CPZ
DZR
FUR
MP
SST
TRZ
AM
APAP
NAPA
NIM
BIR
DPAI
FT
KC
NFT
NZD
RGZ
TMX
log2FC
Mitotoxicant
yes
yes, but no detection at this conc.
no

**Figure 3: Predictive gene expression signature for MRC inhibition.**
**A)** Schematic representation of the relationship between panels B-E. All plots only include genes with a padj < 0.05, log2FC > or < 0.58 and a p-value < 0.05 in the Williams trend test. **B)** Plot based on the gene expression data of all mitochondrial complex inhibitors and separating all genes per complex type. Horizontal bars at the left represent the total number of DEGs per treatment that meet the filtering criteria. Blue bars represent the group of genes unique for CI or CIII inhibition **C)** Plot based on the gene expression data of all mitochondrial complex inhibitors plus all data from the 4 positive adaptive stress controls (60 nM CDDO-me, 1 mg/ml cisplatin, 10 ng/mL TNFα and 12 μM tunicamycin) and separating all genes active inhibitors, inactive inhibitors and positive adaptive stress controls). Horizontal bars at the left represent the total number of DEGs per treatment which meet the filtering criteria. Blue bar represents group of genes unique for all active complex inhibitors **D)** Subset of 382 genes from panel D) separated per active mitochondrial inhibitor. The plot only represents groups of more than 3 genes. Horizontal bars at the left represent the number of DEGs per treatment which meet the filtering criteria and are in the set of 382 probes. Blue bar represents group of genes affected by all active inhibitors. **E)** Heatmap with log2FC values upon exposure to a concentration range of 14 complex inhibitors and the positive adaptive stress controls (60 nM CDDO-me, 1 mg/ml cisplatin, 10 ng/mL TNFα and 12 μM tunicamycin) of the 23 genes effected by all active mitochondrial complex inhibitors and not the positive stress responses controls (from panel E). **F)** Plot including per treatment (CI and CIII inhibitors) the BMD value of the Rho123 data (vertical line) plus the individual BMD value of the 23 probes at 24 h chemical exposure. Both BMD values are determined using BMDexpress software. **G)** Plot including per treatment the BMD value of the OCR basal data ([van der Stel 2020], vertical line) plus the individual BMD value of the 23 probes. Both BMD values are determined using BMDexpress software. **H)** Cellular viability monitored using resazurin reduction 72 h after siRNA transfection (CYP3A5, KLHL24, NOS3, PFKP or siRNA control: kinase pool (KP)) or negative control condition (mock). **I)** Cellular viability monitored using resazurin reduction after 72 h siRNA transfection followed by a concentration range of rotenone for 24 h (CYP3A5, KLHL24, NOS3, PFKP or siRNA control: kinase pool (KP)) or negative control condition (mock). Values are normalized to treatment control (DMSO). **J)** Log2FC data from the TG-GATES database for CDC6, DDC, MPC2, CYP3A5, KLHL24, NOS3 and PFPK in PHH upon 24h exposure to 3 concentrations of DILI-inducing compounds know to also effect the ETC (table 2). **K)** Heatmap with log2FC values from the TG-GATES database for CDC6, DDC, MPC2, CYP3A5, KLHL24, NOS3 and PFPK upon 24h exposure to highest concentration available for DILI-compounds classified by Eakins 2016 (table 2). (* = exceptions are with middle concentration, because highest concentration was more than 100 fold the cMax value). *In vivo* = classification based on literature search presented by Eakins 2016 and *in vitro* = classification based on results in HepG2 by Eakins 2016. Grey classification = concentration presented in the heatmap is lower than the mitotoxic concentration determined by Eakins in HepG2.



To address whether this 7-gene signature could be used in a biomarker approach for flagging of possible mitochondrial toxicity liabilities, we evaluated gene expression data for exposure to chemicals known to cause DILI and available for PHH in the TGGATES database. A list of 156 such chemicals was shortened to focus on 23 chemicals with mitochondrial liabilities in HepG2 cells (Table 2) [Eakins 2016]. 4 out of the 7 selected genes (*CDC6*, *DDC*, *CYP3A5* and *KLHL24*) were similarly affected in PHH as in HepG2 by the chemicals classified as ETC inhibitors (Fig. 3J), except for tamoxifen which did not induce major changes in any gene measured (data not shown). This gene set selected for mitochondrial toxicity via ETC inhibition in HepG2 did not separate DILI compounds with- from those without mitochondrial liabilities in PHH (Fig. 3K).

In summary, using the S1500++ probe set, TempO-Seq could not distinguish active CI from active CIII compounds. However, a gene set was identified whose transcription was specifically affected by mitochondrial toxicants (active CI and CIII inhibitors that affected MMP, ATP production and cell proliferation) and not by other toxicants in HepG2. Gene silencing associated one of these genes, *NOS3*, with adversity in HepG2 cells. A subset of this gene set was also modulated in response to DILI compounds with confirmed ETC inhibitory activity in PHH, but in these cells such a response was also seen with certain compounds not classified as mitochondrial inhibitors.

**Table 1: Gene selected from ETC inhibitor screen**

Table includes information concerning gene name, direction of the transcriptomic change upon ETC inhibitor exposure, full name – function, main location in the cell, organs in which the RNA is present. All gene specific information was collected using genecard.org [Stelzer 2016].

| Gene | Entrez | Gene | Function | Cellular compartment |
|---|---|---|---|---|
| ***Up-regulation*** | | | | |
| ARHGEF12 | 23365 | Rho Guanine Nucleotide Exchange Factor 12 | *Process initiated by extracellular stimuli* | Cytosol, nucleus |
| CYP3A5 | 1577 | Cyp enzyme 3A5 | *Drug metabolism, synthesis of cholesterol, steroids and other lipids* | Endoplasmic reticulum |
| FCER1G | 2207 | Fc Fragment Of IgE Receptor Ig | *Allergic reactions* | Cell membrane |
| FEZ2 | 9637 | Fasciculation And Elongation Protein Zeta 2 | *Axon bundling and elongation* | Nucleus |
| ITGB5 | 3693 | Integrin Subunit Beta 5 | *Cell-surface interaction* | Cell membrane |
| JAK1 | 3716 | Janus Kinase 1 | *Cytokine signal transduction* | Cytosol, nucleus |
| KLHL24 | 54800 | Kelch Like Family Member 24 | *A ubiquitin ligase substrate receptor involved i.a. in keratin stability* | Cytosol, nucleus |
| NOS3 | 4846 | Nitric Oxide Synthase 3 | *Production of signaling molecule nitric oxide (NO)* | All compartments |
| OAS1 | 4938 | 2′-5′-Oligoadenylate Synthetase 1 | *RNA degradation* | Cytosol, nucleus |
| PFKP | 5214 | Phosphofructokinase, Platelet | *Regulation of glycolysis* | Cytosol |
| ***Down-regulation*** | | | | |
| CDC6 | 990 | Cell Division Cycle 6 | *Essential in DNA replication* | All compartments, except for endoplasmic reticulum, endosomes and lysosomes |
| COPZ1 | 22818 | COPI Coat Complex Subunit Zeta 1 | *Autophagy* | Cytosol, golgi |
| DDC | 1644 | Dopa Decarboxylase | *Involved in the production of dopamine, serotonin and tryptamine* | Cytosol |
| KDELR2 | 11014 | KDEL Endoplasmic Reticulum Protein Retention Receptor 2 | *Recycling of proteins between golgi-ER* | Endoplasmic reticulum |
| MAL2 | 114569 | Mal, T Cell Differentiation Protein 2 | *Protein transport* | Cell membrane |
| Brp44/ MCP2 | 25874 | Mitochondrial Pyruvate Carrier 2 | *Pyruvate metabolism, TCA cycle* | Mitochondrion |
| PEX3 | 8504 | Peroxisomal Biogenesis Factor 3 | *Peroxisome biosynthesis* | Peroxisome, endoplasmic reticulum, nucleus |
| PRDX3 | 10935 | Peroxiredoxin 3 | *Mitochondrial antioxidant* | Mitochondria |
| TUBG1 | 7283 | Tubulin Gamma 1 | *Microtubules formation* | Cytoskeleton |
| VAPB | 9217 | VAMP Associated Protein B And C | *Trafficking* | Endoplasmic reticulum, golgi |
| WDR61 | 80349 | WD Repeat Domain 61 | *Regulation transcription* | Cytosol, nucleus |

**Pathway and gene network analysis shows ETC inhibitors trigger responses affecting proliferation, protein homeostasis, and early stress responses**

We next moved from analysis of responses at the individual gene level to analysis of gene networks and pathways, which may enhance translation across model systems. First, we took advantage of previously established weighted gene co-expression network analysis (WGCNA) modules for PHH comprising ~400 gene modules that can be visualized as a toxicogenomics map [Callegaro 2021]. The ETC inhibitor TempO-Seq transcriptomics data obtained in HepG2 was projected on these prior established co-expression modules and used to calculate module eigengene scores (EGSs) to monitor chemical-induced changes in these modules. Concentration dependent up- and down modulation of various modules was observed upon exposure to rotenone and a clear overlap was seen in affected modules upon exposure to the highest non-toxic concentration of rotenone (2 µM) and antimycin (10 µM) (Fig. 4A). The effects of different ETC inhibitors on module eigengenes were highly correlated within CI ($r^2$ = 0.836) and CIII inhibitors ($r^2$ = 0.853) but not within CII inhibitors ($r^2$ = 0.384) (Fig. 4B, Suppl. Fig 4A and B). Moreover, effects on module eigengenes of CI (rotenone) correlated with effects of CIII (antimycin) ($r^2$ = 0.791), but not with effects of CII inhibition (mepronil) ($r^2$ = 0.321) (Fig. 4C, Suppl. Fig 4B). In general, the S1500++ probe set allowed a module coverage of 30-50% and affected genes per module generally overlapped between the exposure to rotenone and antimycin (bold genes in the table of Suppl. Fig. 4C). Comparing all tested chemicals at concentrations just above the BMD of the MMP data did in fact show separation between CI and CIII inhibitors with the exception of antimycin and azoxystrobin that were placed in a CI cluster (Fig. 4D, Suppl. Fig 4D). Of the CII inhibitors, Mepronil was placed in the CIII cluster. Increasing exposure to the highest non-cytotoxic concentrations that far exceeded the effective mitochondrial perturbation level and may cause off-target effects did not enhance CI versus CIII separation but resulted in separation of strong mitotoxicants versus weak/non-mitotoxicants (Fig. 4E, Suppl. Fig 4D). The top 10 upregulated modules for CI and III inhibitors included 7 common modules (Fig. 4F, G and Suppl. Fig. 4C and 5). These modules were associated with oxidative stress (144), signal transduction (149, 158, 248 and 276), metabolism (147, 149 and 248) and transport (149 and 315).

**Table 2: Selection of DILI compounds**

Table includes describes the DILI compound selection based on Eakins 2016. The subdivision mitochondrial toxicant or not *in vivo* is kept similar as previously decided by Eakins *et al* and is based on their literature search. "Mechanism literature" is the mode of action found in literature. "Predicted mechanism" is the mode of action identified by Eakins *et al* using in HepG2. "FDA DILI rank" included the DILI classification as defined by the FDA (#; FDA DILI database[18]). "Exposure info [uM]" includes the cMax as defined by Eakins 2016 *et al* (*), the lowest effective concentration measured in any of the assays of Eakins *et al* (grey = a concentration above the highest concentration tested in TG-GATES) and the 3 concentrations used for the PHH transcriptomics data in the TG-GATES (** [Igarashi 2015]).

| | Compound | Mitochondrial target (*) | | FDA DILI rank (#) | | TGGATES | Exposure info [µM] (*,**) | | | | |
|---|---|---|---|---|---|---|---|---|---|---|---|
| | | Mechanism Literature | Predicted mechanism | Severity | DiliConcern | | cMax | Eakins | low | middle | high |
| Known mitotoxicant | acetaminophen | ETC inhibitor | ETC inhibitor | 5 | Most-DILI-Concern | APAP | 132,25 | 5660 | 200 | 1000 | 5000 |
| | acetylsalicylic acid | ETC inhibitor | Cytotoxicity | NA | NA | no | | | | | |
| | amiodarone | other | Other | 8 | Most-DILI-Concern | AM | 1,17 | 13,4 | 0,28 | 1,4 | 7 |
| | benzbromarone | uncoupler | Uncoupler | 8 | Most-DILI-Concern | BBr | 4,36 | 2,56 | 4 | 20 | 100 |
| | clotrimazole | substrate inhibitor | Substrate inhibitor | 3 | Less-DILI-Concern | no | | | | | |
| | diclofenac | other | Other | 8 | Most-DILI-Concern | DFNa | 6,4 | 235 | 16 | 80 | 400 |
| | entacapone | uncoupler | Substrate inhibitor | 0 | Less-DILI-Concern | no | | | | | |
| | flutamide | ETC inhibitor | ETC inhibitor | 8 | Most-DILI-Concern | FT | 4,59 | 32,5 | 2 | 10 | 50 |
| | ketoconazole | ETC inhibitor | ETC inhibitor | 8 | Most-DILI-Concern | KC | 7 | 2,09 | 0,6 | 3 | 15 |
| | mefloquine | ATP synthase | ETC inhibitor | 7 | Less-DILI-Concern | no | | | | | |
| | menadione | other | Uncoupler | NA | NA | no | | | | | |
| | metformin | ETC inhibitor | none | 0 | Less-DILI-Concern | MFM | 12,39 | NA | 40 | 200 | 1000 |
| | nefazodone | ETC inhibitor | Substrate inhibitor | 8 | Most-DILI-Concern | NZD | 2,61 | 0,6 | 1,2 | 6 | 30 |
| | nimesulide | uncoupler | Other | 8 | Most-DILI-Concern | NIM | 18,05 | 456 | 13,2 | 66 | 330 |
| | nitrofurantoin | ETC inhibitor | ETC inhibitor | 8 | Most-DILI-Concern | NFT | 6 | 48,3 | 5 | 25 | 125 |
| | paraquat | ETC inhibitor | Other | NA | NA | no | | | | | |
| | paroxetine | ETC inhibitor | ETC inhibitor | 8 | Less-DILI-Concern | no | | | | | |
| | perhexiline | Fatty acid oxidation inhibitor | Substrate inhibitor | 8 | Most-DILI-Concern | PH | 2,16 | 6,45 | 0,6 | 3 | 15 |
| | phenformin | ETC inhibitor | ETC inhibitor | NA | NA | no | | | | | |
| | pioglitazone | ETC inhibitor | ETC inhibitor | 3 | Less-DILI-Concern | no | | | | | |
| | primaquine | uncoupler | none | 0 | No-DILI-Concern | no | | | | | |
| | promethazine | ETC inhibitor | Cytotoxicity | 5 | Less-DILI-Concern | no | | | | | |
| | rosiglitazone | ETC inhibitor | ETC inhibitor | 3 | Less-DILI-Concern | RGZ | 0,86 | 5,81 | 12 | 60 | 300 |
| | tamoxifen | ETC inhibitor | ETC inhibitor | 8 | Most-DILI-Concern | TMX | 1,21 | 9,58 | 1 | 5 | 25 |
| | tolcapone | uncoupler | Uncoupler | 8 | Most-DILI-Concern | no | | | | | |
| | troglitazone | ETC inhibitor | ETC inhibitor | 8 | Most-DILI-Concern | no | | | | | |

**Table 2: Selection of DILI compounds** (continued)

| | Compound | Mitochondrial target (*) | | FDA DILI rank (#) | | TGGATES | Exposure info [µM] (*,**) | | | | |
|---|---|---|---|---|---|---|---|---|---|---|---|
| | | Mechanism Literature | Predicted mechanism | Severity | DiliConcern | | cMax | Eakins | low | middle | high |
| No known mitochondrial liability | amitriptyline | none | none | 5 | Less-DILI-Concern | AMT | 0,22 | 12,7 | 0,6 | 3 | 15 |
| | atenolol | none | none | 4 | Less-DILI-Concern | no | | | | | |
| | atorvastatin | none | Other | 5 | Most-DILI-Concern | no | | | | | |
| | azacytidine | none | none | NA | NA | no | | | | | |
| | azathioprine | none | Other | 5 | Most-DILI-Concern | AZP | 1,43 | 200 | 2,92 | 14,6 | 73 |
| | benazepril | none | Cytotoxicity | 4 | Less-DILI-Concern | no | | | | | |
| | betaine | none | none | 0 | No-DILI-Concern | no | | | | | |
| | bosentan | none | Cytotoxicity | 7 | Most-DILI-Concern | no | | | | | |
| | buspirone | none | Substrate inhibitor | 3 | Ambiguous | BPR | 0,01 | 25,1 | 1,2 | 6 | 30 |
| | chloroquine | none | none | 3 | Less-DILI-Concern | no | | | | | |
| | chlorpromazine | none | Cytotoxicity | 2 | Less-DILI-Concern | CPZ | 0,61 | 5,07 | 0,8 | 4 | 20 |
| | clomipramine | none | Substrate inhibitor | 8 | Most-DILI-Concern | CPM | 0,19 | 19,2 | 0,4 | 2 | 10 |
| | clozapine | none | Other | 5 | Most-DILI-Concern | CZP | 0,91 | 14,2 | 2 | 10 | 50 |
| | fialuridine | none | none | 8 | Most-DILI-Concern | no | | | | | |
| | flecainide acetate | none | none | 7 | Less-DILI-Concern | no | | | | | |
| | fluoxetine | none | ETC inhibitor | 3 | Less-DILI-Concern | no | | | | | |
| | fluvastatin | none | ATP synthase | 3 | Less-DILI-Concern | no | | | | | |
| | furosemide | none | none | 2 | Ambiguous | FUR | 11,76 | 500 | 100 | 500 | 2500 |
| | methapyrilene | none | none | NA | NA | MP | 115 | 219 | 24 | 120 | 600 |
| | metoclopramide | none | none | 5 | Less-DILI-Concern | no | | | | | |
| | mibefradil dihydrochloride | none | Uncoupler | NA | NA | no | | | | | |
| | miconazole | none | ETC inhibitor | NA | NA | no | | | | | |
| | nicardipine | none | none | 3 | Ambiguous | no | | | | | |
| | nortriptyline | none | none | 8 | Most-DILI-Concern | no | | | | | |
| | oxybutynin | none | ETC inhibitor | 0 | No-DILI-Concern | no | | | | | |
| | physostigmine | none | none | 0 | No-DILI-Concern | no | | | | | |
| | risperidone | none | ETC inhibitor | 3 | Less-DILI-Concern | no | | | | | |
| | sertraline | none | ETC inhibitor | 3 | Less-DILI-Concern | no | | | | | |
| | simvastatin | none | ETC inhibitor | 3 | Less-DILI-Concern | SST | 0,02 | 5,29 | 1,2 | 6 | 30 |
| | streptomycin | none | none | 0 | No-DILI-Concern | no | | | | | |
| | thioridazine | none | Cytotoxicity | 5 | Less-DILI-Concern | TRZ | 0,55 | 6,04 | 0,6 | 3 | 15 |
| | verapamil | none | Cytotoxicity | 3 | Less-DILI-Concern | no | | | | | |

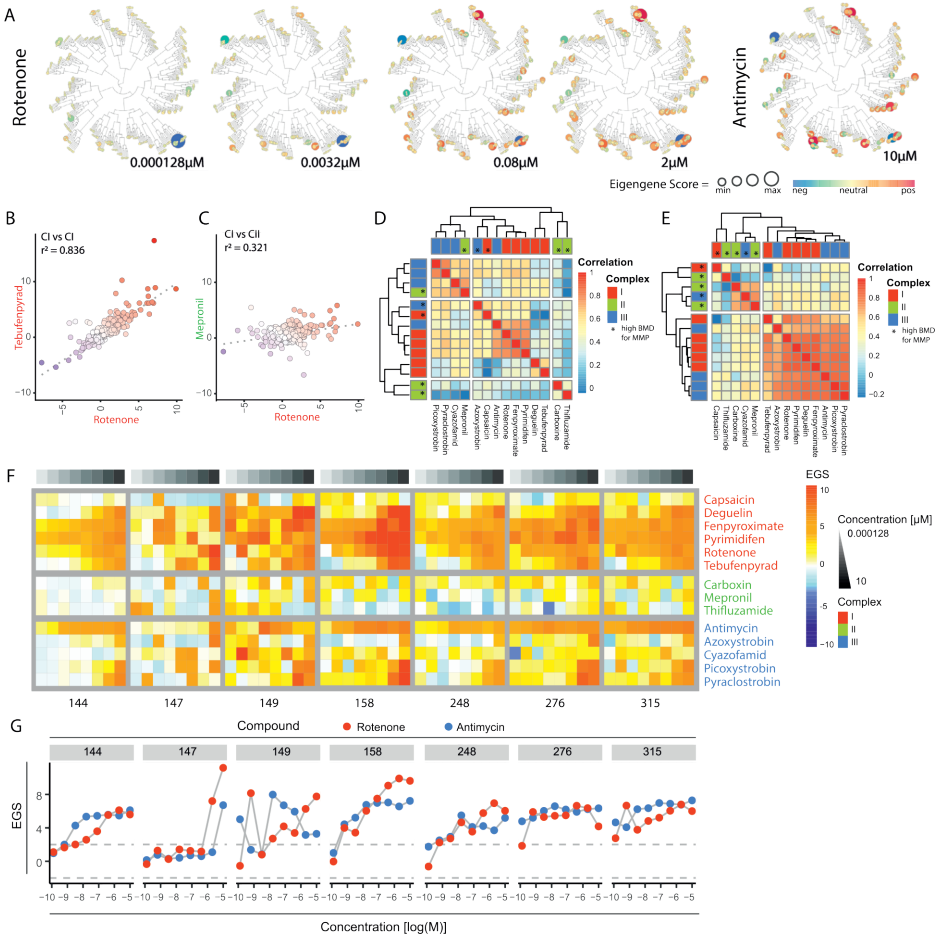


**Figure 4: Gene network activation by MRC inhibitors based on human hepatocyte WGCNA datasets.** **A)** Projection of S1500++ TempO-Seq HepG2 expression data on an established WGCNA map of PHH created from TG-GATES data. 4 panels show the module EGSs upon 24h exposure to 4 concentrations of rotenone. Color range from blue (negative EGS) to red (positive EGS) and are resigned per map. The size of the circle corresponds to the absolute EGS per module. **B and C)** Example correlation plots of the EGS per WGCNA module upon exposure to non-toxic concentrations comparing rotenone (2 µM) to **B)** tebufenpyrad (10 µM) or **C)** mepronil (10 µM). **D)** Correlation plot of all tested ETC inhibitors showing a correlation score based on the EGS scores of all modules per condition. The concentrations selected were a tested concentration above the BMD value of the Rho123 data per treatment (Suppl. fig 4D). This BMD value was determined using BMDexpress. **E)** Correlation plot of all tested ETC inhibitors showing a correlation score based on the EGS scores of all modules per condition. The selected concentration was the highest tested non-toxic concentration per treatment (Suppl. fig 4D). **F)** Heatmap of 7 modules showing Eigengene Scores (EGS) upon 24 h exposure to a concentration range of 14 complex inhibitors. The modules were selected based on being upregulated in both the CI and CIII correlation plot (Suppl. Fig 6A). **G)** Concentration response curves of Eigen Gene Scores (EGS) per selected module upon 24h exposure to rotenone or antimycin. The modules were selected based on being upregulated in both the CI and CIII correlation plot.

We subsequently analyzed GO term enrichment to explore pathways triggered by ETC inhibition. In agreement with the connection to cell proliferation (see Fig. 2F and G) GO term enrichment analysis demonstrated enrichment for perturbation of cell cycle related pathways upon exposure to all CI and III inhibitors (Fig. 5A), as expected in proliferating HepG2 cells. Other GO terms regulated by all CI and III inhibitors included responses

to stress, organelle organization and DNA replication. The top up- and down- regulated genes for these biological processes were mapped in Fig. 5B. The response to stress was captured by changes in metabolism related genes (*GCLC, PPARD, DHRS2, ONECUT1, FABP1*) and induction of oxidative stress responders (*SRXN1, TXNRD1* and *HMOX1*). The GO term organelle organization was mostly driven by changes in the expression of genes involved in cell adhesion and matrix interaction (including amongst others *KRT, CNN1, IRAK2, TUBA1B, MMP3, TIMP2*). The cell cycle term comprised of factors involved in the cell cycle itself (including e.g., *RGCC, DUSP1, PLK3, CDK2, CDC6*), growth factor responses (*IGFBP1, EGFR, FOSL1, TFGB1* and *SMAD3*), DNA replication and related replication control (*GADD54B, POLE2, BRIP1, RMI1* and *FEN*1) and regulation of cell death and differentiation (including *SOX4, MCL1, TRIB3, BMF, BRIC5*).

Our targeted TempO-Seq probe set was biased towards pathways important in toxicology, which could result in an increased threshold for identification of toxicity-related pathways. We next used transcription factor (TF) enrichment analysis, which combines the target gene expression profiles for all measured probes per TF and considers the overall direction of the response, rendering the enrichment less dependent on the number of probes assessed. Again, TF profiles demonstrated a concentration-dependent modulation by CI and CIII inhibitors but not CII ETC inhibitors (Suppl. Fig. 6). Clustering of the enriched TFs resulted in 3 clusters demonstrating a clear concentration dependency based on visual inspection (Fig. 5C and Suppl. Fig. 6). These three TFs clusters belonged to 3 major biological responses: a cluster of downregulated TFs mostly involved in proliferation; a cluster of upregulated TFs involved in inflammation and protein homeostasis; and a cluster of upregulated TFs involved in early stress responses (Fig. 5C).



**Combining TempO-Seq and high content imaging indicates that amino acid response (AAR) is triggered by complex I and III ETC inhibitors**

To allow dynamic monitoring of effects on cell cycle progression, protein homeostasis, and stress responses predicted by the gene- and pathway analyses mentioned above, the expression of P21 (cell cycle arrest), SRXN1 (oxydative stress), and ATF4 and CHOP (ER stress) was monitored using GFP reporter cell lines generated using BAC technology [Wink et al 2014]. Activation of P21 and SRXN1 was minimal for all inhibitors, but clearly upregulated upon exposure to the positive controls (respectively, etoposide and DEM) (Fig. 6A and B, Suppl. Fig. 7). Exposure to both CI and CIII inhibitors, but not CII inhibitors, resulted in a concentration dependent increase in ATF4 (Fig5C, Fig. 6B, Suppl. Fig. 7). The transcription factor ATF4 is involved in protein homeostasis in the endoplasmic reticulum (ER) as well as in mitochondria [Hetz 2012, Melber 2018]. To further explore the possible perturbation of protein homeostasis

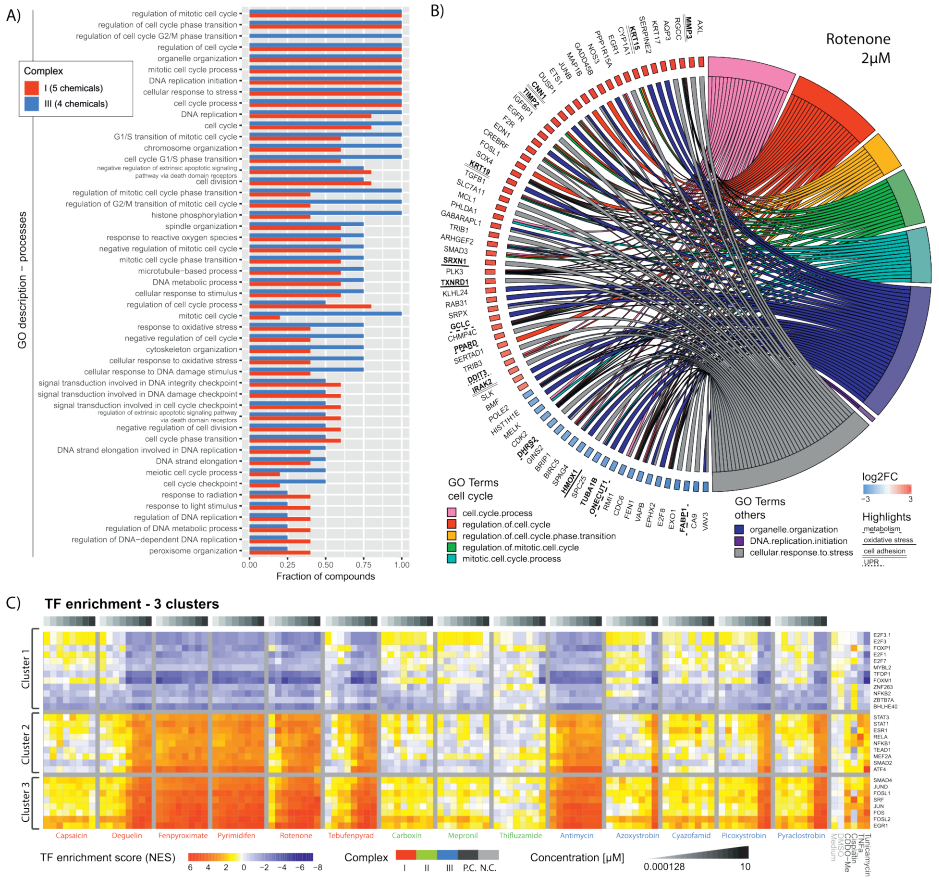


| Cluster 1 (negative regulation) | |
|---|---|
| E2F1, E2F2, E2F3, E2F7 | cell cycle |
| FOXP1 | regulation tissue specific genes |
| MYBL2 | cell cycle progression |
| TFDP1 | cell cycle progression |
| FOXM1 | cell cycle |
| ZNF263 | regulation of transcription |
| NFKB2 | inflammation and immune function |
| ZBTB7A | cell cycle and differentiation |
| BHLHE40 | circadian rhythm and cell differentiation |

| Cluster 2 (positive regulation) | |
|---|---|
| STAT1, STAT3 | normally upregulated upon cytokine and growth factor exposure |
| ESR1 | growth factor response |
| RELA, NFKB1 | inflammation |
| TEAD1 | proliferation and apoptosis |
| MEF2A | muscle related growth ans stress response gens |
| SMAD2 | cell proliferation, apoptosis, and differentiation |
| ATF4 | cAMP response element -> protein/protein interaction |

| Cluster 3 (positive regulation) | |
|---|---|
| SMAD4 | cell proliferation |
| JUND | regulators of cell proliferation, differentiation, and transformation |
| FOSL1, FOSL2 | regulators of cell proliferation, differentiation, and transformation |
| SRF | cell proliferation and differation |
| JUN | dimerizes with c-FOS to create AP1, cell cycle progression |
| FOS | regulators of cell proliferation, differentiation, and transformation |
| EGR1 | growth factor response |

**Figure 5: Transcriptional reprogramming after treatment with agrochemical MRC inhibitors.**
**A)** GO enrichment analysis performed using GOrilla software. Genes considered in the analysis demonstrated a padj <0.05, log2FC < or > 0.58 and p-value of the William trend test < 0.05. The graph only represents GO terms effected by at least 2 compounds of the CI or CIII inhibitors. The blue bar represents CI inhibitors (deguelin, fenpyroximate, pyrimidifen, rotenone and tebufenpyrad) and the red bar represents CIII inhibitors (antimycin, azoxystrobin, picoxystrobin and pyraclostrobin) **B)** Distribution plot of gene expression data upon exposure to 2 µM rotenone. The genes are distributed over the 8 GO-terms affected by all included CI and CIII inhibitors. Only the genes having a log2FC < -2 or < 2 are visualized. **C)** Heatmap of 3 transcription factor enrichment clusters showing normalized enrichment score (NES) upon 24 h exposure to concentration range of 14 complex inhibitors, 4 positive controls (P.C.) (60 nM CDDO-me, 1 mg/ml cisplatin, 10 ng/mL TNFα and 12 µM tunicamycin) and vehicle control (N.C.). Complete cluster of all transcription factors are shown in Suppl. Fig. 4. Transcription factor enrichment study was based on the transcription factor fingerprint in the DoRothEA database and using the viper package for the enrichment assessment. The used confidence parameter in the DoRothEA data set was ABC. Below heatmap are 3 tables including the transcription factors from the 3 clusters plus biological function collected from genecard[17].

and the induction of the related unfolded protein response (UPR), GFP-reporters for BIP (*HSPA5*), CHOP (*DDIT3*) and XBP1 were monitored. Interestingly, XBP1, which is downstream of the UPR sensor IRE1α, was unaffected by ETC inhibition at all non-toxic concentrations. Moreover, while CHOP was upregulated, BIP, a molecular chaperone in the ER was downregulated further arguing against the induction of a UPR (Fig. 6A and B, Suppl. Fig. 7). Overall, the concentration-dependent changes observed with GFP reporters corroborated the TempO-Seq data (Fig. 6C).

Revisiting four ER stress related WGCNA modules (13, 15, 62 and 295; [Callegaro 2021]) in the PHH data mentioned above (Fig. 4), supported the observed difference between the UPR stress inducer tunicamycin and the ETC inhibitors. I.e., deactivation of module 13 (including HSPA5) and activation of module 15 (including ASNS) was observed (Fig. 6D, E and F). The absence of an expected upregulation of module 62 was most likely caused by the lower coverage when using the s1500++ gene set (10.5%). Interestingly, modules 15 and 295 are highly enriched for amino acid biosynthesis and transport. The absence of an effect on XBP1 and the opposite direction of the response for HSPA5/BIP and ATF4 did not support UPR activation but may instead point to nutrient (amino acid) deprivation, which also leads to ATF4 upregulation [Krall 2021, Ye 2010]. Indeed, mRNA of the ATF4 target gene *ASNS*, encoding an enzyme responsible for aspartate to asparagine conversion that is upregulated upon asparagine shortage, showed a 4-fold increase upon exposure to rotenone and antimycin (Fig. 6G).

To explore similarities between responses to mitochondrial toxicants and amino acid deprivation, we analyzed previously published gene expression data for HepG2 exposure to the histidinyl tRNA synthetase inhibitor (HisOH) [Shan 2010]. HisOH simulates amino acid deprivation and activates a response to amino acid starvation, termed the amino acid response (AAR). HisOH exposure resulted in a similar expression pattern of *ATF4* (up regulation) and *HSPA5*/BIP (down regulation) as observed upon rotenone and antimycin exposure (Fig. 6H). In addition, comparisons of the effect on HepG2 RNA expression assessed using microarrays for HisOH [Shan 2010] and rotenone and antimycin (s1500++; our data), demonstrated strikingly similar directionality with only 7 to 8 genes exhibiting an opposite effect upon exposure (Fig. 6I).

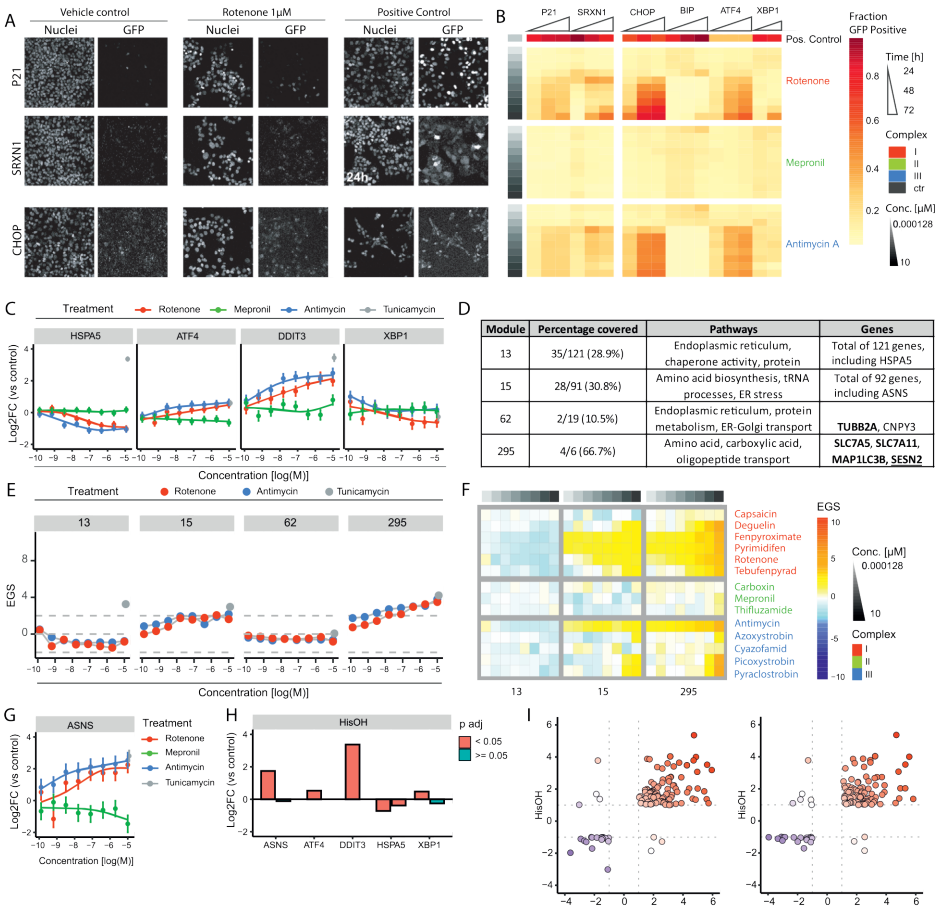


| Module | Percentage covered | Pathways | Genes |
|---|---|---|---|
| 13 | 35/121 (28.9%) | Endoplasmic reticulum, chaperone activity, protein | Total of 121 genes, including HSPA5 |
| 15 | 28/91 (30.8%) | Amino acid biosynthesis, tRNA processes, ER stress | Total of 92 genes, including ASNS |
| 62 | 2/19 (10.5%) | Endoplasmic reticulum, protein metabolism, ER-Golgi transport | **TUBB2A**, CNPY3 |
| 295 | 4/6 (66.7%) | Amino acid, carboxylic acid, oligopeptide transport | **SLC7A5**, **SLC7A11**, **MAP1LC3B**, **SESN2** |

**Figure 6: Effects of various agrochemical MRC inhibitors on cellular stress activation: high content imaging and transcriptomics analysis.**

**A)** Representative pictures of Hoechst and GFP (CHOP-GFP, P21-GFP and SRXN1-GFP) upon 24 or 72 h exposure to the vehicle control, rotenone 1 µM and the positive controls (6 µM tunicamycin of the CHOP-GFP reporter, 25 µM etoposide for the P21-GFP reporter and 0.1 µM DEM for the SRXN1-GFP reporter). **B)** Heatmap of fraction GFP-positive cells for P21-GFP, SRXN1-GFP, CHOP-GFP, BIP-GFP, ATF4-GFP, and XBP1-GFP upon exposure to a concentration range of rotenone, mepronil and antimycin at 24, 48 and 72 h. Positive control compounds included 6 µM tunicamycin of the CHOP-, BIP-, ATF4- and XBP1-GFP reporter, 25 µM etoposide for the P21-GFP reporter and 0.1 µM diethyl maleate (DEM) for the SRXN1-GFP reporter. Cells considered as GFP positive demonstrated an integrated GFP intensity of two times the vehicle control. Values are an mean of 2 or 3 biological replicates. **C)** Concentration response curves of the log2FC ± SE for HSPA5, ATF4, DDIT3 and XBP1 upon exposure to rotenone, mepronil or antimycin. The log2FC value of tunicamycin 6µM is represented as a grey dot. **D)** Table of module 13, 15, 62 and 295 describing: the percentage coverage when projecting the S1500+++ set, pathway enriched pathways of this specific module and the genes measured in that particular module (**bold**: log2FC>0.58 upon exposure to 2 µM rotenone and 10 µM antimycin, <u>underlined</u>: hub gene of this module). The modules were selected based their involvement in the ER stress response [Callegaro 2021]. **E)** Concentration response curves of Eigen Gene Scores (EGS) per selected module upon 24h exposure to rotenone, antimycin or tunicamycin. **F)** Heatmap of 3 modules showing Eigengene Scores (EGS) upon 24 h exposure to a concentration range of 14 complex inhibitors. The modules were selected based on being upregulated in both the CI and CIII correlation plot (Suppl. Fig 6A) or being identified as ER module by Callegaro *et al* [Callegaro 2021]. **G)** Concentration response curves of the log2FC ± SE for ASNS upon exposure to rotenone, mepronil or antimycin. The log2FC value of tunicamycin 6 µM is represented as a grey dot. **H)** log2FC for ASNS, ATF4, DDIT3, HSPA5, XBP1 upon exposure to 5 mM HisOH for 4 h [Shan 2010]. Multiple bars per gene represent single microarray probes. **I)** Correlation plots of HepG2 cells exposed to 5 mM HisOH for 4 h [Shan 2010] and non-toxic concentration of rotenone (2 µM) or antimycin A (10 µM) for 24h. Genes are included with a log2F <-0.58 or > 0.58 and a p-adjusted value below 0.05.

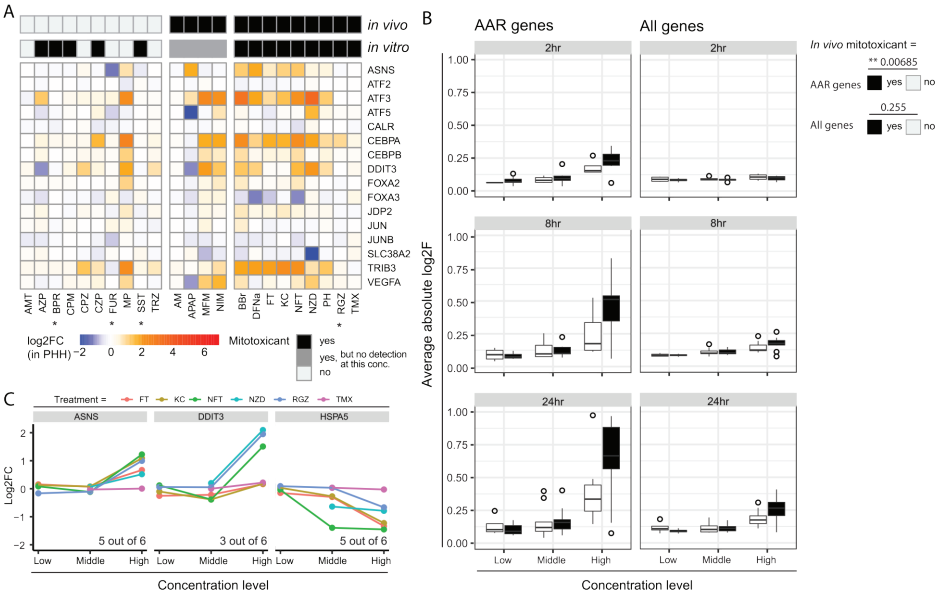


**Figure 7: Extrapolation of electron transport chain (ETC) inhibitor markers to PHH**
**A)** Heatmap of 16 genes involved in the amino acid response [Shan 2010]. The presented values are the log2FC values from the TG-GATES database for the selected genes set upon 24h exposure to highest concentration available for DILI-compounds classified by Eakins 2016 (table 2) (* = exceptions are with middle concentration, because highest concentration was more than 100-fold the cMax value). **B)** Boxplot of the average of the absolute log2FC values of AAR related genes versus "all genes" for all DILI compounds with- versus without *in vivo* mitotoxicant activity at 2, 8 and 24 h exposure to the low, middle, and high concentration. P values were obtained using a generalized linear model of the average abs log2F addressing the following variables: yes/no in vivo mitochondrial toxicant; concentration; time. **C)** Log2FC data from the TG-GATES database for ASNS, DDIT3 and HSPA5 in PHH upon 24h exposure to 3 concentrations of DILI-inducing compounds known to also effect the ETC (table 2).

Lastly, to further evaluate the AAR in the context of mitotoxicants in PHH, expression of genes previously shown to be involved in AAR [Shan 2010] was evaluated in the TG-GATES PHH data for DILI compounds previously assessed for mitochondrial perturbing potential (Table 2, Fig. 7A) [Eakins 2016]. A large proportion of DILI compounds with confirmed *in vivo* and *in vitro* mitotoxic activity affected several of the AAR-related genes. On the other hand, most DILI compounds lacking *in vivo* mitotoxic activity (some of which had also been associated with *in vitro* mitotoxicity) did not affect AAR-related genes. Methapyrilene was a noticeable exception in this group, affecting ~half of the AAR-related genes. Generalized linear regression modeling showed time- and concentration dependent increase in the absolute log2FC for "AAR genes" (time, p=3.74e-05; concentration, p=3.88e-16) and "all genes" (time, p=1.92e-07; concentration, p=5.64e-14) for confirmed *in vivo* mitotoxicitants and non-mitotoxicants. However, whilst the average of the absolute log2FC of the AAR gene set was significantly higher (p=0.00685) for *in vivo* mitotoxicants as compared to the other chemicals at 2, 8, and 24h exposure (Fig 7B; AAR genes) no difference between *in vivo* mitotoxicants and other chemicals was observed for "all genes" in the microarray (Fig 7B; All genes). This suggested that the AAR represents an early response to mitotoxic insults for DILI

compounds in both HepG2 and PHH. In agreement, exposure to ETC inhibiting DILI compounds in most cases affected the expression of genes at the bifurcation between UPR and AAR (*ASNS*, *DDIT3*/CHOP and *HSPA5*/BIP) with similar directionality in PHH as observed upon mitotoxicant exposure in HepG2, further corroborating an AAR in response to ETC inhibition (Fig 7C).

Together, these findings, indicate that active ETC inhibitors trigger cellular signaling pathways including those involved in the evolutionary conserved response to amino acid starvation, AAR. This response appears to be shared between HepG2 and PHH.

## Discussion

In this study we have systematically assessed the perturbation of mitochondrial functioning by a diverse set of agrochemicals that target the electron transport chain (ETC) CI, CII and CIII and its subsequent cellular consequences. Our results indicate that CI inhibiting agrochemicals are most potent as mitotoxicants, followed by CIII inhibitors, while C II inhibitors hardly have any effect. High throughput transcriptomics approaches were identified to be at least as sensitive as mitochondrial integrity and OCR measurements to define biological perturbations by ETC inhibitors. The observed transcriptional alterations demonstrated ETC inhibition related effects rather than complex inhibitor specific effects. Our data indicate that integration of high content imaging approaches and high throughput transcriptomics technology is a powerful approach to provide mechanistic weight-of-evidence to support hazard evaluation of mitochondrial toxicants for full safety assessment.

The majority of studies assessing mitochondrial perturbation in high throughput focus on a few early time points using direct mitochondrial related endpoints to identify potential mitochondrial toxicants [Shah 2016, Wills 2015, Hallinger 2020, Xia 2018, Attene-Ramos 2015]. In contrast, we studied a combination of dynamic imaging-based measurements of mitochondrial functioning and cellular stress signaling responses to unravel the relationship between mitochondrial perturbation and cellular toxicity. By employing a high-content live cell imaging set-up, the temporal dynamics of mitochondrial perturbation were determined by measuring MMP. Assessment of the MMP dynamics upon exposure to a set of mitochondrial ETC inhibitors demonstrated an early onset of concentration-dependent MMP depletion for most CI and CIII inhibitors, delayed perturbation after hydra-methylnon exposure and no/minimal MMP disruption for the CII inhibitors. This indicates direct interaction for most CI and CIII inhibitors and indirect targeting of the mitochondria for hydra-methylnon. Evaluation of the estimated decay time and maximal MMP reduction did not lead to a clear separation of CI and CIII inhibitors. Nevertheless, these parameters can be used to study correlations to other chemical properties, as was demonstrated by the

positive correlation to the logP value. Altogether, these findings illustrate added value of using image-based temporal measurements of mitochondrial functioning to assess mitochondrial perturbation.

The cellular outcome after mitochondrial perturbation depends not only on the strength of the perturbation, but also on the cellular capacity to adapt to this (partial) loss of mitochondrial function. For this purpose, the imaging-based assessment of mitochondrial perturbation was combined with a transcriptomic readout focusing on a broad set of toxicology-related transcripts [Waldmann 2014, Limonciel 2018]. Exposure to both CI and CIII inhibitors triggered major and nearly identical changes in this set of transcripts in a concentration-dependent manner, indicating a generic response upon ETC inhibition instead of complex specific responses. Previous studies have shown that mitochondrial-targeting chemicals can be clustered based on expression profiles of mRNA subsets [Pearson 2016, Simon 2019]. Our broad set of transcripts was used to study the classification of specific and potent CI and CIII inhibitors based on cellular responses upon mitochondrial perturbation. This led to the identification of an ETC inhibition specific gene set that included *CYP3A5, KLHL24, NOS3, PFKP, CDC6, DDC*, and *MPC2*. We verified that these genes were not affected by chemicals well known to induce stress responses, other than ETC inhibition related responses, including DNA damage, reactive oxygen species, unfolded proteins and inflammation. Moreover, the BMC for the onset of gene expression changes was overall lower than the BMC for MMP depletion or OCR decrease. For *CYP3A5, CDC6* and *DDC* no direct link to mitochondrial perturbation has been reported so far. On the other hand, downregulation of *PFKP,* involved in glycolysis, has been reported to result in decreased cellular viability when combined with mitochondrial toxicants [To 2019]. *KLHL24* and *NOS3* are involved in fatty acid metabolism[16] and mitochondria biogenesis, respectively [Nisoli 2006, Nisoli 2004]. Inhibition of *MCP2*, a mitochondrial pyruvate transporter, is reported to result in upregulation of aerobic glycolysis [Li 2017, Schell 2014]. We anticipate that the genes in the ETC inhibition specific set are part of an adaptive response where cells switch from oxidative phosphorylation to glycolysis, increase their fatty acid metabolism and support the production of new mitochondria. Indeed, in particular NOS3 depletion increased the susceptibility of the HepG2 cells to CI inhibition. This gene set may serve as a biomarker panel to flag chemicals and drugs with ETC perturbing potential in early phase high throughput screening using HepG2. However, although regulation by mitotoxicants of this set is confirmed in PHHs, these genes are also sensitive to non-mitotoxicants in this system and can therefore not support mechanistic studies towards the mode of action of various chemicals in PHHs.

Translation of gene expression markers amongst various in vitro models has been proven to be difficult for various liver models [Boess 2003]. Nonetheless, we assume that changes in the expression of groups of genes related to the mode of action of toxicants can be detected across multiple models. The secondary adaptation response will differ depending on the nature of the model being primary material or cell line, including for example the glycolytic capacity of the model in case of mitochondrial toxicants. Toxicity assessment in a tiered testing strategy may start with simple models for larger scale screening to flag toxicants based on model specific markers. Subsequent steps may use HepG2 having a more mitochondria dependent phenotype and enhanced metabolic activity [van der Stel 2020, Hiemstra 2019, Ramaiahgari 2014, Boon 2020] by using 3D cell cultures or improved medium or the use of HepaRG cells having higher levels of metabolism [Gerets 2012].

To gain more quantitative insights into cellular signaling triggered by ETC inhibition and to increase the possibility for translation across *in vitro* models, enrichment of pathways and gene networks was explored. Interestingly, for both CI and CIII inhibitors, the mRNA expression changed for components of the cellular response associated with amino acid deprivation and related responses (AAR) [Krall 2021, Ye 2010, Shan 2010]. Analysis of HepG2 BAC HSPA5/BIP-GFP, ATF4-GFP and CHOP/DDIT3-GFP reporters confirmed the observed mRNA expression changes at the protein level. In addition, the gene encoding an aspartate conversion enzyme that is controlled by the ATF4 transcription factor in the AAR, *ASNS*, is induced after ETC CI or CIII inhibition. Pathway analysis showed, as expected for amino acid deprivation, significant changes in the cell cycle, which was in line with the attenuation of proliferation detected by high-content imaging. To strengthen the evidence concerning amino acid deprivation and to support identification of additional ETC inhibition induced biology, PHH-specific weighted co-regulated gene networks were used, allowing the study of cellular adaptation outside the known biological context [Callegaro 2021, Sutherland 2018]. The projection of our HepG2 transcription data on this PHH network identified co-regulated gene modules that were affected by mitochondrial ETC perturbation. GO-terms related to these modules, as anticipated, included metabolism, oxidative stress responses and mitochondrial trafficking. In addition, assessment of endoplasmic reticulum (ER) stress enriched modules, specifically describing amino acid processes, corroborate the disturbance of protein homeostasis in those cells as well. Moreover, we find that genes known to be involved in the AAR, in general are also affected in PHH upon exposure to DILI compounds with mitochondrial liability *in vivo*. This indicates that AAR may represent a conserved response to ETC inhibition. This observed metabolic adaptation has also been observed in neurons upon mitochondrial toxicity caused by exposure to MMP+ or by mutations in *PINK1* and *PARKIN* [Krug 2014,

Celardo 2017]. In addition, ATF4 and CHOP signaling without a clear UPR response has been observed in the context of muscle disorder [Kaspar 2021]. Notably, the AAR is also linked to the "integrated stress response", that restores balance after amino acid starvation and other types of cellular stress and involves ATF4 [Costa-Mattioli 2020].

Using the ETC inhibitors we aimed to identify mitochondrial specific markers. The identification of ETC inhibition relevant genes and pathways upon exposure to various drug-induced liver injury (DILI) compounds indicate the important role of mitochondria in the occurrence of DILI. In this study only mitochondrial ETC inhibitors for transcriptomics analysis have been used, hence an extension of the chemical set is required to evaluate whether other chemicals, targeting mitochondrial citric acid cycle metabolism, ion homeostasis, mitochondrial coupling or mitophagy, induce a similar generic mitochondrial stress response. Transcriptomic profiling supports besides mitochondrial toxicity marker identification also chemical read across. The two rotenoid CI inhibitors in this study, deguelin and rotenone, exemplify a transcriptomics-based read across approach. Gene co-regulation analysis can strengthen chemical read across by clustering based on similar module activity, which is less dependent on the expression level of single genes [Joseph 2017, Serra 2020]. Furthermore, the overall change in the transcript profiles demonstrates differences in potency between the two rotenoids and the overlap in pathway enrichment, transcription factor activation and gene network module regulation, underlining the similarities in the ETC inhibitor mode of action. To allow the integration of mode of action information and, with that, the identification of mitochondrial perturbation as primary or secondary event in any form of organ toxicity, it is important to enlarge the range of time points used to identify markers or to perform a biologically driven read across.

To summarize, the mechanisms underlying chemical-induced mitochondrial perturbation and cellular signaling were studied using high content imaging and targeted transcriptomics. Both technologies are demonstrated to be suitable to qualify and quantify the effects of ETC inhibitors on mitochondrial and cellular signaling dynamics. By employing pathway and gene network analyses evidence is provided for a response to ETC inhibition that involves the AAR. We envision a tiered testing strategy where high content imaging would identify mitochondrial perturbing chemicals, followed by targeted transcriptomic analysis which identifies subsequent cellular outcomes. Such an approach can provide mechanistic weight-of-evidence to support hazard evaluation of mitochondrial toxicants.

**Funding**
This project has received funding from the European Union's Horizon 2020 research and innovation programme under grant agreement No 681002 (EU-ToxRisk) and the Innovative Medicine Initiative eTRANSAFE project (grant number 777365).

**Conflicts of interest**
The authors declare that they have no conflict of interest.

**Authors' contribution**
WS performed the high content imaging with support of SELD. WS and SD performed the viability and ATP assays. HY performed the phenomenological modeling under supervision of JB. NV and JS collected the TempO-Seq samples. GCal provided support in the assessment of the TGGATES database and performance of the WGCNA analysis. WS analyzed the high content and TempO-Seq data. WS, AF, AW, ML, PJ, BvdW and ED designed the research project and together with GCar and JD supported in the interpretation of the results. The first draft of the manuscript was written by WS and all authors commented on subsequent versions of the manuscript. All authors read and approved the final version of the paper.

# Supplementary material

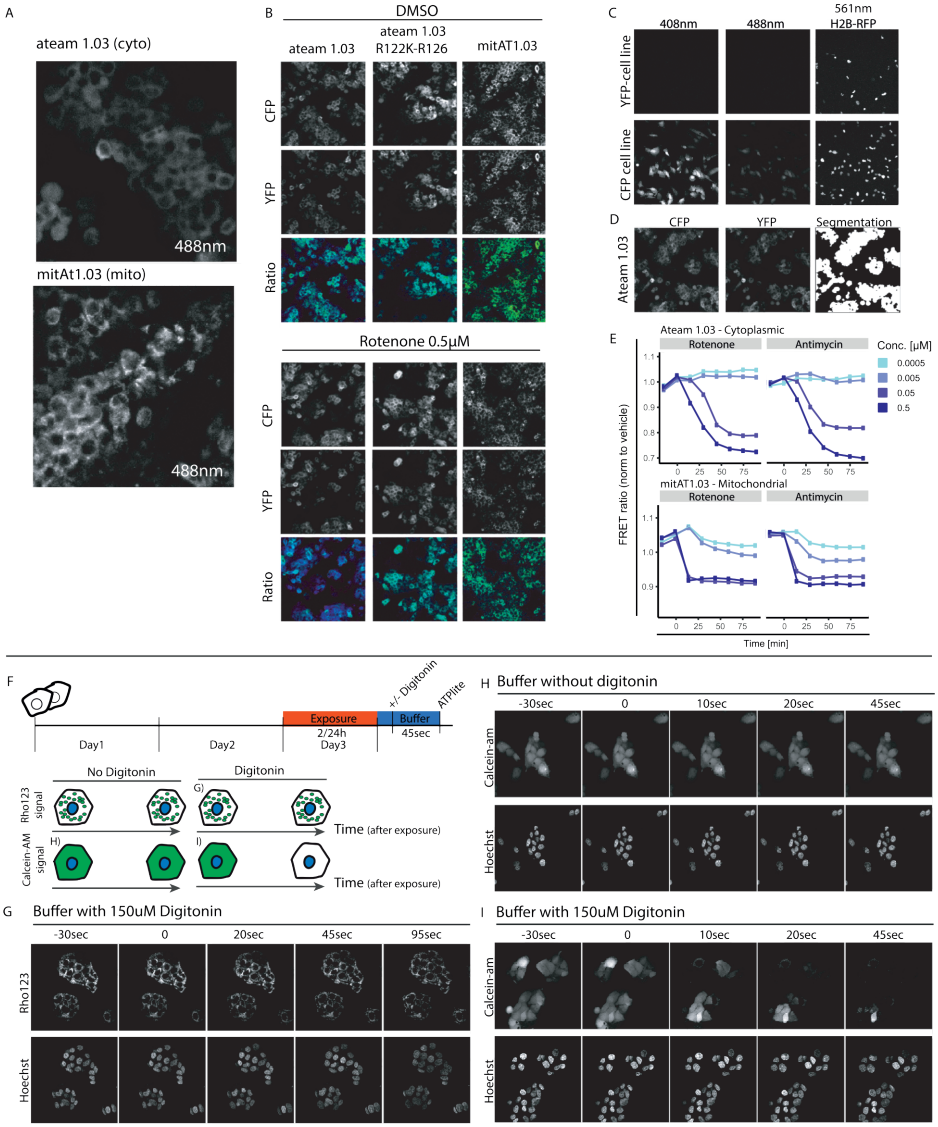


**Supplementary figure 1: Generation and characterization of cytosolic and mitochondrial ATP-biosensors in HepG2 cells.**

**A)** Representative pictures to demonstrate cytoplasmic and mitochondrial localization of respectively ateam1.03 and mitAt1.03. **B)** Representative pictures of the ATP-biosensor in the cytoplasm (normal and mutated) and mitochondria upon 2 h exposure to vehicle control or 0.5 µM rotenone. **C)** Representative images of the Hs578T cell line containing CFP and YFP fluorophores used to adjust imaging settings. **D)** Representative pictures of ATP-biosensor in HepG2 the cytoplasm plus example Ilastik segmentation of the area used for signal quantification. **E)** Quantification of 2$^{nd}$ replicate of the ateam1.03 (cytoplasmic) and mitAt1.03 (mitochondrial) upon exposure to 4 concentrations of rotenone or antimycin. **F)** Representation of the exposure schedule for the ATPlite assay including cell membrane lyses step. Plus schematic representation of change in signal of Rho123 or calcein-AM upon addition of digitonin **G)** Representative pictures of the Rho123 signal upon addition of 150 µM digitonin (digitonin addition at 0 sec). **H)** Representative pictures of the calcein-AM signal upon addition of only buffer (buffer addition at 0 sec). **I)** Representative pictures of the calcein-AM signal upon addition of 150 µM digitonin (digitonin addition at 0 sec).

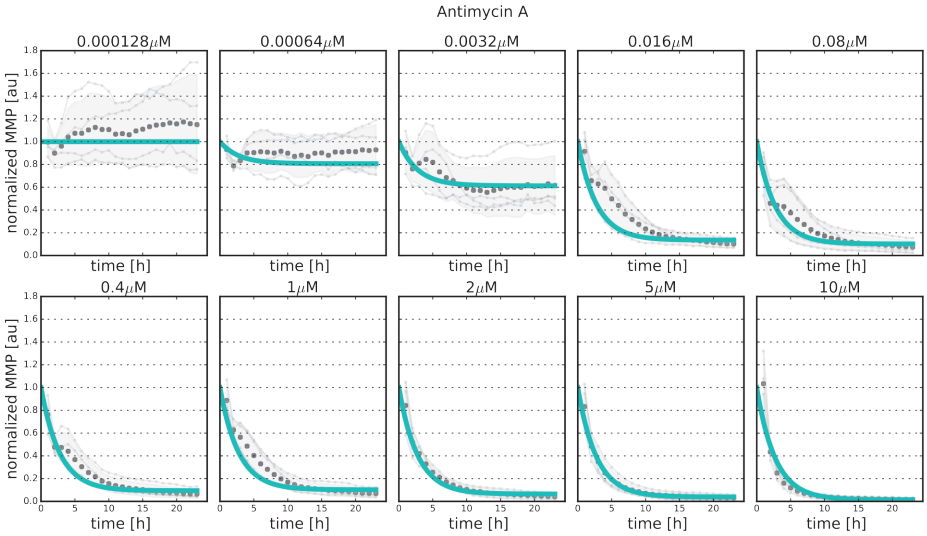


**Supplementary figure 2: Phenomological model fit of mitochondrial membrane potential dynamics**
Representative fit of the Rho123 intensity over time upon exposure to 10 concentrations of antimycin A using the phenomological model. Light grey lines represent data of individual biological replicates, dotted line represents the mean of the 4 biological replicates and the cyan line represents the fitted data.

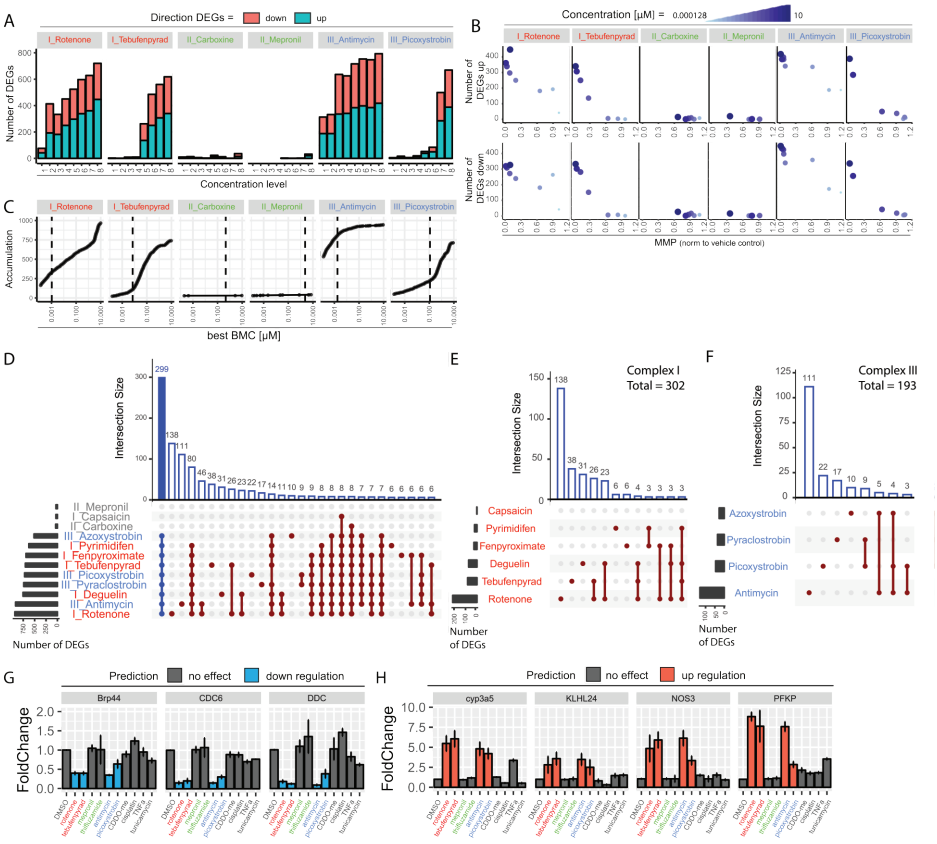


**Supplementary figure 3: Predictive gene expression profiles for MRC inhibition.**
**A)** Concentration response curve of number of DEGs up or down regulated at 24h exposure per treatment. DEGs are considered when padj < 0.05, log2FC > or < 0.58 and the p-values of the Williams trend test < 0.05. Samples were exposed to a concentration range of rotenone, tebufenpyrad, carboxin, mepronil, antimycin or picoxystrobin (concentration range from 0.000128 µM to 10 µM, with steps of factor 5). **B)** Correlation plot comparing MMP to number of DEGs after 24h exposure to a concentration range of rotenone, tebufenpyrad, carboxin, mepronil, antimycin or picoxystrobin (concentration range from 0.000128 µM-10 µM). Values are geometric (MMP) or mean (count) of 4 biological replicates. **C)** Accumulation curves of best BMD values at 24h exposure to rotenone, tebufenpyrad, carboxin, mepronil, antimycin or picoxystrobin calculated per probe using the BMDexpress software. Probes were considered when the p-value of the William trend test < 0.05 (dotted line represents the BMD value of the MMP readout at 24 h). **D)** Plot based on all the gene expression data of all mitochondrial complex inhibitors and separating all genes per individual treatment. Horizontal bars at the left represent the total number of DEGs per treatment which meet the filtering criteria. The vertical bars representing the various group of probes only include groups of more than 6 genes. Blue vertical bar represents the groups of genes affected by all active ETC inhibitors. Grey compound names represent the inactive ETC inhibitors**. E)** Subset of 302 probes from Fig. 6C separated per CI inhibitor. The plot only represents groups of more than 3 genes. **F)** Subset of 193 probes from figure 6C separated per CIII inhibitor. The plot only represents groups of more than 3 genes. **G and H)** Validation using real time PCR of 3 down **(G)** and 4 up **(H)** regulated hits upon exposure to vehicle control, 6 complex inhibitors (2 µM) and the positive adaptive stress response controls (60 nM CDDO-me, 1 mg/ml cisplatin, 10 ng/mL TNFα and 12 µM tunicamycin). Data is represented as mean of 3 biological replicates ± SD.

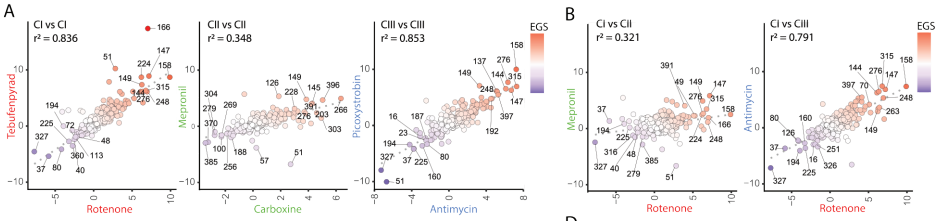


C

| Module | Percentage covered | Pathways | Genes |
|---|---|---|---|
| 144 | 5/11 (45.5%) | oxidative stress | **GCLM**, **TXNRD1, GPAT3, SRXN1,** DCX |
| 147 | 6/11 (54.5%) | Protein metabolism, Insulin signaling | **NRP1**, **SPP1**, NAMPT, **IGF1**, RAB27A, NNMT |
| 149 | 3/10 (30%) | Metabolism, mitochondrial trafficking | **IGFBP1**, **TOMM34**, **S100A16** |
| 158 | 6/10 (60%) | MAPK signaling | **DUSP1**, **KLF6, CYR61**, **MYC, JUN,** TIPARP |
| 248 | 4/7 (57.1%) | Signal transduction, metabolism | **AHR**, **NR3C1,CBLB**, **FZD5** |
| 276 | 3/7 (42.9%) | Signaling (JNK, lipophilic components) | **LRP10, FNDC4**, DUSP22 |
| 315 | 1/6 (16.7%) | Vesicle transport | **CLTB** |

D

| ETC inhibitor | Abb. | Complex | MMP BMD [µM] | Selected conc [µM] | Highest non-toxic conc [µM] |
|---|---|---|---|---|---|
| Capsaicin | CAP | I | NA | 10 | 10 |
| Deguelin | DEG | I | 0.04758 | 0.016 | 10 |
| Fenpyroximate | FPX | I | 0.00067 | 0.0032 | 10 |
| Pyrmidifen | PMD | I | 0.00028 | 0.00064 | 10 |
| Rotenone | ROT | I | 0.00106 | 0.0032 | 2 |
| Tebufenpyrad | TEB | I | 0.00704 | 0.016 | 10 |
| Carboxine | CAR | II | 0.46302 | 2 | 10 |
| Mepronil | MEP | II | 2.33739 | 10 | 10 |
| Thifluzamide | THI | II | 1.76686 | 2 | 10 |
| Antimycin A | AA | III | 0.00177 | 0.0032 | 10 |
| Azoxystrobin | AZO | III | 0.44700 | 2 | 10 |
| Cyazofamid | CYA | III | 4.82265 | 10 | 10 |
| Picoxystrobin | PIC | III | 0.11466 | 0.4 | 10 |
| Pyraclostrobin | PYR | III | 0.20586 | 0.4 | 10 |

**Supplementary figure 4: Gene network activation by MRC inhibitors based on human hepatocyte WGCNA datasets.**

**A)** Correlation plot of the EGS per module comparing upon exposure to a non-toxic concentration (10 µM, except for rotenone it is 2 µM) of 2 representative chemicals of CI, CII or CIII inhibitor. The top modules up and down regulated per correlation are labeled **B)** Correlation plot of the EGS per module comparing upon exposure to a non-toxic concentration (10 µM, except for rotenone it is 2 µM) of rotenone (CI) to mepronil (CII) or antimycin (CIII). The top modules up and down regulated per correlation are labeled. **C)** Table of module 144, 147, 149, 158, 248, 276 and 315 describing: the percentage coverage when projecting the S1500+++ set, pathway enriched pathways of this specific module and the genes measured in that particular module (**bold**: log2FC>0.58 upon exposure to 2 µM rotenone and 10 µM antimycin, underlined: hub gene of this module).**D)** Table depicting the concentration selected in the heatmaps represented in figure 4D and E. Asterisk denotes the chemicals with high BMD values for MMP perturbation.

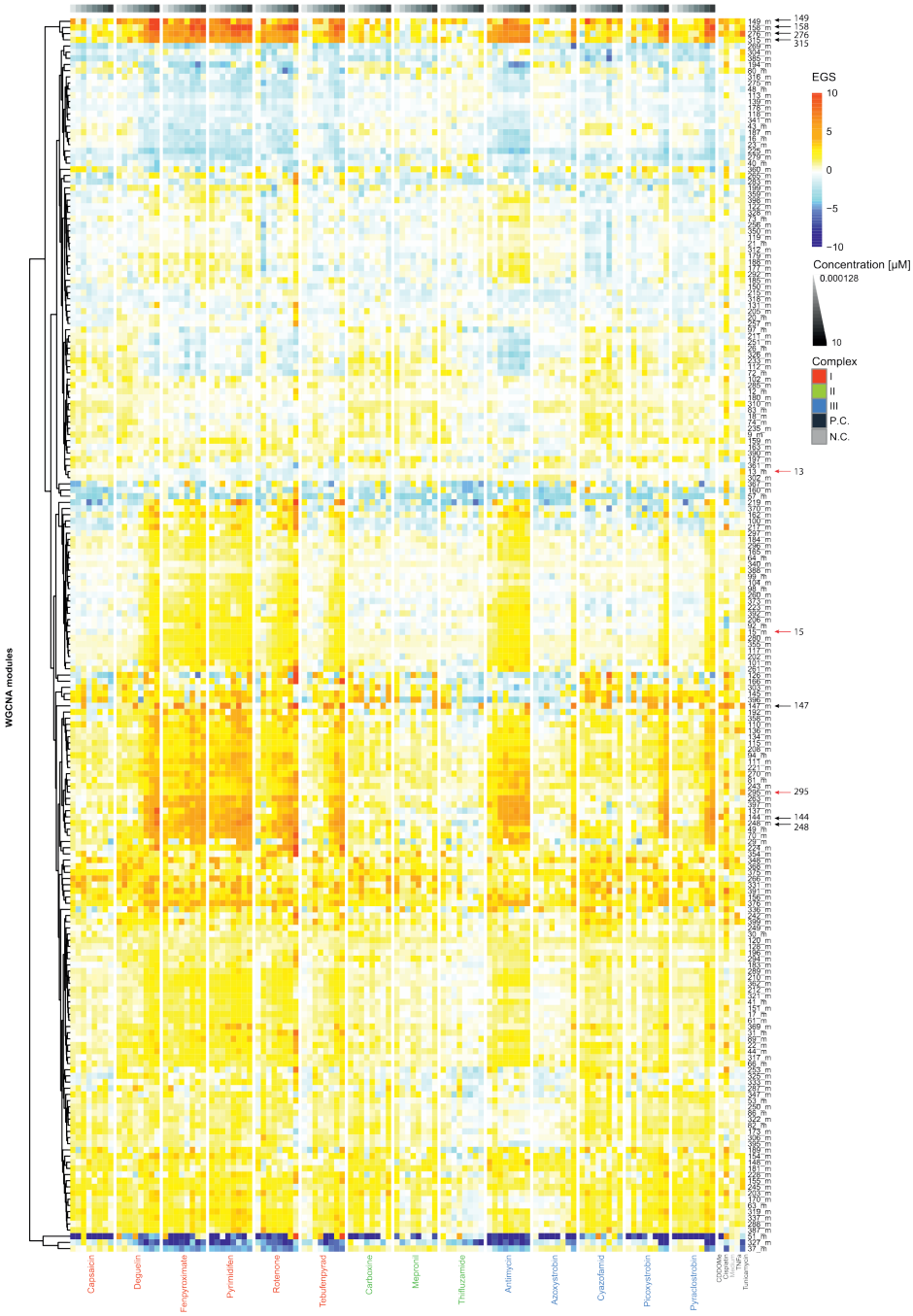


**Supplementary figure 5: Gene network activation by MRC inhibitors based on human hepatocyte WGCNA datasets.**

A clustered heatmap (Pearson correlation) of WGCNA module showing Eigen Gene Scores (EGS) upon 24h exposure to concentration range of 14 complex inhibitors and 4 positive controls (60nM CDDO-me, 1mg/ml cisplatin, 10ng/mL TNFα and 12µM tunicamycin). The included modules do have an EGS of at least 2 in one of the conditions.

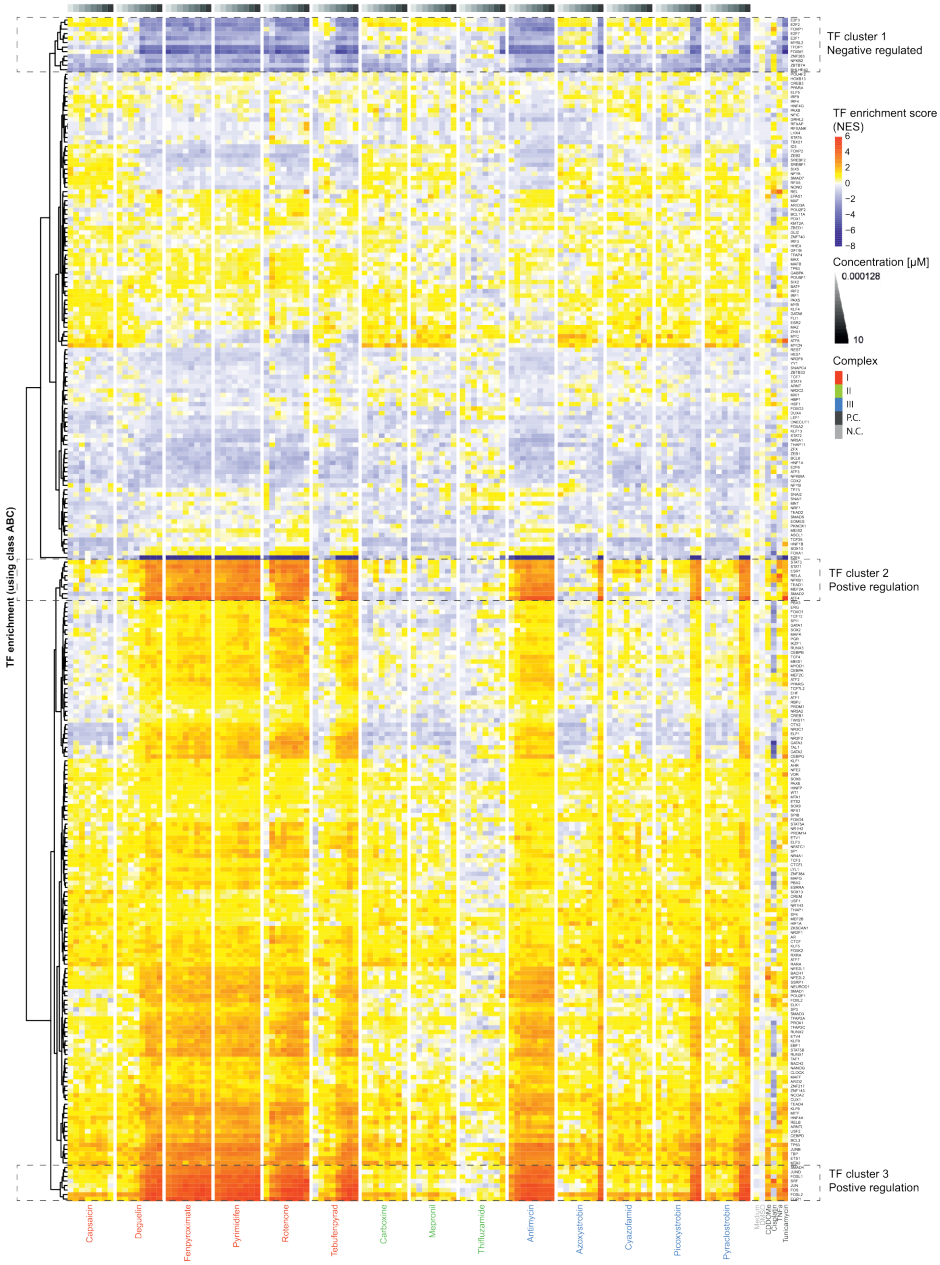


**Supplementary figure 6: Transcriptional reprogramming after treatment with agrochemical MRC inhibitors.**

A clustered heatmap (based on Pearson correlation) of a transcription factor enrichment study showing normalized enrichment score (NES) upon 24h exposure to concentration range of 14 complex inhibitors and 4 positive controls (60 nM CDDO-me, 1 mg/ml cisplatin, 10 ng/mL TNFα and 12 µM tunicamycin). Transcription factor enrichment study was based on the transcription factor fingerprint in the DoRothEA database and using the viper package for the enrichment assessment. The used confidence parameter in the DoRothEA data set was ABC.

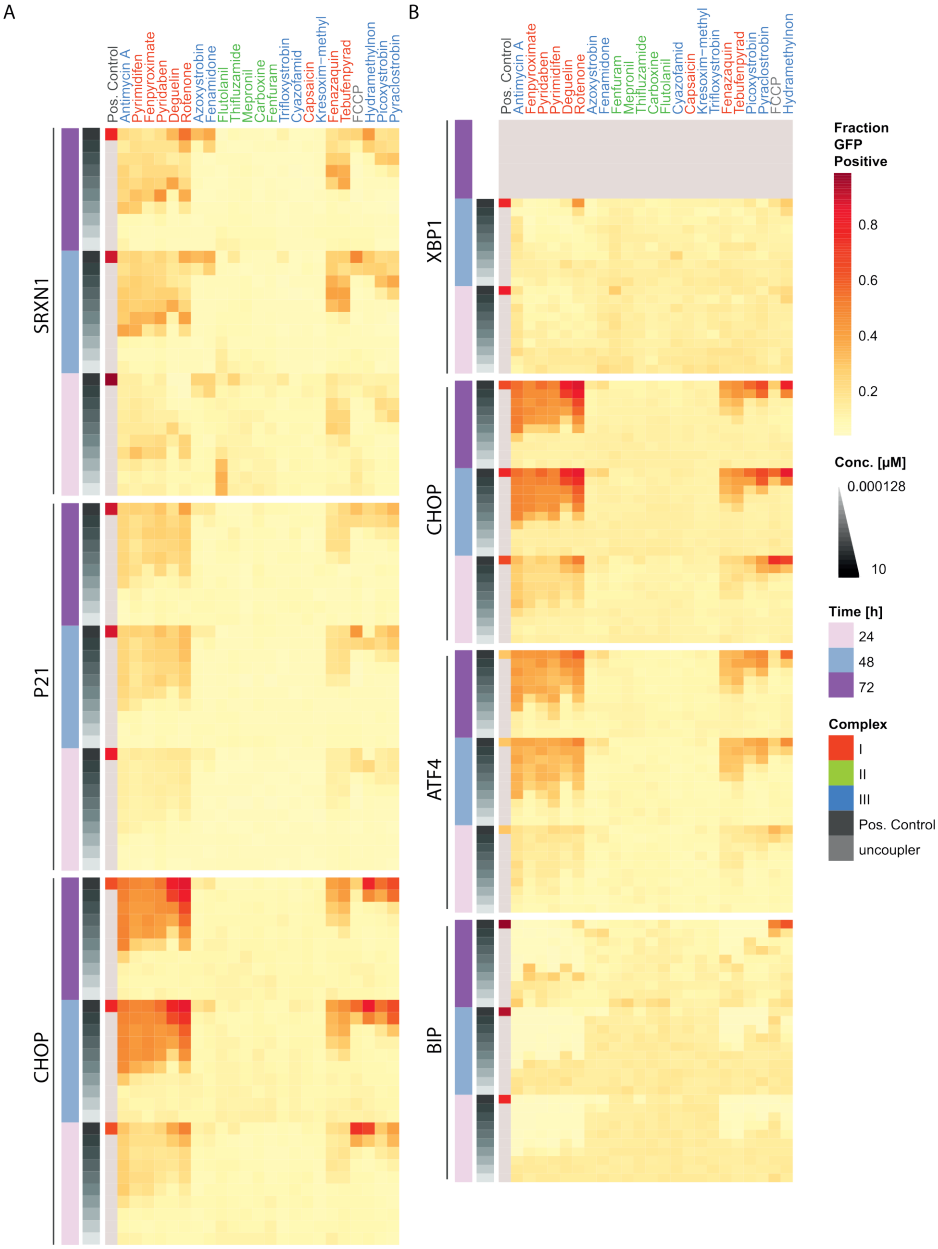


**Supplementary figure 7: Effects of various agrochemical MRC inhibitors on cellular stress response reporter activation.**

**A)** Heatmap of fraction GFP-positive cells for CHOP-GFP, P21-GFP and SRXN1-GFP upon exposure to a concentration range of 22 mitochondrial complex inhibitors at 24, 48 and 72 h. Positive control compounds included 6 µM tunicamycin of the CHOP-GFP reporter, 25 µM etoposide for the P21-GFP reporter and 0.1 µM DEM for the SRXN1-GFP reporter. Cells considered as GFP positive demonstrated an integrated GFP-intensity of two times the vehicle control. Values are a mean of 2 or 3 biological replicates. **B)** Heatmap of fraction GFP-positive cells for BIP-GFP, ATF4-GFP, CHOP-GFP and XBP1-GFP upon exposure to a concentration range of 22 mitochondrial complex inhibitors at 24, 48 and 72 h. Positive control compounds included 6 µM tunicamycin. Cells considered as GFP positive demonstrated an integrated GFP-intensity of two times the vehicle control. Values are a mean of 2 or 3 biological replicates.

**Supplementary table 1: ATP biosensor, CFP and YFP constructs**
Table depicting the plasmids used to create the ATP biosensor and the two constructs used for microscopy calibration.

| Plasmid | Origin | Localization |
|---|---|---|
| pcDNA-ateam1.03 | Gift Imamura | Cytosol |
| pcDNA-mitAT1.03 (pcDNA-CoxVIII2-AT1.03) | Gift Imamura | Mitochondria |
| pcDNA-Ateam 1.03 R122K-R126K | Gift Imamura | Cytosol |
| pECFP-C1 | Clonetech | Cytosol |
| pEYFP-C1 | Clonetech | Cytosol |

**Supplementary table 2: TempO-Seq Probe list**
Table depicting all probes in the S1500++ with information concerning the related gene name, EnsemblID, and if they were in the original S1500 [Mav 2018]. Available in online version of published manuscript.

**Supplementary table 3: RT-qPCR primers**
Table depicting the forward and reverse primers used for validation of the HepG2 ETC fingerprint with RT-qPCR.

| Gene symbol | Forward (F)/ Reverse (R) | Sequence |
|---|---|---|
| Brp44/MPC2 | F | CTACAGGGTTTATTTGGTCAAG |
| | R | AATACGAAAAAGCTGAGAGG |
| CDC6 | F | ATGTAAATCACCTTCTGAGC |
| | R | GTCATCCTGTTACCATCAAC |
| Cyp3a5 | F | CTCCTCTATCTATATGGGACC |
| | R | ATACGTTCCCCACATTTTTC |
| DDC | F | GCTGCAGGAATCAAAAATTG |
| | R | CAACCCTCTGGATAACTTTG |
| KLHL24 | F | AAAGTATATGTTGTCGGTGG |
| | R | AGTATTATCATCAGGTCCTCC |
| NOS3 | F | CATCACCTATGACACCCTC |
| | R | AGCCGCTCCTCTTAATG |
| PFPK | F | ATTTGTGTGCTGGGAATAAG |
| | R | GGAATCCTGTGCTCAAAATC |

# 5

# Mitochondrial fragmentation through OPA1-cleavage in response to ETC inhibition is driven by a combination of reduced ATP and increased MMP

Wanda van der Stel, Huan Yang, Sylvia le Dévédec, Bob van de Water, Joost Beltman, Erik H.J Danen#

*Submitted to Cell. Bio. Toxicol*

**Cells can adjust their mitochondrial morphology by altering the balance between mitochondrial fission and fusion to adapt to stressful conditions. Mitochondria can fuse together upon energy shortage, to enlarge their ATP producing capacity, or they can fragment, to facilitate mitochondrial transport or mitophagy. Such phenotypical alterations could serve as a biomarker for the changes in the underlying mitochondrial processes in the context of chemical-induced toxicity. However, the connection between a chemical perturbation, changes in mitochondrial function, and altered mitochondrial morphology is not well understood. Here, we systematically assessed the effects of distinct classes of electron transport chain (ETC) perturbing agents on mitochondrial membrane potential (MMP), ATP production, mitochondrial morphology, and cell viability using a combination of experimental and computational approaches. Mitochondrial morphology phenotypes were clustered based on high content confocal imaging data and machine learning algorithms and mitochondrial integrity patterns were mapped including temporal and spatial resolutions. Changes in MMP and viability were assessed by imaging and mitochondrial and cellular ATP levels were measured biochemically and using FRET biosensors, and the role of OPA1 post-translational modification as a mechanism connecting functional and morphological adaptation in mitochondria was explored. Our results show that inhibition of mitochondrial ATP production and oxygen consumption rate is insufficient to trigger OPA1 cleavage and mitochondrial fragmentation, whereas the combination of ATP reduction and increase of MMP did provoke a change in mitochondrial morphology. Altogether, our findings connect vital mitochondrial functions and mitochondrial phenotypes that help understanding of cellular toxicity caused by ETC perturbing chemicals.**

**Keywords**: mitochondria, morphology, machine learning, membrane potential, ATP

## Introduction

Mitochondrial malfunctioning plays a role in chemical induced toxicities and various diseases [Pacheu-Grau 2018, Dykens 2007]. Disease-related mitochondrial defects e.g., associated with Parkinson and Alzheimer disease, can be frequently traced back to mutations in genes involved in the major functions of the mitochondria [De Castro 2010, Pacheu-Grau 2018]. Chemical-induced mitochondrial stress stimulates the cell to rearrange its mitochondrial pool and induce adaptive signaling responses in order to cope with reduced cellular functioning [Han 2013]. An inability to recover from the mitochondrial insult, will induce apoptosis and/or necrosis to sacrifice the injured cell. Prolonged stress causing excessive cell death, will result in organ failure [Bock 2009]. Unraveling the concentration- and time-resolved relationships between mitochondrial perturbation and toxicity will provide useful information for chemical safety prediction and provide insight in adaptive and toxic responses to mitochondrial stress.

The type of chemical-insult dictates the type of cellular-mitochondrial responses. Chemicals may directly target key mitochondrial proteins such as electron transport chain (ETC) components or cause cellular stress leading indirectly to damaged mitochondria. In response, mitochondria can trigger a mitochondrial unfolded protein response (UPRmt) to refold incorrectly assembled proteins [Münch 2018, Qureshi 2017], activate mitochondrial biogenesis to increase size and numbers of mitochondria [Jornayvaz 2010, Hock 2009], adapt mitochondrial morphology and remodel ETC to increase oxidative phosphorylation (OXPHOS) capacity [Westermann 2010, Youle 2012], and initiate mitophagy to dispose of malfunctioning mitochondria [Youle 2011, Hamacher-Brady 2016]. The specificity of these mitochondrial responses for certain types of stress could be used to understand and predict the type of chemical-induced perturbation.



Among the mitochondrial responses, morphological remodeling is one of the fastest and most flexible adaptation programs. Even under healthy conditions mitochondria are highly dynamic organelles that constantly adapt their appearance based on the energy demand in various regions of the cells and facilitate mitophagy to get rid of undesired mitochondria [Westermann 2010, Giacomello 2020]. Different mitochondrial morphologies have been recorded in cell lines upon mitochondrial toxicant exposure, including antimycin, FCCP, oligomycin and rotenone [Leonard 2015, Koopman 2005, Koopman 2006, Miyazono 2018]. These morphologies have been classified as puncta, rods, networks, small/large, etc. The presence of larger mitochondrial networks facilitates energy production, because of the increased interconnected membrane surfaces which can support OXPHOS. The formation of smaller mitochondria increases their mobility supporting energy demand in the outer areas of the cells, but also simplifies degradation when desired [Westermann 2010].

Increasing and decreasing mitochondrial surface is achieved by changing the balance between fission and fusion [Seo 2010]. The machinery responsible for fission and fusion consists of a core group of GTPases: DRP1 is mostly responsible for fission and MFN1, MFN2 and OPA1 are responsible for fusion [Westermann 2010]. Fission is achieved by dephosphorylation and polymerization of DRP1 at ER-mitochondrial sites. Fusion of mitochondria is initiated by the outer membrane protein MFN, which connects the outer membranes of two mitochondria and is subsequently followed by fusion of the inner membranes, which is facilitated by OPA1 [Giacomello 2020]. The exact trigger for the activation of the various fission and fusion related GTPases is not completely understood. Some of the GTPase members are activated via post-translational modification including cleavage and phosphorylation [Cribbs 2007, Jahani-Asl 2007, MacVicar2016]. Under healthy conditions, OPA1 is imported into the mitochondria and cleaved by the mitochondrial processing peptidase (MPP) into a long transmembrane protein (long OPA1/ L-OPA1) which supports the fusion process. Stress may activate two proteases, OMA1 and YME1L, that cleave OPA1 resulting in a shorter non-membrane bound form (short OPA1/ S-OPA1), which does not support fusion. Reported triggers that stimulate OPA1 cleavage and inhibit fusion include decreased ATP levels, a drop in mitochondrial membrane potential (MMP), heat shock, and the loss of mitochondrial DNA [Anand 2014, Baker 2014, Ehses 2009, Head 2009, Consolato 2018].

Here, we addressed whether changes in mitochondrial morphology can be coupled to key aspects of mitochondrial function in the context of chemical-induced toxicities. For this purpose, we systematically assessed the effect of distinct classes of ETC perturbing agents in a time- and concentration-resolved manner. We established high-content imaging methods and computational modeling to categorize mitochondrial morphology and monitor changes in ATP levels and MMP dynamics. This data was combined with an analysis of proteolytic cleavage of OPA1 as a key step in mitochondrial fusion. Lastly, we used gene silencing to address the impact of interfering with morphological adaptation on adaptation to mitochondrial stress. Our findings shed light on the dynamic relation between mitochondrial morphology and function in the context of chemical-induced stress and create the opportunity to use mitochondrial morphology changes as a biomarker for the underlying mitochondrial perturbation.

## Materials and Methods

### Chemicals

All tested chemicals were purchased via Sigma Aldrich (Germany): antimycin A (A8674), cyclosporin A (30024), DCCD (D80002), diafenthiuron (31571), oligomycin (O4876), rotenone (R8875). The larger set of chemicals used to study difference between complex inhibitors was obtained via the JRC (Ispra Italy): capsaicin (Cat.

No. M2028), deguelin (D0817), fenpyroximate (31684), pyrimidifen (35999), rotenone (R8875), tebufenpyrad (46438), carboxin (45371), mepronil (33361), thifluzamide (49792, antimycin A (A8674), azoxystrobin (3167), cyazofamid (33874), picoxystrobin (33568), pyraclostrobin (33696. Stocks were created in dimethyl sulfoxide (DMSO) and stored at -80°C/-30°C until further usage. Exposure medium was created at the day of usage and contained a max of 0.2% (v/v) DMSO.

**Cell culture**

All experiments were performed using HepG2 cells purchased from ATCC (American Type Culture Collection, Wesel, Germany). Cells were maintained in complete medium at 37˚C in a 5% CO2 humidified atmosphere. The complete medium consisted of Dulbecco's modified Eagle's medium (DMEM) (Fisher Scientific, 11504496), supplemented with 10% (v/v) FBS (fetal bovine serum), 25 U/ml penicillin and 25 µg/mL streptomycin (FBS; South American, Fisher Scientific, S181L-500 & PenStrep, Fisher Scientific, 15070-063). For experiments that require inhibition of the glycolysis the medium was extra supplemented with 10mM 2-deoxyglycose (2DG) (Sigma-Aldrich, D8375-5G) at the moment of exposure.



**Creation of HepG2 cell lines containing OPA-GFP or ATP-biosensors**

OPA1 fused to GFP was introduced in HepG2 cells using the BAC technology previously optimized in our lab [Wink 2017, Poser 2008]. HepG2 cells containing ATP-biosensors located in the mitochondria or cytoplasm were created using constructs kindly provided by Hiromi Imamura (Precursory Research for Embryonic Science, Japan Science and Technology Agency) [Imamura 2009]. Both for the BAC-GFP and the ATP biosensors constructs, 8ug DNA was introduced using lipofectamine2000 (Fisher Scientific, 11668-027) into 2.000.000 HepG2 cells. Cells were kept on G418 (PAA/Brunschwig chemie, P31-011) selection starting with 0.25mg/ml until confluency followed by 0.5mg/ml until colony formation. Confocal imaging was used to quickly select for GFP positive colonies (both for the OPA1-GFP and the ATP biosensor cell lines). The used OPA1-GFP clone was selected based on protein size in western blot. The used ATP biosensor was selected based on a homogenous expression.

**siRNA transfection**

siRNAs targeting OPA1 (SMARTpool of 4 single siRNAs = MQ-005273-00-0002, siRNA1 = D-005273-01, siRNA2 = D-005273-02, siRNA3 = D-005273-03, siRNA4 = D-005273-04) were purchased from Dharmacon (US). Reverse transfections were performed in 24-wells plates (Costar, 3524) or 96-well screenstar black plate (Greiner Bio-One, 655892, 655866) using 40 or 50nM siRNA and the transfection region INTERFERin (Polyplus, 409-50) in a dilution of 1:1000 or 1:1250. siRNA were

diluted to 1μM in 1x siRNA buffer (Dharmacon, B-002000-UB-100). INTERFERin was diluted 50x in SFM and antibiotic free medium. Upon 5 minutes incubation at RT both solutions were mixed in a 1:3 (siRNA/INTERFERIN) ratio and incubated for 20-30min at RT. Cell mixtures of 476,191 cells/well (24-well) or 23,000 cells/well (96-well) in medium containing FBS and antibiotics were mixed in a ratio of 6.25:1 or 5:1 to the siRNA-INTFERin mixture, respectively. 24h after transfection the medium was refreshed and 72h after transfection chemical exposure followed by the desired readout were performed. Mock and KP (a mixture of 720 siRNA SMARTpools originating from the siGENOME human protein kinase library) were used as controls.

**Confocal live cell imaging and analysis of MMP**

Effects of chemical exposure on MMP was assessed using Rhodamine123 (Rho123) (sigma Aldrich, R8004) using the protocol described previously [van der Stel 2020]. Cells were seeded two days before exposure. At the day of exposure cells were first co-stained with 200ng/μL Hoechst (Life technologies, H1399) and 1μM Rho123 for 75min, followed by a co-staining of 0.2 μM Rho123 and 100nM propidium iodide (PI) (Sigma-Aldrich, P4170) and exposure to the desired concentration of test chemical. Over a period of 24h the signal intensity of Hoechst (408nm), rho123 (448nm) and PI (561nm) were monitored every hour. The nuclei were identified based the Hoechst picture and formed the basis for the assessment of the cytoplasm (n distance around nucleus). Finally, the intensity of the rho123 was assessed in the cytoplasm and the cell death based on the fraction of nuclei that showed co-staining of Hoechst and PI. Part of the MMP data were used for development of a dynamic model and integration with RNA-seq data elsewhere [van der Stel 2021].

**Confocal live cell imaging and analysis of ATP-biosensor**

Effects of chemical exposure upon ATP fluctuations in the cytoplasm and mitochondria of HepG2 cells were assessed using the stabily integrated ATP-biosensor constructs. The experiments were performed as previously described [van der Stel 2020]. Cells were seeded two days before chemical exposure. Imaging was performed every 5minutes starting with two rounds of background measurement, followed by exposures and 2h of imaging. The sensor was exited with the 408nm laser and the FRET ratio was based on the emission at 408 and 488nm. The obtained 408nm images were used to determine the relevant cell area in which the 408 and 488 pixel intensities were determined. Part of the ATP data were integration with RNA-seq data elsewhere [van der Stel 2021].

**Confocal live cell imaging of mitochondrial morphology**

Mitochondrial morphology was monitored using MitoTracker Red CMXRos (cell signaling, 9082) in a life confocal imaging setting. HepG2 cells were seeded with a density of 22.000 cells/well in a 96-wells glass/screenstar black plate (Greiner Bio-One, 655892, 655866). Two days after seeding cells were stained for 60min at 37° C with 200 ng/mL Hoechst 33342 (Life technologies, H1399) and 0.05μM MitoTracker Red. After 60min the medium was replaced with complete DMEM containing 0.013μM MitoTracker Red plus the desired concentration test chemical. The Hoechst and MitoTracker Red signal (respectively 408 and 561nm) were monitored at the desired time points using in total 120x zoom (60x objective plus 2x digital zoom or 40x objective plus 3x zoom) in a Nikon TiE2000 with perfect Focus System and xy-stage (Nikon, Amsterdam, The Netherlands).

**Imaging data analysis for mitochondrial morphology data**

*Nuclei segmentation:* CellProfiler (version 2.1.1 Broad Institute, Cambridge, USA) was used for the identification of nuclear objects. An in-house implemented segmentation module [Di 2012] based on watershed algorithms designed for extra zoom pictures was used to segment nuclear object from Hoechst intensity pictures, which were first equalized using a Gaussian filter.



*Mitochondrial segmentation and feature quantification:* Ilastik version 1.3.2post2 with a pixel classification workflow was used to identify MitoTracker Red positive pixels from background pixels [Berg 2019, Sommer 2011]. The pixel classification workflow consists of: feature selection, training and classification. First, two filters were selected based on visual inspection: *Laplacian of Gaussian* (σ = 3.5) in 2D and *Difference of Gaussians* (σ = 3.5) in 2D. Secondly, fore and background were annotated based on manual inspection of representative MitoTracker Red pictures. Next, a Random Forest classifier is used to classify all pixels into fore and background based on the selected features and annotations. Finally, the output from the pipeline is a "Simple Segmentation" picture, a binary picture with only fore and background classification. Afterwards, a custom python scripts was developed to utilize the Ilastik template in a headless mode, resulting in segmented mitochondrial objects in binary images. Subsequently, four features were used to describe object size and shape: area, perimeter, formfactor and solidity. The area describes the size of the objects in a number of pixels. The perimeter is the number of pixels at the boundary of an object. In the case of object with a hole, the perimeter is the sum of both inner and outer circle (i.e. the total length of the boundary between object and background). The formfactor is defined as $(4 * \pi * Area)/Perimeter$. The solidity is the quantification of the extent to which a shape is convex or concave. It is defined as $Area/ConvexArea$

(ConvexARea = the area enclosed by a convex hull/minimal convex object which can enclose the object).

*Fitting with a Gaussian mixture model:* A Gaussian mixture model (GMM) was applied to classify the segmented mitochondria objects in an unsupervised manner based on the 4 object features. In this way, the objects were divided into two categories, referred to as "fragmented" or "fused". The model was trained using all experimental images of cells exposed to various mitochondrial complex inhibitors and a vehicle control condition at time points ranging from 1h to 24h. The GMM was implemented in python using 100 random starting values for the Gaussians. For each starting value, an expectation–maximization algorithm was utilized to minimize the negative *–log likelihood* of the data. Finally, the model with the lowest negative *–log likelihood* was selected as the best fit. The class to which each mitochondrial object belonged was determined based on the probability for the two classes (i.e., class having the highest probability was selected).

*Statistical test:* To compare control, compound exposure, and siRNA treatment, the ANOVA test combined with a Dunnett test were applied to analyze statistical significance.

*Implementation:* All data analyses were implemented in Linux with python 2.7 with packages scikit-learn for the GMM fitting and prediction, dash for interactive plotting and scipy.stats for statistical testing.

**ATPlite assay and analysis**

ATP levels were assessed in cell lysate upon 2 and 24h chemical exposure as previously described [van der Stel 2020]. Cells were seeded two days before exposure. At the third day cells were stained with Hoechst for 2hours followed by chemical exposure. 1h before the end of the exposure period the cells were imaged to monitor the Hoechst intensity. The Hoechst intensity pictures were used to segment the nuclear objects in every picture and the total nuclear count per image was used to normalized further measurements. After the desired exposure period the medium was replaced by Hanks' buffer including 5 mM HEPES, 250 mM sucrose, 25 mM TRIS, 3 mM EGTA, 5 mM $MgCl_2$, 5 mM succinate and 5 mM glutamate (37 °C, pH 7.3) and for the mitochondrial fraction also supplemented for 30-45sec with 150µM digitonin. ATP content was determined using the ATPlite 1 step Luminscence Assay reagent kit (PerkinElmer, 6016731). ATP data were integration with RNA-seq data elsewhere [van der Stel 2021].

### Western Blot

OPA1-GFP cleavage was monitored using western blot. Cells were plated at a density of 200.000 cells/well in 24wells (Corning, 3524). Two days after seeding the cells were exposed to the test chemical for the desired timespan and lysed using direct lysis in 1x times sample buffer (stock: 1% BromoPhenolBlue (Sigma, B0126-25G) in MQ plus few drops of NaOH to dissolve BPB) supplemented with 5% v/v β-mercaptoethanol (Fisher Scientific, 125472500). Samples were heat-denatured for 10min at 95˚C before usage. Proteins were separated using SDS-PAGE on gels consisting of a running and stacking gel. The running contained per 10ml: 5mL MilliQ, 2.5mL Acrylamide (Bio-Rad, 1610158), 2.5mL Tris (1.5M Tris, with 10% SDS and pH = 8.8), 75µL 10% APS (Ammonium PerSulfate) (Sigma, A3678-25g) and 15µL TEMED (VWR, 17-1312-01). The stacking gel contained per 10mL: 6.1mL MilliQ, 1.3mL Acrylamide, 2.5mL Tris (0.5M Tris, with 10% SDS and pH = 6.8), 75µL 10% APS and 15µL TEMED. The proteins were blotted onto a PVDF membrane (Sigma, IPVH00010) using a wet transfer system. Membranes were incubated in 1% m/v milk in 1%TBS plus Tween20 (Boom, P2287-500mL). Primary and secondary antibodies were diluted in TBS-Tween20, respectively 1:1000 and 1:2000. The used primary antibodies were mouse-anti-GFP (11814460001, Roche) and mouse-anti-tubulin (T-9026, Sigma), detected respectively using goat-anti-mouse-HRP (115-035-003, Jackson) and goat-anti-mouse-Cy5 (115-605-146, Jackson). The horseradish peroxidase activity and Cy5 signal were detected using the Image Quant LAS4000 (GE HealthCare).

### Resazurin assay

The resazurin assay was conducted as previously described (van der Stel 2020). Briefly, the supernatant was replaced, after the assessment of the mitochondrial membrane potential, with 44µM resazurin dissolved in cell culture medium and incubated for 1.5 h in 5% $CO_2$ at 37°C. The colorimetric change upon resazurin reduction was assessed using 540nm excitation and 590nm emission.

## Results

### Analysis pipeline for quantitative categorization of mitochondrial morphology

To assess the link between mitochondrial morphology and mitochondrial perturbation, we assembled an analysis pipeline to classify mitochondrial morphology into two morphology subclasses (“fragmented” and “fused”). To make this pipeline compatible with high throughput data collection and include an unbiased morphology classification, we selected an unsupervised machine learning approach combined with open analysis software (Ilastik and CellProfiler) to segment and assess mitochondrial

objects in living cells (HepG2) stained with MitoTracker Red and imaged using confocal microscopy (Fig. 1A).

Step one of the pipeline included identification of mitochondria from live confocal images in which mitochondria were stained with MitoTracker Red. Ilastik software was used to classify pixels of the MitoTracker Red images into fore- and background (Fig. 1B). In step two, CellProfiler was used to segment mitochondrial objects and quantify 4 features per object: area, perimeter, formfactor and solidity (Fig. 1C). The third step consisted of an unsupervised learning approach using a Gaussian mixture model (GMM) to subdivide segmented mitochondrial objects based on the assessed features into two groups, i.e. fragmented and fused.

The parameter probability prediction from the GMM includes a mean and variance parameter per selected mitochondrial feature for both fragmented and fused mitochondria [Reynolds, 2009] (Fig. 1D). To evaluate the effect of data size on GMM fitting, we monitored the effects on the mean and variance of the Gaussians when changing 3 aspects, i.e., the number of compounds, the number of images and the number of objects. The effect of compound choice was studied using a leave-one-out strategy. The influence of the number of images was tested using 100 randomly selected subsets of the images (each time consisting of half of the images). Similarly, the effect of object number was estimated using only a fraction of all objects pooled from all conditions (using the fraction 1/2, 1/10, and 1/500 of all objects). This analysis showed that the data is sufficient to provide robust parameter estimates for the two mitochondrial classes (Fig. 1D). Moreover, visualization of the four considered features in two-dimensional scatter plots along with their estimated Gaussians demonstrated an excellent fitting performance (Fig. 1E).

**ETC inhibitors disconnect mitochondrial morphology, membrane potential, and ATP production**

To be able to use mitochondrial morphology classification as a toxicity biomarker it is important to understand the relationship between the readout and the biological effect. Alterations of mitochondrial morphology have previously been linked to distinct key functional properties including ATP levels and MMP [Anand 2014, Baker 2014, Ehses 2009, Head 2009, Consolato 2018]. We examined this relationship in the context of 3 known mitochondrial complex inhibitors: Rotenone, Antimycin and Oligomycin, targeting ETC complex I, III, and V, respectively (Fig. 2A).

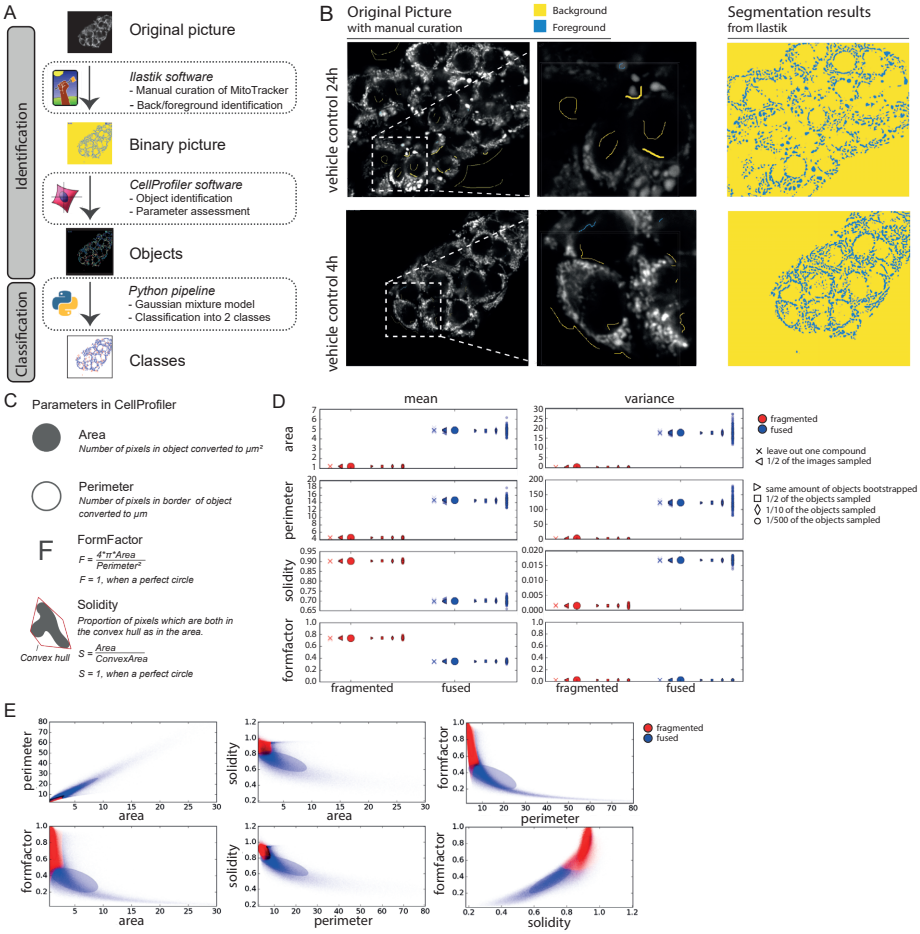


**Figure 1: Quantification of mitochondrial morphology**

**A)** schematic representation of the pipeline used to analyze mitochondrial morphology. The pipeline is designed to assess mitochondrial morphology in an unbiased approach using confocal images of mitochondria stained with MitoTracker Red in HepG2 cells. 1) The intensity pictures are converted to binary pictures using Ilastik software and based on manual curation, 2) Various features are collected of the identified objects using CellProfiler, 3) These features are used to classify all mitochondria into 2 classes using a machine learning approach. **B)** Manual curation of mitochondrial staining in the original MitoTracker Red images using Ilastik and the segmentation result from Ilastik based on the manual curation (yellow = background, blue = foreground). **C)** The selected parameters from CellProfiler software **D)** Effect of the data size on the estimated mean and variance for the four morphological features in the Gaussian mixture model. Red for fragmented mitochondria and blue for fused mitochondria **E)** Scatter plot of two features (area, perimeter, solidity, formfactor) to describe mitochondrial morphology for mixture of two subpopulations. Red for fragmented mitochondria and blue for fused mitochondria. The ellipse kernels represent the Gaussian distribution for the two subpopulations (red for fragmented and blue for fused population. Mean and co-variance info are utilized to draw those ellipses. The contour lines indicating 95% confidence interval of the parameters.

Exposure to a concentration range of oligomycin induced an increase in fragmented mitochondria (Fig. 2B, C). Rotenone treatment did not result in a shift in the identified mitochondrial populations. Antimycin exposure induced a slight decrease in fragmented mitochondria (i.e., an increase in fused mitochondria) at higher concentrations.

Morphological responses were compared to changes in MMP. Rotenone and antimycin each triggered a concentration dependent decrease in MMP (Fig. 2D; 1st column). By contrast, oligomycin stimulated a concentration-dependent increase of the MMP. The latter could be explained by blockage of ATP synthase, causing a proton gradient that is not used for ATP production [Symersky 2012, Hong 2008].

Additionally, morphological responses and MMP dynamics were compared to changes in ATP production. Rotenone, Antimycin and Oligomycin each caused a concentration-dependent drop in ATP levels in the cytoplasm as measured by a cytoplasmic ATP sensor (Fig. 2D; 2nd column; Suppl. fig 1A). Likewise, measurements using an ATP sensor localized to mitochondria showed that exposure to each of these chemicals resulted in a decrease in mitochondrial ATP and this drop was considerably faster than what was observed in the cytoplasmic compartment (Fig. 2D; 3rd column; Suppl. fig 1A). As an alternative approach ATP lite was used to measure overall whole cell ATP levels and ATP in the isolated mitochondrial fraction (Suppl. fig 1B). Both demonstrated a similar concentration-response relationship for Rotenone, Antimycin and Oligomycin as observed with the ATP-biosensors, with the mitochondrial ATP fraction almost completely disappearing upon chemical exposure, when compared to the negative control.

In conclusion, while the three distinct ETC inhibitors caused a similar decrease in mitochondrial ATP production, time and concentration-resolved analysis disconnected the responses at the level of mitochondrial morphology, MMP, and ATP production.

**OPA1 cleavage links ETC inhibition to morphological adaptation**

To address the role of known mitochondrial morphology regulators in the occurrence of the fragmentation phenotype, we silenced the *DRP1, OMA1* and *OPA1* genes and investigated the effect on mitochondrial morphology. Depletion of the fission protein DRP1 resulted as expected in a decrease in the number of fragmented mitochondria (Fig. 3A, B). OPA1 depletion caused a an increase in mitochondrial fragmentation that was pronounced 96h after KD as was also observed with oligomycin. Depletion of the OPA1 regulator OMA1 did not result in a pronounced effect on mitochondria fragmentation. To further investigate the relationship between OPA1 and chemical-induced fragmentation, we developed an OPA1-GFP BAC fusion cell line (Fig. 3C) and used OPA1 silencing to validate the specific detection of long and short OPA1 by GFP antibody in this cell line (Fig. 3D; Suppl. fig 2A). The OPA1-GFP fusion protein localized in mitochondrial like structures in the cell and co-staining using a MitoTracker Red marker demonstrated overlap as expected (Fig. 3E).

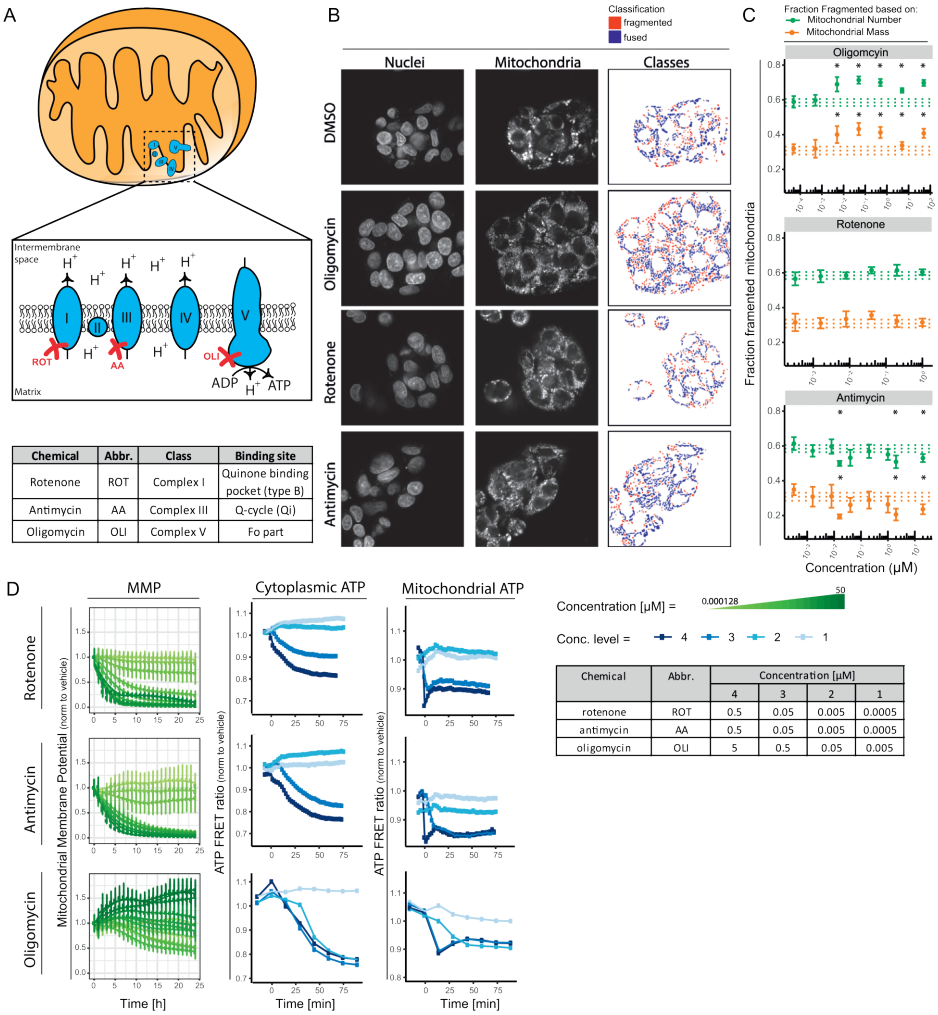


| Chemical | Abbr. | Class | Binding site |
|---|---|---|---|
| Rotenone | ROT | Complex I | Quinone binding pocket (type B) |
| Antimycin | AA | Complex III | Q-cycle (Qi) |
| Oligomycin | OLI | Complex V | Fo part |

| Chemical | Abbr. | Concentration [µM] | | | |
|---|---|---|---|---|---|
| | | 4 | 3 | 2 | 1 |
| rotenone | ROT | 0.5 | 0.05 | 0.005 | 0.0005 |
| antimycin | AA | 0.5 | 0.05 | 0.005 | 0.0005 |
| oligomycin | OLI | 5 | 0.5 | 0.05 | 0.005 |

**Figure 2: Quantitative analysis of ATP and MMP for 3 ETC complex inhibitors**

**A)** Schematic representation of the ETC in mitochondria showing the different complexes involved, the creation of a proton gradient and the synthesis of ATP. Table includes information per compound concerning class and binding site. **B)** Representative confocal imaging pictures of HepG2 cells stained with Hoechst (nuclei) and MitoTracker Red (mitochondria) and exposed for 24h to vehicle control, 1µM rotenone, 1µM antimycin or 5µM oligomycin. The MitoTracker Red pictures were analyzed using the pipeline describe in Fig. 1, which resulted in a distribution into two populations (red = fragmented, blue = fused). **C)** Fraction of mitochondria belonging to the class of fragmented mitochondria following 24h exposure to vehicle control or a concentration range of oligomycin, rotenone or antimycin. The two colors represent two methods: based on the number of identified objects (green) or incorporation of the identified object mass (orange). Data is represented as mean plus SE of three biological replicates. The dotted lines represent the average and SE of the vehicle treatment (0.2 v/v% DMSO). Asterisk represent a p-value < 0.05 for the comparison to the vehicle control. **D)** Quantification of mitochondrial parameters upon exposure to a concentration range of rotenone, antimycin or oligomycin. From left to right: MMP over time after exposure to 10 concentrations ranging from 0.000128 to 50µM (data is represented as a mean of 4 biological replicates ±SD); cellular ATP levels over time upon exposure to 4 concentrations quantified using an ATP-biosensor (the presented data is from one replicate, additional biological replicates are shown in Suppl. fig 2); mitochondrial ATP levels over time upon exposure to 4 concentrations quantified using an ATP-biosensor (the presented data is from one replicate, additional biological replicates are shown in Suppl. fig 2). Table includes the concentrations selected for the ATP-FRET measurements.

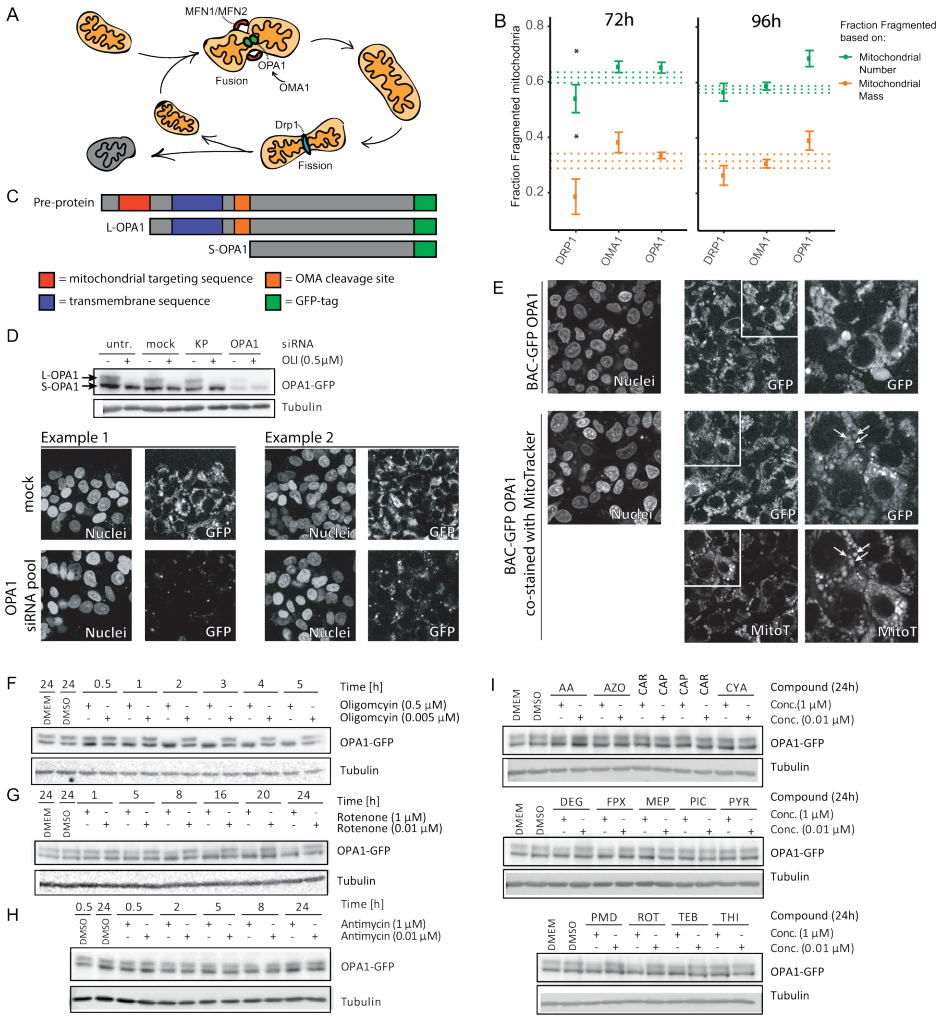


**Figure 3: OPA1 cleavage correlates with mitochondrial fragmentation**

**A)** Picture demonstrating the relationship between the process of fission and fusion and its major players. MFN1/ MFN2 together with the membrane bound form of OPA1 are involved mitochondrial fusion. OMA1 de-activates OPA1 via cleavage. DRP1 together with the endoplasmic reticulum are responsible for mitochondrial fission. **B)** Fraction of mitochondria belonging to the class of fragmented mitochondria 72h or 96h after silencing of *DRP1*, *OMA1* and *OPA1*. The two colors represent two methods for determination of the fraction: based on the number of identified objects (green) or incorporation of the identified object mass (orange). Data is represented as mean plus SE of three or two biological replicates, respectively for 72h and 96h. The dotted lines represent the average and SE of the mock condition. Asterisk represent a p-value < 0.05 for the comparison to the vehicle control (no statistics were performed for the 96h samples). **C)** Scheme demonstrating the different forms of OPA1. **1)** the pre-protein including mitochondrial targeting sequence and transmembrane sequence. **2)** OPA1 is cleaved into L-OPA1 after entering the mitochondria. **3)** L-OPA1 can be cleaved into S-OPA1 by OMA1 resulting in the loss of the transmembrane domain. The creation of a OPA1-GFP fusion protein using BAC technology resulted in a C-terminally tagged protein. **D)** Western blot results for the BAC-GFP OPA1 cell line cultured in absence or presence of oligomycin (0.5µM) in combination with the indicated siRNAs (untr, untreated; mock, transfection reagent only; KP, kinase pool; OPA1, siRNAs targeting *OPA1*). Samples were stained with anti-GFP and anti-tubulin. Lower part: Representative confocal images of HepG2 BAC-GFP OPA1 cells treated with mock or siRNAs targeting *OPA1* and stained with Hoechst (nuclei). **E)** Representative confocal images of the HepG2 BAC-GFP OPA1 reporter cell line demonstrating the overlap of GFP signal and MitoTracker Red. **F)** Western blot results showing GFP and tubulin in HepG2 BAC-GFP OPA1 cells treated with 2 concentrations oligomycin (0.005 or 0.5µM) for 0.5, 1, 2, 3, 4, 5h. **G)** Western blot results showing GFP and tubulin in HepG2 BAC-GFP OPA1 cells treated with 2 concentrations rotenone (0.005 or 0.5µM) for 1, 5, 8, 16, 24h. **H)** Western blot results showing GFP and tubulin in HepG2 BAC-GFP OPA1 cells treated with 2 concentrations antimycin (0.005 or 0.5µM) for 0.5, 2, 5, 8, 24h. **I)** Western blot results showing GFP and tubulin in HepG2 BAC-GFP OPA1 cells treated with 2 concentrations (0.1 or 1µM) of 14 ETC complex inhibitors or controls for 24h.

To investigate how changes in the molecular machinery controlling fission/fusion related to the changes in morphology caused by ETC inhibition, we first focused on oligomycin. The increased fragmentation induced by this compound (Fig. 2B, C) was indeed accompanied by a proteolytic cleavage leading to a loss of the L-OPA variant at 2h (Fig. 3D, F; Suppl. fig 2B, C). We next analyzed post-translational modification of OPA1 in response to rotenone and antimycin that each induced a similar decrease in ATP in the cytoplasm and mitochondria as observed with oligomycin (Fig. 2D; Suppl. fig 1). Like oligomycin, rotenone exposure resulted in a reduction of L-OPA1, albeit less pronounced leaving a residual L-OPA1 expression perhaps explaining the lack of effect of rotenone on mitochondrial morphology (Fig. 3G; Fig. 2D; Suppl. fig 2D). By contrast, but in agreement with its effect on mitochondrial morphology, antimycin exposure failed to induce L-OPA1 cleavage, despite the loss of ATP triggered by this compound (Fig. 3H; Fig. 2D; Suppl. fig 2E). Together, these results indicated that mitochondrial fragmentation in response to ETC inhibition largely correlated with L-OPA1 cleavage, but activation of this process cannot be explained by ATP depletion alone.



**Testing a larger panel of complex I and III inhibitors**

We next compiled a larger set of chemicals all belonging to the classes of complex I and III inhibitors and supplemented this set with 3 complex II inhibitors. Previous work demonstrated that all complex I and III inhibitors, except for capsaicin and cyazofamid, but not complex II inhibitors, attenuated basal oxygen consumption rate (OCR), and specificity for the assigned complexes was confirmed [van der Stel 2020] (Suppl. fig 2F). A 24-hour exposure to concentrations above or around the OCR IC50 value for all active inhibitors did not result in a loss of L-OPA1. We only observed a minimal decrease of L-OPA1 upon exposure to complex I inhibitors pyrimidifen, rotenone and tebufenpyrad (Fig. 3I; Suppl. fig 2G). The absence of major reductions in L-OPA1 levels upon exposure to complex I and III inhibitors further indicated that a drop in ATP and OCR triggered by complex I and III inhibitors, by itself cannot explain OPA1 cleavage. Rather, the complex V inhibitor oligomycin, in addition to ATP and OCR inhibition, must connect to OPA1 cleavage and mitochondrial fragmentation in another manner.

**Complex V inhibition also triggers OPA1 cleavage and mitochondrial fragmentation**

While complex I, III, and V inhibition attenuated ATP levels and OCR, a distinguishing response to the complex V inhibitor oligomycin, as compared to the complex I and III inhibitors, was the increase in MMP in association with OPA1 cleavage and mitochondrial fragmentation. Two other chemicals known to inhibit complex V are DCCD and diafenthiuron (DIA) (Fig. 4A) [Hong 2008, Krieger 2001]. As observed for active complex I and III inhibitors and the complex V inhibitor oligomycin, DCCD and DIA exposures resulted in an ATP decrease although the response was delayed

as compared to other compounds (Fig. 4B row 1 and 2; Suppl. fig 3A, B and C). Like oligomycin, DCCD and DIA triggered an increase in MMP, albeit at later time points as compared to oligomycin and only at lower concentrations (Fig. 4B row 1 and 2). Moreover, a 5h-exposure to 2μM DCCD also resulted in a loss of L-OPA1 and exposure to 2μM DIA resulted in a loss of L-OPA1 after 24h (Fig. 4C; Suppl. fig 3D). Finally, exposure to DCCD and DIA, similar to oligomycin, induced a concentration-dependent increase in the fraction of fragmented mitochondria (Fig. 4B row 1 and 2). These findings showed that the reduction in ATP levels and OCR combined with an increase in MMP that specifically characterized complex V inhibition, may trigger OPA1 cleavage and mitochondrial fragmentation.

**Increase in MMP by itself is insufficient to trigger mitochondrial fragmentation**

To assess if the increase in MMP per se was sufficient to trigger in mitochondrial fragmentation, we included Cyclosporin A (CSA), which affects the MMP via a non-ETC mechanism by blocking the mPTP pore resulting in a reduced exchange/leakage of protons between inner membrane space and mitochondrial matrix [Cassarino 1998, Waldmeier 2002, Mishra 2019]. Exposure to CSA resulted in an increased MMP without any effect upon ATP levels (Fig.4B row 3; Suppl. fig 3A, B and C). CSA treatment did not affect OPA1 cleavage (Fig. 4C; Suppl. fig 3D) and effects on mitochondrial morphology were observed only at the highest concentration tested (Fig. 4B row 3). Visual inspection of the mitochondrial morphology demonstrated that CSA caused a change in organelle structure but not a fragmentation such as observed with Oligomycin, DCCD or DIA exposure (Fig. 4D). These findings indicate that the increase in MMP, by itself is not sufficient to trigger OPA1 cleavage and mitochondrial fragmentation.

**OPA1 depletion similarly triggers mitochondrial fragmentation but does not enhance toxicity of ETC inhibition**

As our findings indicated selective OPA1 cleavage (causing a loss of OPA1 function) in the subset of ETC inhibitors triggering mitochondrial fragmentation, we tested the effect of OPA1 depletion by itself. Silencing *OPA1* resulted in an increase in fragmented mitochondrial objects that was similar to the level induced by Oligomycin (Fig. 5A; compare dashed line in right panel to blue curve in left panel). Combining OPA1 depletion with oligomycin treatment did not further increase mitochondrial fragmentation.

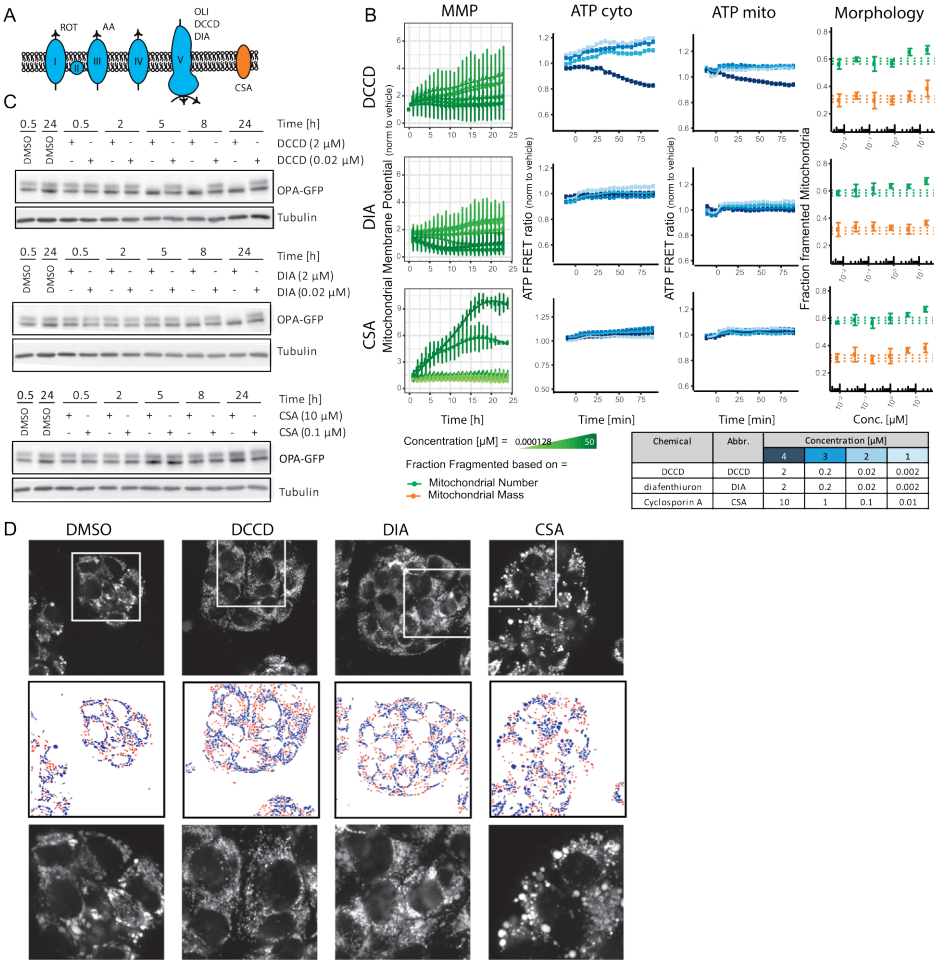


| Chemical | Abbr. | Concentration [µM] | | | |
|---|---|---|---|---|---|
| | | 4 | 3 | 2 | 1 |
| DCCD | DCCD | 2 | 0.2 | 0.02 | 0.002 |
| diafenthiuron | DIA | 2 | 0.2 | 0.02 | 0.002 |
| Cyclosporin A | CSA | 10 | 1 | 0.1 | 0.01 |

**Figure 4: Impact of additional mitochondrial toxicants on mitochondrial function, morphology, and OPA1 cleavage**

**A)** Schematic representation of the molecular target of the different mitochondrial inhibitors used in this study. **B)** Quantification of mitochondrial parameters after exposure to a concentration range of DCCD, DIA and CSA. The panels represent from left to right: mitochondrial membrane potential over time after exposure to 10 concentrations ranging from 0.000128 to 50µM (data is represented as a mean of 4 biological replicates ±SD); cellular ATP levels over time after exposure to 4 concentrations quantified using cytoplasmic ATP-biosensor (presented data is from one replicate, additional biological replicates are shown in Suppl. fig 4); mitochondrial ATP levels over time after exposure to 4 concentrations quantified using mitochondrial-targeted ATP-biosensor (presented data is from one replicate, additional biological replicates are shown in Suppl. fig 4); fraction of mitochondria belonging to the class of fragmented mitochondria after chemical exposure. The two colors represent two methods: based on the number of identified objects (green) or incorporation of the identified object mass (orange). Data is represented as mean plus SE of three biological replicates. The dotted lines represent the average and SE of the DMSO condition. Asterisk represent a p-value < 0.05 for the comparison to the vehicle control. **C)** Western blot results showing GFP and tubulin in HepG2 BAC-GFP OPA1 cells treated with 2 concentrations DCCD (0.02 or 2µM), DIA (0.02 or 2µM) or CSA (0.1 or 10 µM) for 0.5, 2, 8, 24h. **D)** HepG2 cells stained with Hoechst and MitoTracker Red (mitochondria) and exposed 24h to vehicle control, 4µM DCCD, 4µM DIA or 25µM CSA. Top row are representative high confocal imaging pictures. Middle row result of segmentation pipeline demonstrating the distribution into two populations (red = fragmented, blue = fused). Bottom row demonstrates a zoom-in from top panel.

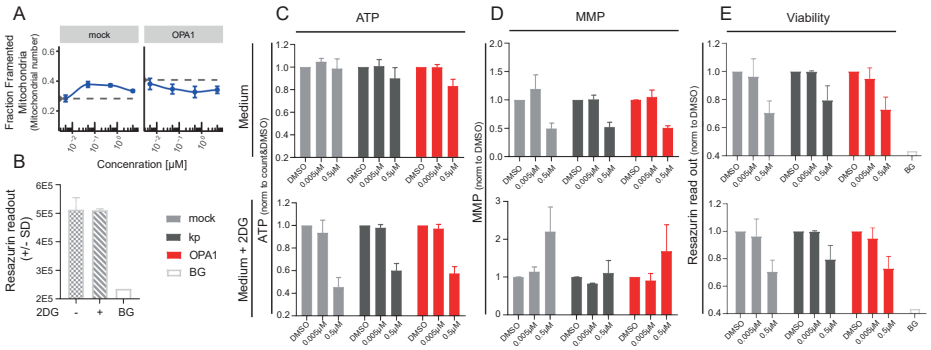


**Figure 5: Effect of OPA1 silencing on mitochondrial morphology, viability, MMP and ATP**
**A)** Fraction of mitochondria belonging to the class of fragmented mitochondria treated 72h with or without *OPA1* siRNAs followed by 24h oligomycin (0.005, 0.05, 0.5 and 5 µM) or vehicle (0.2 v/v% DMSO) exposure. Data is represented as mean fragmented fraction plus SE (based on number of objects identified) of three biological replicates. The dotted lines represent the average of the vehicle exposure. **B)** Quantification of viability based on resazurin conversion for medium with/without 2DG after 96h after KD. Data is representation of mean plus SD of 3 replicates (BG, background signal). **C-E)** Quantification of mitochondrial parameters in cells treated 72h with indicated siRNAs (see legend Fig. 5B) followed by exposure to oligomycin (0.005, 0.5 µM) in medium with/without 2DG. Data is represented as a mean of 3 biological replicates plus SD) **C)** Total cellular ATP levels quantified using ATPlite assay after 5h oligomycin exposure. **D)** Mitochondrial membrane potential at 24h oligomycin exposure. **E)** Quantification of viability based on resazurin conversion after 24h oligomycin exposure.

We assessed whether OPA1 depletion by itself led to toxicity under regular cell culture conditions and in presence of 2-deoxyglucose (2DG) to enforce a strict dependence on mitochondrial respiration. 2DG was added to the medium at a level that did not affect cellular viability per se (Fig. 5B). OPA depletion did not affect ATP levels, MMP, or viability by itself under control or 2DG conditions (Fig. 5C-D). Moreover, the reduction in ATP, the increase in MMP, and the reduced viability observed with 0.5µM oligomycin was not amplified by OPA1 depletion.

Taken together, our findings identify a combination of reduced ATP levels and OCR and increased MMP as the trigger for mitochondrial fragmentation that is observed with exposure to ETC complex V and a subset of complex I and III inhibitors. We find that this combination is intimately connected with OPA1 cleavage and OPA1 silencing is sufficient to trigger a similar mitochondrial fragmentation. This level of fragmentation cannot be assigned to a (mal)adaptive response as OPA1 silencing by itself does not affect viability and fails to (de)sensitize cells to ETC inhibition.

## Discussion

In this work, we assessed the interconnectivity of mitochondrial morphology, MMP, and ATP production in the context of chemical exposure to distinct ETC inhibitors. Our results demonstrate that the different mitochondrial morphologies, fused or fragmented organelles, can be reliably quantified in a high throughput, confocal imaging setup. We identified that changes in ATP or MMP alone could not explain the observed chemical-induced changes in mitochondrial morphology. Our data indicates that the integration

of multiple mitochondrial features in a time- and concentration-dependent approach will improve mechanism-based characterization of mitochondrial toxicants.

Changes in mitochondrial morphology have been linked to alterations in MMP, production of ATP, and other mitochondrial processes [Anand 2014, Baker 2014, Ehses 2009, Head 2009, Consolato 2018]. We combined real time confocal microscopy analysis of mitochondrial morphology, MMP, and ATP levels to assess their temporal relationships in the context of exposure to concentration ranges of ETC complex inhibitors. We used a set of mitochondrial toxicants with a well-defined mode-of-action. The observed mitochondrial objects were quantified based on size and shape descriptors used in earlier studies: area, perimeter, formfactor and solidity [Bondi 2016, Irobi 2012, Rodríguez-Martin 2016]. The use of an unsupervised machine learning pipeline enabled us to separate fragmented and fused objects based on the measured object features. Other have reported a correlation of mitochondrial fission with the perimeter and solidity of the detected objects [Westrate 2014]. The larger variance observed in our data for the size descriptors (area and perimeter) compared to the shape features (solidity and formfactor) indicates that fragmented and fused mitochondria are more easily distinguished by their shape than by their size. Because of the used set of mitochondrial toxicants, the established model is biased towards identification of smaller objects and would benefit from a more diverse set of treatments including those enhancing fusion or inhibiting fission. As an alternative, supervised learning can be employed for mitochondrial classification purposes [Leonard 2015, Peng 2011]. However, supervised learning is based on example mitochondrial objects and requires high resolution images for identification of detailed object features. Our approach is applicable to lower resolution images and therefore fits more readily to high throughput approach. This creates the opportunity to systematically screen large sets of chemicals for their effects upon mitochondrial morphology.



This setup also allowed us to combine high throughput analysis of mitochondrial morphology with other, functional mitochondrial readouts developed for the same imaging format. For this purpose, we focused on MMP using dyes depending on MMP to accumulate in mitochondria and on the production of ATP using ATP biosensors localized in mitochondria or in the cytoplasm. A decrease in MMP [Jones 2017] or a decrease in ATP [Jones 2017] have been reported to drive OPA-mediated changes in morphology. Our findings show that the relationship between MMP, ATP production, and mitochondrial morphology is more complex and, unexpectedly, only ETC complex inhibitors causing an increase in MMP trigger OPA1 cleavage and mitochondrial fragmentation. Importantly, increasing MMP alone by blocking the mPTP pore does not lead to OPA1 cleavage and mitochondrial fragmentation. Instead, a combination of MMP increase with a reduction in ATP production and OCR is what characterizes

the ETC complex I, III, and V inhibitors that trigger mitochondrial fragmentation. Indeed, this subset of ETC complex inhibitors also trigger OPA1 cleavage. Moreover, OPA1 silencing is sufficient to trigger a similar mitochondrial fragmentation. These findings suggest a delicate control of the upstream regulators of OPA1 cleavage such as the protease OMA1, which acts as a sensor for mitochondrial stress [Baker 2014].

We find no evidence that mitochondrial fragmentation associated with OPA1 cleavage represents a (mal)adaptive response. First, OPA1 silencing, which causes a similar level of mitochondrial fragmentation as observed with the subset of ETC complex inhibitors, by itself does not affect ATP production or cell viability. Secondly, OPA1 silencing does not (de)sensitize cells to ETC inhibition. In other *in vitro* and *in vivo* systems, overexpression of OPA1 or another fusion related protein, MFN resulted in protection against mitochondria-related toxicities and disease [Hwang 2014, Alaimo 2014, Patten 2014, Civiletto 2015]. Vice versa, overexpression of the fission protein DRP1 worsened rotenone toxicity in *drosophila* [Hwang 2014] while pharmacological inhibition of Drp1 with mdivi protects cells against oxygen–glucose deprivation [Grohm 2012, Tian 2014]. The reason for the apparent discrepancy between these studies and our own finding is not clear but the modest shift from fusion to fission achieved by OPA1 silencing or by ETC complex inhibition in our study may be tolerated while strong overexpression, a full KO, or pharmacological inhibition of fusion/fission proteins may impact on viability.

In addition to providing new insight in the relationship between different responses to ETC complex inhibition (mitochondrial morphology, MMP, cellular and mitochondrial ATP, cell viability) this study sets the stage for large scale chemical screening using multi-parameter microscopic readouts. The next generation chemical risk assessment paradigm stimulates the use of mechanism-driven studies in which biology-relevant parameters are quantified using sophisticated unbiased assessment methods and integrated into networks of prediction models [Krewski 2014]. The data obtained in this study fits this type of risk assessment, when combined with for instance ordinary differential equations (ODEs) to describe the time and concentration dependency of the ATP and MMP alterations [Yang 2021 submitted, Daun 2008]. Such modeling efforts will result in threshold values describing the concentration, moment in time or the effect size at which one event will trigger the next. This process will benefit from the incorporation of single cell measurements describing multiple events in one cell, which will enable establishment of relationships e.g. between ATP, MMP, and distribution of mitochondrial objects. The time- and concentration-resolved multi-parameter data such as generated in this study can be applied in screening of a wider range of chemicals and provide quantitative data for adverse outcome pathway (AOPs) [Leist 2017].

**Acknowledgements**

This project has received funding from the European Union's Horizon 2020 research and innovation programme under grant agreement No 681002.

We are grateful to Hans de Bont (Leiden University Cell Observatory) for his support & assistance in the morphology microscopy used in this work.

# Supplementary material

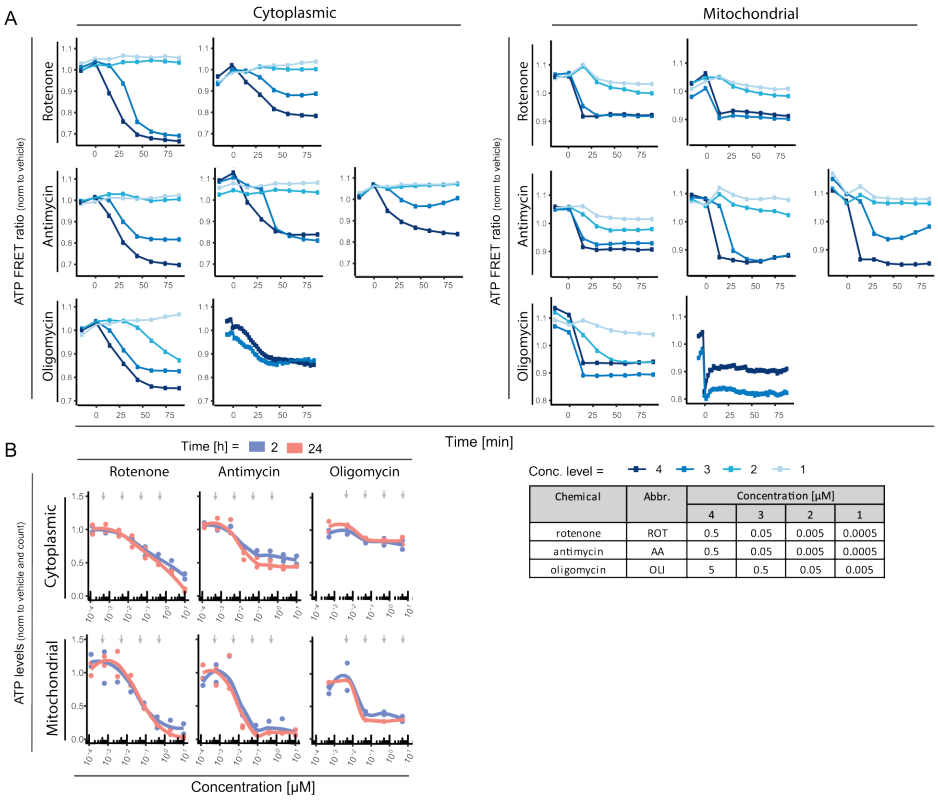


| Chemical | Abbr. | Concentration [µM] | | | |
|---|---|---|---|---|---|
| | | 4 | 3 | 2 | 1 |
| rotenone | ROT | 0.5 | 0.05 | 0.005 | 0.0005 |
| antimycin | AA | 0.5 | 0.05 | 0.005 | 0.0005 |
| oligomycin | OLI | 5 | 0.5 | 0.05 | 0.005 |

**Supplementary figure 1: Quantitative analysis of ATP and MMP for 3 ETC complex inhibitors**
Quantification of mitochondrial parameters after exposure to a concentration range of Rotenone, antimycin and oligomycin. **A)** Cellular and mitochondrial ATP levels over time upon exposure to 4 concentrations quantified using an ATP-biosensor. Individual biological replicates are shown. Table shows concentration 1-4 per compound. **B)** Total cellular and mitochondrial ATP levels measured using ATPlite assay at 2 and 24h exposure to a concentration range of the chemical. Data represents two biological replicates plus fit. Grey arrows represent the concentrations used in Fig2D and suppl. fig 2A.

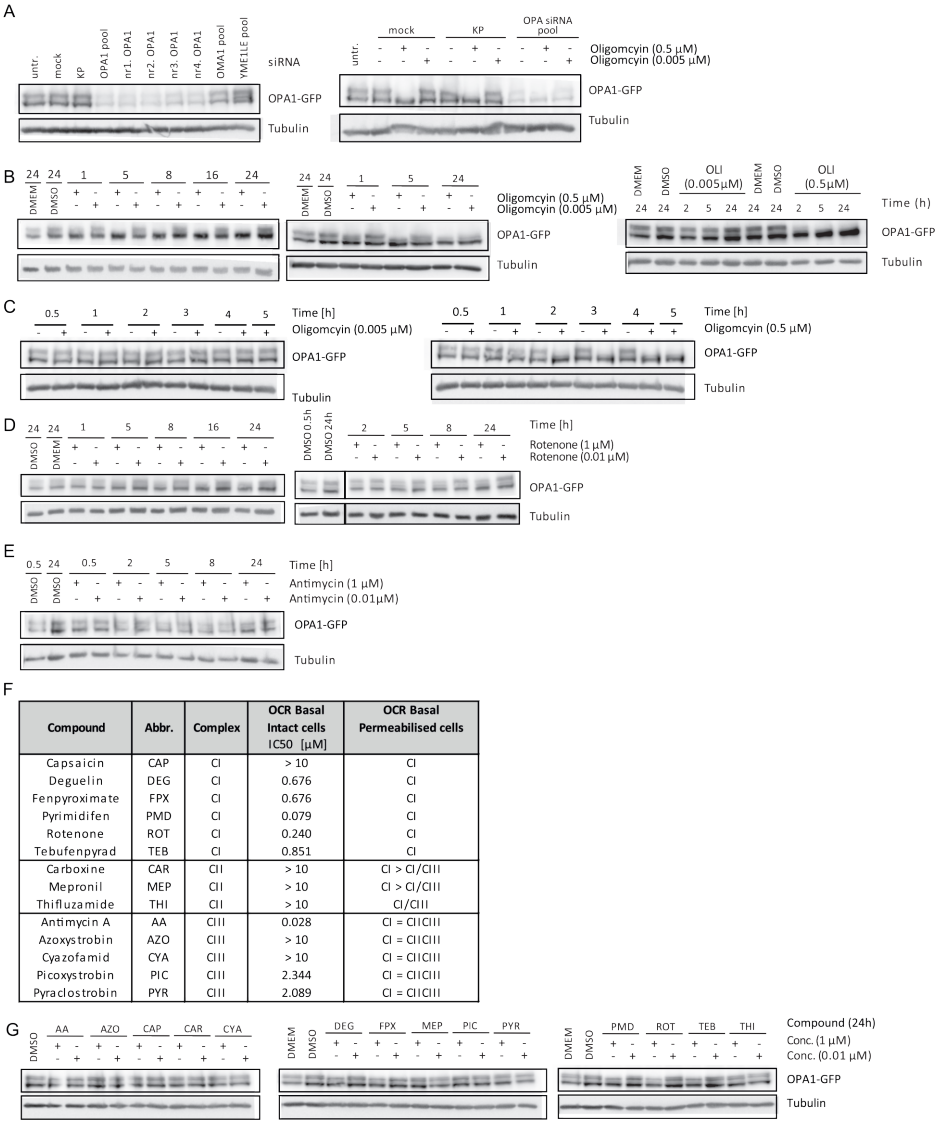


| Compound | Abbr. | Complex | OCR Basal Intact cells IC50 [µM] | OCR Basal Permeabilised cells |
|---|---|---|---|---|
| Capsaicin | CAP | CI | > 10 | CI |
| Deguelin | DEG | CI | 0.676 | CI |
| Fenpyroximate | FPX | CI | 0.676 | CI |
| Pyrimidifen | PMD | CI | 0.079 | CI |
| Rotenone | ROT | CI | 0.240 | CI |
| Tebufenpyrad | TEB | CI | 0.851 | CI |
| Carboxine | CAR | CII | > 10 | CI > CI/CIII |
| Meponil | MEP | CII | > 10 | CI > CI/CIII |
| Thifluzamide | THI | CII | > 10 | CI/CIII |
| Antimycin A | AA | CIII | 0.028 | CI = CIICIII |
| Azoxystrobin | AZO | CIII | > 10 | CI = CIICIII |
| Cyazofamid | CYA | CIII | > 10 | CI = CIICIII |
| Picoxystrobin | PIC | CIII | 2.344 | CI = CIICIII |
| Pyraclostrobin | PYR | CIII | 2.089 | CI = CIICIII |

**Supplementary figure 2: OPA1-GFP cleavage in response to ETC complex inhibitors**
**A)** Left: Western blot results of the BAC-GFP OPA1 cell line after *OPA1* (pool and singles), *OMA1* (pool) and *YME1LE* (pool) siRNA KD (untr, untreated; KP, kinase pool). Samples were stained with anti-GFP and anti-tubulin. Right: Western blot results of the BAC-GFP OPA1 cell line after *OPA1* (pool) siRNA KD (untr, untreated; KP, kinase pool) combined with oligomycin treatment at 2 concentrations (0.005 or 0.5µM). Samples were stained with anti-GFP and anti-tubulin. Samples were stained with anti-GFP and anti-tubulin. **B)** Western blot results showing GFP and tubulin in HepG2 BAC-GFP OPA1 cells treated with 2 concentrations oligomycin (0.005 or 0.5µM) for 1, 2, 5, 8, 16, 24h. **C)** Western blot results showing GFP and tubulin in HepG2 BAC-GFP OPA1 cells treated with 2 concentrations oligomycin (0.005 or 0.5µM) for 0.5, 1, 2, 3, 4, 5h. **D)** Western blot results showing GFP and tubulin in HepG2 BAC-GFP OPA1 cells treated with 2 concentrations rotenone (0.01 or 1µM) for 1, 2, 5, 8, 16, 24h. **E)** Western blot results showing GFP and tubulin in HepG2 BAC-GFP OPA1 cells treated with 2 concentrations antimycin (0.01 or 1µM) for 0.5, 1, 2, 5, 8, 24h. **F)** Table showing OCR results for intact and permeabilized cells (data generated in [van der Stel 2020]). **G)** Western blot results showing GFP and tubulin in HepG2 BAC-GFP OPA1 cells treated with 2 concentrations (0.1 or 1µM) of 14 ETC complex inhibitors or controls for 24h.

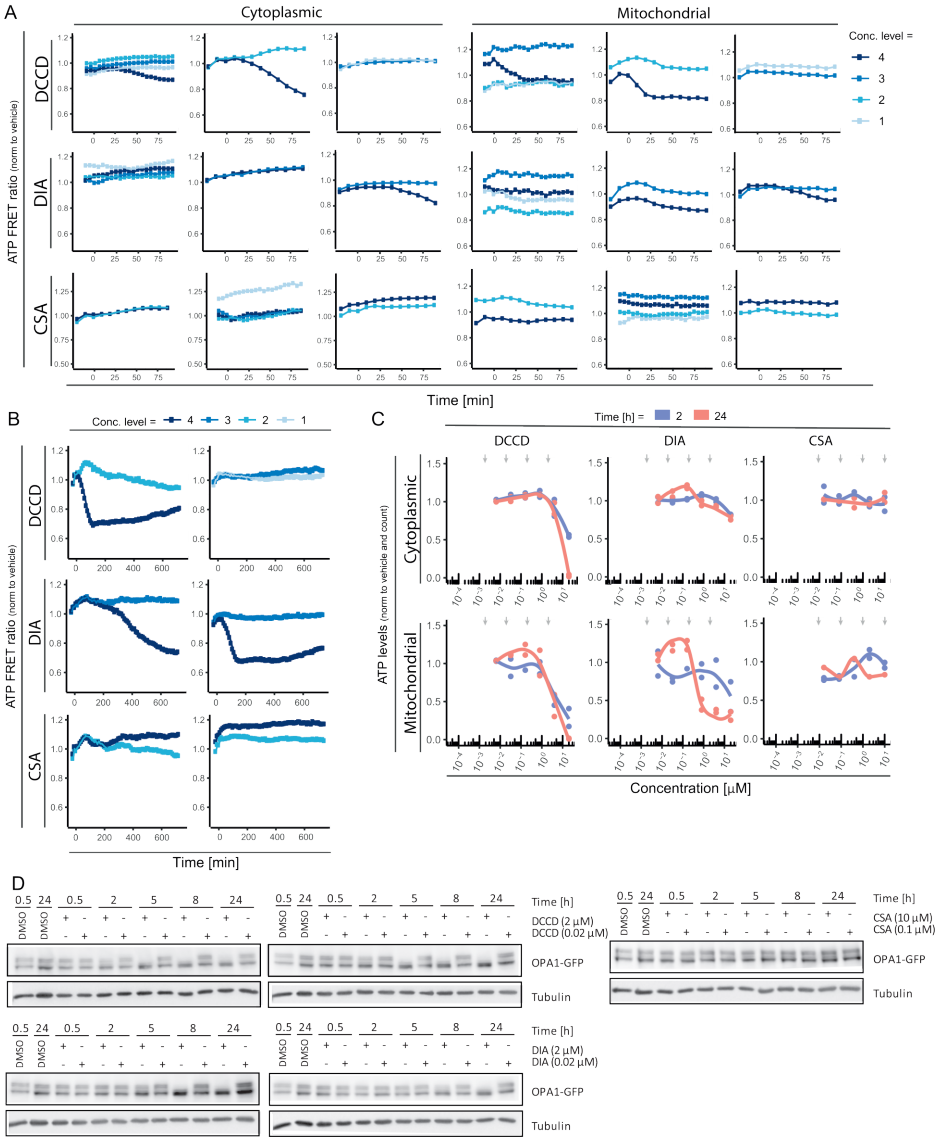


**Supplementary figure 3: Impact of additional mitochondrial toxicants on mitochondrial function, morphology, and OPA1 cleavage**

**A-C)** Quantification of mitochondrial parameters after exposure to a concentration range of DCCD, DIA and CSA. **A)** Cellular and mitochondrial ATP levels over time after exposure to 4 concentrations quantified using the ATP-biosensor (the presented data is from one 2 or 3 biological replicates). **B)** Cellular ATP levels over time (period of 12h) after exposure to 4 concentrations of DCCD, DIA or CSA quantified using cellular ATP-biosensor (the presented data is from one 2 or 3 biological replicates). **C)** Total cellular and mitochondrial ATP levels quantified using ATPlite assay at 2 and 24h exposure to a concentration range of the indicated chemicals. Data represents two biological replicates plus fit. Grey arrows represent the concentrations used in Fig. 4B, C and Suppl. fig 4A. **D)** Western blot results showing GFP and tubulin in HepG2 BAC-GFP OPA1 cells treated with 2 concentrations DCCD (0.02 or 2µM), DIA (0.02 or 2µM) and CSA (0.1 or 10µM) for 0.5, 2, 5, 8, 24h.

## Supplementary information

***Analysis Steps***

*For MitoTracker Red data:*

- M1 obtain two dataframe files about metadata (Experimental information and Picture information),
- M2 run a python script to filter valid data (regarding the spatial resolution and quality of the images),
- M3 run a python script to find MitoTracker Red images (distinguish between nuclear (408nm) and mitochondrial (561nm) images) to segment mitochondria and get morphological features from segmented mitochondria,
- M4 run a python script to fitting a Gaussian mixture model based on all segmented mitochondria or subsampled part of all objects or objects from subsampled images.
- M5 run a python script to quantify response of mitochondria for each treatment based on image-level info, the response could be the fraction of count or mass of either fragmented or fused mitochondria, see details about the quantification in Appendix B.



*For nucleus data:*

- N1 generate a metadata file to instruct cellprofiler concerning the images to be analysed
- N2 run cellprofiler to segment the nuclei and store them as binary images,
- N3 run a python script to count the nuclei (also possible to count nuclei on the boundaries as fractional nuclei based on their size) or quantify the mass of nuclei

***Quantification of classified mitochondria***

*Features concerning identified nuclei:*

- count_nuclei_interior: number of nuclei who do not lie at boundaries
- count_nuclei_boundary: number of nuclei lying at boundaries
- totalMass_interiorNuclei: total mass of nuclei who do not lie at boundaries (based on mass of segmented objects).
- totalMass_boundaryNuclei: total mass of nuclei lying at boundaries (based on mass of segmented objects)
- count_nuclei_factional: number of nuclei by counting the nuclei at boundaries as fractional nuclei (based on mass of segmented objects)

*Features concerning identified mitochondria:*

- nFragmentedMito: number of fragmented mito per image
- nFusedMito: number of fused mito per image
- nTMito: total number of mito per image

- aSumFragmentedMito: sum of mass of fragmented mito per image
- aSumFusedMito: sum of mass of fused mito per image
- fractionFragmentedMitoNumber: fraction of the count of fragmented mito
- fractionFragmentedMitoMass: fraction of the mass of fragmented mito

*Features concerning both:*
- nFragmentedMitoPerCell: number of fragmented mito per cell
- nFusedMitoPerCell number of fused mito per cell
- nTMito: total number of mito per image
- aSumFragmentedMitoPerCell: sum of mass of fragmented mito per cell
- aSumFusedMitoPerCell: sum of mass of fragmented mito per cell
- nFragmentedMitoPerNucleiMass: number of fragmented mito normalized by total mass of nuclei
- nFusedPerNucleiMass: number of fused mito normalized by total mass of nuclei
- aSumFragmentedMitoPerNucleiMass: sum of mass of fragmented mito normalized by total mass of nuclei
- aSumFusedMitoPerNucleiMass: sum of mass of fused mito normalized by total mass of nuclei

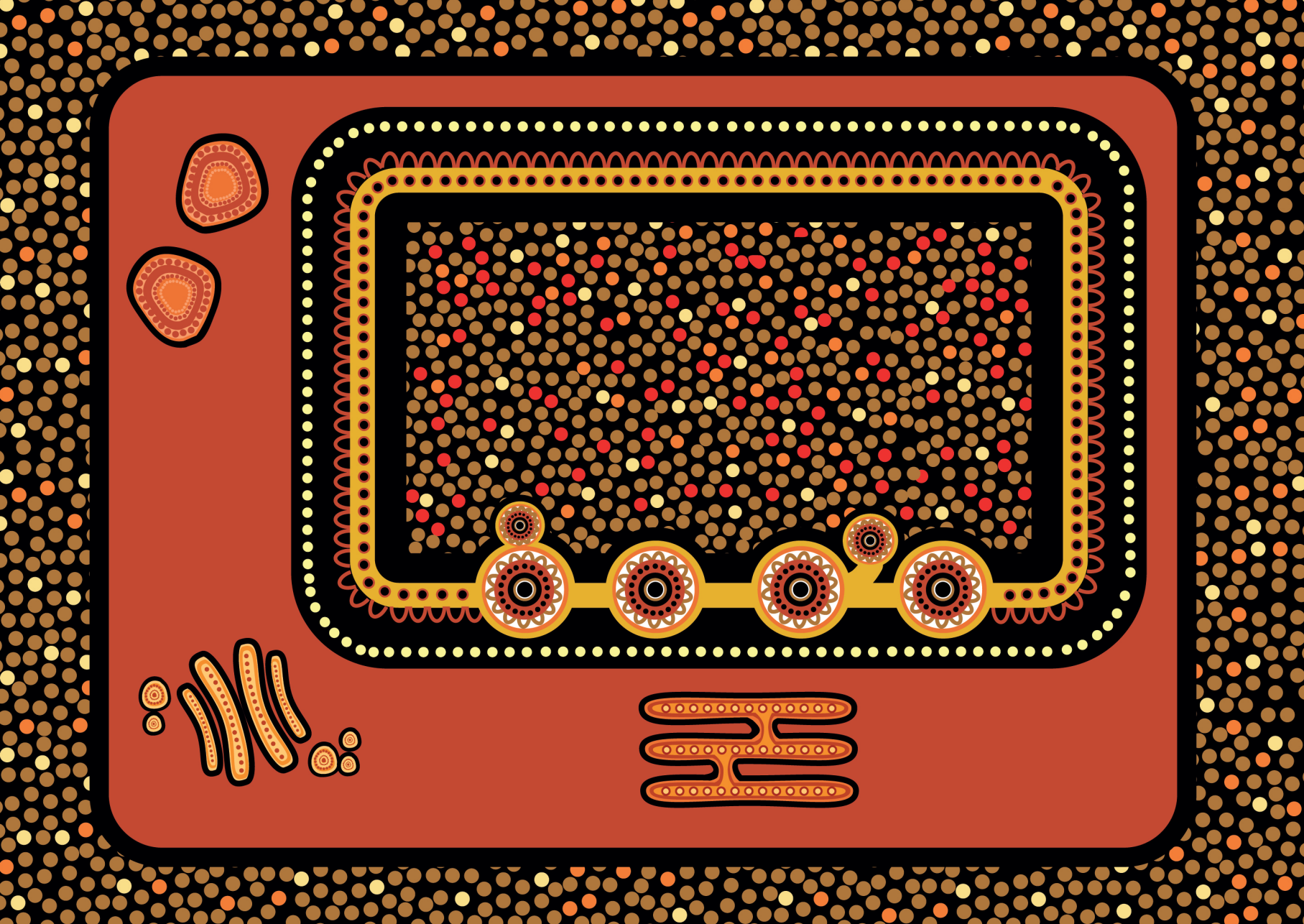

# 6

# Dynamic modeling of mitochondrial membrane potential upon exposure to mitochondrial inhibitors

Huan Yang, Wanda van der Stel, Randy Lee, Caroline Bauch, Sam Bevan, Paul Walker, Bob van de Water, Erik H.J. Danen, Joost B. Beltman#

*Front Pharmacol. 2021 Aug;12:679407; doi: 10.3389/fphar.2021.679407*

**Mitochondria are the main bioenergetic organelles of cells. Exposure to chemicals targeting mitochondria therefore generally results in the development of toxicity. The cellular response to perturbations in cellular energy production is a balance between adaptation, by reorganization and organelle biogenesis, and sacrifice, in the form of cell death. In homeostatic conditions, aerobic mitochondrial energy production requires the maintenance of a mitochondrial membrane potential (MMP). Chemicals can perturb this MMP, and the ex- tent of this perturbation depends both on the pharmacokinetics of the chemicals and on downstream MMP dynamics. Here we obtain a quantitative understanding of mitochondrial adaptation upon exposure to various mitochondrial respiration inhibitors by applying mathematical modeling to partially published high-content imaging time-lapse confocal imaging data, focusing on MMP dynamics in HepG2 cells over a period of 24h. The MMP was perturbed using a set of 24 compounds, either acting as uncoupler or as mitochondrial complex inhibitor targeting complex I, II, III or V. To characterize the effect of chemical exposure on MMP dynamics, we adapted an existing differential equation model and fitted this model to the observed MMP dynamics. Complex III inhibitor data were better described by the model than complex I data. Incorporation of pharmacokinetic decay into the model was required to obtain a proper fit for the uncoupler FCCP. Furthermore, oligomycin (complex V inhibitor) model fits were improved by either combining pharmacokinetic (PK) decay and ion leakage or a concentration-dependent decay. Subsequent mass spectrometry measurements showed that CCP had a significant decay in its PK profile as predicted by the model. Moreover, the measured oligomycin PK profile exhibited only a limited decay at high concentration, whereas at low concentrations the compound remained below the detection limit within cells. This is consistent with the hypothesis that oligomycin exhibits a concentration-dependent decay, jet awaits further experimental verification with more sensitive detection methods. Overall, we show that there is a complex interplay between PK and MMP dynamics within mitochondria and that data-driven modeling is a powerful combination to unravel such complexity.**

**Keywords:** mitochondrial respiration, mitochondrial membrane potential, dynamic modeling, parameter identifiability, uncertainty quantification, high-throughput microscopy imaging

## Introduction

Mitochondria are essential for the regulation of cellular processes including apoptosis, calcium and lipid homeostasis, biogenesis and energy generation (Wojtczak and Zab-locki, 2008). Energy generation in the form of ATP is crucial to support proper functioning of the cell, including active transport, cellular communication and transcription. The process of energy generation is a combination of cytosolic and mitochondrial processes. Within the cytosol, glucose is converted through glycolysis into (net) 2 ATP molecules, 2 NADH molecules and 2 pyruvate molecules. Within mitochondria, pyruvate is the starting material for the tricarboxylic acid (TCA) cycle: Its electrons are used to produce 2 ATP molecules and to reduce NAD to NADH (8 molecules) and FADH to FADH2 (2 molecules). The electrons stored in NADH and FADH2 are transferred via a series of mitochondrial membrane complexes (together termed the electron transport chain (ETC)) to oxygen. This process is called oxidative phosphorylation (OXPHOS). The energy released during the electron transfer over the first 4 complexes (Complex I, II, III and IV) is utilized to create a proton gradient over the membrane separating the mitochondrial intermembrane space from the mitochondrial matrix. This mitochondrial membrane potential (MMP) is then utilized by the fifth complex, an ATP synthase, to generate 32 ATP molecules.



Mitochondrial dysfunction can severely hamper proper cell functioning as it is often accompanied by a reduced ETC efficiency and lowered ATP synthesis (Nicolson, 2014). Inhibition of the mitochondrial complexes and uncoupling of the ETC from the ATP synthase have been observed upon exposure to various drug classes (Dykens et al., 2007; Xia et al., 2018). Mitochondrial malfunctioning resulting from exposure to chemicals will induce cellular signaling pathways involved in adaptation and protection of the cell (Yuan and Kaplowitz, 2013; Atienzar et al., 2016). When the induction of these stress adaptation pathways is insufficient to alleviate the mitochondrial stress, massive mitochondrial failure can occur, resulting in cell death followed by organ failure as can be observed for acute liver failure (ALF) (Yuan and Kaplowitz, 2013).

Four well-known classes of chemicals causing mitochondrial dysfunction, through interference with OXPHOS, are mitochondrial complex I, III and V inhibitors, and uncouplers. Complex I and III inhibitors block electron transfer at the respective ETC complexes, which impedes MMP buildup and thus impairs subsequent ATP generation (Li et al., 2003; Balaban et al., 2005). Uncouplers do not inhibit one of the mitochondrial membrane complexes, but dissipate the MMP by transporting protons from the mitochondrial intermembrane space back to the mitochondrial matrix (Benz and McLaughlin, 1983). As a result, OXPHOS is uncoupled from the ETC leading to low ATP generation. The complex V inhibitor oligomycin binds to the Fo subunit of

the mitochondrial F1-Fo ATP synthase (Symersky et al., 2012). As a consequence, the protons necessary to power ATP synthesis during OXPHOS cannot flow through complex V anymore which causes a reduction of mitochondrial ATP production.

A multitude of compounds with different targets such as the above-mentioned chemical classes can hamper mitochondrial functioning. Currently, a knowledge gap exists for the exact mechanisms of mitochondrial dysfunction on a molecular level as well as subsequent adaptation upon such dysfunction. A promising way forward is to utilize high-throughput measurement techniques to collect dynamic data on the mitochondrial membrane potential (Wink et al., 2017). Moreover, obtaining a quantitative, mechanistic understanding of such in vitro experiments is desirable (Council et al., 2007), which can be achieved through application of dynamic modeling in the form of ordinary differential equation (ODE) models to describe experimental measurements (Kuijper et al., 2017; van Riel, 2006; Yang et al., 2020). Such mechanistic models can be utilized to generate hypotheses and to formally test whether a data set is consistent with these hypotheses (van Riel, 2006; Brodland, 2015). Ideally, this leads to specifically designed follow-up experiments, thus continuing a loop between experimental and in silico work.

Two categories of mechanistic models have previously been established with respect to mitochondrial functioning: biophysical (Cortassa et al., 2003; Beard, 2005; Wu et al., 2007) and holistic models (Ainscow and Brand, 1999; Yang et al., 2015; Bois et al., 2017). Biophysical models are highly detailed and offer the possibility to generate hypotheses on specific biophysical processes taking place in mitochondria. For example, the model by Beard (2005) provides a powerful description of the ETC, as well as of the transport of cations and other substrates. As such, this offers mechanistic insight at the level of individual complexes and of the process of OXPHOS. A downside of this biophysical model is its complexity (17 state variables), which lowers the potential for accurate estimation of the involved parameters. This precludes application of the model to high-throughput toxicity screens where a lot of compounds are evaluated at once. In practice, biophysical models have therefore been optimized for isolated mitochondria, whereas toxicity screens are typically performed with live cells (Wink et al., 2017). Extrapolating the MMP behavior observed for isolated mitochondria to that of entire cells would be a difficult task for which large amounts of data and many validation steps are required.

Holistic models describing the mitochondrial membrane potential are typically simpler than biophysical models and are focused on in vitro to in vivo extrapolation (IVIVE). To investigate the role of mitochondrial functioning for energy metabolism in rat hepatocytes, Ainscow and Brand (1999) performed top-down control analysis by

investigating fluxes of important mitochondrial processes. Another recently proposed holistic ODE model, termed MITOsym (Yang et al., 2015), focused on mitochondrial bioenergetics rather than on the molecular level. The model has seven state variables and contains the most important elements of mitochondrial functioning, including MMP, ATP, glucose and oxygen levels. MITOsym was calibrated using real-time experimental data obtained from a human hepatoma cell line (HepG2).

Here, we develop a flexible model of low complexity that offers mechanistic insight in the cellular adaptations upon exposure to various OXPHOS inhibitors. We first simplified the previously published MITOsym model (Yang et al., 2015) by focusing primarily on modeling of the MMP. We calibrated our model to live-cell microscopy data on MMP dynamics upon exposure to a partially published set of 24 mitochondrial inhibitors (van der Stel et al., 2020) including the classical inhibitors rotenone (complex I inhibitor), antimycin A (complex III inhibitor), oligomycin (complex V inhibitor) and FCCP (uncoupler). The model described the data from ETC complex inhibitors reasonably well, but model extension with intracellular decay was required to describe the MMP response to FCCP and oligomycin. For oligomycin, addition of ion leakage from the mitochondrial intermembrane space to the mitochondrial matrix, or introduction of a concentration-dependent compound decay further improved the fit. We performed mass spectrometry measurements, which confirmed the presence of such decay for FCCP, yet we measured only limited oligomycin decay at high concentrations. At low oligomycin concentrations, compound recovery was below the detection limit. These findings are consistent with a concentration-dependent oligomycin decay explaining the complicated temporal pattern of the MMP for this compound, although more sensitive compound detection methods will be required to experimentally test this hypothesis.



## Material and Methods

### Cell culture

The HepG2 cell line was obtained from ATCC (American Type Culture Collection, Wesel, Germany). We cultivated the cell line in Dulbecco's modified Eagle's medium (DMEM) (cat. No. 11504496, Fisher Scientific) supplemented with 10% (v/v) fetal bovine serum (cat. No. S181L-500, South American, Fisher Scientific) , 25U/ml penicillin and 25µg/mL streptomycin (cat. No. 15070-063, Fisher Scientific). Cells were split every 3 to 5 days and kept at 37°C and 5% CO2.

### Chemicals

All chemicals were purchased from Sigma Aldrich, including FCCP (cas no. 370-86-5, order no. C2920) and oligomycin (cas no. 1404-19-9, order no. O4876). Other chemicals

used for the assessment of various ETC inhibitors were also obtained from Sigma Aldrich, but redistributed by the JRC (Ispra, Italy). This included capsaicin (cas no. 404-86-4 , order no. M2028), deguelin (cas no. 522-17-8, order no. D0817), fenazaquin (cas no. 120928-09-8, order no. 31635), fenpyroximate (cas no. 134098-61-6, order no. 31684), pyridaben (cas no. 96489-71-3, order no. 46047), pyrimidifen (cas no. 105779-78-0, order no. 35999), rotenone (cas no. 83-79-4, order no. R8875), tebufenpyrad (cas no. 119168-77-3, order no. 46438), carboxin (cas no. 5234-68-4, order no. 45371), fenfuram (cas no. 24691-80-3, order no. 45486), flutolanil (cas no. 66332-96-5, order no. N12004), mepronil (cas no. 55814-41-0, order no. 33361), thifluzamide (cas no. 130000-40-7, order no. 49792), antimycin A (cas no. 1397-94-0 , order no. A8674), azoxystrobin (cas no. 215934-32-0, order no. 3167), cyazofamid (cas no. 120116-88-3, order no. 33874), fenamidone (cas no. 161326-34-7, order no. 33965), hydramethylnon (cas. No 67485-29-4, order 35373), kresoxim-methyl (cas. No 143390-89-0, order no. 37899), picoxystrobin (cas no. 117428-22-5, order no. 33568), pyraclostrobin (cas no. 175013-18-0, order no. 33696), trifloxystrobin (cas no. 141517-21-7, order no. 46477). The chemicals were dissolved in dimethyl-sulfoxide (DMSO, Biosolve) and stored at -80°C for long-term storage and -20°C for short-term usage. In all experiments the maximal solvent end concentration was 0.2% (v/v). The MMP, Hoechst and PI measurements were previously published for 21 mitochondrial inhibitors (van der Stel et al., 2020), and these were supplemented with measurements for hydramethylnon, FCCP and oligomycin.

**Confocal imaging**

Cells were seeded at a density of 10.000 cells/well in black µClear 384 well plates (Greiner Bio-One). Two days after seeding, the cells were stained with Hoechst33342 (final conc = 200ng/mL) (cat.no. H1399, Life technologies) and Rhodamine123 (final conc = 1µM) (cat no. R8004-5MG, Sigma Aldrich) for 75min. After 75min the medium (for exact composition see Table S1) was refreshed into medium containing Rhodamine123 at a concentration of 0.2µM) in order to compensate for minor dye loss, yest keeping the dye concentration low to prevent potential toxicity. In addition, at the moment we added Propidium Iodide (conc. = 100nM) (cat. No. P4170, Sigma Aldrich) and the test chemical in the desired concentration. A Nikon TiE2000 with perfect Focus System, xy-stage and incubator (Nikon, Amsterdam, The Netherlands) with 20x objective was used to capture the Hoechst, (408nm), Rho123 (488nm) and PI (561nm) signals every hour.

**Image analysis**

The segmentation of nuclear objects was performed based on Hoechst staining using a WMC segmentation workflow (Di et al., 2012) implemented in ImageJ (version 1.51h).

Segmentation quality depended strongly on the Hoechst intensity and therefore the utilized parameters (Gaussian filter, rolling ball filter and noise filter) were chosen based on visual inspection (see Table S2 for chosen values). Further image processing was performed using CellProfiler (version 2.2.0, broad institute, Cambridge USA). The cytoplasm was identified as the area up to five pixels away from the segmented nuclei, excluding the nuclear pixels themselves. Cells were identified as dead when more than 10% of the segmented pixels of a nucleus were also PI positive. Pixels were identified as PI positive or not using automated thresholding with the maximum correlation threshold (MCT) algorithm applied on the complete image (Padmanabhan et al., 2010). The CellProfiler output was subsequently exported as an HDF5 file and further processed using the R package rhdf5[19].

**Quantification of MMP dynamics**

For each segmented cell, we quantified the intensity of the MMP by calculating the integrated intensity of the Rho123 intensity over the entire cytoplasmic domain. The cytoplasmic integrated intensities for all segmented cells within an image (typically hundreds of cells) approximately follows a log-normal distribution, Fig. S1. Therefore, we extracted the geometric mean of the integrated Rho123 intensities as a representative measure for each biological replicate from one plate, and we repeated this for each time point after exposure to the mitochondrial inhibitors. As reported by Perry *et al* (2011), quenching of the Rho123 dye may occur. Indded we observed a gradual decay in Rho123 dynamics for DMSO control conditions (Fig S2, black lines), yet there were also frequently temporary increase in Rho123 which was presumably due to unpredictable dye uptake dynamics. Because both effects on Rho123 (i.e., quenching and uptake) were plate-dependent, we normalized the Rho123 geometric mean with the DMSO controls on the same plate, i.e., we divided the geometric mean from the treatment condition by the DMSO condition from the same plate for each time point separately, thus largely correcting for these experimental artefacts. Among the biological replicates (N = 3 for oligomycin and N = 4 for all other compounds), we took the arithmetic mean and standard error of the mean.

**Mass Spectrometry sample preparation**

Cells were seeded with a density of 20.000 cells/well in black µClear 96 wells plates (Greiner Bio-One, 655090). The cells were stained with Hoechst33342 for 75min before chemical exposure. Cells were exposed for 2, 8 or 24h to oligomycin (0.005, 0.05, and 0.5µM) and FCCP (0.1, 1 and 10µM). 30min before the end of the exposure period the Hoechst intensity was captured using epi-fluorescence on a Nikon TiE2000 confocal microscope with perfect Focus System, xy-stage and incubator (10x objective, 6x7 montage). Imaging was followed by collection of the supernatant and fixation of the

cells using MeOH after 1x PBS wash. Parallel solution plates with the exposure medium without cells were stored simultaneously with the supernatant at -80°C. The methanol was allowed to evaporate from the fixated cells for approximately 2h. Subsequently, the cells were dissolved in water and the cell lysate was stored at -80°C.

**Quantification of compounds in samples by LC-MS/MS**

Samples exposed to FCCP and oligomycin were analysed on a system consisting of an AcquityTM Bi- nary Solvent Manager (BSM), AcquityTM 4 position heated column manager, 2777 Ultra High Pressure Autosampler and a Xevo TQ MS Triple Quadrupole mass spectrometer (Waters Ltd, Herts, UK). The analysis was performed using an AcquityTM HSS T3 column (1.8 µm) 2.1 x 30 mm (Waters Ltd, Herts, UK) fitted with SecurityGuardTM ULTRA Fully Porous Polar C18 cartridge (Phenomenex, Cheshire, UK). The column was maintained at 40°C and the injection volume was 4µL. The mobile phases for FCCP and oligomycin were 10mM ammonium acetate (mobile phase A) and methanol (mobile phase B). A mobile phase gradient from 0% to 95% mobile phase B was employed over 39 sec. The MS source temperature was 150°C and the desolvation temperature was 650°C. For FCCP the cone voltage was 28V, the collision energy was 20eV, the MRM was 253.06>201.01 and negative ionisation mode was used. For oligomycin the cone voltage was 21V, the collision energy was 10eV, the MRM was 789.54>789.64 and negative ionisation mode was used.

To determine a chromatogram, under certain LC system conditions the compound of interest (analyte) will be separated and elute from the column at a specific retention time. Using the same conditions, if an unknown sample containing the same analyte is injected into the LC system, a peak that corresponds to the analyte would be present with the same retention time. In order to determine the compound quantity present in the sample, the chromatogram is analysed by quantifying the area under the peak, which is directly proportional to the total amount of analyte in the sample. In order to give an absolute quantification a standard curve of the analyte is required.

Separate standard curves were created for FCCP and oligomycin by spiking in known concentrations of these compounds into samples containing water (as was done for the cell lysate samples). For oligomycin, the standard curve showed that at low spike-in concentrations a detection threshold occurred. Therefore, for the cell lysate samples we only incorporated measurements over time for the highest concentration. Because the standard curve was linear above this detection threshold, we directly utilized the measured peak areas for further analysis. The peak areas were adjusted by dividing the values by a machine internal standard value that was determined for each data point separately, and by dividing by the estimated volume of all cells, resulting in a value proportional to the concentration within individual cells. The

nuclear count needed to estimate the cell volume was based on the epi-fluorescent images collected 1h before sample collection, which were analyzed using an in-house macro for ImagePro software version 7.01 (Media Cybernetics). The macro performed intensity segmentation based on a watershed method (filtering on size and shape) after background correction (flatten function and edgefilter). The used parameters for the watershed method included: Intensity threshold = 1000, Meanintensity = 0.1, Edgefilter = 3, RemoveNarrowObjects = TRUE, Minarea = 15 pixels, Maxarea = 4000 pixels). Subsequently, the total volume of the cells was determined based on the nuclear count and a diameter of 30μm. The resulting values were representative for the relative concentration at different time points after exposure. In order to compare experimental measurements to model predictions, we transformed the measurements within cell lysate samples at three time points (2 hr, 8 hr and 24 hr) into ratios relative to earlier time points. For this we considered all possible pairings, i.e. the three ratios 8 hr vs 2 hr, 24 hr vs 8 hr, and 24 hr vs 2 hr.

**Dynamic model of oxidative phosphorylation**

We constructed an ODE model to describe the experimentally observed MMP dynamics by refining the previously published MITOsym model (Yang et al., 2015). Our model has two state variables: oxygen level ([O]) and MMP (Ψ). Compared to the seven variables in the original MITOsym model, we omitted the variables related to glycolysis, because we did not acquire data related to this process. The variables [O] and Ψ were retained because our experiments aimed to measure the MMP, which strongly depends on the oxygen level due to oxygen consumption by complex IV during its oxidation of cytochrome C.



To describe the dynamic changes in the oxygen level, we considered the oxygen supply into mitochondria to take place at a constant rate during our in vitro MMP measurements (set to a value of 0.6, following Yang et al. (2015)). Moreover, in the absence of perturbations, oxygen is consumed at a constant rate that linearly depends on the oxygen level itself by activity of ETC complex IV. In the presence of a complex IV inhibitor, the consumption rate is decreased, which we model with Michaelis-Menten kinetics as

$$\frac{d[O]}{dt} = 0.6 - K_E[O]\frac{K_{Ei}}{K_{Ei} + [D_E]} \tag{1}$$

Here, the second term is the total oxygen consumption rate (OCR), with KE representing the maximal rate of oxygen consumption, $[D_E]$ representing the effective concentration of the applied inhibitor and $K_{Ei}$ representing the inhibitor concentration at which the OCR is half-maximal. Note that our data set did not consist of complex

IV inhibitors, but inhibitors of complex I, II and III are considered to also affect the second term in Eq. (1).

The MMP is built up by proton flow, which occurs in two directions in our model. First, protons are pumped from the mitochondrial matrix into the intermembrane space by complexes I, III and IV, which depends on pyruvate as a main source for the TCA cycle and on oxygen. We describe this by considering the proton flux into the intermembrane space as proportional to the OCR. Second, depletion of the MMP occurs due to ATP synthesis which occurs by complex V along with proton flux back into the matrix. MMP depletion can also occur due to the presence of an uncoupling agent that transports protons into the matrix. Proton depletion due to ATP synthesis and uncoupler activity both follow Michaelis-Menten kinetics in our model. Exposure to an inhibitor of ATP synthesis leads to a decreased MMP depletion rate, which we also describe with Michaelis-Menten kinetics. We incorporate these processes into the equation for Ψ as follows:

$$\frac{d\psi}{dt} = C_f K_E [O] \frac{K_{Ei}}{K_{Ei} + [D_E]} - \frac{V_A\, \psi}{K_A + \psi} \frac{K_{Ai}}{K_{Ai} + [D_A]} - \frac{V_U\, [D_U]}{K_U + [D_U]}\, \psi \qquad (2)$$

Here, $C_f$ is a coefficient that scales the OCR to the rate at which the proton gradient is established, VA is the maximal ATP synthesis rate, $K_A$ is the MMP for which the ATP synthesis rate is half-maximal, $K_{Ai}$ is the concentration at which the inhibition of ATP synthesis is half-maximal for a particular inhibitor, $[D_A]$ is the effective concentration of that ATP synthesis inhibitor, $V_U$ is the maximal proton flux towards the matrix due to uncoupler activity, $K_U$ is the concentration at which uncoupler-mediated proton flux is half-maximal, and $[D_U]$ is the effective concentration of uncoupler. Note that we set $V_U = 1$ and $K_U = 1$, which together with the free parameters for time scaling (see below) and $[D_U]$ was sufficient to describe uncoupler effects.

Although in the current model we consider a fixed relation between the OCR and the rate at which the proton gradient is established (*Cf*), this relation may in reality differ between mitochondrial inhibitors or vary over time. Moreover, the *Cf* parameter, along with other parameters, likely depends on the exact composition of the medium because that could affect cellular respiration processes, such as those relying on NADH. Note that changes in medium composition over time due to uptake of medium components by cells could therefore result in time-varying parameters such as *Cf*. However, the goal of our study was not to study the relation between OCR and MMP in such detail, and would require structured evaluation of the effect of different medium compositions.

**Scaling parameters**

The cells are considered to maintain homeostasis before exposure to any compound. Therefore, we determine the steady state by setting the right hand sides of the ODEs equal to zeros and solving analytically (Supplementary Text). Because the experimentally obtained data are based on image intensity and microscopy settings are such that we are not in the saturating regime for the detectors, the intensity readouts should have a linear relationship with the MMP. Therefore, we introduce two scaling parameters $c_1$ and $c_0$ to map the MMP to the normalized Rho123 intensity (which is measured in arbitrary units):

$$y = c_1\psi + c_0 \tag{3}$$

Quenching of the Rho123 dye278 over time as well as differential dye uptake dynamics between plates led to somewhat unpredictable Rho123 dynamics in DMSO control conditions (also see subsection on 'quantification of MMP dynamics' and black lines in Fig. S2). To prevent this unpredictability from affecting the scaling parameters $c_1$ and $c_2$, we normalized the experimental data for the mitotoxicant-induced Rho123 intensities by the intensities when treated with DMSO (by dividing by the latter). The normalized intensities were subsequently utilized during model calibration to determine the optimal model parameters, including the scaling parameters. Note that only the experimental data and not the simulation data were thus normalized; the scaling parameters were utilized for the latter purpose.



After such normalization of Rho123 intensities, we expected the $c_1$ and $c_0$ parameter values to be the same for all compounds. Therefore, for the exposures at the lowest concentrations for which an MMP response typically does not occur yet, the MMP response normalized to the response to DMSO should be close to 1.0, and the MMP response to the lowest two concentrations should typically be uncorrelated. Indeed, these normalized values were on average around 1.0, but their values ranged from 0.8-1.2, i.e., the variability was relatively large (Fig. S3). Importantly, contrary to the expectation, there was a clear correlation between the normalized MMP values at the lowest2 concentrations (R2 = 059). Thus, the early Rho123 intensity at the lowest two concentrations is compound specific, which could for instance arise from the specific locations of the wells within the plates. Because of this observation, we included separate scaling parameters ($c_1$ and $c_0$) as free parameters for each compound, rather than selecting common scaling parameters across

In addition to scaling parameters $c_1$ and $c_2$, we introduced a parameter r to scale time for both [O] and Ψ, thus controlling the relative rates of change (Supplementary text), and implying that the rate parameters are expressed in arbitrary units.

**Model extensions**

Because for the compound oligomycin (complex V inhibitor) the above model could not qualitatively describe the MMP data, we extended the model with potential-dependent proton leakage for oligomycin only. There is evidence for such leakage for very high MMPs such as those occurring in the presence of oligomycin (Porter and Brand, 1995). Moreover, Berthiaume et al. (2003) reported an overshoot of the MMP upon staining with the dye JC1, and proposed an empirical linear ODE model for the MMP while incorporating proton channel leakiness. Their model-based analysis showed a good fit to the observed MMP during the first 2 hours of increased MMP dynamics. Although proton leakage may depend on the MMP in a non-linear fashion, for slight MMP perturbations a linear relation is a reasonable approximation. Therefore, and inspired by the flux equation for leakage of proton and potassium described by Beard (2005) (Supplementary text), we added leakage to the equation for the MMP in the form of the product term $\alpha(\Psi - \Psi^{o})H(t)$:

$$\frac{d\psi}{dt} = 0.6C_f - \frac{V_A\psi}{K_A + \psi}\frac{K_{Ai}}{K_{Ai} + [D_A]} - \alpha(\psi - \psi^{o})H(t) \tag{4}$$

Here, $\alpha$ is the leakage rate and $\Psi^{o}$ denotes the MMP steady state, ensuring that the steady state is the same as in the original ODE model without leakage. $H(\cdot)$ is a Heaviside function, ensuring that the leakage term is only relevant upon exposure.

For the compounds FCCP and oligomycin, we also studied whether explicit description of the in vitro pharmacokinetics (PK) of the compounds (i.e., a decrease of effective concentrations over time) improves the model fits to the data. To extend the model (Eq. (2)) with such pharmacokinetic decay, we introduced the following function with decay rate $\gamma$:

$$[D_X]_i = [D^{O}{}_X]_i \exp(-\gamma\, t)H(t) \tag{5}$$

Here, $[D^{o}{}_X]_i$ represents the effective concentration in the mitochondrial compartment for one of the inhibitor types (in this case only applied for uncouplers ($[D_U]$) and for ATP synthesis inhibitors $[D_A]$) and index $i$ denotes the applied concentration of the compound in an ascending order. By default we consider a constant decay rate ($\gamma$) that is valid for all concentrations from one compound. For oligomycin, we also consider a model extension in which the compound decay rate is concentration-dependent (Supplementary text).

**Model calibration**

In order to determine suitable model parameters that can explain the dynamics observed from our imaging experiments, parameter selection was done based on MMP measurements. The parameters chosen for optimization included the Michaelis-Menten parameters for ATP synthesis, i.e., $V_A$ and $K_A$, the effective concentrations of inhibitors DX and the scaling parameters $c_1$, $c_0$, and γ. We also consider the case where the parameters $V_A$, $K_A$ and γ are shared across complex I, II and III inhibitors and only the effective concentrations and c1 and c0 are chemical dependent.

Per condition (one single concentration for one compound), the weighted residuals (denoted by R) are defined by the weighted difference between the simulation and the data. Then the sum of $R^2$ quantifies the match between model prediction and observation as follows:

$$R^2 = \sum_{i=1}^{n_t} \frac{\left(y_i^M(\theta) - y_i^D\right)^2}{\sigma_i^2} \tag{6}$$

Here, σ denotes the standard error amongst the replicates, $y^D$ and $y^M(\theta)$ represent experimental observation and model output evaluated with free parameters θ, respectively. We use $i$ to index the time points; in total we have $n_t$ = 23 time points per compound concentration.

To fit the data for an entire set of applied treatment conditions, we minimized the following cost function (i.e. the negative log-likelihood function):

$$\log L(\theta) = \frac{\sum_j^m R_j^2}{2} \tag{7}$$

where the subscript j indexes the treatment condition in a group of m conditions in total.

To estimate the values of the model parameters (θ), we employed a least squares approach with a Trust Region Reflective algorithm and sensitivity equations (Raue et al., 2013). We employed a multi-start approach to find the global minimum of Eq. (7) (Raue et al., 2013), by randomly generating a set of 100 starting values for each free parameter within a broad range. The maximum likelihood estimate was found by ranking the output cost function values amongst all parameter starting values. Best-fitting parameter estimates are provided in Table S3 (for the basic model with separate fitting for the compounds), Table S4 (for the basic model with joint fitting for the compounds), Table S5 (for the model with compound degradation), Table S6 (for the model with compound degradation and ion leakage) and Table S7 (for the model with concentration-dependent compound degradation). Code to simulate the parameterized models is available at https://zenodo.org/record/5140277.

**Statistical tests**

We applied the non-paramteric Kolmogorov_smirnov (KS) test (Massey Jr. 1951) to study which type of ETC complex inhibitor is better described by our model. We perfomrd a KS test for three inhibitor type pairs: I vs II, II vs III, I vs III.

**Profile likelihood and bootstrapping**

In order to identify the limitations of our models with respect to parameter estimation, we inspected the uncertainties in the estimated parameters (Fröhlich et al., 2014). Specifically, we focused on the leakage rate (α; applied for oligomycin) and compound decay rate (γ; applied for FCCP and oligomycin). To this purpose, we applied both a profile likelihood (PL) approach and bootstrapping.

In a PL approach one calculates a confidence interval, yet it also helps to identify parameters that are structurally non-identifiable (Raue et al., 2009; Yang et al., 2016). The confidence interval for a parameter is determined by computing the dependence of the maximum likelihood (i.e., the two-fold logL, or NPL) on the parameter that is being profiled (i.e., fixed at different values). Subsequently, this 'NPL curve' is cut at a threshold of min(NPL) + $x^2(\alpha_{CI}, df = 1)$, i.e., using an underlying $x^2$ distribution at confidence level $\alpha_{CI}$ with 1 degree of freedom (Raue et al., 2009). Note that the invariant property of the maximum likelihood estimate guarantees that the 95% confidence interval of a quantity depending on system parameters can be directly profiled (Moser, 1996). We applied the PL approach and also mathematically analyzed our equations to potentially increase parameter identifiability in refined models (Supplementary text).

Besides the PL approach, we also applied bootstrapping to determine confidence intervals. To achieve this, we generated realistic artificial replicates from the biological replicates as follows: First, we performed 'inter plate bootstrapping' by selecting the same number of biological replicates with replacement as in the original data (note that each biological replicate was on a separate plate). Thus, we sampled four biological replicates at inter plate level for FCCP, and three biological replicates for oligomycin. Second, we applied 'intraplate bootstrapping' to each selected biological replicate. We achieved this by pooling all single-nuclei objects coming from two technical replicates measured from the same well and measured at the same time point. We then sampled from this pool of single-cell data with replacement until we had selected the same number of objects as in the original data. This subset was handled in the same way as the original data, i.e., we calculated the geometric mean for all objects within the subset and applied normalization based on the fluorescence intensities observed for DMSO treatments. As a final step, the mean and standard error (SE) was calculated for the artificially generated replicates at all-

time points. Afterwards we performed parameter estimation to re-fit our model to the bootstrapped data, using the previously obtained optimal parameter values as starting values. In total, we generated 200 bootstrap samples and calculated 95% and 99% confidence intervals based on sample quantiles. This was achieved by utilizing the parameter values obtained at the quantiles (95% and 99%) to conduct ODE simulations that predict the pharmacokinetics of FCCP and oligomycin and thus obtained a 95% confidence interval at each time point.

The model predictions for the relative change in compound level between the time points for which we had experimental measurements can be directly calculated from the estimated value for γ because the effective concentration decays exponentially in our model:

$$R_{T2/T1} = \exp\left(-\gamma(T2 - T1)\right) \tag{8}$$

Here, *T1* and *T2* are the two time points where compound levels are measured. We computed RT 2/T 1 for the three pairs of comparison (*T1* = 2, *T1* = 8), (*T1* = 2, *T2* = 24), and (*T1* = 8, *T2* = 24). Moreover, the 95% and 99% confidence intervals for these ratios were determined either by filling in the PL-based upper and lower values for the estimated γ range, or by filling in the quantile-based estimates resulting from bootstrapping.



## Results

### Construction of an MMP model based on live-cell imaging data

To study the impact of mitochondrial complex inhibitors on the dynamics of the MMP in a live-cell imaging setting, we utilized our previously published data in which HepG2 cells were exposed to a panel of different mitochondrial complex I, II and III inhibitors (van der Stel et al., 2020), and supplemented this with newly generated data for the complex III inhibitor Hydramethylnon, the complex V inhibitor oligomycin and the uncoupler FCCP (Fig. 1). The MMP was monitored every hour for 24h on the basis of the intensity of the dye Rho123, which is sensitive for the membrane potential. We also assessed the effect of chemical exposure on cellular health based on co-staining of hoechst and the cell death marker propidium iodide (see Methods). Exposure scenarios which affected the MMP typically did not induce cell death in the studied period (Fig. S4A-B). Complex III inhibitor Hydramethylnon was an exception; application of this compound at high concentrations did lead to cell death (Fig. S4C).

Based on the experimentally observed MMP dynamics, we next aimed to develop a mathematical model to quantitatively describe the MMP response (Fig. 2). We adapted the previously published MITOsym model (Yang et al., 2015) to a two-state

model (oxygen and the MMP; white boxes in Fig. 2) because we mainly had data on the membrane potential Ψ. In the absence of measurements on other characteristics such as glucose or pyruvate level, we considered those states to be constant, i.e., the flux from pyruvate into OXPHOS (dark grey box in Fig. 2) was considered constant rather than dynamic.

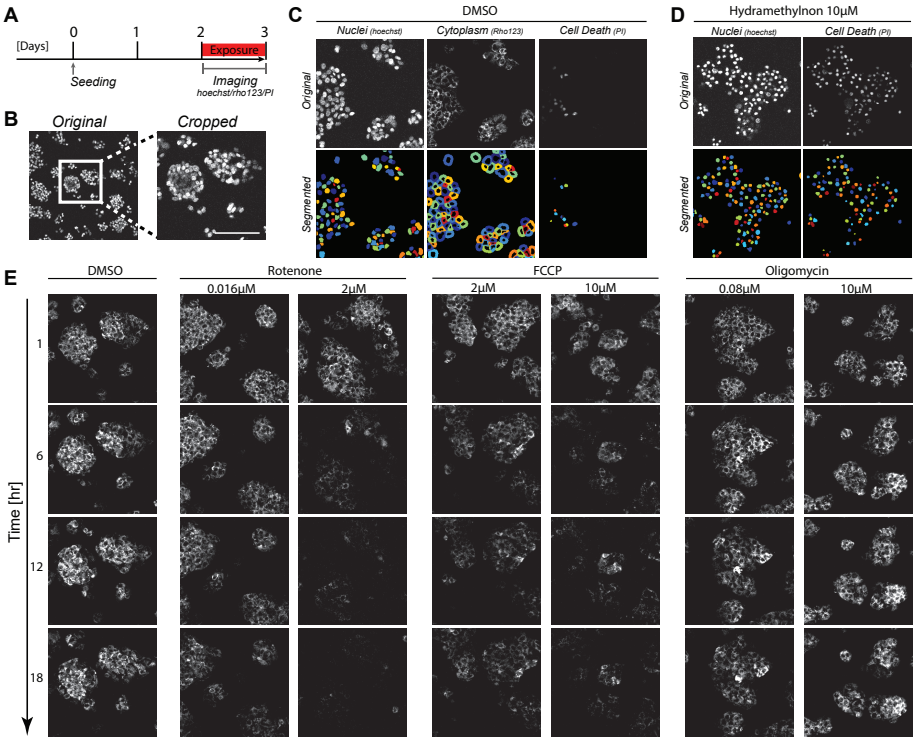


**Figure 1: Image-based measurements over time in HepG2 cells**
**A)** Schematic representation of the experimental set-up. HepG2 cells were imaged for 24h to track Rho123 (MMP), Hoechst (cell nuclei) and PI (necrosis) abundance following 2 days of cell seeding. **B)** Representative images showing original image dimensions and a cropped image. **C-D)** Images of Hoechst, Rho123 and PI staining (top panels) and the resulting segmentation from cellprofiler (bottom panels). Images originate from a vehicle treated condition with 0.2%DMSO for 1h **(C)** or a toxic condition with 10μM hydramethylnon exposure for 24h **(D)**. **E)** Representative Rho123 images over time upon exposure to 0.2% DMSO, Rotenone, Antimycin A or Oligomycin for 1, 6, 12, and 18h.

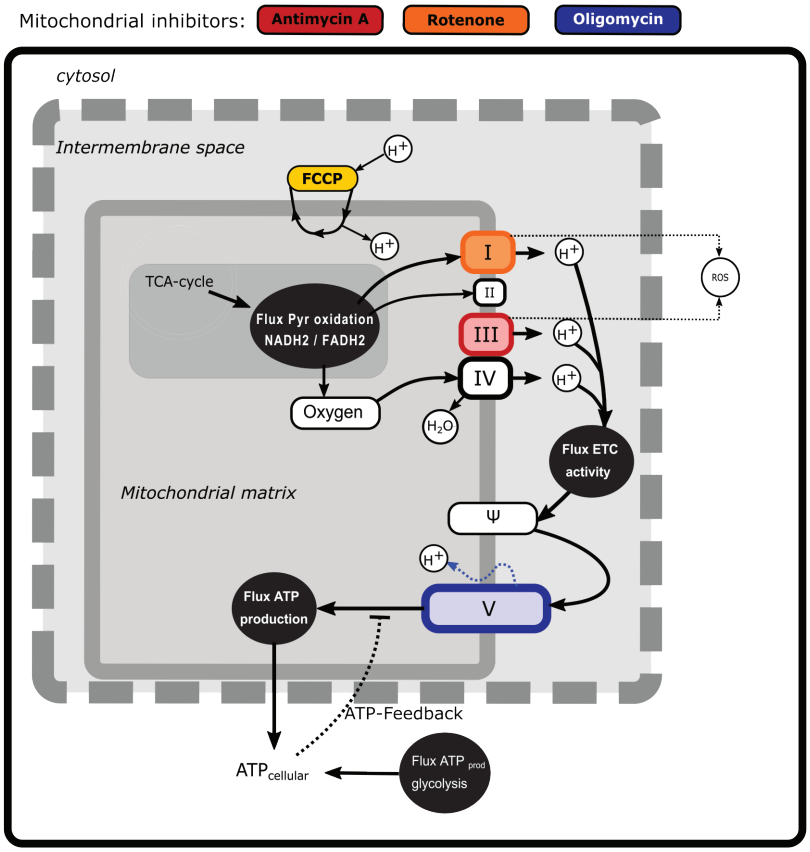


**Figure 2: Scheme illustrating mechanistic information on mitochondrial energy generation and modeled components**.
The state variables that are included in the model (Oxygen and ψ) are shown in the white boxes, while fluxes are depicted by black circles. The non-modelled TCA cycle is indicated in dark gray. The sites of action of four classical mitochondrial inhibitors (FCCP, Antimycin A, Rotenone and Oligomycin) are shown in color.

## Basic model describes exposure to classical ETC inhibitors

We first applied our basic two-state MMP model on the MMP data obtained upon exposure to the classical mitochondrial inhibitors rotenone and antimycin A to test whether it can quantitatively describe the MMP dynamics. We employed maximum likelihood estimation in order to determine the parameters that optimally describe the MMP dynamic data (Fig. 3A). For antimycin A (Fig. 3B; symbols) and rotenone (Fig. 3C; symbols), the data exhibit a gradual decrease of the MMP for low concentrations (e.g., 0.016 μM rotenone), whereas a steep decrease is observed for high concentrations (e.g., 2.0 μM rotenone). Our basic model fitted the MMP dynamics for these inhibitors quite well despite mismatches at some concentrations (Fig. 3B-C, cyan lines). Note that at the lowest concentration antimycin A (Fig. 3B, a substantial deviation of the

model fit to the mean Rho123 intensity of the four replicates occurs, which we attribute to the relatively high variability among the replicates.

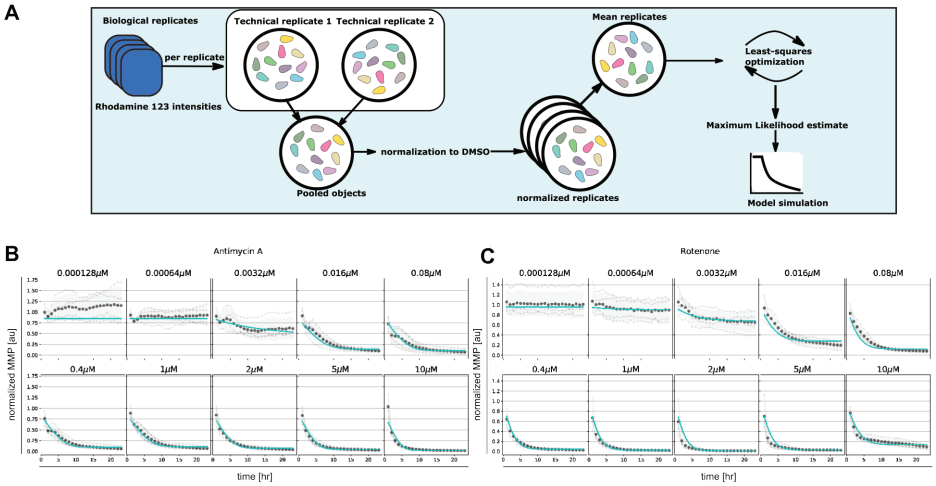


**Figure 3: Model fitting to classical mitochondrial inhibitors Antimycin and Rotenone**.
**A)** Flowchart illustrating the steps for single cell analysis, normalization and model parameter estimation. **B-C)** Quantified MMP dynamics and model fits upon exposure of HepG2 cells to Antimycin **(B)** and Rotenone **(C)** at 10 concentrations. Gray lines and symbols represent individual experimental replicates, black dots and shading represent the mean and standard deviation of all replicates, and cyan lines represent best fits with the basic model. Note that all model parameters are kept free during parameter estimation.

We next asked whether the model could also describe the MMP dynamics for an extensive set of ETC inhibitors affecting either complex I, II or III activity. Inhibitors of complex I and III typically had a large effect on the MMP, whereas complex II inhibitors had only a limited effect. We fitted the data for all compounds either separately, i.e., with all model parameters calibrated per compound (as in (Fig. 3B-C)), or for all compounds at once, i.e., with only the parameters c1 and c0 that map Ψ to the observable y (see Eq. (3)) allowed to vary between the compounds and all other parameters to have the same value across the compounds. In both cases this led to good fits, as illustrated by the examples of deguelin, a complex I inhibitor (Fig. 4A) and azoxystrobin, a complex III inhibitor (Fig. 4B)), which shows the generality of our model with respect to the effect of different ETC inhibitors.

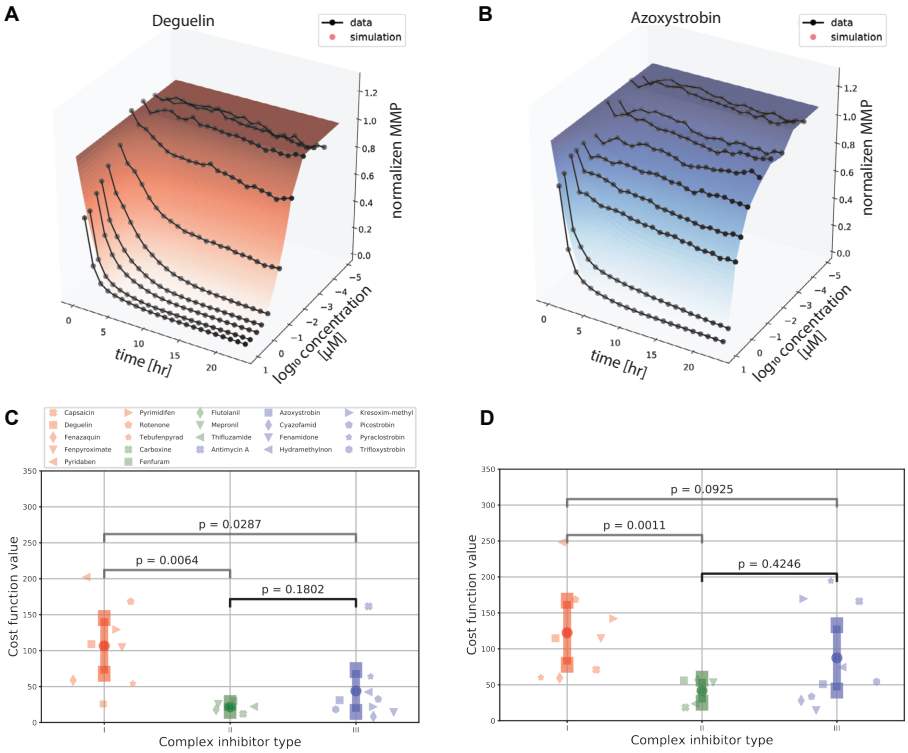


**Figure 4: Comparison of model fits for various ETC inhibitors**.
**A-B)** Landscape of simulated (shaded curved planes) and experimentally determined (gray lines and symbols) concentration-time MMP response following exposure of HepG2 cells to deguelin **(A)** or azoxystrobin **(B)**. Note that in these model fits several parameters were required to be the same across all 22 ETC inhibitors used in the experiments (see Methods). **C-D)** Model fitting performance for all 22 ETC inhibitors (symbols) tackling complex I (red), II (green), or III (blue), using either the combined data for fitting with particular parameters in common **(C)**, or fitting the data for each inhibitor separately with all model parameters kept free **(D)**. The p-values in **(C-D)** are based on a KS test.

We further evaluated the fitting performance amongst classes of ETC inhibitors by comparing the cost function values for the different classes (Fig. 4C-D). We did this both by minimizing the cost function values considering the data sets for each single ETC inhibitor separately (Fig.4C), and considering the joint data set resulting from all 22 ETC inhibitors jointly (Fig. 4D). As expected because of a lower amount of parameters for the more restricted case of fitting all inhibitors jointly, for that fitting approach the cost function values for the same compounds either stay the same or are increased compared to the fits of single ETC inhibitors. There was substantial variability in mean cost function value between compounds, especially for complex I inhibitors. The cost function value was typically lowest for complex II inhibitors, which is likely due to the consistently minimal effects on MMP by such inhibitors. Cost function values for complex I inhibitors were larger than for complex III inhibitors (Fig. 4C-D, with p-values of 0.0287 and 0.0925, respectively), suggesting that there is a qualitative difference in the MMP response between these classes of compounds.

Note that even for the compound with the highest cost function value, i.e., pyridaben, the fit was still reasonably good (Fig. S5A). The relatively high cost function values for some compounds (e.g., for pyridaben, rotenone, and antimycin A) resulted from overall deviations at all time points and concentrations, although perhaps the largest contributions were from the weighted residuals at early time points for high concentrations (Fig. S5B).

For the ETC inhibitors, the model-predicted MMP decrease is expected to coincide with a decreased OCR, for which the model can also generate a prediction that can be compared qualitatively to experimental OCR measurements. To test whether there is indeed such a qualitative match between OCR measurement and simulation, we utilized the parameter estimates for the ETC inhibitors (Table S3) to simulate the OCR, i.e. the second term in Eq. (1). We plotted the simulated OCR at 30 mins for all 22 ETC inhibitors (Fig. S6, blue), following the exposure duration utilized by van der Stel et al. (2020).

For most ETC inhibitors, the simulated OCR either decreased with applied concentration or remained at approximately the same level, which matches the general experimental observations (Fig. S6, black). However, the concentration at which the strongest decrease in OCR occurs and the percentage of OCR inhibition are typically not predicted well by the model. Moreover, for some inhibitors for which the MMP response is almost flat (e.g. fenfuram and capsaicin; not shown), the dependence of simulated OCR on compound concentration exhibited unexpected patterns, which could be due to parameter identifiability issues (see Discussion).

In summary, despite the imperfect nature of the MMP fits and OCR predictions for some compounds, our basic MMP model simulates qualitative features of the OCR well. Moreover, the MMP dynamics upon exposure to all mitochondrial complex inhibitors are described well.

### Compound decay explains MMP dynamics following FCCP and oligomycin exposure

We next asked if our basic MMP model could also describe changes in MMP dynamics upon exposure to compounds that disrupt the MMP through alternative means, i.e., the uncoupler FCCP and the ATP synthase inhibitor oligomycin. Fitting the basic model to MMP measurements for both FCCP (Fig. 5, cyan lines) and oligomycin (Fig.6, cyan lines) showed that the data could not be well described for all concentrations. Specifically, for intermediate and high concentrations of FCCP (1 μM and higher), the MMP first decreased and then started to recover at later time points. This phenomenon cannot be described by our basic model, for which the MMP can only decrease. As

a side note, exposure to low concentrations of FCCP (e.g., 0.000128 μM) seemed to lead to small initial increases of the MMP. However, upon revisiting the unnormalized Rho123 intensities this appeared due to a single replicate out of four replicates in which the MMP response to FCCP exceeded that to DMSO from time points 3 to 24 hours (Fig. S2, replicate 2). Thus, the initial average MMP increase for FCCP should not be interpreted as evidence for MMP hyperpolarization.

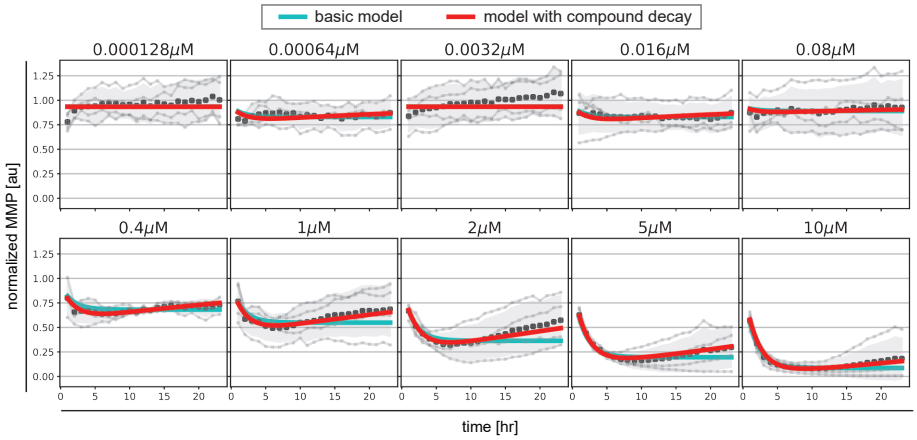


**Figure 5: Model extension with compound degradation is required for good fit to FCCP data**.
MMP data in response to various concentrations of FCCP (gray line and dots indicate individual replicates; black dots and shading indicates the mean of replicates and 95% confidence intervals of means) are shown along with model simulations for best-fitting parameters of the basic model (cyan lines) and of the model extended with compound decay (blue lines).

Such a clear hyperpolarization did occur for oligomycin, for which the MMP initially increased and later decreased. Interestingly, for low concentrations of oligomycin (up to 1.0 μM), the MMP first increased and after 4-6 hours started to decrease, eventually reaching lower values than the initial MMP. For high concentrations of oligomycin (higher than 1.0 μM), the MMP increased and remained at high levels for the entire imaging period. Our basic model can describe an increase of the MMP, which is due to blocking of the proton channel in the ATP synthase, but it cannot explain the late decrease at low oligomycin concentrations.

To investigate which factors are required to quantitatively describe the MMP dynamics observed upon exposure to FCCP and oligomycin, we implemented several extensions to our basic MMP model. First, we introduced pharmacokinetic decay into the model to describe the possibility that compounds either stick to plastic, are not stable over time or are metabolized (controlled by the parameter γ). Second, we considered the possibility of concentration-dependent compound decay (by having different γ parameters for low and high concentrations), which could result from saturation in the processes that lead to such decay. Third, we introduced ion leakage into our model,

because there is evidence for proton or potassium ion leakage from the mitochondrial intermembrane space into the mitochondrial matrix when the MMP is increased above basal level (Beard, 2005) (controlled by the parameter α).

We incorporated these model extensions sequentially, starting with an investigation of the effect of pharmacokinetic decay. For FCCP, model extension with such compound decay was sufficient to quantitatively describe the partial recovery of the MMP at late time points (Fig. 5, red lines). For oligomycin, model extension with compound decay was still insufficient to explain the MMP dynamics (Fig. 6, red lines). However, a model with both compound decay and leakage provided a reasonable description for most concentrations of oligomycin (Fig. 6, black lines). In order to understand why adding leakage to the model led to a better fit, we studied the curvature of the MMP response at its peak and how it depended on the applied oligomycin concentration (Supplementary text). Experimentally, the MMP curvature clearly changed with increasing concentration (Fig. S7A; blue), whereas analytical calculations showed that in the model with only compound decay, the concentration had no effect on curvature (Fig. S7B-C). Addition of leakage to the model led to a qualitative agreement on the curvature change with concentration (Fig. S7A,D; black). The change in curvature with increasing oligomycin concentration also suggested that the decay rate of oligomycin might depend on its concentration. Indeed, addition of concentration- dependent decay to our basic model further improved the fit to the data (Fig. 6, blue lines). Note that in this latter model, ion leakage is not included and there is a different decay rate for the 4 lowest concentrations (γL) and for the 4 highest concentrations (γH ).

We also analyzed structural model identifiability in order to study whether model parameters can be determined uniquely, by performing a profile likelihood analysis (Yang et al., 2016; Raue et al., 2009) on the parameters γ and α (Supplementary text). We found that the compound decay parameter γ is structurally identifiable (Fig. S8), but the ion leakage rate α is not (Fig. S9). Our mathematical analysis further showed that measuring the MMP in an absolute rather than relative manner would make α structurally identifiable (Supplementary text; Fig. S10 and S11). In summary, the conclusion with respect to the presence of ion leakage and its exact quantity awaits further experimental evidence. Nevertheless, application of our model variants to the MMP dynamic data strongly suggests that compound decay takes place both for FCCP and oligomycin, although in the latter case this decay may be concentration dependent.

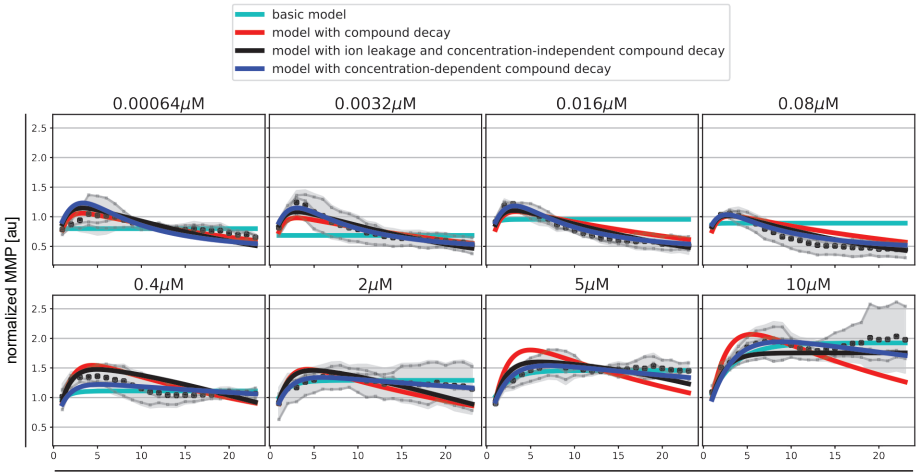


**Figure 6: Model extension with ion leakage and/or compound decay improves the description of Oligomycin data**.
MMP data in response to various concentrations of FCCP (gray line and dots indicate individual replicates; black dots and shading indicates the mean of replicates and 95% confidence intervals of means) are shown along with model simulations for best-fitting parameters of the basic model (cyan lines), of the model extended with concentration independent compound decay (blue lines), of the model with concentration-independent compound decay and ion leakage (red lines), and of the model with concentration-dependent compound decay (purple lines).

6

## LC-MS/MS measurements confirm model-predicted compound decay

In order to further quantify the uncertainty of the decay rate parameters for FCCP and oligomycin (γ), we utilized both a profile likelihood analysis and bootstrapping. For the latter approach, we generated artificial replicates based on intra- and inter-plate variability (Methods). We applied this to our extended model with only compound decay (for FCCP) as well as to the model with compound decay and ion leakage (for oligomycin).

For FCCP, both our bootstrap (Fig. 7A-B) and profile likelihood (Fig. 7C) analysis showed that γ is clearly positive. Thus, the model-predicted amount of FCCP within cells is expected to be substantially less after 24h than at the beginning of the experiment (Fig. 7D). Interestingly, the bootstrap approach returned a more widely distributed γ, with wider confidence intervals at 95% or 99% levels than the profile likelihood approach (compare Fig. 7B and C), presumably because of the variability between replicates. In order to test the model predictions with respect to FCCP decay as an explanation for the behavior of the MMP over time, we quantified the amount of remaining compound within HepG2 cells after exposure to FCCP for 2, 8 and 24 hours by LC-MS/MS, comparing the ratios between these time points (Fig. 7E, dots). This analysis confirmed that substantial FCCP decay occurred on a time scale of hours. In fact, decay was even stronger than predicted by the model when taking into account the confidence interval for the ratios based on the profile likelihood (Fig. 7E, black bars), but fell within the much wider interval resulting from bootstrapping (Fig. 7E, blue bars).

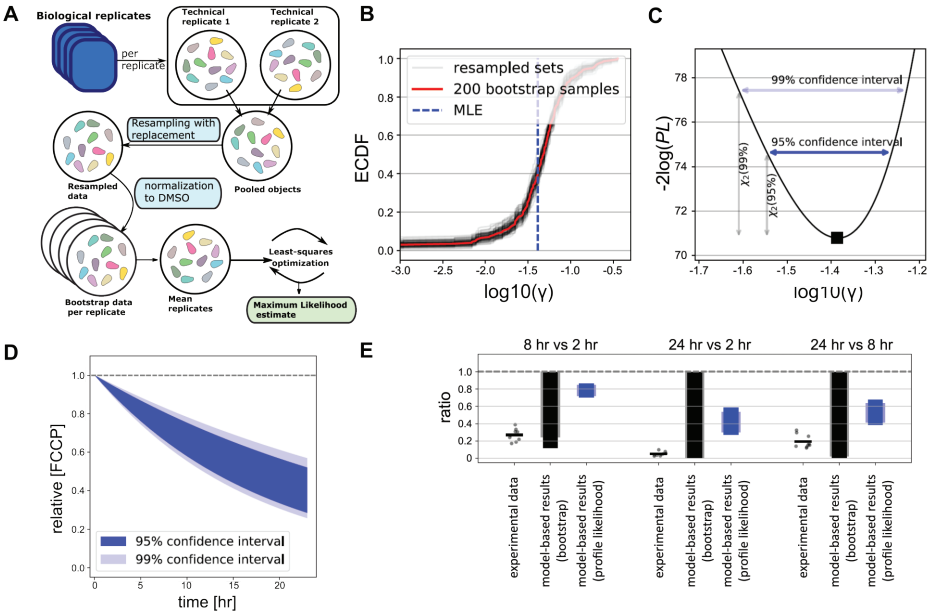


**Figure 7: Intracellular compound measurements confirms FCCP degradation over time**.
**A)** Scheme illustrating our bootstrapping approach. Data from both technical and biological replicates were used to generate artificial data with realistic intra- and inter plate variability (see Methods). Artificial data were used for subsequent model calibration. **B)** Empirically determined cumulative distribution function (ECDF) of the estimated γ values for bootstrapped data. Red line shows ECDF based on all 200 bootstrap samples, gray lines show 100 resampled bootstrap sets (with replacement), and vertical blue dashed line indicates the estimated MLE of the original data. **C)** Profile likelihood for γ, where horizontal dark blue and light blue arrows indicate its 95% and 99% confidence interval. **D)** Model-predicted FCCP dynamics within cells based on 95% (dark blue shading) and 99% confidence interval (light blue shading) of estimated γ, with profile-likelihood-based CIs. **E)** Ratios between time points 2h, 8h and 24h (all possible combinations) of the LC-MS/MS-based intracellular concentrations of FCCP (dots indicate all possible values of the ratios based on separate measurements, and bars indicate the mean of all these ratios) and of the model-based CIs for the ratios. The model-based CIs either result from bootstrapping (gray) or from the profile likelihood analysis (blue), with the dark colors based on 95% CIs and light colors based on 99% CIs.

Application of bootstrapping to the oligomycin data led to a curved ECDF for the leakage parameter α (Fig. 8A), suggesting that this is an identifiable parameter. However, our profile likelihood analysis demonstrated that the leakage rate was not identifiable (Supplementary text; Fig. 8B and S9), confirming earlier work showing that confidence intervals based on bootstrapping cannot be trusted for structurally non-identifiable models (Fröhlich et al., 2014). Mathematical analysis-informed fixation of selected parameters led to an identifiable model (Supplementary text; Fig. S11). Moreover, re-parameterization of the ion leakage parameter (Supplementary text) rendered a well-behaved profile likelihood, both for concentration-independent and -dependent decay γ (Fig. 8C). These two model variants led to quantitatively different model predictions for the oligomycin decay rate (Fig. 8D) and thus of the compound levels over time (Fig. 8E-F). Finally, we measured intracellular concentrations of oligomycin in HepG2 cells by LC-MS/MS after 2h, 8h and 24h of exposure to oligomycin. At high applied concentrations of 0.5 μM, the ratios calculated between

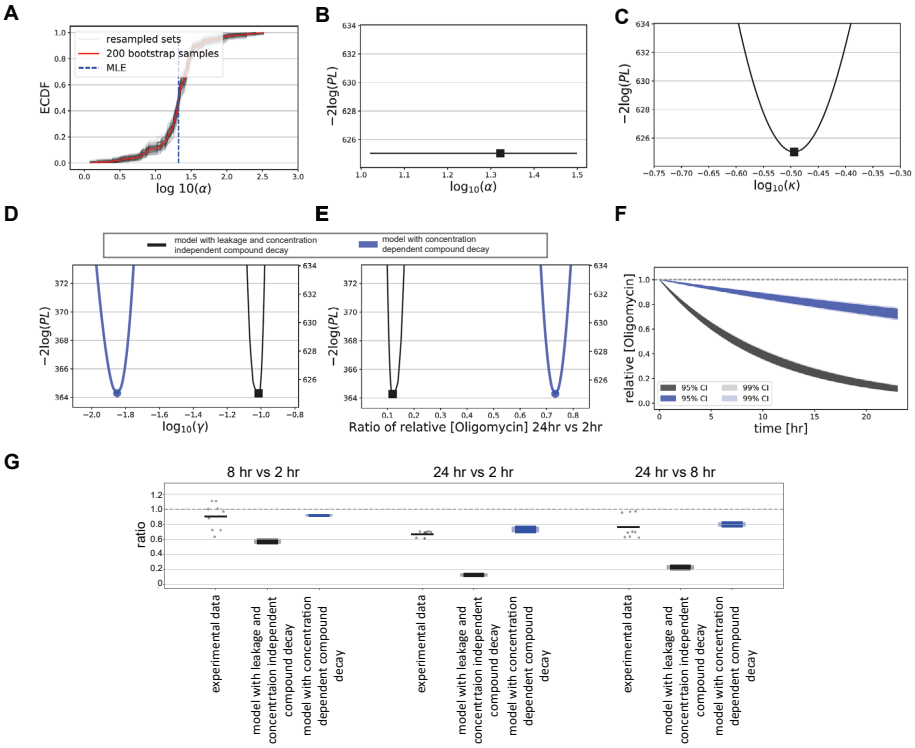


**Figure 8: Uncertainty quantification and measurements for Oligomycin.**
**A)** Empirically determined cumulative distribution function (ECDF) of the estimated values for bootstrapped data. Red line shows ECDF based on all 200 bootstrap samples, gray lines show 100 resampled bootstrap sets (with replacement), and vertical blue dashed line indicates the estimated MLE of the original data. **B)** Profile likelihood for the leakage rate (α), for the model with compound decay and ion leakage is utilized. **C-E)** Profile likelihoods for the fractional measure of leakage (κ) **(C)**, for the Oligomycin degradation rate (γ ) **(D)**, and for the ratio of effective concentrations at 24h and 2h **(E)**. **F)** Model-predicted Oligomycin dynamics within cells based on 95% (dark shadings) and 99% confidence interval (light shadings) of estimated γ values, with profile-likelihood-based CIs. In **(C-F)** either the model is utilized in which the structural un-identifiability of the leakage rate has been solved, with concentration-independent κ (black), or in which κ does depend on the Oligomycin concentration (green and blue, which indicate two local minima). **G)** Ratios between time points 2h, 8h and 24h (all possible combinations) of the LC-MS/MS-based intracellular concentrations of Oligomycin (dots indicate all possible values of the ratios based on separate measurements, and bars indicate the mean of all these ratios) and of the model-based CIs for the ratios. The model-based CIs are based on the profile likelihood analysis for a model with concentration-independent decay (black) or with concentration-dependent decay (blue and green), with the dark colors based on 95% CIs and light colors based on 99% CIs.

these time points suggested a relatively low oligomycin degradation rate with possibly a very limited degradation when comparing the 8h with the 2h time point (Fig. 8G, dots: note that some measurements show a minor increase in oligomycin) Degradation noticeably increased only at a time scale beyond 8h. These data had a large mismatch to predictions for the model with concentration-independent decay and ion leakage (Fig. 8G, black bars). Therefore, we also compared the compound ratios over time to the model with concentration-dependent γ, which matched reasonably well (Fig. 8G, blue bars). At low applied concentrations of 0.005 and 0.05 μM, oligomycin measurements remained below detection levels at all-time point. This finding is

consistent with the hypothesis that oligomycin decay is more rapid at low than at high concentrations, although more sensitive measurements are required to demonstrate this experimentally. In summary, our data and model-based analysis suggests that the complex MMP dynamics observed upon exposure of HepG2 cells to oligomycin could be due to compound decay that varies with the applied concentration. For FCCP, the MMP response is simpler and recovery of the MMP at late time points likely results from FCCP degradation over time.

## Discussion

To quantitatively understand how cells respond to mitochondrial OXPHOS inhibitors in terms of their MMP, we applied a combination of live-cell high-content imaging and dynamical modeling. Here we focused on the MMP resulting from exposure to three classes of OXPHOS inhibitor, involving multiple ETC inhibitors, an uncoupler and an ATP synthase inhibitor. After simplification of a published model describing MMP dynamics (Yang et al., 2015), we could fit data of exposures to 22 compounds. Furthermore, we showed that a likely explanation for the observed MMP recovery at late time points upon exposure to oligomycin and FCCP is that these compounds decay over time, and possibly in a concentration-dependent manner for oligomycin. Such instability may be attributed to intracellular degradation due to the presence of particular enzymes facilitating degradation. Alternatively, compounds may be chemically unstable even in the absence of cells, or become trapped by the plastics of the plate walls. Each of these pharmacokinetic processes may saturate at high concentrations, in which case the decay rate would become concentration-dependent, as could be the case for oligomycin according to our findings. Note that the fact that no MMP recovery occurred for the 22 complex I, II, and III inhibitors and that our basic MMP model fitted well to these data suggests that there is no substantial decay of these compounds during 24 hours. When confronting our set of dynamic MMP models in the future with data for a new compound, we advocate to first calibrate our basic model to these data. Only when clear qualitative mismatches are observed that might be indicative of early MMP increases or late restoration of the MMP to baseline levels, model extensions such as the presented extensions on compound decay should be applied.

Our model does not consider a scenario in which mitochondrial active metabolites are formed over time. Such model extension is straightforward, yet we would advise to apply this only in case two time scales are observed in MMP dynamic data. The effect of metabolites that are formed very fast can likely be described by the current model already, although it will then not be possible to distinguish between effects of metabolites and primary chemicals. Our model also does not consider the scenario

where compounds inhibit multiple mitochondrial complexes. The inhibitors in our current study indeed typically inhibit only one of the complexes in the ETC (van der Stel et al., 2020), although outside the employed concentration range the compounds may inhibit multiple complexes. Other chemicals that are non-selective with respect to the inhibited mitochondrial complexes at low applied concentrations exist (Nadanaciva et al., 2007; Dykens et al., 2008; Felser et al., 2013,0; Grünig et al., 2017), and would be interesting to quantify with our integrated imaging and dynamic modeling approach. Although it is not yet clear whether the MMP resulting from such compounds can also be described with our MMP model, this seems likely because we showed that inhibitors of single complexes are all described with reasonable fit quality. Because there are no obvious distinctive dynamical patterns associated with the different mitochondrial complex inhibitors, this means that our approach is unlikely to be helpful in determining the detailed mode of action of ETC inhibitors. However, for the special case of a compound inhibiting both ATP synthase and complex I or III, the interesting situation might arise where both an MMP decrease and increase might occur. In that case, our models would be helpful in teasing these competing effects apart

The model fits to data for complex III inhibitors were overall slightly better than for complex I inhibitors, which may in part be due to variability of the MMP measurements. We speculate that the current model may also miss some elements that are relevant for some inhibitors to complex I. For example, the rate at which cells take up particular inhibitors within mitochondria may vary between the chemicals, which likely influences the dynamics of the MMP response. Moreover, oxygen is consumed mainly by complex IV activity, and because complex III is closer to complex IV within the ETC than complex I is, this might explain the better fitting result for complex III. Additionally, complex II activity may become different in case of complex I inhibition compared to complex III inhibition, and this may depend on components available in the medium.

Our current model is focused on describing the MMP based on the OCR (i.e. the right hand side of Eq. (1)) and the effect of various ETC inhibitors. Our model could be extended with ATP as a third state variable, i.e., by describing its rate of production and utilization, for instance based on FRET measurements (Imamura et al., 2009). The production of ATP depends on complex V activity which dissipates the MMP whilst synthesizing ATP. Moreover, cytosolic glycolysis generates ATP and cells utilize ATP during their regular activity. Furthermore, there could be feedback from the ATP level back to the oxygen or MMP level. In the original model that we simplified (Yang et al., 2015), several feedback loops were implemented, including a loop from ATP to MMP. Because it is not clear whether the ATP level indeed affects the MMP, it will be important to investigate this by a combination of modeling and experimental ATP level measurements.

With respect to the oxygen level, our model couples an oxygen increase to an MMP increase. Moreover, a decrease of the oxygen consumption rate (OCR) is expected upon exposure to ETC inhibitors, and our model directly implements this (Eq. 2)). We therefore also generated model predictions for the OCR at a single time point (30minutes), which qualitatively matched the experimental observation for the ETC inhibitors at that time point. However, given that oxygen is not utilized for all complexes of the ETC chain, the true relation between OCR level and MMP is likely more complicated than currently implemented. To establish a quantitative match in the future, more detailed temporal OCR measurements would be required. Our current OCR simulations did highlight a potential issue for compounds that hardly affect the MMP, such as complex II inhibitors simulations of the MMP matched the flat experimental data very well, but the simulated OCR decreased greatly at some applied concentrations. This could be due to parameter identifiability issues for $c_1$ and $c_0$ together with other parameters like the effective concentrations [$D_x$]. For example, when $c_1$ approaches zero, tuning of $c_0$ alone could be sufficient to fit to an MMP that remains constant over time. This might be solved by a combination of fixing the value of particular parameters (e.g., $c_1$) and using temporal OCR data for model calibration. Thus, further model refinement is needed to quantitatively describe the OCR quantitatively, which can best be achieved by combining it with detailed OCR measurements. One potential model modification that may be required to quantitatively describe such data is to alter the mathematical term describing the OCR. In our current model, this is implemented as a Michaelis-Menten dependence, but alternative relations might be required. Also for FCCP and oligomycin, the relation between OCR and MMP is likely more complicated than implemented in our current model. For example, the OCR is known to swiftly increase to a maximal level upon FCCP administration and subsequently decreases, while at the same time the MMP primarily decays. Besides further study of the quantitative relation between OCR and MMP for different compounds, reaction oxygen species (ROS) represent an important component to be included in future modeling work. Oxygen and ETC complexes have an important role in the generation of ROS (Liu et al., 2002) and ROS are likewise important for cellular stress responses and adverse effects (Stowe and Camara, 2009; Pereira et al., 2016).

For the complex V inhibitor oligomycin, our model selection approach based on the MMP dynamic data suggested that these dynamics could either be explained by concentration-dependent oligomycin de- cay or by concentration-independent oligomycin decay and ion leakage from the intermembrane space to the mitochondrial matrix in case the MMP increases to values higher than the steady state MMP level. Our subsequent LC-MS/MS quantification showed that the oligomycin decay at high applied concentrations was much lower than expected based on our model with

concentration-independent decay, and that at low applied concentrations oligomycin remained below the detection limit at all-time points. This observation could either be explained by an initial oligomycin concentration that is already very low, or by fast decay at such low concentrations. Although experimental measurements with increased sensitivity will be needed to come to a definite conclusion, we tentatively conclude that the current measurement results are at least consistent with a concentration-dependent oligomycin decay. An alternative explanation is that ion leakage is concentration-dependent. Such leakage at high MMP levels is consistent with previous experimental measurements suggesting a non-linear relation between oligomycin concentration and MMP (Porter and Brand, 1995; Berthiaume et al., 2003). In the biophysical model by Beard (2005), leakage is included as a non-linear relationship between leakage and membrane potential based on the Nernst Equation (Beard, 2005). Although a non-linear mathematical term might thus be more suitable than the linear term that we employed, the model fit is already good with a linear term. Given the difficulty that both oligomycin decay and proton leakage are expected to impact MMP dynamics, it is not possible to fully tease these factors apart based on the current data. Note that other ions besides protons might also contribute to the leakage process and we do not distinguish between these in our model. Further experimental perturbations and integration of such perturbation data into refined mathematical models are required to unravel the ion channels contributing to leakage.



The results were substantially simpler for the uncoupling agent FCCP, where model selection indicated that compound degradation was a potential explanation for the observed MMP dynamics. This prediction qualitatively matched the ratios of the intracellular amount of FCCP experimentally obtained from LC- MS/MS at different time points, although the measurements indicated that FCCP decay may even proceed faster than the model predicted. Therefore, as for oligomycin, a better quantitative match may result from a concentration-dependent instead of -independent decay, yet this would come at the cost of a more complicated model.

Our model is part of a gliding scale of computational models of cellular bioenergetics, that differ in terms of model complexity and purpose. The biophysical model by Beard (2005) is quite detailed, describing the various ETC complexes in mitochondria separately, aiming to quantitatively understand the contribution from these complexes and individual ions to the MMP within individual mitochondria. The model by Yang et al. (2015) is much simpler with respect to MMP, but aims to quantitatively unravel the contribution of glycolysis and oxidative phosphorylation to hepatocellular energetics for cells as a whole, focusing on the OCR and the extracellular acidification rate (ECAR) and how these vary in the context of different media. In a study aiming to describe the effect of a small set of compounds on the MMP, Bois et al. (2017) proposed an

even simpler model with only one ODE, showing that for some compounds this was sufficient to describe the effect on single time-point measurements of the MMP. Here, we designed a model of intermediate complexity, such that it could be calibrated to time courses of MMP measurements for a range of compounds. In the absence of data on downstream effects of the MMP changes such as ATP levels, we did not include these processes in our model, but this can be done in the future in a similar fashion as was done by Yang et al. (2015).

Computational approaches are becoming increasingly important for safety evaluation of chemicals, and dynamical models represent one of the approaches that will be useful for that purpose in the future (Kuijper et al., 2017). Such models represent a so-called quantitative adverse outcome pathway (qAOP) or part thereof. An AOP is a concept frequently used in toxicology to describe a sequence of events (a molecular initiating event and subsequent key events) that is thought to in the end lead to an adverse outcome (Villeneuve et al., 2014a,0). Quantitative versions of such AOPs aim to quantify the links between the events and adverse outcome (Bois et al., 2017). The relative simplicity of our MMP model will facilitate further regulatory usage as part of such a qAOP. The relevant AOP would thus be related to mitochondria, in which MMP loss contributes to mitochondrial malfunctioning (Nicolson, 2014; Terron et al., 2018). In general, qAOPs should be developed in careful consideration of both the biological plausibility and availability of appropriate data. For instance, our work suggests that it might be important to take the potentially complex interplay between PK and early key events (such as MMP decay) into account in mitotoxicity-related qAOPs. Further integration of our model into qAOPs would be useful and could contribute to an integrated tool for exposure-led next generation risk assessment (NGRA) (Dent et al., 2018).

Such model-based tools help to identify thresholds for key events and improve the quantification of key event relationships. In our case, this would for instance involve the relation between MMP and cellular ATP level. Although the AOP is a useful concept for thinking about the events leading to toxicity, in reality an AOP network is likely a more realistic representation (Leist et al., 2017), which is defined as a set of AOPs sharing one key element. As our computational model can capture multiple types of insult to OXPHOS (e.g. inhibition to both complex I and V), further case studies using our model as a basis could help the development of AOP networks to be used during risk assessment (Jarabek and Hines, 2019).

In conclusion, we developed a mathematical model that can be utilized to study mitochondrial dysfunction and that can easily be extended to describe subsequent cellular adaptation. Our model, which was based on the model by Yang et al. (2015) achieved good fits of the MMP dynamics for exposure to mitochondrial ETC inhibitors,

yet an extended model taking into account concentration-independent or -dependent compound decay was needed to properly describe the response to the uncoupler FCCP and ATP synthase inhibitor oligomycin. We also explored the potential role of ion leakage to explain the concentration response to oligomycin, yet based on the currently available data we cannot confirm its occurrence. We cannot exclude that at high concentrations of oligomycin, cellular toxicity affects the MMP dynamic response, although this was not visible in terms of PI staining (Fig. S4). Moreover, in our models we did not consider a potential contribution of ATP synthase operating in reverse, during which ATP would be used to increase the MMP rather than vice versa. Despite these additional processes that may play a role in explaining the MMP dynamics upon oligomycin exposure, our current model-based analysis has generated several hypotheses that can be tested with new experiments. Moreover, in the future our model can be extended further with downstream effects of MMP loss on e.g. cellular ATP levels and cellular adverse outcome. Nevertheless, as emphasized above, the power of the current model lies in its simplicity, which allowed for model calibration to MMP dynamics data. In our opinion model extension is thus primarily useful when appropriate data are available with respect to additional pathway components. Altogether, our work highlights the potential of computational modelling to assist in the quantitative unraveling of mechanisms contributing to mitochondrial toxicity.



**Conflict of interest statement**

CB, SB and PW are employees at Cyprotex Discovery Ltd, a company that develops and provides in vitro assays. Otherwise, the authors declare that the research was conducted in the absence of any commercial or financial relationships that could be construed as a potential conflict of interest.

**Author contributions**

HY, WvdS, BvdW, EHJD and JBB conceptualized the research. RL and HY built the initial version of the computational models, which was refined and finalized by HY. HY performed mathematical analysis to the models. WvdS conducted live-cell confocal microscopy experiments, performed image analysis, and prepared samples for LCMS/MS experiments. CB and SB conducted LCMS/MS experiments. CB, SB, PW, HY, WvdS and JBB analyzed the LCMS/MS data. PW, BvdW, EHJD and JBB supervised the research. HY prepared the first draft with help from RL and WvdS, after which JBB edited and finalized it. All authors read, commented on and approved the manuscript.

**Funding**

This work has received funding from the European Union's Horizon 2020 research and innovation pro- gramme (grant 681002; to PW, BvdW, EHJD and JBB).

## Supplemental information

Supplemental tables 1-7 and supplemental text providing more model details are available using the following link: https://doi.org/10.3389/fphar.2021.679407.

## Supplementary figures

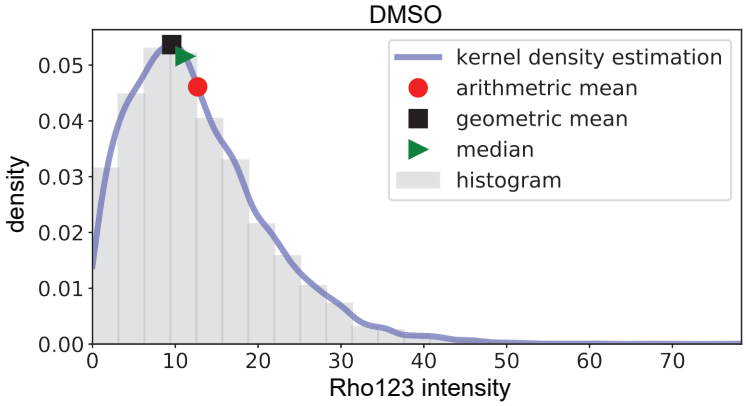


**Supplementary figure 1: Distribution of Rho123 intensity amongst HepG2 cells**.
Binned histogram and estimated density of quantified Rho123 intensities in control DMSO conditions. Also shown are three estimated population means.

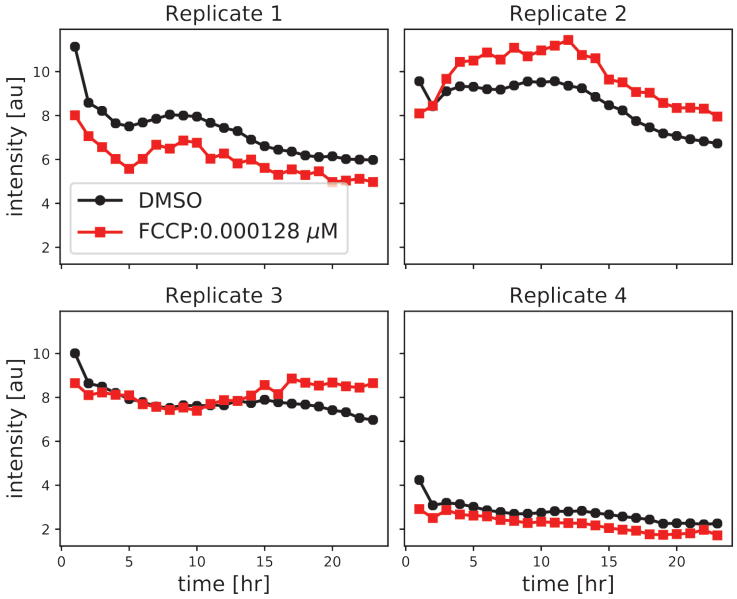


**Supplementary figure 2: Rho123 intensity dynamics upon exposure to DMSO or FCCP at 0.000128 μM**.
Four biological replicates are shown. Note that the data in this plot are not normalized to DMSO controlconditions.

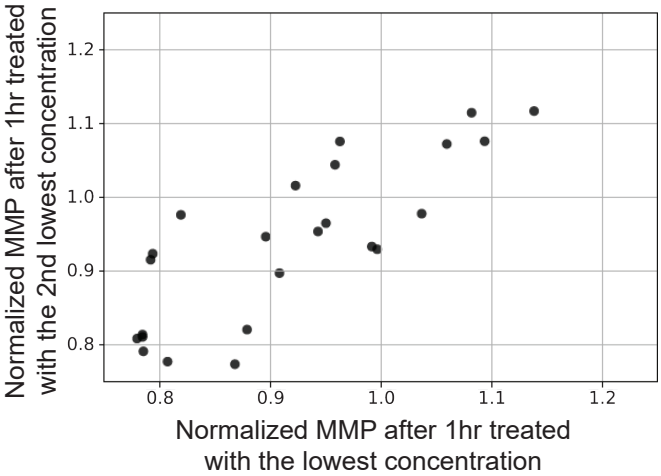


**Supplementary figure 3: Dependence of early MMP measurement at very low concentrations**.
The MMP response at the first measurement time point for the lowest applied concentrations are plotted per compound. Because no correlation is expected for these low concentrations, the presence of such a correlation suggests there are compound-specific effects, which could be related to the well locations in a plate.

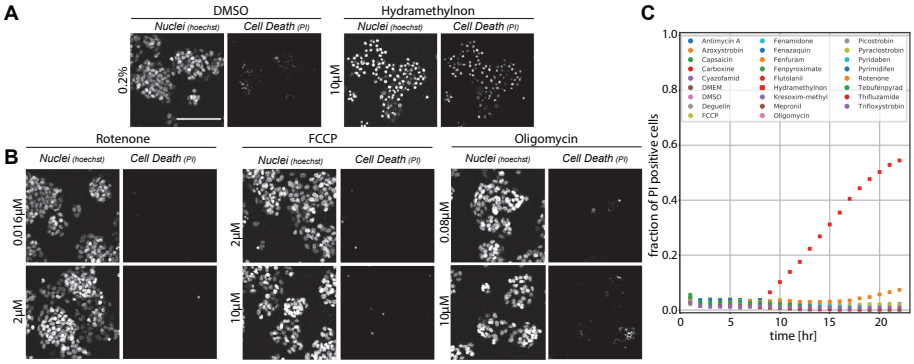


**Supplementary figure 4: Quantification of necrosis in HepG2 cells over time**.
(A-B) Representative confocal microscopy images of Hoechst (cell nuclei) and PI (necrosis) in HepG2 cells at 24h after exposure to vehicle control (0.2% DMSO) or 10μM Hydramethylnon (scale bar: 131.17μm) (A), or of 2 concentrations of Rotenone, Antimcyin A or Oligomycin (B). (C) Quantification of the fraction of PI positive cells during 24h exposure to the highest concentration of the tested compounds (including the 2 controls DMSO and DMEM).

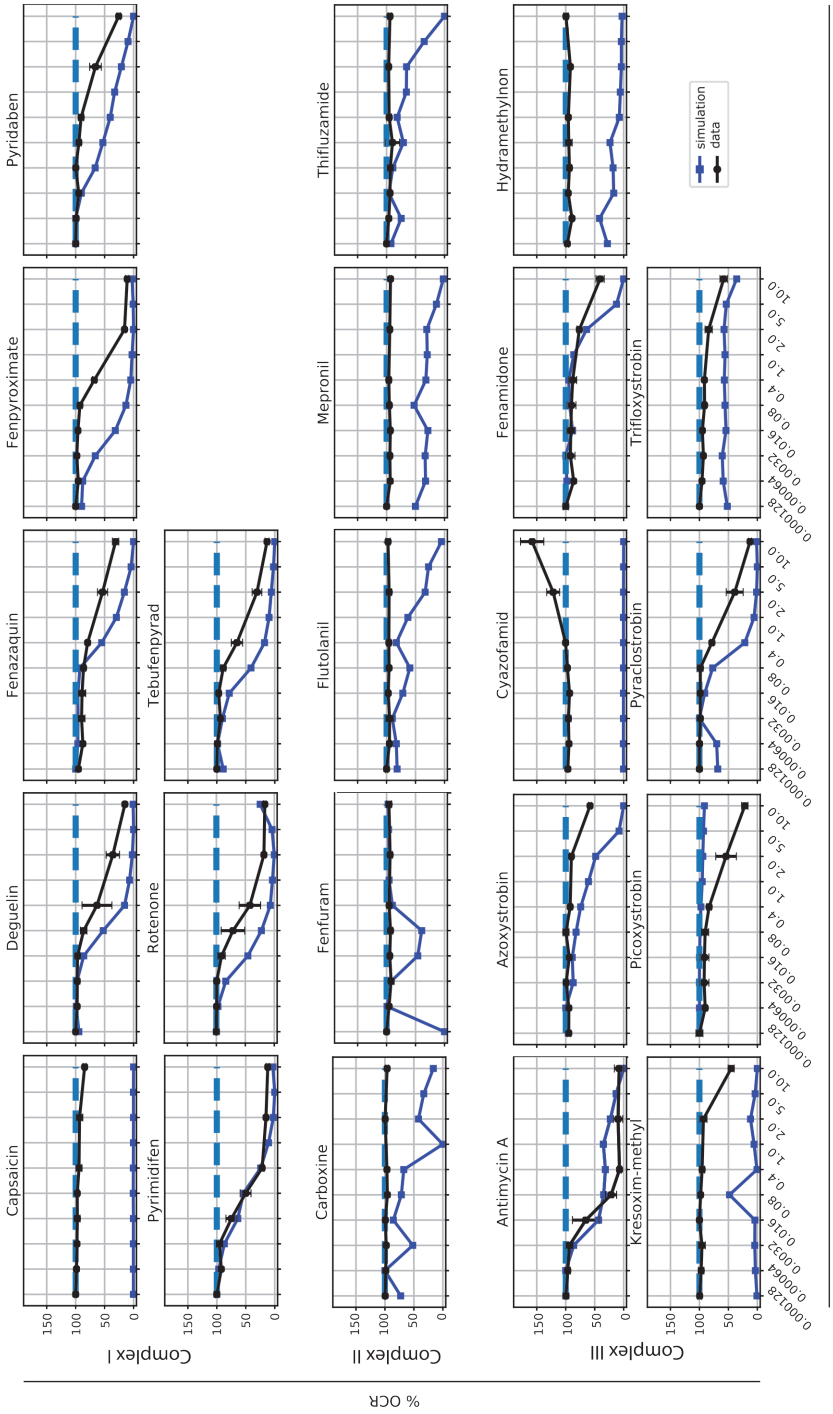


**Supplementary figure 5: Model fitting for compounds with relatively high cost function values.**
(A) Model fit to the MMP dynamics for all applied concentrations of pyridaben, the compound with the highest cost function value amongst all utilized mitochondrial complex inhibitors. (B)Weighted residuals between the model and data for three compounds with relatively high cost function values: rotenone, antimycin A and pyridaben.

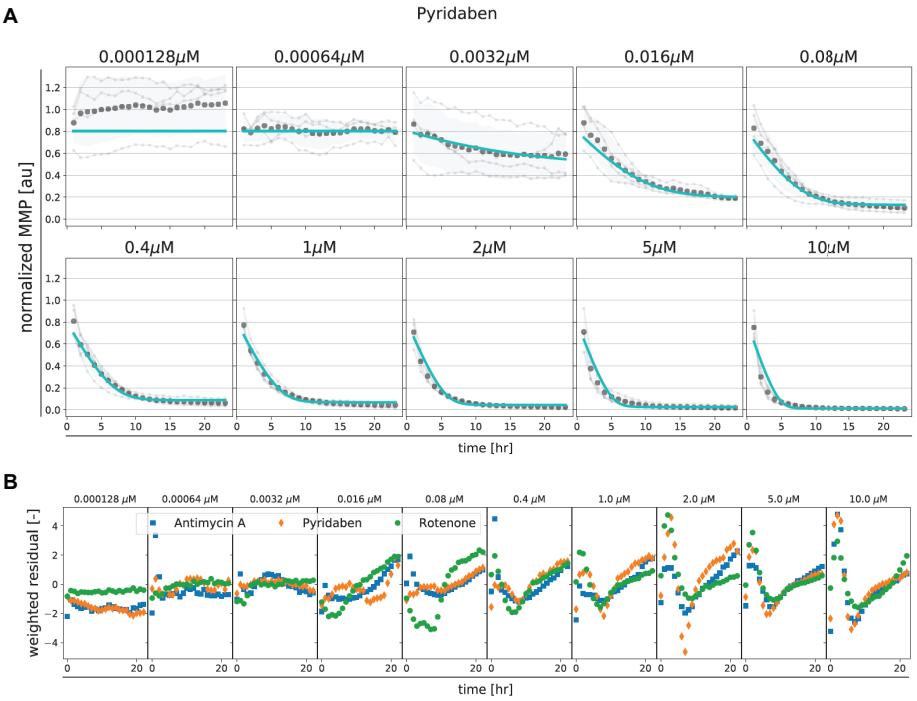


**Supplementary figure 6: Simulated OCR percentages for all ETC inhibitors.**
OCR predictions were based on the parameter estimates in Table S3 for the ETC inhibitors, which were substituted in the mathematical term in Eq. (1) describing the OCR, and evaluated at 30 minutes.

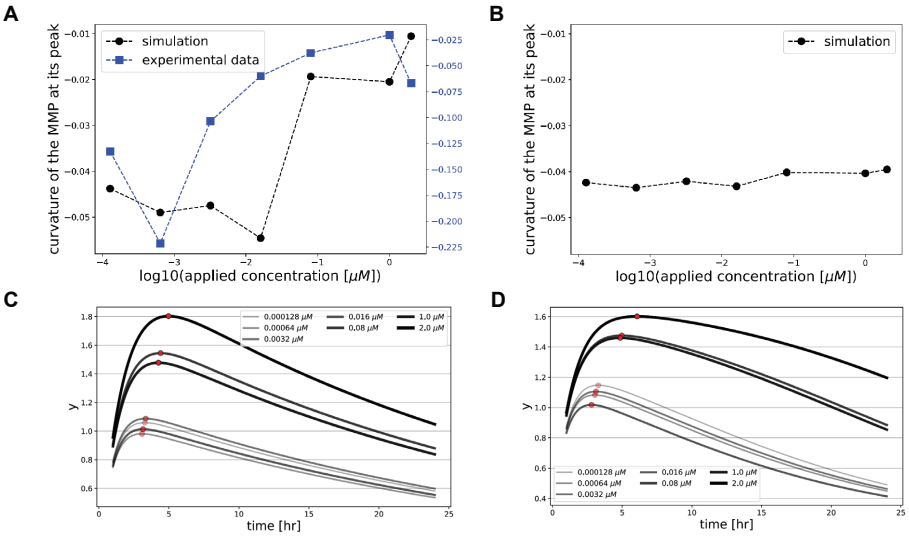


**Supplementary figure 7: Curvature of the MMP response to Oligomycin at its peak**.
(A-B) Relationship between curvature at the MMP response peak and applied Oligomycin concentration. In (A), blue denotes results for the experimental data and black for simulations of the model with compound decay and ion leakage. In (B), results are shown for the model with only compound decay. (C-D) Simulated MMP (y) over time for the model with only compound decay (C) and for the model with both compound decay and ion leakage (D). Red symbols indicate the peaks per simulated concentration.

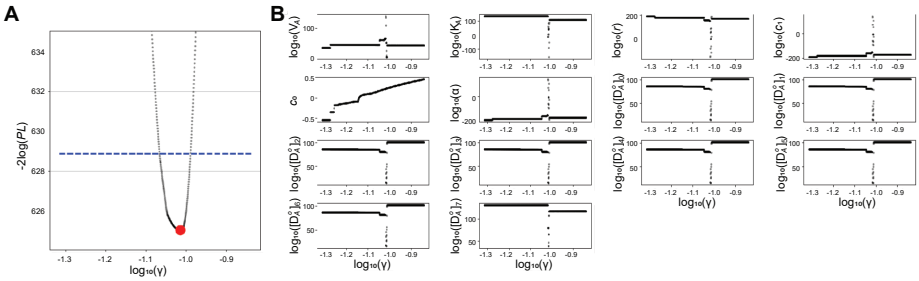


**Supplementary figure 8: Profile likelihood analysis of the decay parameter γ for Oligomycin exposure**. (A) Profile likelihood (-2log(PL); small black dots) for different values of γ, with red dot indicating the MLE. Blue dashed line indicates the location of the 95% confidence interval. (B) Relation between the profiled parameter γ and the other model parameters. The final subpanel again shows the profile likelihood.

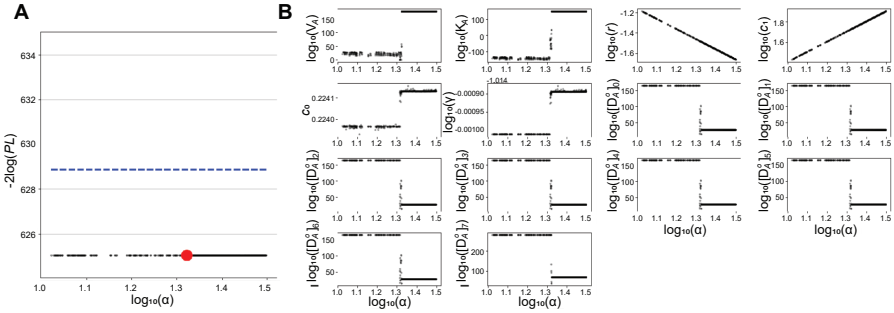


**Supplementary figure 9: Profile likelihood analysis of the ion leakage parameter α for Oligomycin exposure**. (A) Profile likelihood (-2log(PL); small black dots) for different values of γ, with red dot indicating the MLE. Note that the flatness of the curve implies that the parameter is not identifiable. Blue dashed line indicates the location of the 95% confidence interval (which cannot be determined because of the non-identifiability). (B) Relation between the profiled parameter α and the other model parameters. The final subpanel again shows the profile likelihood.

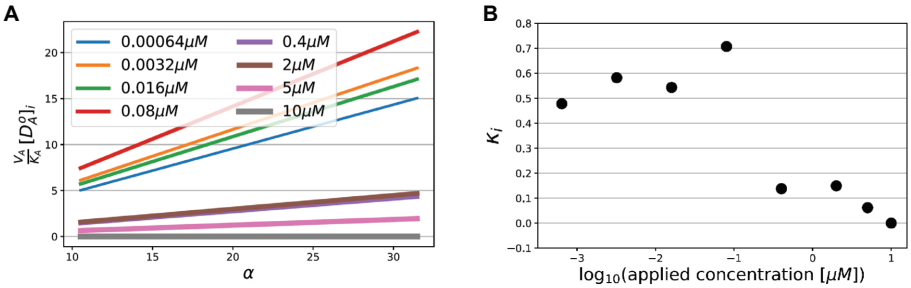


**Supplementary figure 10: Concentration dependence of ratio of leakage and complex V-mediated ion flux**. (A) Relationship between $\frac{V_A}{K_A}[D_A^o]_i^{-1}$ and α during profiling of α. (B) Relationship between the leakage rate/ion flux ratio ($\kappa_i$ values) and the applied concentration (in log10 scale).

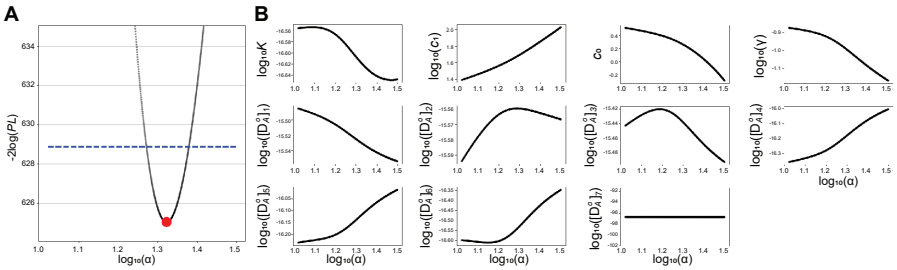


**Supplementary figure 11: Profile likelihood analysis of the ion leakage parameter α for Oligomycin exposure when the parameters $c_1$ and $D_0$ are fixed.**

(A) Profile likelihood (-2log(PL); small black dots) for different values of γ, with red dot indicating the MLE. Blue dashed line indicates the location of the 95% confidence interval. (B) Relation between the profiled parameter α and the other model parameters. The final subpanel again shows the profile likelihood.

# New approach methods (NAMs) supporting read-across:

## two neurotoxicity AOP-based IATA case studies

Wanda van der Stel, Giada Carta, Julie Eakins, Johannes Delp, Ilinca Suciu5, Anna Forsby, Andrea Cediel-Ulloa, Kristina Attoff, Florentina Troger, Hennicke Kamp, Iain Gardner, Barbara Zdrazil, Martijn J. Moné , Gerhard F. Ecker, Manuel Pastor, Jose Carlos Gomes, Andrew White, Erik H.J. Danen, Marcel Leist, Paul Walker, Paul Jennings, Susanne Hougaard Bennekou[#], Bob van de Water[#]

*ALTEX. 2021 Jun; doi:10.14573/altex.2103051*

**Read-across approaches are considered key in moving away from *in vivo* animal testing towards addressing data-gaps using new approach methods (NAMs). Ample successful examples are still required to substantiate this strategy. Here we present and discuss the learnings from two OECD IATA endorsed read-across case studies. They involve two classes of pesticides –rotenoids and strobilurins– each having a defined mode-of-action that is assessed for its neurological hazard by means of an AOP-based testing strategy coupled to toxicokinetic simulations of human tissue concentrations. The endpoint in question is potential mitochondrial respiratory chain mediated neurotoxicity, specifically through inhibition of complex I or III. An AOP linking inhibition of mitochondrial respiratory chain complex I to the degeneration of dopaminergic neurons formed the basis for both cases, but was deployed in two different regulatory contexts. The two cases also exemplify several different read-across concepts: analogue *versus* category approach, consolidated *versus* putative AOP, positive *versus* negative prediction (i.e., neurotoxicity *versus* low potential for neurotoxicity), and structural *versus* biological similarity. We applied a range of NAMs to explore the toxicodynamic properties of the compounds, e.g., *in silico* docking as well as *in vitro* assays and readouts –including transcriptomics– in various cell systems, all anchored to the relevant AOPs. Interestingly, although some of the data addressing certain elements of the read-across were associated with high uncertainty, their impact on the overall read-across conclusion remained limited. Coupled to the elaborate regulatory review that the two cases underwent, we propose some generic learnings of AOP-based testing strategies supporting read-across.**

**Keywords**: *in vitro*, mitochondrial toxicity, neurotoxicity, PBK-modelling, uncertainty analysis

## Introduction

To protect human health, pesticide regulations in Europe (EC 1107/2009) are amongst the most demanding regulations in terms of data requirements [European Parliament and the council, 2009], prescribing *in vivo* mammalian studies [Bennekou et al., 2019]. Even though many pesticides belong to the same pesticidal group, like for example strobilurin fungicides, sulfonyl urea herbicides or pyrethroid insecticides, each of the pesticides still requires a full data package. Pesticide regulation is currently undergoing a Regulatory Fitness and Performance Programme (REFIT) exercise. In this context, the Group of Chief Scientific Advisors to the European Commission recommended that, given the already existing vast amounts of data, read-across approaches are being underutilised across these pesticide groups mainly due to prescriptive data requirements [SAPEA, 2018; EU Scientific advice mechanism, 2018]. In its recent report to the European Parliament [European Parliament and the council, 2020], REFIT estimated that each year up to ~100,000 animals had been used for the testing of pesticides [Busquet et al., 2020]. The use and regulatory acceptance of alternative approaches is crucial to reduce such large-scale *in vivo* vertebrate animal testing in Europe. The US-EPA recently set specific goals towards this end in committing to effectively eliminate mammal testing by 2035 [US-EPA, 2020].



The European Horizon 2020 project EU-ToxRisk aims to provide tools and approaches to replace and reduce animal testing with regard to repeated dose and reproductive toxicity[20]. The EU-ToxRisk project has conducted a series of NAM-supported read-across case studies to explore the utility of these *in silico* and *in vitro* methods to replace *in vivo* testing [Escher et al., 2019]. Read-across is a technique for predicting endpoint information for target substance(s) by using data for the same endpoint(s) from other source substance(s), i.e., by confirming similarity regarding properties relevant for the endpoint in quest between target and source compounds. A total of four case studies were elaborated and reported as integrated approaches to testing and assessment (IATA) and submitted to the OECD IATA Case Studies Project[21]. The case studies underwent rigorous regulatory review by the IATA-project member countries and have been endorsed for publication.

In this paper we present, discuss and compare two of four case studies submitted by the EU-ToxRisk project consortium : *"Identification and characterization of parkinsonian hazard liability of deguelin by an AOP-based testing and read-across approach"* and *"Mitochondrial complex-III-mediated neurotoxicity of azoxystrobin - Read-across to other strobilurins"*. They were chosen since they both involved pesticides groups – respectively rotenoids and strobilurins– and took neurotoxicity as the endpoint with the need for *in vivo* repeat-dose testing described in OECD

guidelines (OECD TG424). The cases studies were recently published on the OECD IATA project website [OECD, 2020a; OECD 2020b]. In addition, both cases are based on an AOP-anchored data-generation strategy supported by physiologically-based kinetic (PBK) modelling. The building of the read-across hypothesis and subsequent testing strategy were to a large extent based on the OECD endorsed AOP *"Inhibition of the mitochondrial complex I of nigra-striatal neurons leads to parkinsonian motor deficits"* [Terron et al., 2018][22].

AOPs represent a sequence of key events (KEs) triggered by chemical exposure, occurring at the molecular, cellular, organ, whole-organism or population level. KEs are causally linked to the adverse outcome (AO), are essential for the progression towards the AO, and should be measurable [Ankley et al., 2010; Villeneuve et al., 2014; Ball et al., 2016]. The OECD runs a programme constructing AOPs and promotes guidance on the use of AOPs in developing IATAs [OECD, 2016], recognizing that AOPs can guide testing of underlying mechanisms, e.g. by using NAMs. In the examples of the two case studies presented here we assembled a battery of *in silico* and *in vitro* NAMs to assess the various KEs in the AOP describing neurotoxicity as a consequence of mitochondrial perturbation. Molecular initiating events (MIEs) interactions were modelled computationally and downstream KEs measured biochemically (e.g., inhibition and perturbation of mitochondrial function and the effects on overall cellular viability, specifically neuronal health). The AOP-based approach was supported by biokinetic and PBK modelling to estimate chemical exposure in the *in vitro* systems and *in vivo*.

## Background information

**Read-across in the assessment of risk/hazard of pesticides targeting mitochondria**
In this manuscript we describe two IATA case studies in which classes of chemicals with a defined mode-of-action (MoA) were assessed for their neurological hazard (table 1).

*Read-across complex I inhibition: rotenoids (Case study 1)*
There is an anticipated hazard for agrochemicals that inhibit complex I (CI) of the mitochondrial respiratory chain to cause toxicity to the nigrostriatal neurons, leading to symptoms that reflect Parkinson's disease. This relationship has been described in a recently OECD endorsed AOP [Terron et al., 2018][22].

One family of pesticides specifically affecting mitochondrial CI are the rotenoids. Two main marketed rotenoids are rotenone and deguelin, which belong to the so-called class of cubé resin pesticides (the root extract from *Lonchocarpus utilis* and *urucu*). The primary pesticidal MoA of rotenoids is the interference with the electron transport chain in mitochondria. Rotenoids inhibit the transfer of electrons from iron-sulfur centers in CI to ubiquinone. This interference affects the creation of usable

cellular energy in the form of ATP and eventually reduces the number of undesired insects and arachnids on treated plants. A similar mode of action is responsible for the piscicidal activity of cubé resin.

Epidemiological studies have indicated that exposure of workers to rotenone was statistically associated with an increased incidence of Parkinson's disease [Dhillon et al., 2008; Tanner et al., 2011]. Moreover, rotenone is used to induce parkinsonian-like phenotypes in experimental animals [Betarbet et al., 2000] and it was also one of the stressors used in developing the aforementioned AOP. It has been reported that deguelin can induce parkinsonian-like phenotypes in rats [Caboni et al., 2004]. Whether deguelin has the same hazard as rotenone for inducing parkinsonian liability in humans is currently unclear.

Through an analogue-based read-across approach using chemicals with high chemical structure and property similarities and identical MoA, we assessed the likelihood of developing parkinsonian liabilities upon exposure to the target chemical deguelin using NAM-derived information from the source chemical rotenone.

*Read-across complex III inhibition: strobilurins (Case study 2)*
Another group of pesticides targets mitochondrial complex III (CIII). Mutations in the CIII proteins are linked to neurodegenerative disorders, but until now no neurological liabilities caused by chemical induced CIII perturbation have been observed in human tissue [Conboy et al., 2018; Ghezzi et al., 2011; Kunii et al., 2015; Mordaunt et al., 2015]. The objective of this case study was to establish the absence of this CIII-mediated neurotoxic potential (as detected with a TG424 study [OECD 1997]) upon exposure to a subset of CIII inhibitors using a biological read-across approach assessing toxicodynamic and toxicokinetic NAM data.

The formation of the read-across category in this study was based on the hypothesis that the selected compounds share similar chemical structure, similar pesticidal MoA, a similar toxicophore, and similar neurotoxic potential as the target compound. The compound set for this assessment encompassed members of the strobilurin fungicides family. The synthetic strobilurin fungicides are derived from the naturally occurring strobilurins A and B. The strobilurins bind to the quinol oxidation site of cytochrome b of mitochondrial CIII. The target chemical was azoxystrobin and the source compounds were pyraclostrobin, picoxystrobin, trifloxystrobin, and kresoxim-methyl. They all have a full toxicological data-package according to European legislation. Thus, this case study applies a category approach based on biological similarity, i.e. compounds sharing a common pesticidal MoA and toxicophore. However, although sharing the same toxicophore, i.e. the E-β-metaoxyacrylate group, the chemicals display less structural similarity than the above-described rotenoid family [Bartlett et al., 2002].

**Table 1:**
**IATA report information**

Consolidated information on the chemicals selected for the read-across case studies assessing complex I inhibition by rotenoids and complex III inhibition by strobilurins. The table follows the structure of the original IATA documents and is subdivided in purpose and analogue information. Purpose depicts the purpose of both read across case studies, the included chemicals (source and target) and the read-across approach. Analogue information describes chemical-specific information concerning physical/chemical properties, *in vivo* ADME, the coupled AOPs and other relevant information collected from external sources (i.e. everything not assessed *in vitro* described in later sections). # = not measured or no information found in literature.

| | | **RX complex I inhibition: rotenoids** |
|---|---|---|
| **Purpose** | **Purpose** | Hazard identification of Parkinson's disease-associated neurological effects caused by complex I inhibitors |
| | **Approaches** | analogue: one TC and one SC |
| | **Target Chemical(s) (TC)** | deguelin |
| | **Read across** | Biological: complex I inhibitors |
| | | Chemical: similarity target and source |
| | **Endpoints** | Parkinsonian motor deficit disorders |
| | **Source Chemical(s) (SC)** | rotenone |

| | | | deguelin | rotenone |
|---|---|---|---|---|
| **Analogue information** | Physchem data | Chemical structure | 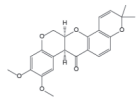 | 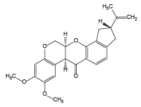 |
| | | MW (g/mol) | 394,423 | 394,423 |
| | | logP | 3.7-5.03 | 4.1-4.65 (pred.) |
| | | water solubility | 1.63e-05 (pred.) | 5.07e-07 (exp.)/ 8.79e-06 (pred.) |
| | | Vapour presure | 1.26e-07 (pred) | 1.08e-07 (pred.) |
| | *In vivo* ADME - oral dosing | Absorption | # | High |
| | | Distribution (brain) | # | # |
| | | Metabolism | Extensive | Extensive (pubchem) |
| | | Excretion | High (pubchem) | Extensive |
| | MoA | | Mitochondrial complex I inhibition | |
| | AOP | | Complex I inhibition leads to Parkinson liabilities | |
| | AOP status | | Endorsed by OECD: AOPwiki AOP number 3 | |
| | Chemical/ biological interaction | | # | well-described in the AOP |
| | Alternative assay results | | # | well-described in the AOP |
| | *In vivo* neurotoxic | | # = data gap | yes (AOP nr. 3) |

**Table 1: IATA report information** (continued)

| **RX complex III inhibition: strobilurins** |
|---|
| Flagging for absence of neurotoxicity caused by complex III inhibitors |
| category: one TC and more SC |
| azoxystobin |
| Biological: complex III inhibitors |
| Chemical: similiarity between strobins, dissimilarity between antimycin and others |
| Low neurotoxic potential |
| pyraclostrobin, picoxystrobin, trifloxystrobin, kresoxim-methlyl, antimycin a |

| azoxystrobin | pyraclostrobin | picoxystrobin | trifloxystrobin | kresoxim-methyl | antimycin A |
|---|---|---|---|---|---|
| 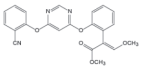 | 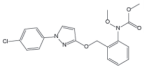 | 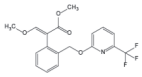 | 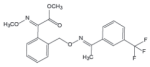 | 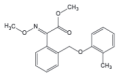 | 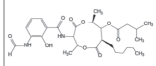 |
| 403,394 | 387,82 | 367,324 | 408,377 | 313,353 | 548,633 |
| 3,7 | 4,1 | 3,6 | 4,9 | 4,1 | 4,75 |
| 1.26e-05 (pred.) | 6.69e-05 (pred.) | 2.95e-05 (pred.) | 4.56e-06 (pred.) | 3.38e-05 (pred.) | # |
| 2,95E-11 | 5.77e-e9 | 8,27E-05 | 3,15E-06 | 1,06E-06 | # |
| High | Moderate | High | Low | Low | # |
| Moderate | Moderate | # | Low | Low | # |
| Extensive | Extensive | Extensive | Extensive | Extensive | # |
| High | Moderate | Extensive | High | High | # |
| Mitochondrial complex III inhibition | | | | | |
| Complex III inhibition leads to neurotoxicity | | | | | |
| Proposed AOP based on AOPwiki AOP nr. 3 | | | | | |
| Strobilurins bind to the quinol oxidation site (Qo) of cytochrome b of complex III. This prevents the electron flow between cytochrome b and cytochrome c, and petrubs NADH oxidation and ATP production in the mitochondria [Bartlett 2002]. | | | | | Antimcyin A binds to the Qi side of complex III [Von Jagow 1986] |
| *In vitro* data in a variaty of cell types plus measurements in zebrafish demonstrated mitochondrial toxicity [OECD 2020b]. Pearson *et al* reported similar effects at gene expression when comparing pyr and tri exposure to various brain diseases. Azo did not cluster with any brain disease [Pearson 2016]. | | | | | *In vitro* data showed upon antimycin A exposure mitochondrial dysfunction and neurotoxic effects [OECD 2020b]. |
| # = data gap | no | # | no | no | There are no test guideline neurotox studies. But some in vivo data indicate neurological development defects [Chang 2003]. |

7

Existing regulatory *in vivo* data was collected for source and target compounds with a focus on ADME properties and neurotoxicity. The source compounds did not show signs of neurotoxicity in neurotoxic studies nor in other repeated dose toxicity studies. In addition to the strobilurin family members, antimycin A –another well-established CIII inhibitor with neurotoxic effects– was included in the chemical set as a reference compound for the MoA. There is also no direct association between antimycin A exposure and neurotoxicity *in vivo* (including humans), possibly due to the potency and acute toxicity of the compound. Furthermore, no accidental exposures of humans to antimycin A have been reported, but acute exposure of animals to antimycin A indicate symptoms that suggest lethality via neuronal perturbations.

**AOPs in the assessment of regulatory questions**

Both IATA case studies are built around the endorsed AOP describing parkinsonian liabilities as a result of chemical-induced perturbation of mitochondrial CI [Terron et al., 2018][22] (figure 1A). The risk assessment of the rotenoid family is described completely in relationship to the OECD AOP curated key events. The assessment of the absence of neurotoxicity for the strobilurin family is anchored to a putative AOP adopted from the mitochondrial complex I AOP, with divergence especially at the MIE and AO (figure 1A). The MIE is described as the chemical interaction with and subsequent inhibition of CIII. Since CIII inhibition, like CI inhibition, perturbs the function of mitochondria we hypothesized that this could also lead to neurotoxicity. In the proposed AOP, mitochondrial dysfunction is directly coupled to neuronal degeneration and subsequently neuronal toxicity. The AO is specified as neuronal without a focus on degeneration of the dopaminergic subgroup of neurons in the human brain.

The endorsed and putative AOP have a common fundamental structure consisting of:

- MIE: binding of the chemical to CI/CIII
- KE1: inhibition of CI/CIII
- KE2: mitochondrial dysfunction
- KE3: impaired proteostasis (only included in the endorsed AOP)
- KE4: neuronal degeneration (specifically dopaminergic neurons in the endorsed AOP)
- KE5: neuro-inflammation (only included in the endorsed AOP)
- AO: parkinsonian motor deficits (endorsed AOP) / neuronal dysfunction (putative AOP)

Next, we describe individual KEs assessed by various *in vitro* and *in silico* methods specific for the associated biological processes (figure 1B and C):

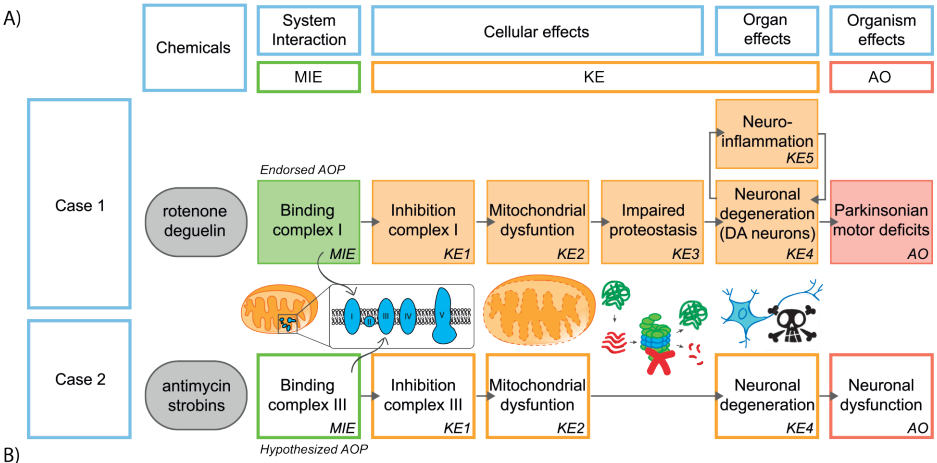


B)

| Replace *in vivo* | NAMs available | Difficult to replace |
|---|---|---|

| Key event | MIE | KE1 | KE2 | KE3 | KE4 | AO |
|---|---|---|---|---|---|---|
| Assay | PK studies<br>Bioavailability | Docking studies<br>Similarity studies | Seahorse assay | MMP assay | Protease activity assay<br>Proteosome activity markers | Viability assays<br>Cell death assay<br>Neuronal health | *In vivo* outcome (NA) |
| Key event | | | | | KE5 | |
| Assay | | | | | No assay included | |

C)

| Assay | Type | Measurement | Technique |
|---|---|---|---|
| Pharmacokinetics (PK) | *in silico/ in vitro* | Chemical distribution within a species | Plasma and tissue concentrations were predicted using physiologically based pharmacokinetic (PBPK) models. |
| Bioavailabiliy | *in silico* | Amount of free chemical in a system | Model predictions (2D steady-state biokinetic model; Fisher 2019) |
| Docking studies | *in silico* | Probability prediction of binding to a receptor | Model predictions (using Schrödinger software) |
| Similarity studies | *in silico* | Structural similairty of chemicals | Predictions (2D = Tanimoto score and 3D = USR-CAT) |
| Seahorse assay (intact cells) | *in vitro* | Mitochondrial respiration | In a seahorse machine: Fluorescent detection of O2 and H+ |
| Seahorse assay (perm. cells) | *in vitro* | Complex specific mitochondrial respiration | In a seahorse machine: Fluorescent detection of O2 and H+ |
| Mitochondrial membrane potential (MMP) assay | *in vitro* | Mitochondrial integrity | Confocal imaging of potential sensitive dye |
| Protease activity assays | *in vitro* | Degradation of protease substrate | Fluorescent measurement of substrate which becomes visible upon cleavage |
| Proteosome activity markers | *in vitro* | Expression of CHOP | Confocal imaging of CHOP coupled to GFP |
| Viability assay | *in vitro* | Viability based on resazurin reduction and ATP level | Assessment of resazurin or ATP levels based respectively on fluorescence and luminescence |
| Neuronal health | *in vitro* | Neuron outgrowth: length of axons and dendrites | Brightfield imaging of neurons |
| | *in vitro* | Neuron degradation: neuronal mass | Brightfield imaging of neurons |

**Figure 1: AOP explanation with NAMs**
**A)** Schematic representation of the AOPs included in both IATA documents: 1) the endorsed AOP (AOPwiki AOP nr.3) describing Parkinson's defects caused by mitochondrial complex I inhibition, and 2) the hypothesized AOP (based on AOPwiki AOP nr.3) describing neuronal degeneration caused by complex III inhibition. **B)** Table depicting the different assays selected to represent the different key events of the AOPs described in **A**. **C)** Table briefly describing the assays from **B** including type of assay, measurement and technique used.

**Methodological considerations**

**MIE: binding of compound to NADH-ubiquinone oxidoreductase (CI) or cytochrome bc1 complex (CIII):** describes the physical allocation of a chemical to the NADH-ubiquinone oxidoreductase (CI) or cytochrome bc1 (CIII) binding pocket. CI of the electron transport chain transfers 2 electrons obtained from NADH oxidation to ubiquinone resulting in its full reduction to ubiquinol [Sharma et al., 2009]. Under normal conditions, CIII of the electron transport chain drives the transfer of electrons from ubiquinol, reduced by CI and succinate dehydrogenase (CII), to cytochrome c [Sarewicz et al., 2015]. Both reactions result in the release of redox energy which is utilized to transport protons from the matrix to the inter-membrane space. The created proton gradient drives the conversion of ADP to ATP by the fifth complex (ATP synthase). The interaction between chemical and receptor can be assessed using docking studies in which the chemical toxicophore of known ligands in combination with crystal structures of the receptor can together provide information on the binding mode and binding efficiency of analogue chemicals. Furthermore, similarity studies based on physical/chemical parameters can provide insights into similarity among chemicals and the likelihood of similarity in binding modes.

**KE1: inhibition of NADH-ubiquinone oxidoreductase or cytochrome bc1 complex:** describes the interference of the inhibitor with CI or CIII, which leads to a decrease or total inhibition of the reduction reactions needed to contribute to the generation of the proton gradient across the mitochondrial membrane. This proton motive force is used by the ATPase (mitochondrial complex V; CV) to produce ATP, prevention of CV activity leads to the total inhibition of oxidative phosphorylation (OXPHOS). To measure and quantify this KE, the Seahorse bioanalyzer was used to measure oxygen consumption rates (OCR) in permeabilized cells. The system is treated with specific substrates and inhibitors of the electron transport chain, allowing for determination of specific sites of inhibition along the chain.

**KE2: mitochondrial dysfunction:** the drop in mitochondrial membrane potential (MMP) following CI or CIII inhibition will lead to total malfunctioning of mitochondria. Thus, the cell is stimulated to switch to other sources of ATP production (like glycolysis) to compensate for the OXPHOS-dependent deficiency in ATP.

*MMP*: Changes in MMP can be monitored with the use of potential dependent fluorescent dyes. Probes such as rhodamine123 or JC-1 accumulate in healthy mitochondria with a polarized membrane. Diminished or changed fluorescence reflect a depolarized MMP as the result of a lost proton gradient over the inner mitochondrial membrane due to electron transport chain inhibition or uncoupling mechanisms (chemically induced or activation of uncoupling proteins).

*Oxygen consumption:* as a consequence of electron transport chain inhibition, oxygen cannot be reduced to water at the level of complex IV. Changes in OCR (mitochondrial respiration) can be measured *in vitro* using the Seahorse bioanalyzer reflecting the level of inhibition of the target complex upon chemical exposure. Measurements of OCR in intact cells provide a physiologically relevant evaluation of direct effect of chemicals on mitochondrial respiration, as well as information on the bioavailability of chemicals in cells. In addition, measurements of OCR in permeabilized cells help assessing the activity of individual complexes of the mitochondrial electron transport chain.

*ATP levels:* inhibition of OXPHOS will eventually lead to ATP depletion when neurons can no longer compensate for the required ATP production via glycolysis. The intracellular ATP content after prolonged/repeated exposure can be measured by the luciferin/luciferase luminescence assay.

*Effects on glycolysis*: as a consequence of perturbation of the mitochondrial respiration, cells will switch to the oxygen-independent glycolysis for ATP production. A measure of this switch is the increase of a glycolysis by-product lactate.

**KE3: impaired proteostasis:** the direct link between mitochondrial dysfunction and impaired proteostasis is still unclear. Nonetheless, in the case of rotenone-induced toxicity, there is indirect *in vivo* evidence of perturbation of cellular proteostasis. Impaired proteostasis is a complex process. Various cellular perturbations can lead to altered handling of proteins. Two important components include the degradation of proteins through the proteasomal system and the disturbed handling of protein, where the latter may cause a so-called unfolded protein response in the endoplasmic reticulum (ER). Both processes can be quantified in *in vitro* systems using the degradation of a fluorescent surrogate substrate of the proteasome or the expression of protein (DDIT3/CHOP) involved in the ER response upon accumulation of unfolded proteins.

**KE4: neuronal degeneration:** lack of functional mitochondria ultimately leads to a drop in cellular ATP levels, increased production of reactive oxygen species (ROS), decreased neurite outgrowth, increased neurite degradation and, eventually, induction of cell death mechanisms.

The subsequent effects observed in neurites (mimicking axons and dendrites), i.e. reduced outgrowth or induced degradation, can be visualised based on changes in morphological features of the cell, for instance by quantifying neurite numbers and length in calcein-stained neurons after chemical exposure. Finally, the decreased viability that results from the drop in ATP can be followed using the resazurin-to-resorufin reduction reaction (a reaction dependent on the metabolic status of the

cell). Another option is to assess the number of dead cells using suitable assays, such as propidium iodide staining of nuclei from necrotic cells.

**KE5: neuro-inflammation:** an inflammatory response to damaged neurons that is characterized by the activation of microglia and astrocytes and the production of pro-inflammatory factors. Persistent inflammation has been observed during the development of parkinsonian liabilities and is thought to contribute to disease progression. In the case studies described here, we did not assess the induction or presence of inflammatory responses. Proper assessment of multifactorial inflammation response requires complex high-level co-culture of multiple cell types, including neurons and glia cells promoting neuroinflammation.

**AO: neuronal toxicity:** prolonged induction of cell death will in the end manifest itself as neurological dysfunction (e.g. neurodegenerative diseases), and rotenoid-induced CI inhibition specifically leads to parkinsonian liabilities. The development of these multi-factorial and slowly developing neurological diseases are difficult to assess using *in vitro* and *in silico* approaches. AOPs are chemical-agnostic. To implement the endorsed/proposed AOP into a risk assessment context and relate the observed *in vitro/in silico* read outs to the *in vivo* observed toxicological outcome, it is important to consider chemical specific properties and the likelihood that a specific AOP will be triggered. Two important chemical specific aspects were assessed in both case studies: biokinetics and pharmacokinetics.

**NAMs used to study MIE and KEs in Case study 1 and 2**

**Cell models:** to assess the likelihood of neurotoxicity upon exposure to rotenoids or strobilurins, we studied the above defined KEs in 4 human cell models using a broad concentration range. The cell models selected for the assessment of the KEs vary per event and include two neuronal cell types (LUHMES and SH-SY5Y cells), a kidney (RPTEC/TERT1) and a liver cell type (HepG2). LUHMES cells are the Lund human mesencephalic cell line differentiated into dopamine-like neurons prior to exposure. SH-SY5Y cells is a human neuroblastoma line demonstrating dopamine-β-hydroxylase activity and can produce relevant neurotransmitters. Both LUHMES and SH-SY5Y cell lines have been used extensively in Parkinson's disease research. RPTEC/TERT1 cells are proximal tubules cells immortalized by a viral integration of hTERT. HepG2 are a hepatocellular carcinoma derived cell line.

***In vitro* assays:** all *in vitro* studies conducted in the 4 different cell models are described in detail in the materials and methods sections of both OECD IATA reports. In summary, LUHMES cells were used to study OCR in permeabilized and intact cells, protease activity (rotenoids only), ATP content, neurite outgrowth, and viability

[Delp et al., 2021]. SH-SY5Y is a human neuroblastoma cell line showing dopamine-β-hydroxylase activity and producing relevant neurotransmitters. Differentiated SH-SY5Y cells were used to study MMP, lactate production, ATP content, neurite degeneration, and viability [Delp et al., 2021]. RPTEC/TERT1 cells are proximal tubules cells immortalized by viral integration of hTERT. RPTEC/TERT1 cells were used to assay for OCR in permeabilized and intact cells, MMP, lactate production, and viability (van der Steel et al., 2020). HepG2 is a hepatocellular carcinoma derived cell line, which we used for measurements of OCR in permeabilized and intact cells, MMP, lactate production, proteasome function (Case study 1), and viability [van der Stel et al., 2020].

**Similarity studies:** three types of chemical similarity scores were included in the two reports: similarity based on 2D (Tanimoto), 3D, or SMART. The Tanimoto score was calculated for structural fingerprints which were created with RDKIT[23] using MACCS keys to represent the chemical specific SMILES collected from US EPA chemical dashboard[24] and one from CHEMID Plus[25] [Leach et al., 2007; Durant et al., 2002]. 3D shape descriptions were determined using USR-CAT based on 10 conformers collected from RDkit [Schreyer et al., 2012]. Finally, similarity was determined based on common SMARTS patterns[26].

**Docking studies:** chemical docking for rotenone and deguelin into mitochondrial CI was performed as previously described by Troger *et al.* [Troger et al., 2020].

**Biokinetic studies:** the relationship between nominal (i.e. added) concentrations in the *in vitro* system and effective concentrations measured in the *in vitro* models, was predicted for all chemicals using an *in silico* model [Fisher et al., 2019]. Measurements of selected chemicals in cells and media were performed for selected chemicals and were compared to *in silico* predictions. Knowledge concerning this relationship between nominal and effective cell concentrations can be used to effectively translate *in vitro* results to *in vivo* conditions (including human).

**TK studies:** Physiologically based (toxico)kinetic (PBK) models in rat or human were constructed to support the IATA case studies using the Simcyp Simulator V17 (Certara UK Limited, Sheffield) using a previously published approach [Albrecht et al., 2019]. The methodology for PBK modelling was based on approaches outlined in WHO guidelines [WHO, 2010]. In brief, a full body PBK model was used with the lung, adipose, bone, brain, heart, kidney, muscle, skin, gastrointestinal tract and liver described as individual tissue compartments. Local sensitivity analyses were conducted for a number of the input parameters used in the PBK model and the effect of changing the input parameters on the plasma AUC of simulated chemicals was calculated. The specific assumptions for the models can be found in the respective IATA report [OECD, 2020a; OECD, 2020b].

**High-content transcriptomics:** effects of chemical exposure on gene expression can give valuable information about toxicological MoA, and can also indicate the point-of-departure for toxicity when a level of chemical exposure has a significant impact on the number of differentially expressed genes (DEGs) [Waldmann at al., 2014]. TempO-Seq analyses of approximately 3,600 genes (toxicologically relevant genes plus tissue relevant markers) was performed after exposure of the 4 cell models to rotenoids and strobilurins [Yeakley et al., 2017; Limonciel et al., 2018; Mav et al., 2018].

## Results

### Read-across complex I inhibition: rotenoids

Assessment of the MIE for rotenone and deguelin was based on *in silico* comparison studies assessing both the docking site and creating a pharmacophore/toxicophore (figure 2, rotenoid, MIE, A&B). The docking approach predicted that rotenone and deguelin have a common binding mode to the NADH-ubiquinone oxidoreductase protein. Furthermore, the created pharmacophore exhibited high similarity for the two chemical structures based on localization of hydrophobic moieties and H-bond acceptors.

Testing for KE1 upon exposure to deguelin and rotenone confirmed that, in LUHMES as well as in HepG2 cells, both inhibitors were selective mitochondrial CI inhibitors (figure 2, rotenoid, KE1, A, B & C and table 2). In both cell lines, rotenone was about 3 times more potent than deguelin in the perturbation of CI. Evaluating CI perturbations based on oxygen consumption readouts revealed that the maximal respiration parameter in intact cells was the most sensitive KE1 readout. Here again rotenone appeared a more potent inhibitor than deguelin.

Potency differences observed in KE1 readouts were also present when assessing mitochondrial integrity as a measure for KE2 (figure 2, rotenoid, KE2, A, B & C and table 2) in SH-SY5Y, HepG2 and RPETC/TERT1 cells. HepG2 and SH-SY5Y revealed a BMC25 for rotenone of about 7-8 times lower than for deguelin. In the case of RPTEC/TERT1 this difference was even a factor of 44. KE1 was also monitored based on the metabolic switch associated with mitochondrial dysfunction. We observed a strongly increased lactate production at lower concentration for rotenone exposure than for deguelin in all tested cell lines (table 2). This effect was most prominent in SHSY5Y cells (rotenone: 0.23 nM; deguelin: 80 nM).

The fourth event (KE3) in the Parkinson's liability AOP describes the perturbation of the proteosome upon chemical exposure. Proteasome activity was assessed based on protease activity and expression of CHOP/DDIT3, a protein involved in impaired protein folding homeostasis responses. Protease inhibition in LUHMES cells displayed similar EC25 values for both deguelin and rotenone (table 2), but rotenone showed a

trend of proteasome perturbation already at lower concentrations (figure 2, rotenoid, KE3, A). Measuring of GFP-CHOP positive HepG2 cells after 24 h exposure showed similar fractions for deguelin and rotenone over the entire concentration range (figure 2, rotenoid, KE3, B). At later time points (48 h and 72 h) a 5-fold difference in GFP-CHOP-positive cells between rotenone and deguelin exposure was observed (figure 2, rotenoid, KE3, C&D and table 2).

The last case study key event (KE4) concerned the measurement of *in vitro* neurite degradation (figure 2, rotenoid, KE4, A&B and table 2) and cell viability (figure 2, rotenoid, KE4, C&D and table 2). Cell viability was assessed based on resazurin reduction in all four models after 24 h of exposure. RPTEC/TERT1 cells demonstrated clear viability perturbation after exposure to deguelin (BMC25 = 398 nM) or rotenone (BMC25 = 102 nM). LUHMES cells demonstrated a viability perturbation upon rotenone exposure (BMC25 = 316 nM) and minimal effects upon deguelin exposure (BMC25 = 9120 nM). Rotenone and deguelin exposures resulted in a slight or no loss of viability in HepG2 and SH-SY5Y cells (for HepG2 and SH-SY5Y, BMC25 > 10,000 nM). We demonstrated that a switch to galactose medium resulted in a clear loss of viability upon exposure to both chemicals, with a lower EC50 value for rotenone [Van der Stel et al., 2020]. The medium switch also resulted in decreased viability for LUHMES cells and SH-SY5Y [Delp et al., 2019].



Effects of chemical exposure on neuronal features were evaluated based on neurite degeneration (measured mean neurite length) in SH-SY5Y or neurite outgrowth (measured neurite area) in LUHMES cells (figure 2, rotenoid, KE4, A&B and table 2). Neurite outgrowth was affected at lower concentrations for rotenone than for deguelin in both cell types. The mean neurite length of SH-SY5Y cells upon deguelin exposure even remained unaffected throughout the used concentration range (up to 10,000 nM).

**Read-across complex III inhibition: strobilurins**

For this case study a series of source chemicals was defined, including various strobilurin family members. Strobilurins were included for which a full data dossier had been evaluated according to European pesticide regulation (110/2007), yielding picoxystrobin, kresoxim-methyl, pyraclosrobin and trifloxystrobin.

**Table 2: Summary of the case studies NAM data.**

| **Summary of data gap filling** | | | **RX complex I inhibition: rotenoids** | |
|---|---|---|---|---|
| **Type of chemical** | | | Target | Source1 |
| **Chemical** | | | Deguelin | Rotenone |
| | Event | Assay | | |
| ***in silico*** | Chemical specific | Similarity 3D | structural modeling complex I | structural modeling complex I |
| | | Permeability (*in humans*) | not in report | not in report |
| | | Absorption (*in humans*) | not in report | not in report |
| | | Distribution (*in humans*) | not in report | not in report |
| | | Metabolism (*in humans*) | not in report | not in report |
| | | Excretion (*in humans*) | not in report | not in report |

| | Key event | Tissue | Assay | Value | |
|---|---|---|---|---|---|
| ***in vivo*** | AO | Brain | *in vivo* indication | # = data gap | Degeneration nigrostriatal dopaminergic neurons |
| ***in vitro*** | KE1 | LUHMES | OCR intact (*) | 1,00E+02 | 2,50E+01 |
| | | LUHMES | OCR perm. (*) | 8,61E+01 | 2,64E+01 |
| | | Liver | OCR perm. (*) | 1,05E+02 | 3,31E+01 |
| | | Liver | OCR intact (b) | 1,58E+02 | 5,01E+01 |
| | | Liver | OCR intact (m) | 2,57E+01 | 1,05E+01 |
| | | Kidney | OCR intact (b) | 1,35E+02 | 1,35E+02 |
| | | Kidney | OCR intact (m) | 3,72E+01 | 2,69E+01 |
| | KE2 | Liver | MMP | 2,40E+01 | 3,00E+00 |
| | | Kidney | MMP | 7,50E+01 | 1,70E+00 |
| | | SH-SY5Y | MMP | 3,35E+02 | 3,45E+01 |
| | | Liver | Lactate | 1,02E+02 | 7,50E+01 |
| | | Kidney | Lactate | 1,91E+02 | 1,82E+02 |
| | | SH-SY5Y | Lactate | <8.00E+01 | 2,30E-01 |
| | KE3 | LUHMES | Protease assay | 6,17E+03 | 6,61E+03 |
| | | Liver | Proteosome (**) | 4,00E+02 | 8,00E+01 |
| | KE4 | Liver | Viability | > 1.00E+4 | > 1.00E+4 |
| | | Kidney | Viability | 3,98E+02 | 1,02E+02 |
| | | SH-SY5Y | Viability | > 1.00E+4 | > 1.00E+4 |
| | | LUHMES | Viability | 9,12E+03 | 3,16E+02 |
| | | LUHMES | NO | 1,15E+03 | 3,80E+01 |
| | | LUHMES | NV | 2,09E+04 | 2,00E+04 |
| | | LUHMES | N ATP | 4,37E+03 | 4,37E+03 |
| | | SH-SY5Y | ND (24h) | > 1.00E+4 | 3,20E+01 |
| | | SH-SY5Y | N tox (24h) | > 1.00E+4 | > 1.00E+4 |
| | Repeat | LUHMES | ND (2x in 10d) | 3,98E+02 | 3,98E+01 |
| | | LUHMES | N tox (2x in 10d) | 1,26E+03 | 3,16E+02 |
| | | SH-SY5Y | ND (2x in 120h) | 3,87E+03 | 2,65E+01 |
| | | SH-SY5Y | N tox (2x in 120h) | 3,14E+03 | 1,22E+02 |

Table summarizes all data collected through *in silico* and *in vitro* methods (as delineated in figure 2). The table is subdivided in in-silico data, *in-vivo* data collected from existing documentation, and *in-vitro* data. The in vitro data is represented as BMC25 (nM) (exceptions (*) = EC50 and (**) = POD). The values are color coded per read-across case study (red low BMC value, green high BMC value). The color code highlights the concentration relationship for both read-across case studies in which the biological closely related KE 2 and KE 3 demonstrated lower BMC values than KE4 and KE5, echoing the AOP concept that more upstream KEs should happen earlier and at lower concentrations. Tissue types included: neuronal (LUHMES and SH-SY5Y), kidney (RPTEC/TERT1) and liver (HepG2).

**Table 2: Summary of the case studies NAM data.** (continued)

| RX complex III inhibition: strobilurins | | | | | |
|---|---|---|---|---|---|
| Target | Source1 | Source2 | Source3 | Source4 | Reference |
| Azoxstrobin | Pyraclostrobin | Picoxystrobin | Trifloxystrobin | Kresoxim-methyl | Antimycin A |
| | | | | | |
| 1,00 | 0,76 | 0,65 | 0,70 | 0,61 | NT |
| High | High | High | High | High | High |
| High | Moderate | High | Low | Moderate | Low |
| Moderate | Moderate | Moderate | Moderate | Moderate | Moderate |
| Extensive | Extensive | Extensive | Extensive | Extensive | Extensive |
| Moderate | Low | Low | Moderate | High | Low |

| Value | | | | | |
|---|---|---|---|---|---|
| # = data gap | Not detected in acute and repeat-dose neurotox. studies | Not detected in standard repeat-dose studies. No neurotox studies available | Not detected in acute neurotox study and neurotox (evaluation of 90 day repeat study) | Not detected in acute and repeat-dose neurotox. studies | No data |
| | | | | | |
| ≤ 5.00E+4 | ≤ 5.00E+4 | ≤ 5.00E+4 | ≤ 5.00E+4 | ≤ 5.00E+4 | 5,00E+02 |
| ≤ 5.00E+4 | ≤ 5.00E+4 | ≤ 5.00E+4 | NT | NT | NT |
| > 1.00E+4 | 3,92E+02 | 4,02E+03 | 5,33E+03 | 6,16E+03 | 1,89E+01 |
| 4,79E+03 | 4,90E+02 | 8,32E+02 | 2,40E+03 | 5,13E+03 | 6,70E+00 |
| 9,33E+03 | 7,24E+02 | 1,12E+03 | 4,68E+03 | 2,69E+03 | 3,39E+00 |
| 3,47E+03 | 4,17E+02 | 2,00E+03 | 1,17E+03 | > 1.00E+4 | 2,34E+01 |
| 1,82E+03 | 1,10E+02 | 1,91E+02 | 1,91E+03 | 5,50E+03 | 4,37E+00 |
| | | | | | |
| 1,12E+03 | 2,88E+02 | 3,89E+02 | > 1.00E+4 | > 1.00E+4 | 3,00E+00 |
| > 1.00E+4 | 7,90E+01 | > 1.00E+4 | 2,57E+03 | > 1.00E+4 | 8,00E-01 |
| 3,25E+03 | 2,96E+02 | 8,32E+03 | 3,63E+02 | 1,35E+03 | 6,60E+01 |
| 2,44E+03 | 1,79E+02 | 4,75E+02 | 9,22E+03 | 1,19E+02 | 7,20E+01 |
| 9,71E+02 | 2,46E+02 | 3,31E+02 | 1,57E+03 | > 1.00E+4 | 1,74E+02 |
| 4,89E+03 | 3,91E+03 | 7,76E+02 | 3,16E+03 | > 1.00E+4 | <8.00E+01 |
| | | | | | |
| not applicable | not applicable | not applicable | not applicable | not applicable | not applicable |
| not applicable | not applicable | not applicable | not applicable | not applicable | not applicable |
| | | | | | |
| > 1.00E+4 | > 1.00E+4 | > 1.00E+4 | > 1.00E+4 | > 1.00E+4 | > 1.00E+4 |
| 5,01E+03 | 4,37E+02 | 8,71E+02 | 6,03E+03 | 7,76E+02 | 3,60E+01 |
| > 1.00E+4 | > 1.00E+4 | > 1.00E+4 | > 1.00E+4 | > 1.00E+4 | > 1.00E+4 |
| > 5.00E+4 | > 5.00E+4 | > 5.00E+4 | > 5.00E+4 | > 5.00E+4 | 2,57E+04 |
| 3,16E+04 | 1,74E+04 | 4,90E+04 | 1,82E+04 | 4,17E+04 | 1,74E+04 |
| > 150000 | 5,25E+04 | > 5.00E+4 | > 5.00E+4 | > 5.00E+4 | >12500 |
| 1,95E+04 | 1,51E+04 | NT | NT | NT | 9,55E+03 |
| > 1.00E+4 | > 1.00E+4 | > 1.00E+4 | > 1.00E+4 | > 1.00E+4 | 1,99E+03 |
| > 1.00E+4 | > 1.00E+4 | > 1.00E+4 | > 1.00E+4 | > 1.00E+4 | > 1.00E+4 |
| | | | | | |
| 2,51E+04 | 3,98E+03 | 1,58E+04 | NT | NT | 1,00E+04 |
| 3,16E+04 | 7,94E+03 | 2,00E+04 | NT | NT | 1,02E+04 |
| > 1.00E+4 | 3,06E+03 | > 1.00E+4 | 2,07E+03 | 7,89E+03 | 4,23E+03 |
| > 1.00E+4 | 5,02E+03 | 9,04E+03 | > 1.00E+4 | > 1.00E+4 | 3,34E+03 |

OCR perm. = oxygen consumption rate in permeabilized cells; OCR intact (b) = oxygen consumption rate in intact cells expressed as basal respiration; OCR intact (m) = oxygen consumption rate in intact cells expressed as maximal respiration; N ATP = neuronal ATP levels; N tox = neuronal toxicity; ND = neurite degeneration; NO = neurite outgrowth; NT = not tested; NV = neuronal viability; 2x in 10 d = 2 times repeated exposure in 10 days; 2x in 120 h = 2 times repeated exposure in 120 h.

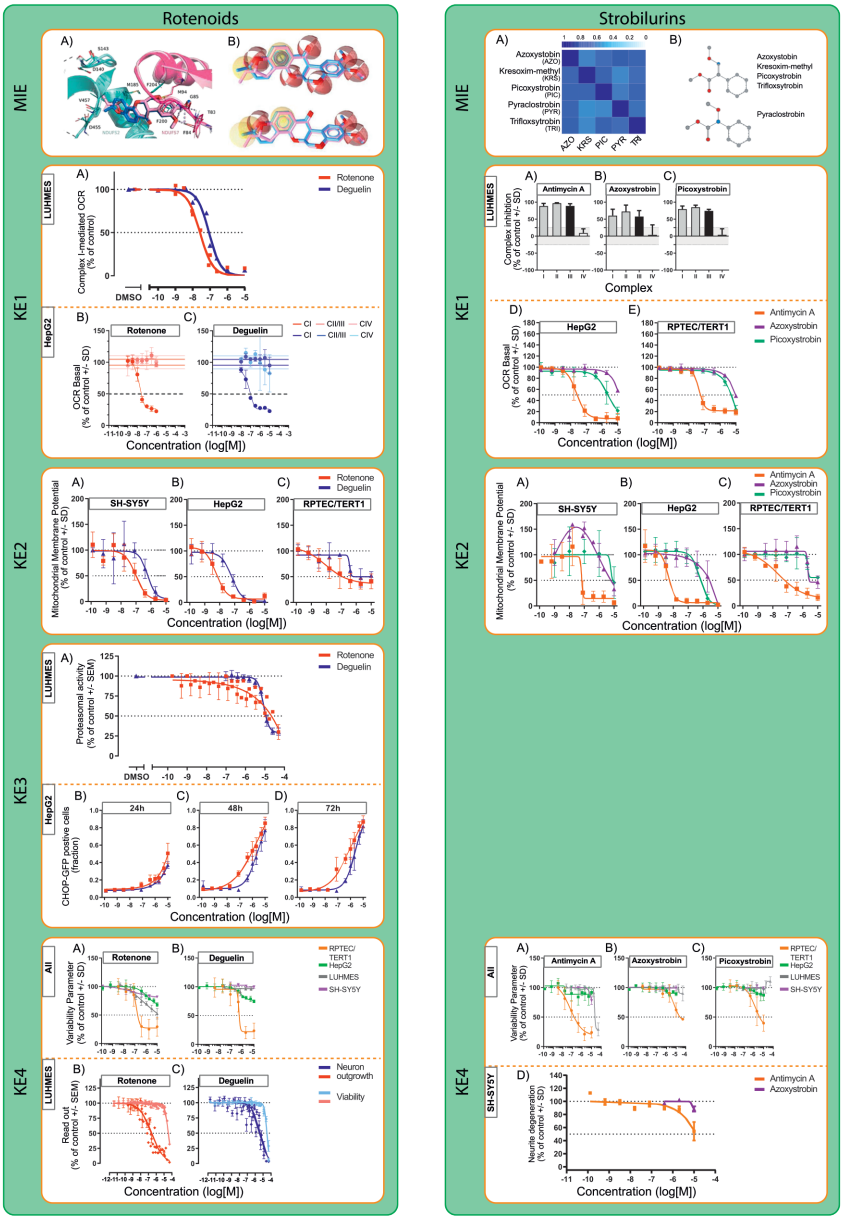


**Figure 2: Rotenoid and strobilurin case study represented as neurotoxicity AOP**

The figure is subdivided in two green panels describing the AOPs and their KEs for the rotenoid and strobilurin case study, which only KEs assessed in the IATA documents being included. The described data is a representation of all collected data and is linked to the BMC values described in Table 2.

**Rotenoids:** in all graphs the color scheme described rotenone in red and deguelin in blue, with exception of KE5 A), in which the different represented cells are depicted in 4 colors). **MIE**: **A)** docking study results describing the proposed common binding mode of 1 (pink sticks) and 2 (blue sticks) and **B)** two possible shared pharmacophores of rotenone and deguelin [Troger 2020]. **KE1**: oxygen consumption rate in permeabilized cells. **A)** Mitochondrial complex I inhibition in LUHMES cells after acute exposure to a concentration range of rotenone (red) and deguelin (blue) [Delp 2021]. Mitochondrial CI, CII/III and CIV inhibition in HepG2 after an acute exposure to **B)** rotenone or **C)** deguelin [van der Stel 2020]. **KE2:** mitochondrial membrane potential (MMP) assay. Effect of a concentration

range of rotenone (red) or deguelin (blue) for 24h upon MMP in **A)** SH-SY5Y, **B)** HepG2 or **C)** RPTEC/TERT1 cells [van der Stel 2020]. **KE3:** proteasome perturbation. **A)** Proteasome activity in LUHMES cells upon 24 h exposure to rotenone (red) or deguelin (blue) [Delp 2021]. Fraction of CHOP-GFP positive HepG2 cells upon exposure to rotenone (red) and deguelin (blue) after **B)** 24 h, **C)** 48 h or **D)** 72 h [Van der Stel 2021 unpublished]. **KE4:** neuronal degeneration. Effects on cell viability measured using resazurin reduction in 4 cell lines RPTEC/TERT1 (orange), HepG2 (green), LUHMES (grey) and SH-SY5Y (purple) after 24h exposure to **A)** rotenone and **B)** deguelin [van der Stel 2020, Delp 201]. Effects upon neurite outgrowth and viability in LUHMES cells after 24 h exposure to **A)** rotenone (pink = viability, red = outgrowth) or **B)** deguelin (light blue = viability, blue = outgrowth) [Delp 2021].
**Strobilurins =** in all graphs the color scheme depicts antimycin A in orange, azoxystrobin in purple and picoxystrobin in green, with exception of KE5 **A)**, in which the different represented cells are depicted in 4 colors. **MIE**: chemical similarity assessment. **A)** 3D similarity score when comparing strobilurin family members represented in a color coded heatmap. **B)** Result of SMART comparison describing structure similarity based on substructures.**KE1:** oxygen consumption rates in permeabilized and intact cells. Complex inhibition assay in permeabilized LUHMES cells after an acute exposure to **A)** antimycin A, **B)** azoxystrobin or **C)** picoxystrobin [Delp 2021]. Effect of an acute antimycin A (orange), azoxystrobin (purple), or picoxystrobin (green) exposure on basal respiration in **D)** HepG2 and **E)** RPTEC/TERT1 cells [van der Stel 2020]. **KE2:** mitochondrial membrane potential (MMP) assay. Effect of 24 h exposure to antimycin A (orange), azoxystrobin (purple), or picoxystrobin (green) upon MMP in **A)** SH-SY5Y, **B)** HepG2 and **C)** RPTEC/TERT1 cells [van der Stel 2020]. **KE4:** neuronal degeneration. Effects on cell viability measured using resazurin reduction in 4 cell lines: RPTEC/TERT1 (orange), HepG2 (green), LUHMES (grey), or SH-SY5Y (purple) after 24 h exposure to **A)** antimycin, **B)** azoxystrobin and **C)** picoxystrobin [van der Stel 2020, Delp 2021]. **D)** Neurite degeneration measured in SH-SY5Y cells after 24 h exposure to antimycin A and azoxystrobin. [Delp 2021].

The likelihood of similar MIEs for the different strobilurin family members was evaluated using *in silico* similarity assessment approaches based on 3D structure and SMART information (figure 2, strobilurin, MIE, A & B and table 2). Comparison of azoxystrobin with the selected strobilurins resulted in comparable 3D similarity scores for all chemicals (ranging from 0.61 to 0.76). This 3D similarity supports the opportunity for performing the read-across. In addition, based on the information contained in the SMART description, we concluded that there is strong conservation of especially the methoxyacrylate moiety within the strobilurin family which also supports our read-across case study.



All performed *in vitro* assays evaluating the following KEs included the target and source chemicals as well as the reference chemical antimycin A. In figure 2 only the results of the target chemical azoxystrobin, source chemical picoxystrobin and reference chemical antimycin A are depicted.

The OCR measured at 50,000 nM in (permeabilized) LUHMES cells confirmed that all chemicals were specific inhibitors of mitochondrial CIII (figure 2, strobilurin, KE1, A, B & C, and table 2). Assessment of CIII-specific inhibition in HepG2 cells demonstrated that pyraclostrobin was the most potent and azoxystrobin the least potent inhibitor (with BMC25 values of 392 nM and > 10,000 nM, respectively) (table 2). Assessment of the effects of chemical exposure on the basal OCR in both HepG2 and RPTEC/TERT1 cells confirmed the potency differences observed in the complex specific assays and the correlated SMART prediction (with pyraclostrobin differing from the others) (figure 2, strobilurin, KE1, D & E and table 2). Furthermore, for both complex-specific and whole-cell assays, antimycin A was a factor 100 to 1000 more effective in perturbing mitochondrial respiration.

Testing for depletion of MMP (KE2) in HepG2, RPTEC/TERT1 and SH-SY5Y after strobilurin exposure also confirmed that pyraclostrobin was the most potent

compound in compromising mitochondrial integrity (table 2). Azoxystrobin and picoxystrobin had similar BMC25 values that were orders of magnitude higher than for antimycin A exposure (figure 2, strobilurin, KE2, A, B &C and table 2).

The final putative KE to be assessed for the strobilurins case study was neuronal degeneration. None of the strobilurins gave rise to a decrease in cell viability in either HepG2, SH-SY5Y nor LUHMES cells (figure 2, strobilurin, KE4, A, B & C and table 2). RPTEC/TERT1 cells showed a decrease in cell viability comparable for azoxystrobin and trifloxystrobin. Exposure to pyraclostrobin, picoxystrobin, and kresoxim-methyl exposure in RPTEC/TERT1 cells resulted in reduced cell viability at ~10-fold lower EC25 than for azoxystrobin. No neuron specific effects (i.e., neurite length differences) were observed after 24 h exposure to strobilurin family members up to 10,000 nM in SH-SY5Y (table 2). In LUHMES cells, effects on neurite outgrowth were observed at higher concentrations, i.e., BMC25 values of 17 and 18 μM for pyraclostrobin and trifloxystrobin and 31, 49 and 42 μM for azoxystrobin, picoxystrobin and kresoxim-methyl, respectively (table 2).

**PBK data**

Biokinetic and PBK models were developed to support both case studies. Rotenone and deguelin have similar physicochemical properties, being neutral compounds with logP values of ~4. Measured human plasma binding and red blood cell distribution of the compounds, as well as the rate of metabolism in human hepatocytes, was similar. Plasma concentrations of rotenone and deguelin were simulated in both humans and rats using PBK models. The simulated unbound plasma exposure of the two compounds in humans was similar, once more supporting the use of rotenone as a source compound for deguelin. Using an *in silico* estimate of protein binding, the volume of distribution and brain concentrations of deguelin predicted by the PBK model were in reasonable agreement (1.3-fold) with observed rat data [Udeani 2001]. Plasma and brain concentrations of rotenone and deguelin were predicted to be similar in rat (within 1.5-fold) for similar administered doses. The biokinetic model predicted that the distribution of rotenone and deguelin within the different *in vitro* systems would vary from system to system (depending on cell numbers and media composition), but would be similar within each system. The *in silico* biokinetic predictions for rotenone agreed well with experimentally measured values. Overall, the biokinetic and PBK modelling supported that the cellular exposure of the two compounds would be comparable when the same dose was applied.

The strobilurin compounds have a range of lipophilicity values (2.5 – 4.5), with azoxystrobin being the least lipophilic. There was a trend for human plasma protein binding with increased lipophilicity, with azoxystrobin having the lowest protein

binding (highest measured fu). The predicted volume of distribution for the compounds was in the range 0.8 – 3 L/kg in humans with similar values being predicted in the rat [Poulin et al., 2002; Berezhkovskiy et al., 2004; Rodgers et al., 2006]. Steady-state brain to plasma distribution ratio was predicted to be 0.4 to 3.9 in the rat across the series of compounds and between 0.98 and 4.4 in humans. Azoxystrobin was in the middle of the range in both species with brain concentrations being predicted to be about 2-fold of those in plasma in both rat and human.

Using *in vitro* metabolism data in human hepatocytes, *in vitro*-to-*in vivo* extrapolation approaches were used to predict the clearance of the compounds. These values ranged from 0.8 to 44 L/h with azoxystrobin having a relatively high predicted clearance (24.4 L/h). Combining the predictions for the volume of distribution and clearance, azoxystrobin was predicted to have the shortest half-life of the compounds in the case study.

Using an allometric approach to scale down the predicted human clearance the rat pharmacokinetics of the compounds was predicted. For picoxystrobin, trifloxystrobin, kresoxim-methyl, azoxystrobin and picoxystrobin the rat PBK models were consistent with available pharmacokinetic data. At oral doses of 10 and 100 mg/kg the total concentrations of azoxystrobin predicted in the rat were within the range of simulated concentrations of the other compounds. However, when free plasma concentrations were considered, azoxystrobin had the highest unbound Cmax; but due to rapid clearance and short half-life the steady state concentrations were lower than –but similar to– those of picoxystrobin.

*In silico* biokinetic modelling predicted that the different compounds would have different cell:nominal concentration ratios in the different experimental systems. Predicted cell:nominal concentration ratios were lowest for azoxystrobin, the most polar of the compounds under consideration. There was reasonable agreement between the predicted and observed concentrations of azoxystrobin in the *in vitro* systems.

**Repeat dosing**

We also considered the necessity of repeated dosing or prolonged exposures for the occurrence of downstream KEs close to the AO, in relationship to the nature of the AO. This is relevant for clinically adverse outcomes like parkinsonian liabilities, which develop as progressive degradation of nigra-striatal dopaminergic brain areas at doses that are not acutely toxic.

Assessment of KE4 following exposure to rotenoids in LUHMES and SH-SY5Y cells (2x exposure, 120 h in total) resulted in similar values for neurite outgrowth compared to single exposures (table 2). However, neurite degeneration was identified in SH-SY5Y cells

upon deguelin exposure in the tested concentration range, which was not observed upon a single 24 h exposure. Notwithstanding, repeated exposure induced cell death at the same concentrations as neurite degeneration where observed (table 2).

For the strobilurins case study repeated exposure yielded a 2 to 4.5-fold increase in sensitivity for the detection of neurite effects in LUHMES cells (table 2). In SH-SY5Y cells, effects on neurite degeneration were within detection range following repeated exposure for all tested strobilurins except for the target chemical azoxystrobin. Only trifloxystrobin had an effect on neuron degeneration at a concentration where viability was not yet affected.

**Transcriptomics**

Follow-up research on both read-across case studies focused on the incorporation of transcriptomics as a promising additional means for enhancing the performance of AOP-based read-across. For this purpose, transcriptomic profiles were collected following 24 h exposures to a broad concentration range of deguelin, rotenone, antimycin A, azoxystrobin, picoxystrobin or pyraclostrobin in all 4 cell lines (LUHMES, SH-SY5Y, RPTEC/TERT1 and HepG2) (figure 3). A cell biological and toxicological relevant target-gene set of >3300 genes was monitored using targeted RNA sequencing-based transcriptomics using TempO-Seq technology (EU-ToxRisk gene panel is an extended version of panel established by the U.S. NIEHS/NTP) [Mav et al., 2018]. Here we will focus on the overall findings; cell type specific results will be discussed in detail in several separate follow-up publications.

Transcripts were considered differentially expressed between treatment condition and solvent control when the fold-change was above 1.5 or below -1.5 and the p-adjusted value was below 0.05. The obtained differentially expressed gene (DEG) profile upon exposure to both rotenoids and strobilurins revealed a strong potency difference. Neuronal cell lines (LUHMES and SH-SY5Y) did not exhibit transcriptomic changes at low concentrations that impact on mitochondrial function and neurite outgrowth. In contrast, HepG2 and RPTEC/TERT1 cells showed earliest changes in gene expression at low concentrations (nM) coinciding with inhibition of CI and III for the respective compounds. Of relevance, some of these genes affected both in HepG2 and RPTEC/TERT1 were related to the ATF4 responsive program that is known to be activated by inhibition of the mitochondrial respiratory chain inhibition including rotenone [Krall et al., 2021]. This is likely part of an adaptive response program to ultimate restore levels of essential amino acids, in particular asparagine. Given that these ATF4-directed programs were not observed in the neuronal cell lines might provide an explanation for the increased sensitivity of the neuronal cells against mitochondrial respiratory chain inhibitors. Further metabolomics analysis of intracellular amino acids levels in

the neuronal cell lines might substantiate this hypothesis. When focusing on the individual HepG2 and RPTEC/TERT1, an increase in DEGs (up or down) occurs at lower concentrations for rotenone exposure compared to deguelin and for antimycin compared to the strobilurins. This observed pattern correlates with the above-described potency differences in the other *in vitro* assays reflecting the AOP KEs.

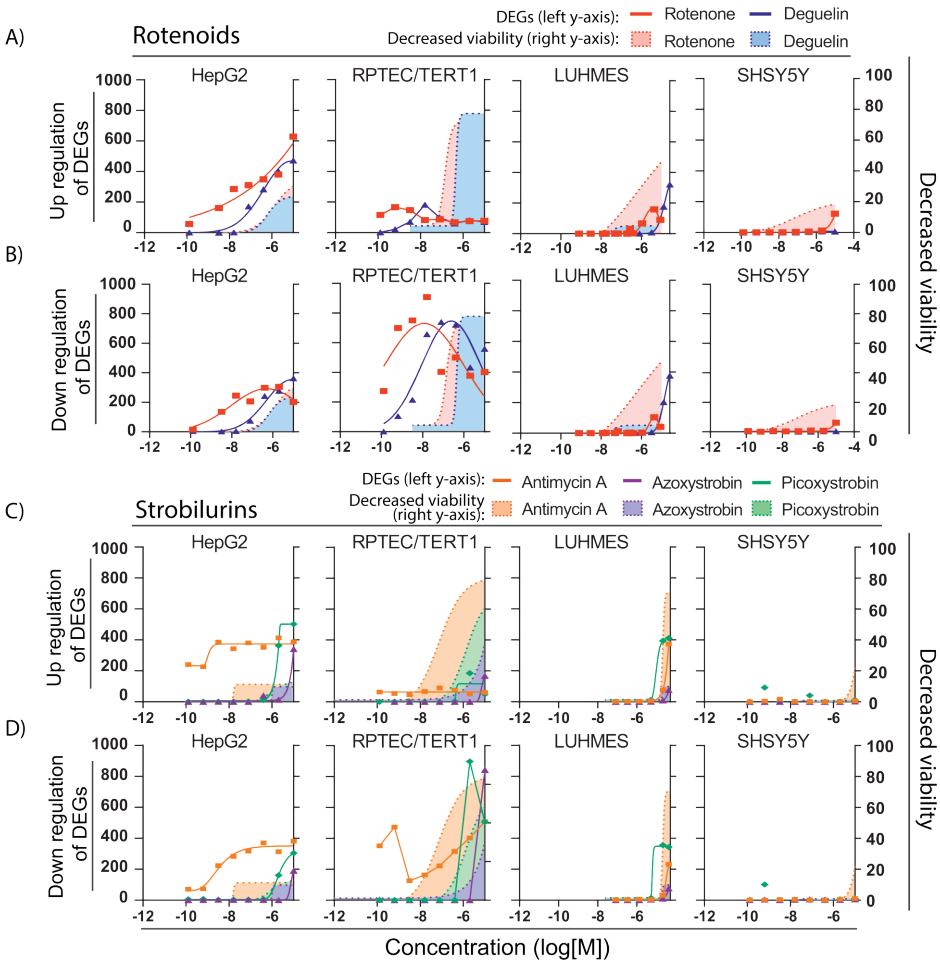


**Figure 3: Targeted transcriptomics using TempO-Seq technology for rotenoid and strobilurin treatment in different test systems.**

The effects on gene expression measured as the number of differentially expressed genes following 24 h exposures to a concentration range of rotenoids (**A** = up and **B** = down) and strobilurins (**C** = up and **D** = down) in HepG2, RPTEC/TERT1, LUHMES, and SH-SY5Y cells. The chemicals included are for the rotenoids: rotenone (red) and deguelin (blue), and for the strobilurins: antimycin A (orange), azoxystrobin (purple) and picoxystrobin (green). Genes included have a p-adjusted value below 0.05 and a log2FC above or below 2. Colored area under graph represent resazurin viability data (also presented in figure 2 in rotenoids/strobilurins KE5).

## Discussion and outlook

This article describes a joint effort to demonstrate the opportunities of performing AOP-based read-across using NAM data with the aim of flagging chemicals for potential neurotoxicity hazards. AOP-based read-across approaches were built around two groups of pesticides targeting mitochondrial complexes, from which we concluded that i) deguelin has a similar MoA as rotenone –but is less potent in its action– allowing for a direct read-across to rotenone to predict parkinsonian liability, and that ii) there is no evidence for a stronger neurotoxic potential of azoxystrobin mediated by a CIII inhibitory MoA as compared to other strobilurins; since source compounds did not show neurotoxicity *in vivo*, it is unlikely that the target compound azoxystrobin is a neurotoxicant via a CIII-mediated mechanism.

The OECD IATA case study template requires a qualitative assessment of the uncertainties for the separate case study elements, conjointly culminating in an overall uncertainty analysis. The various case study elements and their accompanying uncertainties for both the rotenoids and the strobilurins case studies were classified as either low, medium, or high (table 3), as stipulated by the applied 2018 OECD reporting template utilised. This classification pertains to the uncertainty of a used NAM *per se*, but does not explicitly reflect to what extent its result would impact on the overall conclusion of the read-across. Ergo, inclusion of a high-uncertainty methodology may have limited impact on the overall case study conclusions depending on the strength and impact of the other elements/evidence. Practically, based on the experience of the EU-ToxRisk case studies, the OECD IATA Project consortium suggested to discuss the impact of uncertainties on the overall read-across hypothesis and this notion was, in turn, taken up into the OECD template for 2020 [OECD, 2020c]. We will further discuss the main aspects of the uncertainty analysis below.

With one case study relying on an analogy approach and the other on a category approach, the structural boundaries of the read-across by the selected source compounds have different levels of uncertainty. In general, an analogy approach is more uncertain than a category approach which has better defined boundaries based on more negative and positive source compounds.

**Table 3: Summary of the uncertainty evaluation of the various test methods applied in the case studies.**
The table summarizes the uncertainties identified in both IATA case studies subdivided in 15 categories and scored with low, medium or high uncertainty label. TK = toxicokinetics, TD = toxicodynamics, MoA = mode of action

| | | RX complex I inhibition: rotenoids | | RX complex III inhibition: strobilurins | |
|---|---|---|---|---|---|
| **Factor** | | Uncertainty | Comment | Uncertainty | Comment |
| **Structural boundary of the read across** | | Low/Medium | Hig chemical similarity - but based on an analogue approach with only two compounds | TD = Low | Common toxophore and binding site |
| | | | | TK =Medium | Substitutions could affect ADME, but *in vivo* and simulations comparable |
| **Mode of action/AOP** | | Low | OECD endorsed AOP | MoA = Low | strobilurins are desgined to target CIII as their MOA/ AOP putative |
| | | | | AOP = Medium | |
| **Hypothesis** | | Medium | Based on endorsed AOP but predictions based on *in vitro* and *in silico* data | Low | Neurotoxic potential established/CIII inducing NT is high. NAMs covering TK/TD support hypothesis |
| **Similarity of source chemicals for read-across** | | Low | Common toxophore | Low | High 3D similarity with common toxophore |
| **Physical/Chemical properties** | | Low | Structurally highly similar compounds | Medium | Molecular weight & H-bond similar. Target chemical has a lower logP indicating that less reaches the brain |
| **Toxicokinetics** | | Low | Metabolism similar/PBPK predictions similar | *in vivo* = Low | *In vivo* data similar |
| | | | | *in silico* = low | PBPK predictions similar |
| **Similarity of supportive data** | ***in vivo*** | Low | Regulatory *in vivo* data & human data | Low | Regulatory *in vivo* data |
| | ***in vitro*** | Medium | Not OECD validated – but routine assays in the labs | Medium | Not OECD validated – but routine assays in the labs |
| **Number of analogues** | | *Not relevant* | | Low/Medium | Source compounds demonstrating similar negative results. However, only 1 positive compound which was not similar in structure |
| **Quality of end point data** | **Uncertainty of the assay** | Medium | Reported according to ToxTemp/DB-ALM. *In silico* models not validated externally | Low/Medium | Reported according to ToxTemp/DB-ALM. *In silico* models not validated externally |
| | **Following proposed AOP** | Low/Medium | AOP endorsed but with the described uncertainties | High | AOP – putative |
| | **KEof the AOPs reflected by assays** | Low/Medium | Low uncertainty for all, except proteosomal activity | Medium | Uncertainty whether assays can predict neurotoxicity |
| **Similarity of endpoint data (among source compound(s))** | | Low/Medium | Similar for all assays except one | Low | No signs of in vivo neurotoxicity of source chemical. High similarity *in vitro* between source and target |
| **Concordance and weight of evidence for justifying the hypothesis** | | Low | Combined data support that rotenone and deguelin have similar behavior in the various test methods but different potency | Low | The target compound is biologically comparable to the source compounds |
| **Overall** | | Low | Based on the uncertainty of the above factors and their impact on prediction | Low/Medium | Based on the uncertainty of the above factors and their impact on the prediction |

In case of the category-based strobilurins read-across, compounds were all defined by a common toxicophore, although the overall chemical similarity was modest. Unsurprisingly, chemical similarities displayed low Tanimoto scores. However, similarity among the strobilurins was higher when based on the 3D-features of the molecules. This lack of structural similarity was considered unlikely to have significant repercussions on the overall read-across, as biological similarities (TK & TD properties) were comparable. Regarding physicochemical similarities of the strobilurins, the logP of azoxystrobin was lower than that of the source compounds. The impact of this difference was nevertheless assessed as low on the overall read-across conclusion, since the lower logP value would indicate that the compound is less prone to reach the brain in comparison to source compounds with higher logP values.

In case of the analogue-based rotenoid read across, chemical similarity between deguelin and rotenone is high for both structural and physicochemical properties. The similarity between target and source chemicals was further supported by the similarity in the determined pharmacophore and for the CI docking.

In both case studies, uncertainties related to the toxicokinetic behaviour of the compounds were considered low based on *in silico* TK simulations from PBK models. These estimates were further supported by a sensitivity analysis where the impact of the various input values in the PBK model on total plasma AUC in humans and rats was assessed [OECD, 2020a; OECD, 2020b].

As both case studies relied on non-guideline *in vitro* data, formal validation of the assays is not available. This could constitute a high uncertainty. However, most assays were part of a consortium-wide reviewed description document [Krebs et al., 2019] and some were described using DB-ALM documentation [EC, 2019]. All methods were internally validated and assay types are commonly used to address mitochondrial functioning of *in vitro* systems.

Both case studies were built using an AOP as the guiding structure for the selection of assays supporting the assessment of the relationship between MoA (mitochondrial complex inhibition) and adversity (the neurological dysfunction). The uncertainty related to the MoA/AOP is low for the rotenoid case study, as the used AOP has been fully developed and has been endorsed by the OECD; overall AOP uncertainty was gauged as being low[22]. Moreover, one of the stressor compounds for developing the AOP was rotenone, further reducing the uncertainty regarding the relevance of the AOP.

This contrasts the putative AOP on which strobilurins testing strategy relied. The AOP is postulated mainly based on antimycin A data where very little *in vivo* and human data was available [OECD, 2020a; OECD, 2020b]. Notwithstanding, we recently

showed that AOP#3 from AOP-wiki can be expanded to inhibitors of mitochondrial function, specifically CIII inhibitors [Delp et al., 2021].

Several observations were made regarding the approach of linking *in vitro* and *in silico* assays to different KEs of AOPs. When testing for early KEs it is not necessary to use cells directly related to the adverse endpoint in question, if the studied cellular biochemistry was also observed in other cell types (e.g., the mitochondrial respiratory chain). For late KE testing –close to the AO– it is difficult to define "adversity" *in vitro*, using multiple read-outs from different assays reducing the uncertainty. This was exemplified when measuring viability, neurodegeneration and neurite outgrowth, which are all closely related to the human AO as they assess processes related to neuronal integrity.

Also, it has been established that assays used are not only sensitive to mitochondrial toxicity but are also capable of detecting a wide array of MoAs [Delp et al., 2019]. A broad biological coverage of testing is helpful in addressing the question whether other MoAs/AOPs would be needed to be addressed for the read-across. Another observation was, when the hazard concerned an adverse outcome like parkinsonian motor deficits, being an endpoint not routinely picked up in regulatory studies [Ockleford et al., 2017], then an AOP-based read-across approach with robust late KE assays might provide higher confidence than a standard regulatory study, in this case the OECD TG424.



Incorporation of assays monitoring a broader range of possible biological events, like the use of transcriptomics, into an AOP-based read-across could both support the assessment of single KEs or the complete AOP as well as reduce uncertainties originating from other measurement. Firstly, gene expression of individual genes can be linked to the process specific for KEs to assess changes over the length of the AOP. Incorporation of concentration and time factors will help support causal relationship studies. This approach could also be reverted specifically in a read-across context by assessing differences and similarities in gene expression patterns upon exposures to closely related chemicals. The sets of genes can be used as fingerprints for the assessment of other chemicals. Using the approach in the assessment of the gene expression patterns upon exposure to all included CI and CIII inhibitors did not result in the identification of CI or CIII unique genes in HepG2 cells (unpublished Van der Stel). This means that transcriptomics in this particular case would suffice for MIE identification or studies concerning the MIE specifically but rather indicate mitochondrial toxicity in general. Secondly, transcriptomics could support the assessment of a large range of biological pathways that would be activated by mitochondrial toxicants and at multiple levels (sensor, transcription factors and target

genes), which would be labour intensive when done with single assays. We observed no specific modulation of transcriptional programs at low toxic concentrations of the CI and CIII inhibitors in neuronal cells, indicating we likely have not missed unexpected biological perturbations during our assessment. In HepG2 and RPTEC cells transcriptional changes were observed at similar concentrations that affected mitochondrial function.

Previously obtained data provides evidence for the link between our KE4 and the occurrence of neuronal dysfunction and more specifically degradation of dopaminergic neurons in the substantia nigra. The observed specific degradation of neurons originates from a limited capacity to compensate the reduced ATP production by upregulation of glycolysis [Almeida et al., 2001; Almeida et al., 2004; Herrrero-Mendez et al., 2009; Terron et al., 2018]. Moreover, the dopaminergic neurons located in the substantia nigra have a higher energy demand compared to other catecholaminergic neurons in the brain, because of their length, highly branched phenotype and the presence of high numbers of synapses. In addition, they exhibit calcium-dependent autonomous pace-making activity, which has been demonstrated to require more energy than similar activities relying on potassium [Schildknecht et al., 2017]. The combination of this unique architecture and the calcium dependent pace-making activities result in a low residual energy capacity, which makes this cell type very susceptible to cell death caused by a reduction or absence of mitochondrial energy production. At last, hydrophobic toxicants tend to accumulate into the brain, which increases the risk of toxicity upon prolonged low level exposures for neurons.

All together, we have shown that the practical application of an AOP approach through integration of specific technologies and test systems that reflect the AOP MIE and KEs, might find broader application in a read-across safety assessment of structurally related substances.

Based on the learnings from an elaborate OECD IATA case study project regulatory review panel of the two case studies, some more generic learnings on an AOP–based testing strategy supporting read-across can be proposed:

- Anchoring a testing strategy to AOPs is useful since the relevance of endpoints tested is by this means established. When an AOP is not available or it is not well-consolidated, it is necessary to describe and justify the scientific rationale in detail. However, in all cases it is still necessary to address whether other MoAs would be relevant for the problem formulation.
- When testing for a KE, it can be useful to apply different assays to observe consistency, unless one assay has already been established as adequate

- An analogue approach can be justified based on low uncertainty around most of the elements of the read-across.
- A read-across based on not only structural similarity but also biological similarity can be justified by a broad biological coverage of late KE assays together with toxicokinetic data.
- Although, it is recognized that a low toxicity hypothesis is more difficult to underpin (it is difficult to justify when testing is sufficient for regulatory decision-making), it is possible to address this if the problem formulation is narrow and well-defined. In this context, it is useful to provide data on reference compounds to demonstrate that the testing strategy works.

**Conflict of interest**

The authors declare that there is no conflict of interest

**Acknowledgements**

This work was supported by the European Union's Horizon 2020 research and innovation programme under Grant agreement no. 681002 (EU-ToxRisk). Parts of this work contributed to two IATA Case Studies projects – *"Identification and characterization of parkinsonian hazard liability of deguelin by an AOP-based testing and read across approach"* – and – *"Mitochondrial complex-III-mediated neurotoxicity of azoxystrobin - Read-across to other strobilurins"* – [OECD, 2020a; OECD, 2020b].

# 8

# Discussion and future perspective

Perturbation of cellular homeostasis is a major cause of organ toxicity occurring upon chemical exposure. Malfunctioning of one of the most important cellular organelles, the mitochondria, is observed upon exposure to 15% of 10,000 environmental chemicals (TOX library) [Attene-Ramos 2015, Xia 2018]. Testing for chemical-induced mitochondrial malfunctioning is becoming more prominent during the development of chemicals and is largely based on proper functioning of vital mitochondrial processes, like respiration and metabolism [Dykens 2007, Dykens 2014]. Despite the current testing strategy, mitochondrial perturbations are still observed upon exposure to existing environmental chemicals, signifying the need for improvements in risk assessment. We hypothesized that the use of a more mechanism-driven testing approach that also monitors the overall cellular responses, besides functioning of the vital mitochondrial processes, will strengthen the prediction of potential mitochondrial toxicity during chemical risk assessment.

## Mechanism-based research links mitochondrial perturbation to cellular adversity

Organ toxicity is the result of both perturbation of the mitochondrial proteins and enzymes followed by a (partial) loss of their function and the incapability of the cell/tissue to overcome this. Assessment of changes in cellular behavior upon perturbation of mitochondrial processes will improve the identification of conditions leading to cellular adaptation or toxicity. To enable proper classification of generic, chemical class- and substance-specific effects, a comprehensive characterization of vital mitochondrial processes, cellular behavior and toxicity is required.

Vital mitochondrial process can generally be subdivided in 6 processes, as reviewed in **chapter 2**: metabolism, respiration, protein homeostasis, morphology dynamics, calcium homeostasis and mitophagy. The assays monitoring proper functioning of these mitochondrial processes should allow us to discriminate between normal fluctuations (non-toxic conditions) and a perturbed state (toxic conditions), and ideally provide scaled results, matching the potency of chemicals. This information supports flagging of chemicals that require further testing. In addition, the ability to separate mitochondrial toxicants with different modes-of-action will support the use of more tailored risk assessment pipelines, with specific testing steps only relevant for subgroups of chemicals. In **chapter 3**, we focused on the evaluation of well-known biochemical assays for vital mitochondrial functions, which monitor (complex-specific) respiration, mitochondrial integrity, glycolytic capacity and cell viability for mitochondrial transport inhibitors. These assays were all capable of discriminating inactive (e.g., complex II inhibitors) and active chemicals (e.g., complex I and III inhibitors) and could be used to determine potency differences within the group of

active chemicals. ToxCast and Tox21 have used similar approaches, confirming that these assays can identify different classes of mitochondrial electron transport chain inhibitors [Xia 2018, Willw 2015, Hallinger 2020]. Others have demonstrated that mitochondrial membrane potential readouts for a large set of chemicals allowed the identification of chemical structure clusters with increased risk for mitochondrial-related toxicity [Attene-Ramos 2015]. Nonetheless, this data did not differentiate classes of mitochondrial toxicants and likely identified only the most potent structures. Identification of inhibitors that have low potency or that demonstrate only partial inhibition remains important in case of prolonged exposure (i.e., a low dose of agro-chemicals) or upon exposure to mixtures (i.e., a combination of drugs and food additives), which could result in accumulative or even synergistic effects [Nandipati 2016, Vasan 2020].

Cellular behavior upon perturbation of vital mitochondrial processes can be monitored based on cellular signaling indicating, among others, the initiation of adaptation responses and induction of cell death. The emerging opportunities that come with the omics technologies allow us to study cellular signaling based on information gathered: at gene, protein and metabolite level, from any cell system, at any moment in time and for any chemical concentration [Brockheimer 2017, Heijne 2005]. We examined the relationship between mitochondrial perturbation and cellular signaling using targeted transcriptomics (**chapter 4**). The overall concentration-dependent change in expression of the set of toxicology relevant transcripts illustrated that we can distinguish chemical potencies based on the transcriptome profiles. The study of the up- and down-regulated transcripts did not allow separation of the chemicals targeting the different protein complexes responsible for mitochondrial respiration, which indicates a shared cellular response upon exposure to this class of chemicals [Pearson 2016, Simon 2019]. The incorporation of chemicals with other mode-of-actions (mitochondrial metabolism and morphology), multiple time points (covering primary and secondary responses) and the use of the whole transcriptome is required to study the clustering behavior of different classes of mitochondrial toxicants and will support studies that aim to distinguish between the primary targets of all chemical classes.

Based on our work and that from others, we envision that the ultimate assay design for testing the relationship between mitochondrial events and cellular toxicity should incorporate multiple readouts in one run such that their relative influence can be studied. A set of consecutive readouts could be an early drop in ATP levels monitored using ATP-FRET (used in **chapter 4 and 5**), followed by the up- or downregulation of relevant downstream fluorophore-labeled proteins and eventually the induction of cell death markers at a later stage. Alternatively, a set of concurrent readouts addressing multiple features of one cellular response, or several features of different cellular

responses will strengthen the identification of toxic conditions. These combined high-content imaging approaches are only limited by the number of available lasers, compatibility of the used fluorophores and the resolution required to capture the studied biological process. The use of these single cell measurements will allow the identification of exact thresholds amongst the various subsequent events occurring between mitochondrial perturbation and toxicity, which will help to understand why one cell survives and another cell will not.

Single cell concurrent measurements are already commonly used in a sequencing context [Hwang 2018]. The sequencing captures both nuclear and mitochondrial genome-driven gene expression and the co-expression patterns of both have been used to understand occurrence and development of mitochondrial diseases [Lareau 2020]. These patterns could also be used to understand possible adaptive or adverse responses upon exposure to chemicals targeting mitochondrial genes and/or proteins. In the last decades, single cell sequencing and imaging-based readouts are integrated in one assessment pipeline to link phenotypic readouts, like protein expression and morphology, to concurrent transcriptomic changes. This approach relies on sequencing of single cells that were selected based on interesting phenotypes or were stained for interesting markers after collection [Binan 2016, Liu 2020]. In this way, imaging-based selection of cells with specific mitochondrial phenotypes and concurrent single cell sequencing enables linking of different mitochondrial appearances to the expression of relevant proteins (**chapter 5**).

Altogether, this work demonstrated that using a tiered testing strategy that monitors mitochondrial processes followed by detailed assessment of cellular signaling will provide valuable information to unravel the relationship between mitochondrial perturbation and cellular adversity, which will support identification of both potent and less pronounced mitochondrial toxicants.

## Mechanism-based studies enable the use of a variety of in vitro cell models

Nowadays toxicology and chemical risk assessment is focused on reducing the animal burden in all phases of chemical development and evaluation. Since 2013, the use of products tested on animals is completely banned in the cosmetic field and the use of alternative testing methods is preferred and promoted in the context of chemical assessment under REACH [European Committee 2009, European Committee 2006]. The choice of cell system to use in alternative testing methods influences the throughput, relevance and complexity of the outcome. The outcome of especially mitochondria-related readouts can vary between cell systems, because of large differences in mitochondrial mass and need for mitochondrial respiration

[Pagliarini 2008, Wang 2010]. Nevertheless, the use of a tiered mechanism-driven testing strategy allows the use of all available models; this requires proper selection for readouts relevant for the used cell type and its complexity.

The first tier in the assessment of mitochondrial toxicity includes the study of chemical-target interaction. The molecular structures of mitochondrial targets are assumed to be comparable between different human cell types. This implies that any cell type, independent of its origin or need for mitochondrial respiration, could be used to assess the potency of chemicals for interaction with mitochondrial targets in high-throughput formats assessing large sets of chemicals. We demonstrated that HepG2 cells do support the assessment of complex-specific inhibition of respiration, loss of mitochondrial integrity and decreased ATP production (**chapter 3, 4, 6 and 7**). Moreover, related changes in downstream signaling processes could be picked-up with HepG2 cells that do not exhibit toxicity, indicating HepG2 is "fit-for-purpose" to analyze these early events.

These "simple" models, like HepG2 cells, can be forced to rely more on mitochondrial respiration. We achieved this via inhibition of glycolysis, which resulted in an increase in the observed cellular toxicity. This new phenotype better resembled the effects observed in cell lines that already rely more on mitochondrial respiration, like RPTEC-TERT1 (**chapter 3 and 4**, Delp 2019). Another option is to increase the complexity of model systems by changing the culture environment via the introduction of an extracellular matrix. In **chapter 3**, we demonstrated that HepG2 cells cultured in 3D protein matrices establish a different phenotype including the reduction of glycolysis-related factors. Furthermore, exposure to electron transport chain inhibitors, specifically complex I inhibitors, led to toxicity already in response to a single dose.



Nevertheless, certain human tissues are more susceptible towards mitochondrial perturbation upon chemical exposure and therefore require extra attention in follow-up research. Differences between tissues arise from their reliance on mitochondrial respiration or high energy demand as is observed for respectively neurons and muscles. To enable proper assessment of mitochondrial toxicity, it is necessary to incorporate *in vitro* assays monitoring readouts specific for proper functioning of these susceptible tissues. In **chapter 7** and related work [Delp 2020], we additionally monitored the outgrowth and degradation of neurons to capture central nervous system specific effects. It is clearly demonstrated that chemicals known to induce neuronal disorders, like rotenone, also display a more pronounced effect in the susceptible tissues. Assessment of specific muscle function can be achieved *in vitro* by assessing myotube formation via morphological features, immunofluorescence staining and their adhesion to each other and cell culture materials [Ishikawa 2019, Murphy 2016].

More advanced model systems for mitochondrial, or any type of toxicity studies, are models that capture a form of higher tissue complexity. This higher complexity can be achieved by using multiple tissues (organ-on-a-chip), multiple cell types (micro tissues) or multiple cell lines derived from one genetic background (IPSCs technology). Organ-on-a-chip combines multiple tissues to enable monitoring of metabolism and signaling in the development of toxicity [Bavli 2016]. This combination will create a more realistic homeostasis between different substrates and metabolites involved in mitochondrial respiration and regulation of glycolysis. Micro tissues will support the study of interactions within one tissue, to understand why particular cell types are more vulnerable and how intercellular signaling is involved in the development of toxicity. This concept combined with IPSCs was explored in the form of a "mini brain" and could provide valuable information into the relationship between mitochondrial perturbation and neurological disorders [Govindan 2021]. Moreover, IPSCs differentiated into multiple cell lineages enables more in-depth studies when creating tissues with different mitochondrial mass (kidney, cardio, liver, and neuro) from the same genetic background [Shi 2017].

To summarize, the integration of specific *in vitro* models into the different steps of a tiered testing strategy enables flagging of chemicals in early stages using simple cell models followed by testing for specific toxicity in susceptible tissues or upon prolonged exposure using tissue relevant and more complex systems. The proper use of these *in vitro* methodologies will help to move from complete *in vivo* testing strategies to more hybrid forms in which *in vitro* work will reduce the required number of test animals, and ultimately to a chemical risk assessment without the need of animals.

## Integration of in vitro and in silico strengthens mitochondrial perturbation prediction

The use of quantitative rather than qualitative mechanistic information facilitates the development of toxicity prediction models assessing the probability that chemical exposure will result in cellular adversity. *In silico* simulations enable the generation of detailed mathematical descriptions of experimental data allowing intra- or extrapolation to untested conditions, which will indicate if a chemical is safe or not and inform about required further testing.

Understanding the exact relationship between the degree of mitochondrial perturbation and the balance of cellular adaptation or adversity is required to enable the identification of mitochondrial toxicants in general, but specifically for chemicals that have a less pronounced effect.

To facilitate the identification of these adversity thresholds, it is essential to describe the observed changes in mitochondrial functioning. In **chapter 4 and 6**, we monitored mitochondrial perturbation using temporal high content imaging of mitochondrial membrane potential fluctuations in detail. We described the time-dynamics using *in silico* approaches based on a phenomenological model and an ordinary differential equation (ODE) model. Others employed ODE models to describe the relationship between mitochondrial DNA and mitochondrial morphology [Kornick 2019], the interaction between $Ca^{2+}$ homeostasis and mitochondrial swelling [Moshkforoush 2019, Efendiev 2020], and the balance between all mitochondrial metabolites [Bazil 2010]. The obtained parameters from both phenomological and ODE models could serve as a classification of hazardous and non-hazardous chemicals. Nevertheless, ODE descriptors fit best in a biology-driven assessment.

Moreover, the use of machine learning approaches, supervised or unsupervised, help to establish tools in which information obtained from *in vitro* and *in silico* approaches together support chemical clustering and as a result improved classification. In **chapter 5**, we used unsupervised machine learning algorithms to classify the mitochondrial morphology phenotypes into two sub-groups. The unbiased algorithm enables the assessment of the change in distribution between the two mitochondrial types of mitochondrial morphology upon chemical exposure. A combination of processes, including MMP and ATP, should be perturbed before mitochondrial fragmentation occurred, rather than only a decrease in MMP [Jones 2017]. Machine learning approaches to classify mitochondria morphologies are also exploited by others using both supervised and unsupervised assessment to classify mitochondrial phenotypes [Zahedi 2018, Fisher 2020]. Using high resolution images, they achieved the characterization of fragmented and tubular objects, though when integrating morphology features into a high-content analysis pipeline, the use of lower resolution pictures is standard practice. Therefore, in **chapter 5** we focused on the discrimination of clear differences rather than identification of detailed structures. The next step in understanding the implications of mitochondrial morphology change for the development of toxicity is to link the phenotypes besides to mitochondrial processes also to the dynamics of morphology machinery proteins. Others already demonstrated that changed expressions of these machinery proteins can be both protective and disruptive upon exposure to several known mitochondrial inhibitors [Hwang 2014, Alaimo 2014, Patten 2014, Civiletto 2015, Grohm 2012, Tian 2014, Jones 2017].

The incorporation of these *in silico* approaches into *in vitro* testing platforms allow detailed quantification of chemical-induced temporal, spatial and concentration-dependent change in mitochondrial parameters, including ATP, MMP and mitochondrial morphology. We envision that combining this approach with the

quantitative description of cellular behavior upon chemical exposure will support prediction of toxicity upon a broad variety of exposure scenarios.

## Chemical risk assessment revisited?

Incorporation of *in vitro*-based mechanistic studies into chemical risk assessment requires broad acceptance amongst regulatory agencies. To achieve this, new methodologies need to gain trust and successful examples are vital in this process. Integration of new methodologies into the identification of the risk a chemical poses for human health can be done at various levels of the assessment process, including hazard and exposure assessments.

Chemical risk assessment attempts to estimate the hazard of a particular chemical by its identification and characterization. Hazard identification for mitochondrial toxicants can be performed both bottom-up or top-down. A bottom-up approach is based on biochemical assays focusing on known mitochondrial targets, such as respiration, metabolism, or morphology. This approach can be used to identify chemicals that completely perturb particular targets or to flag chemicals that demonstrate less pronounced effects but could be of risk in combined or prolonged exposures. A top-down approach is built around the cellular response, for instance transcriptomic profiles, observed upon mitochondrial target perturbation and could flag chemicals that induce responses known to be linked to levels of mitochondrial perturbation above the cells capacity to adapt.

Hazard characterization takes it a step further and focuses on understanding the temporal, concentration, and spatial relationship among the mode-of-actions and the occurrence of adversities. It assesses the risk of a chemical upon acute vs prolonged exposure, the concentration at which adaptation turns into adversity and the effects of an accumulated dose in specific tissues. In this case more complex *in vitro* model systems, for instance, the 3D spheroids or IPSC based cell systems can support the study of different dosing regimens. In addition, systems specific for mitochondrial susceptive tissues, like neurons and muscles, help to identify chemicals which both interfere with the mitochondrial targets and perturb susceptible tissue-specific features.

The complete risk characterization also requires a likelihood estimation if a person or a specific group of people will be exposed to a dose that would pose a threat to their health. This is based on expected exposure levels based on intake and exposure levels that will induce toxicity. The hazardous exposure levels are generally determined based on *in vivo* toxicity assessments combined with a range of safety factors assessing inter- and intra-species variations, duration of exposure and the output used to define an effect. Reduction of uncertainty or even only identification

of the existing uncertainty in the safety factors will create more confidence in the obtained information and potentially reduces the large numbers of animal studies [EFSA 2018, Bokkers 2017].

The *in vitro* approaches discussed in this thesis are not capable of replacing all exposure related data obtained from *in vivo* tests. Especially the assessment of various exposure scenarios and tissue interactions are challenging to mimic *in vitro*. Nevertheless, mechanistic studies could support in reducing the safety factors concerning the identification of the effect levels (point of departure = PoD). The PoD is based on an observed first effective dose (lowest/no observed effect level = LOAEL/NOAEL) or modelled based on the complete tested dose range (benchmark dose = BMD) both obtained from *in vivo* studies. *In vitro* assays, in particular will help to identify relevant concentration ranges, which will focus and reduce follow-up experiments *in vivo*. *In vivo* relevant doses can be extrapolated from *in vitro* concentration ranges for any desired (mitochondrial-related) readout when using bioavailability studies to determine the *in vitro* available concentration [Fisher 2019] and PBPK modeling to translate this into an *in vivo* available dose [Shebley 2018] (as we performed in **chapter 7** and related work [OECD 2020a, OECD 2020b, OECD 2019, Van der Stel 2021 submitted, Escher 2021 submitted]).

Finally, the detailed mitochondrial toxicity data obtained with *in vitro* mechanistic studies, especially with the broad omics assessments, also support the identification of the expected type(s) of adversity in humans. This informs us about the possible susceptive users and the features which should be monitored to timely identify possible mitochondrial perturbation during development phases and possibly thereafter.



## Concluding remarks

Altogether, this thesis contributes to the integration of *in vitro* mitochondrial-related toxicity assessment into chemical risk assessment. We evaluated existing and new mitochondrial toxicity biomarkers for their potential application in high-content imaging approaches and established a transcriptomic analysis pipeline that supports more mechanism-driven assessment of the relationship among mitochondrial perturbation, cellular adaptation and adversity. Ultimately, our *in vitro* mitochondrial toxicity strategy will support safer use of chemicals and reduce the animal burden to achieve this goal.

# A

# Appendix

References
Abbreviations
Nederlandse Samenvatting
List of publications
About the author

# References


Abozguia, K., Clarke, K., Lee, L., et al. (2006). Modification of myocardial substrate use as a therapy for heart failure. Nature Clinical Practice Cardiovascular Medicine, 3(9), 490–498. https://doi.org/10.1038/ncpcardio0583

Aghamaali, M. R., Jafarian, V., Sariri, R., et al. (2011). Cloning, sequencing, expression and structural investigation of mnemiopsin from mnemiopsis leidyi: An attempt toward understanding Ca 2+- regulated photoproteins. Protein Journal, 30(8), 566–574. https://doi.org/10.1007/s10930-011-9363-8

Aigner, A., Buesen, R., Gant, T., et al. (2016). Advancing the use of noncoding RNA in regulatory toxicology: Report of an ECETOC workshop. Regulatory Toxicology and Pharmacology, 82, 127–139. https://doi.org/10.1016/j.yrtph.2016.09.018

Ainscow, E. K., & Brand, M. D. (1999). Top-down control analysis of ATP turnover, glycolysis and oxidative phosphorylation in rat hepatocytes. European Journal of Biochemistry, 263(3), 671–685. https://doi.org/10.1046/j.1432-1327.1999.00534.x

Akimzhanov, A. M., & Boehning, D. (2011). Monitoring dynamic changes in mitochondrial calcium levels during apoptosis using a genetically encoded calcium sensor. Journal of Visualized Experiments, 50, 2578. https://doi.org/10.3791/2579

Alaimo, A., Gorojod, R. M., Beauquis, J., et al. (2014). Deregulation of mitochondria-shaping proteins Opa-1 and Drp-1 in manganese-induced apoptosis. PLoS ONE, 9(3), e91848. https://doi.org/10.1371/journal.pone.0091848

Alberts, B., Johnson, A., Lewis, J., et al. (2002). Molecular biology of the cell. New York: Garland Science.

Alexander, C., Votruba, M., Pesch, U. E. A., et al. (2000). OPA1, encoding a dynamin-related GTPase, is mutated in autosomal dominant optic atrophy linked to chromosome 3q28. Nature Genetics, 26(2), 211–215. https://doi.org/10.1038/79944

Almeida, A., Moncada, S., & Bolaños, J. (2004). Nitric oxide switches on glycolysis through the AMP protein kinase and 6-phosphofructo-2-kinase pathway. Nature Cell Biology, 6(1), 45–51. https://doi.org/10.1038/NCB1080

Alvarez, M. J., Shen, Y., Giorgi, F. M., et al. (2016). Functional characterization of somatic mutations in cancer using network-based inference of protein activity. Nature Genetics, 48(8), 838–847. https://doi.org/10.1038/ng.3593

Anand, R., Wai, T., Baker, M. J., et al. (2014). The i-AAA protease YME1L and OMA1 cleave OPA1 to balance mitochondrial fusion and fission. Journal of Cell Biology, 204(6), 919–929. https://doi.org/10.1083/jcb.201308006

Anderson, N. M., Mucka, P., Kern, J. G., et al. (2018). The emerging role and targetability of the TCA cycle in cancer metabolism. Protein and Cell, 9(2), 216–237. https://doi.org/10.1007/s13238-017-0451-1

Anderson, R. E., Tan, W. K., Martin, H. S., et al. (1999). Effects of glucose and PaO2 modulation on cortical intracellular acidosis, NADH redox state, and infarction in the ischemic penumbra. Stroke, 30(1), 160–170. https://doi.org/10.1161/01.STR.30.1.160

Angrish, M. M., McQueen, C. A., Cohen-Hubal, E., et al. (2017). Mechanistic toxicity tests based on an adverse outcome pathway network for hepatic steatosis. Toxicological Sciences, 159(1), 159–169. https://doi.org/10.1093/TOXSCI/KFX121

Ankley, G. T., Bennett, R. S., Erickson, R. J., et al. (2010). Adverse outcome pathways: A conceptual framework to support ecotoxicology research and risk assessment. Environmental Toxicology and Chemistry, 29(3), 730–741. https://doi.org/10.1002/etc.34

Aschauer, L., Gruber, L. N., Pfaller, W., et al. (2013). Delineation of the Key Aspects in the Regulation of Epithelial Monolayer Formation. Molecular and Cellular Biology, 33(13), 2535–2550. https://doi.org/10.1128/MCB.01435-12

Ashburner, M., Ball, C. A., Blake, J. A., et al. (2000). Gene ontology: Tool for the unification of biology. In Nature Genetics (Vol. 25, Issue 1, pp. 25–29). https://doi.org/10.1038/75556

Aslam, B., Basit, M., Nisar, M. A., et al. (2017). Proteomics: Technologies and their applications. In Journal of Chromatographic Science (Vol. 55, Issue 2, pp. 182–196). https://doi.org/10.1093/chromsci/bmw167

Atienzar, F. A., Blomme, E. A., Chen, M., et al. (2016). Key Challenges and Opportunities Associated with the Use of in Vitro Models to Detect Human Dili: Integrated Risk Assessment and Mitigation Plans. In BioMed Research International. Hindawi Limited. https://doi.org/10.1155/2016/9737920

Attene-Ramos, M. S., Huang, R., Michael, S., et al. (2015). Profiling of the Tox21 Chemical Collection for Mitochondrial Function to Identify Compounds that Acutely Decrease Mitochondrial Membrane Potential. Environmental Health Perspectives, 123(1), 49–56. https://doi.org/10.1289/ehp.1408642

Auguie, B. (2017). gridExtra: Miscellaneous Functions for "Grid" Graphics. R package version 2.3. https://CRAN.R-project.org/package=gridExtra

Babson, A., & Phillips, G. (1965). A rapid colorimetric assay for serum lactic dehydrogenase. Clinica Chimica Acta; International Journal of Clinical Chemistry, 12(2), 210–215. https://doi.org/10.1016/0009-8981(65)90032-X

Baderna, V., Schultz, J., Kearns, L. S., et al. (2020). A novel AFG3L2 mutation close to AAA domain leads to aberrant OMA1 and OPA1 processing in a family with optic atrophy. Acta Neuropathologica Communications, 29(8), 93. https://doi.org/10.1186/s40478-020-00975-w

Baird, G. S., Zacharias, D. A., & Tsien, R. Y. (1999). Circular permutation and receptor insertion within green fluorescent proteins. Proc Natl Acad Sci USA, 96(20), 11241–11246. https://doi.org/10.1073/pnas.96.20.11241

Bakayan, A., Domingo, B., Vaquero, C. F., et al. (2017). Fluorescent Protein–photoprotein Fusions and Their Applications in Calcium Imaging. In Photochemistry and Photobiology (Vol. 93, Issue 2, pp. 448–465). Blackwell Publishing Inc. https://doi.org/10.1111/php.12682

Baker, M. J., Lampe, P. A., Stojanovski, D., et al. (2014). Stress-induced OMA1 activation and autocatalytic turnover regulate OPA1-dependent mitochondrial dynamics. EMBO Journal, 33(6), 578–593. https://doi.org/10.1002/embj.201386474

Balaban, R. S., Nemoto, S., & Finkel, T. (2005). Mitochondria, oxidants, and aging. In Cell (Vol. 120, Issue 4, pp. 483–495). Cell Press. https://doi.org/10.1016/j.cell.2005.02.001

Balestrino, R., & Schapira, A. H. V. (2020). Parkinson disease. In European Journal of Neurology (Vol. 27, Issue 1, pp. 27–42). https://doi.org/10.1111/ene.14108

Ball, A. L., Kamalian, L., Alfirevic, A., et al. (2016). Identification of the additional mitochondrial liabilities of 2-hydroxyflutamide when compared with its parent compound, flutamide in HepG2 cells. Toxicological Sciences, 153(2), 341–351. https://doi.org/10.1093/toxsci/kfw126

Ball, N., Cronin, M., Shen, J., et al. (2016). Toward Good Read-Across Practice (GRAP) guidance. ALTEX, 33(2), 149–166. https://doi.org/10.14573/ALTEX.1601251

Banaji, M., Mallet, A., Elwell, C. E., et al. (2010). Modelling of mitochondrial oxygen consumption and NIRS detection of cytochrome oxidase redox state. Advances in Experimental Medicine and Biology, 662, 285–291. https://doi.org/10.1007/978-1-4419-1241-1_41

Bannuscher, A., Hellack, B., Bahl, A., et al. (2020). Metabolomics profiling to investigate nanomaterial toxicity in vitro and in vivo. Nanotoxicology, 14(6), 807–826. https://doi.org/10.1080/17435390.2020.1764123

Barbour, J. A., & Turner, N. (2014). Mitochondrial stress signaling promotes cellular adaptations. In International Journal of Cell Biology. https://doi.org/10.1155/2014/156020

Bartett, D. W., Clough, J. M., Godfrey, C. R. A., et al. (2001). Understanding the strobilurin fungicides. In Pesticide Outlook (Vol. 12, Issue 4, pp. 143–148). https://doi.org/10.1039/b106300f

Bartlett, D., Clough, J., Godwin, J., et al. (2002). The strobilurin fungicides. Pest Management Science, 58(7), 649–662. https://doi.org/10.1002/PS.520

Battistoni, M., Di Renzo, F., Menegola, E., et al. (2019). Quantitative AOP based teratogenicity prediction for mixtures of azole fungicides. Computational Toxicology, 11, 72–81. https://doi.org/10.1016/j.comtox.2019.03.004

Battogtokh, G., Choi, Y. S., Kang, D. S., et al. (2018). Mitochondria-targeting drug conjugates for cytotoxic, anti-oxidizing and sensing purposes: current strategies and future perspectives. Acta Pharmaceutica Sinica B, 8(6), 862–880. https://doi.org/10.1016/j.apsb.2018.05.006

Bavli, D., Prill, S., Ezra, E., et al. (2016). Real-time monitoring of metabolic function in liver-onchip microdevices tracks the dynamics of Mitochondrial dysfunction. Proceedings of the National Academy of Sciences of the United States of America, 113, E2231–E2240. https://doi.org/10.1073/pnas.1522556113

Bazil, J. N., Buzzard, G. T., & Rundell, A. E. (2010). Modeling Mitochondrial Bioenergetics with Integrated Volume Dynamics. PLoS Computational Biology, 6(1), e1000632. https://doi.org/10.1371/journal.pcbi.1000632

Beard, D. A. (2005). A biophysical model of the mitochondrial respiratory system and oxidative phosphorylation. PLoS Computational Biology, 1(4), 0252–0264. https://doi.org/10.1371/journal.pcbi.0010036

Befroy, D. E., Rothman, D. L., Petersen, K. F., et al. (2012). 31P-magnetization transfer magnetic resonance spectroscopy measurements of in vivo metabolism. In Diabetes (Vol. 61, Issue 11, pp. 2669–2678). Diabetes. https://doi.org/10.2337/db12-0558

Ben-Hail, D., Palty, R., & Shoshan-Barmatz, V. (2014). Measurement of mitochondrial Ca2+ transport mediated by three transport proteins: VDAC1, the NA+/CA2+ exchanger, and the CA2+ uniporter. Cold Spring Harbor Protocols, 2014(2), 161–166. https://doi.org/10.1101/pdb.top066241

Bennekou, S. (2019). Moving towards a holistic approach for human health risk assessment - Is the current approach fit for purpose? EFSA Journal. European Food Safety Authority, 17(Suppl 1). https://doi.org/10.2903/J.EFSA.2019.E170711

Benz, R., & McLaughlin, S. (1983). The molecular mechanism of action of the proton ionophore FCCP (carbonylcyanide p-trifluoromethoxyphenylhydrazone). Biophysical Journal, 41(3), 381–398. https://doi.org/10.1016/S0006-3495(83)84449-X

Berezhkovskiy, L. (2004). Volume of distribution at steady state for a linear pharmacokinetic system with peripheral elimination. Journal of Pharmaceutical Sciences, 93(6), 1628–1640. https://doi.org/10.1002/JPS.20073

Berg, J., Hung, Y. P., & Yellen, G. (2009). A genetically encoded fluorescent reporter of ATP:ADP ratio. Nature Methods, 6(2), 161–166. https://doi.org/10.1038/nmeth.1288

Berg, S., Kutra, D., Kroeger, T., et al. (2019). ilastik: interactive machine learning for (bio)image analysis. Nature Methods, 16(12), 1226–1232. https://doi.org/10.1038/s41592-019-0582-9

Berman, S. B., Pineda, F. J., & Hardwick, J. M. (2008). Mitochondrial fission and fusion dynamics: The long and short of it. In Cell Death and Differentiation (Vol. 15, Issue 7, pp. 1147–1152). Cell Death Differ. https://doi.org/10.1038/cdd.2008.57

Berthiaume, F., MacDonald, A. D., Kang, Y. H., et al. (2003). Control analysis of mitochondrial metabolism in intact hepatocytes: Effect of interleukin-1β and interleukin-6. Metabolic Engineering, 5(2), 108–123. https://doi.org/10.1016/S1096-7176(03)00010-7

Betarbet, R., Sherer, T. B., MacKenzie, G., et al. (2000). Chronic systemic pesticide exposure reproduces features of Parkinson's disease. Nature Neuroscience, 3(12), 1301–1306. https://doi.org/10.1038/81834

Bhatt, D. P., Chen, X., Geiger, J. D., et al. (2012). A sensitive HPLC-based method to quantify adenine nucleotides in primary astrocyte cell cultures. Journal of Chromatography B: Analytical Technologies in the Biomedical and Life Sciences, 889–890, 110–115. https://doi.org/10.1016/j.jchromb.2012.02.005

Binan, L., Mazzaferri, J., Choquet, K., et al. (2016). Live single-cell laser tag. Nature Communications, 7(1), 1–8. https://doi.org/10.1038/ncomms11636

Bobko, A. A., Dhimitruka, I., Eubank, T. D., et al. (2009). Trityl-based EPR probe with enhanced sensitivity to oxygen. Free Radical Biology and Medicine, 47(5), 654–658. https://doi.org/10.1016/j.freeradbiomed.2009.06.007

Bock, F. J., & Tait, S. W. G. (2020). Mitochondria as multifaceted regulators of cell death. In Nature Reviews Molecular Cell Biology (Vol. 21, Issue 2, pp. 85–100). https://doi.org/10.1038/s41580-019-0173-8

Boelsterli, U. A. (2003). Mechanistic Toxicology: The Molecular Basis of How Chemicals Disrupt Biological Targets. Taylor & Francis.

Boelsterli, U. A., & Lim, P. L. K. (2007). Mitochondrial abnormalities-A link to idiosyncratic drug hepatotoxicity? Toxicology and Applied Pharmacology, 220(1), 92–107. https://doi.org/10.1016/j.taap.2006.12.013

Boess, F., Kamber, M., Romer, S., et al. (2003). Gene expression in two hepatic cell lines, cultured primary hepatocytes, and liver slices compared to the in vivo liver gene expression in rats: Possible implications for toxicogenomics use of in vitro systems. Toxicological Sciences, 73(2), 386–402. https://doi.org/10.1093/toxsci/kfg064

Bois, F. Y., Ochoa, J. G. D., Gajewska, M., et al. (2017). Multiscale modelling approaches for assessing cosmetic ingredients safety. Toxicology, 392, 130–139. https://doi.org/10.1016/j.tox.2016.05.026

Bokkers, B. G. H., Mengelers, M. J., Bakker, M. I., et al. (2017). APROBA-Plus: A probabilistic tool to evaluate and express uncertainty in hazard characterization and exposure assessment of substances. Food and Chemical Toxicology, 110, 408–417. https://doi.org/10.1016/j.fct.2017.10.038

Bollard, M. E., Contel, N. R., Ebbels, T. M. D., et al. (2010). NMR-based metabolic profiling identifies biomarkers of liver regeneration following partial hepatectomy in the rat. Journal of Proteome Research, 9(1), 59–69. https://doi.org/10.1021/pr900200v

Bondi, H., Zilocchi, M., Mare, M. G., et al. (2016). Dopamine induces mitochondrial depolarization without activating PINK1-mediated mitophagy. Journal of Neurochemistry, 136(6), 1219–1231. https://doi.org/10.1111/jnc.13506

Bonora, M., Giorgi, C., Bononi, A., et al. (2013). Subcellular calcium measurements in mammalian cells using jellyfish photoprotein aequorin-based probes. Nature Protocols, 8(11), 2105–2118. https://doi.org/10.1038/nprot.2013.127

Boon, R., Kumar, M., Tricot, T., et al. (2020). Amino acid levels determine metabolism and CYP450 function of hepatocytes and hepatoma cell lines. Nature Communications, 11(1). https://doi.org/10.1038/S41467-020-15058-6

Bouhifd, M., Hartung, T., Hogberg, H. T., et al. (2013). Review: Toxicometabolomics. In Journal of Applied Toxicology (Vol. 33, Issue 12, pp. 1365–1383). https://doi.org/10.1002/jat.2874

Bouillot, S., Reboud, E., & Huber, P. (2018). Functional consequences of calcium influx promoted by bacterial pore-forming Toxins. In Toxins (Vol. 10, Issue 10, p. 387). https://doi.org/10.3390/toxins10100387

Bricker, D. K., Taylor, E. B., Schell, J. C., et al. (2012). A mitochondrial pyruvate carrier required for pyruvate uptake in yeast, Drosophila, and humans. Science, 337(6090), 96–100. https://doi.org/10.1126/science.1218099

Brockmeier, E. K., Hodges, G., Hutchinson, T. H., et al. (2017). The role of omics in the application of adverse outcome pathways for chemical risk assessment. Toxicological Sciences, 158(2), 252–262. https://doi.org/10.1093/toxsci/kfx097

Brodie, E. J., Zhan, H., Saiyed, T., et al. (2018). Perrault syndrome type 3 caused by diverse molecular defects in CLPP. Scientific Reports, 8(1), 12862. https://doi.org/10.1038/s41598-018-30311-1

Brodland, G. W. (2015). How computational models can help unlock biological systems. In Seminars in Cell and Developmental Biology (Vols. 47–48, pp. 62–73). Academic Press. https://doi.org/10.1016/j.semcdb.2015.07.001

Bross, P., & Fernandez-Guerra, P. (2016). Disease-associated mutations in the HSPD1 gene encoding the large subunit of the mitochondrial HSP60/HSP10 chaperonin complex. In Frontiers in Molecular Biosciences (Vol. 3, p. 49). https://doi.org/10.3389/fmolb.2016.00049

Brunmair, B., Staniek, K., Gras, F., et al. (2004). Thiazolidinediones, Like Metformin, Inhibit Respiratory Complex I: A Common Mechanism Contributing to Their Antidiabetic Actions? Diabetes, 53(4), 1052–1059. https://doi.org/10.2337/diabetes.53.4.1052

Buesen, R., Chorley, B. N., da Silva Lima, B., et al. (2017). Applying 'omics technologies in chemicals risk assessment: Report of an ECETOC workshop. Regulatory Toxicology and Pharmacology, 91 Suppl(Suppl 1), S3–S13. https://doi.org/10.1016/j.yrtph.2017.09.002

Bulthuis, E. P., Adjobo-Hermans, M. J. W., Willems, P. H. G. M., et al. (2019). Mitochondrial Morphofunction in Mammalian Cells. In Antioxidants and Redox Signaling (Vol. 30, Issue 18, pp. 2066–2109). https://doi.org/10.1089/ars.2018.7534

Bushel, P. R., Paules, R. S., & Auerbach, S. S. (2018). A Comparison of the TempO-Seq S1500+ Platform to RNA-Seq and Microarray Using Rat Liver Mode of Action Samples. Frontiers in Genetics, 9(485). https://doi.org/10.3389/fgene.2018.00485

Busquet, F., A, K., C, R., et al. (2020). New European Union statistics on laboratory animal use - what really counts! ALTEX, 37(2), 167–186. https://doi.org/10.14573/ALTEX.2003241

Buzkova, J., Nikkanen, J., Ahola, S., et al. (2018). Metabolomes of mitochondrial diseases and inclusion body myositis patients: treatment targets and biomarkers. EMBO Molecular Medicine, 10(12), e9091. https://doi.org/10.15252/emmm.201809091

Caboni, P., Sherer, T., Zhang, N., et al. (2004). Rotenone, deguelin, their metabolites, and the rat model of Parkinson's disease. Chemical Research in Toxicology, 17(11), 1540–1548. https://doi.org/10.1021/TX049867R

Callegaro, G., Kunnen, S. J., Trairatphisan, P., et al. (2021). The human hepatocyte TXG-MAPr: WGCNA transcriptomic modules to support mechanism-based risk assessment. BioRxiv, 2021.05.17.444463. https://doi.org/10.1101/2021.05.17.444463

Cannon, J., Tapias, V., Na, H., et al. (2009). A highly reproducible rotenone model of Parkinson's disease. Neurobiology of Disease, 34(2), 279–290. https://doi.org/10.1016/J.NBD.2009.01.016

Carbon, S., Douglass, E., Good, B. M., et al. (2021). The Gene Ontology resource: enriching a GOld mine. Nucleic Acids Research, 49(D1), D325–D334. https://doi.org/10.1093/nar/gkaa1113

Carlson, M. (2019). org.Hs.eg.db: Genome wide annotation for Human. R package version 3.8.2. https://bioconductor.org/packages/release/data/annotation/html/org.Hs.eg.db.html

Carr, D. ported by Nicholas Lewin-Koh, Martin Maechler and contains copies of lattice functions written by Deepayan Sarkar (2021). hexbin: Hexagonal Binning Routines. R package version 1.28.2. https://CRAN.R-project.org/package=hexbin

Cassarino, D. S., Swerdlow, R. H., Parks, J. K., et al. (1998). Cyclosporin A increases resting mitochondrial membrane potential in SY5Y cells and reverses the depressed mitochondrial membrane potential of Alzheimer's disease cybrids. Biochemical and Biophysical Research Communications, 248(1), 168–173. https://doi.org/10.1006/bbrc.1998.8866

Celardo, I., Lehmann, S., Costa, A. C., et al. (2017). dATF4 regulation of mitochondrial folate-mediated one-carbon metabolism is neuroprotective. Cell Death & Differentiation 2017 24:4, 24(4), 638–648. https://doi.org/10.1038/cdd.2016.158

Chan, E. Y. L., & McQuibban, G. A. (2013). The mitochondrial rhomboid protease: Its rise from obscurity to the pinnacle of disease-relevant genes. In Biochimica et Biophysica Acta - Biomembranes (Vol. 1828, Issue 12, pp. 2916–2925). https://doi.org/10.1016/j.bbamem.2013.05.012

Chandel, N. S. (2014). Mitochondria as signaling organelles. In BMC Biology (Vol. 22, Issue 2, pp. 204–206). https://doi.org/10.1186/1741-7007-12-34

Chang, T., Horal, M., Jain, S., et al. (2003). Oxidant regulation of gene expression and neural tube development: Insights gained from diabetic pregnancy on molecular causes of neural tube defects. Diabetologia, 46(4), 538–545. https://doi.org/10.1007/S00125-003-1063-2

Chang, W., Wickham, H. (2020). ggvis: Interactive Grammar of Graphics. R package version 0.4.7. https://CRAN.R-project.org/package=ggvis

Chang, W., Cheng, J., Allaire, J.J., Sievert, C., Schloerke, B., Xie, Y., Allen, J., McPherson, J., Dipert, A., Borges, B. (2021). shiny: Web Application Framework for R. R package version 1.6.0. https://CRAN.R-project.org/package=shiny

Chen, C., Stephenson, M. C., Peters, A., et al. (2018). 31P magnetization transfer magnetic resonance spectroscopy: Assessing the activation induced change in cerebral ATP metabolic rates at 3 T. Magnetic Resonance in Medicine, 79(1), 22–30. https://doi.org/10.1002/mrm.26663

Chen, H., & Chan, D. C. (2009). Mitochondrial dynamics-fusion, fission, movement, and mitophagy-in neurodegenerative diseases. Human Molecular Genetics, 18(R2), R169–R176. https://doi.org/10.1093/hmg/ddp326

Chen, L., Zhong, F., & Zhu, J. (2020). Bridging targeted and untargeted mass spectrometry-based metabolomics via hybrid approaches. In Metabolites (Vol. 10, Issue 9, p. 348). https://doi.org/10.3390/metabo10090348

Christen, T., Bouzat, P., Pannetier, N., et al. (2014). Tissue oxygen saturation mapping with magnetic resonance imaging. Journal of Cerebral Blood Flow and Metabolism, 34(9), 1550–1557. https://doi.org/10.1038/jcbfm.2014.116

Civiletto, G., Varanita, T., Cerutti, R., et al. (2015). Opa1 overexpression ameliorates the phenotype of two mitochondrial disease mouse models. Cell Metabolism, 21(6), 845–854. https://doi.org/10.1016/j.cmet.2015.04.016

Clark, L. C., Wolf, R., Granger, D., et al. (1953). Continuous recording of blood oxygen tensions by polarography. Journal of Applied Physiology, 6(3), 189–193. https://doi.org/10.1152/jappl.1953.6.3.189

Conboy, E., Selcen, D., Brodsky, M., et al. (2018). Novel Homozygous Variant in TTC19 Causing Mitochondrial Complex III Deficiency with Recurrent Stroke-Like Episodes: Expanding the Phenotype. Seminars in Pediatric Neurology, 26, 16–20. https://doi.org/10.1016/J.SPEN.2018.04.003

Consolato, F., Maltecca, F., Tulli, S., et al. (2018). m-AAA and i-AAA complexes coordinate to regulate OMA1, the stress-activated supervisor of mitochondrial dynamics. Journal of Cell Science, 131(7), jcs213546. https://doi.org/10.1242/jcs.213546

Contag, C. H., Spilman, S. D., Contag, P. R., et al. (1997). Visualizing Gene Expression in Living Mammals Using a Bioluminescent Reporter. Photochemistry and Photobiology, 66(4), 523–531. https://doi.org/10.1111/j.1751-1097.1997.tb03184.x

Cortassa, S., Aon, M. A., Marbán, E., et al. (2003). An integrated model of cardiac mitochondrial energy metabolism and calcium dynamics. Biophysical Journal, 84(4), 2734-2755. https://doi.org/10.1016/S0006-3495(03)75079-6

Costa-Mattioli, M., & Walter, P. (2020). The integrated stress response: From mechanism to disease. Science (New York, N.Y.), 368(6489). https://doi.org/10.1126/SCIENCE.AAT5314

Craig, A., Sidaway, J., Holmes, E., et al. (2006). Systems toxicology: Integrated genomic, proteomic and metabonomic analysis of methapyrilene induced hepatotoxicity in the rat. Journal of Proteome Research, 5(7), 1586–1601. https://doi.org/10.1021/pr0503376

Cribbs, J. T., & Strack, S. (2007). Reversible phosphorylation of Drp1 by cyclic AMP-dependent protein kinase and calcineurin regulates mitochondrial fission and cell death. EMBO Reports, 8(10), 939–944. https://doi.org/10.1038/sj.embor.7401062

Crouch, S. P. M., Kozlowski, R., Slater, K. J., et al. (1993). The use of ATP bioluminescence as a measure of cell proliferation and cytotoxicity. Journal of Immunological Methods, 160(1), 81–88. https://doi.org/10.1016/0022-1759(93)90011-U

Cui, Y., & Paules, R. S. (2010). Use of transcriptomics in understanding mechanisms of drug-induced toxicity. Pharmacogenomics, 11(4), 573–585. https://doi.org/10.2217/pgs.10.37

Da Cunha, F. M., Torelli, N. Q., & Kowaltowski, A. J. (2015). Mitochondrial Retrograde Signaling: Triggers, Pathways, and Outcomes. In Oxidative Medicine and Cellular Longevity (Vol. 2015, p. 482582). https://doi.org/10.1155/2015/482582

Danhier, P., & Gallez, B. (2015). Electron paramagnetic resonance: A powerful tool to support magnetic resonance imaging research. Contrast Media and Molecular Imaging, 10(4), 266–281. https://doi.org/10.1002/cmmi.1630

Daun, S., Rubin, J., Vodovotz, Y., et al. (2008). Equation-based models of dynamic biological systems. Journal of Critical Care, 23(4), 585–594. https://doi.org/10.1016/j.jcrc.2008.02.003

Davis, J. M., Ekman, D. R., Skelton, D. M., et al. (2017). Metabolomics for informing adverse outcome pathways: Androgen receptor activation and the pharmaceutical spironolactone. Aquatic Toxicology, 184, 103–115. https://doi.org/10.1016/j.aquatox.2017.01.001

De Castro, I. P., Martins, L. M., & Tufi, R. (2010). Mitochondrial quality control and neurological disease: An emerging connection. Expert Reviews in Molecular Medicine, 12, e12. https://doi.org/10.1017/S1462399410001456

De Vos, K. J., & Sheetz, M. P. (2007). Visualization and Quantification of Mitochondrial Dynamics in Living Animal Cells. Methods in Cell Biology, 80, 627–682. https://doi.org/10.1016/S0091-679X(06)80030-0

DeBerardinis, R. J., & Chandel, N. S. (2020). We need to talk about the Warburg effect. In Nature Metabolism (Vol. 2, Issue 2, pp. 127–129). Nature Research. https://doi.org/10.1038/s42255-020-0172-2

Degli Esposti, M. (1998). Inhibitors of NADH-ubiquinone reductase: an overview. Biochimica et Biophysica Acta, 1364(2), 222–235. https://doi.org/10.1016/S0005-2728(98)00029-2

Degli Esposti, M., & Ghelli, A. (1994). The mechanism of proton and electron transport in mitochondrial complex I. Biochimica et Biophysica Acta, 1187(2), 116–120. https://doi.org/10.1016/0005-2728(94)90095-7

Delettre, C., Lenaers, G., Griffoin, J. M., et al. (2000). Nuclear gene OPA1, encoding a mitochondrial dynamin-related protein, is mutated in dominant optic atrophy. Nature Genetics, 26(2), 207–210. https://doi.org/10.1038/79936

Delp, J., Cediel-Ulloa, A., Suciu, I., et al. (2021). Neurotoxicity and underlying cellular changes of 21 mitochondrial respiratory chain inhibitors. Archives of Toxicology, 95(2), 591–651. https://doi.org/10.1007/s00204-020-02970-5

Delp, J., Funke, M., Rudolf, F., et al. (2019). Development of a neurotoxicity assay that is tuned to detect mitochondrial toxicants. Archives of Toxicology, 93(6), 1585–1608. https://doi.org/10.1007/s00204-019-02473-y

Dempsey, J. L., & Cui, J. Y. (2017). Long non-coding RNAs: A novel paradigm for toxicology. In Toxicological Sciences (Vol. 155, Issue 1, pp. 3–21). https://doi.org/10.1093/toxsci/kfw203

Dent, M., Amaral, R. T., Da Silva, P. A., et al. (2018). Principles underpinning the use of new methodologies in the risk assessment of cosmetic ingredients. Computational Toxicology, 7, 20–26. https://doi.org/10.1016/J.COMTOX.2018.06.001

Depaoli, M. R., Bischof, H., Eroglu, E., et al. (2019). Live cell imaging of signaling and metabolic activities. In Pharmacology and Therapeutics (Vol. 202, pp. 98–119). Elsevier Inc. https://doi.org/10.1016/j.pharmthera.2019.06.003

Detaille, D., Guigas, B., Leverve, X., et al. (2002). Obligatory role of membrane events in the regulatory effect of metformin on the respiratory chain function. Biochemical Pharmacology, 63(7), 1259–1272. https://doi.org/10.1016/S0006-2952(02)00858-4

Dey, K., Bazala, M. A., & Kuznicki, J. (2020). Targeting mitochondrial calcium pathways as a potential treatment against Parkinson's disease. Cell Calcium, 89, 102216. https://doi.org/10.1016/j.ceca.2020.102216

Dhillon, A. S., Tarbutton, G. L., Levin, J. L., et al. (2008). Pesticide/environmental exposures and Parkinson's disease in East Texas. Journal of Agromedicine, 13(1), 37–48. https://doi.org/10.1080/10599240801986215

Di Virgilio, F., Pinton, P., & Falzoni, S. (2016). Assessing extracellular ATP as danger signal in vivo: The pmeluc system. In Methods in Molecular Biology (Vol. 1417, pp. 115–129). Humana Press Inc. https://doi.org/10.1007/978-1-4939-3566-6_7

Di, Z., Herpers, B., Fredriksson, L., et al. (2012). Automated Analysis of NF-κB Nuclear Translocation Kinetics in High-Throughput Screening. PLoS ONE, 7(12), e52337. https://doi.org/10.1371/journal.pone.0052337

Diepart, C., Verrax, J., Calderon, P. B., et al. (2010). Comparison of methods for measuring oxygen consumption in tumor cells in vitro. Analytical Biochemistry, 396(2), 250–256. https://doi.org/10.1016/j.ab.2009.09.029

Dikoglu, E., Alfaiz, A., Gorna, M., et al. (2015). Mutations in LONP1, a mitochondrial matrix protease, cause CODAS syndrome. American Journal of Medical Genetics, Part A, 167(7), 1501–1509. https://doi.org/10.1002/ajmg.a.37029

diMauro, S., & Vivo, D. C. De. (1999). Diseases of Mitochondrial Metabolism. In Basic: Neurochemistry: Molecular, Cellular and Medical Aspects (Vol. 6). Lippincott-Raven. https://www.ncbi.nlm.nih.gov/books/NBK27914/

Divakaruni, A. S., Paradyse, A., Ferrick, D. A., et al. (2014). Analysis and interpretation of microplate-based oxygen consumption and pH data. In Methods in Enzymology (Vol. 547, Issue C, pp. 309–354). Academic Press Inc. https://doi.org/10.1016/B978-0-12-801415-8.00016-3

Dmitriev, R. I., & Papkovsky, D. B. (2012). Optical probes and techniques for O 2 measurement in live cells and tissue. In Cellular and Molecular Life Sciences (Vol. 69, Issue 12, pp. 2025–2039). Cell Mol Life Sci. https://doi.org/10.1007/s00018-011-0914-0

Dolman, N. J., Chambers, K. M., Mandavilli, B., et al. (2013). Tools and techniques to measure mitophagy using fluorescence microscopy. In Autophagy (Vol. 9, Issue 11, pp. 1653–1662). Taylor and Francis Inc. https://doi.org/10.4161/auto.24001

Doull's, & Casarett. (2008). Toxicology The Basic Science of Poisons. In McGraw-Hill. https://doi.org/10.1036/0071470514

Dowle, M., Srinivasan, A., (2021). data.table: Extension of `data.frame`. R package version 1.14.0. https://CRAN.R-project.org/package=data.table

Dreier, D. A., Mello, D. F., Meyer, J. N., et al. (2019). Linking Mitochondrial Dysfunction to Organismal and Population Health in the Context of Environmental Pollutants: Progress and Considerations for Mitochondrial Adverse Outcome Pathways. Environmental Toxicology and Chemistry, 38(8), 1625–1634. https://doi.org/10.1002/etc.4453

Durand, F., & Hoogenraad, N. (2017). Assessing mitochondrial unfolded protein response in mammalian cells. In Methods in Molecular Biology (Vol. 1567, pp. 363–378). Humana Press Inc. https://doi.org/10.1007/978-1-4939-6824-4_22

Durant, J., Leland, B., Henry, D., et al. (2002). Reoptimization of MDL keys for use in drug discovery. Journal of Chemical Information and Computer Sciences, 42(6), 1273–1280. https://doi.org/10.1021/CI010132R

Dykens, J. A., Jamieson, J. D., Marroquin, L. D., et al. (2008). In vitro assessment of mitochondrial dysfunction and cytotoxicity of nefazodone, trazodone, and buspirone. Toxicological Sciences, 103(2), 335–245. https://doi.org/10.1093/toxsci/kfn056

Dykens, J. A., Marroquin, L. D., & Will, Y. (2007). Strategies to reduce late-stage drug attrition due to mitochondrial toxicity. In Expert Review of Molecular Diagnostics (Vol. 7, Issue 2, pp. 161–175). Expert Rev Mol Diagn. https://doi.org/10.1586/14737159.7.2.161

Dykens, J. A., & Will, Y. (2007). The significance of mitochondrial toxicity testing in drug development. Drug Discovery Today, 12(17–18), 777–785. https://doi.org/10.1016/j.drudis.2007.07.013

Dykens, J. A., & Will, Y. (2008). Drug-Induced Mitochondrial Dysfunction. Drug-Induced Mitochondrial Dysfunction, 1–616. https://doi.org/10.1002/9780470372531

Eakins, J., Bauch, C., Woodhouse, H., et al. (2016). A combined in vitro approach to improve the prediction of mitochondrial toxicants. Toxicology in Vitro, 34, 161–170. https://doi.org/10.1016/j.tiv.2016.03.016

Eden, E., Navon, R., Steinfeld, I., et al. (2009). GOrilla: A tool for discovery and visualization of enriched GO terms in ranked gene lists. BMC Bioinformatics, 10, 48. https://doi.org/10.1186/1471-2105-10-48

Efendiev, M. A., Otani, M., & Eberl, H. J. (2020). Mathematical Analysis of a PDE-ODE Coupled Model of Mitochondrial Swelling with Degenerate Calcium Ion Diffusion. Society for Industrial and Applied Mathematics, 52(1), 543–569. https://doi.org/10.1137/18M1227421

EFSA (2018) Benford D,Halldorsson T, Jeger MJ, Knutsen HK, More S, Naegeli H, Noteborn H, Ockleford C, Ricci A, Rychen G,Schlatter JR, Silano V, Solecki R, Turck D, Younes M, Craig P, Hart A, Von Goetz N, Koutsoumanis K,Mortensen A, Ossendorp B, Martino L, Merten C, Mosbach-Schulz O and Hardy A, 2018. Guidance on Uncertainty Analysis in Scientific Assessments. EFSA Journal 2018;16(1):5123, 39 pp https://doi.org/10.2903/j.efsa.2018.5123

Ehses, S., Raschke, I., Mancuso, G., et al. (2009). Regulation of OPA1 processing and mitochondrial fusion by m-AAA protease isoenzymes and OMA1. Journal of Cell Biology, 187(7), 1023–1036. https://doi.org/10.1083/jcb.200906084

Else, A. J., Barnes, S. J., Danson, M. J., et al. (1988). A new spectrophotometric assay for citrate synthase and its use to assess the inhibitory effects of palmitoyl thioesters. Biochemical Journal, 251(3), 803–807. https://doi.org/10.1042/bj2510803

Emwas, A. H. M. (2015). The strengths and weaknesses of NMR spectroscopy and mass spectrometry with particular focus on metabolomics research. Methods in Molecular Biology, 1277, 161–193. https://doi.org/10.1007/978-1-4939-2377-9_13

Escher, S., Kamp, H., Bennekou, S., et al. (2019). Towards grouping concepts based on new approach methodologies in chemical hazard assessment: the read-across approach of the EU-ToxRisk project. Archives of Toxicology, 93(12), 3643–3667. https://doi.org/10.1007/S00204-019-02591-7

Eskelinen, E. L., Reggiori, F., Baba, M., et al. (2011). Seeing is believing: The impact of electron microscopy on autophagy research. In Autophagy (Vol. 7, Issue 9, pp. 935–956). Taylor and Francis Inc. https://doi.org/10.4161/auto.7.9.15760

Esser, L., Quinn, B., Li, Y., et al. (2004). Crystallographic studies of quinol oxidation site inhibitors: a modified classification of inhibitors for the cytochrome bc(1) complex. Journal of Molecular Biology, 341(1), 281–302. https://doi.org/10.1016/J.JMB.2004.05.065

Esser, L., Yu, C., & Xia, D. (2014). Structural basis of resistance to anti-cytochrome $bc_1$ complex inhibitors: implication for drug improvement. Current Pharmaceutical Design, 20(5), 704–724. https://doi.org/10.2174/13816128200514021416332 7

Esterhuizen, K., van der Westhuizen, F. H., & Louw, R. (2017). Metabolomics of mitochondrial disease. In Mitochondrion (Vol. 35, pp. 97–110). https://doi.org/10.1016/j.mito.2017.05.012

EU Scientific advice mechanism (2018) EU Authorisation Processes of Plant Protection Products – From a Scientific Point of View. Publications Office of the EU, Luxembourg. https://doi.org/10.2777/238919

European Commission, Joint Research Centre (JRC) (2019): EURL ECVAM dataset on alternative methods to animal experimentation (DB-ALM). PID: http://data.europa.eu/89h/b7597ada-148d-4560-9079-ab0a5539cad3

European committee (2006) Regulation (EC) No 1907/2006 of the European Parliament and of the Council of 18 December 2006 concerning the Registration, Evaluation, Authorisation and Restriction of Chemicals (REACH), establishing a European Chemicals Agency, amending Directive 1999/45/EC and repealing Council Regulation (EEC) No 793/93 and Commission Regulation (EC) No 1488/94 as well as Council Directive 76/769/EEC and Commission Directives 91/155/EEC, 93/67/EEC, 93/105/EC and 2000/21/EC, https://eur-lex.europa.eu/legal-content/EN/TXT/?uri=CELEX:32006R1907

European committee (2009) Regulation (EC) No 1223/2009 of the European Parliament and of the Council of 30 November 2009 on cosmetic products (recast)
https://eur-lex.europa.eu/legal-content/EN/TXT/?uri=CELEX:02009R1223-20190813
(found via: https://ec.europa.eu/growth/sectors/cosmetics/animal-testing_en)

European Parliament and the council (2009), Regulation (EC) No 1107/2009 of the European Parliament and of the Council of 21 October 2009 concerning the placing of plant protection products on the market and repealing Council Directives 79/117/EEC and 91/414/EEC (OJ L 309, 24.11.2009, p. 1) http://data.europa.eu/eli/reg/2009/1107/oj

European Parliament and the council (2020) Evaluation of Regulation (EC) No 1107/2009 on the placing of plant protection products on the market and of Regulation (EC) No 396/2005 on maximum residue levels of pesticides. Brussels https://eur-lex.europa.eu/legal-content/EN/TXT/PDF/?uri=CELEX:52020DC0208&from=EN

Fahrner, J. A., Liu, R., Perry, M. S., et al. (2016). A novel de novo dominant negative mutation in DNM1L impairs mitochondrial fission and presents as childhood epileptic encephalopathy. American Journal of Medical Genetics, Part A, 170(8), 2002–2011. https://doi.org/10.1002/ajmg.a.37721

Fazzini, F., Schöpf, B., Blatzer, M., et al. (2018). Plasmid-normalized quantification of relative mitochondrial DNA copy number. Scientific Reports, 8(1). https://doi.org/10.1038/s41598-018-33684-5

Felser, A., Blum, K., Lindinger, P. W., et al. (2013). Mechanisms of hepatocellular toxicity associated with dronedarone - A comparison to amiodarone. Toxicological Sciences, 131(2), 480–490. https://doi.org/10.1093/toxsci/kfs298

Felser, A., Lindinger, P. W., Schnell, D., et al. (2014). Hepatocellular toxicity of benzbromarone: Effects on mitochondrial function and structure. Toxicology, 324, 136–146. https://doi.org/10.1016/j.tox.2014.08.002

Fernandes, J., Chandler, J. D., Lili, L. N., et al. (2019). Transcriptome analysis reveals distinct responses to physiologic versus toxic manganese exposure in human neuroblastoma cells. In Frontiers in Genetics (Vol. 10, p. 676). https://doi.org/10.3389/fgene.2019.00676

Fernandez-Fernandez, S., Almeida, A., & Bolaños, J. P. (2012). Antioxidant and bioenergetic coupling between neurons and astrocytes. Biochemical Journal, 443(1), 3-11. https://doi.org/10.1042/BJ20111943

Ferrick, D. A., Neilson, A., & Beeson, C. (2008). Advances in measuring cellular bioenergetics using extracellular flux. In Drug Discovery Today (Vol. 13, Issues 5–6, pp. 268–274). Drug Discov Today. https://doi.org/10.1016/j.drudis.2007.12.008

Fischer, C. A., Besora-Casals, L., Rolland, S. G., et al. (2020). MitoSegNet: Easy-to-use Deep Learning Segmentation for Analyzing Mitochondrial Morphology. IScience, 23(10), 101601. https://doi.org/10.1016/j.isci.2020.101601

Fisher, C., Siméon, S., Jamei, M., et al. (2019). VIVD: Virtual in vitro distribution model for the mechanistic prediction of intracellular concentrations of chemicals in in vitro toxicity assays. Toxicology in Vitro, 58, 42–50. https://doi.org/10.1016/j.tiv.2018.12.017

Florez-Sarasa, I., Ribas-Carbo, M., Del-Saz, N. F., et al. (2016). Unravelling the in vivo regulation and metabolic role of the alternative oxidase pathway in C3 species under photoinhibitory conditions. The New Phytologist, 212(1), 66–79. https://doi.org/10.1111/nph.14030

Fonteriz, R. I., de la Fuente, S., Moreno, A., et al. (2010). Monitoring mitochondrial [Ca2+] dynamics with rhod-2, ratiometric pericam and aequorin. Cell Calcium, 48(1), 61–69. https://doi.org/10.1016/j.ceca.2010.07.001

Foran, C. M., Rycroft, T., Keisler, J., et al. (2019). A modular approach for assembly of quantitative adverse outcome pathways. Altex, 36(3), 353–362. https://doi.org/10.14573/altex.1810181

Forred, B. J., Daugaard, D. R., Titus, B. K., et al. (2017). Detoxification of mitochondrial oxidants and apoptotic signaling are facilitated by thioredoxin-2 and peroxiredoxin-3 during hyperoxic injury. PLoS ONE, 12(1), e0168777. https://doi.org/10.1371/journal.pone.0168777

Friedman, J. R., & Nunnari, J. (2014). Mitochondrial form and function. Nature, 505(7483), 335–343. https://doi.org/10.1038/nature12985

Fröhlich, F., Theis, F. J., & Hasenauer, J. (2014). Uncertainty analysis for non-identifiable dynamical systems: Profile likelihoods, bootstrapping and more. Lecture Notes in Computer Science (Including Subseries Lecture Notes in Artificial Intelligence and Lecture Notes in Bioinformatics), 8859, 61–72. https://doi.org/10.1007/978-3-319-12982-2_5

From, A. H. L., & Ugurbil, K. (2011). Standard magnetic resonance-based measurements of the pi¡ATP rate do not index the rate of oxidative phosphorylation in cardiac and skeletal muscles. American Journal of Physiology - Cell Physiology, 301(1). https://doi.org/10.1152/ajpcell.00345.2010

Fromenty, B. (2019). Inhibition of mitochondrial fatty acid oxidation in drug-induced hepatic steatosis. In Liver Research (Vol. 3, Issues 3–4, pp. 157–169). https://doi.org/10.1016/j.livres.2019.06.001

Gan, C.-S., Chong, P. K., Pham, T. K., et al. (2007). Technical, experimental, and biological variations in isobaric tags for relative and absolute quantitation (iTRAQ). Journal of Proteome Research, 6(2), 821–827. https://doi.org/10.1021/pr060474i

Gao, X., Wen, X., Esser, L., et al. (2003). Structural basis for the quinone reduction in the bc1 complex: a comparative analysis of crystal structures of mitochondrial cytochrome bc1 with bound substrate and inhibitors at the Qi site. Biochemistry, 42(30), 9067–9080. https://doi.org/10.1021/BI0341814

Garaschuk, O., Griesbeck, O., & Konnerth, A. (2007). Troponin C-based biosensors: A new family of genetically encoded indicators for in vivo calcium imaging in the nervous system. In Cell Calcium (Vol. 42, Issues 4–5, pp. 351–361). Elsevier Ltd. https://doi.org/10.1016/j.ceca.2007.02.011

Garcia-Alonso, L., Ibrahim, M., Turei, D., et al. (2018). Benchmark and integration of resources for the estimation of human transcription factor activities. Genome Res. , 29(8), 1363–1375. https://doi.org/10.1101/337915

Garrido, C., Galluzzi, L., Brunet, M., et al. (2006). Mechanisms of cytochrome c release from mitochondria. Cell Death and Differentiation, 13, 1423–1433. https://doi.org/10.1038/sj.cdd.4401950

Gautier, L., Cope, L., Bolstad, B. M., et al. (2004). Affy - Analysis of Affymetrix GeneChip data at the probe level. Bioinformatics, 20(3), 307–315. https://doi.org/10.1093/bioinformatics/btg405

Gawlowski, T., Suarez, J., Scott, B., et al. (2012). Modulation of dynamin-related protein 1 (DRP1) function by increased O-linked-β-N-acetylglucosamine modification (O-GlcNAc) in cardiac myocytes. Journal of Biological Chemistry, 287(35), 30024–30034. https://doi.org/10.1074/jbc.M112.390682

Geiger, T., Wisniewski, J. R., Cox, J., et al. (2011). Use of stable isotope labeling by amino acids in cell culture as a spike-in standard in quantitative proteomics. Nature Protocols, 6(2), 147–157. https://doi.org/10.1038/nprot.2010.192

Georgakopoulos, N. D., Wells, G., & Campanella, M. (2017). The pharmacological regulation of cellular mitophagy. In Nature Chemical Biology (Vol. 13, Issue 2, pp. 136–146). https://doi.org/10.1038/nchembio.2287

Gerencser, A. A., Neilson, A., Choi, S. W., et al. (2009). Quantitative microplate-based respirometry with correction for oxygen diffusion. Analytical Chemistry, 81(16), 6868–6878. https://doi.org/10.1021/ac900881z

Gerets, H. H. J., Tilmant, K., Gerin, B., et al. (2012). Characterization of primary human hepatocytes, HepG2 cells, and HepaRG cells at the mRNA level and CYP activity in response to inducers and their predictivity for the detection of human hepatotoxins. Cell Biology and Toxicology, 28(2), 69–87. https://doi.org/10.1007/s10565-011-9208-4

Ghezzi, D., Arzuffi, P., Zordan, M., et al. (2011). Mutations in TTC19 cause mitochondrial complex III deficiency and neurological impairment in humans and flies. Nature Genetics, 43(3), 259–263. https://doi.org/10.1038/NG.761

Ghosh, R., Goswami, S. K., Feitoza, L. F. B. B., et al. (2016). Diclofenac induces proteasome and mitochondrial dysfunction in murine cardiomyocytes and hearts. International Journal of Cardiology, 223, 923–935. https://doi.org/10.1016/j.ijcard.2016.08.233

Giacomello, M., Pyakurel, A., Glytsou, C., et al. (2020). The cell biology of mitochondrial membrane dynamics. Nature Reviews Molecular Cell Biology, 21(4), 204–224. https://doi.org/10.1038/s41580-020-0210-7

Giedt, R. J., Fumene Feruglio, P., Pathania, D., et al. (2016). Computational imaging reveals mitochondrial morphology as a biomarker of cancer phenotype and drug response. Scientific Reports, 6, 32985. https://doi.org/10.1038/srep32985

Giglia-Mari, G., Zotter, A., & Vermeulen, W. (2011). DNA damage response. Cold Spring Harbor Perspectives in Biology, 3(1), a000745. https://doi.org/10.1101/cshperspect.a000745

Gijbels, E., Vilas-Boas, V., Annaert, P., et al. (2020). Robustness testing and optimization of an adverse outcome pathway on cholestatic liver injury. Archives of Toxicology, 94(4), 1151–1172. https://doi.org/10.1007/s00204-020-02691-9

Giorgi, C., Agnoletto, C., Bononi, A., et al. (2012). Mitochondrial calcium homeostasis as potential target for mitochondrial medicine. In Mitochondrion (Vol. 12, Issue 1, pp. 77–85). https://doi.org/10.1016/j.mito.2011.07.004

Giorgi, C., Marchi, S., & Pinton, P. (2018). The machineries, regulation and cellular functions of mitochondrial calcium. In Nature Reviews Molecular Cell Biology (Vol. 19, Issue 11, pp. 713–730). https://doi.org/10.1038/s41580-018-0052-8

Gomes, S. I. L., Roca, C. P., Scott-Fordsmand, J. J., et al. (2019). High-throughput transcriptomics: Insights into the pathways involved in (nano) nickel toxicity in a key invertebrate test species. Environmental Pollution, 245, 131–140. https://doi.org/10.1016/j.envpol.2018.10.123

Gong, Z., Tas, E., & Muzumdar, R. (2014). Humanin and age-related diseases: A new link? Frontiers in Endocrinology, 5, 210. https://doi.org/10.3389/fendo.2014.00210

Gonzalez-Coloma, A., Reina, M., Diaz, C. E., et al. (2013). Natural Product-Based Biopesticides for Insect Control. In Reference Module in Chemistry, Molecular Sciences and Chemical Engineering. Elsevier. https://doi.org/10.1016/B978-0-12-409547-2.02770-0

Goodwin, W. H. (2015). DNA: Mitochondrial DNA. In Encyclopedia of Forensic and Legal Medicine: Second Edition (pp. 351–358). Elsevier Inc. https://doi.org/10.1016/B978-0-12-800034-2.00155-5

Görlach, A., Bertram, K., Hudecova, S., et al. (2015). Calcium and ROS: A mutual interplay. In Redox Biology (Vol. 6, pp. 260–271). https://doi.org/10.1016/j.redox.2015.08.010

Govindan, S., Batti, L., Osterop, S. F., et al. (2021). Mass Generation, Neuron Labeling, and 3D Imaging of Minibrains. Frontiers in Bioengineering and Biotechnology, 8, 1436. https://doi.org/10.3389/fbioe.2020.582650

Grandl, M., & Schmitz, G. (2010). Fluorescent high-content imaging allows the discrimination and quantitation of E-LDL-induced lipid droplets and Ox-LDL-generated phospholipidosis in human macrophages. Cytometry Part A, 77(3), 231–242. https://doi.org/10.1002/cyto.a.20828

Griesbeck, O., Baird, G. S., Campbell, R. E., et al. (2001). Reducing the environmental sensitivity of yellow fluorescent protein. Mechanism and applications. Journal of Biological Chemistry, 276(31), 29188–29194. https://doi.org/10.1074/jbc.M102815200

Grohm, J., Kim, S. W., Mamrak, U., et al. (2012). Inhibition of Drp1 provides neuroprotection in vitro and in vivo. Cell Death and Differentiation, 19(9), 1446–1458. https://doi.org/10.1038/cdd.2012.18

Grünig, D., Felser, A., Bouitbir, J., et al. (2017). The catechol-O-methyltransferase inhibitors tolcapone and entacapone uncouple and inhibit the mitochondrial respiratory chain in HepaRG cells. Toxicology in Vitro, 42, 337-347. https://doi.org/10.1016/j.tiv.2017.05.013

Grynkiewicz, G., Poenie, M., & Tsien, R. Y. (1985). A new generation of Ca2+ indicators with greatly improved fluorescence properties. In Journal of Biological Chemistry (Vol. 260, Issue 6, pp. 3440–3450). Elsevier. https://doi.org/10.1016/s0021-9258(19)83641-4

Gu, X., & Manautou, J. E. (2012). Molecular mechanisms underlying chemical liver injury. In Expert Reviews in Molecular Medicine (Vol. 14, p. e4). https://doi.org/10.1017/S1462399411002110

Gugiatti, E., Tenca, C., Ravera, S., et al. (2018). A reversible carnitine palmitoyltransferase (CPT1) inhibitor offsets the proliferation of chronic lymphocytic leukemia cells. In Haematologica (Vol. 103, Issue 11, pp. e531–e536). https://doi.org/10.3324/haematol.2017.175414

Guo, J., Nguyen, H. T., Ito, S., et al. (2018). In ovo exposure to triclosan alters the hepatic proteome in chicken embryos. Ecotoxicology and Environmental Safety, 165, 495–504. https://doi.org/10.1016/j.ecoenv.2018.09.043

Haber, L. T., Dourson, M. L., Allen, B. C., et al. (2018). Benchmark dose (BMD) modeling: current practice, issues, and challenges. In Critical Reviews in Toxicology (Vol. 48, Issue 5, pp. 387–415). https://doi.org/10.1080/10408444.2018.1430121

Halestrap, A. P. (2009). What is the mitochondrial permeability transition pore? In Journal of Molecular and Cellular Cardiology (Vol. 46, Issue 6, pp. 821–831). https://doi.org/10.1016/j.yjmcc.2009.02.021

Halevy, R., Shtirberg, L., Shklyar, M., et al. (2010). Electron spin resonance micro-imaging of live species for oxygen mapping. Journal of Visualized Experiments, 42, 2122. https://doi.org/10.3791/2122

Hallinger, D. R., Lindsay, H. B., Friedman, K. P., et al. (2020). Respirometric screening and characterization of mitochondrial toxicants within the toxcast phase i and II chemical libraries. Toxicological Sciences, 176(1), 715–192. https://doi.org/10.1093/toxsci/kfaa059

Hamacher-Brady, A., & Brady, N. R. (2016). Mitophagy programs: Mechanisms and physiological implications of mitochondrial targeting by autophagy. In Cellular and Molecular Life Sciences (Vol. 73, Issue 4, pp. 775–795). https://doi.org/10.1007/s00018-015-2087-8

Hammerling, B. C., Najor, R. H., Cortez, M. Q., et al. (2017). A Rab5 endosomal pathway mediates Parkin-dependent mitochondrial clearance. Nature Communications, 8, 14050. https://doi.org/10.1038/ncomms14050

Han, D., Dara, L., Win, S., et al. (2013). Regulation of drug-induced liver injury by signal transduction pathways: Critical role of mitochondria. In Trends in Pharmacological Sciences (Vol. 34, Issue 4, pp. 243–253). https://doi.org/10.1016/j.tips.2013.01.009

Harder, Z., Zunino, R., & McBride, H. (2004). Sumo1 Conjugates Mitochondrial Substrates and Participates in Mitochondrial Fission. Current Biology, 14(4), 340–345. https://doi.org/10.1016/j.cub.2004.02.004

Harris, G., Eschment, M., Orozco, S. P., et al. (2018). Toxicity, recovery, and resilience in a 3D dopaminergic neuronal in vitro model exposed to rotenone. Archives of Toxicology, 92(8), 2587–2606. https://doi.org/10.1007/s00204-018-2250-8

Hartung, T. (2016). Making big sense from big data in toxicology by read-across. Altex, 33(2), 83–93. https://doi.org/10.14573/altex.1603091

Harwig, M. C., Viana, M. P., Egner, J. M., et al. (2018). Methods for imaging mammalian mitochondrial morphology: A prospective on MitoGraph. Analytical Biochemistry, 552, 81–99. https://doi.org/10.1016/j.ab.2018.02.022

Head, B., Griparic, L., Amiri, M., et al. (2009). Inducible proteolytic inactivation of OPA1 mediated by the OMA1 protease in mammalian cells. Journal of Cell Biology, 187(7), 959–966. https://doi.org/10.1083/jcb.200906083

Heijne, W. H. M., Kienhuis, A. S., Van Ommen, B., et al. (2005). Systems toxicology: Applications of toxicogenomics, transcriptomics, proteomics and metabolomics in toxicology. In Expert Review of Proteomics (Vol. 2, Issue 5, pp. 767–780). https://doi.org/10.1586/14789450.2.5.767

Heim, N., & Griesbeck, O. (2004). Genetically Encoded Indicators of Cellular Calcium Dynamics Based on Troponin C and Green Fluorescent Protein. Journal of Biological Chemistry, 279(14), 14280–14286. https://doi.org/10.1074/jbc.M312751200

Heinonen, S., Buzkova, J., Muniandy, M., et al. (2015). Impaired mitochondrial biogenesis in adipose tissue in acquired obesity. Diabetes, 64(9), 3135–3145. https://doi.org/10.2337/db14-1937

Hemmerich, J., Troger, F., Füzi, B., et al. (2020). Using Machine Learning Methods and Structural Alerts for Prediction of Mitochondrial Toxicity. Molecular Informatics, 39(5), e2000005. https://doi.org/10.1002/minf.202000005

Hetz, C. (2012). The unfolded protein response: Controlling cell fate decisions under ER stress and beyond. In Nature Reviews Molecular Cell Biology (Vol. 13, Issue 2, pp. 89–102). https://doi.org/10.1038/nrm3270

Hiemstra, S., Ramaiahgari, S., Wink, S., et al. (2019). High-throughput confocal imaging of differentiated 3D liver-like spheroid cellular stress response reporters for identification of drug-induced liver injury liability. Archives of Toxicology, 93(10), 2895–2911. https://doi.org/10.1007/S00204-019-02552-0

Hock, M. B., & Kralli, A. (2009). Transcriptional Control of Mitochondrial Biogenesis and Function. Annual Review of Physiology, 71, 177–2023. https://doi.org/10.1146/annurev.physiol.010908.163119

Hodneland Nilsson, L. I., Nitschke Pettersen, I. K., Nikolaisen, J., et al. (2015). A new live-cell reporter strategy to simultaneously monitor mitochondrial biogenesis and morphology. Scientific Reports, 5. https://doi.org/10.1038/srep17217

Holley, A. K., Bakthavatchalu, V., Velez-Roman, J. M., et al. (2011). Manganese superoxide dismutase: Guardian of the powerhouse. In International Journal of Molecular Sciences (Vol. 12, Issue 10, pp. 7114–7162). https://doi.org/10.3390/ijms12107114

Hong, S., & Pedersen, P. L. (2008). ATP Synthase and the Actions of Inhibitors Utilized To Study Its Roles in Human Health, Disease, and Other Scientific Areas. Microbiology and Molecular Biology Reviews, 72(4), 590–641. https://doi.org/10.1128/mmbr.00016-08

Horsefield, R., Yankovskaya, V., Sexton, G., et al. (2006). Structural and computational analysis of the quinone-binding site of complex II (succinate-ubiquinone oxidoreductase): a mechanism of electron transfer and proton conduction during ubiquinone reduction. The Journal of Biological Chemistry, 281(11), 7309–7316. https://doi.org/10.1074/JBC.M508173200

Hothorn, T., Bretz, F., & Westfall, P. (2008). Simultaneous inference in general parametric models. Biometrical Journal. Biometrische Zeitschrift, 50(3), 346–363. https://doi.org/10.1002/BIMJ.200810425

Hsieh, A. Y. Y., Budd, M., Deng, D., et al. (2018). A Monochrome Multiplex Real-Time Quantitative PCR Assay for the Measurement of Mitochondrial DNA Content. Journal of Molecular Diagnostics, 20(5), 612–620. https://doi.org/10.1016/j.jmoldx.2018.05.001

Huang, L., Sun, G., Cobessi, D., et al. (2006). 3-nitropropionic acid is a suicide inhibitor of mitochondrial respiration that, upon oxidation by complex II, forms a covalent adduct with a catalytic base arginine in the active site of the enzyme. The Journal of Biological Chemistry, 281(9), 5965–5972. https://doi.org/10.1074/JBC.M511270200

Huber, W., von Heydebreck, A., Sueltmann, H., Poustka, A.,Vingron, M., (2002) Variance Stabilization Applied to Microarray Data Calibration and to the Quantification of Differential Expression. Bioinformatics 18, S96-S104, https://bioconductor.org/packages/release/bioc/html/vsn.html

Huizing, M., Ruitenbeek, W., Thinnes, F. P., et al. (1996). Deficiency of the voltage-dependent anion channel: A novel cause of mitochondriopathy. Pediatric Research, 39(5), 760–765. https://doi.org/10.1203/00006450-199605000-00003

Huynh, F. K., Green, M. F., Koves, T. R., et al. (2014). Measurement of fatty acid oxidation rates in animal tissues and cell lines. In Methods in Enzymology (Vol. 542, pp. 391–405). Academic Press Inc. https://doi.org/10.1016/B978-0-12-416618-9.00020-0

Hwang, B., Lee, J. H., & Bang, D. (2018). Single-cell RNA sequencing technologies and bioinformatics pipelines. In Experimental and Molecular Medicine (Vol. 50, Issue 8, p. 96). Nature Publishing Group. https://doi.org/10.1038/s12276-018-0071-8

Hwang, R. Der, Wiemerslage, L., LaBreck, C. J., et al. (2014). The neuroprotective effect of human uncoupling protein 2 (hUCP2) requires cAMP-dependent protein kinase in a toxin model of Parkinson's disease. Neurobiology of Disease, 69, 180–191. https://doi.org/10.1016/j.nbd.2014.05.032

Hynes, J., Floyd, S., Soini, A. E., et al. (2003). Fluorescence-based cell viability screening assays using water-soluble oxygen probes. Journal of Biomolecular Screening, 8(3), 264–272. https://doi.org/10.1177/1087057103008003004

Hynes, J., Marroquin, L. D., Ogurtsov, V. I., et al. (2006). Investigation of drug-induced mitochondrial toxicity using fluorescence-based oxygen-sensitive probes. Toxicological Sciences, 92(1), 186–200. https://doi.org/10.1093/toxsci/kfj208

Igarashi, Y., Nakatsu, N., Yamashita, T., et al. (2015). Open TG-GATEs: A large-scale toxicogenomics database. Nucleic Acids Research, 43, D921–D927. https://doi.org/10.1093/nar/gku955

Ikuhiro, K., Paul, K. M., & Hyder, F. (2004). Dynamic Imaging of Perfusion and Oxygenation by Functional Magnetic Resonance Imaging. Journal of Cerebral Blood Flow & Metabolism, 24(12), 1369–1381. https://doi.org/10.1097/01.wcb.0000141501.12558.9b

Imamura, H., Huynh Nhat, K. P., Togawa, H., et al. (2009). Visualization of ATP levels inside single living cells with fluorescence resonance energy transfer-based genetically encoded indicators. Proceedings of the National Academy of Sciences of the United States of America, 106(37), 15651–15656. https://doi.org/10.1073/pnas.0904764106

Indiveri, C., Iacobazzi, V., Tonazzi, A., et al. (2011). The mitochondrial carnitine/acylcarnitine carrier: Function, structure and physiopathology. Molecular Aspects of Medicine, 32(4–6), 223–233. https://doi.org/10.1016/j.mam.2011.10.008

Inouye, S., & Tsuji, F. I. (1993). Cloning and sequence analysis of cDNA for the Ca2+-activated photoprotein, clytin. FEBS Letters, 315(3), 343–346. https://doi.org/10.1016/0014-5793(93)81191-2

Irobi, J., Holmgren, A., Winter, V. De, et al. (2012). Mutant HSPB8 causes protein aggregates and a reduced mitochondrial membrane potential in dermal fibroblasts from distal hereditary motor neuropathy patients. Neuromuscular Disorders, 22(8), 699–711. https://doi.org/10.1016/j.nmd.2012.04.005

Ishikawa, K., Yoshida, K., Kanie, K., et al. (2019). Morphology-Based Analysis of Myoblasts for Prediction of Myotube Formation. SLAS Discovery, 24(1), 47–56. https://doi.org/10.1177/2472555218793374

Jacobs, L. J. A. M., de Wert, G., Geraedts, J. P. M., et al. (2006). The transmission of OXPHOS disease and methods to prevent this. In Human Reproduction Update (Vol. 12, Issue 2, pp. 119–136). https://doi.org/10.1093/humupd/dmi042

Jafarian, V., Sariri, R., Hosseinkhani, S., et al. (2011). A unique EF-hand motif in mnemiopsin photoprotein from Mnemiopsis leidyi: Implication for its low calcium sensitivity. Biochemical and Biophysical Research Communications, 413(2), 164–170. https://doi.org/10.1016/j.bbrc.2011.08.022

Jahani-Asl, A., & Slack, R. S. (2007). The phosphorylation state of Drp1 determines cell fate. In EMBO Reports (Vol. 8, Issue 10, pp. 912–913). https://doi.org/10.1038/sj.embor.7401077

Jarabek, A. M., & Hines, D. E. (2019). Mechanistic integration of exposure and effects: advances to apply systems toxicology in support of regulatory decision-making. In Current Opinion in Toxicology (Vol. 16, pp. 83–92). Elsevier B.V. https://doi.org/10.1016/j.cotox.2019.09.001

Jassal, B., Matthews, L., Viteri, G., et al. (2020). The reactome pathway knowledgebase. Nucleic Acids Research, 48(D1), D498–D503. https://doi.org/10.1093/nar/gkz1031

Jennings, P., Koppelstaetter, C., Aydin, S., et al. (2007). Cyclosporine A induces senescence in renal tubular epithelial cells. American Journal of Physiology - Renal Physiology, 293(3), F831–F838. https://doi.org/10.1152/ajprenal.00005.2007

Jennings, P., Koppelstaetter, C., Pfaller, W., et al. (2004). Assessment of a new cell culture perfusion apparatus for in vitro chronic toxicity testing part 1: Technical description. Altex, 21(2), 51–60.

Johansson, H. K. L., Svingen, T., Boberg, J., et al. (2020). Calretinin is a novel candidate marker for adverse ovarian effects of early life exposure to mixtures of endocrine disruptors in the rat. Archives of Toxicology, 94(9), 1241–1250. https://doi.org/10.1007/s00204-020-02697-3

Johnson, J., Walsh, M., Bockus, B., et al. (1981). Monitoring of relative mitochondrial membrane potential in living cells by fluorescence microscopy. The Journal of Cell Biology, 88(3), 526–535. https://doi.org/10.1083/JCB.88.3.526

Johnson, J., Walsh, M., & Chen, L. (1980). Localization of mitochondria in living cells with rhodamine 123. Proc Nat Acad Sci USA, 77(2), 990–994. https://doi.org/10.1073/PNAS.77.2.990

Jones, A. J. Y., & Hirst, J. (2013). A spectrophotometric coupled enzyme assay to measure the activity of succinate dehydrogenase. Analytical Biochemistry, 442(1), 19–23. https://doi.org/10.1016/j.ab.2013.07.018

Jones, E., Gaytan, N., Garcia, I., et al. (2017). A threshold of transmembrane potential is required for mitochondrial dynamic balance mediated by DRP1 and OMA1. Cellular and Molecular Life Sciences, 74(7), 1347–1363. https://doi.org/10.1007/s00018-016-2421-9

Jornayvaz, F. R., & Shulman, G. I. (2010). Regulation of mitochondrial biogenesis. Essays in Biochemistry, 47, 69–84. https://doi.org/10.1042/BSE0470069

Joseph, P. (2017). Transcriptomics in toxicology. Food and Chemical Toxicology, 109, 650–662. https://doi.org/10.1016/j.fct.2017.07.031

Jourdain, A., & Martinou, J. C. (2010). Mitochondrial dynamics: Quantifying mitochondrial fusion in vitro. BMC Biology, 8, 99. https://doi.org/10.1186/1741-7007-8-99

Jovaisaite, V., & Auwerx, J. (2015). The mitochondrial unfolded protein response-synchronizing genomes. In Current Opinion in Cell Biology (Vol. 33, pp. 74–81). https://doi.org/10.1016/j.ceb.2014.12.003

Kamalian, L., Chadwick, A. E., Bayliss, M., et al. (2015). The utility of HepG2 cells to identify direct mitochondrial dysfunction in the absence of cell death. Toxicology in Vitro, 29(4), 732–740. https://doi.org/10.1016/j.tiv.2015.02.011

Kamentsky, L., Jones, T. R., Fraser, A., et al. (2011). Improved structure, function and compatibility for cellprofiler: Modular high-throughput image analysis software. Bioinformatics, 27(8), 1179–1180. https://doi.org/10.1093/bioinformatics/btr095

Kanehisa, M., & Goto, S. (2000). KEGG: Kyoto Encyclopedia of Genes and Genomes. In Nucleic Acids Research (Vol. 28, Issue 1, pp. 27–30). https://doi.org/10.1093/nar/28.1.27

Karbowski, M., Cleland, M. M., & Roelofs, B. A. (2014). Photoactivatable green fluorescent protein-based visualization and quantification of mitochondrial fusion and mitochondrial network complexity in living cells. In Methods in Enzymology (Vol. 547, Issue C, pp. 57–73). Academic Press Inc. https://doi.org/10.1016/B978-0-12-801415-8.00004-7

Kaspar, S., Oertlin, C., Szczepanowska, K., et al. (2021). Adaptation to mitochondrial stress requires CHOP-directed tuning of ISR. Science Advances, 7(22), eabf0971. https://doi.org/10.1126/SCIADV.ABF0971

Katayama, H., Kogure, T., Mizushima, N., et al. (2011). A sensitive and quantitative technique for detecting autophagic events based on lysosomal delivery. Chemistry and Biology, 18(8), 1042–1052. https://doi.org/10.1016/j.chembiol.2011.05.013

Kaufmann, P., Török, M., Hänni, A., et al. (2005). Mechanisms of benzarone and benzbromarone-induced hepatic toxicity. Hepatology, 41(4), 925-935. https://doi.org/10.1002/hep.20634

Kennedy, A. S., Raleigh, J. A., Perez, G. M., et al. (1997). Proliferation and hypoxia in human squamous cell carcinoma of the cervix: First report of combined immunohistochemical assays. International Journal of Radiation Oncology Biology Physics, 37(4), 897–905. https://doi.org/10.1016/S0360-3016(96)00539-1

Kennedy, S. (2002). The role of proteomics in toxicology: Identification of biomarkers of toxicity by protein expression analysis. In Biomarkers (Vol. 7, Issue 4, pp. 269–290). https://doi.org/10.1080/13547500210127318

Kerr, D., Grahame, G., & Nakouzi, G. (2012). Assays of pyruvate dehydrogenase complex and pyruvate carboxylase activity. Methods in Molecular Biology, 837, 93–119. https://doi.org/10.1007/978-1-61779-504-6_7

Ki, S. S., Jeong, J. M., Kim, S. H., et al. (2002). A case of neurotoxicity following 5-fluorouracil-based chemotherapy. The Korean Journal of Internal Medicine, 17(1), 73–77. https://doi.org/10.3904/kjim.2002.17.1.73

Kim, J. H., Ahn, J. H., Barone, P. W., et al. (2010). A luciferase/single-walled carbon nanotube conjugate for nearInfrared fluorescent detection of cellular ATP. Angewandte Chemie - International Edition, 49(8), 1456–1459. https://doi.org/10.1002/anie.200906251

Kitada, T., Asakawa, S., Hattori, N., et al. (1998). Mutations in the parkin gene cause autosomal recessive juvenile parkinsonism. Nature, 392(6676), 605–608. https://doi.org/10.1038/33416

Kluckova, K., Sticha, M., Cerny, J., et al. (2015). Ubiquinone-binding site mutagenesis reveals the role of mitochondrial complex II in cell death initiation. Cell Death and Disease, 6(5). https://doi.org/10.1038/cddis.2015.110

Kohonen, P., Parkkinen, J. A., Willighagen, E. L., et al. (2017). A transcriptomics data-driven gene space accurately predicts liver cytopathology and drug-induced liver injury. Nature Communications, 8. https://doi.org/10.1038/ncomms15932

Kolde, R., (2019). pheatmap: Pretty Heatmaps. R package version 1.0.12. https://CRAN.R-project.org/package=pheatmap

Koopman, W. J. H., Verkaart, S., Visch, H. J., et al. (2005). Inhibition of complex I of the electron transport chain causes O 2-.-mediated mitochondrial outgrowth. American Journal of Physiology - Cell Physiology, 288(6), 1440–1450. https://doi.org/10.1152/ajpcell.00607.2004

Koopman, W. J. H., Visch, H. J., Smeitink, J. A. M., et al. (2006). Simultaneous quantitative measurement and automated analysis of mitochondrial morphology, mass, potential, and motility in living human skin fibroblasts. Cytometry Part A, 69(1), 1–2. https://doi.org/10.1002/cyto.a.20198

Korga, A., Ostrowska, M., Iwan, M., et al. (2019). Inhibition of glycolysis disrupts cellular antioxidant defense and sensitizes HepG2 cells to doxorubicin treatment. FEBS Open Bio, 9(5), 959–972. https://doi.org/10.1002/2211-5463.12628

Kornick, K., Bogner, B., Sutter, L., et al. (2019). Population Dynamics of Mitochondria in Cells: A Minimal Mathematical Model. Frontiers in Physics, 7, 146. https://doi.org/10.3389/fphy.2019.00146

Krall, A., Mullen, P., Surjono, F., et al. (2021). Asparagine couples mitochondrial respiration to ATF4 activity and tumor growth. Cell Metabolism, 33(5), 1013-1026.e6. https://doi.org/10.1016/J.CMET.2021.02.001

Krebs, A., Nyffeler, J., Karreman, C., et al. (2020). Determination of benchmark concentrations and their statistical uncertainty for cytotoxicity test data and functional in vitro assays. ALTEX, 37(1), 155–163. https://doi.org/10.14573/ALTEX.1912021

Krebs, A., Waldmann, T., Wilks, M., et al. (2019). Template for the description of cell-based toxicological test methods to allow evaluation and regulatory use of the data. ALTEX, 36(4), 682–699. https://doi.org/10.14573/ALTEX.1909271

Krewski, D., Westphal, M., Andersen, M. E., et al. (2014). A framework for the next generation of risk science. In Environmental Health Perspectives (Vol. 122, Issue 8, pp. 796–805). https://doi.org/10.1289/ehp.1307260

Krieger, R. I. (2001). Handbook of Pesticide Toxicology. In Handbook of Pesticide Toxicology. Elsevier. https://doi.org/10.1016/b978-0-12-426260-7.x5000-9

Krug, A. K., Gutbier, S., Zhao, L., et al. (2014). Transcriptional and metabolic adaptation of human neurons to the mitochondrial toxicant MPP +. Cell Death & Disease 2014 5:5, 5(5), e1222–e1222. https://doi.org/10.1038/cddis.2014.166

Kühl, I., Miranda, M., Atanassov, I., et al. (2017). Transcriptomic and proteomic landscape of mitochondrial dysfunction reveals secondary coenzyme Q deficiency in mammals. ELife, 6, e30952. https://doi.org/10.7554/eLife.30952

Kuijper, I. A., Yang, H., Van De Water, B., et al. (2017). Unraveling cellular pathways contributing to drug-induced liver injury by dynamical modeling. In Expert Opinion on Drug Metabolism and Toxicology (Vol. 13, Issue 1, pp. 5–17). Taylor and Francis Ltd. https://doi.org/10.1080/17425255.2017.1234607

Kunii, M., Doi, H., Higashiyama, Y., et al. (2015). A Japanese case of cerebellar ataxia, spastic paraparesis and deep sensory impairment associated with a novel homozygous TTC19 mutation. Journal of Human Genetics, 60(4), 187–191. https://doi.org/10.1038/JHG.2015.7

Kwon, K. A., Kwon, H.-C., Kim, M. C., et al. (2010). A Case of 5-Fluorouracil Induced Encephalopathy. Cancer Research and Treatment, 42(2), 118–120. https://doi.org/10.4143/crt.2010.42.2.118

Labib, S., Williams, A., Yauk, C. L., et al. (2016). Nano-risk Science: Application of toxicogenomics in an adverse outcome pathway framework for risk assessment of multi-walled carbon nanotubes. Particle and Fibre Toxicology, 13, 15. https://doi.org/10.1186/s12989-016-0125-9

Lai, J. C. K., DiLorenzo, J. C., & Sheu, K. F. R. (1988). Pyruvate dehydrogenase complex is inhibited in calcium-loaded cerebrocortical mitochondria. Neurochemical Research, 13(11), 1043–1048. https://doi.org/10.1007/BF00973148

Lareau, C. A., Ludwig, L. S., Muus, C., et al. (2020). Massively parallel single-cell mitochondrial DNA genotyping and chromatin profiling. Nature Biotechnology, 39(4), 451–461. https://doi.org/10.1038/s41587-020-0645-6

Lee, D. H., Kim, S. Y., & Hong, J. I. (2004). A fluorescent pyrophosphate sensor with high selectivity over ATP in water. Angewandte Chemie - International Edition, 43(36), 4777–4780. https://doi.org/10.1002/anie.200453914

Lee, E. H., Kim, S., Choi, M. S., et al. (2019). Gene networking in colistin-induced nephrotoxicity reveals an adverse outcome pathway triggered by proteotoxic stress. International Journal of Molecular Medicine, 43(3), 1343–1355. https://doi.org/10.3892/ijmm.2019.4052

Lee, Y. C., Bååth, J. A., Bastle, R. M., et al. (2018). Impact of Detergents on Membrane Protein Complex Isolation. Journal of Proteome Research, 17(1), 348–358. https://doi.org/10.1021/acs.jproteome.7b00599

Leist, M., Ghallab, A., Graepel, R., et al. (2017). Adverse outcome pathways: opportunities, limitations and open questions. Archives of Toxicology, 91(11), 3477–3505. https://doi.org/10.1007/s00204-017-2045-3

Lemasters, J. J., & Ramshesh, V. K. (2007). Imaging of Mitochondrial Polarization and Depolarization with Cationic Fluorophores. In Methods in Cell Biology (Vol. 80, pp. 283–295). Methods Cell Biol. https://doi.org/10.1016/S0091-679X(06)80014-2

Leonard, A. P., Cameron, R. B., Speiser, J. L., et al. (2015). Quantitative analysis of mitochondrial morphology and membrane potential in living cells using high-content imaging, machine learning, and morphological binning. Biochim Biophys Acta, 1853(2), 348–360. https://doi.org/10.1016/j.bbamcr.2014.11.002

Li, H., Zhu, X., Yang, W., et al. (2014). Comparative kinetics of Qi site inhibitors of cytochrome bc1 complex: picomolar antimycin and micromolar cyazofamid. Chemical Biology & Drug Design, 83(1), 71–80. https://doi.org/10.1111/CBDD.12199

Li, L., Wang, C., Yang, H., et al. (2017). Metabolomics reveal mitochondrial and fatty acid metabolism disorders that contribute to the development of DKD in T2DM patients. Molecular BioSystems, 13(11), 2392–2400. https://doi.org/10.1039/c7mb00167c

Li, N., Ragheb, K., Lawler, G., et al. (2003). Mitochondrial complex I inhibitor rotenone induces apoptosis through enhancing mitochondrial reactive oxygen species production. Journal of Biological Chemistry, 278(10), 8516–8525. https://doi.org/10.1074/jbc.M210432200

Li, Y., Li, X., Kan, Q., et al. (2017). Mitochondrial pyruvate carrier function is negatively linked to Warburg phenotype in vitro and malignant features in esophageal squamous cell carcinomas. Oncotarget, 8(1), 1058–1073. https://doi.org/10.18632/oncotarget.13717

Liepinsh, E., Makrecka, M., Kuka, J., et al. (2014). Selective inhibition of OCTN2 is more effective than inhibition of gamma-butyrobetaine dioxygenase to decrease the availability of l-carnitine and to reduce myocardial infarct size. Pharmacological Research, 85, 33–38. https://doi.org/10.1016/j.phrs.2014.05.002

Limonciel, A., Aschauer, L., Wilmes, A., et al. (2011). Lactate is an ideal non-invasive marker for evaluating temporal alterations in cell stress and toxicity in repeat dose testing regimes. Toxicology in Vitro : An International Journal Published in Association with BIBRA, 25(8), 1855–1862. https://doi.org/10.1016/J.TIV.2011.05.018

Limonciel, A., G, A., G, C., et al. (2018). Comparison of base-line and chemical-induced transcriptomic responses in HepaRG and RPTEC/TERT1 cells using TempO-Seq. Archives of Toxicology, 92(8), 2517–2531. https://doi.org/10.1007/S00204-018-2256-2

Lindon, J. C., Keun, H. C., Ebbels, T. M. D., et al. (2005). The Consortium for Metabonomic Toxicology (COMET): Aims, activities and achievements. In Pharmacogenomics (Vol. 6, Issue 7, pp. 691–699). https://doi.org/10.2217/14622416.6.7.691

Ling, N. (2003). Rotenone - A review of its toxicity and use for fisheries management. Science for Conservation.

Liu, X., Xu, J., Lv, Y., et al. (2013). An ATP-selective, lanthanide complex luminescent probe. Dalton Transactions, 42(27), 9840–9846. https://doi.org/10.1039/c3dt50986a

Liu, Y., Fiskum, G., & Schubert, D. (2002). Generation of reactive oxygen species by the mitochondrial electron transport chain. Journal of Neurochemistry, 80(5), 780–787. https://doi.org/10.1046/j.0022-3042.2002.00744.x

Liu, Y., Jin, M., Wang, Y., et al. (2020). MCU-induced mitochondrial calcium uptake promotes mitochondrial biogenesis and colorectal cancer growth. Signal Transduction and Targeted Therapy, 5(1), 59. https://doi.org/10.1038/s41392-020-0155-5

Liu, Y., Villamena, F. A., Sun, J., et al. (2009). Esterified trityl radicals as intracellular oxygen probes. Free Radical Biology and Medicine, 46(7), 876–883. https://doi.org/10.1016/j.freeradbiomed.2008.12.011

Liu, Z., Yuan, J., Lasorella, A., et al. (2020). Integrating single-cell RNA-seq and imaging with SCOPE-seq2. Scientific Reports, 10(1), 1–15. https://doi.org/10.1038/s41598-020-76599-w

Longo, D., Yang, Y., Watkins, P., et al. (2016). Elucidating Differences in the Hepatotoxic Potential of Tolcapone and Entacapone With DILIsym(®), a Mechanistic Model of Drug-Induced Liver Injury. CPT: Pharmacometrics & Systems Pharmacology, 5(1), 31–39. https://doi.org/10.1002/PSP4.12053

Longo, N., Amat Di San Filippo, C., & Pasquali, M. (2006). Disorders of carnitine transport and the carnitine cycle. Am J Med Genet C - Semin Med Genet, 142C(2), 77–85. https://doi.org/10.1002/ajmg.c.30087

Los, F. C. O., Randis, T. M., Aroian, R. V., et al. (2013). Role of Pore-Forming Toxins in Bacterial Infectious Diseases. Microbiol Mol Biol Rev, 77(2), 173–207. https://doi.org/10.1128/mmbr.00052-12

Love, M. I., Huber, W., & Anders, S. (2014). Moderated estimation of fold change and dispersion for RNA-seq data with DESeq2. Genome Biology, 15(12), 550. https://doi.org/10.1186/s13059-014-0550-8

Lowe, R., Shirley, N., Bleackley, M., et al. (2017). Transcriptomics technologies. PLoS Computational Biology, 13(5), e1005457. https://doi.org/10.1371/journal.pcbi.1005457

Lümmen, P. (1998). Complex I inhibitors as insecticides and acaricides. Biochim Biophys Acta, 1364(2), 287-296. https://doi.org/10.1016/S0005-2728(98)00034-6

Lynch, M., & Marinov, G. K. (2015). The bioenergetic costs of a gene. Proceedings of the National Academy of Sciences of the United States of America, 112(51), 15690–15695. https://doi.org/10.1073/pnas.1514974112

Ma, Y., Wang, W., Devarakonda, T., et al. (2020). Functional analysis of molecular and pharmacological modulators of mitochondrial fatty acid oxidation. Scientific Reports, 10(1), 1450. https://doi.org/10.1038/s41598-020-58334-7

MacVicar, T., & Langer, T. (2016). OPA1 processing in cell death and disease - the long and short of it. In Journal of Cell Science (Vol. 129, Issue 12, pp. 2297–2306). https://doi.org/10.1242/jcs.159186

Maekawa, H., Inoue, T., Ouchi, H., et al. (2019). Mitochondrial Damage Causes Inflammation via cGAS-STING Signaling in Acute Kidney Injury. Cell Reports, 29(5), 1261–1273. https://doi.org/10.1016/j.celrep.2019.09.050

Manfredi, G., Yang, L., Gajewski, C. D., et al. (2002). Measurements of ATP in mammalian cells. Methods, 26(4), 317–326. https://doi.org/10.1016/S1046-2023(02)00037-3

Manzoni, C., Kia, D. A., Vandrovcova, J., et al. (2018). Genome, transcriptome and proteome: The rise of omics data and their integration in biomedical sciences. Briefings in Bioinformatics, 19(2), 286–302. https://doi.org/10.1093/BIB/BBW114

Markova, S. V., Burakova, L. P., Golz, S., et al. (2012). The light-sensitive photoprotein berovin from the bioluminescent ctenophore Beroe abyssicola: A novel type of Ca 2+-regulated photoprotein. FEBS Journal, 279(5), 856–870. https://doi.org/10.1111/j.1742-4658.2012.08476.x

Markova, S. V., Vysotski, E. S., Blinks, J. R., et al. (2002). Obelin from the bioluminescent marine hydroid Obelia geniculata: Cloning, expression, and comparison of some properties with those of other Ca2+-regulated photoproteins. Biochemistry, 41(7), 2227–2236. https://doi.org/10.1021/bi0117910

Marroquin, L. D., Hynes, J., Dykens, J. A., et al. (2007). Circumventing the crabtree effect: Replacing media glucose with galactose increases susceptibility of hepG2 cells to mitochondrial toxicants. Toxicological Sciences, 97(2), 539–547. https://doi.org/10.1093/toxsci/kfm052

Martens, M., Ammar, A., Riutta, A., et al. (2021). WikiPathways: connecting communities. Nucleic Acids Research, 49(D1), D613–D621. https://doi.org/10.1093/nar/gkaa1024

Martens, M., Verbruggen, T., Nymark, P., et al. (2018). Introducing WikiPathways as a Data-Source to Support Adverse Outcome Pathways for Regulatory Risk Assessment of Chemicals and Nanomaterials. Frontiers in Genetics, 9, 661. https://doi.org/10.3389/fgene.2018.00661

Martin, W. F., Garg, S., & Zimorski, V. (2015). Endosymbiotic theories for eukaryote origin. In Philos Trans R Soc B Biolo Sci (Vol. 370, Issue 1678, p. 20140330). https://doi.org/10.1098/rstb.2014.0330

Massey, F. J. (1951). The Kolmogorov-Smirnov Test for Goodness of Fit. Journal of the American Statistical Association, 46(253), 68. https://doi.org/10.2307/2280095

Mathon, C., Bovard, D., Dutertre, Q., et al. (2019). Impact of sample preparation upon intracellular metabolite measurements in 3D cell culture systems. Metabolomics, 15(6), 92. https://doi.org/10.1007/s11306-019-1551-0

Mav, D., Shah, R. R., Howard, B. E., et al. (2018). A hybrid gene selection approach to create the S1500+ targeted gene sets for use in high-throughput transcriptomics. PLoS ONE, 13(2), e0191105. https://doi.org/10.1371/journal.pone.0191105

McKenzie, M., Lim, S. C., & Duchen, M. R. (2017). Simultaneous measurement of mitochondrial calcium and mitochondrial membrane potential in live cells by fluorescent microscopy. Journal of Visualized Experiments, 2017(119), 55166. https://doi.org/10.3791/55166

McKim, J. M., & Erickson, R. J. (1991). Environmental Impacts on the Physiological Mechanisms Controlling Xenobiotic Transfer across Fish Gills. Physiological Zoology, 64(1), 39–67. https://doi.org/10.1086/physzool.64.1.30158513

Mclafferty, F. W. (1980). Tandem Mass Spectrometry (MS/MS): A Promising New Analytical Technique for Specific Component Determination in Complex Mixtures. Accounts of Chemical Research, 13(2), 33–39. https://doi.org/10.1021/ar50146a001

Meeusen, S. L., & Nunnari, J. (2007). Mitochondrial fusion in vitro. Methods in Molecular Biology (Clifton, N.J.), 372, 461–466. https://doi.org/10.1007/978-1-59745-365-3_32

Mehta, M. M., Weinberg, S. E., & Chandel, N. S. (2017). Mitochondrial control of immunity: Beyond ATP. In Nature Reviews Immunology (Vol. 17, Issue 10, pp. 608–620). https://doi.org/10.1038/nri.2017.66

Melber, A., & Haynes, C. M. (2018). UPR mt regulation and output: A stress response mediated by mitochondrial-nuclear communication. In Cell Research (Vol. 28, Issue 3, pp. 281–295). https://doi.org/10.1038/cr.2018.16

Memon, A. A., Zöller, B., Hedelius, A., et al. (2017). Quantification of mitochondrial DNA copy number in suspected cancer patients by a well optimized ddPCR method. Biomolecular Detection and Quantification, 13, 32–39. https://doi.org/10.1016/j.bdq.2017.08.001

Mercer, T. R., Neph, S., Dinger, M. E., et al. (2011). The human mitochondrial transcriptome. Cell, 146(4), 645–658. https://doi.org/10.1016/j.cell.2011.06.051

Merritt II, J. L., Norris, M., & Kanungo, S. (2018). Fatty acid oxidation disorders. Annals of Translational Medicine, 6(24), 473–473. https://doi.org/10.21037/atm.2018.10.57

Merry, T. L., & Ristow, M. (2016). Mitohormesis in exercise training. Free Radical Biology and Medicine, 98, 123–130. https://doi.org/10.1016/j.freeradbiomed.2015.11.032

Meyer, J. N., Hartman, J. H., & Mello, D. F. (2018). Mitochondrial Toxicity. Toxicological Sciences, 162(1), 15–23. https://doi.org/10.1093/toxsci/kfy008

Meyer, J. N., Leung, M. C. K., Rooney, J. P., et al. (2013). Mitochondria as a target of environmental toxicants. In Toxicological Sciences (Vol. 134, Issue 1, pp. 1–17). https://doi.org/10.1093/toxsci/kft102

Meyer, J. N., Leuthner, T. C., & Luz, A. L. (2017). Mitochondrial fusion, fission, and mitochondrial toxicity. Toxicological Science, 134(1), 1–17. https://doi.org/10.1016/j.tox.2017.07.019

Microsoft Corporation, Weston, S. (2020). doParallel: Foreach Parallel Adaptor for the 'parallel' Package. R package version 1.0.16. https://CRAN.R-project.org/package=doParallel

Mik, E. G., Johannes, T., Zuurbier, C. J., et al. (2008). In vivo mitochondrial oxygen tension measured by a delayed fluorescence lifetime technique. Biophysical Journal, 95(8), 3977–3990. https://doi.org/10.1529/biophysj.107.126094

Minta, A., Kao, J. P. Y., & Tsien, R. Y. (1989). Fluorescent indicators for cytosolic calcium based on rhodamine and fluorescein chromophores. Journal of Biological Chemistry, 264(14), 8171–8178. https://doi.org/10.1016/s0021-9258(18)83165-9

Mishra, J., Davani, A. J., Natarajan, G. K., et al. (2019). Cyclosporin A Increases Mitochondrial Buffering of Calcium: An Additional Mechanism in Delaying Mitochondrial Permeability Transition Pore Opening. Cells, 8(9), 1052. https://doi.org/10.3390/cells8091052

Miyawaki, A., Griesbeck, O., Heim, R., et al. (1999). Dynamic and quantitative Ca2+ measurements using improved cameleons. Proceedings of the National Academy of Sciences of the United States of America, 96(5), 2135–2140. https://doi.org/10.1073/pnas.96.5.2135

Miyawaki, A., Llopis, J., Heim, R., et al. (1997). Fluorescent indicators for Ca2+ based on green fluorescent proteins and calmodulin. Nature, 388(6645), 882–887. https://doi.org/10.1038/42264

Miyazono, Y., Hirashima, S., Ishihara, N., et al. (2018). Uncoupled mitochondria quickly shorten along their long axis to form indented spheroids, instead of rings, in a fission-independent manner. Scientific Reports, 8(1), 350. https://doi.org/10.1038/s41598-017-18582-6

Monaghan, R. M., & Whitmarsh, A. J. (2015). Mitochondrial Proteins Moonlighting in the Nucleus. In Trends in Biochemical Sciences (Vol. 40, Issue 12, pp. 728–735). https://doi.org/10.1016/j.tibs.2015.10.003

Morciano, G., Sarti, A. C., Marchi, S., et al. (2017). Use of luciferase probes to measure ATP in living cells and animals. Nature Protocols, 12(8), 1542–1562. https://doi.org/10.1038/nprot.2017.052

Mordaunt, D., Jolley, A., Balasubramaniam, S., et al. (2015). Phenotypic variation of TTC19-deficient mitochondrial complex III deficiency: a case report and literature review. American Journal of Medical Genetics. Part A, 167(6), 1330–1336. https://doi.org/10.1002/AJMG.A.36968

Moser, B. K. (1996). Maximum Likelihood Estimation and Related Topics. In Linear ModelsProbability and Mathematical Statistics (pp. 105–129). Elsevier. https://doi.org/10.1016/b978-012508465-9/50006-5

Moshkforoush, A., Ashenagar, B., Tsoukias, N. M., et al. (2019). Modeling the role of endoplasmic reticulum-mitochondria microdomains in calcium dynamics. Scientific Reports, 9(1), 1–16. https://doi.org/10.1038/s41598-019-53440-7

Münch, C. (2018). The different axes of the mammalian mitochondrial unfolded protein response. In BMC Biology (Vol. 16, Issue 1, p. 81). https://doi.org/10.1186/s12915-018-0548-x

Murphey, W. H., Barnaby, C., Lin, F. J., et al. (1967). Malate dehydrogenases. II. Purification and properties of Bacillus subtilis, Bacillus stearothermophilus, and Escherichia coli malate dehydrogenases. Journal of Biological Chemistry, 242(7), 1548–1559. https://pubmed.ncbi.nlm.nih.gov/4960671/

Murphy, S. M., Kiely, M., Jakeman, P. M., et al. (2016). Optimization of an in vitro bioassay to monitor growth and formation of myotubes in real time. Bioscience Reports, 36(3), e00330. https://doi.org/10.1042/BSR20160036

Murrell, P., (2015). compare: Comparing Objects for Differences. R package version 0.2-6. https://CRAN.R-project.org/package=compare

Muschet, C., Möller, G., Prehn, C., et al. (2016). Removing the bottlenecks of cell culture metabolomics: fast normalization procedure, correlation of metabolites to cell number, and impact of the cell harvesting method. Metabolomics, 12(10), 151. https://doi.org/10.1007/s11306-016-1104-8

Mushtaq, M. Y., Choi, Y. H., Verpoorte, R., et al. (2014). Extraction for metabolomics: Access to the metabolome. In Phytochemical Analysis (Vol. 25, Issue 4, pp. 291–306). https://doi.org/10.1002/pca.2505

Nadanaciva, S., Bernal, A., Aggeler, R., et al. (2007). Target identification of drug induced mitochondrial toxicity using immunocapture based OXPHOS activity assays. Toxicology in Vitro, 21(5), 902–911. https://doi.org/10.1016/j.tiv.2007.01.011

Nadanaciva, S., Dykens, J., Bernal, A., et al. (2007). Mitochondrial impairment by PPAR agonists and statins identified via immunocaptured OXPHOS complex activities and respiration. Toxicology and Applied Pharmacology, 223(3), 277–287. https://doi.org/10.1016/J.TAAP.2007.06.003

Nagai, T., Sawano, A., Eun Sun Park, et al. (2001). Circularly permuted green fluorescent proteins engineered to sense Ca2+. Proc Natl Acad Sci USA, 98(6), 3197–3202. https://doi.org/10.1073/pnas.051636098

Nakai, J., Ohkura, M., & Imoto, K. (2001). A high signal-to-noise ca2+ probe composed of a single green fluorescent protein. Nature Biotechnology, 19(2), 137–141. https://doi.org/10.1038/84397

Nandipati, S., & Litvan, I. (2016a). Environmental exposures and Parkinson's disease. In Int J Environ Res Public Health (Vol. 13, Issue 9, p. 881). https://doi.org/10.3390/ijerph13090881

Naven, R. T., Swiss, R., Klug-Mcleod, J., et al. (2013). The development of structure-activity relationships for mitochondrial dysfunction: Uncoupling of oxidative phosphorylation. Toxicological Sciences, 131(1), 271–278. https://doi.org/10.1093/toxsci/kfs279

Nelson, D. L., & Cox, M. M. (2017). Lehninger Principles of Biochemistry. In W.H. Freeman and Company (Vol. 7).

Neuwirth, E., (2014). RColorBrewer: ColorBrewer Palettes. R package version 1.1-2. https://CRAN.R-project.org/package=RColorBrewer

Nicolson, G. L. (2014). Mitochondrial dysfunction and chronic disease: Treatment with natural supplements. Integrative Medicine (Boulder), 13(4), 35–43. /pmc/articles/PMC4566449/

Nisoli, E., & Carruba, M. O. (2006). Nitric oxide and mitochondrial biogenesis. Journal of Cell Science, 119, 2855–2865. https://doi.org/10.1242/jcs.03062

Nisoli, E., Clementi, E., Carruba, M. O., et al. (2007). Defective mitochondrial biogenesis: A hallmark of the high cardiovascular risk in the metabolic syndrome? In Circulation Research (Vol. 100, Issue 6, pp. 795–806). https://doi.org/10.1161/01.RES.0000259591.97107.6c

Nisoli, E., Falcone, S., Tonello, C., et al. (2004). Mitochondrial biogenesis by NO yields functionally active mitochondria in mammals. Proc Natl Acad Sci USA, 101(47), 16507–16512. https://doi.org/10.1073/pnas.0405432101

Nonnenmacher, Y., Palorini, R., d'Herouël, A. F., et al. (2017). Analysis of mitochondrial metabolism in situ: Combining stable isotope labeling with selective permeabilization. Metabolic Engineering, 43(Pt B), 147–155. https://doi.org/10.1016/j.ymben.2016.12.005

Nymark, P., Rieswijk, L., Ehrhart, F., et al. (2018). A Data Fusion Pipeline for Generating and Enriching Adverse Outcome Pathway Descriptions. Toxicological Sciences, 62(1), 264–275. https://doi.org/10.1093/toxsci/kfx252

OECD (1997), Test No. 424: Neurotoxicity Study in Rodents, OECD Guidelines for the Testing of Chemicals, Section 4, OECD Publishing, Paris, https://doi.org/10.1787/9789264071025-en

OECD(2016).Guidance document for the use of adverse outcome pathways in developing integrated approaches to testing and assessment (IATA), Series on Testing & Assessment No.260, Paris, ENV/JM/MONO(2016)67http://www.oecd.org/officialdocuments/publicdisplaydocumentpdf/?cote=env/jm/mono(2016)67&doclanguage=en

OECD (2019) Prediction of a 90 day repeated dose toxicity study (OECD 408) for 2-Ethylbutyric acid using a read-across approach from other branched carboxylic acids: Series on testing and assessment no. 324, ENV/JM/MONO(2020)20, https://www.oecd.org/chemicalsafety/risk-assessment/iata-integrated-approaches-to-testing-and-assessment.htm

OECD (2020a). van der Stel, W., Bennekou, S. H., Carta, G., Eakins, J., Delp, J., Forsby, A., Kamp, H., Gardner, I., Zdradil, B., Pastor, M., Gomes, J. C., White, A., Steger-Hartmann, T., Danen, E. H. J., Leist, M., Walker, P., Jennings, P., & van de Water, B. (2020). Case study on the use of integrated approaches to testing and assessment for identification and characterisation of parkinsonian hazard liability of deguelin by an aop-based testing and read across approach: Series on Testing and Assessment No. 326, ENV/JM/MONO(2020)22. https://orbit.dtu.dk/en/publications/case-study-on-the-use-of-integrated-approaches-to-testing-and-ass-2

OECD (2020b). Bennekou, S. H., van der Stel, W., Carta, G., Eakins, J., Delp, J., Forsby, A., Kamp, H., Gardner, I., Zdradil, B., Pastor, M., Gomes, J. C., White, A., Steger-Hartmann, T., Danen, E. H. J., Leist, M., Walker, P., Jennings, P., & van de Water, B. (2020). Case study on the use of integrated approaches to testing and assessment for mitochondrial complex-iii-mediated neurotoxicity of azoxystrobin - read-across to other strobilurins: Series on testing and assessment no. 327, ENV/JM/MONO(2020)23 o
https://orbit.dtu.dk/en/publications/case-study-on-the-use-of-integrated-approaches-to-testing-and-ass

OECD (2020c), Report on considerations form case studies on integrated approaches for testing and assessment (IATA), Series on Testing & Assessment No.328, Paris, ENV/JM/MONO(2020)24 http://www.oecd.org/officialdocuments/publicdisplaydocumentpdf/?cote=env/jm/mono(2020)24&doclanguage=en

Ockleford, C., Adriaanse, P., Berny, P., et al. (2017). Investigation into experimental toxicological properties of plant protection products having a potential link to Parkinson's disease and childhood leukaemia. EFSA Journal. European Food Safety Authority, 15(3), e04691. https://doi.org/10.2903/J.EFSA.2017.4691

Ohkura, M., Matsuzaki, M., Kasai, H., et al. (2005). Genetically encoded bright Ca2+ probe applicable for dynamic Ca2+ imaging of dendritic spines. Analytical Chemistry, 77(18), 5861–5869. https://doi.org/10.1021/ac0506837

Oki, N. O., Farcal, L., Abdelaziz, A., et al. (2019). Integrated analysis of in vitro data and the adverse outcome pathway framework for prioritization and regulatory applications: An exploratory case study using publicly available data on piperonyl butoxide and liver models. Toxicology in Vitro, 54, 23–32. https://doi.org/10.1016/j.tiv.2018.09.002

Okun, J., Lümmen, P., & Brandt, U. (1999). Three classes of inhibitors share a common binding domain in mitochondrial complex I (NADH:ubiquinone oxidoreductase). The Journal of Biological Chemistry, 274(5), 2625–2630. https://doi.org/10.1074/JBC.274.5.2625

Olszewska, A., & Szewczyk, A. (2013). Mitochondria as a pharmacological target: Magnum overview. In IUBMB Life (Vol. 65, Issue 3, pp. 273–281). https://doi.org/10.1002/iub.1147

Ong, S. E., & Mann, M. (2007). A practical recipe for stable isotope labeling by amino acids in cell culture (SILAC). Nature Protocols, 1(6), 2650–2660. https://doi.org/10.1038/nprot.2006.427

Oonthonpan, L., Rauckhorst, A. J., Gray, L. R., et al. (2019). Two human patient mitochondrial pyruvate carrier mutations reveal distinct molecular mechanisms of dysfunction. JCI Insight, 5(13), e126132. https://doi.org/10.1172/jci.insight.126132

Ouellet, M., Guillebaud, G., Gervais, V., et al. (2017). A novel algorithm identifies stress-induced alterations in mitochondrial connectivity and inner membrane structure from confocal images. PLoS Computational Biology, 13(6), e1005612. https://doi.org/10.1371/journal.pcbi.1005612

Owen, M. R., Doran, E., & Halestrap, A. P. (2000). Evidence that metformin exerts its anti-diabetic effects through inhibition of complex 1 of the mitochondrial respiratory chain. Biochemical Journal, 384(Pt 3), 607–614. https://doi.org/10.1042/0264-6021:3480607

Özalp, V. C., Nielsen, L. J., & Olsen, L. F. (2010). An aptamer-based nanobiosensor for real-time measurements of ATP dynamics. ChemBioChem, 11(18), 2538–2541. https://doi.org/10.1002/cbic.201000500

Pacheu-Grau, D., Rucktaeschel, R., & Deckers, M. (2018). Mitochondrial dysfunction and its role in tissue-specific cellular stress. Cell Stress, 2(8), 184–199. https://doi.org/10.15698/cst2018.07.147

Padmanabhan, K., Eddy, W. F., & Crowley, J. C. (2010). A novel algorithm for optimal image thresholding of biological data. Journal of Neuroscience Methods, 193(2), 380–384. https://doi.org/10.1016/j.jneumeth.2010.08.031

Pagès, H., Carlson, M., Falcon, S., Li, N. (2020). AnnotationDbi: Manipulation of SQLite-based annotations in Bioconductor. R package version 1.52.0, https://bioconductor.org/packages/AnnotationDbi

Pagliarini, D. J., Calvo, S. E., Chang, B., et al. (2008). A Mitochondrial Protein Compendium Elucidates Complex I Disease Biology. Cell, 134(1), 112–123. https://doi.org/10.1016/j.cell.2008.06.016

Palikaras, K., Lionaki, E., & Tavernarakis, N. (2018). Mechanisms of mitophagy in cellular homeostasis, physiology and pathology. In Nature Cell Biology (Vol. 20, Issue 9, pp. 1013–1022). https://doi.org/10.1038/s41556-018-0176-2

Palmer, A. E., & Tsien, R. Y. (2006). Measuring calcium signaling using genetically targetable fluorescent indicators. Nature Protocols, 1(3), 1057–1065. https://doi.org/10.1038/nprot.2006.172

Pan, D., Lindau, C., Lagies, S., et al. (2018). Metabolic profiling of isolated mitochondria and cytoplasm reveals compartment-specific metabolic responses. Metabolomics, 14(5), 59. https://doi.org/10.1007/s11306-018-1352-x

Park, L. C. H., Calingasan, N. Y., Sheu, K. F. R., et al. (2000). Quantitative α-ketoglutarate dehydrogenase activity staining in brain sections and in cultured cells. Analytical Biochemistry, 277(1), 86–93. https://doi.org/10.1006/abio.1999.4359

Patergnani, S., & Pinton, P. (2015). Mitophagy and mitochondrial balance. Methods in Molecular Biology (Clifton, N.J.), 1241, 181–194. https://doi.org/10.1007/978-1-4939-1875-1_15

Patten, D. A., Wong, J., Khacho, M., et al. (2014). OPA1-dependent cristae modulation is essential for cellular adaptation to metabolic demand. The EMBO Journal, 33(22), 2676–2691. https://doi.org/10.15252/embj.201488349

Paupe, V., & Prudent, J. (2018). New insights into the role of mitochondrial calcium homeostasis in cell migration. Biochem Biophys Res Commun, 500(1), 75–86. https://doi.org/10.1016/j.bbrc.2017.05.039

Pearson, B. L., Simon, J. M., McCoy, E. S., et al. (2016). Identification of chemicals that mimic transcriptional changes associated with autism, brain aging and neurodegeneration. Nature Communications, 7, 11173. https://doi.org/10.1038/ncomms11173

Pearson, B., Simon, J., McCoy, E., et al. (2016). Identification of chemicals that mimic transcriptional changes associated with autism, brain aging and neurodegeneration. Nature Communications, 7, 11173. https://doi.org/10.1038/NCOMMS11173

Peng, J. Y., Lin, C. C., Chen, Y. J., et al. (2011). Automatic morphological subtyping reveals new roles of caspases in mitochondrial dynamics. PLoS Computational Biology, 7(10), e1002212. https://doi.org/10.1371/journal.pcbi.1002212

Penjweini, R., Andreoni, A., Rosales, T., et al. (2018). Intracellular oxygen mapping using a myoglobin-mCherry probe with fluorescence lifetime imaging. Journal of Biomedical Optics, 23(10), 1–14. https://doi.org/10.1117/1.jbo.23.10.107001

Pereira, E. J., Smolko, C. M., & Janes, K. A. (2016). Computational models of reactive oxygen species as metabolic byproducts and signal-transduction modulators. In Frontiers in Pharmacology (Vol. 7, p. 457). Frontiers Media S.A. https://doi.org/10.3389/fphar.2016.00457

Perry, S. W., Norman, J. P., Barbieri, J., et al. (2011). Mitochondrial membrane potential probes and the proton gradient: A practical usage guide. In BioTechniques (Vol. 50, Issue 2, pp. 98–115). Biotechniques. https://doi.org/10.2144/000113610

Pessayre, D., Fromenty, B., Berson, A., et al. (2012). Central role of mitochondria in drug-induced liver injury. Drug Metabolism Reviews, 44(1), 34–87. https://doi.org/10.3109/03602532.2011.604086

Peter, B., Waddington, C. L., Oláhová, M., et al. (2018). Defective mitochondrial protease LonP1 can cause classical mitochondrial disease. Human Molecular Genetics, 27(10), 1743-1753. https://doi.org/10.1093/hmg/ddy080

Pfanner, N., Warscheid, B., & Wiedemann, N. (2019). Mitochondrial proteins: from biogenesis to functional networks. In Nature Reviews Molecular Cell Biology (Vol. 20, Issue 5, pp. 267–284). https://doi.org/10.1038/s41580-018-0092-0

Pfleger, J., He, M., & Abdellatif, M. (2015). Mitochondrial complex II is a source of the reserve respiratory capacity that is regulated by metabolic sensors and promotes cell survival. Cell Death & Disease, 6(7). https://doi.org/10.1038/CDDIS.2015.202

Phillips, J. R., Svoboda, D. L., Tandon, A., et al. (2019). BMD Express 2: Enhanced transcriptomic dose-response analysis workflow. Bioinformatics, 35(10), 1780–1782. https://doi.org/10.1093/bioinformatics/bty878

Phillips, M. J., & Voeltz, G. K. (2016). Structure and function of ER membrane contact sites with other organelles. In Nature Reviews Molecular Cell Biology (Vol. 17, Issue 2, pp. 69–82). https://doi.org/10.1038/nrm.2015.8

Pietzke, M., Zasada, C., Mudrich, S., et al. (2014). Decoding the dynamics of cellular metabolism and the action of 3-bromopyruvate and 2-deoxyglucose using pulsed stable isotope-resolved metabolomics. Cancer & Metabolism, 2, 9. https://doi.org/10.1186/2049-3002-2-9

Pirzada, N. A., Ali, I. I., & Dafer, R. M. (2000). Fluorouracil-induced neurotoxicity. Annals of Pharmacotherapy, 34(1), 35–38. https://doi.org/10.1345/aph.18425

Popov, L.-D., & Simionescu, N. (2020). Mitochondrial biogenesis: An update. J Cell Mol Med, 24(9), 4892–4899. https://doi.org/10.1111/jcmm.15194

Porceddu, M., Buron, N., Roussel, C., et al. (2012). Prediction of liver injury induced by chemicals in human with a multiparametric assay on isolated mouse liver mitochondria. Toxicological Sciences, 129(2), 332–345. https://doi.org/10.1093/toxsci/kfs197

Porter, R. K., & Brand, M. D. (1995). Mitochondrial proton conductance and H+/O ratio are independent of electron transport rate in isolated hepatocytes. Biochemical Journal, 310(2), 379–382. https://doi.org/10.1042/bj3100379

Poser, I., Sarov, M., Hutchins, J. R. A., et al. (2008). BAC TransgeneOmics: A high-throughput method for exploration of protein function in mammals. Nature Methods, 5(5), 405–415. https://doi.org/10.1038/nmeth.1199

Poulin, P., & Theil, F. (2002). Prediction of pharmacokinetics prior to in vivo studies. 1. Mechanism-based prediction of volume of distribution. Journal of Pharmaceutical Sciences, 91(1), 129–156. https://doi.org/10.1002/JPS.10005

Prudent, J., & McBride, H. M. (2017). The mitochondria–endoplasmic reticulum contact sites: a signalling platform for cell death. In Current Opinion in Cell Biology (Vol. 47, pp. 52–63). https://doi.org/10.1016/j.ceb.2017.03.007

Puigvert, J. C., Von Stechow, L., Siddappa, R., et al. (2013). Systems biology approach identifies the kinase Csnk1a1 as a regulator of the DNA damage response in embryonic stem cells. Science Signaling, 6(259), ra5. https://doi.org/10.1126/scisignal.2003208

Puschmann, A., Fiesel, F. C., Caulfield, T. R., et al. (2017). Heterozygous PINK1 p.G411S increases risk of Parkinson's disease via a dominant-negative mechanism. Brain, 140(1), 98–117. https://doi.org/10.1093/brain/aww261

Qin, C., Yang, G., Yang, J., et al. (2020). Metabolism of pancreatic cancer: Paving the way to better anticancer strategies. In Molecular Cancer (Vol. 19, Issue 1, p. 50). BioMed Central Ltd. https://doi.org/10.1186/s12943-020-01169-7

Quirós, P. M., Mottis, A., & Auwerx, J. (2016). Mitonuclear communication in homeostasis and stress. In Nature Reviews Molecular Cell Biology (Vol. 17, Issue 4, pp. 213-226). Nature Publishing Group. https://doi.org/10.1038/nrm.2016.23

Qureshi, M. A., Haynes, C. M., & Pellegrino, M. W. (2017). The mitochondrial unfolded protein response: Signaling from the powerhouse. In Journal of Biological Chemistry (Vol. 292, Issue 33, pp. 13500–13506). https://doi.org/10.1074/jbc.R117.791061

Rabilloud, T., & Lescuyer, P. (2015). Proteomics in mechanistic toxicology: History, concepts, achievements, caveats, and potential. In Proteomics (Vol. 15, Issues 5–6, pp. 1051–1074). https://doi.org/10.1002/pmic.201400288

Rajendran, M., Dane, E., Conley, J., et al. (2016). Imaging adenosine triphosphate (ATP). In Biological Bulletin (Vol. 231, Issue 1, pp. 73–84). Marine Biological Laboratory. https://doi.org/10.1086/689592

Ramaiahgari, S., den Braver, M., Herpers, B., et al. (2014). A 3D in vitro model of differentiated HepG2 cell spheroids with improved liver-like properties for repeated dose high-throughput toxicity studies. Archives of Toxicology, 88(5), 1083–1095. https://doi.org/10.1007/S00204-014-1215-9

Rana, P., Aleo, M. D., Gosink, M., et al. (2019). Evaluation of in Vitro Mitochondrial Toxicity Assays and Physicochemical Properties for Prediction of Organ Toxicity Using 228 Pharmaceutical Drugs. In Chemical Research in Toxicology (Vol. 32, Issue 1, pp. 156–167). https://doi.org/10.1021/acs.chemrestox.8b00246

Rao, V. K., Carlson, E. A., & Yan, S. S. (2014). Mitochondrial permeability transition pore is a potential drug target for neurodegeneration. In Biochimica et Biophysica Acta - Molecular Basis of Disease (Vol. 1842, Issue 8, pp. 1267–1272). https://doi.org/10.1016/j.bbadis.2013.09.003

Rasola, A., & Bernardi, P. (2011). Mitochondrial permeability transition in Ca2+-dependent apoptosis and necrosis. In Cell Calcium (Vol. 50, Issue 3, pp. 222–233). https://doi.org/10.1016/j.ceca.2011.04.007

Ratti, M., Lampis, A., Ghidini, M., et al. (2020). MicroRNAs (miRNAs) and Long Non-Coding RNAs (lncRNAs) as New Tools for Cancer Therapy: First Steps from Bench to Bedside. In Targeted Oncology (Vol. 15, Issue 3, pp. 261–278). https://doi.org/10.1007/s11523-020-00717-x

Raue, A., Kreutz, C., Maiwald, T., et al. (2009). Structural and practical identifiability analysis of partially observed dynamical models by exploiting the profile likelihood. Bioinformatics, 25(15), 1923–1929. https://doi.org/10.1093/bioinformatics/btp358

Raue, A., Schilling, M., Bachmann, J., et al. (2013). Lessons Learned from Quantitative Dynamical Modeling in Systems Biology. PLoS ONE, 8(9), e74335. https://doi.org/10.1371/journal.pone.0074335

Rauthan, M., & Pilon, M. (2015). A chemical screen to identify inducers of the mitochondrial unfolded protein response in C. elegans. Worm, 4(4), e1096490. https://doi.org/10.1080/21624054.2015.1096490

Reddy, P. H. (2014). Increased mitochondrial fission and neuronal dysfunction in Huntington's disease: Implications for molecular inhibitors of excessive mitochondrial fission. In Drug Discovery Today (Vol. 19, Issue 7, pp. 951–955). https://doi.org/10.1016/j.drudis.2014.03.020

Reisch, A. S., & Elpeleg, O. (2007). Biochemical Assays for Mitochondrial Activity: Assays of TCA Cycle Enzymes and PDHc. In Methods in Cell Biology (Vol. 80, pp. 199–222). Methods Cell Biol. https://doi.org/10.1016/S0091-679X(06)80010-5

Reynolds, D. (2009). Gaussian Mixture Models. In Encyclopedia of Biometrics (pp. 659–663). Springer US. https://doi.org/10.1007/978-0-387-73003-5_196

Ribeiro, S. M., Giménez-Cassina, A., & Danial, N. N. (2015). Measurement of mitochondrial oxygen consumption rates in mouse primary neurons and astrocytes. Methods in Molecular Biology, 1241, 59–69. https://doi.org/10.1007/978-1-4939-1875-1_6

Ritchie, M. E., Phipson, B., Wu, D., et al. (2015). Limma powers differential expression analyses for RNA-sequencing and microarray studies. Nucleic Acids Research, 43(7), e47. https://doi.org/10.1093/nar/gkv007

Rizzuto, R., Simpson, A. W. M., Brini, M., et al. (1992). Rapid changes of mitochondrial Ca2+ revealed by specifically targeted recombinant aequorin. Nature, 358(6384), 325–327. https://doi.org/10.1038/358325a0

Rodgers, T., & Rowland, M. (2006). Physiologically based pharmacokinetic modelling 2: predicting the tissue distribution of acids, very weak bases, neutrals and zwitterions. Journal of Pharmaceutical Sciences, 95(6), 1238–1257. https://doi.org/10.1002/JPS.20502

Rodrigues, R. M., Kollipara, L., Chaudhari, U., et al. (2018). Omics-based responses induced by bosentan in human hepatoma HepaRG cell cultures. Archives of Toxicology, 92(6), 1939–1952. https://doi.org/10.1007/s00204-018-2214-z

Rodríguez-Enríquez, S., Juárez, O., Rodríguez-Zavala, J. S., et al. (2001). Multisite control of the Crabtree effect in ascites hepatoma cells. European Journal of Biochemistry, 268(8), 2512-2519. https://doi.org/10.1046/j.1432-1327.2001.02140.x

Rodríguez-Martín, T., Pooler, A. M., Lau, D. H. W., et al. (2016). Reduced number of axonal mitochondria and tau hypophosphorylation in mouse P301L tau knockin neurons. Neurobiology of Disease, 85, 1-10. https://doi.org/10.1016/j.nbd.2015.10.007

Ron, D., & Walter, P. (2007). Signal integration in the endoplasmic reticulum unfolded protein response. In Nature Reviews Molecular Cell Biology (Vol. 8, Issue 7, pp. 519–529). https://doi.org/10.1038/nrm2199

Rosenberger, C., Rosen, S., Paliege, A., et al. (2009). Pimonidazole adduct immunohistochemistry in the rat kidney: Detection of tissue hypoxia. Methods in Molecular Biology, 466, 161–174. https://doi.org/10.1007/978-1-59745-352-3_12

Ross, M. F., Da Ros, T., Blaikie, F. H., et al. (2006). Accumulation of lipophilic dications by mitochondria and cells. Biochemical Journal, 400(1), 199–208. https://doi.org/10.1042/BJ20060919

Rowland, A. A., & Voeltz, G. K. (2012). Endoplasmic reticulum-mitochondria contacts: Function of the junction. In Nature Reviews Molecular Cell Biology (Vol. 13, Issue 10, pp. 607–625). https://doi.org/10.1038/nrm3440

RStudio Team. (2016). RStudio: Integrated Development for R. 2016.

Rudis, B., Bolker, B., Schulz, J., (2017). ggalt: Extra Coordinate Systems, 'Geoms', Statistical Transformations, Scales and Fonts for 'ggplot2'. R package version 0.4.0. https://CRAN.R-project.org/package=ggalt

Rumsey, W. L., Vanderkooi, J. M., & Wilson, D. F. (1988). Imaging of phosphorescence: A novel method for measuring oxygen distribution in perfused tissue. Science, 241(4873), 1649–1651. https://doi.org/10.1126/science.3420417

Ruprecht, J., Yankovskaya, V., Maklashina, E., et al. (2009). Structure of Escherichia coli succinate:quinone oxidoreductase with an occupied and empty quinone-binding site. The Journal of Biological Chemistry, 284(43), 29836–29846. https://doi.org/10.1074/JBC.M109.010058

Rustin, P., Bourgeron, T., Parfait, B., et al. (1997). Inborn errors of the Krebs cycle: A group of unusual mitochondrial diseases in human. Biochim Biophys Acta, 1361(2), 185–197. https://doi.org/10.1016/S0925-4439(97)00035-5

Sabbaha, H. N., & Stanley, W. C. (2002). Partial fatty acid oxidation inhibitors: A potentially new class of drugs for heart failure. In European Journal of Heart Failure (Vol. 4, Issue 1, pp. 3–6). https://doi.org/10.1016/S1388-9842(01)00183-0

Sacks, W., Esser, A. H., & Sacks, S. (1991). Inhibition of pyruvate dehydrogenase complex (PDHC) by antipsychotic drugs. Biological Psychiatry, 29(2), 176–182. https://doi.org/10.1016/0006-3223(91)90046-O

Salabei, J., Gibb, A., & Hill, B. (2014). Comprehensive measurement of respiratory activity in permeabilized cells using extracellular flux analysis. Nature Protocols, 9(2), 421–438. https://doi.org/10.1038/NPROT.2014.018

Samanta, K., Mirams, G. R., & Parekh, A. B. (2018). Sequential forward and reverse transport of the Na+ Ca2+ exchanger generates Ca2+ oscillations within mitochondria. Nature Communications, 9(1), 156. https://doi.org/10.1038/s41467-017-02638-2

Sandoval-Acuña, C., Lopez-Alarcón, C., Aliaga, M. E., et al. (2012). Inhibition of mitochondrial complex i by various non-steroidal anti-inflammatory drugs and its protection by quercetin via a coenzyme Q-like action. Chemico-Biological Interactions, 199(1), 18-28. https://doi.org/10.1016/j.cbi.2012.05.006

Sangar, M. C., Bansal, S., & Avadhani, N. G. (2010). Bimodal targeting of microsomal cytochrome P450s to mitochondria: Implications in drug metabolism and toxicity. In Expert Opinion on Drug Metabolism and Toxicology (Vol. 6, Issue 10, pp. 1231–1251). https://doi.org/10.1517/17425255.2010.503955

SAPEA, Science Advice for Policy by European Academies. (2018) Improving authorisation processes for plant protection products in Europe: a scientific perspective on the potential risks to human health. Berlin: SAPEA. https://doi.org/10.26356/plantprotectionproducts

Sarewicz, M., & Osyczka, A. (2015). Electronic connection between the quinone and cytochrome C redox pools and its role in regulation of mitochondrial electron transport and redox signaling. Physiological Reviews, 95(1), 219–243. https://doi.org/10.1152/PHYSREV.00006.2014

Sargsyan, A., Cai, J., Fandino, L. B., et al. (2015). Rapid parallel measurements of macroautophagy and mitophagy in mammalian cells using a single fluorescent biosensor. Scientific Reports, 5, 12397. https://doi.org/10.1038/srep12397

Satoh, T., Miyoshi, H., Sakamoto, K., et al. (1996). Comparison of the inhibitory action of synthetic capsaicin analogues with various NADH-ubiquinone oxidoreductases. Biochimica et Biophysica Acta, 1273(1), 21–30. https://doi.org/10.1016/0005-2728(95)00131-X

Schell, J. C., Olson, K. A., Jiang, L., et al. (2014). A role for the mitochondrial pyruvate carrier as a repressor of the warburg effect and colon cancer cell growth. Molecular Cell, 56(3), 400–413. https://doi.org/10.1016/j.molcel.2014.09.026

Schmidt, A., Kellermann, J., & Lottspeich, F. (2005). A novel strategy for quantitative proteomics using isotope-coded protein labels. Proteomics, 5(1), 4–15. https://doi.org/10.1002/pmic.200400873

Schreyer, A., & T, B. (2012). USRCAT: real-time ultrafast shape recognition with pharmacophoric constraints. Journal of Cheminformatics, 4(1), 27. https://doi.org/10.1186/1758-2946-4-27

Schuler, F., Yano, T., S, D. B., et al. (1999). NADH-quinone oxidoreductase: PSST subunit couples electron transfer from iron-sulfur cluster N2 to quinone. Proceedings of the National Academy of Sciences of the United States of America, 96(7), 4149–4153. https://doi.org/10.1073/PNAS.96.7.4149

Schwab, M. A., Kölker, S., Van Den Heuvel, L. P., et al. (2005). Optimized spectrophotometric assay for the completely activated pyruvate dehydrogenase complex in fibroblasts. Clinical Chemistry, 51(1), 151–160. https://doi.org/10.1373/clinchem.2004.033852

Seabold, S., & Perktold, J. (2010). Statsmodels: Econometric and Statistical Modeling with Python. Proceedings of the 9th Python in Science Conference. https://doi.org/10.25080/majora-92bf1922-011

Seo, A. Y., Joseph, A. M., Dutta, D., et al. (2010). New insights into the role of mitochondria in aging: Mitochondrial dynamics and more. In Journal of Cell Science (Vol. 123, Issue Pt 15, pp. 2533–2542). https://doi.org/10.1242/jcs.070490

Serra, A., Fratello, M., Cattelani, L., et al. (2020). Transcriptomics in Toxicogenomics, Part III: Data Modelling for Risk Assessment. In Nanomaterials (Vol. 4, pp. 708–710). https://doi.org/10.3390/nano10040708

Shah, I., Woodrow Setzer, R., Jack, J., et al. (2016). Using toxcastTM data to reconstruct dynamic cell state trajectories and estimate toxicological points of departure. Environmental Health Perspectives, 124(7), 910–919. https://doi.org/10.1289/ehp.1409029

Shan, J., Lopez, M. C., Baker, H. V., et al. (2010). Expression profiling after activation of amino acid deprivation response in HepG2 human hepatoma cells. Physiological Genomics, 41(3), 315–327. https://doi.org/10.1152/physiolgenomics.00217.2009

Sharma, L., Lu, J., & Bai, Y. (2009). Mitochondrial respiratory complex I: structure, function and implication in human diseases. Current Medicinal Chemistry, 16(10), 1266–1277. https://doi.org/10.2174/092986709787846578

Shebley, M., Sandhu, P., Emami Riedmaier, A., et al. (2018). Physiologically Based Pharmacokinetic Model Qualification and Reporting Procedures for Regulatory Submissions: A Consortium Perspective. Clinical Pharmacology & Therapeutics, 104(1), 88–110. https://doi.org/10.1002/cpt.1013

Shi, Y., Inoue, H., Wu, J. C., et al. (2017). Induced pluripotent stem cell technology: A decade of progress. In Nature Reviews Drug Discovery (Vol. 16, Issue 2, pp. 115–130). Nature Publishing Group. https://doi.org/10.1038/nrd.2016.245

Shiio, Y., & Aebersold, R. (2006). Quantitative proteome analysis using isotope-coded affinity tags and mass spectrometry. Nature Protocols, 1(1), 139–145. https://doi.org/10.1038/nprot.2006.22

Shoshan-Barmatz, V., & Mizrachi, D. (2012). VDAC1: from structure to cancer therapy. Frontiers in Oncology, 29(2), 164. https://doi.org/10.3389/fonc.2012.00164

Shpilka, T., & Haynes, C. M. (2018). The mitochondrial UPR: Mechanisms, physiological functions and implications in ageing. In Nature Reviews Molecular Cell Biology (Vol. 19, Issue 2, pp. 109–120). https://doi.org/10.1038/nrm.2017.110

Sierotzki, H., & Scalliet, G. (2013). A review of current knowledge of resistance aspects for the next-generation succinate dehydrogenase inhibitor fungicides. Phytopathology, 103(9), 880–887. https://doi.org/10.1094/PHYTO-01-13-0009-RVW

Sies, H., Berndt, C., & Jones, D. P. (2017). Oxidative Stress: Annual Review of Biochemistry. Annual Review of Biochemistry, 86, 715–748. https://doi.org/10.1146/annurev-biochem-061516-045037

Simon, J. M., Paranjape, S. R., Wolter, J. M., et al. (2019). High-throughput screening and classification of chemicals and their effects on neuronal gene expression using RASL-seq. Scientific Reports, 9(1), 4529. https://doi.org/10.1038/s41598-019-39016-5

Smirnova, E., Griparic, L., Shurland, D. L., et al. (2001). Dynamin-related protein Drp1 is required for mitochondrial division in mammalian cells. Molecular Biology of the Cell, 12(8), 2245–2256. https://doi.org/10.1091/mbc.12.8.2245

Smith, A. C., Eyassu, F., Mazat, J. P., et al. (2017). MitoCore: A curated constraint-based model for simulating human central metabolism. BMC Systems Biology, 11(1), 114. https://doi.org/10.1186/s12918-017-0500-7

Smith, L. C., Lavelle, C. M., Silva-Sanchez, C., et al. (2018). Early phosphoproteomic changes for adverse outcome pathway development in the fathead minnow (Pimephales promelas) brain. Scientific Reports, 8(1), 10212. https://doi.org/10.1038/s41598-018-28395-w

Smith, L., Villaret-Cazadamont, J., Claus, S. P., et al. (2020). Important considerations for sample collection in metabolomics studies with a special focus on applications to liver functions. In Metabolites (Vol. 10, Issue 3, p. 104). https://doi.org/10.3390/metabo10030104

Sommer, C., Straehle, C., Kothe, U., et al. (2011). Ilastik: Interactive learning and segmentation toolkit. Proceedings - International Symposium on Biomedical Imaging, 230–233. https://doi.org/10.1109/ISBI.2011.5872394

Spagou, K., Wilson, I. D., Masson, P., et al. (2011). HILIC-UPLC-MS for exploratory urinary metabolic profiling in toxicological studies. Analytical Chemistry, 83(1), 382–390. https://doi.org/10.1021/ac102523q

Späth, M. R., Bartram, M. P., Palacio-Escat, N., et al. (2019). The proteome microenvironment determines the protective effect of preconditioning in cisplatin-induced acute kidney injury. Kidney International, 95(2), 333–349. https://doi.org/10.1016/j.kint.2018.08.037

Speidel, D. (2015). The role of DNA damage responses in p53 biology. In Archives of Toxicology (Vol. 89, Issue 4, pp. 501–517). https://doi.org/10.1007/s00204-015-1459-z

Stelzer, G., Rosen, N., Plaschkes, I., et al. (2016). The GeneCards suite: From gene data mining to disease genome sequence analyses. Current Protocols in Bioinformatics, 54, 1.30.1-1.30.33. https://doi.org/10.1002/cpbi.5

Stowe, D. F., & Camara, A. K. S. (2009). Mitochondrial reactive oxygen species production in excitable cells: Modulators of mitochondrial and cell function. In Antioxidants and Redox Signaling (Vol. 11, Issue 6, pp. 1373–1414). Antioxid Redox Signal. https://doi.org/10.1089/ars.2008.2331

Strauss, K. A., Jinks, R. N., Puffenberger, E. G., et al. (2015). CODAS syndrome is associated with mutations of LONP1, encoding mitochondrial AAA+ lon protease. American Journal of Human Genetics, 96(1), 121–135. https://doi.org/10.1016/j.ajhg.2014.12.003

Suárez-Rivero, J., Villanueva-Paz, M., de la Cruz-Ojeda, P., et al. (2016). Mitochondrial Dynamics in Mitochondrial Diseases. Diseases, 5(1), 1. https://doi.org/10.3390/diseases5010001

Sutherland, J. J., Webster, Y. W., Willy, J. A., et al. (2018). Toxicogenomic module associations with pathogenesis: A network-based approach to understanding drug toxicity. Pharmacogenomics Journal, 18(3), 377–390. https://doi.org/10.1038/tpj.2017.17

Symersky, J., Osowski, D., Walters, D. E., et al. (2012a). Oligomycin frames a common drug-binding site in the ATP synthase. Proc Natl Acad Sci USA, 109(35), 13961–13965. https://doi.org/10.1073/pnas.1207912109

Symersky, J., Osowski, D., Walters, D. E., et al. (2012b). Oligomycin frames a common drug-binding site in the ATP synthase. Proc Natl Acad Sci USA, 109(35), 13961–13965. https://doi.org/10.1073/pnas.1207912109

Takahashi, E., Takano, T., Nomura, Y., et al. (2006). In vivo oxygen imaging using green fluorescent protein. American Journal of Physiology - Cell Physiology, 291(4), C781–C787. https://doi.org/10.1152/ajpcell.00067.2006

Tanner, C., Kamel, F., Ross, G., et al. (2011). Rotenone, paraquat, and Parkinson's disease. Environmental Health Perspectives, 119(6), 866–872. https://doi.org/10.1289/EHP.1002839

Tanner, C. M., Ross, G. W., Jewell, S. A., et al. (2009). Occupation and risk of parkinsonism: A multicenter case-control study. Archives of Neurology, 66(9), 1106–1113. https://doi.org/10.1001/archneurol.2009.195

Tarca, A. L., Carey, V. J., Chen, X. wen, et al. (2007). Machine learning and its applications to biology. In PLoS computational biology (Vol. 3, Issue 6, p. e116). https://doi.org/10.1371/journal.pcbi.0030116

Terron, A., Bal-Price, A., Paini, A., et al. (2018). An adverse outcome pathway for parkinsonian motor deficits associated with mitochondrial complex I inhibition. Archives of Toxicology, 92(1), 41–82. https://doi.org/10.1007/S00204-017-2133-4

Thomas, B., & Flint Beal, M. (2007). Parkinson's disease. In Human Molecular Genetics (Vol. 16, Issue Spec No. 2, pp. R183–R194). https://doi.org/10.1093/hmg/ddm159

Tian, Q., Stepaniants, S. B., Mao, M., et al. (2004). Integrated genomic and proteomic analyses of gene expression in mammalian cells. Molecular and Cellular Proteomics, 3(10), 960–969. https://doi.org/10.1074/mcp.M400055-MCP200

Tian, Y., Li, B., Shi, W. Z., et al. (2014). Dynamin-related protein 1 inhibitors protect against ischemic toxicity through attenuating mitochondrial ca2+ uptake from endoplasmic reticulum store in PC12 cells. International Journal of Molecular Sciences, 15(2), 3172–3185. https://doi.org/10.3390/ijms15023172

Tilmant, K., Gerets, H., De Ron, P., et al. (2018). In vitro screening of cell bioenergetics to assess mitochondrial dysfunction in drug development. Toxicology in Vitro : An International Journal Published in Association with BIBRA, 52, 374–383. https://doi.org/10.1016/J.TIV.2018.07.012

Titz, B., Elamin, A., Martin, F., et al. (2014). Proteomics for systems toxicology. In Computational and Structural Biotechnology Journal (Vol. 11, Issue 18, pp. 73–90). https://doi.org/10.1016/j.csbj.2014.08.004

To, T. L., Cuadros, A. M., Shah, H., et al. (2019). A Compendium of Genetic Modifiers of Mitochondrial Dysfunction Reveals Intra-organelle Buffering. Cell, 179(5), 1222-1238.e17. https://doi.org/10.1016/j.cell.2019.10.032

Tocilescu, M., Zickermann, V., Zwicker, K., et al. (2010). Quinone binding and reduction by respiratory complex I. Biochimica et Biophysica Acta, 1797(12), 1883–1890. https://doi.org/10.1016/J.BBABIO.2010.05.009

Troger, F., Delp, J., Funke, M., et al. (2020). Identification of mitochondrial toxicants by combined in silico and in vitro studies – A structure-based view on the adverse outcome pathway. Computational Toxicology, 14, 100123. https://doi.org/10.1016/J.COMTOX.2020.100123

Tulli, S., Del Bondio, A., Baderna, V., et al. (2019). Pathogenic variants in the AFG3L2 proteolytic domain cause SCA28 through haploinsufficiency and proteostatic stress-driven OMA1 activation. Journal of Medical Genetics, 56(8), 499–511. https://doi.org/10.1136/jmedgenet-2018-105766

Uchinomiya, S., Matsunaga, N., Kamoda, K., et al. (2020). Fluorescence detection of metabolic activity of the fatty acid beta oxidation pathway in living cells. Chemical Communications, 56(20), 3023–3026. https://doi.org/10.1039/c9cc09993j

Udeani, G., Zhao, G., Shin, Y., et al. (2001). Pharmacokinetics of deguelin, a cancer chemopreventive agent in rats. Cancer Chemotherapy and Pharmacology, 47(3), 263–268. https://doi.org/10.1007/S002800000187

Um, J. H., Kim, Y. Y., Finkel, T., et al. (2018). Sensitive measurement of mitophagy by flow cytometry using the pH-dependent fluorescent reporter mt-Keima. Journal of Visualized Experiments, 2018(138). https://doi.org/10.3791/58099

US-EPA, United States Environmental Protection Agency (2020). New approach methods work plan: Reducing use of animals in chemical testing. U.S. Environmental Protection Agency, Washington, DC. EPA 615B2001 https://www.epa.gov/sites/production/files/2020-06/documents/epa_nam_work_plan.pdf

Valente, E. M., Abou-Sleiman, P. M., Caputo, V., et al. (2004). Hereditary early-onset Parkinson's disease caused by mutations in PINK1. Science, 304(5674), 1158–1160. https://doi.org/10.1126/science.1096284

Van Den Bogert, C., Spelbrink, J. N., & Dekker, H. L. (1992). Relationship between culture conditions and the dependency on mitochondrial function of mammalian cell proliferation. Journal of Cellular Physiology, 152(3), 632–638. https://doi.org/10.1002/jcp.1041520323

van der Stel, W., Carta, G., Eakins, J., Darici, S., Delp, J., A, F., et al. (2020). Multiparametric assessment of mitochondrial respiratory inhibition in HepG2 and RPTEC/TERT1 cells using a panel of mitochondrial targeting agrochemicals. Archives of Toxicology, 94(8), 2707–2729. https://doi.org/10.1007/S00204-020-02792-5

van Ravenzwaay, B., Cunha, G. C. P., Leibold, E., et al. (2007). The use of metabolomics for the discovery of new biomarkers of effect. Toxicology Letters, 172(1–2), 21–28. https://doi.org/10.1016/j.toxlet.2007.05.021

Van Ravenzwaay, B., Herold, M., Kamp, H., et al. (2012). Metabolomics: A tool for early detection of toxicological effects and an opportunity for biology based grouping of chemicals-From QSAR to QBAR. Mutation Research - Genetic Toxicology and Environmental Mutagenesis, 746(2), 144–150. https://doi.org/10.1016/j.mrgentox.2012.01.006

van Ravenzwaay, B., Sperber, S., Lemke, O., et al. (2016). Metabolomics as read-across tool: A case study with phenoxy herbicides. Regulatory Toxicology and Pharmacology, 81, 288–304. https://doi.org/10.1016/j.yrtph.2016.09.013

van Riel, N. A. W. (2006). Dynamic modelling and analysis of biochemical networks: Mechanism-based models and model-based experiments. In Briefings in Bioinformatics (Vol. 7, Issue 4, pp. 364–374). Brief Bioinform. https://doi.org/10.1093/bib/bbl040

Van Summeren, A., Renes, J., Van Delft, J. H. M., et al. (2012). Proteomics in the search for mechanisms and biomarkers of drug-induced hepatotoxicity. In Toxicology in Vitro (Vol. 26, Issue 3, pp. 373–385). https://doi.org/10.1016/j.tiv.2012.01.012

Vander Heiden, M. G., Cantley, L. C., & Thompson, C. B. (2009). Understanding the warburg effect: The metabolic requirements of cell proliferation. In Science (Vol. 324, Issue 5930, pp. 1029–1033). https://doi.org/10.1126/science.1160809

Vasan, K., Werner, M., & Chandel, N. S. (2020). Mitochondrial Metabolism as a Target for Cancer Therapy. In Cell Metabolism (Vol. 32, Issue 3, pp. 341–352). Cell Press. https://doi.org/10.1016/j.cmet.2020.06.019

Villeneuve, D., D, C., N, G.-R., et al. (2014). Adverse outcome pathway (AOP) development I: strategies and principles. Toxicological Sciences : An Official Journal of the Society of Toxicology, 142(2), 312–320. https://doi.org/10.1093/TOXSCI/KFU199

Villeneuve, D. L., Crump, D., Garcia-Reyero, N., et al. (2014a). Adverse outcome pathway (AOP) development I: Strategies and principles. Toxicological Sciences, 142(2), 312–320. https://doi.org/10.1093/toxsci/kfu199

Villeneuve, D. L., Crump, D., Garcia-Reyero, N., et al. (2014b). Adverse outcome pathway development II: Best practices. Toxicological Sciences, 142(2), 321–330. https://doi.org/10.1093/toxsci/kfu200

Vinken, M. (2013). The adverse outcome pathway concept: A pragmatic tool in toxicology. In Toxicology (Vol. 312, pp. 158–165). https://doi.org/10.1016/j.tox.2013.08.011

von Jagow, G., & TA, L. (1986). Use of specific inhibitors on the mitochondrial bc1 complex. Methods in Enzymology, 126(C), 253–271. https://doi.org/10.1016/S0076-6879(86)26026-7

von Stechow, L., Ruiz-Aracama, A., van de Water, B., et al. (2013). Identification of Cisplatin-Regulated Metabolic Pathways in Pluripotent Stem Cells. PLoS ONE, 8(10), e76476. https://doi.org/10.1371/journal.pone.0076476

Voos, W., & Röttgers, K. (2002). Molecular chaperones as essential mediators of mitochondrial biogenesis. In Biochim Biophys Acta (Vol. 1592, Issue 1, pp. 51-62). https://doi.org/10.1016/S0167-4889(02)00264-1

Vowinckel, J., Hartl, J., Butler, R., et al. (2015). MitoLoc: A method for the simultaneous quantification of mitochondrial network morphology and membrane potential in single cells. Mitochondrion, 24, 77–86. https://doi.org/10.1016/j.mito.2015.07.001

Vuckovic, D. (2012). Current trends and challenges in sample preparation for global metabolomics using liquid chromatography-mass spectrometry. In Analytical and Bioanalytical Chemistry (Vol. 403, Issue 6, pp. 1523–1548). https://doi.org/10.1007/s00216-012-6039-y

Waldeck-Weiermair, M., Gottschalk, B., Madreiter-Sokolowski, C. T., et al. (2019). Development and Application of Sub-Mitochondrial Targeted Ca2 + Biosensors. Frontiers in Cellular Neuroscience, 13, 449. https://doi.org/10.3389/fncel.2019.00449

Waldmann, T., Rempel, E., Balmer, N. V., König, A., et al. (2014). Design principles of concentration-dependent transcriptome deviations in drug-exposed differentiating stem cells. Chemical Research in Toxicology, 27(3), 408–420. https://doi.org/10.1021/tx400402j

Waldmeier, P. C., Feldtrauer, J. J., Qian, T., et al. (2002). Inhibition of the mitochondrial permeability transition by the nonimmunosuppressive cyclosporin derivative NIM811. Molecular Pharmacology, 62(1), 22–29. https://doi.org/10.1124/mol.62.1.22

Wallace, D. C., & Chalkia, D. (2013). Mitochondrial DNA genetics and the heteroplasmy conundrum in evolution and disease. Cold Spring Harbor Perspectives in Biology, 5(11), a021220. https://doi.org/10.1101/cshperspect.a021220

Wan, B., LaNoue, K. F., Cheung, J. Y., et al. (1989). Regulation of citric acid cycle by calcium. Journal of Biological Chemistry, 64(23), 13430–13439.

Wang, A., Costello, S., Cockburn, M., et al. (2011). Parkinson's disease risk from ambient exposure to pesticides. European Journal of Epidemiology, 26(7), 547–555. https://doi.org/10.1007/s10654-011-9574-5

Wang, L., Yuan, L., Zeng, X., et al. (2016). A Multisite-Binding Switchable Fluorescent Probe for Monitoring Mitochondrial ATP Level Fluctuation in Live Cells. Angewandte Chemie - International Edition, 55(5), 1773–1776. https://doi.org/10.1002/anie.201510003

Wang, X. D., & Wolfbeis, O. S. (2014). Optical methods for sensing and imaging oxygen: Materials, spectroscopies and applications. In Chemical Society Reviews (Vol. 43, Issue 10, pp. 3666–3761). Royal Society of Chemistry. https://doi.org/10.1039/c4cs00039k

Wang, Z. M., Ying, Z., Bosy-Westphal, A., et al. (2010). Specific metabolic rates of major organs and tissues across adulthood: Evaluation by mechanistic model of resting energy expenditure. American Journal of Clinical Nutrition, 92(6), 1369–1377. https://doi.org/10.3945/ajcn.2010.29885

Ward, J. H. (1963). Hierarchical Grouping to Optimize an Objective Function. Journal of the American Statistical Association, 236–244. https://doi.org/10.1080/01621459.1963.10500845

West, A. P., Khoury-Hanold, W., Staron, M., et al. (2015). Mitochondrial DNA stress primes the antiviral innate immune response. Nature, 520(7548), 553–557. https://doi.org/10.1038/nature14156

Westermann, B. (2010). Mitochondrial fusion and fission in cell life and death. In Nature Reviews Molecular Cell Biology (Vol. 11, Issue 12, pp. 872–884). https://doi.org/10.1038/nrm3013

Westrate, L. M., Drocco, J. A., Martin, K. R., et al. (2014). Mitochondrial morphological features are associated with fission and fusion events. PLoS ONE, 9(4), e95265. https://doi.org/10.1371/journal.pone.0095265

Wetmore, B. A., & Merrick, B. A. (2004). Toxicoproteomics: Proteomics applied to toxicology and pathology. In Toxicologic Pathology (Vol. 32, Issue 6, pp. 619–642). https://doi.org/10.1080/01926230490518244

Wickham, H., (2007). Reshaping Data with the reshape Package. Journal of Statistical Software, 21(12), 1-20. URL http://www.jstatsoft.org/v21/i12/.

Wickham, H., (2011). The Split-Apply-Combine Strategy for Data Analysis. Journal of Statistical Software, 40(1), 1-29. URL http://www.jstatsoft.org/v40/i01/.

Wickham, H., (2016), ggplot2: Elegant Graphics for Data Analysis. Springer-Verlag New York, https://CRAN.R-project.org/package=ggplot2

Wickham, H., Bryan, J., (2019). readxl: Read Excel Files. R package version 1.3.1. https://CRAN.R-project.org/package=readxl

Wickham, H., (2019). stringr: Simple, Consistent Wrappers for Common String Operations. R package version 1.4.0. https://CRAN.R-project.org/package=stringr

Wickham, H., Seidel, D., (2020). scales: Scale Functions for Visualization. R package version 1.1.1. https://CRAN.R-project.org/package=scales

Wickham, H., (2020). tidyr: Tidy Messy Data. R package version 1.1.2. https://CRAN.R-project.org/package=tidyrWill, Y., & Dykens, J. (2014). Mitochondrial toxicity assessment in industry-a decade of technology development and insight. Expert Opinion on Drug Metabolism and Toxicology, 10(8), 1061–1067. https://doi.org/10.1517/17425255.2014.939628

Wickham, H., François, R., Henry, L., Müller, K., (2021). dplyr: A Grammar of Data Manipulation. R package version 1.0.4. https://CRAN.R-project.org/package=dplyr

Wiederschain, G. Y. (2011). The Molecular Probes handbook. A guide to fluorescent probes and labeling technologies. Biochemistry (Moscow), 76(11), 1276–1276. https://doi.org/10.1134/s0006297911110101

Will, Y., & Dykens, J. (2014). Mitochondrial toxicity assessment in industry-a decade of technology development and insight. In Expert Opinion on Drug Metabolism and Toxicology (Vol. 10, Issue 8, pp. 1061–1067). https://doi.org/10.1517/17425255.2014.939628

Will, Y., Hynes, J., Ogurtsov, V. I., et al. (2007). Analysis of mitochondrial function using phosphorescent oxygen-sensitive probes. Nature Protocols, 1(6), 2563–2572. https://doi.org/10.1038/nprot.2006.351

Will, Y., Shields, J. E., & Wallace, K. B. (2019). Drug-induced mitochondrial toxicity in the geriatric population: Challenges and future directions. In Biology (Vol. 8, Issue 2, p. 32). https://doi.org/10.3390/biology8020032

Williams, B. B., Khan, N., Zaki, B., et al. (2010). Clinical electron paramagnetic resonance (EPR) oximetry using India ink. Advances in Experimental Medicine and Biology, 662, 149–156. https://doi.org/10.1007/978-1-4419-1241-1_21

Williams, E. G., Wu, Y., Jha, P., et al. (2016). Systems proteomics of liver mitochondria function. Science, 352(6291), aad0189. https://doi.org/10.1126/science.aad0189

Wills, L. P., Beeson, G. C., Hoover, D. B., et al. (2015). Assessment of ToxCast phase II for mitochondrial liabilities using a high-throughput respirometric assay. Toxicological Sciences, 146(2), 226–234. https://doi.org/10.1093/toxsci/kfv085

Wilmes, A., Bielow, C., Ranninger, C., et al. (2015). Mechanism of cisplatin proximal tubule toxicity revealed by integrating transcriptomics, proteomics, metabolomics and biokinetics. Toxicology in Vitro, 30(1 Pt A), 117–127. https://doi.org/10.1016/j.tiv.2014.10.006

Wilmes, A., Limonciel, A., Aschauer, L., et al. (2013). Application of integrated transcriptomic, proteomic and metabolomic profiling for the delineation of mechanisms of drug induced cell stress. Journal of Proteomics, 79, 180–194. https://doi.org/10.1016/j.jprot.2012.11.022

Wilson, T., & Woodland Hastings, J. (1998). Bioluminescence. In Annual Review of Cell and Developmental Biology (Vol. 14, pp. 197–230). Annu Rev Cell Dev Biol. https://doi.org/10.1146/annurev.cellbio.14.1.197

Wink, S., Hiemstra, S., Herpers, B., et al. (2017). High-content imaging-based BAC-GFP toxicity pathway reporters to assess chemical adversity liabilities. Archives of Toxicology, 91(3), 1367–1383. https://doi.org/10.1007/s00204-016-1781-0

Wink, S., Hiemstra, S., Huppelschoten, S., et al. (2014). Quantitative high content imaging of cellular adaptive stress response pathways in toxicity for chemical safety assessment. In Chemical Research in Toxicology (Vol. 27, Issue 3, pp. 338–355). https://doi.org/10.1021/tx4004038

Wink, S., Hiemstra, S. W., Huppelschoten, S., et al. (2018). Dynamic imaging of adaptive stress response pathway activation for prediction of drug induced liver injury. Archives of Toxicology, 92(5), 1797–1814. https://doi.org/10.1007/s00204-018-2178-z

Witten, D., (2019). PoiClaClu: Classification and Clustering of Sequencing Data Based on a Poisson Model. R package version 1.0.2.1. https://CRAN.R-project.org/package=PoiClaClu

Wittenberg, J. B. (1970). Myoglobin-facilitated oxygen diffusion: role of myoglobin in oxygen entry into muscle. In Physiological reviews (Vol. 50, Issue 4, pp. 559–636). https://doi.org/10.1152/physrev.1970.50.4.559

Wojtczak, L., & Zabłocki, K. (2008). Basic Mitochondrial Physiology in Cell Viability and Death. In Drug-Induced Mitochondrial Dysfunction (pp. 1–35). John Wiley & Sons, Inc. https://doi.org/10.1002/9780470372531.ch1

Wolters, J. E. J., Van Herwijnen, M. H. M., Theunissen, D. H. J., et al. (2016). Integrative "-Omics" Analysis in Primary Human Hepatocytes Unravels Persistent Mechanisms of Cyclosporine A-Induced Cholestasis. Chemical Research in Toxicology, 29(12), 2164–2174. https://doi.org/10.1021/acs.chemrestox.6b00337

Wood, E., Latli, B., & Casida, J. E. (1996). Fenazaquin Acaricide Specific Binding Sites in NADH: Ubiquinone Oxidoreductase and Apparently the ATP Synthase Stalk. Pesticide Biochemistry and Physiology, 54(2), 135–145. https://doi.org/10.1006/PEST.1996.0017

World Health Organization (2010) International Programme on Chemical Safety & Inter-Organization Programme for the Sound Management of Chemicals. Characterization and application of physiologically based phamacokinetic models in risk assessment.https://apps.who.int/iris/handle/10665/44495

Wu, C. C., Luk, H. N., Lin, Y. T. T., et al. (2010). A Clark-type oxygen chip for in situ estimation of the respiratory activity of adhering cells. Talanta, 81(1–2), 228–234. https://doi.org/10.1016/j.talanta.2009.11.062

Wu, F., Yang, F., Vinnakota, K. C., et al. (2007). Computer modeling of mitochondrial tricarboxylic acid cycle, oxidative phosphorylation, metabolite transport, and electrophysiology. Journal of Biological Chemistry, 282(34), 24525–24537. https://doi.org/10.1074/jbc.M701024200

Xia, M., Huang, R., Shi, Q., et al. (2018a). Comprehensive analyses and prioritization of Tox21 10K chemicals affecting mitochondrial function by in-depth mechanistic studies. Environmental Health Perspectives, 126(7), 077010. https://doi.org/10.1289/EHP2589

Xu, Z., Singh, N. J., Lim, J., et al. (2009). Unique sandwich stacking of pyrene-adenine-pyrene for selective and ratiometric fluorescent sensing of ATP at physiological pH. Journal of the American Chemical Society, 131(42), 15528–15533. https://doi.org/10.1021/ja906855a

Yaginuma, H., Kawai, S., Tabata, K. V., et al. (2014). Diversity in ATP concentrations in a single bacterial cell population revealed by quantitative single-cell imaging. Scientific Reports, 4, 6522. https://doi.org/10.1038/srep06522

Yang, H., Meijer, H. G. E., Buitenweg, J. R., et al. (2016). Estimation and identifiability of model parameters in human nociceptive processing using yes-no detection responses to electrocutaneous stimulation. Frontiers in Psychology, 7, 1884. https://doi.org/10.3389/fpsyg.2016.01884

Yang, H., Niemeijer, M., van de Water, B., et al. (2020). ATF6 Is a Critical Determinant of CHOP Dynamics during the Unfolded Protein Response. IScience, 23(2), 100860. https://doi.org/10.1016/j.isci.2020.100860

Yang, Y., Nadanaciva, S., Will, Y., et al. (2015). MITOsym®: A mechanistic, mathematical model of hepatocellular respiration and bioenergetics. Pharmaceutical Research, 32(6), 1975–1992. https://doi.org/10.1007/s11095-014-1591-0

Ye, J., Kumanova, M., Hart, L. S., et al. (2010). The GCN2-ATF4 pathway is critical for tumour cell survival and proliferation in response to nutrient deprivation. EMBO Journal, 29(12), 2082–2096. https://doi.org/10.1038/emboj.2010.81

Yeakley, J., Shepard, P., Goyena, D., et al. (2017). A trichostatin A expression signature identified by TempO-Seq targeted whole transcriptome profiling. PloS One, 12(5). https://doi.org/10.1371/JOURNAL.PONE.0178302

Yen, K., Lee, C., Mehta, H., et al. (2012). The emerging role of the mitochondrial-derived peptide humanin in stress resistance. In Journal of Molecular Endocrinology (Vol. 50, Issue 1, pp. R11–R19). https://doi.org/10.1530/JME-12-0203

Yépez, V. A., Kremer, L. S., Iuso, A., et al. (2018). OCR-Stats: Robust estimation and statistical testing of mitochondrial respiration activities using seahorse xf analyzer. PLoS ONE, 13(7), e0199938. https://doi.org/10.1371/journal.pone.0199938

Yi, H. S., Chang, J. Y., & Shong, M. (2018). The mitochondrial unfolded protein response and mitohormesis: A perspective on metabolic diseases. In Journal of Molecular Endocrinology (Vol. 61, Issue 3, pp. R91–R105). https://doi.org/10.1530/JME-18-0005

Youle, R. J., & Narendra, D. P. (2011). Mechanisms of mitophagy. Nature Reviews Molecular Cell Biology, 12(1), 9–14. https://doi.org/10.1038/nrm3028

Youle, R. J., & Van Der Bliek, A. M. (2012). Mitochondrial fission, fusion, and stress. In Science (Vol. 337, Issue 6098, pp. 1062–1065). https://doi.org/10.1126/science.1219855

Yuan, L., & Kaplowitz, N. (2013). Mechanisms of drug-induced liver injury. In Clinics in Liver Disease (Vol. 17, Issue 4, pp. 507–518). W.B. Saunders. https://doi.org/10.1016/j.cld.2013.07.002

Yumnamcha, T., Devi, T. S., & Singh, L. P. (2019). Auranofin Mediates Mitochondrial Dysregulation and Inflammatory Cell Death in Human Retinal Pigment Epithelial Cells: Implications of Retinal Neurodegenerative Diseases. Frontiers in Neuroscience, 13, 1065. https://doi.org/10.3389/fnins.2019.01065

Zachar, Z., Marecek, J., Maturo, C., et al. (2011). Non-redox-active lipoate derivates disrupt cancer cell mitochondrial metabolism and are potent anticancer agents in vivo. Journal of Molecular Medicine, 89(11), 1137–1148. https://doi.org/10.1007/s00109-011-0785-8

Zahedi, A., On, V., Phandthong, R., et al. (2018). Deep Analysis of Mitochondria and Cell Health Using Machine Learning. Scientific Reports, 8(1), 1–15. https://doi.org/10.1038/s41598-018-34455-y

Zeileis, A., Fisher, J. C., Hornik, K., et al. (2020). Colorspace: A toolbox for manipulating and assessing colors and palettes. Journal of Statistical Software. https://doi.org/10.18637/jss.v096.i01

Zgheib, E., Gao, W., Limonciel, A., et al. (2019). Application of three approaches for quantitative AOP development to renal toxicity. Computational Toxicology, 11, 1–13. https://doi.org/10.1016/j.comtox.2019.02.001

Zhang, H., Chen, Q. Y., Xiang, M. L., et al. (2009). In silico prediction of mitochondrial toxicity by using GA-CG-SVM approach. Toxicology in Vitro, 23(1), 134–140. https://doi.org/10.1016/j.tiv.2008.09.017

Zhao, P., Wang, L., Zhu, X., et al. (2010). Subnanomolar inhibitor of cytochrome bc1 complex designed by optimizing interaction with conformationally flexible residues. Journal of the American Chemical Society, 132(1), 185–194. https://doi.org/10.1021/JA905756C

Zhao, X. Y., Lu, M. H., Yuan, D. J., et al. (2019). Mitochondrial dysfunction in neural injury. In Frontiers in Neuroscience (Vol. 13, p. 30). https://doi.org/10.3389/fnins.2019.00030

Zhao, Y., Araki, S., Wu, J., et al. (2011). An expanded palette of genetically encoded Ca2+ indicators. Science, 333(6051), 1888–1891. https://doi.org/10.1126/science.1208592

Zhao, Y., & Jensen, O. N. (2009). Modification-specific proteomics: Strategies for characterization of post-translational modifications using enrichment techniques. In Proteomics (Vol. 9, Issue 20, pp. 4632–4641). https://doi.org/10.1002/pmic.200900398

Zhong, X., da Silveira e Sá, R. de C., & Zhong, C. (2017). Mitochondrial biogenesis in response to chromium (VI) toxicity in human liver cells. International Journal of Molecular Sciences, 18(9), 1877. https://doi.org/10.3390/ijms18091877

Zhong, Y., Li, X., Yu, D., et al. (2015). Application of mitochondrial pyruvate carrier blocker UK5099 creates metabolic reprogram and greater stem-like properties in LnCap prostate cancer cells in vitro. Oncotarget, 6(35), 37758–37769. https://doi.org/10.18632/oncotarget.5386

Zhou, Y., Zhang, S., He, H., et al. (2018). Design and synthesis of highly selective pyruvate dehydrogenase complex E1 inhibitors as bactericides. Bioorganic and Medicinal Chemistry, 26(1), 84–95. https://doi.org/10.1016/j.bmc.2017.11.021

Zhou, Z., Austin, G., Young, L., et al. (2018). Mitochondrial Metabolism in Major Neurological Diseases. Cells, 7(12), 229. https://doi.org/10.3390/cells7120229

Zoeteweij, J. P., Van De Water, B., De Bont, H. J. G. M., et al. (1994). Mitochondrial K+ as modulator of Ca2+-dependent cytotoxicity in hepatocytes. Novel application of the K+-sensitive dye PBFI (K+-binding benzofuran isophthalate) to assess free mitochondrial K+ concentrations. Biochemical Journal, 299(Pt 2), 539–543. https://doi.org/10.1042/bj2990539

Züchner, S., Mersiyanova, I. V., Muglia, M., et al. (2004). Mutations in the mitochondrial GTPase mitofusin 2 cause Charcot-Marie-Tooth neuropathy type 2A. Nature Genetics, 36(5), 449–451. https://doi.org/10.1038/ng1341

Zukunft, S., Prehn, C., Röhring, C., et al. (2018). High-throughput extraction and quantification method for targeted metabolomics in murine tissues. Metabolomics, 14(1), 18. https://doi.org/10.1007/s11306-017-1312-x

# Websites


1. https://www.khanacademy.org/science/biology/membranes-and-transport/active-transport/a/active-transport, accessed April 2021
2. https://www.khanacademy.org/science/biology/cell-signaling/mechanisms-of-cell-signaling/a/intracellular-signal-transduction, accessed April 2021
3. https://aopwiki.org/aops; accessed April 2021
4. https://www.oecd.org/chemicalsafety/testing/adverse-outcome-pathways-molecular-screening-and-toxicogenomics.htm; accessed April 2021
5. https://www.uniprot.org/uniprot/Q9Y5U8; accessed April 2021
6. https://www.malacards.org/card/mitochondrial_pyruvate_carrier_deficiency; accessed April 2021
7. https://www.genecards.org/cgi-bin/carddisp.pl?gene=MPC2&keywords=MPC2; accessed April 2021
8. https://ghr.nlm.nih.gov/condition/pyruvate-dehydrogenase-deficiency; accessed April 2021
9. https://clinicaltrials.gov/ct2/home; accessed April 2021
10. https://www.ncbi.nlm.nih.gov/nuccore/NC_012920.1; accessed April 2021
11. https://www.frac.info/; (FRAC poster 2021 (R) accessed April 2021
12. https://medlineplus.gov/genetics/condition/charcot-marie-tooth-disease/#inheritance; accessed April 2021
13. http://amp.pharm.mssm.edu/Harmonizome/gene_set/Glycolysis/PANTHER+Pathways; accessed October 2021
14. http://brainarray.mbni.med.umich.edu/Brainarray/Database/CustomCDF/genomic_curated_CDF.asp; HGU133Plus2 array version, accessed June 2021.
15. https://github.com/mcs07/PubChemPy; accessed October 2021
16. https://amp.pharm.mssm.edu/archs4/gene/KLHL24; accessed October 2021
17. https://www.genecards.org/; accessed October 2021
18. https://www.fda.gov/science-research/liver-toxicity-knowledge-base-ltkb/drug-induced-liver-injury-rank-dilirank-dataset; accessed October 2021
19. https://bioconductor.org/packages/release/bioc/html/rhdf5.html; accessed 1 June2021
20. https://www.eu-toxrisk.eu/, accessed March 2021
21. http://www.oecd.org/chemicalsafety/risk-assessment/iata-integrated-approaches-to-testing-and-assessment.htm; accessed March 2021
22. https://aopwiki.org/aops/3; accessed June 2021
23. http://www.rdkit.org/; accessed March 2021
24. http://comptox.epa.gov/dashboard; accessed March 2021
25. http://chem.nlm.nih.gov/chemidplus/; accessed March 2021
26. https://smartsview.zbh.uni-hamburg.de/; accessed March 2021

# Abbreviations

| | |
|---|---|
| 2D | two-dimensional |
| 3D | three-dimensional |
| 2DG | 2-deoxy glucose |
| AA | antimycin a |
| ADP | adenosine diphosphate |
| AIC | akaike information criterion |
| AOP | adverse outcome pathway |
| APS | ammonium persulfate |
| ATP | adenosine triphosphate |
| AZO | azoxystrobin |
| BAC | bacterial artificial chromosome |
| BMC | bench mark concentration |
| CAP | capsaicin |
| CAR | carboxin |
| CDDO-me | bardoxolone methyl |
| cDNA | complementary DNA |
| CFP | cyan fluorescent protein |
| cMax | maximal concentration in plasm |
| CSA | cyclosporine a |
| CYA | cyazofamid |
| cyt | cytoplasmic |
| DCCD/DCC | N,N'-Dicyclohexylcarbodiimide |
| DDR | DNA damage response |
| DEG | differential expressed genes (transcriptomics context) |
| DEG | deguelin (compoun context) |
| DEM | diethyl maleate |
| DIA | diafenthiuron |
| DILI | drug-induced liver injury |
| DMEM | dulbecco's modified eagle's medium |
| DMSO | dimethyl sulfoxide |
| DNA | deoxyribonucleic acid |
| EC50 | half maximal effective concentration |
| EGS | eigengene Score |
| ER | Endoplasmic reticulum |
| ETC | electron transport chain |
| FAO | Fatty acid oxidation |
| FBS | fetal bovine serum |
| FC | fold change |
| FCCP | Carbonyl cyanide 4-(trifluoromethoxy) phenylhydrazone |
| FP | Fluorophore/ fluorescent protein |
| FPX | fenpyroximate |
| FRET | fluorescence resonance energy transfer |
| Gal | galactose |
| GFP | green fluorescent protein |
| Glu | glucose |
| GO | gene ontology |
| IC50 | half maximal inhibitory concentration |
| IF | Immuno fluorescence |
| KD | knock down |
| KP | kinase pool |
| MEP | mepronil |
| mito | mitochondria |
| MMP | mitochondrial membrane potential |
| mt | mitochondrial |
| N.C. | negative control |
| NES | normalized enrichment score |
| nuc | nuclear |
| O/N | overnight |
| OCR | oxygen consumption rate |
| N.C. | negative control |
| NES | normalized enrichment score |
| O/N | overnight |
| OCR | oxygen consumption rate |
| OLI | oligomycin |
| OSR | oxidative stress response |
| OXPHOS | oxidative phosphorylation |
| P.C. | positive control |
| padj | adjusted p-value |
| PBS | phosphate-buffered saline |
| PCR | polymerase chain reaction |
| PenStrep | penicillin-streptomycin |
| PHH | primary human hepatocytes |
| PI | propidium iodide |
| PIC | pixocystrobin |
| PMD | pyrimidifen |
| pme | Plasma-membrane-targeted |
| PVDF | polyvinylidene difluoride |
| PYR | pyraclostrobin |
| Rho123 | rhodamine123 |
| RNA | ribonucleic acid |
| ROS | reactive oxygen species |
| ROT | rotenone |
| RT | room temperature |
| SD | standard deviation |
| siRNA | small interfering RNA |
| TEB | tebufenpyrad |
| TF | transcription factor |
| TGGATES | Toxicogenomics Project-Genomics Assisted Toxicity Evaluation System |
| THI | thifluzamide |
| TNFa | tumour necrosis factor alpha |
| TP | time point |
| untr | untreated |
| UPR | unfolded protein response |
| VAL | valinomycin |
| WB | Western blot |
| WGCNA | weighted gene correlation network analysis |
| YFP | yellow fluorescent protein |

## Nederlandse Samenvatting

Een ongewenst effect van blootstelling aan chemische substanties zoals medicijnen, pesticiden, industriele grondstoffen en cosmetica, is het ontstaan van schade aan cruciale organen. In veel gevallen is deze schade terug te leiden tot de verstoring van verschillende organellen in de cel. Een van de belangrijkste organellen van de cel zijn de mitochondriën. De meeste cellen in het menselijk lichaam zijn in het bezit van honderden mitochondriën, die samen verantwoordelijk zijn voor de productie van energie, opslag en constructie van bouwstoffen en de regulatie van celdood. Verstoring van deze processen door langdurige lage of acute hoge blootstelling aan chemicaliën leidt tot celdood, weefsel schade en uiteindelijk orgaanletsel. In de laatste jaren heeft de industrie verschillende studies geintroduceerd om orgaanletsel te voorkomen door vroegtijdig nieuwe subtanties die mitochondriële schade veroorzaken op te sporen. Om deze vroegtijdige risicio analyse te verbeteren is het van groot belang om de relatie tussen mitochondriële schade en de uiteindelijke uitkomst voor mensen en dier beter te begrijpen. Deze kennis draagt bij aan de verbetering en hervorming van de mitochondriële risicobeoordeling voor zowel bestaande als nieuwe chemische substanties.

Mitochondriën zijn opgebouwd uit een dubbel membraan welke een geladen compartiment omsluit. Daarnaast bezitten mitochondriën verschillende enzymen die betrokken zijn bij de omzetting van xenobiotica naar metabolieten. Al deze factoren maken dat chemische substanties, zowel de oorspronkelijke stof als de metabolieten, sneller ophopen in mitochondriën dan in andere cel organellen. Schade aan een fractie van de mitochondriën zal niet onmiddelijk leiden tot ernstige weefsel- of orgaan schade sinds de mate van cellulaire toxiciteit vooral afhangt van de hoeveelheid beschadigde mitochondriën per cel en de snelheid waarmee de totale popluatie van mitochondriën kan herstellen. De cel en zijn mitochondriën bezitten verschillende adaptieve stress responses die de cel mogelijkheden biedt om te herstellen. De beschikbare responsen zijn onder anderen mechanismen die de hoeveelheid reactieve elementen verminderen of beschadede eiwitten kunnen herstellen. Daarnaast kunnen mitochondriën hun morfologie veranderen: door het fuseren van individuele organellen of fragmentere van 1 organel in meerderen, kan DNA en eiwitten worden uitgewisseld of beschadigde delen worden afgesplitst zodat deze delen specifiek kunnen worden afgebroken. Al deze systemen maken dat de cel een beperkte hoeveelheid stress intern kan afhandelen. Als de hoeveelheid stress en daarmee dus schade te groot wordt, dan zal de cel celdood programma's activeren om daarmee het weefsel of het orgaan in zijn geheel te kunnen beschermen. Echter, langdurig geringe of acute schade kunnen beiden leiden tot grote hoeveelheden celdood en daarmee uiteindelijk ook toch tot orgaan schade.

Sommige organen zijn gevoeliger voor het ontwikkelen van mitochondrieel gerelateerde problemen dan andere. Dit zijn organen die veel energie nodig hebben voor het uitvoeren van hun functie, zoals hart, de nieren en spieren, maar ook weefsels die volledig afhankelijk zijn van mitochondriën voor de energie productie, zoals neuronen. Tot slot zijn de organen die betrokken zijn bij het verwerken van alle opgenomen stoffen, zoals de nieren en de lever, ook extra gevoelig vanwegen de verhoogde blootstelling aan chemische stoffen en hun metabolieten.

In dit proefschrift bestuderen wij de rol van mitochondriën in de ontwikkeling van cellulaire schade na blootstelling aan chemische substantie, in het bijzonder landbouwchemicaliën. Hierbij hebben wij met verschillende technieken het functioneren van de mitochondriën en de cel in kaart gebracht, om vervolgens deze informatie te kunnen gebruiken in de risico beoordeling van chemische substanties.

In **hoofdstuk 2** hebben we de zes meest belangrijke mitochondriële processen, die verstoord kunnen raken in mitochondriën gerelateerd letsel, gedefinieerd aan de hand van de ontwikkeling van menselijke ziekten veroorzaakt door mutaties in eiwitten betrokken bij deze processen. We bespreken de huidige *in vitro* methoden om deze processen te bestuderen. Tot slot bespreken we de mogelijkheid om deze methoden te gebruiken in verschillende cel modelen in de context van adverse outcome pathways (AOP) om zo kennis te genereren die bruikbaar voor de risicobeoordeling van bestaande en nieuwe chemische substanties.

In **hoofdstuk 3** hebben we meerdere landbouwchemicaliën, die zijn ontworpen om specifiek de mitochondriële energie productie te verstoren in ongedierte, getest op hun verstorende werking in human mitochondriën. Voor deze vergelijkingsstudie hebben we gekozen voor 2 humane cel types die gerelateerd zijn aan organen met verhoogde gevoeligheid voor: HepG2 als lever-achtig celtype en RPTEC-TERT1 als nier-achtig celtype. Wij hebben hier de verstoring van mitochondriën bestudeerdt door gebruik te maken van een set bekende mitochondriële remmers in meerdere assays die momenteel beschikbaar zijn voor het visualiseren en bestuderen van mitochondriën.

De remmers verstoren mitochondriële energie productie door een interactie aan te gaan met 1 van de 5 betrokken eiwitcomplexen. Gebruikmakend van de geselecteerde assays hebben wij duidelijk het verschil in potentie tussen de remmers van eiwitcomplex I en III laten zien. Daarnaast werd het duidelijk dat het meten van de mitochondriële ademhaling de meest gevoelige waarneming is in beide celtypes. De blootstelling aan complex II remmers heeft geen gevolgen in deze celtypes. Het aanpassen van de kweek-condities door middel van het vervangen van het medium of de introductie van een artficiële extracellulaire matrix leidde tot verhoogde

sensitiviteit van de HepG2 cellen, voornamelijk bij blootstelling aan mitochondriële complex I remmers.

In **hoofdstuk 4** hebben wij ons specifiek gericht op mechanistisch onderzoek om de interactie tussen mitochondriën en de cell ten tijde van mitochondriële schade te ontrafelen. De chemicaliën als beschreven in hoofdstuk 3 zijn ingezet in in een combinatie van microscopie- en genexpressie assays voor zowel mitochondriële als cellulaire metingen. Met deze opzet was het mogelijk om de effecten van chemicaliën op mitochondriële integriteit en cellulaire gezondheid te koppelen aan veranderingen in gen expressie. Aan de hand van verschillende gen expressie analysis waren wij niet in staat om complex I- of complex III-specifieke genexpressie patronen of unieke genen te identificeren. Het was wel mogelijk om een set genen te selecteren die uniek was voor de verstoring van mitochondriën in het algemeen. Het genexpressie profiel komt overeen met de waarnemingen van de membraan integriteits metingen en mitochondriele ademhaling. Daarnaast hebben we onderzocht of deze set van genen in staat was om mitochondriële verstoring te detecteren in een nieuwe set chemicaliën, waarvan bekend is dat zij leverschade veroorzaken. De set van genen voorspelde correct de correlatie tussen de mitochondriële membraan integriteit en gen expressie voor 4 van de 5 geteste chemicaliën. Tot slot konden we vaststellen dat het uitschakelen van enkele van deze genen leidde tot meer celdood, nadat mitochondriële schade was opgetreden.

Eerder hebben we aangegeven dat het belangrijk is om de betrokkenheid van mitochondriën in cellulaire schade te kunnen visualiseren en dit het liefst te kunnen doen in een vroeg stadium van de risico beoordeling. In **hoofdstuk 5** hebben we de potentie van mitochondriële morfologie als mogelijke indicator voor mitochondriële schade bekeken. Daarnaast hebben we de relatie tussen mitochondriële morphologie en andere mitochondriële metingen zoals het ATP niveau, het mitochondriële membraan potentiaal (MMP) en de levensvatbaarheid bestudeerd. Ten eerste hebben we een analyse methode opgezet om objectief grote hoeveelheden microscopie data te analyseren en de aanwezige mitochondriën te classificeren als gefuseerd of gefragmenteerd. Deze analyse methode kon worden gebruikt om de waargenomen morfologie te kwantificeren. Het blijkt dat gefragmenteerd mitochondriën vooral ontstaan na blootselling aan complex V en niet aan complex I of III remmers welke allen leiden tot een afname in het ATP niveau, maar een verschillend effect hebben op MMP. Het verschil in morfologische verandering kon worden relateerd aan het optreden van specifieke veranderingen in een eiwit, namelijk OPA1. Tot slot hebben we gekeken naar de relatie van meerdere eiwitten die betrokken zijn bij de morfologische veranderingen en verschillende mitochondriële meeting zoals het ATP niveau, MMP en levensvatbaarheid na blootstelling aan oligomycin.

In het laatste experimentele **hoofdstuk 6**, hebben we de effecten van mitochondriële ademhaling remmers op de MM- dynamiek bestudeerd aan de hand van computationele modellen. Door gebruik te maken van concentrati-e en tijds-afhankelijk data konden we de afname in MMP na blootstelling met complex I-, II- en III-remmers moduleren. Gebaseerd op de geobserveerde afwijking tussen the model en de experimentele data na blootstelling met een uncoupler (FCCP) en een complex V remmer (oligomycin) konden we het model verbeteren door de toevoeging van proton lekkage en farmacokinetiek.

In **hoofdstuk 7** hebben we de verkregen *in vitro* en *in silico* data opgenomen in een risico beoordeling die zich specifiek focust op de vergelijking van chemische substanties met vergelijkbare chemische en biologische eigenschappen. In deze risico beoordeling is alle beschikbare data gekoppeld aan biologische gebeurtenissen die zijn omschreven in een bestaand of een nieuw voorgestelde adverse outcome pathway (AOP). Een AOP is een lineare beschrijving van een toxicologisch proces aan de hand van opeenvolgende gebeurtenissen, beginnend bij de interactie van een chemische stof met het biologische systeem tot uiteindelijk de ontwikkeling van orgaanschade. We bespreken in dit hoofdstuk twee pesticiden en beredeneren aan de hand van *in vitro* en *in silico* data de waarschijnlijkheid dat zij een risico vormen voor het ontwikkelen van neuronale schade door middel van verstoring van de mitochondriën.

Dit proefschrift vergroot de kennis omtrent de bijdragen van mitochondriën en mitochondriële communicatie in de ontwikkeling orgaanschade. Verder hebben wij verschillende methoden voor de beoordeling van mitochondriën geëvalueerd en in de context geplaatst van risicobeoordeling van chemische substanties. We zijn gestart met het ontwikkelen van high-content methoden om in de toekomst mogelijk sneller en betrouwbaarder mitochondriële verstoring te detecteren en de risico beoordeling uit te voeren aan de hand van biologisch en mechanistisch relevant bewijs.

## List of Publications

*Multiparametric assessment of mitochondrial respiratory inhibition in HepG2 and RPTEC/TERT1 cells using a panel of mitochondrial targeting agrochemicals.*
**W. van der Stel**[1], G. Carta[1], J. Eakins, S. Darici, J. Delp, A. Forsby, S. Hougaard Bennekou, I. Gardner, M. Leist, E.H.J. Danen, P. Walker, B. Van de Water, P. Jennings
[1] Authors contributed equally
Archives of Toxicology, 2020, https://doi.org/10.1007/s00204-020-02849-5

*Mapping the cellular response to electron transport chain inhibitors reveals selective signaling networks triggered by mitochondrial perturbation*
**W. van der Stel**, H. Yang, N.G. Vrijenhoek, J.P. Schimming, G. Callegaro, G. Carta, S. Darici, J. Delp, A. Forsby, A. White, S. le Dévédec, M. Leist, P. Jennings, J. Beltman, B. van de Water, E. H.J. Danen
Archives of Toxicology, 2021, doi: 10.1007/s00204-021-03160-7

*Mitochondrial fragmentation through OPA1-cleavage in response to ETC inhibition is driven by a combination of reduced ATP and increased MMP*
**W. van der Stel**, H. Yang, S. le Dévédec, B. van de Water, J.J. Beltman, E.H.J Danen
Cell Biology and Toxicology, 2021, Submitted

*Dynamic modeling of mitochondrial membrane potential upon exposure to mitochondrial inhibitors*
H. Yang, **W. van der Stel**, R. Lee, C. Bauch, S. Bevan, P. Walker, B. van de Water, E.H.J Danen, J.J. Beltman
Frontiers in Pharmacology, 2021, https://doi.org/10.3389/fphar.2021.679407

*New approach methods (NAMs) supporting read-across: two neurotoxicity AOP-based IATA case studies*
**W. van der Stel**, G. Carta, J. Eakins, J. Delp, I. Suciu, A. Forsby, A. Cediel-Ulloa, K. Attoff, F. Troger, H. Kamp, I. Gardner, B. Zdrazil, M. Moné, G.F. Ecker, M. Pastor, J.C. Gomes, A. White, E.H.J. Danen, M. Leist, P. Walker, P. Jennings, S. Hougaard Bennekou, B. van de Water
ALTEX, 2021, https://doi.org/10.14573/altex.2103051

*Case study on the use of integrated approaches to testing and assessment for identification and characterisation of parkinsonian hazard liability of deguelin by an aop-based testing and read across approach: Series on Testing and Assessment No. 326*
**W. van der Stel**, S. Hougaard Bennekou, G. Carta, J. Eakins, J. Delp, A. Forsby, H. Kamp, I. Gardner, B. Zdradil, M. Pastor, J.C. Gomes, A. White, T. Steger-Hartman, E.H.J. Danen, M. Leist, P. Walker, P. Jennings, B. van de Water
OECD platform, 2020, URL: https://orbit.dtu.dk/en/publications/case-study-on-the-use-of-integrated-approaches-to-testing-and-ass-2

*Case study on the use of integrated approaches to testing and assessment for mitochondrial complex-iii-mediated neurotoxicity of azoxystrobin - read-across to other strobilurins: Series on testing and assessment no. 327*
S. Hougaard Bennekou, **W. van der Stel**, G. Carta, J. Eakins, J. Delp, A. Forsby, H. Kamp, I. Gardner, B. Zdradil, M. Pastor, J.C. Gomes, A. White, T. Steger-Hartman, E.H.J. Danen, M. Leist, P. Walker, P. Jennings, B. van de Water
OECD platform, 2020, URL: https://orbit.dtu.dk/en/publications/case-study-on-the-use-of-integrated-approaches-to-testing-and-ass

*Development of a Neurotoxicity Assay That Is Tuned to Detect Mitochondrial Toxicants*
J. Delp, M. Funke, F. Rudolf, A. Cediel, S. Hougaard Bennekou, **W. van der Stel**, G. Carta, P. Jennings, C. Toma, I. Gardner, B. van de Water, A. Forsby, M. Leist
Achieves of Toxicology, 2019, DOI: 10.1007/s00204-019-02473-y

*Identification of mitochondrial toxicants by combined in silico and in vitro studies – A structure-based view on the adverse outcome pathway*
F. Troger, J. Delp, M. Funke, **W. van der Stel**, C. Colas, M. Leist, B. van de Water, G.F. Ecker
Computational Toxicology, 2020, https://doi.org/10.1016/j.comtox.2020.100123

*Neurotoxicity and underlying cellular changes of 21 mitochondrial respiratory chain inhibitors*
J. Delp, A. Cediel-Ulloa, I. Suciu, P. Kranaster, B. van Vugt-Lussenburg, V. Kos, **W. van der Stel**, G. Carta, S. Bennekou, P. Jennings, B. van de Water, A. Forsby, M. Leist
Archives of Toxicology, 2021, https://doi.org/10.1007/s00204-020-02970-5

*Physiologically relevant estrogen receptor alpha pathway reporters for single cell imaging-based carcinogenic hazard assessment of estrogenic compounds*
B. Duijndam, A. Goudriaan, T. van den Hoorn, **W. van der Stel**, S. le Dévédec, P. Bouwman, J.W. van der Laan, B. van de Water
Toxicological Sciences, 2021, https://doi.org/10.1093/toxsci/kfab037

*A quantitative AOP of mitochondrial toxicity based on data from three cell lines*
T. Cleo, W. Gao, J. Delp, G. Carta, **W. van der Stel**, M. Leist, P. Jennings, B. van de Water, F. Bois
Toxicological Sciences, 2021, Submitted

*Evaluation of an imaging-based in vitro screening platform for estrogenic activity with OECD reference chemicals*
B. Duijndam, M. Tedeschi, **W. van der Stel**, T. van den Hoorn, B. van der Burg, P. Bouwman, J.W. van der Laan, B. van der Water
Toxicology in Vitro, 2021, Submitted

*A systematic high throughput transcriptomics and phenotypic screening approach to classify the pro-oxidant mode-of-action of a large class of phenolic compounds*
L.J.M. Bischoff, J.P. Schimming, **W. van der Stel**, M. Niemeijer, S. Escher, G. Callegaro, S.J. ter Braak, J.P. Langenberg, D. Noort, B. van de Water
Ready for submission

## About the author

Wanda van der Stel was born in Dordrecht, on the 4th of October 1991. She complete her VWO diploma with a major in Natuur en Techniek plus Gezondheid (Nature & Technique and Nature & Heath) with an addition subject of art at the Stedelijk Dalton Lyceum. At the Leiden University she obtained her bachelor and master degree in Bio-Pharmaceutical Sciences. During her master program she contributed to the research assessing TNFα signaling dynamics in drug induced liver injury (DILI) at the division of Drug Discovery and Safety (DDS) at the Leiden Academic Center of Drug Research (LACDR). Her second internship was at the DKFZ in Heidelberg , Germany continuing the research in the field of DILI, but now assessing the effects of liver toxicants on the transcription and translocation of IL6 and downstream signaling components. During her literature study she summarized the current knowledge in the field of vaccine administration in the battle of eradication of polio. After acquiring her master degree, she started as a PhD under the supervision of Prof. Erik Danen and prof. Bob van de Water and assessing *High throughput approaches to unravel key events in mitochondrial adverse outcome pathways*. Currently, she is employed as post-doctoral researcher in the lab of Bob van de Water to set up a high throughput Crispr screening facility.